TESE DE DOUTORAMENTO

Drivers of hydrological extremes in current and future climates: the role of atmospheric moisture transport

Luis Gimeno Sotelo

2024

"Mención internacional"

Universidade Vigo

EIDO
Escola Internacional
de Doutoramento

Universida de Vigo

Escola Internacional de Doutoramento

Luis Gimeno Sotelo

TESE DE DOUTORAMENTO

Drivers of hydrological extremes in current and future climates: the role of atmospheric moisture transport

Dirixida por:

Dr. Sergio Martín Vicente Serrano

Dr. David Barriopedro Cepero

2024

"Mención internacional"

Campus Universitario de Ourense, Universidade de Vigo

Departamento de Física Aplicada | Environmental Physics Laboratory (EPhysLab)

Luis Gimeno Sotelo (luis.gimeno-sotelo@uvigo.gal)

Universidade Vigo

Escola Internacional de Doutoramento

Dr. Sergio Martín Vicente Serrano e Dr. David Barriopedro Cepero, profesores de investigación do Consello Superior de Investigacións Científicas (CSIC):

FAN CONSTAR que o presente traballo, titulado ***"Drivers of hydrological extremes in current and future climates: the role of atmospheric moisture transport"*** que presenta Luis Gimeno Sotelo para a obtención do título de Doutor pola Universidade de Vigo con Mención Internacional, foi elaborado baixo a súa dirección no programa de doutoramento *"Auga, sustentabilidade e desenvolvemento"* baixo a modalidade de compendio de publicacións.

Ourense, 18 de xullo de 2024

Os directores da tese de doutoramento

Dr. Sergio Martín Vicente Serrano　　　　Dr. David Barriopedro Cepero

Acknowledgements

I would like to express my gratitude to all the people who have supported me during the development of this thesis in the different aspects of my life: my supervisors, colleagues, family and friends. I especially thank:

- Sergio and David: for their constant advice.

- My father: for always being there.

- Raquel, Isidro and Sancho: for putting up with me during these years.

- Patricia: for letting me know what love is.

- Corina: for showing me the culture of hard work.

- Coral, Marina and Santi: for being much more than cousins.

- Julia, Miguel Ángel and my aunts and uncles: for the nice family times we spend together.

- José Carlos: for being a fantastic colleague and friend.

- Gleisis, Carlos Javier, José and Claudia: for being great friends and the wonderful moments we have lived over the last years.

- Rogert and Milica: for the nice collaborations we have done during my PhD period.

- Marta: for helping me a lot with the teaching work.

- Emanuele and Jakob: for learning a lot from them during my visit to Leipzig.

I acknowledge the funding from the *Ministerio de Ciencia, Innovación y Universidades* and *Agencia Estatal de Investigación* (*MICIU/AEI /10.13039/501100011033*), and the *Fondo Social Europeo Plus (FSE+)*, under the PhD Grant PRE2022-101497. This work is supported by the SETESTRELO project (grant no. PID2021-122314OB-I00), funded by the *MICIU/AEI /10.13039/501100011033* and by the *Fondo Europeo de Desarrollo Regional (FEDER), Unión Europea (UE)*. As a member of the EPhysLab research group, I acknowledge the support by *Xunta de Galicia* under the Project ED431C2021/44 (*Programa de Consolidación e Estructuración de Unidades de Investigación Competitivas (Grupos de Referencia Competitiva)* and *Consellería de Cultura, Educación e Universidade*). This thesis has also been possible thanks to the computing resources and technical support provided by *CESGA (Centro de Supercomputación de Galicia)* and *RES (Red Española de Supercomputación)*.

CONTENTS

RESUMEN

Los extremos meteorológicos y climáticos son una amenaza constante para la sociedad, tanto en términos de salud como económicos, y un buen entendimiento de los mismos es crucial para el próspero desarrollo de la Humanidad. Son de gran interés aquellos relacionados con el ciclo del agua, como las sequías, que ha sido el más mortal en las últimas décadas, o aquellos asociados a precipitaciones extremas, los más costosos económicamente. A pesar de la complejidad en la definición de ambos extremos, estos fenómenos siempre están asociados a excesos o ausencias de precipitación. La escala temporal en la que se desarrollan es diferente, puesto que la precipitación extrema se suele estudiar en escalas cortas (como la subdiaria o la diaria) y las sequías a escalas mayores (por ejemplo, la mensual o la estacional). En todo caso, existen varios tipos de sequía (meteorológica, agrícola, hidrológica, socioeconómica o ecológica), dependiendo del ámbito al que se refiere, siendo la sequía meteorológica, asociada a déficits de precipitación, aquella que es objeto de estudio en esta tesis. Así, en este trabajo doctoral se pretende avanzar en el conocimiento de los factores que afectan a las precipitaciones extremas y a las sequías meteorológicas a escala global, tanto en el clima presente como en el futuro, centrando la atención en el papel que juega el transporte de humedad atmosférica.

El transporte de vapor de agua en la atmósfera es un componente clave del ciclo hidrológico global. La atmósfera recibe vapor de agua de la superficie de la Tierra fundamentalmente de la evaporación oceánica (y en mucha menor medida de los continentes), y es transportado, afectando a los regímenes de precipitación a escala global. Las áreas en las que, climatológicamente, la evaporación excede a la precipitación definen

las principales regiones fuentes de humedad, y son principalmente oceánicas, aunque también hay fuentes terrestres muy relevantes como las cuencas del río Amazonas o el Congo. Existen determinados mecanismos atmosféricos que son responsables del transporte de humedad a escala global, destacando los ríos atmosféricos y los chorros de niveles bajos. Los ríos atmosféricos son corredores largos y estrechos de humedad en la troposfera que no tienen posiciones geográficas permanentes y están frecuentemente asociados a los ciclones extratropicales, siendo los más relevantes en el transporte del vapor de agua que llega a las latitudes medias. Las principales regiones continentales de ocurrencia de ríos atmosféricos incluyen las costas Pacífica y Atlántica de Norte América, la costa Atlántica de Europa, la costa Pacífica de Asia, y el suroeste de Sudamérica, Sudáfrica y Australia. En cambio, los chorros de niveles bajos son importantes en regiones tropicales y subtropicales, tienen una posición geográfica semi-permanente y se caracterizan por fuertes vientos en la baja troposfera, fundamentalmente por la noche. Uno de los más estudiados, el de las Grandes Llanuras, principalmente activo en verano, transporta vapor de agua desde el Golfo de México hasta las Grandes Llanuras de Norte América y es responsable de aproximadamente un tercio del vapor de agua total que llega al territorio continental de Estados Unidos.

El papel del transporte de humedad en la ocurrencia de precipitaciones es clave, ya que el vapor de agua total contenido en una columna de aire en un momento dado no suele ser suficiente para mantener la ocurrencia de precipitación, siendo necesario un aporte constante de humedad desde el exterior. Así, los excesos y déficits de transporte de humedad suelen estar asociados a extremos hidrometeorológicos, influyendo en precipitaciones extremas y sequías, respectivamente. Además de la necesidad de humedad atmosférica disponible para la generación de precipitaciones, también es necesario un mecanismo que fuerce el ascenso del aire. Los ascensos del aire pueden producirse por forzamiento orográfico o por inestabilidad atmosférica, ocurriendo esta última a muy diferentes escalas espacio-temporales, desde escalas de tormentas y mesoescalares, que deben su inestabilidad fundamentalmente a causas termodinámicas, como a escala sinóptica en sistemas meteorológicos como frentes o ciclones extratropicales, que deben su inestabilidad fundamentalmente a causas dinámicas. La influencia relativa de la inestabilidad atmosférica con respecto al contenido de humedad es también un tema relevante. Así, para que ocurra precipitación extrema debe alcanzarse un determinado valor de inestabilidad atmosférica, pero, una vez alcanzado éste, la magnitud de la precipitación extrema depende más de la humedad atmosférica disponible que del valor de la inestabilidad.

Como consecuencia del calentamiento global, el aire puede almacenar una mayor cantidad de vapor de agua debido al aumento de las temperaturas, según la relación de Clausius-Clapeyron, que corresponde a un aumento del 6-7% por cada 1 K de aumento de temperatura. En este marco de calentamiento, tanto las precipitaciones extremas como el transporte de humedad a nivel global también aumentarían siguiendo dicha relación termodinámica, aunque pueden existir diferencias regionales debidas a cambios en la circulación atmosférica, es decir, a factores dinámicos. Si bien se prevé que la mayor parte de la superficie mundial experimente cambios en las precipitaciones extremas al ritmo de la relación de Clausius-Clapeyron, hay algunas regiones en las que los factores dinámicos desempeñan un papel importante, pudiendo aumentar estas precipitaciones extremas más rápido o más despacio que el ritmo dictado por la relación de Clausius-Clapeyron. En cuanto a los mecanismos de transporte de humedad, también se prevén cambios con el calentamiento global, de tal manera que, por ejemplo, se prevé que los ríos atmosféricos transporten una mayor cantidad de humedad, se produzcan con más frecuencia y su ubicación se desplace hacia los polos. Mientras que en el clima histórico ya se ha observado una tendencia general al aumento de las precipitaciones extremas, los cambios en las sequías meteorológicas son más inciertos. Aunque las proyecciones futuras basadas en modelos climáticos muestran un aumento en la frecuencia de las condiciones secas en algunas regiones del planeta, son pocas las áreas en las que dicha tendencia se ha observado ya en el clima presente.

El objetivo de esta tesis es cuantificar el papel del transporte de humedad en las precipitaciones extremas y las sequías meteorológicas en el clima actual y futuro, siguiendo un enfoque probabilístico. Estas complejas relaciones requieren técnicas estadísticas avanzadas, como las tomadas de la Teoría de Valores Extremos o las cópulas. Estas versátiles técnicas fueron diseñadas específicamente para captar el comportamiento de los valores más altos (o más bajos) de las variables estudiadas, así como los distintos tipos de dependencia existentes entre ellas. Para llevar a cabo los análisis pretendidos, se necesitan datos de precipitación y de transporte de humedad en rejilla, obtenidos de las bases de datos más apropiadas para cada estudio específico. Para los estudios centrados en clima presente, los datos de precipitación se obtuvieron de bases de datos basadas en observaciones y de los reanálisis del Centro Europeo de Previsiones Meteorológicas a Medio Plazo, mientras que para estudiar el clima futuro, se utilizaron datos de un modelo climático de la Fase 6 del Proyecto de Intercomparación de Modelos Acoplados. Utilizando datos de reanálisis y de dicho modelo climático, el transporte de humedad se cuantificó desde un enfoque Euleriano para los estudios de precipitación extrema y desde una aproximación Lagrangiana en los relacionados con la ocurrencia de sequía. Esta aproximación Lagrangiana permitió estimar la contribución a la precipitación en una región determinada procedente de la humedad de una fuente dada. Para estudiar la relación entre las sequías meteorológicas y los déficits de las contribuciones a la precipitación de las fuentes de humedad consideradas, se utilizaron índices estandardizados, que permiten realizar comparaciones en el espacio y el tiempo.

En cuanto a los resultados obtenidos, primeramente se identificaron las regiones en las que el transporte de humedad ejerce una mayor influencia sobre la precipitación diaria extrema en el clima presente. Se obtuvo que el transporte de humedad ejerce una influencia débil en las regiones tropicales, donde ya existe una gran cantidad de humedad y las contribuciones de humedad procedentes de regiones exteriores no son necesarias para que se produzcan precipitaciones extremas. Sin embargo, en las zonas subtropicales y extratropicales se encontró que el transporte de humedad tiene una mayor influencia en las precipitaciones extremas, principalmente vinculada a los patrones de los principales mecanismos de transporte de humedad. De hecho, las regiones de mayor ocurrencia de estos mecanismos se corresponden estrechamente con las zonas de influencia del componente dinámico del transporte de humedad en las precipitaciones extremas. Dicho componente, íntimamente relacionado con la circulación atmosférica, se espera que juegue un papel clave para comprender los cambios en la relación entre el transporte de humedad y las precipitaciones extremas en un contexto de calentamiento global.

Adicionalmente, se demostró que la ocurrencia simultánea de valores extremos de transporte de humedad y precipitación está claramente influenciada por los ríos atmosféricos en sus regiones de ocurrencia. Se encontró que existe una elevada probabilidad de extremos concurrentes, junto con valores razonablemente altos de transporte de humedad y precipitación, en las regiones donde los ríos atmosféricos tocan tierra. El análisis específico de estas regiones mostró que existen probabilidades más altas de extremos concurrentes en el hemisferio norte que en el sur, siendo especialmente notables en la costa del Pacífico de América del Norte. Además, los porcentajes más altos de ocurrencia de ríos atmosféricos en los días de extremos concurrentes de transporte de humedad y precipitación se encontraron en esas regiones de ocurrencia de ríos atmosféricos (superiores al 90%), y la influencia de su penetración en zonas continentales interiores fue claramente visible (con porcentajes superiores al 75%). Sin embargo, en la mayoría de las regiones tropicales (incluidas las zonas monzónicas), los porcentajes de ocurrencia de ríos atmosféricos en los días de extremos simultáneos de transporte de humedad y precipitación no superaron el 50%, lo que refleja una baja relación de los ríos atmosféricos con la ocurrencia de extremos simultáneos en estas regiones. En general, se detectó un ligero descenso en los porcentajes de ocurrencia de ríos atmosféricos en los días de extremos concurrentes de transporte de humedad y precipitación en el clima presente, una vez eliminados los posibles efectos de El Niño-Oscilación del Sur. Este descenso, que es especialmente marcado en las costas norteamericanas (tanto del Atlántico como del Pacífico) en invierno, puede ser visto como un resultado preliminar sobre los efectos del calentamiento global en la relación de los ríos atmosféricos con los extremos concurrentes de transporte de humedad y precipitación.

La importancia de los extremos de transporte de humedad en la ocurrencia de precipitaciones extremas se analizó en función de otros dos factores fundamentales: el agua precipitable (contenido de vapor de agua en la columna de aire) y la velocidad vertical, que representan factores termodinámicos y dinámicos que afectan a la precipitación extrema. Se calculó la probabilidad condicional de precipitaciones extremas para todas las combinaciones de valores extremos y no extremos de los tres factores estudiados para el clima actual. En primer lugar, se comprobó que al menos uno de los factores debe ser extremo para que se produzcan precipitaciones de elevada intensidad. Además, se demostró que, a escala mundial, las condiciones extremas en la velocidad vertical favorecen notablemente la aparición de precipitaciones extremas. Sin embargo, el agua precipitable es el factor más relevante para la ocurrencia de precipitación extrema en regiones subtropicales, y el transporte de humedad el principal factor en las regiones de ocurrencia de ríos atmosféricos. En cuanto a las combinaciones de dos factores extremos, la más ventajosa es la de valores extremos de velocidad vertical y agua precipitable, con transporte de humedad no extremo. De hecho, esta combinación de dos factores está asociada a probabilidades de precipitación extrema similares o incluso superiores a la de los tres factores extremos. Existen claras diferencias latitudinales en cuanto a la combinación dominante para la ocurrencia de precipitaciones extremas. En la mayoría de las zonas extratropicales, especialmente en regiones situadas en el interior de los continentes, la combinación de agua precipitable y velocidad vertical es dominante, ya que en esas zonas el transporte de humedad no es tan necesario para la ocurrencia de precipitaciones extremas, teniendo en cuenta la mayor influencia de las fuentes locales de humedad, fundamentalmente a través de procesos de evapotranspiración. Sin embargo, en zonas subtropicales, donde los flujos de humedad son climatológicamente divergentes, la combinación de tres factores es dominante. En esas regiones, la presencia de valores extremos de transporte horizontal de humedad junto con un contenido extremo de vapor de agua en la columna atmosférica implica un aumento de la inestabilidad debido a la convergencia del flujo de humedad en niveles bajos (lo contrario de las condiciones climatológicas), favoreciendo consecuentemente las precipitaciones extremas. La combinación de los tres impulsores en condiciones extremas es también la más ventajosa en la Antártida, donde el transporte de humedad es necesario debido a los bajos valores de humedad local debidos a las bajas temperaturas que allí se registran. En menor medida, la combinación de velocidad vertical extrema y transporte de humedad, en condiciones de agua precipitable no extrema, es la más relevante en algunas zonas de la costa de Norteamérica y Europa en invierno, lo que puede interpretarse en términos del papel de los ríos atmosféricos en la ocurrencia de precipitaciones extremas en esas regiones.

Se demostró que la contribución a la precipitación del conjunto de las zonas oceánicas y terrestres mundiales, además de las trece principales fuentes climatológicas de humedad del planeta, guarda una estrecha relación con la ocurrencia de sequías meteorológicas. En la mayoría de las regiones del mundo, se estimó que la probabilidad condicional de ocurrencia de sequías, dado un déficit de contribución a la precipitación de la totalidad de las áreas oceánicas o de la totalidad de las áreas terrestres, es superior al 10%, siendo evidente la huella de los principales mecanismos de transporte de humedad en las regiones asociadas a mayores probabilidades de sequía (superiores al 15%, 20% o 25%). Muchas zonas continentales interiores del mundo muestran una fuerte relación entre los déficits de contribución de origen terrestre y la ocurrencia de sequías meteorológicas, lo que se asocia a un papel destacado de los procesos de reciclaje y de propagación de las sequías. En cuanto al análisis de las trece principales fuentes de humedad globales, el patrón espacial de las áreas de dominancia de cada fuente (entendidas como las áreas en las que la probabilidad de sequía dado un déficit de contribución de esa fuente es la más alta) se asemeja a los patrones de ocurrencia de precipitación y precipitación extrema asociados a cada fuente. Se encontraron tres regiones clave en las que el déficit de contribución de una única fuente de humedad está altamente relacionado con la ocurrencia de sequía en las escalas temporales de uno y tres meses (probabilidad de sequía superior al 20%): centro-este de Norteamérica (déficit de la fuente del Mar Caribe y Golfo de México), sudeste de Sudamérica (fuente del Amazonas), y este de Europa (fuente del Mediterráneo). En esas regiones, donde la relación entre los déficits de transporte de humedad y la ocurrencia de sequías es fuerte, la probabilidad de sequía asociada a valores específicos de los déficits de contribución concuerda razonablemente bien con la severidad de las sequías observadas, lo que puede servir como punto de partida para mejorar la predicción de las sequías en esas regiones.

En nueve regiones mundiales en la que se prevé un aumento en la magnitud de la sequía en el futuro, la relación entre los déficits de contribución a la precipitación de la fuente de humedad específica dominante y la ocurrencia de sequías demostró ser generalmente fuerte, entendiendo por fuente dominante aquella en la que la probabilidad de sequía asociada a un déficit de contribución es la más alta. Sin embargo, en la mayoría de los casos, las probabilidades de sequía obtenidas fueron sólo ligeramente superiores a las obtenidas considerando las principales fuentes de humedad del planeta. Se comprobó que la fuente dominante no siempre coincide con la fuente con mayor porcentaje de contribución a la precipitación. Entre las regiones en las que no coinciden la fuente dominante y la más contribuyente, destacan aquellas áreas, en su mayoría extratropicales, en las que las fuentes dominantes son oceánicas y las más contribuyentes son terrestres. En estas regiones, una baja contribución de la fuente oceánica implica una baja contribución de la fuente terrestre a un ritmo más rápido que en las zonas húmedas de los trópicos, donde hay una fuerte evapotranspiración y los procesos de reciclaje son muy relevantes en escalas de tiempo cortas. Así, en dichas zonas de no coincidencia, debido a ese rápido efecto cascada desde un déficit de la fuente oceánica al de la fuente terrestre, las fuentes oceánicas tienen una mayor influencia en la ocurrencia de sequías que las terrestres, a pesar de ser estas últimas las más contribuyentes.

Con respecto a la región euromediterránea en clima futuro, se prevé que la influencia del transporte de humedad en la ocurrencia de precipitaciones extremas y sequías meteorológicas aumente, con mayor intensidad para las sequías que para las precipitaciones extremas. De hecho, se ha demostrado que la concurrencia entre ríos atmosféricos y precipitación extrema condiciona altamente la relación entre el transporte de humedad y la ocurrencia de precipitaciones extremas en la región. Un mayor porcentaje de concurrencia entre ríos atmosféricos y precipitaciones extremas explicaría el aumento previsto de la dependencia entre el transporte de humedad y las precipitaciones extremas que se observa para mediados del siglo XXI en la estación invernal. Sin embargo, teniendo en cuenta las condiciones estables de la concurrencia de ríos atmosféricos y precipitaciones extremas para finales de siglo en invierno, y la disminución de la dependencia entre transporte de humedad y precipitación extrema que se prevé en ese periodo, es necesario considerar los cambios en otros mecanismos relacionados con la inestabilidad atmosférica. Así, el desacoplamiento previsto entre ríos atmosféricos y ciclones extratropicales con el calentamiento global implicaría que la inestabilidad atmosférica no estaría asociada a la ocurrencia de futuros ríos atmosféricos en los mismos términos que en el clima actual, con la consiguiente disminución de la dependencia entre transporte de humedad y precipitación extrema a finales de siglo. En cuanto a la influencia de los déficits de contribución a la precipitación de las principales fuentes de humedad oceánicas de la región euromediterránea en la ocurrencia de sequías meteorológicas, se constató un notable aumento de dicha relación. Se demostró que el patrón de la fuente de humedad dominante se prevé bastante estable en el clima futuro, siendo la fuente de humedad del Océano Atlántico Norte dominante en la parte occidental de la región, y el Mar Mediterráneo en las partes central y oriental, de forma coherente con el patrón climático actual. Considerando el déficit de contribución de la fuente de humedad dominante a lo largo de la región euromediterránea, las probabilidades de sequía han aumentado considerablemente, pasando de estar entre el 5% y el 20% en el clima actual a ser del orden del 30% en casi toda la región, y del 60% en zonas como Turquía, los Balcanes y la Península Ibérica. Este aumento general de la influencia del transporte de humedad desde el océano en la ocurrencia de sequías debe entenderse en el contexto de un marcado descenso de los niveles de almacenamiento de agua terrestre. En consonancia con las proyecciones obtenidas para la mayoría de los modelos de cambio climático actuales, se prevé una disminución de la humedad del suelo (representativa de los niveles de almacenamiento de agua terrestre) en la zona euromediterránea. En consecuencia, cabe esperar que la evapotranspiración disminuya en el futuro, con una reducción de la importancia de las fuentes locales de humedad para las precipitaciones en la región. Así pues, se espera que los déficits de contribución a la precipitación de las fuentes de humedad oceánicas de la región euromediterránea desempeñen un papel más notable en la ocurrencia de sequías en dicha región en el futuro.

En esta tesis se han abordado numerosos aspectos relacionados con la relación entre el transporte de humedad y la ocurrencia de precipitaciones extremas y sequías meteorológicas, con importantes implicaciones. Especialmente, se han determinado las regiones del mundo en las que la influencia del transporte de humedad sobre esos extremos hidrometeorológicos es mayor, y se ha cuantificado la magnitud de dicha influencia. Este hallazgo puede suponer un notable avance en la capacidad predictiva de dichos fenómenos extremos, considerando que el transporte de humedad, muy ligado a la circulación atmosférica a gran escala, puede ser más predecible por los modelos que la precipitación, más asociada a procesos a pequeña escala. Puede ser especialmente útil para mejorar la predicción de las sequías que se desarrollan en una escala temporal más corta que las habituales o los cambios repentinos de eventos húmedos a secos y viceversa. Esta tesis supone también un avance en la comprensión del papel que jugarán los ríos atmosféricos en la dependencia entre el transporte de humedad y las precipitaciones extremas en el futuro en la región euromediterránea, así como de los cambios que se esperan en la relación entre los déficits de contribución a la precipitación de las fuentes oceánicas y la ocurrencia de sequías meteorológicas en dicha región.

ABSTRACT

Weather and climate extremes are a constant threat to society, both in terms of health and economics, and a good understanding of them is crucial for the prosperous development of humankind. Of greatest interest are those related to the water cycle, such as droughts, the deadliest in recent decades, or those associated with extreme precipitation, the costliest economically. Despite the complexity in defining both extremes, these phenomena are always associated with excesses or absences of precipitation. The time scale on which they develop is different, since extreme precipitation is usually studied on short scales (such as sub-daily or daily) and droughts on larger scales (e.g. monthly or seasonal). In any case, there are several types of drought (meteorological, agricultural, hydrological, socioeconomic or ecological), depending on the area to which it refers, being meteorological drought, associated with precipitation deficits, the one that is the subject of study in this thesis. Thus, this doctoral work aims to advance in the knowledge of the factors that affect extreme precipitation and meteorological droughts on a global scale, both in present and future climates, focusing on the role played by atmospheric moisture transport.

The transport of water vapour in the atmosphere is a key component of the global hydrological cycle. The atmosphere receives water vapour from the Earth's surface primarily from ocean evaporation (and to a much lesser extent from the continents), and it is transported affecting precipitation regimes on a global scale. The areas where, climatologically, evaporation exceeds precipitation define the main moisture source regions, and are mainly oceanic, although there are also very relevant terrestrial sources such as the Amazon or Congo river basins. There are certain atmospheric mechanisms

that are responsible for the transport of moisture on a global scale, most notably atmospheric rivers and low-level jets. Atmospheric rivers are long, narrow corridors of moisture in the troposphere that do not have permanent geographical positions and are frequently associated with extratropical cyclones, being the most relevant in the transport of water vapour reaching the mid-latitudes. The main continental regions of atmospheric river occurrence include the Pacific and Atlantic coasts of North America, the Atlantic coast of Europe, the Pacific coast of Asia, and southwestern South America, South Africa and Australia. In contrast, low-level jets are important in tropical and subtropical regions, have a semi-permanent geographical position and are characterised by strong winds in the lower troposphere, mainly at night. One of the most studied, the Great Plains low-level jet, mainly active in summer, transports water vapour from the Gulf of Mexico to the Great Plains of North America and is responsible for about one third of the total water vapour reaching the continental United States.

The role of moisture transport in the occurrence of precipitation is key, since the total water vapour contained in an air column at any given time is usually not sufficient to maintain the occurrence of precipitation, requiring a constant supply of moisture from outside. Thus, moisture transport excesses and deficits are often associated with hydrometeorological extremes, leading to extreme precipitation and droughts, respectively. In addition to the need for available atmospheric moisture for precipitation generation, a mechanism to force air lift is also necessary. Air lift can occur due to orographic forcing or atmospheric instability, the latter occurring at very different spatio-temporal scales, from storm and mesoscale scales that owe their instability primarily to thermodynamic causes to synoptic scales in weather systems such as fronts or extratropical cyclones, which owe their instability primarily to dynamical causes. The relative influence of atmospheric instability with respect to moisture content is also a relevant issue. Thus, for extreme precipitation to occur, a certain value of atmospheric instability must be reached, but once this is reached, the magnitude of extreme precipitation depends more on the available atmospheric humidity than on the instability value.

As a consequence of global warming, the air may store more water vapour due to rising temperatures, according to the Clausius-Clapeyron relationship, which corresponds to an increase of 6-7% for every 1 K increase in temperature. In this warming framework, global precipitation extremes and moisture transport would also increase following this thermodynamic relationship, although there may be regional differences due to changes in atmospheric circulation, i.e. dynamic factors. While most of the global surface is expected to experience changes in precipitation extremes at the rate of the Clausius-Clapeyron relationship, there are some regions where dynamic factors play an important role, and these precipitation extremes may increase faster or slower than the rate dictated by the Clausius-Clapeyron relationship. In terms of moisture transport mechanisms, changes are also expected with global warming, such that, for example, atmospheric rivers are expected to transport more moisture, occur more frequently and their location is expected to shift polewards. While a general trend of increasing precipitation extremes has already been observed in historical climate, expected changes in meteorological droughts are more uncertain. Although projections based on climate models agree on increasing dry conditions in some regions of the planet in future climate, there are few areas where such a trend has already been observed in the present climate.

The aim of this thesis is to quantify the role of moisture transport in extreme precipitation and meteorological droughts in current and future climate, following a probabilistic approach. These complex relationships require advanced statistical techniques, such as those borrowed from Extreme Value Theory or copulas. These versatile techniques were specifically designed to capture the behaviour of the highest (or lowest) values of the studied variables, as well as the different types of dependence between them. In order to carry out the intended analyses, precipitation and moisture transport grid data are needed, obtained from the most appropriate databases for each specific study. For the present climate studies, precipitation data were obtained from observation-based databases and reanalyses of the European Centre for Medium-Range Weather Forecasts, while for the future climate studies, data from a climate model from the Coupled Model Intercomparison Project Phase 6 were used. Using reanalysis and climate model data, moisture transport was quantified from a Eulerian approach for extreme precipitation studies and from a Lagrangian approach for drought occurrence studies. This Lagrangian approach allowed estimating the contribution to the precipitation in a given region from the moisture from a given source. In order to study the relationship between meteorological droughts and contribution to precipitation deficits from the moisture sources considered, standardised indices were used, allowing spatio-temporal comparisons.

In terms of the obtained results, firstly, the regions where moisture transport has the greatest influence on extreme daily precipitation in the present climate were identified. It was found that moisture transport has a weak influence in tropical regions, where a large amount of moisture is already present and moisture contributions from outside regions are not necessary for extreme precipitation to occur. However, in subtropical and extratropical areas, moisture transport was found to have a stronger influence on precipitation extremes, mainly linked to the patterns of the main moisture transport mechanisms. In fact, the regions of greatest occurrence of these mechanisms correspond closely to the areas of influence of the dynamic component of moisture transport on extreme precipitation. This component, closely related to atmospheric circulation, is expected to play a key role in understanding changes in the relationship between moisture transport and extreme precipitation under global warming.

Additionally, it was shown that the simultaneous occurrence of extreme values of moisture transport and precipitation is clearly influenced by the atmospheric rivers in their regions of occurrence. It was found that high probabilities of concurrent extremes together with reasonably high values of moisture transport and precipitation occur mainly in regions where atmospheric rivers make landfall. A specific analysis of these regions showed that higher probabilities of concurrent extremes are found in the northern hemisphere than in the southern hemisphere, being especially high on the Pacific coast of North America. In addition, the highest percentages of atmospheric river occurrence on days of concurrent extremes of moisture transport and precipitation were found in these regions of atmospheric river occurrence (above 90%), and the influence of their penetration into inland continental areas was clearly visible (with percentages above 75%). However, in most tropical regions (including monsoon areas), the percentages of occurrence of atmospheric rivers on days of simultaneous moisture transport and precipitation extremes did not exceed 50%, reflecting a low relationship of atmospheric rivers with the occurrence of simultaneous extremes in these regions. In general, a slight decrease in the occurrence of atmospheric rivers on days of concurrent extremes of moisture transport and precipitation was detected in the present climate after the removal of possible El Niño-Southern Oscillation effects. This decrease, which is especially marked along the North American coasts (both Atlantic and Pacific) in winter, can be seen as a preliminary result on the effects of global warming on the relationship of atmospheric rivers with the concurrent extremes of moisture transport and precipitation.

The importance of moisture transport extremes in the occurrence of extreme precipitation was analysed in terms of two other fundamental drivers: precipitable water (water vapour content in the air column) and vertical velocity, which represent thermodynamic and dynamic factors affecting extreme precipitation, respectively. The conditional probability of extreme precipitation was calculated for all combinations of extreme and non-extreme values of the three studied drivers for the current climate. First, it was found that at least one of the drivers must be extreme for extreme precipitation to occur. In addition, it was shown that, on a global scale, vertical velocity is the driver that, when extreme, most favours the occurrence of extreme precipitation. However, precipitable water is the most relevant for the occurrence of extreme precipitation in subtropical regions, and moisture transport in the regions of occurrence of atmospheric rivers. As for the combinations of two extreme drivers, the most advantageous is that of extreme values of vertical velocity and precipitable water, with non-extreme moisture transport. In fact, this two-driver combination is associated with similar or even higher extreme precipitation probabilities than that of the three extreme drivers. There are clear latitudinal differences in the dominant combination for the occurrence of extreme precipitation. In most extratropical areas, especially in regions located in the interior of continents, the combination of precipitable water and vertical velocity is dominant, since in these areas moisture transport is not as necessary for the occurrence of extreme precipitation, given the greater influence of local moisture sources, primarily through evapotranspiration processes.

However, in subtropical areas, where moisture fluxes climatologically diverge, the combination of the three drivers is dominant. In these regions, the presence of extreme values of horizontal moisture transport together with extreme water vapour content in the atmospheric column implies an increase in instability due to the convergence of moisture fluxes at low levels (the opposite of climatological conditions), consequently favouring extreme precipitation. The combination of the three drivers under extreme conditions is also the most advantageous in Antarctica, where moisture transport is necessary due to the low local humidity values owing to the low temperatures there. To a lesser extent, the combination of extreme vertical velocity and moisture transport, under non-extreme precipitable water conditions, is the most relevant in some coastal areas of North America and Europe in winter, which can be interpreted in terms of the role of atmospheric rivers in the occurrence of extreme precipitation in those regions.

The contribution to precipitation from the whole global oceanic and terrestrial areas and from the thirteen major climatological moisture sources was shown to be closely related to the occurrence of meteorological droughts. In most regions of the world, the conditional probability of drought occurrence given a deficit in the contribution to precipitation from the whole oceanic or the whole terrestrial areas was estimated to be greater than 10%, with the footprint of the major moisture transport mechanisms evident in regions associated with higher drought probabilities (greater than 15%, 20% or 25%). Many inland continental areas of the world show a strong relationship between contribution deficits of terrestrial origin and the occurrence of meteorological droughts, which is associated with a prominent role of recycling and drought propagation processes. As for the analysis of the thirteen major global moisture sources, the spatial pattern of the areas of dominance of each source (understood as the areas where the probability of drought given a contribution deficit from that source is the highest) resembles the patterns of precipitation and extreme precipitation occurrence associated with each source. Three key regions were found where the contribution deficit from a single moisture source is highly associated with drought occurrence on the one- and three-month timescales (drought probability greater than 20%): central-east North America (contribution deficit from the Caribbean Sea and Gulf of Mexico source), south-east South America (Amazon source), and east Europe (Mediterranean source). In these regions, where the relationship between moisture transport deficits and drought occurrence is strong, the probability of drought associated with specific values of contribution deficits agrees reasonably well with the severity of observed droughts, which can serve as a starting point for improving the predictability of droughts in these regions.

In nine world regions where drought magnitude is expected to increase in the future, the relationship between contribution to precipitation deficits from the dominant specific moisture source and drought occurrence was shown to be generally strong. The dominant source for drought occurrence was considered to be the moisture source where the probability of drought associated with a contribution deficit from that source is the highest. However, in most cases, the estimated drought probabilities were only slightly higher than those obtained considering the main global moisture sources. It was found that the dominant source does not always coincide with the source with the highest percentage contribution to precipitation. Among the regions where the dominant and the most contributing source do not coincide, there is a noteworthy situation, corresponding to areas, mostly extratropical, where the dominant sources are oceanic and the most contributing sources are terrestrial. In these regions, a low contribution from the oceanic source implies a low contribution from the terrestrial source at a faster rate than in the humid zones of the tropics, where there is strong evapotranspiration and recycling processes are very relevant on short time scales. Thus, in such non-coincidence areas, due to this rapid cascade effect from a deficit of the oceanic source to that of the terrestrial source, oceanic sources have a greater influence on the occurrence of droughts than terrestrial sources, despite the latter being the most contributing ones.

With respect to the Euromediterranean region in the future climate, the influence of moisture transport on the occurrence of extreme precipitation and meteorological droughts is expected to increase, with greater intensity for droughts than for extreme precipitation. The concurrence between atmospheric rivers and extreme precipitation was shown to highly influence the relationship between moisture transport and extreme precipitation in the region. A higher concurrence between atmospheric rivers and extreme precipitation would explain the expected increase in the dependence between moisture transport and extreme precipitation observed for the mid-21st century in winter. However, given the stable conditions projected for the concurrence of atmospheric rivers and extreme precipitation at the end of the century in winter and the decrease in the dependence between moisture transport and extreme precipitation in that period, it is necessary to consider changes in other mechanisms related to atmospheric instability. Thus, the projected decoupling between atmospheric rivers and extratropical cyclones with global warming would imply that atmospheric instability would not be associated with the occurrence of future atmospheric rivers in the same terms as in the current climate, with a consequent decrease in the dependence between moisture transport and extreme precipitation at the end of the century. Regarding the influence of contribution to precipitation deficits from the major oceanic moisture sources of the Euromediterranean region on the occurrence of meteorological droughts, a marked increase in this relationship was found. It was shown that the dominant moisture source pattern is expected to be fairly stable in the future climate, with the North Atlantic Ocean moisture source being dominant in the western part of the region, and the Mediterranean Sea in the central and eastern parts, consistent with the current climate pattern. Considering the contribution deficit from the dominant moisture source at each point of the Euromediterranean region, the drought probability notably increased from 5%-20% in the current climate to around 30% in most of the region, and 60% in areas such as Turkey, the Balkans and the Iberian Peninsula. This general increase in the influence of moisture transport from the ocean on drought occurrence should be understood in the context of a marked decline in terrestrial water storage levels. In line with the projections obtained for most climate models, a decrease in soil moisture (representative of terrestrial water storage levels) is projected for the Euromediterranean area. Consequently, evapotranspiration is expected to decrease in the future, with a reduction in the importance of local moisture sources for the precipitation in the region. Thus, contribution to precipitation deficits from the oceanic moisture sources of the Euromediterranean region are expected to play a more prominent role in the occurrence of future droughts there.

This thesis has addressed many aspects related to the relationship between moisture transport and the occurrence of extreme precipitation and meteorological droughts, with important implications. In particular, the world regions where the influence of moisture transport on these hydrometeorological extremes is greatest has been determined, and the magnitude of this influence has been quantified. This finding may represent a notable advance in the predictability of such extreme events, considering that moisture transport, which is closely linked to large-scale atmospheric circulation, may be more predictable by models than precipitation, which is more associated with small-scale processes. It may be especially useful in order to improve the predictability of droughts that develop on a shorter time scale than usual or the predictability of sudden changes from wet to dry events and vice versa. This thesis also advances the understanding of the role that atmospheric rivers will play in the dependence between moisture transport and extreme precipitation in the future in the Euromediterranean region, as well as the expected changes in the relationship between contribution to precipitation deficits from oceanic sources and the occurrence of meteorological droughts in that region.

LIST OF TABLES

LIST OF ACRONYMS

AED	Atmospheric Evaporative Demand
AIC	Akaike Information Criterion
AMO	Atlantic Multidecadal Oscillation
AR	Atmospheric River
CC	Clausius-Clapeyron
CESM2	Community Earth System Model Version 2
CLLJ	Caribbean Low-Level Jet
CMIP6	Coupled Model Intercomparison Project Phase 6
CPC	Climate Prediction Center
CWD	Consecutive Wet Days
ECMWF	European Centre for Medium-Range Weather Forecasts
ENSO	El Niño-Southern Oscillation
ETCCDI	Expert Team on Climate Change Detection and Indices
EVT	Extreme Value Theory
FLEXPART	FLEXible PARTicle model
GEV	Generalized Extreme Value model
GMST	Global Mean Surface Temperature
GPLLJ	Great Plains Low-Level Jet
IPART	Image-Processing-based Atmospheric River Tracking
IPCC	Intergovernmental Panel on Climate Change
ISSN	International Standard Serial Number
ITCZ	Intertropical Convergence Zone
IVT	Integrated Vapor Transport
IWV	Integrated Water Vapor
JCR	Journal Citation Reports
LLJ	Low-Level Jet
MSWEP	Multi-Source Weighted-Ensemble Precipitation
NAO	North Atlantic Oscillation
PDO	Pacific Decadal Oscillation
PRCPTOT	Total Precipitation

SALLJ	South American Low-Level Jet
SDII	Simple Daily Intensity Index
SPEI	Standardised Precipitation Evapotranspiration Index
SPI	Standardised Precipitation Index
SSP	Shared Socioeconomic Pathway
WMO	World Meteorological Organization
WRF	Weather Research and Forecast

1
Introduction

1.1 Motivation

Knowledge of weather and climate phenomena is crucial for our society, with a remarkable interest in extreme events and their projected changes in the future (*Seneviratne et al., 2021*). Heatwaves, cold spells, heavy rainfall, floods, droughts, wildfires or extreme storms are examples of weather and climate extremes, associated with serious health, ecological and economic damages (*Jahn, 2015*; *Bell et al., 2018*; *Van de Pol et al., 2017*). It is estimated that weather, climate and water hazards caused 2.06 million deaths and US$ 3.6 trillion in economic losses from 1970 to 2019 (*WMO, 2021*). Among them, droughts are the deadliest ones, associated with 650,000 deaths during that period, and storms (US$ 521 billion) and floods (US$ 115 billion) are the costliest ones from an economic point of view. Both storms (including tropical cyclones, extratropical storms and convective storms) and floods have in common that they are frequently related to the occurrence of extreme precipitation, that is, precipitation values that are unusually high. Thus, understanding the drivers of extreme precipitation and droughts and how they will evolve in the future merits a special focus.

Extreme precipitation is characterised by the short time scale in which it can occur, and hence precipitation data is usually accumulated for a time period between hours to several days. There are 10 indices recommended by the Expert Team on Climate Change Detection and Indices (ETCCDI) that account for extreme precipitation (*Zhang et al.,* *2011*; *Gimeno et al., 2022*). Some indices are threshold-based, that is, they count the number of days with precipitation greater than a given pre-specified threshold (for example, 10 or 20 mm; they are denoted as R10mm and R20mm, respectively). Other indices refer to the maximum precipitation values over a time period. The maximum daily precipitation, denoted as Rx1day, or the maximum of the 5-day accumulated precipitation, denoted as Rx5day, are examples of this kind of indices. Other ones are based on percentiles, which are more adequate for spatiotemporal comparisons (such as the R95p or R99p, referring to the total precipitation corresponding to days greater than the 95th or 99th percentiles, respectively). However, extreme precipitation may also be quantified in terms of the duration of the event, as the maximum number of consecutive wet days (CWD), considering a day as wet if precipitation is greater than 1 mm. The total annual precipitation coming from wet days is also quantified (PRCPTOT). Additionally, the ratio between the total precipitation and the number of wet days is a useful index (SDII), providing information about the precipitation intensity. As an alternative to these nonparametric indices, other approaches for defining extreme precipitation include the use of parametric techniques, such as those derived from the Extreme Value Theory (EVT) (*Coles, 2001*). However, it is not straightforward to select the threshold for considering a precipitation value as extreme, and subsequent analyses may be highly dependent on that selection (*Beguería, 2005*). For further information about extreme precipitation indices, the reader is referred to the second section of the supplementary paper 1 (*Gimeno et al., 2022*).

PAPER S1, Section 2: Gimeno, L., Sorí, R., Vázquez, M., Stojanovic, M., Algarra, I., Eiras-Barca, J., **Gimeno-Sotelo, L.**, & Nieto, R. (2022). Extreme precipitation events. *WIREs Water*, 9(6), e1611. https://doi.org/10.1002/wat2.1611

The concept of drought is multidimensional (*Vicente-Serrano, 2016*), and the idea of a single definition is not realistic (*Lloyd-Hughes, 2014*). Droughts, understood as periods with insufficient water, are usually based on a longer time scale than extreme precipitation, from monthly to yearly. The types of droughts differ on the study focus (*Wilhite and Glantz, 1985*): precipitation (meteorological), yields (agricultural), streamflow, reservoirs or groundwater (hydrological), and people's needs or economic demands (socioeconomic). When droughts refer to damages in ecosystems as a consequence of reduced water resources the term “ecological drought” is used (*Crausbay et al., 2017*). Precipitation deficits are key in drought occurrence (*McKee et al., 1993*), but drought severity may be exacerbated when the demand of water from the atmosphere (that is, the atmospheric evaporative demand, AED) increases (*Vicente-Serrano et al., 2020*). When they accumulate in time, soil moisture deficits may occur and therefore crop failures may take place, as well as reduced streamflow and groundwater, with subsequent socioeconomic and ecological implications (*Zhang et al., 2022*; *Vicente-Serrano et al., 2021*). Droughts are usually identified in terms of negative anomalies from long-term normal conditions, using standardised indices that allow spatiotemporal comparisons (*Slette et al., 2020*). From a climatological point of view, two relevant drought indices are the Standardised Precipitation Index (SPI; *McKee et al., 1993*), exclusively based on precipitation data, and the Standardised Precipitation Evapotranspiration Index (SPEI; *Vicente-Serrano et al., 2010*), which accounts for the differences between precipitation and AED. To calculate these indices, precipitation data (or the differences between precipitation and AED) are accumulated over a period of n months. For example, time scales of $n = 1, 3, 6$, or 12 months may be used depending on the aim of the analysis, that is, short-duration droughts or longer ones. Using those indices, a drought event may be identified as the period during which the considered index is beyond a given threshold (*Fleig et al., 2006*; *Tallaksen et al., 1997*), chosen according to a predefined severity.

One of the main drivers of extreme precipitation and meteorological droughts is the atmospheric moisture transport, which is a key component of the global water cycle (*Trenberth et al., 2007*). The atmosphere receives water vapour from the Earth's surface mainly through evaporation from the ocean, and to a much smaller extent from the continents (*Quante and Matthias, 2006*). World regions where, climatologically, evaporation exceeds precipitation are considered as the major moisture sources of the planet (*Gimeno et al., 2010a*), most of them oceanic areas (such as the North Atlantic Ocean or the Mediterranean Sea), although there are key terrestrial sources such as the Amazon or Congo river basins. Water vapour may be transported from moisture sources to other areas where precipitation may occur (moisture sinks) through moisture transport mechanisms, being the major ones the atmospheric rivers (ARs) and low-level jets (LLJs) (*Gimeno et al., 2016*). The most relevant mechanism for moisture arrival in the midlatitudes are the ARs, long and narrow moisture corridors in the troposphere, with non-permanent geographical positions, usually associated to extratropical cyclones (*Zhu and Newell, 1998*; *Gimeno et al., 2014*; *Gimeno et al., 2021a*). The main regions of landfalling AR occurrence include the North American Pacific and Atlantic coasts, the European Atlantic coast, the Pacific Asian coast, and the Southwest of South America, South Africa and Australia (*Algarra et al., 2020*). LLJs are important in tropical and subtropical areas, their position is semi-permanent and are characterised by strong winds at the lower troposphere, especially at night (*Algarra et al., 2019*). One of the most studied low-level jet systems is the Great Plains LLJ (GPLLJ), which is mainly active in summer. It transports moisture from the Gulf of Mexico to the American Great Plains and is responsible for about one third of the total atmospheric moisture arriving in the continental United States (*Helfand and Schubert, 1995*). Other well-researched LLJs are the South American one (SALLJ), which transports moisture from the Amazon to La Plata river basins (*Marengo et al., 2004*); the Caribbean one (CLLJ, or Intra-Americas LLJ; *Amador, 2008*), mainly affecting Central America; or the CHOCO LLJ (*Sierra et al., 2021*), transporting moisture along the Pacific South-American coast and penetrating Colombia. Extensive information about the role of atmospheric moisture transport in extreme precipitation occurrence and the associated mechanisms can be found in the sixth section of the supplementary paper 1 (*Gimeno et al., 2022*).

PAPER S1, Section 6: Gimeno, L., Sorí, R., Vázquez, M., Stojanovic, M., Algarra, I., Eiras-Barca, J., **Gimeno-Sotelo, L.**, & Nieto, R. (2022). Extreme precipitation events. *WIREs Water*, 9(6), e1611. https://doi.org/10.1002/wat2.1611

The role of atmospheric moisture transport in precipitation occurrence is key, since the total water vapour contained in an air column at a given time is generally not enough to maintain precipitation, and a constant supply of moisture from outside is needed (*Trenberth et al., 2003*). Thus, moisture transport excesses and deficits are often associated with hydrometeorological extremes, influencing extreme precipitation (*Vázquez et al., 2020*) and droughts (*Drumond et al., 2019*), respectively. Apart from the necessity of available atmospheric moisture for precipitation generation, a mechanism that forces the air to rise is also needed. Air ascents may occur due to orographic forcing or due to atmospheric instability, for example due to convection processes or meteorological systems such as cyclones. However, the relative influence of atmospheric instability on precipitation occurrence with respect to moisture content is different for extreme precipitation and droughts. For extreme precipitation, it strongly depends on the available atmospheric moisture, although a certain value of atmospheric instability should be reached (*Kunkel et al., 2020*). Instead, the lack of atmospheric instability is key for drought occurrence (*Trenberth et al., 1988*).

As a consequence of global warming, the water-holding capacity of the atmosphere increases, that is, the air can store a greater amount of water vapour due to the higher temperatures, according to the Clausius-Clapeyron (CC) relationship, which corresponds to a 6-7% increase per 1 K increase in the global mean surface temperature (GMST). Under this warming framework, extreme precipitation would also increase following the CC relationship (*Trenberth et al., 2003*). The general increasing trend in extreme precipitation has already been observed in the historical climate (*Sun et al., 2021*), using Rx1day and Rx5day data from 14,796 stations, each of them having at least 30 years of record for the period 1900–2018. It was found that the change in extreme precipitation per 1 K increase in GMST was 6.6% for Rx1day and 5.7% for Rx5day, being consistent with the CC relationship, in line with earlier work (*Westra et al., 2013*). For the 1900–2018 period, more than two-thirds of stations showed increasing trends in extreme precipitation, and the intensification was evident in many regions, including central and eastern North America, northern Central America, northern Europe and eastern Asia. However, uncertainties exist in regions with poor data coverage such as Africa and South America. For further information about the trends in extreme precipitation with global warming, as well as the underlying physical processes, the reader is referred to the fourth and fifth sections of the supplementary paper 1 (*Gimeno et al., 2022*).

PAPER S1, Sections 4 and 5: Gimeno, L., Sorí, R., Vázquez, M., Stojanovic, M., Algarra, I., Eiras-Barca, J., **Gimeno-Sotelo, L.**, & Nieto, R. (2022). Extreme precipitation events. *WIREs Water*, 9(6), e1611. https://doi.org/10.1002/wat2.1611

Increases in atmospheric moisture lead to an intensification of the global water cycle (*Held and Soden, 2006*), including moisture transport. Although both extreme precipitation and moisture transport are projected to increase with global warming at the CC rate due to the previously explained thermodynamic effect, regional differences may exist due to changes in the atmospheric circulation, that is, dynamic factors (*Pfahl et al., 2017*, for extreme precipitation; *O'Brien et al., 2022,* for moisture transport). In regions where dynamic factors play an important role, extreme precipitation may increase faster (super-CC) or slower (sub-CC) than the CC rate (*John et al., 2022*). The super-CC regions are mainly limited to the equatorial area, in line with stronger convection over the Intertropical Convergence Zone (ITCZ) core, and the sub-CC regions encompass subtropical anticyclonic areas, where subsidence is projected to increase in the future (*Douville et al., 2021*). Further information about how the changes in the thermodynamic and dynamic factors are projected to affect extreme precipitation in a warmer climate, as well as the changes in the dependence between them, can be found in the supplementary paper 2 (*Gimeno-Sotelo et al., 2024a*). Regarding moisture transport mechanisms, changes are also projected under global warming For example, ARs will carry a higher amount of moisture, occur more frequently, and will be shifted poleward (*Payne et al., 2020*). LLJs will also undergo changes in intensity and location, such as a westward expansion of the CLLJ and the SALLJ (*Torres-Alavez et al., 2021*).

PAPER S2: **Gimeno-Sotelo, L.**, Bevacqua, E., Fernández-Alvarez, J. C., Barriopedro, D., Zscheischler, J., & Gimeno, L. (2024a). Projected changes in extreme daily precipitation linked to changes in precipitable water and vertical velocity in CMIP6 models. *Atmospheric Research*, 304. https://doi.org/10.1016/j.atmosres.2024.107413

When it comes to changes in meteorological droughts, there are only a few regions (central Europe, southern South Africa and southwestern Australia) where significant drying (decreasing trends in SPI) are observed for the period 1900-2020 (*Vicente-Serrano et al., 2022*). However, a larger number of regions are projected to undergo an increase in meteorological drought duration and intensity in the future (*Ukkola et al., 2020*). Central America, Chile, the Amazon, southern and western Africa, the Mediterranean and southern Australia are among the regions where meteorological droughts are projected to be longer in the future. Drought intensity is also projected to increase in Central America, Chile, the Amazon, western Africa and the Mediterranean, as well as in other regions such as central Europe, central Africa, southeast Asia, the United States and western Russia. In southern Africa and Australia, future droughts are projected to increase in duration, but they will not be more intense. In supplementary paper 3 (*Gimeno-Sotelo et al., 2024b*), a comprehensive analysis of the projected changes of different types of droughts under a high anthropogenic emission scenario can be found.

PAPER S3: **Gimeno-Sotelo, L.**, El Kenawy, A., Franquesa, M., Noguera, I., Fernández-Duque, B., Domínguez-Castro, F., Peña-Angulo, D., Reig, F., Sorí, R., Gimeno, L., Nieto, R. & Vicente-Serrano, S. M. (2024b). Assessment of the global relationship of different types of droughts in model simulations under high anthropogenic emissions. *Earth's Future*, 12, e2023EF003629. https://doi.org/10.1029/2023EF003629

The aim of this thesis is to quantify the role of moisture transport in extreme precipitation and meteorological droughts in the present and future climates, following a probabilistic approach. These complex relationships require advanced statistical techniques. Thus, extreme value analysis (*Coles, 2001*) and copula models (*Nelsen, 2006*) are used for this purpose. These versatile techniques were specifically designed for capturing the behaviour of the highest (or lowest) values of the studied variables, and the different types of dependence existing between pairs of variables. Moreover, this work is novel in the analysis of the relationship between moisture transport and the studied hydrometeorological phenomena using a compound event framework (*Zscheischler et al., 2018*; *Bevacqua, et al., 2021*).

The link between moisture transport and extreme precipitation is tackled first for the present climate. The world regions where moisture transport has a strongest influence on precipitation maxima are identified. Next, the simultaneous occurrence of moisture transport and extreme precipitation is explored in terms of ARs, one of the major moisture transport mechanisms, as explained before. Afterwards, the influence of moisture transport on extreme precipitation is studied jointly with other precipitation drivers, namely the water vapour content and vertical velocity.

The role of moisture transport in drought occurrence is analysed in terms of the relationship between the contribution to precipitation deficit from a given moisture source and the occurrence of drought in a sink region. First, for the present climate, the drought probabilities associated with the contribution to precipitation deficits from the major moisture sources of the planet (as well as the whole oceanic and land global areas) are analysed. Afterwards, having determined the world regions with projected drought trends under a high greenhouse gas emission scenario, the drought probability associated with deficits in moisture supply from specific sources of those regions is studied for the present climate.

The assessment of future changes in hydrometeorological extremes over the Euromediterranean region is a topic of major concern. Therefore, the influence of moisture transport on both extreme precipitation and meteorological droughts in the Euromediterranean region is assessed for the present and future climates, under a high greenhouse gas emission scenario. That region is highly relevant with respect to the role of moisture transport in those hydrometeorological extremes. ARs exert a great influence on extreme precipitation in its Atlantic coast (*Lavers and Villarini, 2013*), and similar structures are also relevant in the northern Mediterranean coast (*Lorente-Plazas et al., 2020*). Thus, this thesis assesses future changes in the concurrence between ARs and extreme precipitation. The Mediterranean is also a hotspot region in terms of meteorological droughts, as projections indicate that they will be longer and more intense in the future (*Ukkola et al., 2020*). Considering the two major oceanic moisture sources affecting that region (the North Atlantic Ocean and the Mediterranean Sea), the projected changes in the drought probability associated with a contribution deficit from those sources are unravelled in this thesis.

1.2 Thesis structure

This thesis, which results from a compendium of five scientific papers and one submitted manuscript, is structured in six chapters:

This **Chapter 1** presents a brief overview of the role of moisture transport in extreme precipitation and droughts, both in present and future climates, as well as the structure of the thesis.

Chapter 2 describes the general and specific objectives of the thesis.

Chapter 3 provides information about the data and methodology used to fulfil those objectives.

Chapter 4 contains the five scientific papers and the submitted manuscript that are included in the main text of the thesis.

Chapter 5 discusses the key results of the thesis.

Chapter 6 encompasses the general conclusions and future work.

The supplementary material contains three scientific papers and the supplementary material of the five articles (and the submitted manuscript) included in the main text, as well as that of the three supplementary articles.

2
Objectives

2.1 General objectives

The **main objective** of this thesis is to determine the influence of moisture transport on the occurrence of hydrometeorological extremes, particularly in daily precipitation extremes and meteorological droughts, both in the present and future climates. This main objective is articulated into two general objectives:

General objective 1: Determine the influence of moisture transport on **extreme daily precipitation**. For this objective, moisture transport was quantified from a Eulerian perspective at a grid scale.

General objective 2: Study the influence of moisture transport deficits on **meteorological droughts**. For this objective, moisture transport was quantified from a Lagrangian perspective, estimating the contribution to the precipitation in a region from its major (or specific) moisture sources.

2.2 Specific objectives

Within the framework of these two general objectives, several specific objectives are pursued, which contribute to one (or the two) general objectives defined above:

Specific objective 1.1: Determine the world regions where moisture transport exerts a greater influence on extreme daily precipitation on a global scale in the present climate, quantifying the magnitude of the relationship. The results are described in the article *"Where does the link between atmospheric moisture transport and extreme precipitation matter?"* (Gimeno-Sotelo and Gimeno, 2023), published in the journal *Weather and Climate Extremes*, and included in Section 4.1.

Specific objective 1.2: Analyse the relationship of concurrent extremes of moisture transport and extreme daily precipitation with the occurrence of ARs on a global scale in the present climate. This was addressed in the article *"Concurrent extreme events of atmospheric moisture transport and continental precipitation: The role of landfalling atmospheric rivers"* (Gimeno-Sotelo and Gimeno, 2022), published in the journal *Atmospheric Research*, and included in Section 4.2.

Specific objective 1.3: Quantify the influence of moisture transport on extreme daily precipitation with respect to other drivers, namely precipitable water and vertical velocity. The combinations of drivers that most favour the occurrence of extreme daily precipitation are analysed. This objective was tackled in the article *"Combinations of drivers that most favor the occurrence of daily precipitation extremes"* (Gimeno-Sotelo et al., 2023), published in the journal *Atmospheric Research*, and included in Section 4.3.

Specific objective 2.1: Study the influence of the deficits in the contribution to precipitation from the major moisture sources of the planet (as well as the whole global oceanic and terrestrial areas) on the occurrence of meteorological droughts in the present climate. It is addressed in the article *"Unravelling the origin of the atmospheric moisture deficit that leads to droughts"* (Gimeno-Sotelo et al., 2024d), published in the journal *Nature Water*, and included in Section 4.4.

Specific objective 2.2: Analyse the importance of specific moisture sources in the occurrence of meteorological droughts in the regions with projected increase in drought magnitude with global warming. This question is pursued in the article *"Nexus between the deficit in moisture transport and drought occurrence in regions with projected drought trends"* (Gimeno-Sotelo et al., 2024e), published in the journal *Environmental Research Letters*, and included in Section 4.5.

Specific objective 3: Study the future projected changes in the influence of moisture transport on extreme daily precipitation and meteorological droughts over the Euromediterranean region. It is addressed in the submitted manuscript *"The increasing influence of atmospheric moisture transport on hydrometeorological extremes in the Euromediterranean region with global warming"* (Gimeno-Sotelo et al., 2024c), included in Section 4.6.

3
Data and Methodology

3.1 Data used

In this subsection a brief description of the data used in the different studies that are included in this thesis is provided, making a distinction between the data sets used for the analysis of present and future climates.

Present climate

Precipitation

In *Gimeno-Sotelo and Gimeno (2023)* (Section 4.1) and *Gimeno-Sotelo et al. (2023)* (Section 4.3), daily precipitation data from the ERA5 reanalysis (*Hersbach et al., 2020*) at 0.5° resolution is used for the period 1981-2020. Reanalyses are products that combine information from observations and short-range weather forecasts through a data assimilation process, being suitable for global studies in the present climate. They provide data for the entire planet, especially reliable from the 1980s, when satellite data started to be massively assimilated. However, reanalyses have some limitations, especially in regions with less observational data, complex orography or where small-scale convective processes take place. The ERA5 reanalysis is the latest reanalysis from the European Centre for Medium-Range Weather Forecasts (ECMWF) and has been shown to be reasonably adequate for hydroclimatic applications (*Nogueira, 2020*; *Rivoire et al., 2021*; *Lavers et al., 2022*). Specifically, it is highly reliable for extreme precipitation occurring in extratropical regions and the winter season, which is the main scope of study in this thesis. A comprehensive discussion about the advantages and uncertainties associated with data from the ERA5 reanalysis can be found in Section 4.1.

Where possible, precipitation data from a data set other than reanalysis has been employed to avoid using the same data source as for moisture transport calculation. This is the case of *Gimeno-Sotelo and Gimeno (2022)* (Section 4.2), in which precipitation data from the ERA5 reanalysis are not used because it may influence the results of the analysis of concurrent extremes of atmospheric moisture transport and precipitation. Thus, daily precipitation data from the Climate Prediction Center Global Unified Gauge-Based Analysis (CPC; *Xie et al., 2007*) is used for the period 1981-2017, at a spatial resolution of 0.5°. CPC is a global gridded product based on station data and an interpolation algorithm to deal with orography. The use of the CPC dataset in Section 4.2 is also justified by the focus of the study on the regions of occurrence of landfalling ARs, which are mostly located in extratropical areas with a dense station network.

However, the use of reanalysis data for precipitation is preferable for studies dealing with the future climate. In this case, climate model outputs are utilised, and, for validation purposes, it is necessary to employ the same data source for precipitation and moisture transport in the present climate. Thus, in *Gimeno-Sotelo et al. (2024c)* (Section 4.6), the Weather Research and Forecast (WRF-ARW) model, Version 3.8.1 (*Skamarock et al., 2008*) is used to obtain dynamically downscaled data from the ERA5 reanalysis (WRF-ERA5 data). In that Section, WRF-ERA5 precipitation data at a spatial resolution of 20 km are used for the analysis of the Euromediterranean region (30°N- 50°N; 15°W-35°E) in the historical period (1985-2014), following the simulation scheme described in *Fernández-Alvarez et al. (2023a)*. Accordingly, the use of ERA5 reanalysis in Section 4.1 enables the comparison of the results obtained in Section 4.6.

Regarding drought analysis, in *Gimeno-Sotelo et al. (2024d)* (Section 4.4) and *Gimeno-Sotelo et al. (2024e)* (Section 4.5), monthly precipitation data from the Multi-Source Weighted-Ensemble Precipitation dataset (MSWEP; *Beck et al., 2019*) is used for the 1980-2018 period at 0.5° and 0.1° resolutions, respectively. MSWEP is a global precipitation product that combines data from different sources (gauge-based, satellite and reanalysis) and outperforms other precipitation datasets; see Section 4.4 for further details. The use of MSWEP data instead of other datasets that are only based on observations is because in Section 4.4 and Section 4.5 special attention is given to regions with low station density, such as the Amazon or Congo river basins, where observational data does not allow a reliable drought analysis.

Regardless of the precipitation dataset used in each specific study, CPC, MSWEP and reanalyses from the ECMWF have a reasonable concordance with other precipitation products, with the main discrepancies occurring in regions with complex orography, tropical areas, northern Africa, and some high-latitude regions (such as northern North America or Greenland); see *Sun et al. (2018)* for a review.

Moisture transport

For the analysis of the relationship between moisture transport and extreme precipitation, moisture transport is computed in a Eurelian way using the vertically integrated moisture transport (IVT). This is a grid-point metric which is widely used for that purpose (*Gimeno et al., 2012*). It is defined as follows:

$$IVT = \sqrt{\left(\frac{1}{g}\int_{p_s}^{p_t} q\, u\, dp\right)^2 + \left(\frac{1}{g}\int_{p_s}^{p_t} q\, v\, dp\right)^2} = \sqrt{{IVT_u}^2 + {IVT_v}^2}\,,$$

where g refers to gravitational acceleration, q to specific humidity, u and v to the eastwards and northwards wind components, and p_s and p_t to the surface and top pressure levels considered, respectively. It is important to note that considering pressure levels above 300 hPa has a negligible impact on the value of IVT (*Ratna et al., 2016*), so integrating over the whole atmospheric column (as in Sections 4.1, 4.2 and 4.3) or up to 300 hPa (as in Section 4.6) should provide almost identical results. In Sections 4.1, 4.2 and 4.3, daily IVT values are obtained from the ERA5 reanalysis at 0.5° resolution, whereas Section 4.6 uses the high-resolution WRF-ERA5 data (20 km).

Regarding the analysis of the influence of contribution to precipitation deficits from the moisture sources of a region and the occurrence of meteorological droughts there, moisture transport is estimated following a Lagrangian approach (*Stohl and James, 2004, 2005*). In Sections 4.4 and 4.5, the outputs from the FLEXPART v9.0 dispersion model (FLEXible PARTicle model; *Stohl et al., 2005*; *Pisso et al., 2019*) are used for the period 1980-2018, based on data from the ERA-Interim reanalysis (*Dee et al., 2011*), the predecessor reanalysis of ERA5 from the ECMWF. This Lagrangian approach divides the atmosphere into approximately two million air particles and tracks forward the particles departing from a given source region and reaching each grid point of the target region. The method accounts for the changes in specific humidity ($\frac{dq}{dt}$) every six hours along an optimal time by grid defined in *Nieto and Gimeno (2021)*. For each grid point of area A in the target region, the balance between evaporation (E) and precipitation (P) is estimated by means of the vertically aggregated sum of the changes in specific humidity of the particles reaching that point, as follows:

$$E - P = \frac{\sum m \frac{dq}{dt}}{A},$$

where m is the mass of each air particle (assumed as constant). At each grid point, a negative value of (E-P) represents the contribution to the precipitation there from the considered moisture source (the modulus of that value is used for practical reasons).

In Section 4.4 the whole oceanic and continental global areas are used as moisture sources (the database obtained by *Nieto and Gimeno, 2021* is used), as well as the major moisture sources of the planet (already identified in *Gimeno et al., 2010a*). The major global moisture sources considered in that Section include eleven oceanic moisture sources (the North Pacific Ocean, the South Pacific Ocean, the Caribbean Sea and Gulf of Mexico, the North Atlantic Ocean, the South Atlantic Ocean, the Mediterranean Sea, the Agulhas Current region, the Red Sea, the Zanzibar Current and Arabian Sea region, the Indian Ocean, and the Coral Sea) and two continental ones (the Amazon and Congo River basins); see Fig. 2 in *Gimeno-Sotelo et al. (2024d).* Monthly global data for contribution to precipitation from the considered moisture sources were obtained for the 1980-2018 period at 0.5° resolution.

In Section 4.5, the specific moisture sources of nine world regions where the magnitude of meteorological drought events is projected to increase in the future under a high anthropogenic emission scenario (Shared Socioeconomic Pathway 5-8.5; SSP5-8.5) are used. This scenario represents a radiative forcing of 8.5 W/m^2 for 2100 (*O'Neill et al., 2016*). The nine target regions are central America, northern and northeastern Brazil, the Amazon, southwestern South America, the western and eastern Mediterranean, southern Africa, and southwestern Australia (see Fig.1 in *Gimeno-Sotelo et al.,2024e*), and their specific moisture sources are identified following a Lagrangian approach analogous to that defined above, but in a backward direction (see Fig.2 in *Gimeno-Sotelo et al.,2024e*). Those specific moisture sources are regions where, climatologically, evaporation exceeds precipitation, that is, positive values of (E-P) are found. The monthly contribution to precipitation in a given target region from each of its specific moisture sources is obtained for the period 1980-2018.

In Section 4.6, the contribution to precipitation from three major moisture sources is considered: the North Atlantic Ocean, the Mediterranean Sea and the Caribbean Sea and Gulf of Mexico. The first two are the major moisture sources of the Euromediterranean region (Section 4.4), and the third one is another relevant source for the Iberian Peninsula (*Gimeno et al., 2010b*). In Section 4.6 a Lagrangian approach similar to that in Sections 4.4 and 4.5 is applied to ERA5 data and the FLEXPART-WRF model (*Brioude et al., 2013*) to obtain the contribution to precipitation from these moisture sources in the historical climate (1985-2014) at a spatial resolution of 20 km.

The Lagrangian approach used in this thesis for obtaining the contribution to precipitation data from a given moisture source, and for determining the specific moisture sources of a given region has been successfully employed in a large number of publications (see *Gimeno et al., 2020b* for a review).

Other drivers of extreme precipitation

Apart from moisture transport, other important drivers of extreme precipitation are also considered in this thesis, namely precipitable water and vertical velocity.

In Sections 4.1 and 4.3, daily precipitable water data is obtained from the ERA5 reanalysis for the period 1981-2020 at 0.5° resolution. This metric represents the total amount of water vapour contained along the atmospheric column over each grid point. It is also known as vertically integrated water vapor (IWV), and is defined as follows:

$$IWV = \frac{1}{g}\int_{p_s}^{p_t} q\,dp,$$

where g refers to gravitational acceleration, q to specific humidity, and p_s and p_t to the surface and top pressure levels considered, respectively.

In Section 4.3, the ERA5 reanalysis is also used to obtain daily data of vertical velocity at 500 hPa at 0.5° resolution for the period 1981-2020. Vertical velocity is defined as "$-\omega$", where $\omega = \frac{dp}{dt}$, with p referring to atmospheric pressure. Positive values of "$-\omega$" indicate upward motion, so this metric represents atmospheric instability. It captures instability better on a synoptic scale (100-1000 km) than on the mesoscale (10-100 km), being more reliable in extratropical than in tropical regions (*O'Gorman and Schneider, 2009*).

Atmospheric river occurrence

In Section 4.2, the AR database by *Guan and Waliser (2015)* is used to obtain daily data of AR occurrence for the period 1981-2017 at 0.5° resolution. That database was constructed using ERA-Interim reanalysis data and has a spatial resolution of 1.5°. Taking this into account, if an atmospheric river is detected in a 1.5° grid point, it is considered to occur in all the 0.5° grid points included there.

In Section 4.6, daily data of AR occurrence at 20 km resolution over the Euromediterranean region for the historical climate (1985-2014) is obtained using the Image-Processing-based Atmospheric River Tracking (IPART) method (*Xu et al., 2020*). This approach has been shown more adequate for studying projected changes with global warming, as is the case of Section 4.6, and was already applied in *Fernández-Alvarez et al. (2023b)* for AR detection in the Iberian Peninsula.

Future climate

In Section 4.5, nine world regions are identified where the magnitude of meteorological drought events is projected to increase from 1850 to 2100. To do so, monthly precipitation data are obtained from 18 models of the Coupled Model Intercomparison Project Phase 6 (CMIP6) experiment (*Eyring et al., 2016*); the list of the models used can be found in Section 4.5. Data is interpolated at a common 2.5° resolution grid for the historical period (1850-2014) and the future period under the SSP5-8.5 scenario (2015-2100).

The Community Earth System Model Version 2 (CESM2; *Danabasoglu, 2020*) from the CMIP6 experiment is used in Section 4.6. As for the ERA5 reanalysis data, the WRF-ARW model, Version 3.8.1, is applied to dynamically downscale the CESM2 data at a spatial resolution of 20 km (WRF-CESM2 data). Three time periods are analysed (historical: 1985-2014; mid-21st century: 2036-2065; end-21st century: 2071-2100), considering a future climate under the SSP5-8.5 scenario. The procedure to obtain moisture transport data for the three studied periods uses dynamically downscaled data from the CESM2 model and is analogous to that employed for the dynamically downscaled ERA5 data. For the analysis of the relationship between moisture transport and extreme precipitation in the future, moisture transport is quantified using the IVT metric. Additionally, the AR occurrence data is obtained using the IPART method. Regarding the moisture transport data for meteorological drought analysis, the contribution to precipitation from the North Atlantic Ocean, the Mediterranean Sea and the Caribbean Sea and Gulf of Mexico is obtained using the FLEXPART-WRF model, as described above.

3.2 Methodology used

In this subsection, an overview of the main statistical methods used in this thesis is given, with special emphasis on those related to extreme value analysis and copulas, which are the key advanced statistical methods of this thesis.

Drought and contribution to precipitation indices calculation

In order to study the relationship between moisture transport deficits and the occurrence of meteorological droughts, standardized indices are highly necessary, as they allow spatiotemporal comparisons (*Slette et al., 2020*). In this case, considering that moisture transport is mainly related to precipitation occurrence, and with the aim of isolating that influence, the SPI (*McKee et al., 1993*) is used, which is based on precipitation data only. SPI values are obtained by fitting a gamma distribution to the precipitation series of each month of the year in an independent way and transforming the data to obtain standard normal values. The precipitation data of each month may be accumulated over the previous months. That is, different time scales may be used to obtain the indices. In this thesis, the 1-month time scale is preferably used (Sections 4.4, 4.5 and 4.6), which indicates that the monthly precipitation is not accumulated. This time scale accounts for short-term droughts, which is more reasonable for the analysis of the influence of moisture transport deficits, considering that the residence time of water vapour is usually 3-10 days (*Gimeno et al., 2021b*). However, in Section 4.4, the 3-month time scale is also used, which means that the precipitation value of month m represents the accumulated precipitation over the [m-2, m] interval, therefore accounting for seasonal droughts. Regardless of the time scale used, because of its standard normal nature, SPI values higher or lower than zero indicate wet or dry conditions, respectively. Using the contribution to precipitation data from the studied moisture sources, analogous indices to SPI are obtained (denoted as SPIc).

Non-stationary Generalized Extreme Value methods for extreme precipitation analysis

In this thesis, the annual maxima method from the Extreme Value Theory (EVT) (*Coles, 2001*, *Beirlant et al., 2006*) is used to analyse precipitation maxima as a function of its drivers. Non-stationary Generalized Extreme Value (GEV) models are used to estimate the influence that each driver has on extreme precipitation. This approach is used in Section 4.1 to study the influence of moisture transport on annual precipitation maxima in the period 1981-2020 and independently for each season. In Section 4.6, it is also applied to analyse the projected changes in the influence of moisture transport on extreme precipitation in the Euromediterranean region with global warming, for the winter and summer seasons. It is assumed that the annual precipitation maxima (represented by the variable Y) follow a GEV distribution:

$$G(y;\ \mu,\sigma,\gamma) = \exp\left\{-[1+\gamma\frac{y-\mu}{\sigma}]^{-1/\gamma}\right\}\ \text{, with } 1+\gamma\frac{y-\mu}{\sigma} > 0,$$

where y represents a value of Y and μ, σ and γ are the location, scale and shape parameters of the distribution, respectively. The non-stationary approach consists of expressing the parameters as a function of a covariate (for example IVT). In Sections 4.1 and 4.6, the non-stationarity is included in the location and scale parameters as linear functions of IVT, as follows: $\mu(IVT) = \beta_0 + \beta_1 IVT$ and $\sigma(IVT) = \theta_0 + \theta_1 IVT$. Additionally, in Section 4.1, non-stationary GEV models are analogously fitted including IWV and the ratio between IVT and IWV (IVT/IWV) as covariates, representing the thermodynamic and dynamic components of moisture transport, respectively. In this thesis, special attention is given to the β_1 coefficient, as it quantifies the influence that the studied covariate exerts on the precipitation maxima magnitude. Using maximum likelihood estimation, asymptotic confidence intervals can be found for the model coefficients (*Casella and Berger, 2024*), and a coefficient is found to be significant (at a given significance level) if the associated confidence interval does not contain the zero value. The goodness of fit of the non-stationary GEV models is assessed using diagnostic plots, as recommended by *Coles (2001)*; further information about the goodness-of-fit assessment can be found in Section 4.1.

A fitted non-stationary GEV model for precipitation maxima as a function of a covariate (a driver) can be used for estimating a *n*-year return level, that is, a value that, on average, is exceeded once every *n* years, for a given value of the driver. In Section 4.1, the driver influence is quantified as the variation percentage in the 20-year return level of precipitation maxima between a low and a high value of the studied driver (10th percentile and 90th percentile, respectively). High values of this metric indicate a strong influence of that driver on the precipitation maxima.

Copulas for probability estimation

In this thesis we make use of techniques from the copula theory (*Nelsen, 2006*; *Joe, 2014*; *Shemyakin and Kniazev, 2017*) to study the relationship between pairs of variables and estimating different probabilities of interest. This is the approach that is followed in Section 4.2, 4.4, 4.5 and 4.6. Copulas excel in capturing the joint behaviour of a pair of variables, accounting for different shapes, symmetries, and dependence patterns, including dependence between the extreme values of the distributions (tail dependence).

They are becoming increasingly popular in the hydroclimatic literature because many studies are focused on extreme events, for which sophisticated statistical methods are required in order to unravel complex relationships between the variables (see *Tootoonchi et al., 2022* for a review).

A copula is basically the joint distribution function of a pair of random variables that follow a uniform distribution with a mean of 0 and standard deviation of 1. Copulas have a key property, which is that the joint distribution function of a pair of continuous random variables can be written as a function of a copula and the univariate distribution functions of each variable of the pair (marginal distributions). That property is known as the Sklar´s theorem (*Sklar, 1959*). There are several types of copula models and in this thesis the analysis is based on a set of copula types that account for a wide variety of dependence patterns, namely the Gaussian, Student-t, Frank, Gumbel, Clayton and Joe copulas, as well as the independence one (reflecting the pattern of two unrelated variables); see their expressions in Section 4.2. Those copula types are fitted using bivariate data: in Section 4.2, IVT and precipitation data; in Sections 4.4, 4.5 and 4.6, SPI and SPIc (that is, the drought index used in this thesis and the standardized contribution to precipitation from a given moisture source). Having fitted those copula models following a semi-parametric approach (see Section 4.2 for further information about the parameter estimation procedure), the best copula model according to the Akaike Information Criterion is selected (AIC; *Akaike, 1974*). The goodness of fit of the copula models can be assessed using a variety of statistical tests; for example, a Cramér-von Mises one (see *Genest et al., 2009*) as in Section 4.2, or that by *Huang and Prokhorov (2014)* based on White´s information matrix equality (*White, 1982*), as in Section 4.4, 4.5 and 4.6.

The selected copula model is used to estimate the probabilities of interest. For example, in Section 4.2, the probability of the simultaneous occurrence of extreme values of IVT and precipitation is estimated using copula models, taken extreme as the 90th percentile of each variable:

$$P\left(IVT \geq q90_{IVT}, prec \geq q90_{prec}\right),$$

where *prec* refers to precipitation, and $q90_{IVT}$ and $q90_{prec}$ to the 90th percentile of IVT and precipitation, respectively.

Additionally, in Sections 4.4, 4.5 and 4.6, copula models are used in order to estimate the conditional probability of meteorological drought occurrence (SPI lower than its 5th percentile) given an equivalent contribution to precipitation deficit from a moisture source (SPIc lower than its 5th percentile):

$$P(SPI \leq -1.64 \mid SPIc \leq -1.64),$$

where this threshold (-1.64) refers to the 5th percentile of the standard normal distribution.

For additional information about the technical details of the probability estimation procedure, the reader is referred to Sections 4.2 and 4.4.

4
Set of publications

This chapter comprises five published scientific articles and one submitted manuscript, listed in Table 1, tackling each of the specific objectives of the thesis. The quality indicators of the journals in which the articles were published are shown in Table 2, corresponding to the Journal Citation Reports (JCR) of the year 2023 (latest information available at the time of writing this thesis).

Table 1. Information about the five publications and the submitted manuscript included in Chapter 4.

Title	Authors	Year	Journal
“Where does the link between atmospheric moisture transport and extreme precipitation matter?”	**Gimeno-Sotelo, L.**, and Gimeno, L.	2023	*Weather and Climate Extremes*
“Concurrent extreme events of atmospheric moisture transport and continental precipitation: The role of landfalling atmospheric rivers”	**Gimeno-Sotelo, L.**, & Gimeno, L.	2022	*Atmospheric Research*
“Combinations of drivers that most favor the occurrence of daily precipitation extremes”	**Gimeno-Sotelo, L.**, Bevacqua, E., & Gimeno, L.	2023	*Atmospheric Research*
“Unravelling the origin of the atmospheric moisture deficit that leads to droughts”	**Gimeno-Sotelo, L.**, Sorí, R., Nieto, R., Vicente-Serrano, S. M., & Gimeno, L.	2024	*Nature Water*
“Nexus between the deficit in moisture transport and drought occurrence in	**Gimeno-Sotelo, L.**, Stojanovic, M., Sorí, R., Nieto,	2024	*Environmental Research Letters*

regions with projected drought trends”	R., Vicente-Serrano, S. M., & Gimeno, L.		
“The increasing influence of atmospheric moisture transport on hydrometeorological extremes in the Euromediterranean region with global warming”	**Gimeno-Sotelo, L.**, Fernández-Alvarez, J. C., Nieto, R., Vicente-Serrano, S. M., & Gimeno, L.	2024	Submitted manuscript

Table 2. Information about the journals where the articles in Chapter 4 were published, for those journals included in the Journal Citation Reports of the year 2023.

Journal	*Weather and Climate Extremes*	*Atmospheric Research*	*Environmental Research Letters*
ISSN	2212-0947	0169-8095	1748-9326
Region	NETHERLANDS	NETHERLANDS	ENGLAND
Publisher	ELSEVIER	ELSEVIER SCIENCE INC	Institute of Physics Publishing Ltd
Impact Factor	6.1	4.5	5.8
Quartile (Category)	Q1 (METEOROLOGY & ATMOSPHERIC SCIENCES)	Q1 (METEOROLOGY & ATMOSPHERIC SCIENCES)	Q1 (METEOROLOGY & ATMOSPHERIC SCIENCES)

4.1 Regions where atmospheric moisture transport influences extreme precipitation

The first article included in this chapter is entitled “**Where does the link between atmospheric moisture transport and extreme precipitation matter?**” by **Gimeno-Sotelo, L.**, and Gimeno, L., and was published in the journal *Weather and Climate Extremes* in 2023.

Weather and Climate Extremes 39 (2023) 100536

Contents lists available at ScienceDirect

Weather and Climate Extremes

journal homepage: www.elsevier.com/locate/wace

Where does the link between atmospheric moisture transport and extreme precipitation matter?

Luis Gimeno-Sotelo, Luis Gimeno *

Centro de Investigación Mariña, Universidade de Vigo, Environmental Physics Laboratory (EPhysLab), Ourense, Spain

ARTICLE INFO

Keywords:
Extreme precipitation
Moisture transport
Extreme value analysis

ABSTRACT

Atmospheric moisture transport is the primary component of the atmospheric branch of the water cycle, and its anomalies strongly influence drought and precipitation extremes. We utilised the full geographical and temporal spectrum of the ERA-5 reanalysis data and extreme value theory to identify regions where the atmospheric moisture transport, quantified as local integrated moisture vertical transport (IVT), influences daily extreme precipitation, and where this influence has a relevant dynamic component, which may alter the dependency between IVT and extreme precipitation as temperatures increase with climate change. We showed that this dependency is weak or negligible in tropical regions and strong but nonuniform in extratropical regions. Its influence is much greater in areas where the main moisture transport mechanisms occur, namely, atmospheric rivers, low-level jets, and tropical cyclones. The dynamic component of IVT, linked to wind, is highly consequential in regions with landfalling atmospheric rivers, landfalling tropical cyclones, or moisture-transporting low-level jets.

1. Introduction

Few topics bring as much consensus in the scientific community as the importance of the mechanisms of extreme precipitation and how they are influenced by climate change (Douville et al., 2021; Seneviratne et al., 2021; Caretta and Pörtner, 2022). In fact, extreme precipitation, in addition to being the main cause of floods and their dramatic socio-economic impacts, also arouses an important theoretical interest in relation to the mechanisms causing its intensification in response to a warming climate. Despite limitations in defining extreme precipitation periods and its various behaviours in tropical or extratropical regions (Zhang et al., 2019), a robust signal indicates that extreme precipitation increases globally with temperature, following the thermodynamic constraints imposed by the water-holding capacity of the atmosphere but varying regionally owing to atmospheric dynamical changes (O'Gorman, 2015; Bao et al., 2017).

Depending on the selected temporal and spatial domains, extreme precipitation can be caused by multiple meteorological systems. On the synoptic scale, tropical cyclones and monsoon lows in the tropics and baroclinic systems such as extratropical cyclones, warm conveyor belts, and fronts in the extratropics are the most prominent. The only common factors between these systems are the production of atmospheric instability with strong vertical motion and the potential for intense moisture transport to a region of extreme precipitation (De Vries, 2021). It is very difficult to generate intense precipitation with the sole humidity contained in the atmospheric column; strong and sustained moisture contributions are required from outside regions (Trenberth et al., 2003), in some cases very remote (Insua-Costa et al., 2022). Hence, great importance has been given to the main global mechanisms of moisture transport, namely the atmospheric rivers in the extratropics and the low-level jets (LLJs) in tropical regions (Gimeno et al., 2016).

Among the various methods of quantifying moisture transport (see Gimeno et al., 2012 for a review) the Eulerian scheme based on the integrated moisture vertical transport (IVT) has been the most widespread in extreme precipitation analyses, mainly due to its use in the identification and characterization of the atmospheric rivers (ARs) (Zhu and Newell, 1998; Gimeno et al., 2014; Payne et al., 2020). ARs are organised structures with high IVT that extend thousands of kilometres in length and a few hundred kilometres in width; they are responsible for approximately 90% of the meridional moisture transport from the subtropics to the extratropics (Zhu and Newell, 1998). Many global and regional studies have analysed the link between the current and future frequencies and intensities of ARs and precipitation extremes (e.g., at a global scale (Waliser and Guan, 2017), for the regional-scale current

* Corresponding author.
E-mail address: l.gimeno@uvigo.es (L. Gimeno).

https://doi.org/10.1016/j.wace.2022.100536
Received 22 May 2022; Received in revised form 1 December 2022; Accepted 3 December 2022
Available online 6 December 2022

climate (Lavers and Villarini, 2013; Ralph and Dettinger, 2012), and for the future climate (Gao et al., 2016; Whan et al., 2020). However, the relationship between IVT and extreme precipitation is not restricted only to the occurrence of ARs. There are values of IVT that are not categorised as ARs owing to the size of the structure (e.g., in the Mediterranean area including the Alpine region (Lorente-Plazas et al., 2020; Mahlstein et al., 2019)), the magnitude of the IVT, or the mechanism responsible for the high IVT values (e.g., tropical cyclones or LLJs-Gimeno et al., 2016-). Therefore, local IVT-extreme precipitation relationships have also been considered, so the IVT has been used as a precursor for extreme precipitation (Froidevaux and Martius, 2016) or to attribute singular extreme events to climate change (Reid et al., 2021). Notably, the IVT field is much more predictable than the precipitation field (Lavers et al., 2014, 2016), thereby increasing its already broad relevance.

Ultimately, the IVT is a product of humidity and wind; therefore, its values and sensitivity to climate change depend on those of humidity (thermodynamic component) and wind (dynamic component). This dichotomy translates into different influences from “windy ARs” versus “wet ARs”. For example, in the west coast of the US, a main region for AR occurrence, more rainfall is associated with windy ARs than with wet ARs, but the latter is associated with higher AR frequency (Gonzales et al., 2020). In terms of sensitivity to climate change and, in particular, increases in global temperature, the thermodynamic component will follow the global dependence on humidity given by the Clausius–Clapeyron relationship, while the dynamic component will exhibit regional behaviours linked to changes in the atmospheric general circulation. For example, considering the end-of-century projections for a temperature increase of 3.5 °C, the thermodynamic component of the IVT increases uniformly worldwide at a rate of 20–40% per century, whereas the dynamic component decreases by 5–15% in the tropics and mid-latitudes and increases by a similar amount in polar regions (O'Brien et al., 2022).

However, the strength of the relationship between IVT and precipitation extremes varies greatly depending on the method chosen to define extreme precipitation and the IVT value and extension thresholds, as well as the region or season. There are regions where IVT has very little influence on precipitation extremes and others where its influence is decisive. Moreover, in the latter, the nexus may be more associated with either the thermodynamic or dynamic component of the IVT. Here, we utilised the full geographical and temporal spectrum of the state-of-the-art fifth-generation atmospheric reanalysis (ERA-5) data and the extreme value theory to model the relationships between daily extreme precipitation and IVT. This enabled us to determine where, when, and to what extent the relationship between IVT and extreme precipitation is important globally. Additionally, considering their importance in the context of climate change, we estimated the relative influence of the two IVT components, dynamic and thermodynamic, respectively represented by IVT/IWV and IWV, where IWV refers to the integrated water vapor along the atmospheric column, often referred to as precipitable water.

2. Data and methods

2.1. Data

We used data from the ERA-5 reanalysis (Hersbach, H. et al., 2020) -the most recent reanalysis from the European Centre for Medium-Range Weather Forecasts-to obtain daily values of precipitation, integrated moisture vertical transport (IVT) and integrated water vapor (IWV) for the period 1981–2020 at 0.5° resolution. IVT and IWV are defined as follows, in terms of the specific humidity, the eastward component of wind (u) and the northward component of wind (v):

$$IVT = \sqrt{\left(\frac{1}{g}\int_{\Omega} q\, u\, dp\right)^2 + \left(\frac{1}{g}\int_{\Omega} q\, v\, dp\right)^2} = \sqrt{IVT_u^2 + IVT_v^2} \quad \text{and}$$

$$IWV = \frac{1}{g}\int_{\Omega} q\, u\, dp \quad ,$$

where Ω refers to the entire atmospheric column and g to gravitational acceleration. The use of the entire atmospheric column is due to computational convenience, taking into account that the variables “total column water vapor” (IWV), “vertical integral of eastward water vapor flux” (IVT_u) and “vertical integral of northward water vapor flux” (IVT_v) from the ERA-5 reanalysis are so defined.

The main reason why the ERA-5 reanalysis was used in this study is because its primary aim was to identify the regions worldwide where the relationship between IVT and extreme precipitation is more intense on a global scale, and this reanalysis provides us with gridded data at a suitably high resolution for the meteorological interpretation of the worldwide and large-region results. To analyse how the link between the variables under study varies seasonally, the data were organised into four different sets according to the season: December–February (Northern Hemisphere Winter), March–May (Northern Hemisphere Spring), June–August (Northern Hemisphere Summer), and September–November (Northern Hemisphere Autumn).

2.2. Assessment of ERA-5 to evaluate daily and extreme precipitation and IWV

Reanalyses combine observations and circulation models to reconstruct past data with regular spatial and temporal resolution covering the entire globe, which is its main advantage and reason for its great use. Thus, they can generate data where there were no observations, the reason for their great success, but also the source of their strongest uncertainties. This forces us to be especially careful in its use and indicate where reanalyses are more appropriate and where less, especially in the use of daily and extreme data.

ERA-5 is the latest reanalysis generated by the European Centre for Medium-Range Weather Forecasts (Hersbach et al., 2020), and far exceeds its predecessor ERA-interim, and practically all reanalyses in use in quality for the study of the hydrological cycle (Nogueira, 2020). Due to its construction process, based on a circulation model, one of its strong points is the good reproduction of the large-scale general circulation of the atmosphere and it can be expected that it reproduces well its extremes, but it is more difficult to affirm that reproduces well daily and extreme values of precipitation and water column.

ERA-5 has been used since its launch in 2018 and there are not many previous assessment studies of daily precipitation and water column values at a global level, although there are some regional ones, especially linked to some type of precipitation -e.g. Hénin et al. (2018) in the Iberian Peninsula, Amjad et al. (2020) in Turkey, Bandhauer et al. (2022) in several European regions, Timmermans et al. (2019) or Xu et al. (2019) in the USA, Gleixner et al. (2020) in East Africa or Jiang et al. (2020) in Chinese mainland-. However, there are two global studies (Rivoire et al., 2021 for precipitation and Eiras Barca et al., 2022 for water column) that assess ERA-5 daily data against satellite data and one (Lavers et al., 2022) that assesses ERA5 daily precipitation data against gauge-based precipitation observations. They can help us to indicate where ERA-5 has more problems in reproducing daily and extreme precipitation and water column data and therefore the results of our study should be taken with caution.

Rivoire et al., 2021 assessed daily precipitation in ERA-5 against CMORPH satellite data (Joyce et al., 2004) over the entire globe for the period January 1979 to December 2018 in a regular grid with 0.25° resolution. To do this, they analysed the co-occurrence of precipitation extremes quantified by the hit rate, adjusting the extreme distributions using a generalized Pareto distribution for each grid point and calculating the Kullback–Leibler divergence to quantify the distance between the entire EGPDs obtained from ERA-5 and the observations. In this study, it was concluded that ERA-5 and CMORPH precipitation intensity agree well over the midlatitudes and disagree over the tropics in all seasons. A view of the hit rate for events greater than the 95th percentile between ERA-5 and CMORPH (figure C2 in Rivoire et al., 2021) shows values that are higher than 70% in practically all the regions of interest in our study.

Lavers et al. (2022) used daily precipitation observations from 5 637 stations from 2001 to 2020 to assess daily precipitation in ERA-5, using the nearest neighbor approach to match the closest ERA-5 grid point to a station and the mean, the standard deviation of the differences and the Stable Equitable Error in Probability Space (SEEPS) score (Rodwell et al., 2010; Haiden et al., 2012) to estimate errors. They showed that the smallest ERA-5 errors occurred during winter in the extratropics and the largest in the tropics mostly across the Maritime Continent. An analysis of four extreme precipitation events showed a general agreement between the precipitation patterns from ERA-5 and the observations, although there are some limitations associated with strong convection and orography. The authors concluded that for both daily data and extreme precipitation events, ERA-5 is more skillful in the extratropics than in the tropics, and in extratropics during winter than during summer because of the convective systems.

Eiras-Barca et al. (2022) assessed daily ERA-5 integrated vertical water vapor column (IWV) data against the new Total Column Vater Vapor Data Record (CDR-2 (v2)) —developed by the European Space Agency (ESA) in coordination with the Satellite Application Facility on Climate Monitoring (CM SAF), for a unified grid of 0.5° × 0.5° and the period July 2002–December 2017. The study was done globally but with a focus on regions of critical interest for moisture transport mechanisms (almost 40 000 atmospheric river (AR) and nocturnal low-level jet (NLLJ) events were identified on a global scale between 2002 and 2017). Results show low bias between ERA-5 versus CDR-2 in the regions of interest of our study (generally less than ±2 kg m−2) and temporal correlations in the IWV fields above 0.8 in most areas. The highest disagreement was reported in the main tropical rainforest regions, which in general are not areas of critical interest for moisture transport phenomena.

Recently, an extension to the 50s has been made for the ERA-5 reanalysis (Bell et al., 2021), which would allow the period of record to be extended. This would substantially reduce the impact of sampling variability on the fitted extreme value distributions by increasing the annual maxima sample size. However, the extension of the ERA-5 reanalysis to 1950 is a new product and is still in the testing phase due to the large uncertainties it has in the upper air. Because the massive assimilation of satellite data occurs in the operational phase, since 1979, the vast majority of assimilable data at different vertical levels are those derived from radiosondes with limited spatial coverage. IVT is an extraordinarily sensitive variable to this since it integrates zonal and meridional winds and specific humidity data at multiple vertical levels, so a quality product cannot be expected. The extension to the 50s indeed incorporates some satellite data before the operational era, but in any case, they are very limited and do not guarantee adequate minimum spatial and temporal coverage. Therefore, introducing data before 1979 into our analysis would disturb the results, making them more uncertain, that is why we have limited the analysis to the most reliable period since 1980.

2.3. Statistical methods

We relied on the annual maxima method from the Extreme Value Theory (EVT). For extensive information about this method, see e.g. Coles (2001) and Beirlant et al. (2004). In short, for a given variable, the method consists of fitting a GEV distribution to the sample of the maximum annual values of that variable. Let Y be the random variable corresponding to the annual maxima of the variable under study; according to the annual maxima method, the distribution function of Y is assumed to have the following expression (GEV distribution function):

$$G(y;\ \mu,\sigma,\gamma)=\exp\left\{-\left[1+\gamma\frac{y-\mu}{\sigma}\right]^{-1/\gamma}\right\}\text{with } 1+\gamma\frac{y-\mu}{\sigma}>0$$

where y is a value of the random variable Y, and $\mu\in\mathbb{R}, \sigma>0,$ and $\gamma\in\mathbb{R}$ are the location, scale, and shape parameter of that distribution, respectively. The parameter μ quantifies the central tendency of the distribution, σ refers to its dispersion, and γ indicates whether the distribution is bounded and, if not, how "thick" the tail of the distribution is. If $\gamma<0$, the distribution is bounded. If $\gamma>0,$ it is unbounded and has a "heavy" tail; if $\gamma\to 0$, it is also unbounded and has an exponential tail. In the latter case, the GEV reduces to the Gumbel distribution, which takes the form:

$$G(y;\ \mu,\sigma)=\exp\left\{-\exp\left[-\frac{y-\mu}{\sigma}\right]\right\}.$$

It is possible to express μ and σ in terms of a covariate z (non-stationary approach), for example, as linear functions: $\mu(z)=\beta_0+\beta_1 z$ and $\sigma(z)=\theta_0+\theta_1 z$.

For each season between 1981 and 2020, linearly detrended precipitation, IVT, IVT/IWV and IWV data were used to fit non-stationary GEV models to the annual maxima of precipitation at each grid point, considering separately the covariates IVT, IVT/IWV, and IWV (these covariates were centred and scaled before being used for the model fitting). The use of linearly detrended data is justified by the fact that the aim of this study is to assess the influence that these covariates have on extreme precipitation, regardless of the trends that the variables may have. Although the analysis is performed by means of linearly detrended data, it has been checked that the effect of removing trends is negligible in this study, as the use of detrended or non-detrended data produces very similar results in this case. The location and scale parameters were expressed as linear functions of the respective covariate, and the resulting coefficients $\beta_0, \beta_1, \theta_0$ and θ_1 , as well as the shape parameter γ , were estimated using maximum likelihood fitting using the software *R* (R Core Team, 2022; namely the *ismev* package -Heffernan and Stephenson, 2018). This estimation method enables the construction of asymptotic confidence intervals based on the normal approximation; see Casella and Berger (2002) for a theoretical explanation of maximum likelihood estimators and their asymptotic properties. Using confidence intervals, the significance of the coefficients β_0, β_1, θ_0 and θ_1 can be assessed; for a given confidence level, if the value 0 is contained in the confidence interval of a coefficient, that coefficient is judged not to be statistically significant at that level.

Regarding the assessment of the goodness of fit of the non-stationary GEV models, as pointed out in Coles (2001), there is not homogeneity in the distributional assumptions for each observation, that is, for each value of the covariate the parameters of the extreme value model take different values. Therefore, goodness-of-fit tests, which are common in the stationary case, are not simple to apply in the non-stationary one. Thus, following indications from Coles (2001), for $Y_z \sim GEV(\mu(z),\sigma(z),\gamma)$, we defined the standardized variables $\widetilde{Y}_z=\frac{1}{\widehat{\gamma}}\log\left\{1+\widehat{\gamma}\left(\frac{Y_z-\widehat{\mu}(z)}{\widehat{\sigma}(z)}\right)\right\}$, which are standard-Gumbel distributed, and produced probability and quantile plots of the observed $\widetilde{y}_z$ with respect to that distribution. The probability plot is constructed as follows: $\left\{\frac{i}{m+1},\exp(-\exp(-\widetilde{y}_{(i)}));\ i=1,\dots,m\right\}$

and the quantile plot:

$$\left\{\widetilde{y}_{(i)},-\log\left(-\log\left(\frac{i}{m+1}\right)\right);\ i=1,\dots,m\right\}$$

where $\widetilde{y}_{(1)},\dots,\widetilde{y}_{(m)}$ are the ordered values of the $\widetilde{y}_z$.

Having constructed these diagnostic plots, the goodness of fit of the non-stationary GEV models is assessed by means of the linearity of the points in those plots. As such, to have a metric that allows the assessment of global gridded data, we computed the R^2 of the linear regression model which is associated to each plot, for all the non-stationary GEV models that were fitted.

Having fitted a GEV model to the annual maxima of precipitation, it is possible to estimate a *m*-year return level, which is the value of maximum precipitation which is exceeded on average once every *m* years. In a non-stationary framework with a covariate z, letting z^* be a fixed value for that covariate, the estimated *m*-year return level ($\widehat{y_m}$) can be calculated from the quantile function of the GEV distribution (denoted as $G^{\leftarrow}$) as follows:

$$\widehat{y_m} = G^{\leftarrow}\left(1 - \frac{1}{m}\ ;\ \widehat{\mu}(z^*), \widehat{\sigma}(z^*), \widehat{\gamma}\right)$$

where $\widehat{\mu}(z)$, $\widehat{\sigma}(z)$, and $\widehat{\gamma}$ refer to the estimated parameters of a non-stationary GEV model with location and scale parameters as a function of z (note that it is a conditional extreme value model). In this framework, the return levels estimates are conditional on specific realizations of the covariate, that is, a *m*-year return level is interpreted as a value that is exceeded once every 20 years when the covariate equals z^*.

In this study, we computed the percentage of variation in the estimated 20-year return level of maximum precipitation between a low and a high value of a given driver of that variable; thus, the 10th percentile and the 90th percentile of the centred and scaled covariates IVT, IVT/IWV, and IWV were calculated. High percentages in a region indicate that the corresponding covariate has a high influence on the precipitation maxima in that region. The computation of the estimated return levels was performed using the *R* package *evd* (Stephenson, 2002).

3. Results

3.1. Maximum precipitation and IVT: a first approach

A simple and intuitive way to visualise the fact that extreme precipitation is not related to extreme IVT everywhere in the same way is to show the patterns of the highest daily precipitation for the full analysed period, P_h, and the averaged IVT for the corresponding day, IVTp (Fig. 1; see Supplementary Fig. 1 for intermediate seasons).

A fundamental difference can be observed between the two patterns. In general, the P_h pattern is visually comparable with those of the mean precipitation or extreme precipitation above high percentiles (Supplementary Fig. 2 top), with the principal maxima in the Intertropical Convergence Zone (ITCZ) moving seasonally and secondary maxima in regions of occurrence of extratropical cyclones in both hemispheres with regional distinctions linked to tropical cyclones and monsoon circulations.

The IVTp pattern is no longer as similar to that of the mean or extreme IVT at high percentiles (Supplementary Fig. 2 bottom). Within the general pattern, there are coincidences in the extratropical regions of high IVT ("IVT storm tracks"), which migrate towards the poles in the summer of each hemisphere, and in the regions of very high IVT values that occur in June–August in the Indian monsoon region and the east coast of Asia; however, equatorial IVT maxima are not observed in the IVTp field, neither in the equatorial band of the Pacific easterly trade winds nor in the north-eastern South American continent. In large parts of the coincident regions, the IVTp value is notably above that of the 95th percentile, which indicates that very extreme IVT values correspond to the day of absolute maximum precipitation; therefore, a strong relationship exists between extreme precipitation and IVT in these

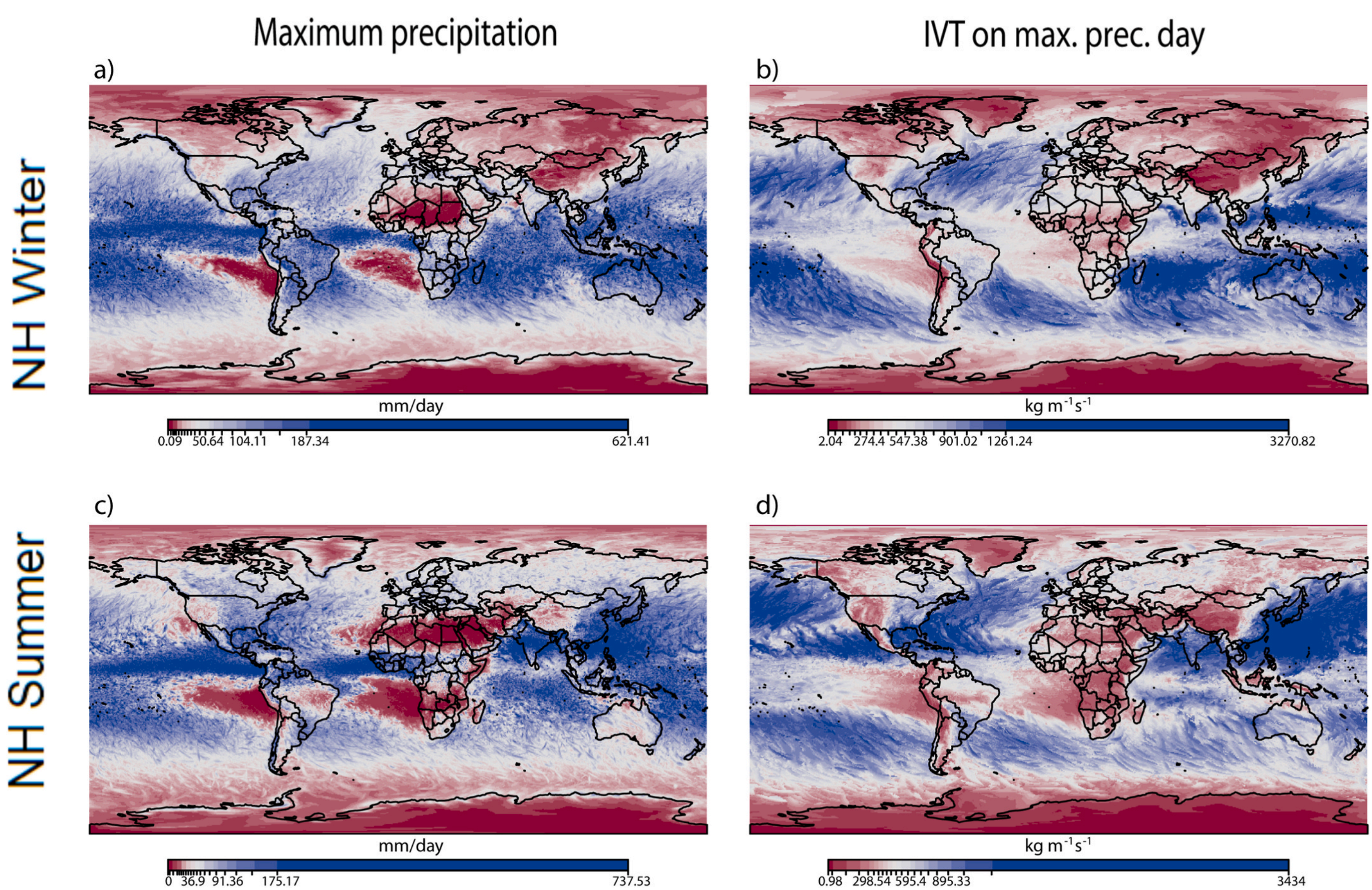

Fig. 1. Highest daily precipitation value and corresponding daily-averaged IVT value for a) and b) Northern Hemisphere Winter (December–February) and c) and d) Northern Hemisphere Summer (June–August), for the period 1981–2020.

regions.

Additionally, a careful visual analysis reveals the filamentous structures of the IVTp maxima, indicating that, in many cases, these values occurred on the same day through the same moisture transport structure. For example, this is very visible during both December–February and June–August in storm track regions owing to ARs (see Fig. 7 in Guan and Waliser, 2015) or during June–August in the North Atlantic owing to tropical cyclones (see Fig. 1 in Bloemendaal et al., 2020). The high coincidence in the IVTp maxima with P_h in the subtropical bands of maximum LLJs occurrence (see Fig. 4 in Algarra et al., 2019) is also noticeable. Therefore, the comparison between the P_h and IVTp patterns indicates that the relationship between extreme precipitation and IVT seems to be highly dependent upon the occurrence of the main global moisture transport mechanisms, namely ARs, LLJs, and tropical cyclones (Gimeno et al., 2016).

3.2. Regions and seasons in which IVT influences precipitation maxima

As described in Subsection 2.3, for each season, a non-stationary generalized extreme value (GEV) model was fitted to the annual precipitation maxima, allowing the location and scale parameters of the GEV distribution to vary linearly with IVT, IVT/IWV, and IWV. The goodness of fit of those models was assessed by means of the R^2 values for the linear models associated with the probability and quantile plots that were constructed as explained in Subsection 2.3; see Supplementary Figures 3,4 and 5. As can be seen from those figures, the R^2 values are very high (very close to 1) almost everywhere (and in every region of interest) for every season. Thus, these results indicate that the non-stationary GEV models that were fitted are adequate.

The location parameter (μ) of the GEV distribution measures the magnitude of the extreme precipitation and, considering that μ is expressed as a linear function of each covariate z, the slope (β_1) provides us with valuable information about the influence that this covariate has on the precipitation maxima. Fig. 2 (for intermediate seasons, see Supplementary Fig. 6) shows the maximum likelihood estimates for β_1 for the fitted GEV models, considering IVT and IVT/IWV separately as a covariate. For notation simplicity, those estimates are denoted by $\widehat{\beta}_{IVT}$ and $\widehat{\beta}_{IVT/IWV}$. Only significant values of $\widehat{\beta}_{IVT}$ and $\widehat{\beta}_{IVT/IWV}$ were plotted, and their significance was assessed in terms of their normal approximation confidence intervals (see Subsection 2.3). From this figure, we quantified the influence that IVT and its dynamic component, IVT/IWV, had on precipitation maxima.

The $\widehat{\beta}_{IVT}$ pattern (Fig. 2a,c) shows overlapping occurrences of the main moisture transport mechanisms (Fig. 3). Thus, in general, this relationship was strong in the subtropical regions of both hemispheres, practically null in the tropical regions, and moderate in the extratropical regions; in the latter case, it oscillated between an almost negligible relationship in the Southern Hemisphere (due to the minimal presence of continental regions) to a stronger one in the Northern Hemisphere. Additionally, the influence of ARs was observed in a continuous subtropical band of strong influence along the coastal regions of the continents and extending to high latitudes, including the polar ones, with greater intensity during their respective winters. Tropical cyclones influenced a strong relationship between IVT and extreme precipitation in all areas of TC occurrence in their corresponding summers. The influence of LLJs was apparent in the monsoon regions of the Asian

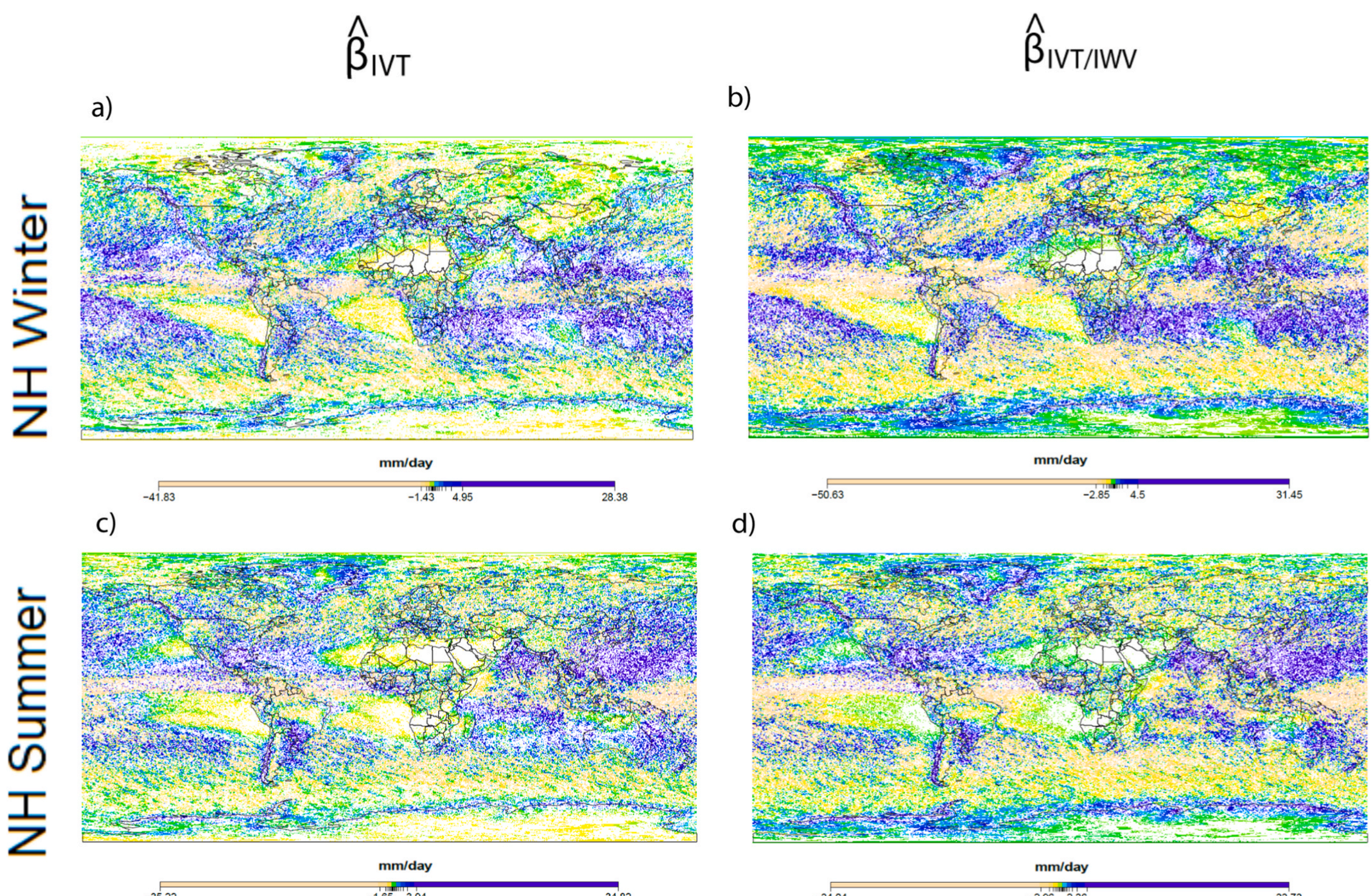

Fig. 2. Spatial patterns of the significant values of the estimated coefficient that represents the influence of IVT (a) and c)) and IVT/IWV (b) and d)) on maximum precipitation according to the GEV analysis (95% confidence level), for Northern Hemisphere Winter (December–February) and Northern Hemisphere Summer (June–August), respectively, for the period 1981–2020.

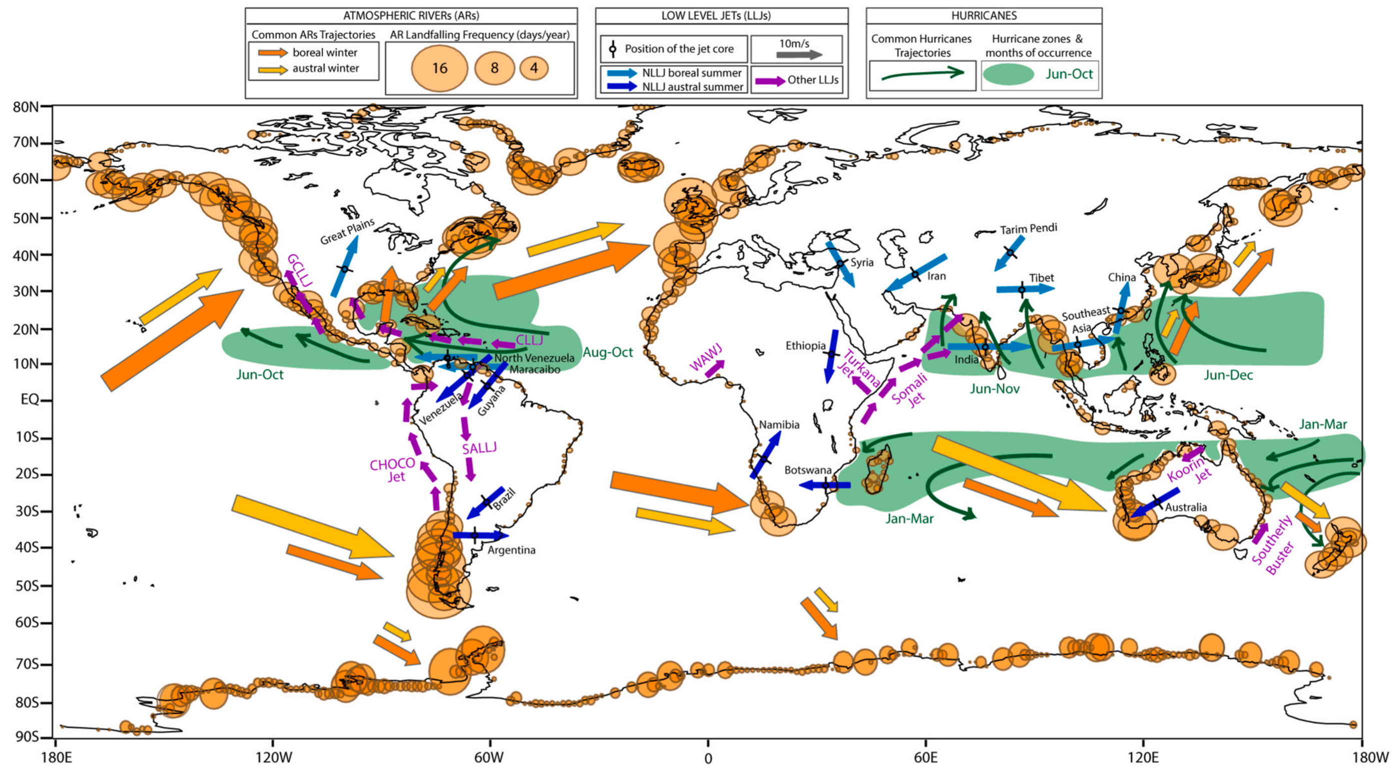

Fig. 3. Main regions where atmospheric rivers (ARs), low-level jets (LLJs), and tropical cyclones (TCs) occur. This figure was adapted from Gimeno et al. (2016). Orange arrows indicate the direction of ARs and orange circles show the frequency of landfalling ARs (days/year), based on Guan and Waliser (2015). Locations of nocturnal LLJs, as described by Rife et al. (2010), are shown as blue arrows, and their names are also displayed. The size of the arrow is scaled to the speed in the core of the jet. Green areas and dates indicate the regions and periods of tropical cyclone occurrence (Source: International Best Track Archive for Climate Stewardship, NOAA (Knapp et al., 2010)). (For interpretation of the references to colour in this figure legend, the reader is referred to the Web version of this article.)

continent during June–August, and in the south-eastern region of the South American continent.

This pattern is much more notable when the influence of the dynamic component of the IVT, calculated as $\widehat{\beta}_{IVT/IWV}$, is examined (Fig. 2b,d). At a continental level, this dynamic component influences extreme precipitation in the main regions where ARs make landfall (Fig. 3), such as the western North American, European, or South American coasts during their respective winters; in regions where TCs make landfall during summers, such as the North American and south-eastern Asian coasts; and in regions where LLJs cross continents, such as those associated with the Indian monsoon or the easternmost branch of the South American low-level jet.

In the remaining regions where IVT influences extreme precipitation, this influence is exclusively due to the thermodynamic component of the IVT, associated with the IWV (Supplementary Fig. 7). This supplementary figure represents the significant values of $\widehat{\beta}_{IWV}$, that is, the estimate of the slope (β_1) considering IWV as the covariate.

3.3. *Contribution of the dynamic component of IVT to the precipitation maxima*

The dynamic component of IVT, estimated as the ratio IVT/IWV, represents the vertically averaged wind, weighted by the specific humidity at each height. Its variations are related to changes in the magnitude of moisture-transporting winds; hence, they are linked to changes in atmospheric circulation.

Fig. 4 shows a finer regional analysis than Fig. 2, by representing the percentage change in the estimated 20-year return levels of the maximum precipitation when the covariate IVT/IWV is low and high (the 10th and 90th percentiles). This represents the change in the maximum precipitation value that is expected to occur on average once every 20 years, for a high versus a low dynamic component of IVT (it is important to remind that the return levels estimates are conditional on specific realizations of the covariate).

As can be seen in Fig. 4, there are regions in which changes were approximately 50% or higher. These occurred during the boreal winter on the west coast of North America, west coast of the Mediterranean, east coast of southern Africa, and central and western Australia. During the boreal summer, areas of relevant change were observed along the coasts of the Gulf of Mexico, the Caribbean, and Australia, the central regions of South America, and the north-western Indian subcontinent. It is in these regions that the greatest modifications of the relationship between IVT and extreme precipitation can be expected in a changing climate. These changes have already been observed in the present warming climate. A recent study observed changes in the estimated probability of concurrent IVT and precipitation extremes in most AR-landfall regions when comparing a recent (warmer) period versus a previous (colder) period (Gimeno-Sotelo and Gimeno, 2022).

4. Discussion and conclusion

We identified regions where atmospheric moisture transport, quantified as IVT, influences the daily extreme precipitation. Moreover, we determined where this influence has a relevant dynamic component, which may cause the relationship between IVT and extreme precipitation to change due to increased temperatures linked to climate change. Three important conclusions can be drawn from the study:

- The relationship between the IVT and extreme daily precipitation is very weak or even negligible in tropical regions. Because very high values of water vapor already exist in the tropics, a continuous and high external moisture contribution is not necessary to provide water vapor for extreme precipitation. In situations of atmospheric

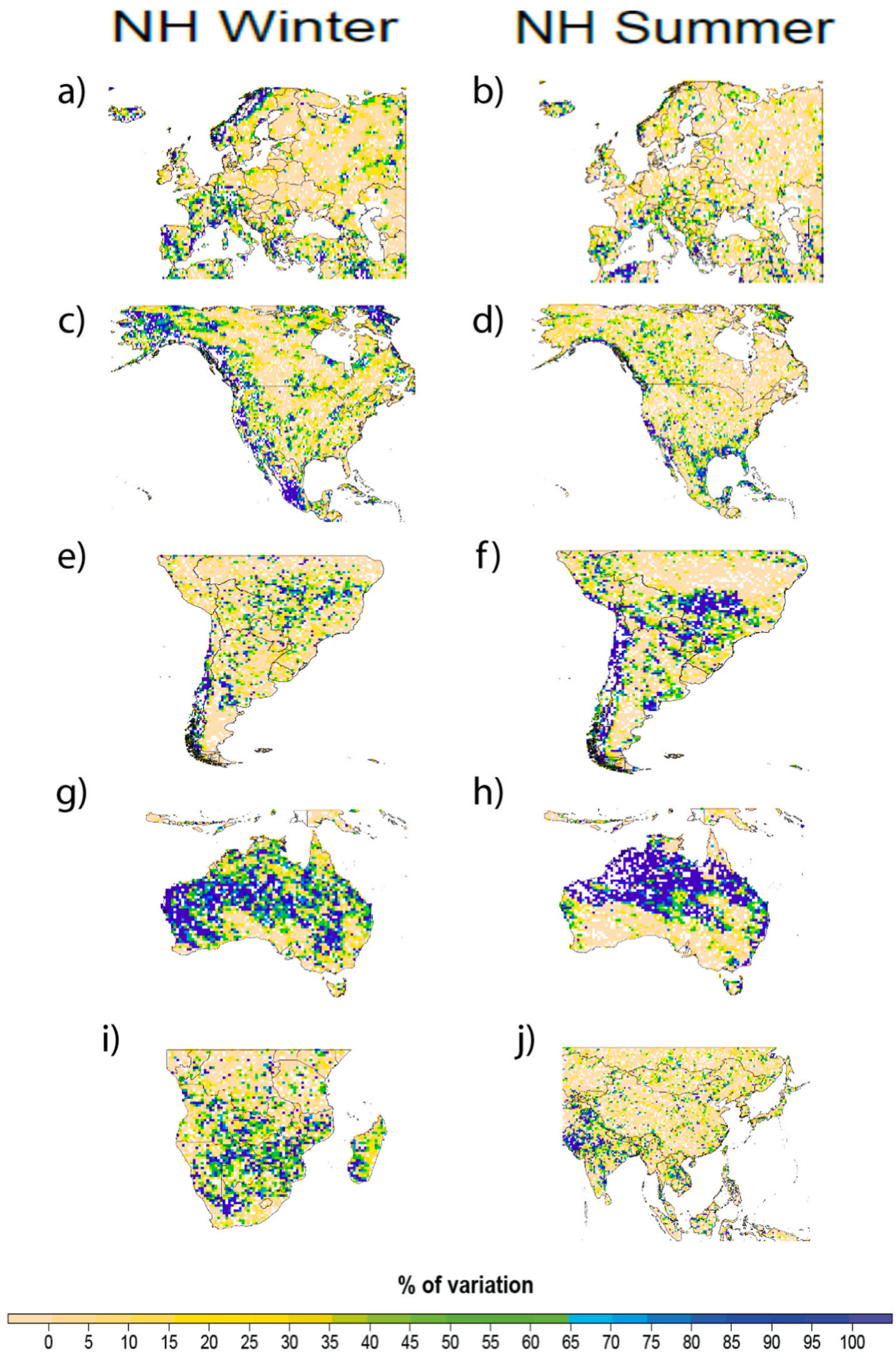

Fig. 4. Spatial pattern of the percentage of variation for the estimated 20-year return levels of maximum precipitation between the 10th and 90th percentiles of IVT/IWV, for the period 1981–2020. (a), (c), (e), and (g) refer to the results for Europe, North America, South America, and Australia during Northern Hemisphere Winter (December–February); b), d), f), and h) indicate the same regions during Northern Hemisphere Summer (June–August). i) corresponds to Southern Africa during NH Winter, and j) refers to the Asian monsoon region during NH Summer.

instability, the necessary water vapor to potentially generate extreme precipitation is already present. This agrees with the auxiliary results presented in this article concerning the dependence of IWV on extreme precipitation and the results reached in a recent paper, where a strong relationship between extremes of IWV and extreme daily precipitation was demonstrated (Kim et al., 2022).

- In extratropical regions, IVT strongly influences extreme precipitation, but not uniformly. Its influence is much greater in areas where the main modes of moisture transport occur, namely: (i) in the extensions of the subtropical band of moisture transport towards high latitudes in coastal regions, thereby revealing a signature of the ARs; (ii) in the regions and seasons of occurrence of tropical cyclones; and (iii) in the areas where strong low-level jet systems occur, which are frequently associated with monsoon circulations. In the polar regions of both hemispheres, the influence is restricted to the ARs.
- The dynamic component of IVT, linked to the wind, is highly important in the relationship between IVT and extreme precipitation in many regions of great meteorological and socioeconomic interest, such as: (i) the primary regions where ARs make landfall, including the west coasts of North America, South America, and Europe; (ii) the main regions of tropical cyclone landfalls, such as the southeast coast of North America, the Caribbean, and southeast Asia; and (iii) the regions influenced by large LLJs that transport moisture, such as the Indian monsoon region and southern South America. In these regions, the importance of the thermodynamic component of the IVT, associated with the IWV, decreases; Kim et al., 2022 also noted this, finding a smaller impact from the IWV on non-tropical extreme

precipitation events, except for continental areas of America and Eurasia that are far inland.

Our study has important practical implications deriving from the identification of regions and seasons during which studying the relationship between IVT and extreme precipitation is particularly important. This also implies that the study of the predictability of IVT in these specific regions and seasons can improve the predictability of daily precipitation extremes in those regions.

However, this study also has important theoretical implications. In the regions where the dynamic component of the IVT is important for extreme precipitation, the magnitude of the relationship between IVT and extreme precipitation may be more altered by climate change. As humidity, which defines the thermodynamic component of the IVT, will influence both IVT and extreme precipitation similarly, in those regions where the dynamic component of the IVT is important, we should expect greater changes in the dependence between IVT and extreme precipitation in the future.

This study has some limitations associated with the quality of the reanalysis precipitation data, which is generally low for regions with less dense instrument networks. Additionally, the coarse resolution of the data of the reanalysis necessitated further regional analysis in areas with complex orography or where small-scale convective processes are relevant. In particular, ERA-5 should be used carefully to study extreme precipitation over the tropics and IWV in the main tropical rainforest regions, but its confidence is high in the regions (extratropical) and seasons (winter) where the main results of our study are reached. Furthermore, the sample size may be seen as an important limitation (see Li et al., 2019) because, for each season, we used 40 annual precipitation maxima for model fitting; therefore, the parameter estimates may have been affected by sampling variability, as noted by Su and Smith (2021). If the period of reliable worldwide gridded data for IVT and precipitation were larger, the obtained results for the GEV analysis would be more robust. A comprehensive validation of the quality of the daily data of winds and specific humidity in the upper air of the recently released extension of ERA-5 to the 50s is clearly necessary for this purpose.

CRediT authorship contribution statement

Luis Gimeno-Sotelo: Formal analysis, Visualization, Writing – original draft, Writing – review & editing. **Luis Gimeno:** Conceptualization, Resources, Writing – original draft, Writing – review & editing, Supervision, Funding acquisition.

Declaration of competing interest

The authors declare that they have no known competing financial interests or personal relationships that could have appeared to influence the work reported in this paper.

Data availability

ERA-5 reanalysis data are publicly available and can be obtained from https://cds.climate.copernicus.eu.

Acknowledgements

This work is part of the SETESTRELO project (grant no. PID2021-122314OB-I00) funded by the Ministerio de Ciencia e Innovación, Spain. The EPhysLab group was co-funded by Xunta de Galicia, Consellería de Cultura, Educación e Universidade, under project ED431C 2021/44 "Programa de Consolidación e Estructuración de Unidades de Investigación Competitivas". Luis Gimeno-Sotelo was supported by a UVigo PhD grant ("Axudas para contratos predoutorais da Universidade de Vigo"). The authors would like to especially thank Raquel Nieto for her assistance in the design of the figures, and Iago Algarra and Marta Vázquez for downloading necessary data for the study.

Appendix A. Supplementary data

Supplementary data to this article can be found online at https://doi.org/10.1016/j.wace.2022.100536.

References

Algarra, I., Eiras-Barca, J., Nieto, R., Gimeno, L., 2019. Global climatology of nocturnal low-level jets and associated moisture sources and sinks. Atmos. Res. 229, 39–59. https://doi.org/10.1016/j.atmosres.2019.06.016.

Amjad, M., Yilmaz, M.T., Yucel, I., Yilmaz, K.K., 2020. Performance evaluation of satellite- and model-based precipitation products over varying climate and complex topography. J. Hydrol. 584 (February), 124707 https://doi.org/10.1016/j.jhydrol.2020.124707.

Bandhauer, M., Isotta, F., Lakatos, M., Lussana, C., Båserud, L., Izsák, B., Szentes, O., Tveito, O.E., Frei, C., 2022. Evaluation of daily precipitation analyses in E-OBS (v19.0e) and ERA5 by comparison to regional high-resolution datasets in European regions. Int. J. Climatol. 42 (2), 727–747. https://doi.org/10.1002/joc.7269.

Bao, J., Sherwood, S.C., Alexander, L.V., Evans, J.P., 2017. Future increases in extreme precipitation exceed observed scaling rates. Nat. Clim. Change 7 (2), 128–132. https://doi.org/10.1038/nclimate3201.

Beirlant, J., Goegebeur, Y., Segers, J., Teugels, J.L., 2004. Statistics of Extremes: Theory and Applications. John Wiley & Sons, Chichester.

Bell, B., Hersbach, H., Simmons, A., Berrisford, P., Dahlgren, P., Horányi, A., et al., 2021. The ERA5 global reanalysis: preliminary extension to 1950. Q. J. R. Meteorol. Soc. 147 (741), 4186–4227. https://doi.org/10.1002/qj.4174. Available from:

Bloemendaal, N., et al., 2020. Generation of a global synthetic tropical cyclone hazard dataset using STORM. Sci. Data 7 (1), 1–12. https://doi.org/10.1038/s41597-020-0381-2.

Caretta, M.A., et al., 2022. Water. In: Climate Change 2022: Impacts, Adaptation, and Vulnerability. Contribution of Working Group II to the Sixth Assessment Report of the Intergovernmental Panel on Climate Change [Pörtner, H.O. , et al.]. Cambridge University Press (in press).

Casella, G., Berger, R.L., 2002. Statistical Inference, second ed. Duxbury Press, Pacific Grove.

Coles, S., 2001. An Introduction to Statistical Modeling of Extreme Values. Springer, London.

De Vries, A.J., 2021. A global climatological perspective on the importance of Rossby wave breaking and intense moisture transport for extreme precipitation events. Weather and Climate Dynamics 2 (1), 129–161. https://doi.org/10.5194/wcd-2-129-2021.

Douville, H., et al., 2021. Water cycle changes. In: Climate Change 2021: The Physical Science Basis. Contribution of Working Group I to the Sixth Assessment Report of the Intergovernmental Panel on Climate Change [Masson-Delmotte, V., et al.]. Cambridge University Press (in press).

Eiras-Barca, J., Algarra, I., Nieto, R., Schröder, M., Hegglin, M.I., Gimeno, L., 2022. Analysis of the main source regions of moisture transport events with the new ESA CCI/CM-SAF Total Column Water Vapour Climate Data Record (v2). Q. J. R. Meteorol. Soc. https://doi.org/10.1002/qj.4358.

Froidevaux, P., Martius, O., 2016. Exceptional integrated vapour transport toward orography: an important precursor to severe floods in Switzerland. Q. J. R. Meteorol. Soc. 142 (698), 1997. https://doi.org/10.1002/qj.2793, 201.

Gao, Y., Lu, J., Leung, L.R., 2016. Uncertainties in projecting future changes in atmospheric rivers and their impacts on heavy precipitation over Europe. J. Clim. 29 (18), 6711–6726, 2016. https://www.jstor.org/stable/26385654.

Gimeno, L., et al., 2012. Oceanic and terrestrial sources of continental precipitation. Rev. Geophys. 50, 4. https://doi.org/10.1029/2012RG000389.

Gimeno, L., Nieto, R., Vázquez, M., Lavers, D.A., 2014. Atmospheric rivers: a mini-review. Front. Earth Sci. 2, 2. https://doi.org/10.3389/feart.2014.00002.

Gimeno, L., et al., 2016. Major mechanisms of atmospheric moisture transport and their role in extreme precipitation events. Annu. Rev. Environ. Resour. 41, 117–141. https://doi.org/10.1146/annurev-environ-110615-085558.

Gimeno-Sotelo, L., Gimeno, L., 2022. Concurrent extreme events of atmospheric moisture transport and continental precipitation: the role of landfalling atmospheric rivers. Atmos. Res. 278, 106356 https://doi.org/10.1016/j.atmosres.2022.106356.

Gleixner, S., Demissie, T., Diro, G.T., 2020. Did ERA5 improve temperature and precipitation reanalysis over East Africa? Atmosphere 11 (9), 996–1019. https://doi.org/10.3390/atmos11090996.

Gonzales, K.R., Swain, D.L., Barnes, E.A., Diffenbaugh, N.S., 2020. Moisture-versus wind-dominated flavors of atmospheric rivers. Geophys. Res. Lett. 47, 23. https://doi.org/10.1029/2020GL090042.

Guan, B., Waliser, D.E., 2015. Detection of atmospheric rivers: evaluation and application of an algorithm for global studies. J. Geophys. Res. Atmos. 120 (24), 12514–12535. https://doi.org/10.1002/2015JD024257.

Haiden, T., Rodwell, M.J., Richardson, D.S., Okagaki, A., Robinson, T., Hewson, T.D., 2012. Intercomparison of global model precipitation forecast skill in 2010/11 using the SEEPS score. Mon. Weather Rev. 140, 2720–2733. https://doi.org/10.1175/MWR-D-11-00301.1.

Heffernan, J.E., Stephenson, A.G., 2018. Ismev: an introduction to statistical modeling of extreme values. R package version 1.42. https://CRAN.R-project.org/package=ismev.
Hénin, R., Liberato, M., Ramos, A., Gouveia, C., 2018. Assessing the use of satellite-based estimates and high-resolution precipitation datasets for the study of extreme precipitation events over the Iberian Peninsula. Water 10 (11), 1688. https://doi.org/10.3390/w10111688.
Hersbach, H., et al., 2020. The ERA5 global reanalysis. Q. J. R. Meteorol. Soc. 146 (730), 1999–2049. https://doi.org/10.1002/qj.3803.
Insua-Costa, D., Senande-Rivera, M., Llasat, M.C., Miguez-Macho, G., 2022. A global perspective on western Mediterranean precipitation extremes. npj Climate and Atmospheric Science 5 (1), 1–7. https://doi.org/10.1038/s41612-022-00234-w.
Jiang, Q., Li, W., Fan, Z., He, X., Sun, W., Chen, S., et al., 2020. Evaluation of the ERA5 reanalysis precipitation dataset over Chinese Mainland. J. Hydrol., 125660 https://doi.org/10.1016/j.jhydrol.2020.125660. October.
Joyce, R.J., Janowiak, J.E., Arkin, P.A., Xie, P., 2004. CMORPH: a method that produces global precipitation estimates from passive microwave and infrared data at high spatial and temporal resolution. J. Hydrometeorol. 5 (3), 487–503. https://doi.org/10.1175/1525-7541(2004)005⟨0487:CAMTPG⟩2.0.CO;2.
Kim, S., Sharma, A., Wasko, C., Nathan, R., 2022. Linking total precipitable water to precipitation extremes globally. Earth's Future 10, e2021EF002473. https://doi.org/10.1029/2021EF002473.
Knapp, K.R., et al., 2010. NCDC International Best Track Archive for Climate Stewardship (IBTrACS) Project, Version 3. NOAA National Centers for Environmental Information. https://doi.org/10.7289/V5NK3BZP.
Lavers, D.A., Villarini, G., 2013. The nexus between atmospheric rivers and extreme precipitation across Europe. Geophys. Res. Lett. 40 (12), 3259–3264. https://doi.org/10.1002/grl.50636.
Lavers, D.A., Pappenberger, F., Zsoter, E., 2014. Extending medium-range predictability of extreme hydrological events in Europe. Nat. Commun. 5 (1), 1–7. https://doi.org/10.1038/ncomms6382.
Lavers, D.A., Pappenberger, F., Richardson, D.S., Zsoter, E., 2016. ECMWF Extreme Forecast Index for water vapor transport: a forecast tool for atmospheric rivers and extreme precipitation. Geophys. Res. Lett. 43 (22), 11–852. https://doi.org/10.1002/2016GL07132.
Lavers, D.A., Simmons, A., Vamborg, F., M, J., 2022. An evaluation of ERA5 precipitation for climate monitoring. Q. J. R. Meteorol. Soc. 1–14. https://doi.org/10.1002/qj.4351. Available from:
Li, C., Zwiers, F., Zhang, X., Li, G., 2019. How much information is required to well constrain local estimates of future precipitation extremes? Earth's Future 7 (1), 11–24.
Lorente-Plazas, R., et al., 2020. Unusual atmospheric-river-like structures coming from Africa induce extreme precipitation over the western Mediterranean Sea. J. Geophys. Res. Atmos. 125, 2. https://doi.org/10.1029/2019JD031280.
Mahlstein, I., Bhend, J., Spirig, C., Martius, O., 2019. Developing an automated medium-range flood awareness system for Switzerland based on probabilistic forecasts of integrated water vapor fluxes. Weather Forecast. 34 (6), 1759–1776. https://doi.org/10.1175/WAF-D-18-0189.1.
Nogueira, M., 2020. Inter-comparison of ERA-5, ERA-interim and GPCP rainfall over the last 40 years: process-based analysis of systematic and random differences. J. Hydrol. 583 (August 2019), 124632 https://doi.org/10.1016/j.jhydrol.2020.124632.
O'Brien, T.A., et al., 2022. Increases in future AR count and size: overview of the ARTMIP Tier 2 CMIP5/6 experiment. J. Geophys. Res. Atmos. 127, 6. https://doi.org/10.1029/2021JD036013.
O'Gorman, P.A., 2015. Precipitation extremes under climate change. Curr. Clim. Change Rep. 1 (2), 49–59. https://doi.org/10.1007/s40641-015-0009-3.
Payne, A.E., et al., 2020. Responses and impacts of atmospheric rivers to climate change. Nat. Rev. Earth Environ. 1 (3), 143–157. https://doi.org/10.1038/s43017-020-0030-5.
R Core Team. R, 2022. A Language and Environment for Statistical Computing. R Foundation for Statistical Computing, Vienna, Austria. URL. https://www.R-project.org/.
Ralph, F.M., Dettinger, M.D., 2012. Historical and national perspectives on extreme West Coast precipitation associated with atmospheric rivers during December 2010. Bull. Am. Meteorol. Soc. 93 (6), 783–790. https://doi.org/10.1175/BAMS-D-11-00188.1.
Reid, K.J., O'Brien, T.A., King, A.D., Lane, T.P., 2021. Extreme water vapor transport during the March 2021 sydney floods in the context of climate projections. Geophys. Res. Lett. 48, 22. https://doi.org/10.1029/2021GL095335.
Rife, D.L., Pinto, J.O., Monaghan, A.J., Davis, C.A., Hannan, J.R., 2010. Global distribution and characteristics of diurnally varying low-level jets. J. Clim. 23 (19), 5041–5064. https://doi.org/10.1175/2010JCLI3514.1.
Rivoire, P., Martius, O., Naveau, P., 2021. A comparison of moderate and extreme ERA-5 daily precipitation with two observational data sets. Earth Space Sci. 8, e2020EA001633 https://doi.org/10.1029/2020EA001633.
Rodwell, M.J., Richardson, D.S., Hewson, T.D., Haiden, T., 2010. A new equitable score suitable for verifying precipitation in numerical weather prediction. Q. J. R. Meteorol. Soc. 136, 1344–1363. https://doi.org/10.1002/qj.656.
Seneviratne, S.I., et al., 2021. Weather and climate extreme events in a changing climate. In: Climate Change 2021: The Physical Science Basis. Contribution of Working Group I to the Sixth Assessment Report of the Intergovernmental Panel on Climate Change [Masson-Delmotte, V., et al.]. Cambridge University Press (Press).
Stephenson, A.G., 2002. Evd: extreme value distributions. R. News 2 (2), 31–32. URL: https://CRAN.R-project.org/doc/Rnews/.
Su, Y., Smith, J.A., 2021. An atmospheric water balance perspective on extreme rainfall potential for the contiguous US. Water Resour. Res. 57, 4. https://doi.org/10.1029/2020WR028387.
Timmermans, B., Wehner, M., Cooley, D., O'Brien, T., Krishnan, H., 2019. An evaluation of the consistency of extremes in gridded precipitation data sets. Clim. Dynam. 52 (11), 6651–6670. https://doi.org/10.1007/s00382-018-4537-0.
Trenberth, K.E., Dai, A., Rasmussen, R.M., Parsons, D.B., 2003. The changing character of precipitation. Bull. Am. Meteorol. Soc. 84 (9), 1205–1218. https://doi.org/10.1175/BAMS-84-9-1205.
Waliser, D., Guan, B., 2017. Extreme winds and precipitation during landfall of atmospheric rivers. Nat. Geosci. 10 (3), 179–183. https://doi.org/10.1038/ngeo2894.
Whan, K., Sillmann, J., Schaller, N., Haarsma, R., 2020. Future changes in atmospheric rivers and extreme precipitation in Norway. Clim. Dynam. 54 (3), 2071–2084. https://doi.org/10.1007/s00382-019-05099-z.
Xu, X., Frey, S.K., Boluwade, A., Erler, A.R., Khader, O., Lapen, D.R., Sudicky, E., 2019. Evaluation of variability among different precipitation products in the Northern Great Plains. J. Hydrol.: Reg. Stud. 24 (May), 100608 https://doi.org/10.1016/j.ejrh.2019.100608.
Zhang, W., Villarini, G., Wehner, M., 2019. Contrasting the responses of extreme precipitation to changes in surface air and dew point temperatures. Climatic Change 154 (1), 257–271. https://doi.org/10.1007/s10584-019-02415-8.
Zhu, Y., Newell, R.E., 1998. A proposed algorithm for moisture fluxes from atmospheric rivers. Mon. Weather Rev. 126 (3), 725–735.

4.2 The role of atmospheric rivers in linking atmospheric moisture transport and extreme precipitation

The second article included in this chapter is entitled "**Concurrent extreme events of atmospheric moisture transport and continental precipitation: The role of landfalling atmospheric rivers**" by **Gimeno-Sotelo, L.**, & Gimeno, L., and was published in the journal *Atmospheric Research* in 2022.

Atmospheric Research 278 (2022) 106356

Contents lists available at ScienceDirect

Atmospheric Research

journal homepage: www.elsevier.com/locate/atmosres

Concurrent extreme events of atmospheric moisture transport and continental precipitation: The role of landfalling atmospheric rivers

Luis Gimeno-Sotelo *, Luis Gimeno

Centro de Investigación Mariña, Universidade de Vigo, Environmental Physics Laboratory (EPhysLab), Campus da Auga, 32004, Ourense, Spain

ARTICLE INFO

Keywords:
Extreme precipitation
Moisture transport
Atmospheric rivers
Concurrent extremes
Copulas

ABSTRACT

An analysis of concurrent extreme events of continental precipitation and Integrated Water Vapor Transport (IVT) is crucial to our understanding of the role of the major global mechanisms of atmospheric moisture transport, including that of the landfalling Atmospheric Rivers (ARs) in extratropical regions. For this purpose, gridded data on CPC precipitation and ERA-5 IVT at a spatial resolution of 0.5° were used to analyse these concurrent events, covering the period from Winter 1980/1981 to Autumn 2017. For each season, and for each point with more than 400 non-dry days, several copula models were fitted to model the joint distribution function of the two variables. At each of the analysed points, the best copula model was used to estimate the probability of a concurrent extreme. At the same time, within the sample of observed concurrent extremes, the proportion of days with landfalling ARs was calculated for the whole period and for two 15-year sub-periods, one earlier period and one more recent (warmer) period. Three metrics based on copulas were used to analyse carefully the influence of IVT on extreme precipitation in the main regions of occurrence of AR landfall. The results show that the probability of occurrence of concurrent extremes is strongly conditioned by the dynamic component of the IVT, the wind. The occurrence of landfalling ARs accounts for most of the concurrent extreme days of IVT and continental precipitation, with percentages of concurrent extreme days close to 90% in some seasons in almost all the known regions of maximum occurrence of landfalling ARs, and with percentages greater than 75% downwind of AR landfall regions. This coincidence was lower in tropical regions, and in monsoonal areas in particular, with percentages of less than 50%. With a few exceptions, the role of landfalling ARs as drivers of concurrent extremes of IVT and continental precipitation tends to show a decrease in recent (warmer) periods. For almost all the landfalling AR regions with high or very high probabilities of achieving a concurrent extreme, there is a general trend towards a lower influence of IVT on extreme continental precipitation in recent (warmer) periods.

1. Introduction

Atmospheric moisture transport is the essence of the atmospheric branch of the hydrological cycle, and has crucial importance in precipitation on the continents, in terms of both its average values (Gimeno et al., 2010, 2012, 2020; van der Ent et al., 2010; van der Ent and Savenije, 2013) and its extremes (Vázquez et al., 2020; Liu et al., 2020; De Vries, 2021). Intensifications (or reductions) in transported moisture can result in precipitation anomalies and flooding (or drought) when these are high (or low) (Gimeno et al., 2016; Drumond et al., 2019; Liu et al., 2020). The role of moisture transport is even more important in extreme precipitation. According to a simple approximation, extreme precipitation scales with moisture content and with some indicator of atmospheric instability, being much more sensitive to the former (Emori and Brown, 2005; Nie et al., 2018). Extreme precipitation requires a certain threshold of atmospheric instability, once it is reached the value of extreme precipitation increases as the water vapor content increases (Emori and Brown, 2005; Kunkel et al., 2020). From the amount of water vapor in an air column at a given time, it is not possible to know how much water vapor is involved in precipitation, the water vapor in the column is changing, it is necessary to know how much water vapor transported from the surrounding areas converges in the column. In fact, for actual extreme precipitation events, the amount of precipitation is much greater than the highest amount of moisture measured in the air column at a given time, indicating that, depending on the time scale taken to define the water vapor content, the convergence of water vapor

* Corresponding author.
E-mail address: luis.gimeno-sotelo@uvigo.es (L. Gimeno-Sotelo).

https://doi.org/10.1016/j.atmosres.2022.106356
Received 4 February 2022; Received in revised form 23 June 2022; Accepted 20 July 2022
Available online 26 July 2022

is the most determining factor in the amount of moisture that will result in precipitation (Benton and Estoque, 1954; Mo et al., 2021). Large moisture transports do not guarantee large moisture convergence. If a large amount of moisture is transported into an air column from one side and the same amount is removed out of the column from the other side, then the net contribution of this moisture transport to precipitation is zero. On the other hand, if the amount of moisture being transported into the air column is larger than the amount being transported out of the column, then we have a net contribution of the moisture transport to the precipitation. In other words, moisture transport influences extreme precipitation when converges, which can be caused by multiple mechanisms, meteorologically as complex as convergence associated with baroclinic developments or as simple as that resulting from orographic forcing. As a large moisture transport will not always imply extreme precipitation, it is of obvious interest to know where and when this occurs. The relationship between moisture transport, moisture content, and extreme precipitation must therefore be intense and of great importance, not just in hydro-meteorological terms, but also in terms of climate change, because the three parameters all scale approximately with temperature following a thermodynamic constraint imposed by the Clausius-Clapeyron equation (Held and Soden, 2006; Bao et al., 2017); specifically, they grow around 6–7% for each degree of increase in atmospheric surface temperature.

If moisture transport is quantified as vertically integrated water vapor transport (IVT), a local measure of the moisture advected horizontally in the atmosphere, the simultaneous occurrence of extreme IVT and extreme precipitation must be spatially and temporally diverse throughout the world because most of the moisture is transported via two major mechanisms of atmospheric moisture transport, Low Level Jets (LLJs) in tropical and subtropical regions and Atmospheric Rivers (ARs) in subtropical and extratropical areas (Gimeno et al., 2016). The first of these structures, LLJs, have semi-permanent positions with well defined but distant moisture sources, regions of IVT maxima, and moisture sinks, where the precipitation associated with the system is the highest (Algarra et al., 2019). The distance between areas of strong IVT and precipitation associated with LLJs means that the influence that IVT should have on extreme precipitation (at grid scale) may not be that strong. This problem of distance is not seen in the other major mechanism of moisture transport, ARs, which are non-permanent narrow and long corridors of moisture in the atmosphere (Zhu and Newell, 1994; Gimeno et al., 2014; Ralph et al., 2018). ARs are generally, though not always, associated with extratropical cyclones (Gimeno et al., 2021), and are characterized and even frequently defined by high values of IVT (Neiman et al., 2008). They are closely related to heavy precipitation associated mainly with baroclinic development and orographic forcing (Ralph et al., 2006; Ralph and Dettinger, 2011; Ralph et al., 2016; Tan et al., 2021; Dettinger et al., 2015; Gimeno et al., 2014; Mukherjee and Mishra, 2021a). Landfalling AR occurrence shows intraseasonal variations and preferential areas of occurrence (Guan and Waliser, 2015; Algarra et al., 2020), therefore in the areas and preferred seasons of landfalling AR occurrence, a very high occurrence of concurrent extremes of IVT and continental precipitation may be expected. In this context, the analysis of those concurrent extremes is of crucial importance in understanding the role of the landfalling ARs as a major mechanism behind continental precipitation extremes.

The analysis of concurrent extremes, defined as the simultaneous occurrence of extreme values of at least two variables, is a topic of recent and intense interest. Most studies have focused on variables whose extreme joint occurrence is linked with natural hazards, such as storm surges and heavy precipitation (e.g. Wahl et al., 2015; Bevacqua et al., 2019), droughts and heatwaves (e.g. Mazdiyasni and AghaKouchak, 2015) or precipitation and extreme wind (e.g. Martius et al., 2016; Zscheischler et al., 2021). A more meteorological derivation of these phenomena implies an understanding of the role of specific meteorological systems in the genesis of these concurrent extremes, hence the existence of various studies of the relationship between concurrent wind and precipitation and extratropical cyclones (e.g. Owen et al., 2021 for Europe or Messmer and Simmonds, 2021 at a global scale), with fronts only or with combined cyclones and fronts (Catto and Dowdy, 2021). The present study is set against this conceptual background of concurrent extremes.

In our present investigation we will make use of copulas in order to model the joint distribution function of IVT and continental precipitation. This is very common in environmental research (see e.g., Cong and Brady, 2012; Reddy and Ganguli, 2012; Zscheischler and Seneviratne, 2017; Lazoglou and Anagnostopoulou, 2019). Our analysis is carried out at each point on a global grid, separately for each season. At each analysed point, the best copula model is used to estimate the probability of a concurrent extreme of the two variables. Furthermore, within the sample of observed concurrent extremes, the proportion of days with landfalling ARs is also calculated. For those regions with the highest occurrence of landfalling ARs, we also use copula models to estimate the conditional probability of achieving an extreme precipitation event for a given value of IVT, and the IVT value for a given conditional probability of extreme precipitation.

The aim of the present study is to gain an insight of the role of landfalling ARs in the occurrence of concurrent extreme events of atmospheric moisture transport and continental precipitation. One previous study is relevant and merits special attention. Waliser and Guan (2017) estimated the impact of ARs on extremes of 10-m wind and precipitation and found, among other results of note, that ARs are associated with about 50% of concurrent extremes across most mid-latitude regions. IVT is the variable we use to compute moisture transport, and while this depends on wind it also depends on moisture, and furthermore it is computed for the whole vertical column and not just at 10 m. There are many other differences between our study and that of Waliser and Guan (2017), both methodological (e.g., our use of copulas to deal with concurrent extremes) and conceptual (e.g., we focus on the role of the extremes of IVT, which provide high values of moisture content and are thus related to extreme precipitation). Their results are nevertheless of great interest in comparison with ours.

2. Data

2.1. IVT and precipitation

We obtained daily IVT and precipitation data at a spatial resolution of 0.5° for the period 1981–2017. Precipitation data were obtained from the Climate Prediction Center Global Unified Gauge-Based Analysis (CPC) (Xie et al., 2007). CPC is a gauge-based product, which assimilates daily reports from more than 30,000 stations, and uses an optimal interpolation algorithm that accounts for orography. CPC is well known to have the advantage of a high station density with any limitations in the gauge network density, which is poor over tropical Africa and Antarctica. IVT, as defined in (1), was calculated from data obtained from the European Centre for Medium-Range Weather Forecasts Reanalysis ERA-5 (Hersbach et al., 2020), where q is the specific humidity, $\mathbf{U}$ is the horizontal wind field, and Ω refers to the integration over the whole tropospheric column. Daily values of IVT were obtained by computing the daily mean of all hourly values between 0:00 UTC and 23:00 UTC of the corresponding date.

$$IVT = \frac{1}{g}\left|\left(\int_{\Omega} q\mathbf{U}dp\right)\right| \tag{1}$$

The CPC data set was based on station reports plus interpolation, and has an important advantage compared with the use of precipitation obtained directly from ERA-5 reanalysis. Because our aim is to study the simultaneous occurrence of extremes of IVT and precipitation, and the former is calculated from the reanalysis, the use of precipitation data also obtained from the reanalysis could result in a concurrent extreme due partly to the use of the same model to construct the reanalysis.

However, the CPC daily precipitation database has the disadvantage that different countries have different EOD (End of Day) hours. The selection of ERA-5 to calculate IVT rather than any other reanalysis is because of the well-known reliability of the reanalysis produced by the European Centre for Medium-Range Weather Forecasts for hydrological applications (e.g., Xu et al., 2019; Tarek et al., 2020). Fig. 1 shows the total number of days with nonzero precipitation at each grid point for December–January-February (top) and June–July-August (bottom) and Fig. S1 for intermediate seasons (March–April-June and September–October-November). The annual precipitation frequency map (not shown) visually compares well with previous analogous maps by Sun et al. (2006), their Fig. 1) and Beck et al. (2019), their Fig. 8a).

2.2. Occurrence of landfalling ARs

The daily occurrence of landfalling ARs for each continental 0.5° grid point for the period 1981–2017 was estimated from the AR database developed by Guan and Waliser (2015). This database applies thresholds of IVT intensity and geometric conditions to ERA-Interim reanalysis data (Dee et al., 2011) to identify the locations of ARs at a global scale. Its time resolution is 6 h time step (00:00; 06:00; 12:00; and 18:00 UTC), and if at any of the 4 times along the day the AR was detected, that day was considered as an AR day. Because the spatial resolution of this database is 1.5°, all the 0.5° grid-points included in any 1.5° grid-point considered as an AR were also considered in the same way. Fig. 2 shows the total number of occurrences of landfalling ARs at each grid point for December–January-February (top) and June–July-August (bottom), and Fig. S2 shows the same data for intermediate seasons March–April-June and September–October-November. The plots show the known occurrence of landfalling ARs, with maxima in the extratropical North Atlantic/Pacific, southeastern Pacific, and South Atlantic, and the most frequent landfalling ARs along the west coasts of Europe, North America, and southern South America (Guan and Waliser, 2015; Algarra et al., 2020).

3. Methods

As specified in Section 1, the statistical analysis in this study is based on **copula theory**. A comprehensive description of this theory is given in Nelsen (2006), Joe (2014) and Shemyakin and Kniazev (2017). We now

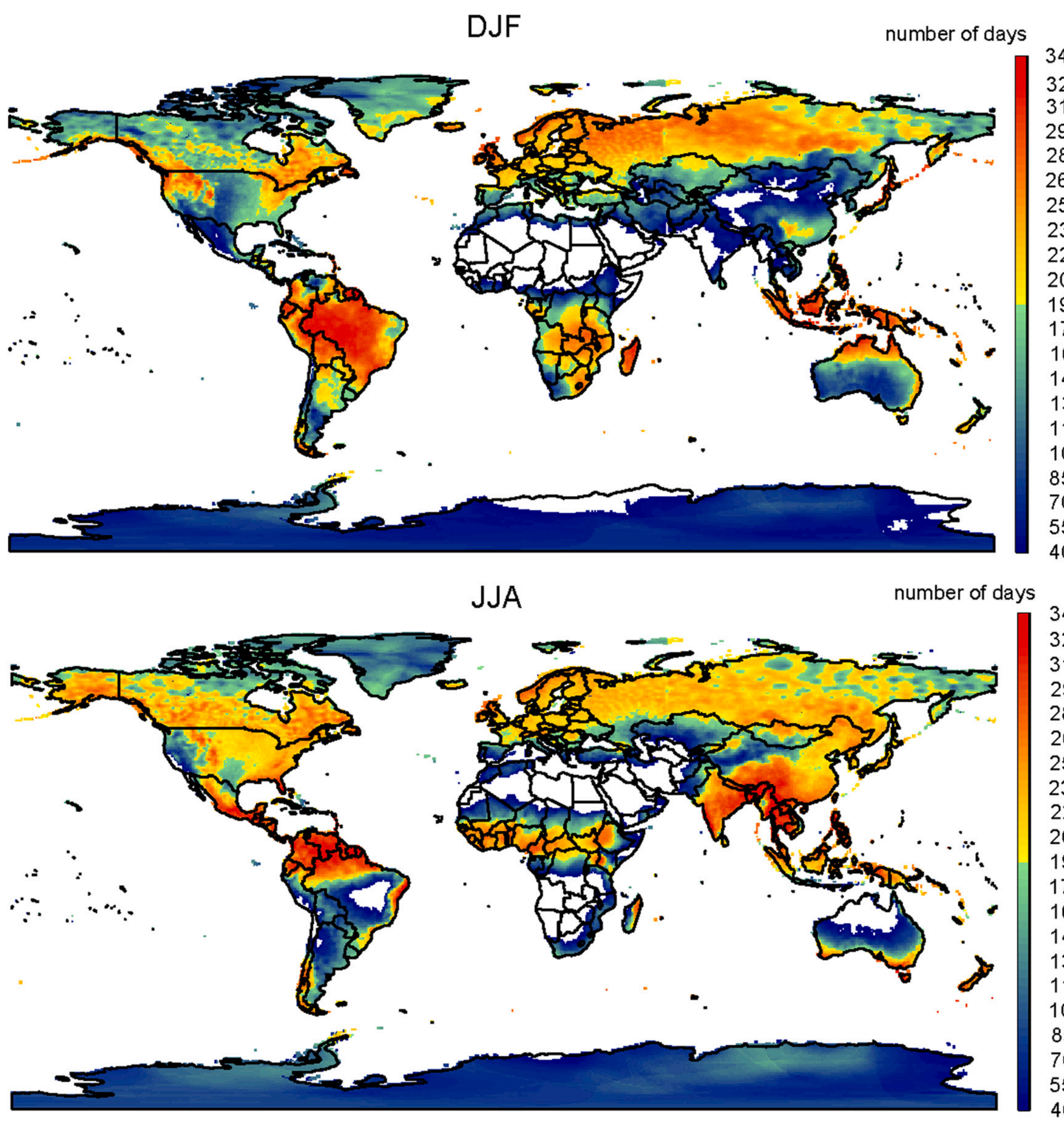

Fig. 1. Total number of days for the period 1981–2017 with nonzero precipitation at each grid point for December–January-February (top) and June–July-August (bottom).

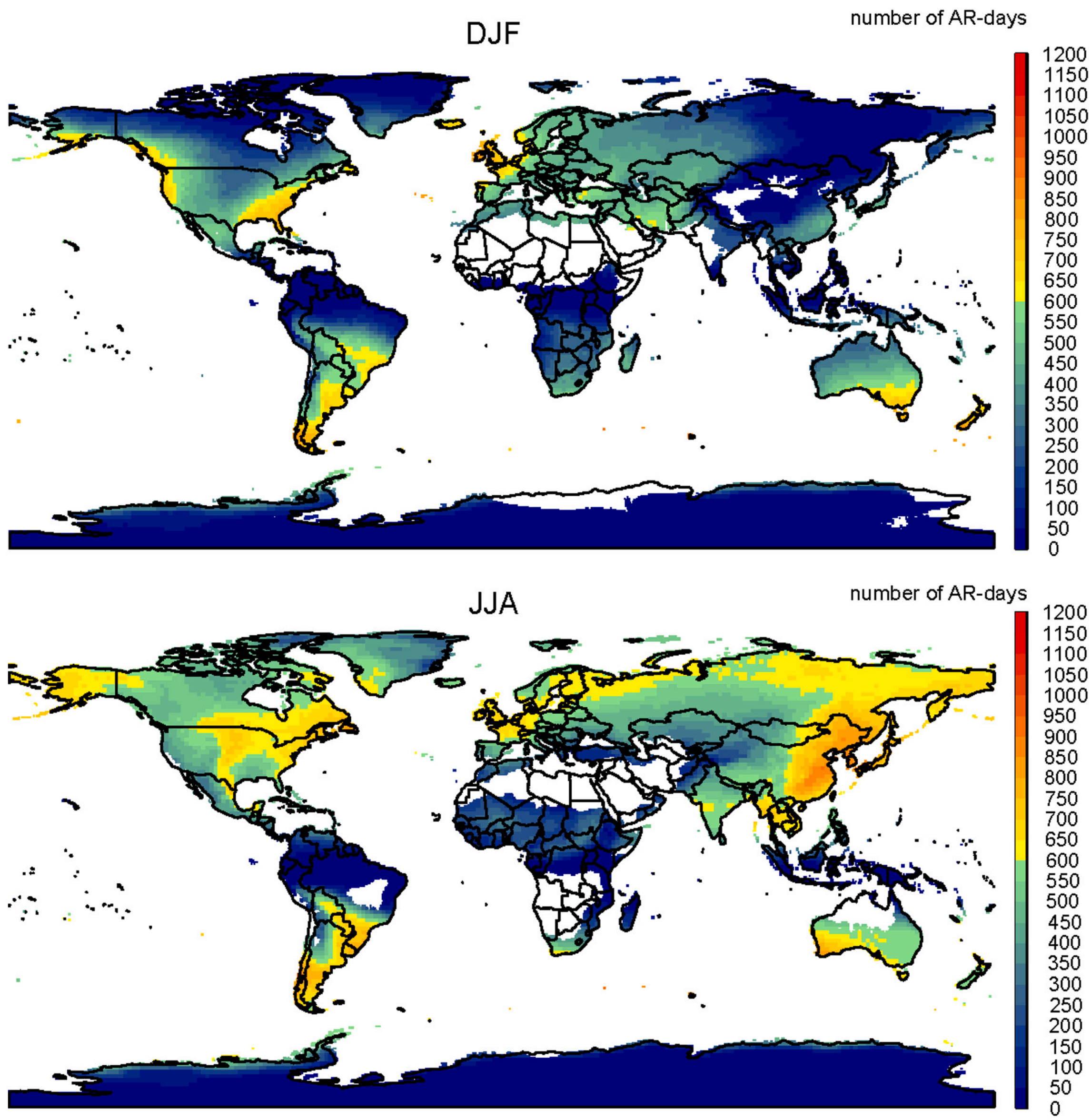

Fig. 2. Number of days of occurrence of landfalling ARs for the period 1981–2017 at each grid point, for December–January-February (top) and June–July-August (bottom).

present a brief summary of some of the most pertinent aspects.

3.1. The concept of copula

Let (U, V) be a random pair with U and V following a uniform distribution with a mean of 0 and a standard deviation of 1. A copula C is its joint distribution function, i.e.:

$$C(u,v) = P(U \leq u, V \leq v), \quad u, v \in (0,1). \tag{2}$$

For two continuous variables X and Y with arbitrary distribution functions F and G respectively, the joint distribution function of (X, Y), denoted by H, can be written as a function of a copula and the marginal distributions, according to **Sklar's Theorem** (Sklar (1959)):

$$H(x,y) = P(X \leq x, Y \leq y) = C(F(x), G(y)), \quad x, y \in \mathbb{R} \tag{3}$$

In our case F and G will be estimated non-parametrically (the corresponding empirical distribution functions will be used), therefore the choice of an appropriate model for the copula C results directly in a model for the joint distribution H.

Copula models. The copula models used here belong to the Elliptical and Archimedean families.

Regarding **Elliptical** copulas, Gaussian and Student-*t* types will be used:

- *Gaussian copula*:

$$C(u,v;\rho) = \Phi_\rho\left(\Phi^{-1}(u), \Phi^{-1}(v)\right), \quad u, v \in (0,1), \tag{4}$$

where $\Phi^{-1}(.)$ is the inverse of the distribution function of a standard normal distribution and $\Phi_\rho(.,.)$ is the joint distribution function of a standard bivariate normal distribution with Pearson's linear correlation coefficient ρ.

- *Student-t copula*:

$$C(u,v;\eta,\rho) = T_{\eta\rho}\left(T_\eta^{-1}(u), T_\eta^{-1}(v)\right), \quad u, v \in (0,1), \tag{5}$$

where $T_\eta^{-1}(.)$ is the inverse of the distribution function of the Student-*t* distribution with η degrees of freedom and $T_{\eta\rho}(.,.)$ is the joint distribution function of a bivariate Student-*t* distribution with η degrees of freedom and Pearson's linear correlation coefficient ρ.

With respect to the **Archimedian** copulas used in this article, Table 1 lists the expressions of the models.

The *independence copula* will also be used:

$$C(u,v) = uv, \quad u,v \in (0,1). \tag{6}$$

3.2. Using copulas to study concurrent extremes

Let $U = F(X)$ and $V = G(Y)$ be the uniform-transformed random variables and (u,v) the bivariate threshold (on the uniform scale). In order to analyse the joint extremal behaviour of the variables in our study, we focus on the probability that both variables exceed the corresponding threshold (see Salvadori and De Michele, 2004):

$$p_{AND} = P(U > u, V > v) = 1 - u - v + C(u,v) \tag{7}$$

We also make use of the conditional probability of one variable exceeding a threshold, given a fixed value of the other variable. This has the following expression (Salvadori and De Michele, 2004):

$$p_{COND} = P(V > v | U = u) = 1 - \frac{\partial}{\partial u} C(u,v) \tag{8}$$

3.3. Parameter estimation

Let us consider an observed sample $((x_1,y_1),\dots,(x_n,y_n))$ of the studied pair (X,Y). The question is then of how this information can be used to estimate the parameters of the copula models. There are several methods of estimation (see Joe, 2014; Shemyakin and Kniazev, 2017), and in this article our analysis will be based on the **semi-parametric** approach:

1. Pseudo-observations $\{(\widehat{u}_i,\widehat{v}_i), i = 1,2,\dots,n\}$ are computed, where $\widehat{u}_i := \frac{n}{n+1}\widehat{F}(x_i)$ and $\widehat{v}_i := \frac{n}{n+1}\widehat{G}(y_i)$, with $\widehat{F}$ and $\widehat{G}$ being the empirical distribution functions of X and Y, respectively.
2. The resulting estimator, the Maximum Pseudo-Likelihood Estimator (MPLE), can be calculated as follows: $\widehat{\boldsymbol{\theta}} = \mathrm{argmax}\sum_{i=1}^{n} log(c(\widehat{u}_i\widehat{v}_i)\,|\boldsymbol{\theta})$, where $\boldsymbol{\theta}$ is the parameter vector of the copula model and $c(.,.)$ is the copula density function, defined as $c(u,v) = \frac{\partial^2 C}{\partial u \partial v} = \frac{\partial^2 C}{\partial v \partial u}, \quad u,v \in (0,1)$.

3.4. Copulas with precipitation data

As in this study precipitation data is used, it is important to take into account that, before fitting the copula, a relevant pretreatment is convenient. Precipitation is a variable that contains a large number of zero values, and those values have the same rank (there are ties in the data). As stated in the review by Tootoonchi et al. (2022), ties can cause bias in the copula, and there are different ways of dealing with this problem. Among others, one way is removing from the sample those zero values. That is the option that was chosen in this article, as those zero values are not interesting at all in this study because the focus is on the concurrent extremes. Therefore, in this article, the sample of (IVT, precipitation) always refers to the days of nonzero precipitation. However, the quantile-based thresholds for the variables were calculated including the days of zero precipitation because zeros are also observed values, and it was decided to use them for that purpose.

Table 1
Archimedian copulas used in this article.

Model	C(*u*,*v*)	$\alpha\in$
Frank	$-\frac{1}{\alpha}log\left(\frac{1-e^{-\alpha}-(1-e^{-\alpha u})(1-e^{-\alpha v})}{1-e^{-\alpha}}\right)$	$\mathbb{R}\backslash\{0\}$
Gumbel	$\exp[-\{(-\log(u))^{\alpha}+(-\log(v))^{\alpha}\}^{1/\alpha}]$	$[1,\infty)$
Clayton	$\max\{(u^{-\alpha}+v^{-\alpha}-1)^{-1/\alpha},0\}$	$[-1,\infty)\backslash\{0\}$
Joe	$1-[(1-u)^{\alpha}+(1-v)^{\alpha}-(1-u)^{\alpha}(1-v)^{\alpha}]^{\frac{1}{\alpha}}$	$[1,\infty)$

4. Results and discussion

4.1. Worldwide analysis of concurrent extremes

The simplest way of defining concurrent extremes of two variables (in our case IVT and continental precipitation) involves counting the number of days on which a quantile-based threshold for the two variables is exceeded, in our case this is the 90th percentile (Fig. 3 for December–January-February (top) and June–July-August (bottom) and supplementary Fig. S3 for intermediate seasons). The general distribution of number of concurrent extremes seems to show that it is highly conditioned by the dynamic component of the IVT, the wind (Martius et al., 2016), and the orientation of coasts and mountain ranges versus the atmospheric general flux. Values are low in the deep tropics, where precipitation is mainly convective, and not favoured by strong horizontal winds and moisture transport. The number of concurrent extremes shows an increase in extratropical regions, reaching higher values along the coast of the continents, mainly on the windward side of North-South oriented mountain ranges due to orographic forcing. Precipitation over these regions is derived mainly from extratropical cyclones, characterized simultaneously by high winds, and therefore strong moisture transport, and precipitation (Messmer and Simmonds, 2021). Baroclinic activity is more intense during winter, and consequently the number of concurrent extremes is higher in extratropical regions in the corresponding winter than in summer. This general pattern is disturbed regionally by the action of meteorological structures associated with strong moisture transport, in which high humidity is combined with low-level wind. Examples of this are the high values of concurrent extremes in the NE Brazilian region in JJA affected by Low-Level Jet (LLJ) systems (Braz et al., 2021), or the moderate values in the SE of North America in JJA affected by tropical cyclones (Liu et al., 2021). To sum up, maxima of concurrence of extremes are found on extratropical continental coasts during winter, mostly affected by ARs with regional fingerprints of other major mechanisms of atmospheric moisture transport such as LLJs or tropical cyclones and the orographic forcing by large mountain barriers. The absolute number of concurrent extremes is in part dependent on the number of precipitation days (Fig. 1 and S1) because IVT occurs every day, so the presence of low values in the tropics, where the number of precipitation days is very high, implies a very low extremal dependence. For extratropical latitudes over the Northern Hemisphere with many precipitation days, a very high number of concurrent extremes may not mean that the extremal dependence is so high.

At this point, it is interesting to know the geographical distribution of the values of the 90th percentiles of IVT and continental precipitation.

Fig. 4 shows the 90th percentile values of IVT ($q90_{IVT}$) for December–January-February (top) and June–July-August (bottom) (values for intermediate seasons are shown in Fig. S4). The global distribution reveals low values over the polar regions and areas with high topography, and high values over tropical and extratropical coasts dominated by tropical easterlies and storm tracks. A more detailed inspection of the regions of maximum occurrence reveals that these regions coincide with the main areas of occurrence of landfalling ARs, such as the Californian or Western European coasts and the main LLJ systems, as clearly seen in the Great Plains in North America or along the Andes in South America (Gimeno et al., 2016; De Vries, 2021). However, and as expected, the absolute maxima are linked to the Asian monsoon in the wet season (JJA). It is also clear that in extratropical regions in the Northern Hemisphere, extreme values of IVT are lower for the Pacific than for the Atlantic coasts, with a clear contrast between the American Pacific coast and the American and European Atlantic coasts, which are three of the most important regions of occurrence of landfalling ARs. This is the case for both summer and winter. In the Southern Hemisphere, higher extreme values of IVT occur on the Australian coasts than on the South

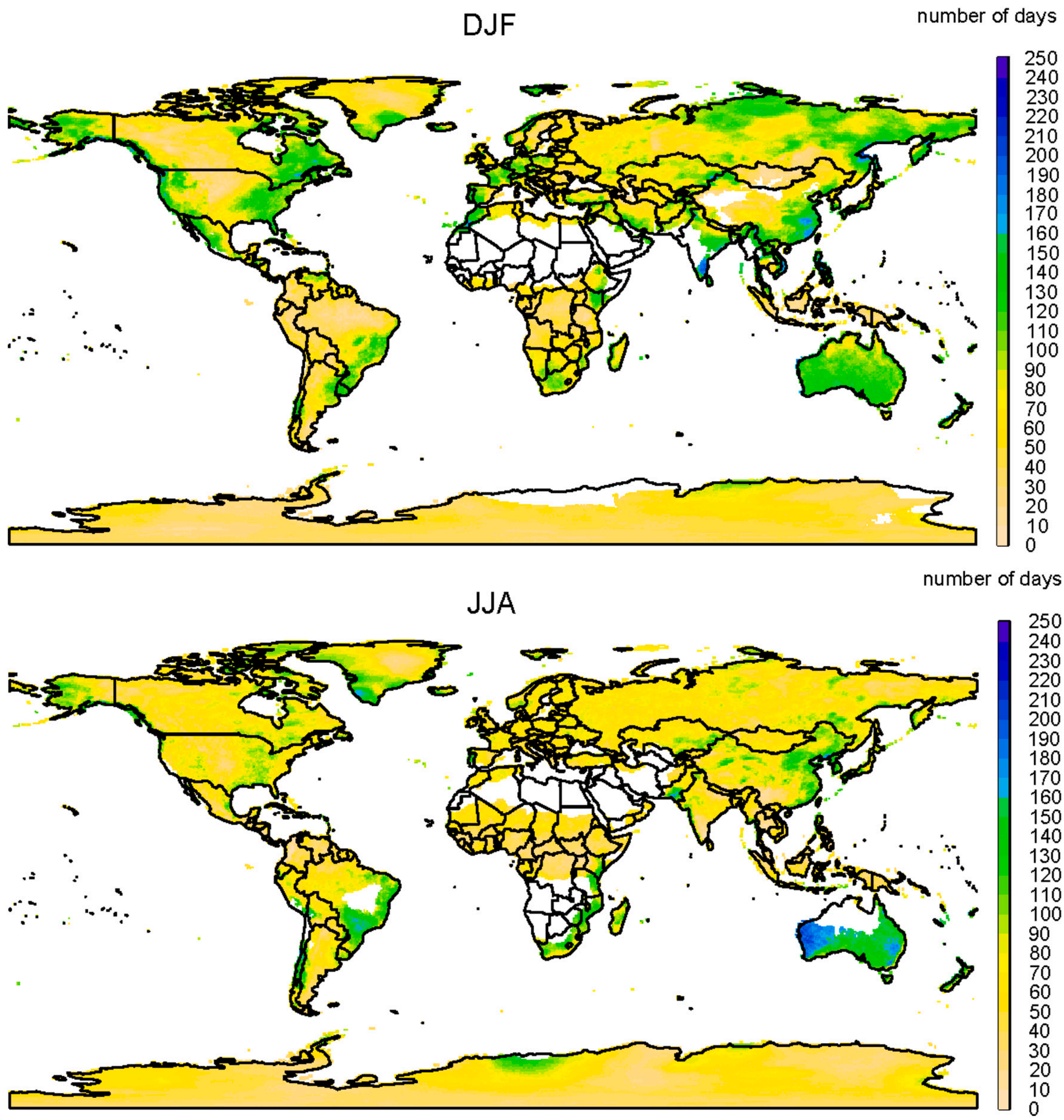

Fig. 3. Number of days exceeding the bivariate threshold ($q90_{IVT}$, $q90_{prec}$) for December–January-February (top) and June–July-August (bottom) for the period 1981–2017. The quantiles were calculated including the days of zero precipitation.

African or Chilean coasts, even though all three are at similar latitudes.

Fig. 5 shows the 90th percentile of daily continental precipitation ($q90_{prec}$) for December–January-February (top) and June–July-August (bottom) (intermediate seasons are shown in Fig. S5). The annual distribution of $q90_{prec}$ (not shown) is visually comparable with previous equivalent maps by Dietzsch et al. (Dietzsch et al., 2017, their Fig. 5c and d) and Beck et al. (Beck et al., 2019, their Fig. 7a). In general, the pattern is quite similar to annual mean precipitation, with maximum values along the Intertropical Convergence Zone (ITCZ), varying seasonally with its movement, and over monsoonal regions during the wet season. Secondary maxima occur in regions of extra-tropical cyclone tracks on North-west American or European west coasts during the boreal winter or on the coasts of New Zealand and Chile during the austral winter. Areas of occurrence of other meteorological systems that produce extreme precipitation events are also identified as local maxima in Fig. 5, such as areas of occurrence of tropical cyclones (e.g., on the North American east coast during boreal summer) or Mesoscale Convective Systems (e.g., the Plata river basins during the austral winter). The large area of high $q90_{prec}$ over the Amazon region is in part due to high values over the region but is also partly due to the limited number of precipitation gauges, implying a loss of variance due to the effects of interpolation (Haberlandt, 2007).

The spatial distribution of concurrent extremes shown in Fig. 3 is related partly to the local number of precipitation days, so it is convenient to estimate the probability of achieving a concurrent extreme of IVT and continental precipitation.

The copula models presented in Section 3 were fitted to the IVT and precipitation data introduced in Section 2, for the sample of nonzero precipitation days. That is, for each season (December-January-February, March-April-May, June-July-August, September-October-November), we fitted for each grid point with more than 400 days of nonzero precipitation the following copula models to the pair (IVT, precipitation): a Gaussian, a Student-*t*, a Frank, a Gumbel, a Clayton, a Joe and an independence copula. We chose to consider only those grid points because a sample size of more than 400 bivariate observations allowed us to work comfortably with copulas. For the parameter estimation, we used the semi-parametric approach explained in Section 3. Among those copula models that were fitted, only the best one according

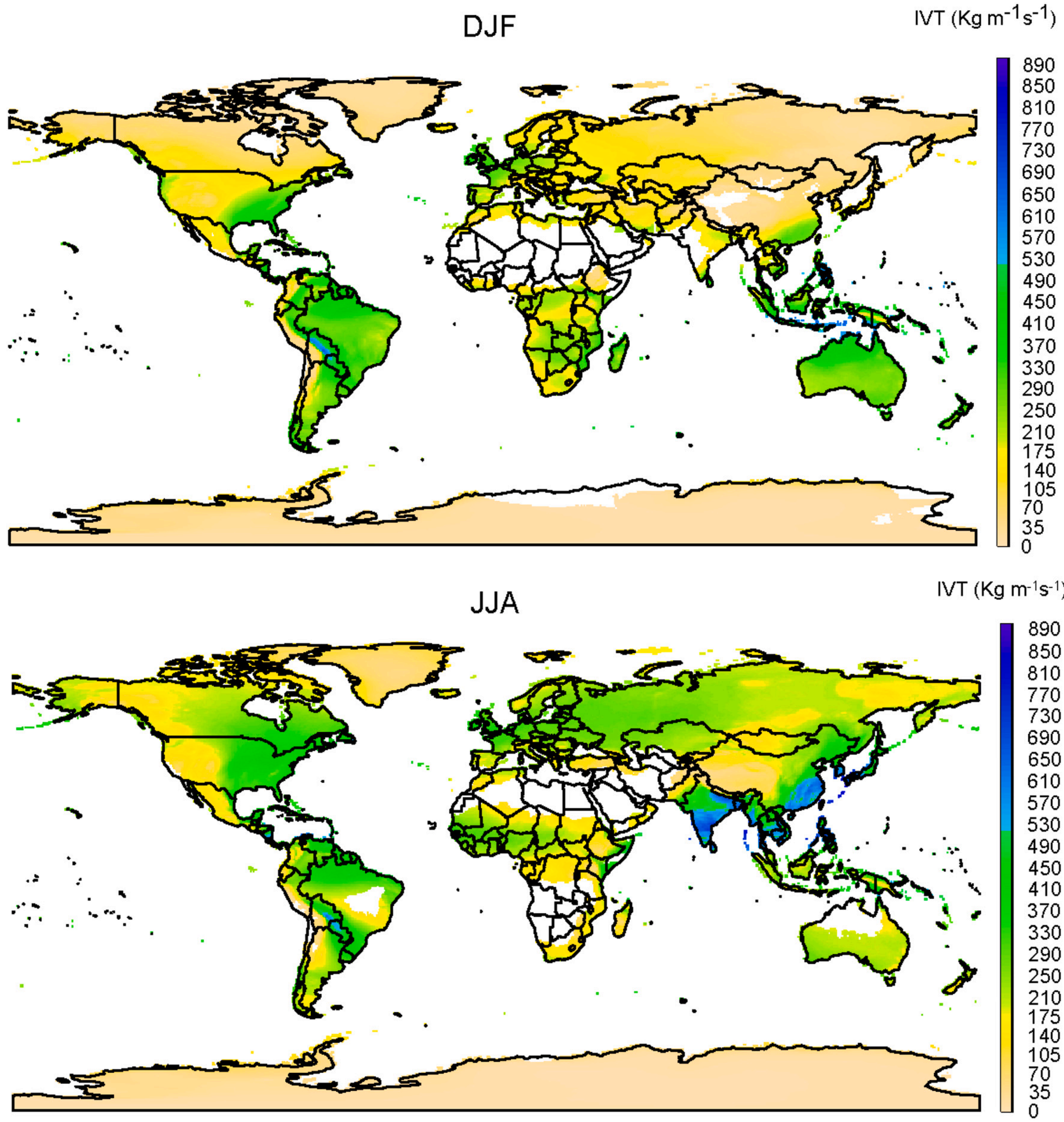

Fig. 4. 90th percentile of IVT for December–January-February (top) and June–July-August (bottom) for the period 1981–2017. It was calculated including the days of zero precipitation.

to the AIC (Akaike, 1974) was considered for our analysis (the one with the lowest AIC value). In Fig. S9 it is possible to see the best fitted copula model for the pair (IVT,precipitation) at each grid point for each season.

In Fig. 6 we show the estimated probability of concurrent extremes computed according to (7) using the copula model with the lowest AIC value for each grid point, for December-January-February and June-July-August (the results for intermediate seasons can be found in Fig. S6). With the exception of regions of occurrence of landfalling ARs, monsoonal areas, and regions influenced by LLJs, the estimated probability of joint extremes is less than 4%. The general distribution of maxima of estimated probability resembles the number of concurrent extremes, but there are some differences linked mostly to the number of precipitation days. Therefore, maxima of around 40% of probability are shown in monsoonal areas during the dry season. This effect is particularly visible in DJF for the Asian and North American monsoonal regions, and in JJA for the Australian and South America monsoonal regions, although it is also visible with a lower intensity for the African monsoonal regions. Another effect of accounting for the number of days of precipitation is observed in the north-south gradient of probability in regions of occurrence of landfalling ARs. Thus, for DJF on the Atlantic-European-North African coasts there is a decrease in probability from values of the order of 25% on the Moroccan coasts to 4% on the Scandinavian ones. A similar decrease is seen on the American Pacific coast from California to Northern Canada. Maxima of probability are again evident in polar regions of landfalling ARs, with values higher than 25% in the Antarctica in JJA and somewhat lower, of the order of 8%, in Alaska and Kamchatka in DJF.

A joint analysis of Figs. 3 and 6, which account for the concurrent extremes and their probability, and Figs. 4 and 5, which account for the thresholds of IVT and precipitation used to define their extremes, reveals regions with very high values of both IVT and precipitation, where the probability of occurrence of concurrent extremes is very low, such as the ITCZ or monsoonal regions in the wet season. On the other hand, there are regions with a high probability of concurrent extremes but with low values of IVT and precipitation, such as the polar regions or the monsoonal regions in the dry season. Moderate-to-high probabilities of occurrence of concurrent extremes accompanied by moderately high values of IVT and precipitation occur mainly in the areas of occurrence

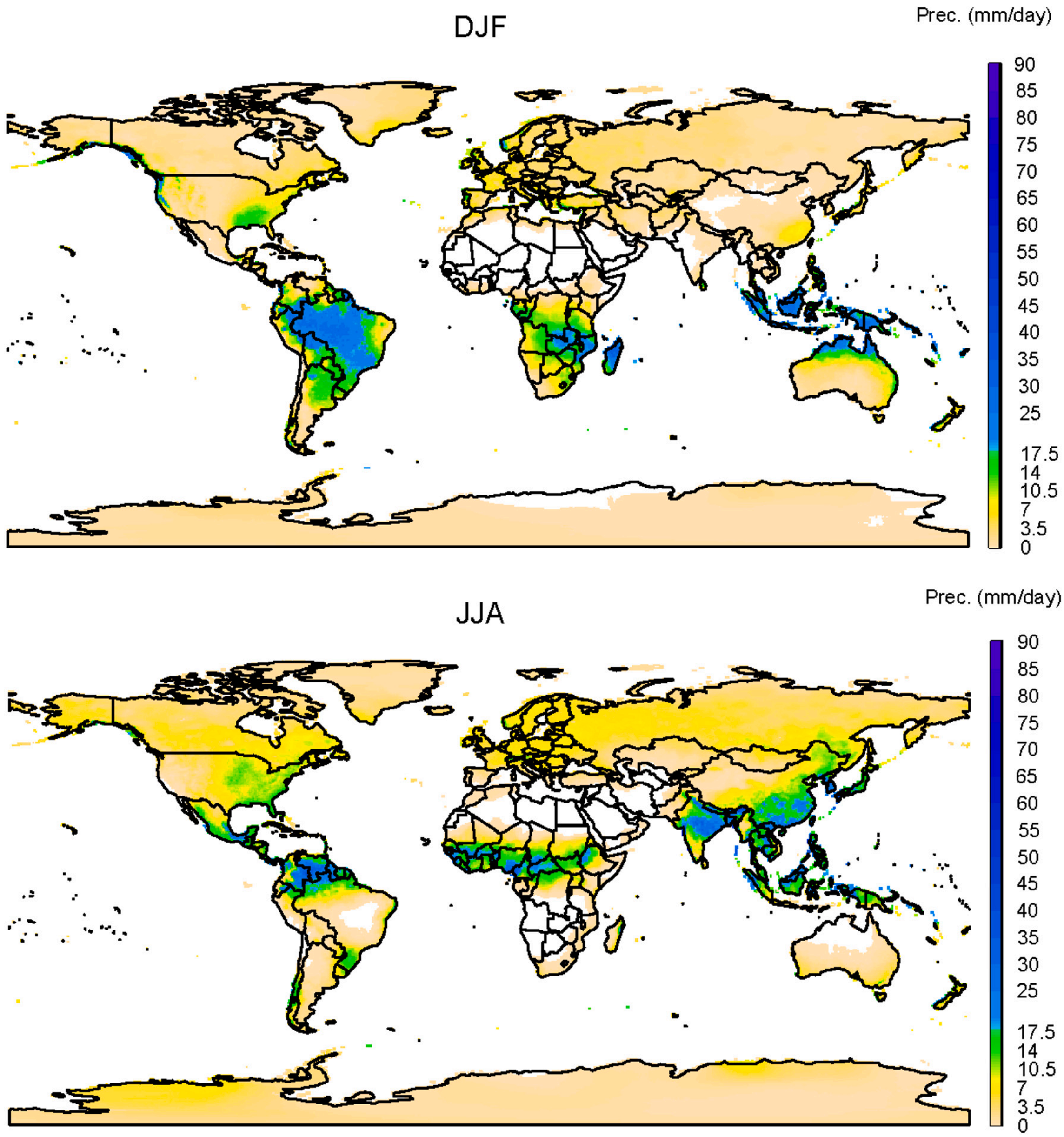

Fig. 5. 90th percentile of continental precipitation for December–January-February (top) and June-July-August (bottom) for the period 1981–2017. It was calculated including the days of zero precipitation.

of landfalling ARs (Fig. 2). We focus on these regions in the next section.

4.2. AR landfalling regions: concurrent extremes and conditional probabilities

Fig. 7 shows the percentage of concurrent extreme days of IVT and continental precipitation that coincide with the occurrence of landfalling ARs, for December–January-February, for the whole period 1981–2017, and for two 15-year sub-periods, an earlier period and a more recent warmer period, in order to investigate the potential effects of recent warming. Fig. 8 and Figs. S7 and S8 are the equivalent to Fig. 7 for June-July-August, March-April-May and September-October-November respectively. In many studies, the period covered by reanalysis has been split in order to study differences between them based on the idea that the period since 2001 has been considerably warmer than the preceding period, 1980–2000 (a detailed justification of this approach with ERA5 data is shown in Mukherjee and Mishra (2021b)). Because the ENSO greatly affects the transport of moisture (Castillo et al., 2014; Kim et al., 2019; Xiong and Ren, 2021), in order to define the two sub-periods we have removed the 6 years of strongest ENSO for each season (the 3 most intense El Niñno and the 3 most intense La Niña according to the Extended Multivariate ENSO Index and available at https://psl.noaa.gov/enso/climaterisks/years/top24enso.html).

Therefore, for **December-January-February**, the *earlier period* corresponds to: 1981, 1982, 1984, 1985, 1986, 1987, 1988, 1990, 1991, 1993, 1994, 1995, 1996, 1997 and 1999; and the *later period* to: 2002, 2003, 2004, 2005, 2006, 2007, 2008, 2009, 2010, 2012, 2013, 2014, 2015, 2016 and 2017.

In the case of **June-July-August**, the *earlier period* refers to: 1981, 1982, 1984, 1985, 1986, 1990, 1991, 1992, 1993, 1994, 1995, 1996, 1998, 1999 and 2000; and the *later period* to: 2002, 2003, 2004, 2005, 2006, 2007, 2008, 2009, 2011, 2012, 2013, 2014, 2015, 2016 and 2017.

Considering the whole period, percentages lower than 50% occur in tropical regions and over the Asian plateaus, and are higher in practically all extratropical and polar regions. Percentages higher than 90%

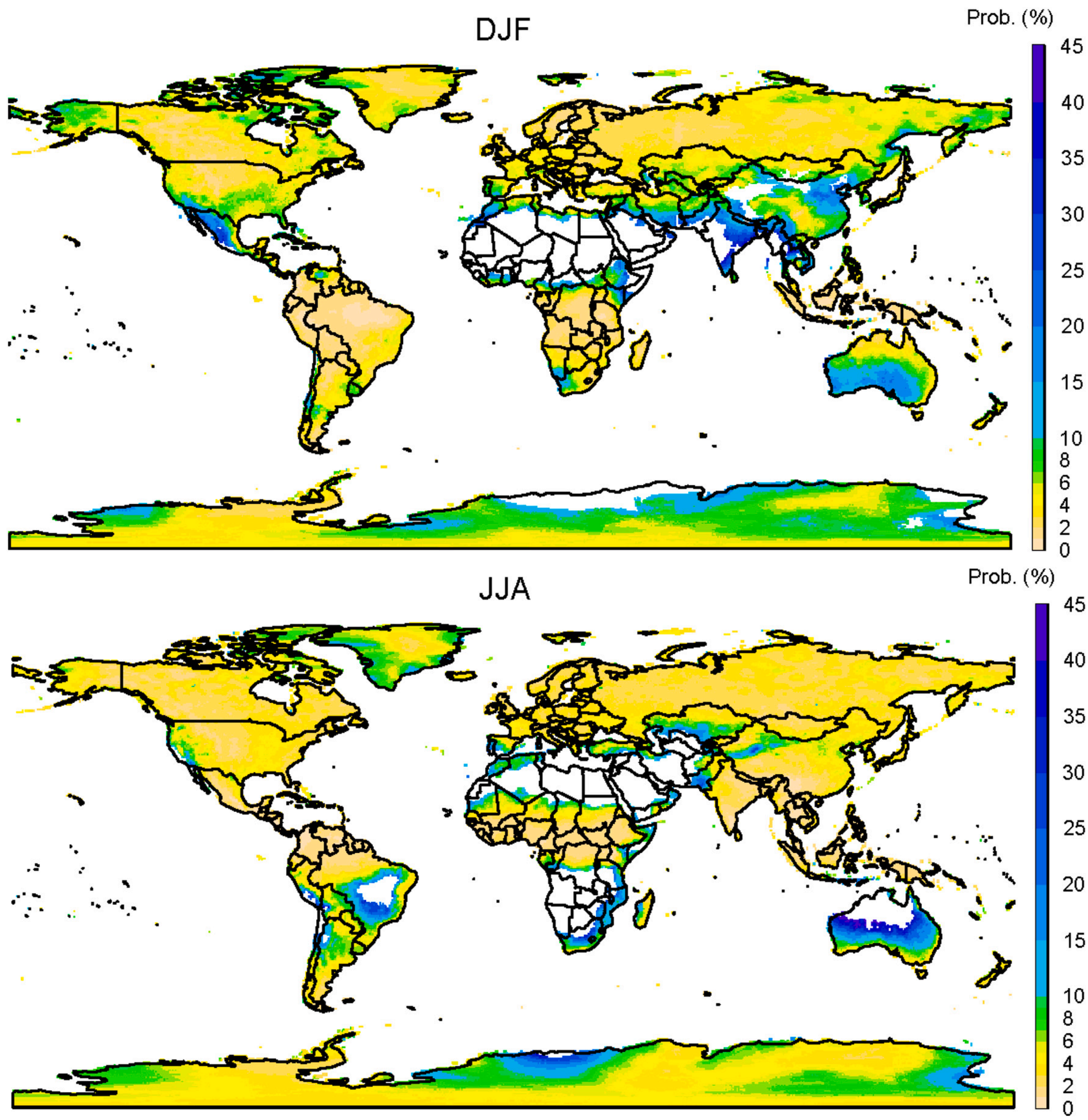

Fig. 6. Estimated probability of achieving a concurrent extreme of IVT and continental precipitation (percent), for December-January-February and June-July-August for the period 1981–2017. It is computed using the copula model with the lowest AIC value for each grid point. The quantile-based thresholds were calculated including the days of zero precipitation.

occur in some seasons of the year in all the known regions of maximum occurrence of landfalling ARs, the North American Pacific, the European Atlantic, the Asian Pacific, the Southern Australian, South African, and South American coasts. Large continental regions downwind of these regions of preferential occurrence of landfalling ARs show percentages greater than 75%, reflecting the effect on inland penetration of ARs (Rutz et al., 2015; Lavers and Villarini, 2015; Nayak and Villarini, 2018; Ralph et al., 2019; Eiras-Barca et al., 2021). There are no percentages higher than 50% in any season in the monsoon regions, where the concurrence between IVT and precipitation is high, showing that in these regions both the definition of ARs and their effects are diffuse (Gimeno et al., 2021). In both hemispheres, the percentage is higher in autumn and winter than in spring and summer, with the exception of the Asian Pacific coasts. There are regions such as Iran where the concurrence of extreme IVT and precipitation is moderate or low but the percentage that coincide with landfalling ARs is high, reaching values close to 90% in spring and winter, and other regions such as the Antarctic around zero longitude where the opposite applies. A comparison with Waliser and Guan (2017), who used the same AR database, shows a high concordance in the regions they found with a high proportion of separate wind extremes and precipitation extremes associated with ARs, although with lower percentages in their study, partially due to their use of a more restrictive 98th percentile as the threshold for defining extremes.

The differences in the percentage of concurrent extreme days of IVT and continental precipitation that coincide with the occurrence of landfalling ARs between the earlier and more recent periods seem to reflect a spatially asymmetric variation. The general trend is towards a decrease in recent (warmer) periods, with a reduction in the percentage over the Pacific and Atlantic North American coasts (which is very marked during winter) and in the Southern Hemisphere regions (also more evident in the austral winter). There is no apparent change for the Pacific Asian coasts, and a slight regional increase on the European Atlantic coasts (e.g., British Isles in winter and the Iberian Peninsula in autumn). Although there could be factors other than warming and the ENSO (partially excluded from this study) that differentiate earlier and later sub-periods; for instance, there was a change in the Atlantic Multidecadal Oscillation (AMO) phase from negative to positive in the mid-

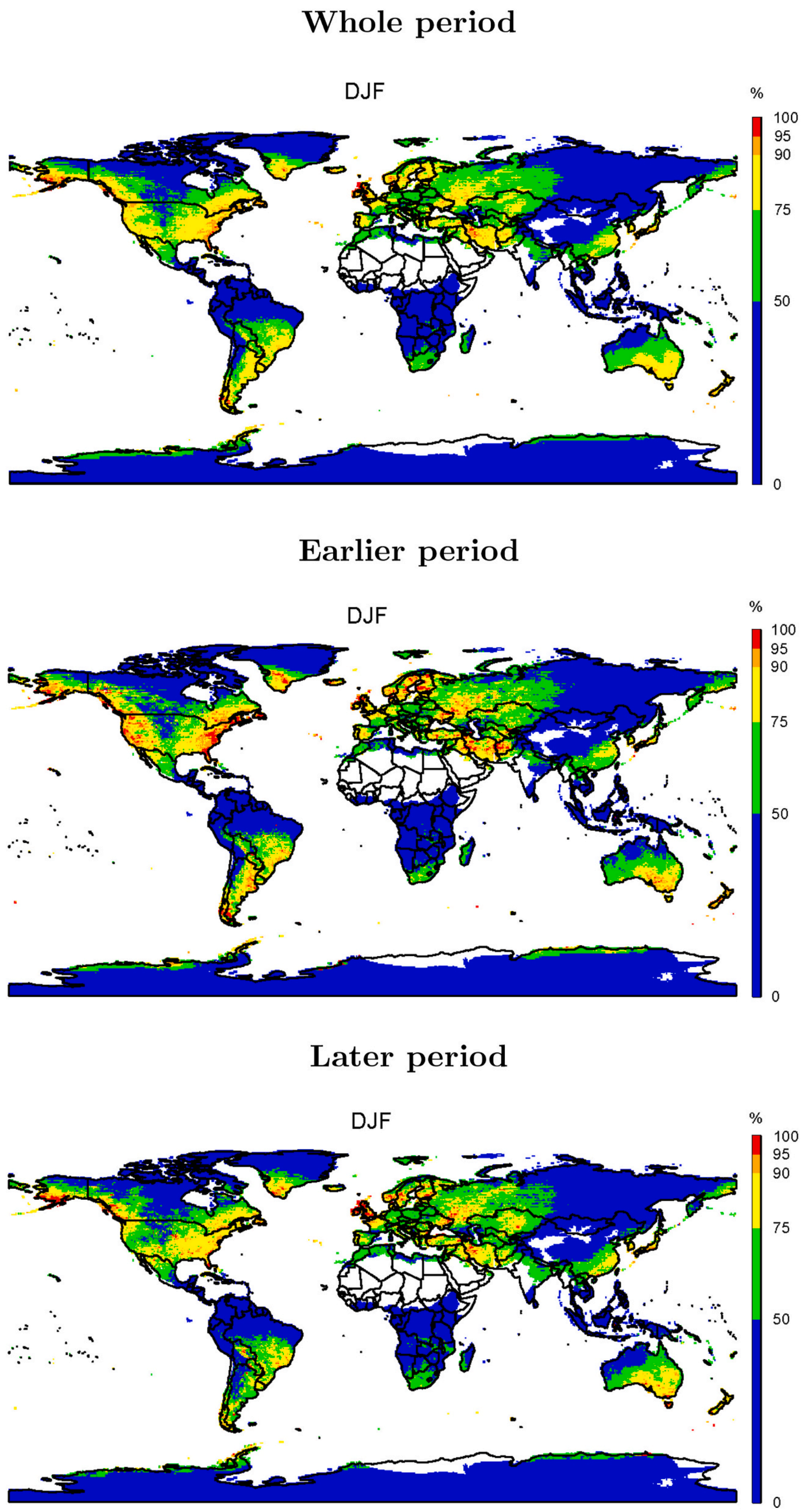

Fig. 7. Percentage of concurrent extreme days of IVT and continental precipitation that coincide with the occurrence of landfalling ARs, for **December-January-February**, for the whole period 1981–2017, and the earlier and later studied periods.

nineties Trenberth et al. (2021) or the phase shift of the Pacific Decadal Oscillation (PDO) at the end of the twentieth century (Li et al., 2020); the results point to a slight reduction with warming of the role of ARs as mechanism behind the concurrent extremes of IVT and continental precipitation. There are some physical factors that support this hypothesis, based on the thermodynamic responses of the hydrological cycle to global warming. Although the number of ARs and the moisture transported by them is predicted by models to increase with warming (Espinoza et al., 2018; Massoud et al., 2019; Payne et al., 2020), the IVT associated with ARs increases in the models at lower rates than the

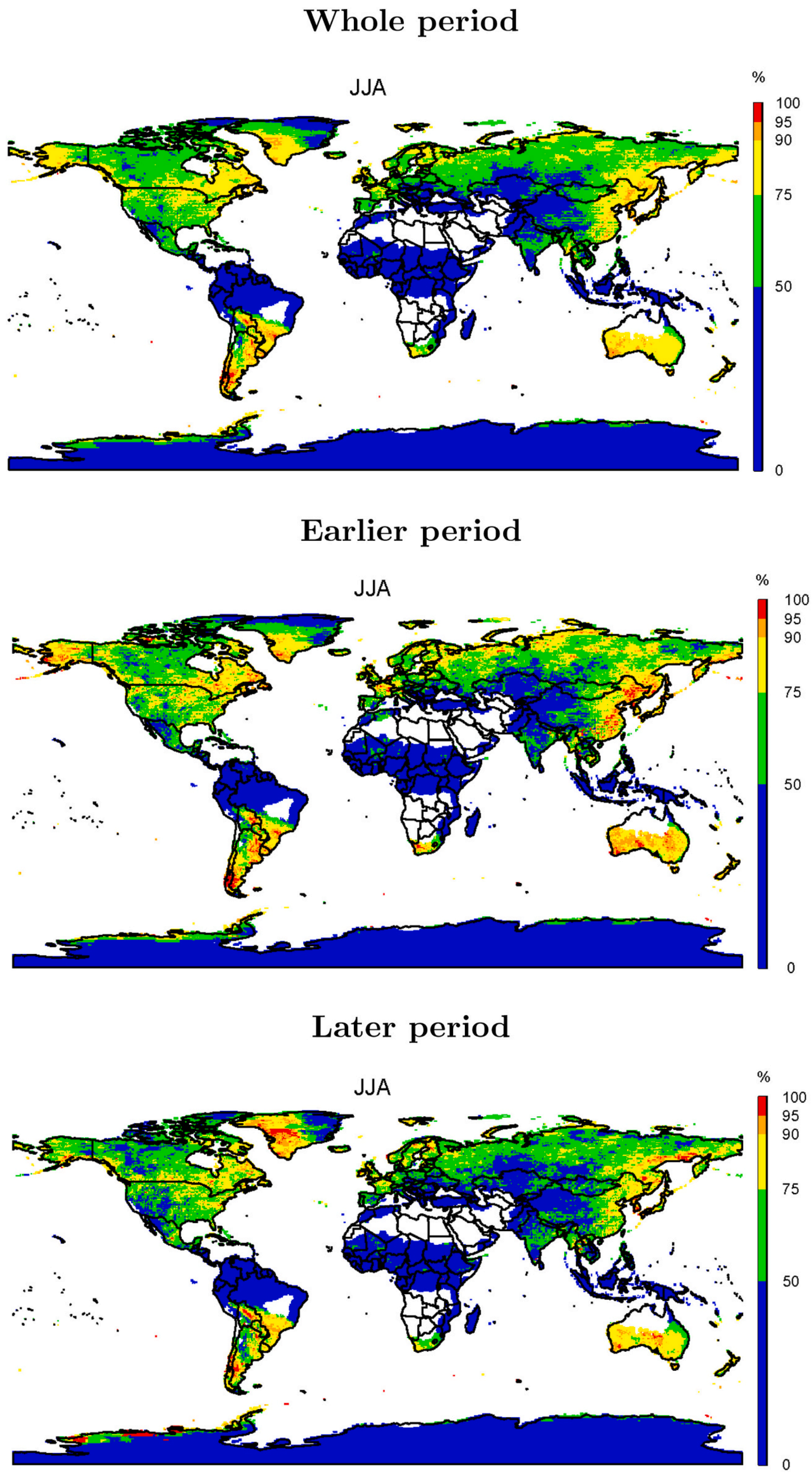

Fig. 8. Percentage of concurrent extreme days of IVT and continental precipitation that coincide with the occurrence of landfalling ARs, for **June-July-August**, for the whole period 1981–2017, and the earlier and later studied periods.

integrated water vapor associated with ARs (McClenny et al., 2020). As extreme precipitation increases with water vapor content (Emori and Brown, 2005; Kunkel et al., 2020), it is possible that there could be changes in extreme precipitation at higher rates than in the extreme IVT, with a consequent decrease in the simultaneous occurrence of extreme events of IVT and continental precipitation and a reduction in the importance of landfalling ARs as a major mechanism behind these concurrent extremes. In any case, extreme precipitation efficiency is something more complex, depending more closely to the moisture flux convergence and column relative humidity, rather than on the IVT and the integrated water vapor (IWV).

At this point, it is useful to make use of copulas to analyse carefully the influence that IVT has on extreme continental precipitation in the main regions of landfalling ARs (Fig. 9, adapted from Fig. 1 in Algarra

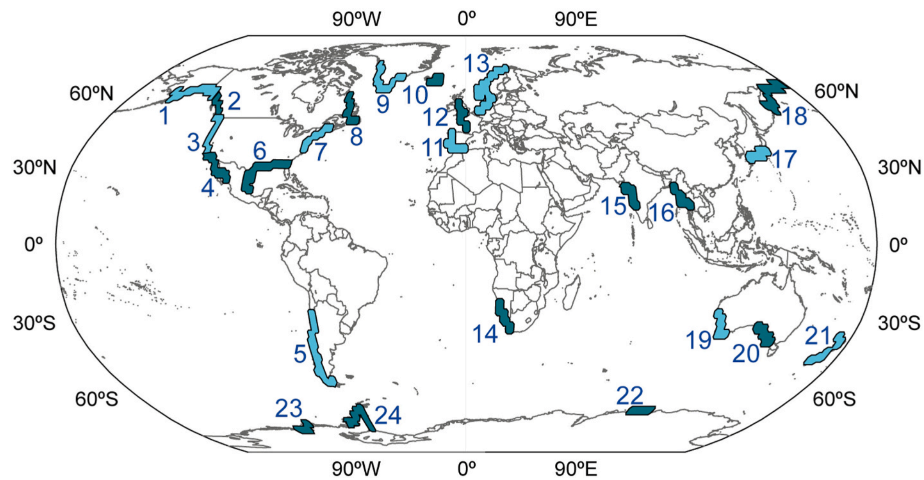

Fig. 9. Regions of maximum occurrence of landfalling ARs adapted from Fig. 1 in Algarra et al. (2020). The differential shading does not have any meaning, it is simply to differentiate between the key AR regions.

et al., 2020). For that purpose, we also used daily series of IVT and precipitation, but in this case they were averaged over the corresponding AR landfalling region. Again, for the reasons explained in Section 3, the copulas are fitted to the sample of nonzero precipitation days, and for the computation of the quantile-based thresholds for the variables the days with zero precipitation are included. In Table 2, it is possible to find three metrics for each region for the whole period and for the two sub-periods:

I) $P(IVT \geq q90_{IVT}, Prec \geq q90_{prec})$, which is the estimated probability of achieving a concurrent extreme of IVT and precipitation, computed using (7).

II) $P(Prec \geq q90_{prec} | IVT = 250)$, which is the estimated conditional probability of precipitation exceeding its corresponding 90th percentile, for a value of IVT equal to 250 $\mathrm{kg\,m^{-1}\,s^{-1}}$, computed using (8). That value of IVT represents a threshold commonly used to identify ARs (e.g., Ralph et al., 2019; Eiras-Barca et al., 2021).

III) x s.t. $P(Prec \geq q90_{prec} | IVT = x) = 0.5$, which is the estimated value of IVT for which the probability of precipitation exceeding its corresponding 90th percentile equals 0.5.

The copula models that were used in order to compute the metrics in Table 2 are included in Table S1. They correspond to the fitted copula

Table 2
Results of the analysis of the IVT and continental precipitation averaged over the main AR landfalling regions. The metrics were calculated for the whole period 1981–2017, and the earlier and later studied periods, using the best fitted copula model in each case (according to the AIC).

Reg.	Season	Metric I			Metric II			Metric III		
		Whole	Earlier	Later	Whole	Earlier	Later	Whole	Earlier	Later
1	DJF	0.04	0.05	0.03	0.69	0.91	0.47	193.00	167.45	258.51
2	DJF	0.05	0.05	0.05	0.54	0.54	0.56	234.31	225.85	234.28
3	DJF	0.05	0.07	0.05	0.43	0.64	0.39	269.90	232.45	289.07
4	DJF	0.07	0.07	0.06	0.82	0.79	0.78	183.58	197.47	194.72
	JJA	0.03	0.02	0.03	0.35	0.25	0.41	343.85	339.09	343.85
5	JJA	0.03	0.03	0.03	0.59	0.72	0.44	223.51	201.87	263.21
6	DJF	0.03	0.04	0.03	0.18	0.21	0.17	454.07	388.88	535.51
	JJA	0.04	0.02	0.04	0.13	0.13	0.14	358.21	427.89	361.00
7	DJF	0.04	0.05	0.03	0.18	0.19	0.18	453.14	403.88	766.43
8	DJF	0.05	0.03	0.05	0.61	0.32	0.71	215.63	NaN	194.53
9	DJF	0.04	0.03	0.04	0.78	1.00	0.71	150.79	156.43	153.69
10	DJF	0.03	0.03	0.03	0.27	0.31	0.24	456.62	414.03	476.50
11	DJF	0.05	0.06	0.04	0.36	0.37	0.35	318.06	302.25	325.15
12	DJF	0.04	0.05	0.03	0.20	0.22	0.21	383.14	377.13	NaN
13	DJF	0.03	0.04	0.03	0.39	0.73	0.34	NaN	199.25	NaN
14	JJA	0.04	0.03	0.07	0.35	0.29	0.89	NaN	NaN	163.35
15	DJF	0.02	NA	NA	0.77	NA	NA	96.40	NA	NA
	JJA	0.04	0.02	0.05	0.03	0.03	0.04	680.09	1013.64	671.84
16	DJF	0.08	0.05	0.09	0.64	0.41	0.69	190.10	417.53	167.33
	JJA	0.03	0.03	0.03	0.04	0.04	0.05	800.26	794.70	767.69
17	DJF	0.04	0.04	0.05	0.32	0.30	0.33	333.35	338.23	328.32
18	DJF	0.04	0.04	0.04	0.83	1.00	0.80	133.79	127.00	123.12
19	JJA	0.04	0.05	0.04	0.31	0.33	0.28	402.70	343.42	NaN
20	JJA	0.03	0.04	0.03	0.29	0.34	0.23	NaN	NaN	NaN
21	JJA	0.05	0.05	0.04	0.51	0.63	0.40	248.81	213.20	284.57
22	JJA	0.05	0.04	0.05	0.34	0.59	0.35	NaN	171.02	NaN
23	JJA	0.03	0.05	0.00	0.90	0.52	0.06	164.56	90.11	NaN
24	JJA	0.03	0.03	0.03	0.94	0.94	0.97	188.17	133.06	143.41

NA (Not Available): The number of days of nonzero precipitation in the corresponding period is lower or equal to 400.
NaN (Not a Number): There is not a value x such that $P(Prec \geq q90_{prec} | IVT = x) = 0.5$ in the corresponding period.

types with the lowest AIC value in each case.

These metrics were calculated for the corresponding winter of each AR landfalling region except for monsoonal regions, where both summer and winter were taken into account. The analysis of the whole period shows that in general terms, areas of landfalling ARs in the Northern Hemisphere have higher probabilities of achieving a concurrent extreme of IVT and continental precipitation than areas in the Southern Hemisphere, with maxima of 0.05 over the Pacific American coasts, The Canadian Atlantic, and the Iberian Peninsula, most of which are extratropical regions. That is, in these regions, among the total sample, 5% of values correspond to a simultaneous occurrence of extreme IVT and extreme precipitation, understanding by "extreme" the value of the corresponding 90th percentile of the variable (calculated including also the days of zero precipitation). In the Southern Hemisphere, the probabilities are higher in the Australian AR regions than in the American or African ones. In Polar AR regions, there are high probabilities of around 0.04 in the Northern Hemisphere but these are lower over the Antarctic AR regions, at around 0.02, the lowest among all the areas of AR landfall. AR monsoonal regions have moderate (around 0.03) probabilities of achieving a concurrent extreme of IVT and precipitation. These results have logical correspondence with the other two metrics: a) the lower probability of achieving a concurrent extreme of IVT and precipitation, b) the higher conditional probability of extreme precipitation for a value of IVT equal to 250 $\mathrm{kg\,m^{-1}s^{-1}}$, and c) the lower IVT for which the probability of precipitation exceeding its corresponding 90th percentile equals 0.5. We illustrate the meaning of these two metrics with an example. Region 3 (Californian coast) has a similar latitude to region 11 (Iberian Peninsula) and a lower latitude than region 1 (Alaska). For a day with a value of IVT of 250 $\mathrm{kg\,m^{-1}s^{-1}}$, which is typical of an AR, it is far more likely that the precipitation was extreme in California (43%) than in the Iberian Peninsula (36%), but much less likely than in Alaska (69%). Similarly, it is necessary to have a lower IVT in California (269.90 $\mathrm{kg\,m^{-1}s^{-1}}$) than in the Iberian Peninsula (318.08 $\mathrm{kg\,m^{-1}s^{-1}}$) but higher than in Alaska (193 $\mathrm{kg\,m^{-1}s^{-1}}$) to achieve a scenario where for two days of nonzero precipitation, one is an extreme precipitation day. This shows, again, that the strong latitudinal IVT gradient and the contrast from one region to another must be taken into account in the identification of ARs (Guan and Waliser, 2015; Reid et al., 2020), and in the characterisation of their strength and impacts (Ralph et al., 2019; Eiras-Barca et al., 2021).

The analysis of the three metrics by sub-period confirms the results presented in Fig. 7. Almost all the AR landfalling regions with high or very high probabilities of concurrent extremes of IVT and continental precipitation (South Africa and Japan regions are the only exceptions) show a general tendency towards lower occurrence of simultaneous extremes in recent (warmer) periods. In one example in particular, for region 3 (California coasts) from the earlier period to the more recent warmer period, the estimated probability of achieving a concurrent extreme was reduced from 7% to 5%. In that region, the probability of an extreme precipitation day given an IVT of 250 $\mathrm{kg\,m^{-1}s^{-1}}$ was reduced from 64% to 39% and it is necessary to have about 57 $\mathrm{kg\,m^{-1}s^{-1}}$ more of IVT to achieve a scenario where for two days of nonzero precipitation, one is an extreme precipitation day. An IVT of 250 $\mathrm{kg\,m^{-1}s^{-1}}$ implies a near certainty of extreme precipitation in Northern Hemisphere polar regions in the earlier period but not in the more recent (warmer) period. In any of the regions of higher AR landfalling occurrence, such as the Atlantic European coast, we estimated that only about one third of the days with this IVT value were associated with extreme precipitation in the recent (warmer) period.

4.3. Additional comments on the statistical analysis

The statistical analysis of this study was mainly performed using the *R* package *VineCopula* (Nagler et al., 2020). The code used to obtain the results presented in this article is available from the authors upon reasonable request.

When using copulas, it is advisable to assess the impact that the autocorrelation between the observations has on the results. In our study, for each grid point, we repeated the statistical analysis selecting every third observation of the series, and the same was done for every fifth observation, in a similar way to Naveau et al. (2016). The results remained essentially unchanged from using the complete series, so we decided to keep all the observations in order to have a larger sample.

We also investigated the effect that the trend of the IVT and precipitation series had on our analysis. Both the IVT and precipitation series were linearly detrended and the results were completely analogous to the ones obtained for the non-detrended series, so we also opted to keep the original data.

For the copula models that were used to compute the metrics in Table 2, a Cramér–von Mises goodness-of-fit test was performed in each case (see Genest et al., 2009), by means of the *R* package *gofCopula* (Okhrin et al., 2021). The null hypothesis that the copula model fits well to the data was not rejected at significance level 0.05 in all the cases. Therefore, we can conclude that those models were appropriate for the calculations that were carried out.

5. Conclusions

This paper offers an analysis of the concurrent extremes of vertically integrated water vapor transport (a local measure of moisture transport) and precipitation on the continents, the main aim being an understanding of the role played by landfalling atmospheric rivers, and whether this role has changed in the current warming climate.

The main conclusions reached in this work can be summarised in five main points, as follows:

- Copula models were a very useful tool for the analysis of the concurrent extremes of IVT and precipitation. On the one hand, for the worldwide analysis at grid-point level, they enabled us to estimate the probability of simultaneous occurrence of extreme values of the variables. On the other hand, for the in-depth analysis in the AR landfalling regions, we also made use of copulas to calculate two additional metrics: the estimated conditional probability of extreme precipitation for a value of IVT which represents a threshold commonly used to identify ARs, and the estimated value of IVT that is necessary to reach a scenario in which for two days of nonzero precipitation, one is an extreme precipitation day.
- The pattern of the absolute number of concurrent extremes of IVT and continental precipitation is very similar to the one corresponding to wind and precipitation: low in the tropics and growing in subtropical and extratropical regions, reaching its highest values along the coast of the continents in regions where atmospheric rivers occur. It is also possible to recognize the regional action of other meteorological structures associated with strong moisture transport, such as low-level jets or tropical cyclones.
- The estimated probability of achieving a concurrent extreme of IVT and continental precipitation shows a similar pattern to the one corresponding to the absolute number of concurrent extremes, but intensifies as the number of precipitation days reduces. This is visible in the high probabilities in monsoonal areas during the dry season or the north-south gradient of probability in the regions of occurrence of landfalling ARs. Simultaneous high probabilities of occurrence of concurrent extremes together with moderately high values of IVT and precipitation occur mostly in regions of landfalling ARs.
- Landfalling ARs occurrence accounts for most of the concurrent extreme days of IVT and continental precipitation. Percentages of AR landfalling occurrence with respect to the concurrent extreme days reach values close to 90% in some seasons of the year in almost all the known regions of maximum occurrence of landfalling ARs, with percentages greater than 75% downwind of AR landfalling regions. This coincidence is low in tropical regions and in particular in monsoonal areas, with percentages lower than 50%. A careful

copula-based analysis performed in the regions of maximum occurrence of landfalling ARs confirms that in Northern Hemisphere AR landfalling areas there are higher probabilities of achieving a concurrent extreme of IVT and precipitation than in the AR landfalling regions in the Southern Hemisphere. Moreover, the analysis enabled us to find that absolute maxima of probability occur over the Pacific American coasts, the Canadian Atlantic and the Iberian Peninsula, that only moderate probabilities occur over AR monsoonal regions, and that these are low over Antarctic AR regions.
- The role of landfalling ARs as drivers of concurrent extremes of IVT and continental precipitation is not the same for the two sub-periods of the study, one earlier and another more recent (warmer) period. The general tendency is towards a decrease in the influence of landfalling ARs in recent (warmer) periods, which is especially marked over the Pacific and Atlantic North American coasts during winter. This is evident both from the percentage of concurrent extreme days of IVT and continental precipitation that coincide with the occurrence of landfalling ARs and from the analysis of three copula-derived metrics.

A logical evolution of this study and possible future work would be to study, similarly to what has been done in this article, the concurrence between extreme precipitation and extreme moisture transport convergence, quantified as convergence of IVT. The moisture transport by itself will only be linked to extreme precipitation if there is an instability mechanism that forces the water vapor to rise, which in any case would inevitably result in a high convergence of the integrated water vapor flux value. As most of the moisture is confined at low levels, a high IVT convergence value implies ascents, and therefore IVT convergence implies both moisture arrival at a place and ascent, that is why its relationship with precipitation (and extreme precipitation) must necessarily be stronger than that between precipitation and the moisture transport itself (Mo et al., 2021). Some of the results reached in this paper, such as the general tendency towards a decrease in the influence of landfalling ARs in recent (warmer) periods, may be better understood if the causal linkage between moisture transport and precipitation through moisture transport convergence is taken into account.

This study has some limitations associated with i) the quality of the precipitation data, mainly associated with the density of the gauge network, this being particularly poor over tropical Africa and Antarctica; ii) the coarse resolution of the data of the reanalysis, which precludes a detailed regional analysis in areas with complex orography or where small-scale convective processes are relevant; iii) the fact that our daily IVT values do not follow the different EOD hours of the daily CPC precipitation values; iv) the deïinition of the concurrent extremes, herein the local 90th percentile, which is low compared with the 99th percentile more commonly used to define very rare extremes, but necessary in our case to permit large enough samples to relate seasonality to AR landfalling occurrence; v) the sample size of the two sub-periods used for the analysis of the IVT and continental precipitation averaged over the main AR landfalling regions, which is relatively small (only 15 years), so the findings shown in that part of the study should be understood as a preliminary approach to the analysis of the effects of global warming on the concurrent extremes of IVT and continental precipitation, a topic that requires the use of climate change models to be fully tackled.

As suggested by Zscheischler et al. (2021), studies based on reanalysis should be compared with others using higher resolution models when compound precipitation and wind (in our case IVT) extremes are studied over complex terrain. This is the object of our further research, where a twofold nesting WRF simulation will be used to study the concurrent extremes of IVT and precipitation for current and future climates at a 6-km resolution for Western European coasts, a region of high AR landfalling occurrence.

CRediT authorship contribution statement

Luis Gimeno-Sotelo: Formal analysis, Visualization, Writing – original draft, Writing – review & editing. **Luis Gimeno:** Conceptualization, Resources, Writing – original draft, Writing – review & editing, Supervision, Funding acquisition.

Declaration of Competing Interest

The authors declare that they have no known competing financial interests or personal relationships that could have appeared to influence the work reported in this paper.

Acknowledgements

Both authors acknowledge the financial support received from the Spanish Government within the LAGRIMA Project (Grant No. RTI2018-095772-B-I00) and the support obtained from the Xunta de Galicia, under project ED431C 2021/44 "Programa de Consolidación e Estructuración de Unidades de Investigación Competitivas". The authors also acknowledge Bin Guan and Iago Algarra for providing data necessary for this research. Funding for open access charge: Universidade de Vigo/CISUG

Appendix A. Supplementary data

Supplementary data to this article can be found online at https://doi.org/10.1016/j.atmosres.2022.106356.

References

Akaike, H., 1974. A new look at the statistical model identification. IEEE Trans. Autom. Control 19, 716–723.
Algarra, I., Eiras-Barca, J., Nieto, R., Gimeno, L., 2019. Global climatology of nocturnal low-level jets and associated moisture sources and sinks. Atmos. Res. 229, 39–59.
Algarra, I., Nieto, R., Ramos, A.M., Eiras-Barca, J., Trigo, R.M., Gimeno, L., 2020. Significant increase of global anomalous moisture uptake feeding landfalling atmospheric rivers. Nat. Commun. 11, 1–7.
Bao, J., Sherwood, S.C., Alexander, L.V., Evans, J.P., 2017. Future increases in extreme precipitation exceed observed scaling rates. Nat. Clim. Chang. 7, 128–132.
Beck, H.E., Wood, E.F., Pan, M., Fisher, C.K., Miralles, D.G., Van Dijk, A.I., McVicar, T.R., Adler, R.F., 2019. MSWEP V2 global 3-hourly 0.1 precipitation: methodology and quantitative assessment. Bull. Am. Meteorol. Soc. 100, 473–500.
Benton, G.S., Estoque, M.A., 1954. Water-vapor transfer over the north American continent. J. Meteorol. 11, 462–477.
Bevacqua, E., Maraun, D., Vousdoukas, M.I., Voukouvalas, E., Vrac, M., Mentaschi, L., Widmann, M., 2019. Higher probability of compound flooding from precipitation and storm surge in Europe under anthropogenic climate change. Sci. Adv. 5, eaaw5531.
Braz, D.F., Ambrizzi, T., Da Rocha, R.P., Algarra, I., Nieto, R., Gimeno, L., 2021. Assessing the moisture transports associated with nocturnal low-level jets in continental South America. Front. Environ. Sci. 9, 657764.
Castillo, R., Nieto, R., Drumond, A., Gimeno, L., 2014. The role of the ENSO cycle in the modulation of moisture transport from major oceanic moisture sources. Water Resour. Res. 50, 1046–1058.
Catto, J.L., Dowdy, A., 2021. Understanding compound hazards from a weather system perspective. Weather Clim. Extrem. 32, 100313.
Cong, R.-G., Brady, M., 2012. The interdependence between rainfall and temperature: copula analyses. Sci. World J. 2012.
De Vries, A.J., 2021. A global climatological perspective on the importance of Rossby wave breaking and intense moisture transport for extreme precipitation events. Weather Clim. Dynam. 2, 129–161.
Dee, D.P., Uppala, S., Simmons, A., Berrisford, P., Poli, P., Kobayashi, S., Andrae, U., Balmaseda, M., Balsamo, G., Bauer, d. P., et al., 2011. The ERA-Interim reanalysis: configuration and performance of the data assimilation system. Q. J. R. Meteorol. Soc. 137, 553–597.
Dettinger, M.D., Ralph, F.M., Lavers, D.A., 2015. Setting the stage for a global science of atmospheric rivers. EOS, Earth Space Sci. News 96.
Dietzsch, F., Andersson, A., Ziese, M., Schröder, M., Raykova, K., Schamm, K., Becker, A., 2017. A global ETCCDI-based precipitation climatology from satellite and rain gauge measurements. Climate 5, 9.
Drumond, A., Stojanovic, M., Nieto, R., Vicente-Serrano, S.M., Gimeno, L., 2019. Linking anomalous moisture transport and drought episodes in the IPCC reference regions. Bull. Am. Meteorol. Soc. 100, 1481–1498.
Eiras-Barca, J., Ramos, A.M., Algarra, I., Vázquez, M., Dominguez, F., Miguez-Macho, G., Nieto, R., Gimeno, L., Taboada, J., Ralph, F.M., 2021. European West Coast

atmospheric rivers: a scale to characterize strength and impacts. Weather Clim. Extrem. 31, 100305.
Emori, S., Brown, S., 2005. Dynamic and thermodynamic changes in mean and extreme precipitation under changed climate. Geophys. Res. Lett. 32.
Espinoza, V., Waliser, D.E., Guan, B., Lavers, D.A., Ralph, F.M., 2018. Global analysis of climate change projection effects on atmospheric rivers. Geophys. Res. Lett. 45, 4299–4308.
Genest, C., Rémillard, B., Beaudoin, D., 2009. Goodness-of-fit tests for copulas: a review and a power study. Insurance: Mathem. Econom. 44, 199–213.
Gimeno, L., Drumond, A., Nieto, R., Trigo, R.M., Stohl, A., 2010. On the origin of continental precipitation. Geophys. Res. Lett. 37.
Gimeno, L., Stohl, A., Trigo, R.M., Dominguez, F., Yoshimura, K., Yu, L., Drumond, A., Durán-Quesada, A.M., Nieto, R., 2012. Oceanic and terrestrial sources of continental precipitation. Rev. Geophys. 50.
Gimeno, L., Nieto, R., Vázquez, M., Lavers, D.A., 2014. Atmospheric rivers: a mini-review. Front. Earth Sci. 2, 2.
Gimeno, L., Dominguez, F., Nieto, R., Trigo, R., Drumond, A., Reason, C.J., Taschetto, A. S., Ramos, A.M., Kumar, R., Marengo, J., 2016. Major mechanisms of atmospheric moisture transport and their role in extreme precipitation events. Annu. Rev. Environ. Resour. 41, 117–141.
Gimeno, L., Vázquez, M., Eiras-Barca, J., Sor, R., Stojanovic, M., Algarra, I., Nieto, R., Ramos, A.M., Durán-Quesada, A.M., Dominguez, F., 2020. Recent progress on the sources of continental precipitation as revealed by moisture transport analysis. Earth Sci. Rev. 201, 103070.
Gimeno, L., Algarra, I., Eiras-Barca, J., Ramos, A.M., Nieto, R., 2021. Atmospheric river, a term encompassing different meteorological patterns. Wiley Interdiscip. Rev. Water e1558.
Guan, B., Waliser, D.E., 2015. Detection of atmospheric rivers: Evaluation and application of an algorithm for global studies. J. Geophys. Res.-Atmos. 120, 12514–12535.
Haberlandt, U., 2007. Geostatistical interpolation of hourly precipitation from rain gauges and radar for a large-scale extreme rainfall event. J. Hydrol. 332, 144–157.
Held, I.M., Soden, B.J., 2006. Robust responses of the hydrological cycle to global warming. J. Clim. 19, 5686–5699.
Hersbach, H., Bell, B., Berrisford, P., Hirahara, S., Horányi, A., Muñoz-Sabater, J., Nicolas, J., Peubey, C., Radu, R., Schepers, D., et al., 2020. The ERA5 global reanalysis. Q. J. R. Meteorol. Soc. 146, 1999–2049.
Joe, H., 2014. Dependence Modeling with Copulas. CRC Press.
Kim, H.-M., Zhou, Y., Alexander, M.A., 2019. Changes in atmospheric rivers and moisture transport over the Northeast Pacific and western North America in response to ENSO diversity. Clim. Dyn. 52, 7375–7388.
Kunkel, K.E., Stevens, S.E., Stevens, L.E., Karl, T.R., 2020. Observed climatological relationships of extreme daily precipitation events with precipitable water and vertical velocity in the contiguous United States. Geophys. Res. Lett. 47, e2019GL086721.
Lavers, D.A., Villarini, G., 2015. The contribution of atmospheric rivers to precipitation in Europe and the United States. J. Hydrol. 522, 382–390.
Lazoglou, G., Anagnostopoulou, C., 2019. Joint distribution of temperature and precipitation in the Mediterranean, using the Copula method. Theor. Appl. Climatol. 135, 1399–1411.
Li, S., Wu, L., Yang, Y., Geng, T., Cai, W., Gan, B., Chen, Z., Jing, Z., Wang, G., Ma, X., 2020. The Pacific Decadal Oscillation less predictable under greenhouse warming. Nat. Clim. Chang. 10, 30–34.
Liu, B., Tan, X., Gan, T.Y., Chen, X., Lin, K., Lu, M., Liu, Z., 2020. Global atmospheric moisture transport associated with precipitation extremes: Mechanisms and climate change impacts. Wiley Interdiscip. Rev. Water 7, e1412.
Liu, Q., Li, T., Zhou, W., 2021. Impacts of multi-timescale circulations on meridional moisture transport. J. Clim. 34, 8065–8085.
Martius, O., Pfahl, S., Chevalier, C., 2016. A global quantification of compound precipitation and wind extremes. Geophys. Res. Lett. 43, 7709–7717.
Massoud, E., Espinoza, V., Guan, B., Waliser, D., 2019. Global climate model ensemble approaches for future projections of atmospheric rivers. Earth's Future 7, 1136–1151.
Mazdiyasni, O., AghaKouchak, A., 2015. Substantial increase in concurrent droughts and heatwaves in the United States. Proc. Natl. Acad. Sci. 112, 11484–11489.
McClenny, E.E., Ullrich, P.A., Grotjahn, R., 2020. Sensitivity of atmospheric river vapor transport and precipitation to uniform sea surface temperature increases. J. Geophys. Res.-Atmos. 125, e2020JD033421.
Messmer, M., Simmonds, I., 2021. Global analysis of cyclone-induced compound precipitation and wind extreme events. Weather Clim. Extrem. 32, 100324.
Mo, R., So, R., Brugman, M.M., Mooney, C., Liu, A.Q., Jakob, M., Castellan, A., Vingarzan, R., 2021. Column relative humidity and primary condensation rate as two useful supplements to atmospheric river analysis. Water Resour. Res. 57, e2021WR029678.
Mukherjee, S., Mishra, A.K., 2021a. Cascading effect of meteorological forcing on extreme precipitation events: role of atmospheric rivers in southeastern US. J. Hydrol. 601, 126641.
Mukherjee, S., Mishra, A.K., 2021b. Increase in compound drought and heatwaves in a warming world. Geophys. Res. Lett. 48, e2020GL090617.
Nagler, T., Schepsmeier, U., Stoeber, J., Brechmann, E.C., Graeler, B., Erhardt, T., 2020. VineCopula: Statistical Inference of Vine Copulas. URL. https://CRAN.R-project.org/package=VineCopula.
Naveau, P., Huser, R., Ribereau, P., Hannart, A., 2016. Modeling jointly low, moderate, and heavy rainfall intensities without a threshold selection. Water Resour. Res. 52, 2753–2769.
Nayak, M.A., Villarini, G., 2018. Remote sensing-based characterization of rainfall during atmospheric rivers over the Central United States. J. Hydrol. 556, 1038–1049.
Neiman, P.J., Ralph, F.M., Wick, G.A., Lundquist, J.D., Dettinger, M.D., 2008. Meteorological characteristics and overland precipitation impacts of atmospheric rivers affecting the West Coast of North America based on eight years of SSM/I satellite observations. J. Hydrometeorol. 9, 22–47.
Nelsen, R.B., 2006. An Introduction to Copulas. Springer Science & Business Media.
Nie, J., Sobel, A.H., Shaevitz, D.A., Wang, S., 2018. Dynamic amplification of extreme precipitation sensitivity. Proc. Natl. Acad. Sci. 115, 9467–9472.
Okhrin, Ostap, Trimborn, Simon, Waltz, Martin, April 27, 2021. gofCopula: Goodness-of-Fit Tests for Copulae. Available at SSRN: https://ssrn.com/abstract=3560825.
Owen, L.E., Catto, J.L., Stephenson, D.B., Dunstone, N.J., 2021. Compound precipitation and wind extremes over Europe and their relationship to extratropical cyclones. Weather Clim. Extrem. 33, 100342.
Payne, A.E., Demory, M.-E., Leung, L.R., Ramos, A.M., Shields, C.A., Rutz, J.J., Siler, N., Villarini, G., Hall, A., Ralph, F.M., 2020. Responses and impacts of atmospheric rivers to climate change. Nat. Rev. Earth Environ. 1, 143–157.
Ralph, F.M., Dettinger, M.D., 2011. Storms, floods, and the science of atmospheric rivers. EOS Trans. Am. Geophys. Union 92, 265–266.
Ralph, F.M., Neiman, P.J., Wick, G.A., Gutman, S.I., Dettinger, M.D., Cayan, D.R., White, A.B., 2006. Flooding on California's Russian River: role of atmospheric rivers. Geophys. Res. Lett. 33.
Ralph, F.M., Cordeira, J.M., Neiman, P.J., Hughes, M., 2016. Landfalling atmospheric rivers, the Sierra Barrier Jet, and extreme daily precipitation in northern California's upper Sacramento River watershed. J. Hydrometeorol. 17, 1905–1914.
Ralph, F.M., Dettinger, M.D., Cairns, M.M., Galarneau, T.J., Eylander, J., 2018. Defining "atmospheric river": How the Glossary of Meteorology helped resolve a debate. Bull. Am. Meteorol. Soc. 99, 837–839.
Ralph, F.M., Rutz, J.J., Cordeira, J.M., Dettinger, M., Anderson, M., Reynolds, D., Schick, L.J., Smallcomb, C., 2019. A scale to characterize the strength and impacts of atmospheric rivers. Bull. Am. Meteorol. Soc. 100, 269–289.
Reddy, M.J., Ganguli, P., 2012. Bivariate flood frequency analysis of Upper Godavari River flows using Archimedean copulas. Water Resour. Manag. 26, 3995–4018.
Reid, K.J., King, A.D., Lane, T.P., Short, E., 2020. The sensitivity of atmospheric river identification to integrated water vapor transport threshold, resolution, and regridding method. J. Geophys. Res.-Atmos. 125, e2020JD032897.
Rutz, J.J., Steenburgh, W.J., Ralph, F.M., 2015. The inland penetration of atmospheric rivers over western North America: a Lagrangian analysis. Mon. Weather Rev. 143, 1924–1944.
Salvadori, G., De Michele, C., 2004. Frequency analysis via copulas: theoretical aspects and applications to hydrological events. Water Resour. Res. 40.
Shemyakin, A., Kniazev, A., 2017. Introduction to Bayesian Estimation and Copula Models of Dependence. Wiley Online Library.
Sklar, M., 1959. Fonctions de repartition an dimensions et leurs marges. Publ. Inst. Statist. Univ. Paris 8, 229–231.
Sun, Y., Solomon, S., Dai, A., Portmann, R.W., 2006. How often does it rain? J. Clim. 19, 916–934.
Tan, Y., Yang, S., Zwiers, F., Wang, Z., Sun, Q., 2021. Moisture budget analysis of extreme precipitation associated with different types of atmospheric rivers over western north america. Clim. Dyn. 1–17.
Tarek, M., Brissette, F.P., Arsenault, R., 2020. Evaluation of the ERA5 reanalysis as a potential reference dataset for hydrological modelling over North America. Hydrol. Earth Syst. Sci. 24, 2527–2544.
Tootoonchi, F., Sadegh, M., Haerter, J.O., Räty, O., Grabs, T., Teutschbein, C., 2022. Copulas for hydroclimatic analysis: a practice-oriented overview. Wiley Interdiscip. Rev. Water 9, e1579.
Trenberth, K., Zhang, R., et al., 2021. The Climate Data Guide: Atlantic Multi-decadal Oscillation (AMO). Last modified 05 Jun 2021. Retrieved from. https://climatedataguide.ucar.edu/climate-data/atlantic-multi-decadal-oscillation-amo.
van der Ent, R.J., Savenije, H.H., 2013. Oceanic sources of continental precipitation and the correlation with sea surface temperature. Water Resour. Res. 49, 3993–4004.
van der Ent, R.J., Savenije, H.H., Schaefli, B., Steele-Dunne, S.C., 2010. Origin and fate of atmospheric moisture over continents. Water Resour. Res. 46.
Vázquez, M., Nieto, R., Liberato, M.L., Gimeno, L., 2020. Atmospheric moisture sources associated with extreme precipitation during the peak precipitation month. Weather Clim. Extrem. 30, 100289.
Wahl, T., Jain, S., Bender, J., Meyers, S.D., Luther, M.E., 2015. Increasing risk of compound flooding from storm surge and rainfall for major US cities. Nat. Clim. Chang. 5, 1093–1097.
Waliser, D., Guan, B., 2017. Extreme winds and precipitation during landfall of atmospheric rivers. Nat. Geosci. 10, 179–183.
Xie, P., Chen, M., Yang, S., Yatagai, A., Hayasaka, T., Fukushima, Y., Liu, C., 2007. A gauge-based analysis of daily precipitation over East Asia. J. Hydrometeorol. 8, 607–626.
Xiong, Y., Ren, X., 2021. Influences of Atmospheric Rivers on North Pacific Winter precipitation: climatology and dependence on ENSO condition. J. Clim. 34, 277–292.
Xu, X., Frey, S.K., Boluwade, A., Erler, A.R., Khader, O., Lapen, D.R., Sudicky, E., 2019. Evaluation of variability among different precipitation products in the Northern Great Plains. J. Hydrol. Region. Stud. 24, 100608.

Zhu, Y., Newell, R.E., 1994. Atmospheric rivers and bombs. Geophys. Res. Lett. 21, 1999–2002.
Zscheischler, J., Seneviratne, S.I., 2017. Dependence of drivers affects risks associated with compound events. Sci. Adv. 3, e1700263.
Zscheischler, J., Naveau, P., Martius, O., Engelke, S., Raible, C.C., 2021. Evaluating the dependence structure of compound precipitation and wind speed extremes. Earth Syst. Dynam. 12, 1–16.

4.3 The relative importance of atmospheric moisture transport in extreme precipitation compared to other drivers

The third article of this chapter is entitled "**Combinations of drivers that most favor the occurrence of daily precipitation extremes**" by **Gimeno-Sotelo, L.**, Bevacqua, E., & Gimeno, L., and was published in the journal *Atmospheric Research* in 2023.

Atmospheric Research 294 (2023) 106959

Contents lists available at ScienceDirect

Atmospheric Research

journal homepage: www.elsevier.com/locate/atmosres

Combinations of drivers that most favor the occurrence of daily precipitation extremes

Luis Gimeno-Sotelo [a,*], Emanuele Bevacqua [b], Luis Gimeno [a]

[a] Centro de Investigación Mariña, Universidade de Vigo, Environmental Physics Laboratory (EPhysLab), Campus da Auga, 32004 Ourense, Spain
[b] Department of Computational Hydrosystems, Helmholtz Centre for Environmental Research, 04318 Leipzig, Germany

ARTICLE INFO

Keywords:
Extreme precipitation
Precipitable water
Moisture transport
Atmospheric instability

ABSTRACT

Previous studies indicate atmospheric instability, total column water vapor, and horizontal moisture transport as major drivers of precipitation extremes, however little is known about how the combination of these drivers affects precipitation extremes across the world. Here, using daily data from the ERA-5 reanalysis spanning the period 1981–2020, we identified the combinations of extreme values for these three major drivers that enhance the probability of daily precipitation extremes on a global scale. Our findings show that extreme daily precipitation is practically impossible without any of these drivers being extreme. Atmospheric instability is the primary driver of precipitation extremes, meaning that, among the three cases of the drivers being extreme in isolation, extreme atmospheric instability is associated with the highest average probability of extreme precipitation over landmasses (29% during December–February, 32% during June–August). When considering the combination of two drivers being simultaneously extreme, joint extremes of atmospheric instability and total column water vapor (and non-extreme horizontal moisture transport) lead to the highest probability of extreme precipitation (69% during December–February, 70% during June–August), which is similar to the probability under three drivers in extreme conditions (67% and 72%). Our results point to a latitudinal variation of the combination that leads to the highest probability of extreme precipitation. In subtropics, the case of the three extreme drivers dominates, whereas in extratropical regions, the dominant combination is that of the joint extremes of atmospheric instability and total column water vapor (and non-extreme horizontal moisture transport). By providing information on the most important drivers of precipitation extremes worldwide, these results can serve as a basis for evaluating precipitation extremes in climate models and understanding projected changes, which is vital for developing robust risk assessments.

1. Introduction

An unequivocal consequence of global warming is the change in precipitation extremes (Douville et al., 2021; Seneviratne et al., 2021; Caretta et al., 2022). With considerable spatial variability, these changes have already been documented for the current climate (e.g. Donat et al., 2016 or Sun et al., 2021) and are projected for future climates (e.g. Westra et al., 2014 or Bao et al., 2017). Behind these changes, there is a thermodynamical cause affecting precipitation extremes everywhere in the world: the increase of extreme precipitation with the increase of the water-holding capacity of the air, which grows at a rate of 6–7% per degree of warming according to the Clausius–Clapeyron relationship (Soden and Held, 2006; Allen and Ingram, 2002). Additionally, there is a dynamic cause: changes in atmospheric circulation and, therefore, in the convergence of atmospheric moisture, which modulate regional extreme precipitation (O'Gorman, 2015; Bao et al., 2017). Depending on the region, such a dynamic effect can enhance or dampen the thermodynamically-driven increase (Pfahl et al., 2017). Thermodynamical and dynamic contributions to changes in extreme precipitation can be well represented with the drivers studied in this article, i.e., atmospheric instability, mostly accounting for dynamic contribution; total column water vapor, mostly accounting for thermodynamical contribution; and horizontal moisture transport, accounting for both dynamic and thermodynamical contributions.

Although the relationship between extreme precipitation and moisture is complex (Neelin et al., 2022), in the first approximation, extreme precipitation broadly scales with moisture content and any indicator of atmospheric instability, such as *vertical velocity*. Unlike total

* Corresponding author.
E-mail address: luis.gimeno-sotelo@uvigo.es (L. Gimeno-Sotelo).

https://doi.org/10.1016/j.atmosres.2023.106959
Received 11 April 2023; Received in revised form 17 June 2023; Accepted 5 August 2023
Available online 9 August 2023

precipitation (e.g., annual or seasonal precipitation), daily extreme precipitation is more sensitive to moisture content than to atmospheric instability (Emori and Brown, 2005; Nie et al., 2018). The exceedance of an atmospheric instability threshold is required for extreme precipitation to occur; however, once this threshold is reached, extreme precipitation increases with increasing water vapor content (Emori and Brown, 2005; Kunkel et al., 2020a). To study precipitation extremes, moisture content can be quantified from the *vertically-integrated water vapor or precipitable water (IWV)*, a variable of great climatic interest as a promising covariate for projecting extreme precipitation in future climates. In a recent study, Kim et al. (2022) pointed out three advantages of considering total water vapor content: its dependence on temperature in general, its estimation from satellites and models, good agreement with radiosonde observations as opposed to precipitation, and its higher correlation with precipitation compared to other covariates, such as surface air temperature or dew point temperature (Roderick et al., 2020).

The relationship between total precipitation and the IWV is often approximated as linear based on simple considerations of the mass balance equation (Hagos et al., 2021; Hagos et al., 2021; Kim et al., 2022), however this relationship is not linear and may vary in different locations and seasons. Some regional studies have shown strong positive correlations between extreme precipitation and IWV, for example for Australia (Roderick et al., 2019) and the contiguous United States (Kunkel et al., 2020b). However, this strong correlation does not seem sufficient to justify the change in extreme precipitation, as shown for extremes in Australia by Bao et al. (2017). Likewise, the linear relationship has also been questioned, for instance Kunkel et al. (2020a) showed that under very high amounts of water vapor, as occurs in regions closer to the tropics or in hot seasons, the increase in daily extreme precipitation is disproportionately larger than the increase in IWV. Such non-linearities highlight the relevance of accounting for changes in dynamical processes when studying precipitation extreme changes. Accordingly, in a recent global study, Kim et al. (2022) found within the tropics a very strong relationship between daily extreme precipitation and IWV only outside of the rainforests; in the extratropical regions (regions outside 30° latitudes, except the interior of North America and North Asia) the relationship is very weak. Overall, they concluded that the IWV is a good driver of daily extreme precipitation in the tropics and is better in hot than cold seasons but not for extratropical regions, where it is necessary to consider other factors such as horizontal moisture transport, which were not considered in their study.

One major reason for the weak influence of the IWV on extreme precipitation in some regions and seasons is the fact that it is not possible to determine how much water vapor is involved in precipitation simply from the amount of water vapor in a column of air at any given time. In fact, the water vapor in the column changes continuously, hence the convergence of water vapor into the column from the surrounding area needs to be considered. Accordingly, the highest amount of moisture measured in the air column at a given time is always much less than the amount of precipitation during actual extreme precipitation events (Trenberth et al., 2003). This indicates that, depending on the time scale used to define the IWV, a constant supply of humidity from the outside, i.e. high *horizontal moisture transport*, is required to maintain high moisture in the atmospheric column. Therefore, on a daily scale, that is when – on average – the amount of extreme precipitation is twice the amount of water vapor (Kunkel et al., 2020a), horizontal moisture transport must be considered as a scaling variable to explain extreme precipitation.

In extratropical regions, it is extremely difficult to generate intense precipitation with only the humidity contained in the atmospheric column. For the occurrence of precipitation extremes, large and sustained contributions of water vapor are required from regions outside the air column (Trenberth et al., 2003; Gimeno et al., 2010), which are often very remote regions (Insua-Costa et al., 2022). Horizontal moisture transport is not spatially or temporally homogeneous, but there are some major horizontal moisture transport mechanisms, namely atmospheric rivers (ARs), low-level jets (LLJs), and tropical cyclones (TCs) (Gimeno et al., 2016) that make the relationship between horizontal moisture transport and extreme precipitation spatially and temporally diverse. There are many ways to quantify horizontal moisture transport (see Gimeno et al., 2012 for a review), most of which are based on *vertically-integrated horizontal moisture transport (IVT)*. IVT is widely used, for example for the identification and characterization of ARs, which are phenomena closely associated with extreme precipitation in extratropical regions (Zhu and Newell, 1998; Gimeno et al., 2014; Payne et al., 2020; Gimeno-Sotelo and Gimeno, 2022). In a recent global study of the relationship between IVT and extreme precipitation on a daily scale using extreme value analysis, Gimeno-Sotelo and Gimeno (2023) showed that the dependence between IVT and extreme precipitation is very weak or negligible in tropical regions, but important in extratropical regions, especially in those where the main mechanisms of horizontal moisture transport are effective, which encompasses some of the areas with the greatest productive economy and population on the planet.

Overall, in the first approximation, daily extreme precipitation may have a very diverse spatial and seasonal dependence on three drivers: atmospheric instability, the water vapor column, and horizontal moisture transport. This study examines how the combination of these three drivers affects extreme precipitation on a global scale. Identifying the combination of drivers that favor extreme precipitation in each region and season will serve both for the design of process-oriented diagnostics (POD) related to extreme precipitation for the evaluation of climate models and as a basis to determine the predominant role of thermodynamical or dynamic factors in changes in extreme precipitation.

2. Data and methods

We used the ERA-5 reanalysis (Hersbach et al., 2020) for the period 1981–2020 to obtain daily data for the following variables at a 0.5° resolution: precipitation, vertically-integrated horizontal moisture transport (IVT), vertically-integrated water vapor (IWV), and vertical velocity at 500 hPa. IWV (also known as precipitable water or total column water vapor) and vertical velocity at 500 hPa were directly obtained from the reanalysis, whereas IVT was computed as the vertical integral of eastward and northward water vapor flux (IVT_u and IVT_v, respectively). The IWV and IVT can be expressed as follows:

$$IWV = \frac{1}{g}\int_{\Omega} q\, dp,$$

$$IVT = \sqrt{\left(\frac{1}{g}\int_{\Omega} q\, u\, dp\right)^2 + \left(\frac{1}{g}\int_{\Omega} q\, v\, dp\right)^2} = \sqrt{IVT_u^{\,2} + IVT_v^{\,2}},$$

where q refers to specific humidity, u to zonal wind, v to meridional wind, g to gravitational acceleration, and Ω to the entire atmospheric column. Please note that in this article vertical velocity refers to "-ω", where $\omega = \frac{dp}{dt}$, and p refers to the atmospheric pressure, i.e., "-ω" is the measure that is used for representing atmospheric instability (Holton, 1973).

In this study, using ERA-5 reanalysis data allows for analyzing the relationship between extreme precipitation and the extremes of the three studied drivers (i.e., IWV, IVT and vertical velocity) on a global scale. The limitations of using reanalysis data for these variables have been comprehensively discussed in previous studies (Gimeno-Sotelo et al., 2022, Gimeno-Sotelo and Gimeno, 2023). As explained in Gimeno-Sotelo and Gimeno, 2023, we use ERA-5 data only for the period 1981–2020 because the recently released backward extension up to 1950 does not provide reliable IVT data.

To study the effect of seasonality on the obtained results, the analysis was performed independently for the boreal and austral winters, i.e. December–February (DJF) and June–August (JJA), respectively. For each of the analyzed seasons, we define an extreme value of a variable when the variable is larger than its corresponding 95th percentile (computed for the corresponding season within the period 1981–2020), and vice-versa for non-extreme values. We also tested that using different thresholds (90th and 98th percentile) does not substantially affect the results. Successively, based on empirical counting, we estimate the conditional probability of extreme precipitation for all combinations of extreme and non-extreme conditions of the drivers. Specifically, we consider the following combinations of drivers:

i) the three drivers being non-extreme, which is the reference case here.
ii) one driver being extreme and the other two drivers being non-extreme.
iii) two drivers being extreme and the other driver being non-extreme.
iv) the three drivers being extreme.

The conditional probability of extreme precipitation for a given combination of drivers in extreme conditions is estimated as the ratio between the number of days in which both extreme precipitation (Pcp_{ext}) and the combination of drivers occurred, and the total number of days in which the combination occurred, that is:

$$\widehat{P}(Pcp_{ext}|combination\ of\ extreme\ drivers) = \frac{\#\{Pcp_{ext}, combination\ of\ extreme\ drivers\}}{\#\{combination\ of\ extreme\ drivers\}},$$

where "#" refers to the number of elements of a set.

Among the combinations considered (those with only one extreme driver, those with two extreme drivers, or all the combinations), the dominant combination is the one that maximises the conditional probability of extreme precipitation.

To quantify the influence of extreme conditions of the drivers on precipitation extremes, we compute the difference between the probability associated with the cases (ii-iv) and the probability associated with the reference case under no extreme drivers (i). Statistical significance for these differences is assessed using a test based on continuity-corrected score intervals (see Method 11 in Newcombe, 1998), using R software (R Core Team, 2022), namely the function *prop.test()*; see Supplementary Method for further details.

3. Results and discussion

We begin by analyzing the estimated probability of occurrence of extreme daily precipitation when none of the three drivers (IWV, IVT, and vertical velocity) is extreme. In line with the physically-based choice of the precipitation drivers, probabilities are very low, in particular, they are smaller than or equal to 5% (the value expected under the independence of precipitation extreme occurrence from the drivers) over virtually all (>99.9%) landmasses in DJF and JJA. This result indicates that at least one of the three drivers must be extreme for daily precipitation extremes to occur. In the following subsections, we analyze the extent to which precipitation extremes occurs when one, two, or all three drivers are extreme.

3.1. Only one extreme driver

Fig. 1 shows which is the *dominant driver* of precipitation extremes over different regions, i.e. which among the three drivers being extreme in isolation maximise the probability of precipitation extremes. In general, vertical velocity is the most frequent dominant driver. IWV dominates in tropical and subtropical regions, with the exception of the central axis of the ITCZ, while IVT dominates in the regions where atmospheric rivers occur (Gimeno et al., 2016). Specifically, extreme vertical velocity dominates over 59% of global landmasses in DJF (65% in JJA), while IWV dominates over only 26% of landmasses in DJF (27% in JJA) and extreme IVT over 15% of landmasses in DJF (8% in JJA).

Fig. 2 shows the differences between the estimated probability of extreme daily precipitation when only one of the three drivers is extreme and the probability in the reference case of no extreme drivers. The absolute values of the conditional probabilities related to the three conditions in Fig. 2 are shown in Fig. S1.

In line with Fig. 1, Fig. 2 shows that the highest deviations from the reference case are found when vertical velocity is extreme, and the other two drivers are not. That is, vertical velocity is the main driver of precipitation extremes, especially over landmasses, where precipitation extremes are most impactful. Probabilities differ significantly from the reference case in most regions worldwide (Fig. 2a,b), except for the subtropical oceanic areas and some continental areas where extreme instability by itself does not guarantee the occurrence of extreme precipitation. Low probabilities are found in subtropical oceanic subsidence regions (Fig. S1a,b), which are areas with very low precipitation, with the greatest effect in the corresponding summer. In the rest of the oceanic areas, high probabilities (40%–60%) are generally observed with even higher values (60%–80%) in some areas of the Intertropical Convergence Zone (ITCZ). Over landmasses, the pattern is heterogeneous, including regions with high probabilities (40%–60%), such as the continental areas of the ITCZ, the Amazon and Congo basins, the east of the North American and Asian continents, and the interior of the European continent in summer.

Regarding the case of only extreme IVT (Fig. 2c,d) and only extreme IWV (Fig. 2e,f), the probability of precipitation extremes is also significantly different from that in the reference case in many regions. In the case of only extreme IVT, probabilities in the order of 40%–60% are found in winter in some regions affected by atmospheric rivers, such as the west coast of North America, Norway, and the east coast of Russia (Fig. S1c). Specifically, these high values mark very well atmospheric rivers' oceanic track and landfalling areas (Fig. 2c,d). The strong relationship between IVT and extreme precipitation and its link with the occurrence of atmospheric rivers has already been revealed in recent studies by Gimeno-Sotelo and Gimeno (2022, 2023). In the case of only extreme IWV, we found probabilities of 40%–60% in the entire tropical and subtropical regions (with values reaching 60%–80% locally), except for the ITCZ axis, where it is low (Fig. S1e,f). This result agrees with the recent work by Kim et al. (2022), indicating that IWV is necessary for extreme precipitation to occur in tropical regions; in extratropical regions, extreme IWV in isolation does not guarantee extreme precipitation, as additional drivers are required.

3.2. Two extreme drivers

Despite the dominant contribution of vertical velocity to precipitation extremes (Fig. 1), all drivers contribute to a certain extent to extreme precipitation (Fig. 2). Hence, the combination of two drivers in extreme conditions may enhance the occurrence of precipitation extremes. As shown in Fig. 3, the dominant combination of two drivers is extreme vertical velocity and IWV (and non-extreme IVT). Such a combination dominates over 76% of global landmasses in DJF and 78% in JJA. However, in some areas of maximum occurrence of atmospheric rivers, such as the coastal areas of western North America and Europe, the combination of extreme vertical velocity and IVT (and non-extreme IWV) dominates – this combination dominates over 17% and 16% of global landmasses in DJF and JJA, respectively.

We find that the probability of extreme daily precipitation increases greatly when two of the three drivers involved are extreme and the other is not (Figs. 4 and S2). Notably, the values of the difference of probabilities with respect to the reference case are typically higher than those associated with only one driver in extreme conditions (compare Fig. 2 with Fig. 4).

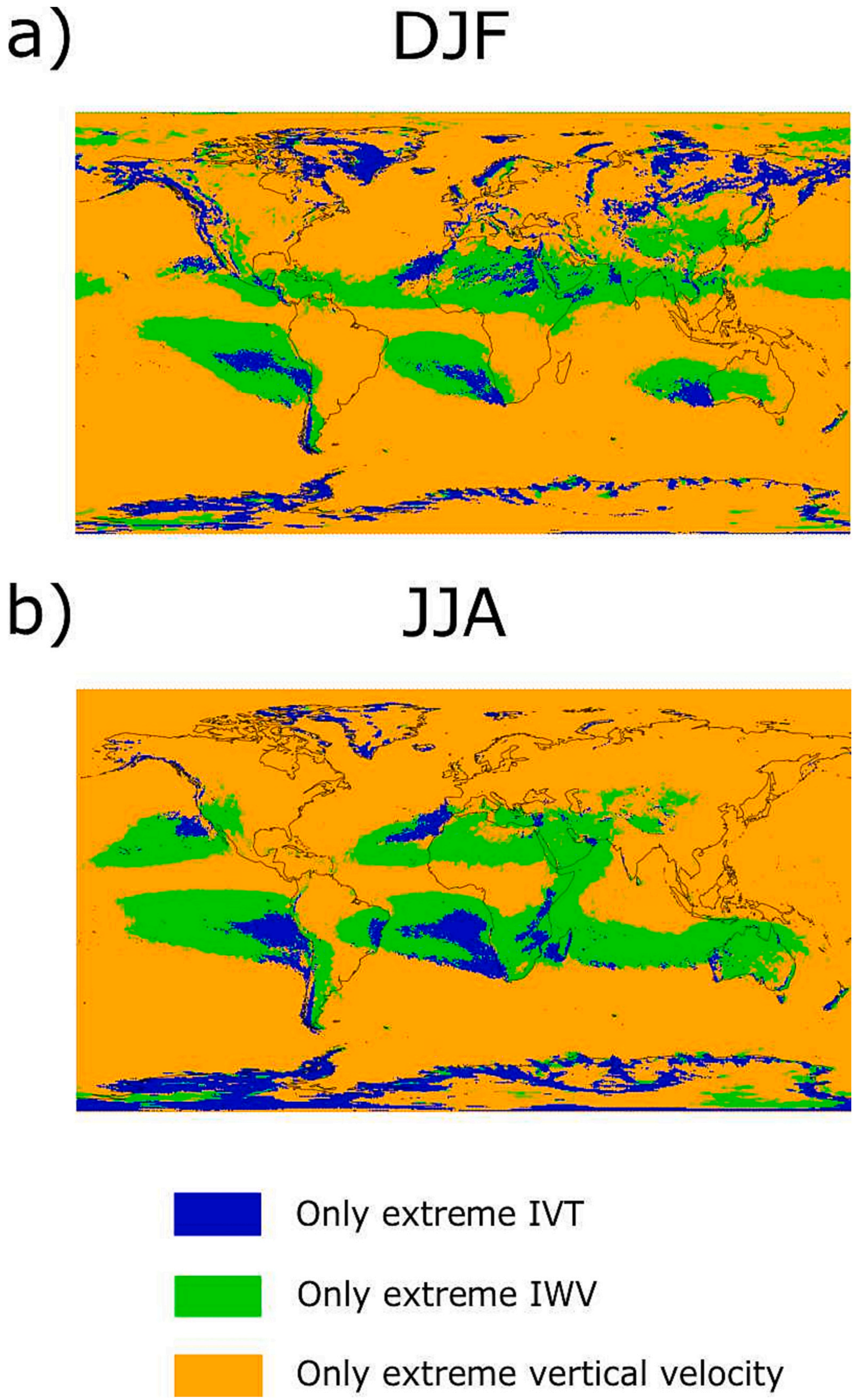

Fig. 1. Spatial pattern of the dominant driver of precipitation extremes, that is the combination of one extreme driver in isolation with the highest associated extreme precipitation probability, for a) December–February and b) June–August.

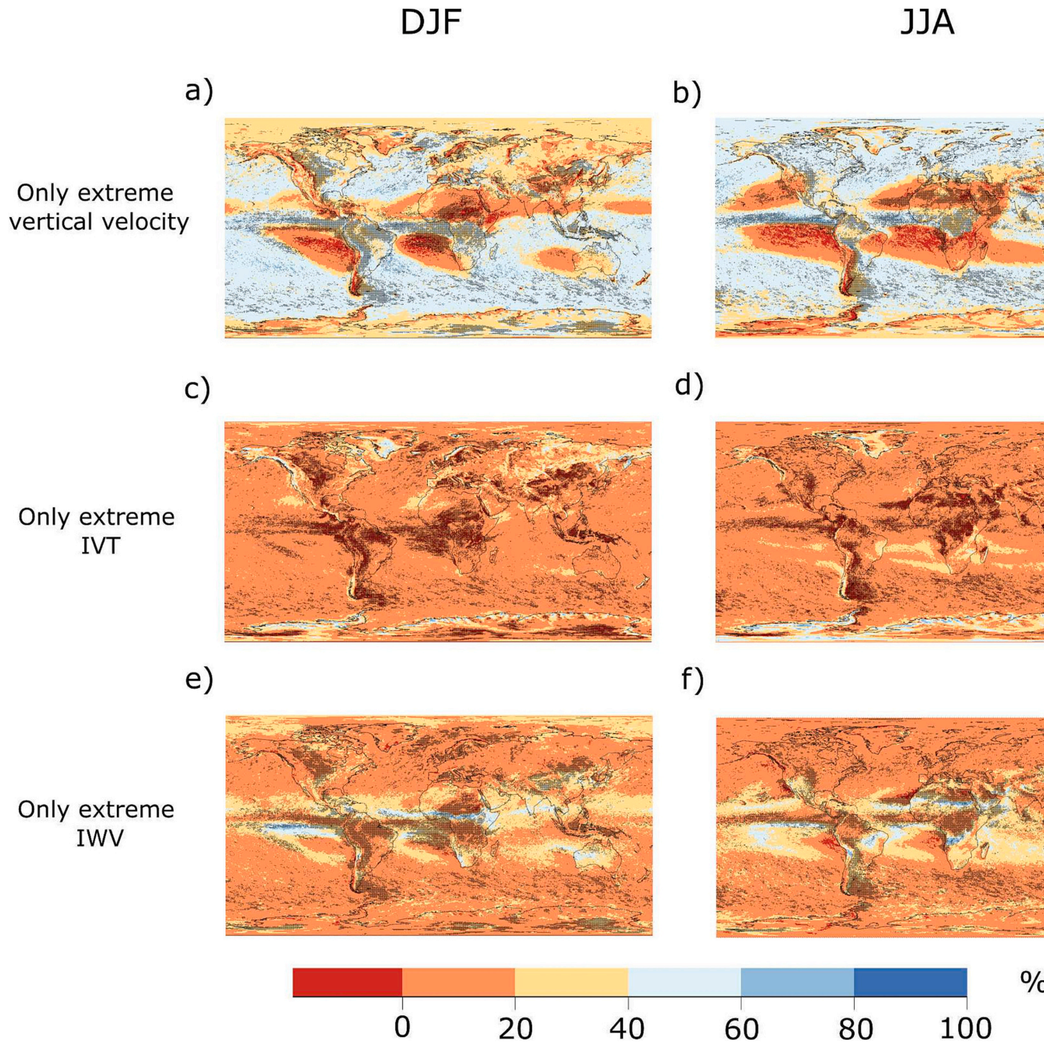

Fig. 2. Difference between the conditional probabilities of extreme precipitation for the combinations of one extreme driver in isolation and the conditional probability in the reference case, i.e. when the three drivers are not extreme. Grid points without stippling are those whose values are significantly different from 0 at 95% confidence level. a), b) Refer to the combination of only extreme vertical velocity; c), d) only extreme IVT; and e), f) only extreme IWV, for December–February and June–August, respectively.

The combination of extreme vertical velocity and IVT, under non-extreme IWV (Fig. 4a,b) leads to more areas of non-significant differences with respect to the reference case compared to the combination of extreme vertical velocity and IWV (Fig. 4c,d). These non-significant differences for the combination of extreme vertical velocity and IVT are especially remarkable over inner continental areas. Globally, the combination of extreme vertical velocity and IVT is associated with a lower probability of precipitation extremes (60–80%; see Fig. S2a,b) than the case of extreme vertical velocity and IWV (80%–100%; see Fig. S2c,d), which is the combination of two extreme drivers that leads to the highest probabilities of precipitation extremes. Accordingly, areas of low probability are also more extended in the former than in the latter situation.

In the extratropics, combined vertical velocity and IVT extremes increase the probability of precipitation extremes substantially (compared to individual extreme drivers in isolation). This indicates that atmospheric dynamics play a very important role in the genesis of precipitation extremes in the extratropics through large-scale weather systems, such as extratropical cyclones or fronts; however, they are only really relevant when there is sufficient moisture advection (IVT) to guarantee high values of moisture in the column (Gimeno et al., 2010; Kunkel et al., 2012).

Regarding the combined extremes of vertical velocity and IWV, under non-extreme IVT, probabilities are significantly different from the reference case in most regions, with the exceptions of the areas affected by subtropical anticyclones and coastal regions with high orography, e. g. north-western North America, south-western South America, and Norway (Fig. 4c,d).

The situation for the other combination of drivers, i.e. extreme IVT and IWV (and non-extreme vertical velocity), is different (Fig. 4e,f, and Fig. S2e,f). Probabilities are generally lower than in the case of the other combinations of two drivers (with most regions with values below 40%). The highest probabilities are found in the subtropics (with values between 60% and 80% in many of these areas). Subtropics are the greatest moisture sources of the planet (Gimeno et al., 2012), climatologically characterized by the strongest evaporation minus precipitation areas over the world, i.e., the highest climatological values of divergence of moisture fluxes. The situation of extremely high IVT and IWV in those regions implies the reverse of the climatological conditions, that is, the convergence of moisture fluxes. As moisture is maximum at low levels, convergence of moisture fluxes implies convergence of winds at low levels which is associated strongly in subtropical regions with atmospheric instability and consequently extreme precipitation (Mo et al., 2021). This is revealed under non-extreme vertical velocity (being high but not necessarily extreme), with probabilities of extreme precipitation being reasonably high, and is much more evident under extreme vertical

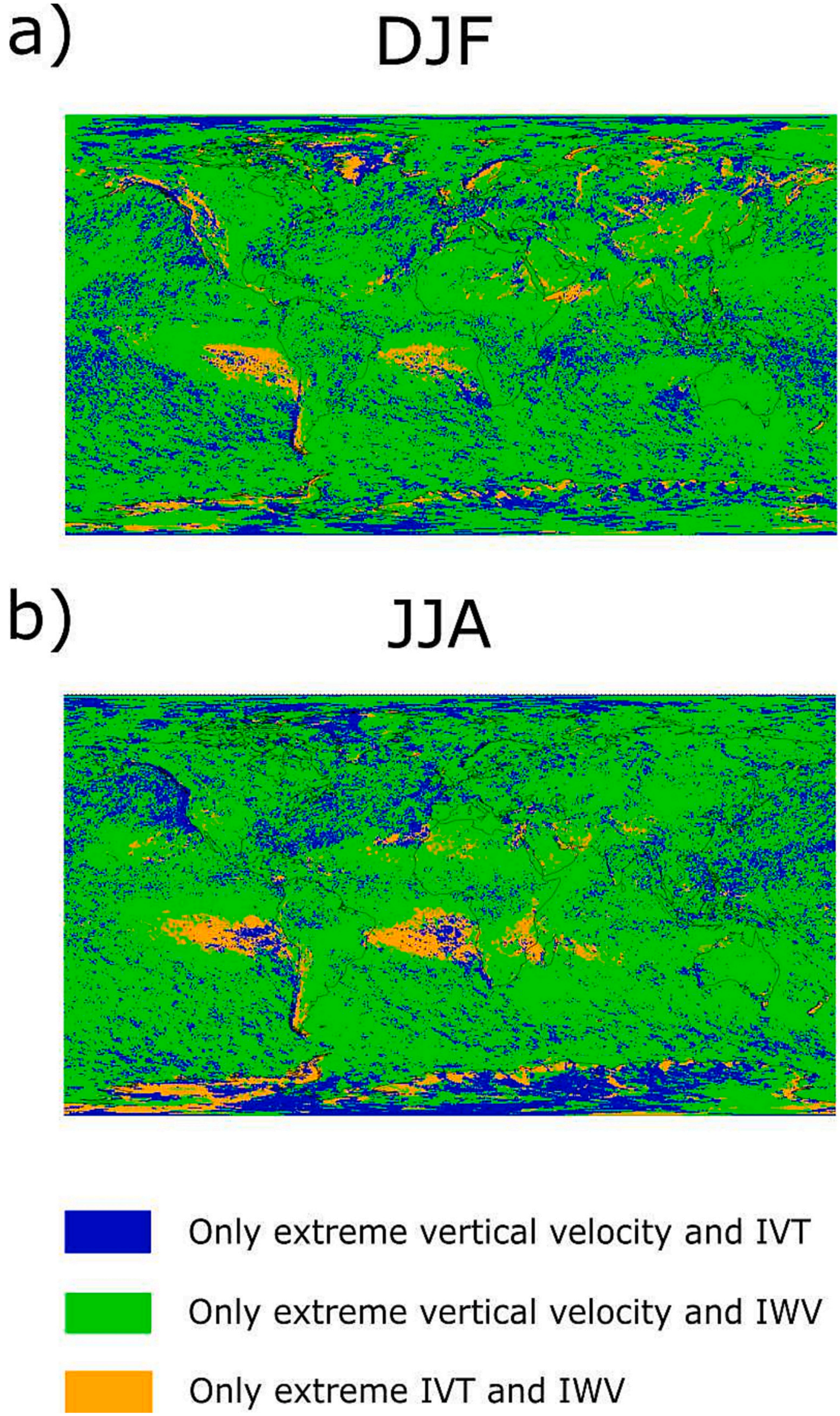

Fig. 3. Spatial pattern of the combination of two extreme drivers associated with the highest extreme precipitation probability for each grid point, for a) December–February and b) June–August.

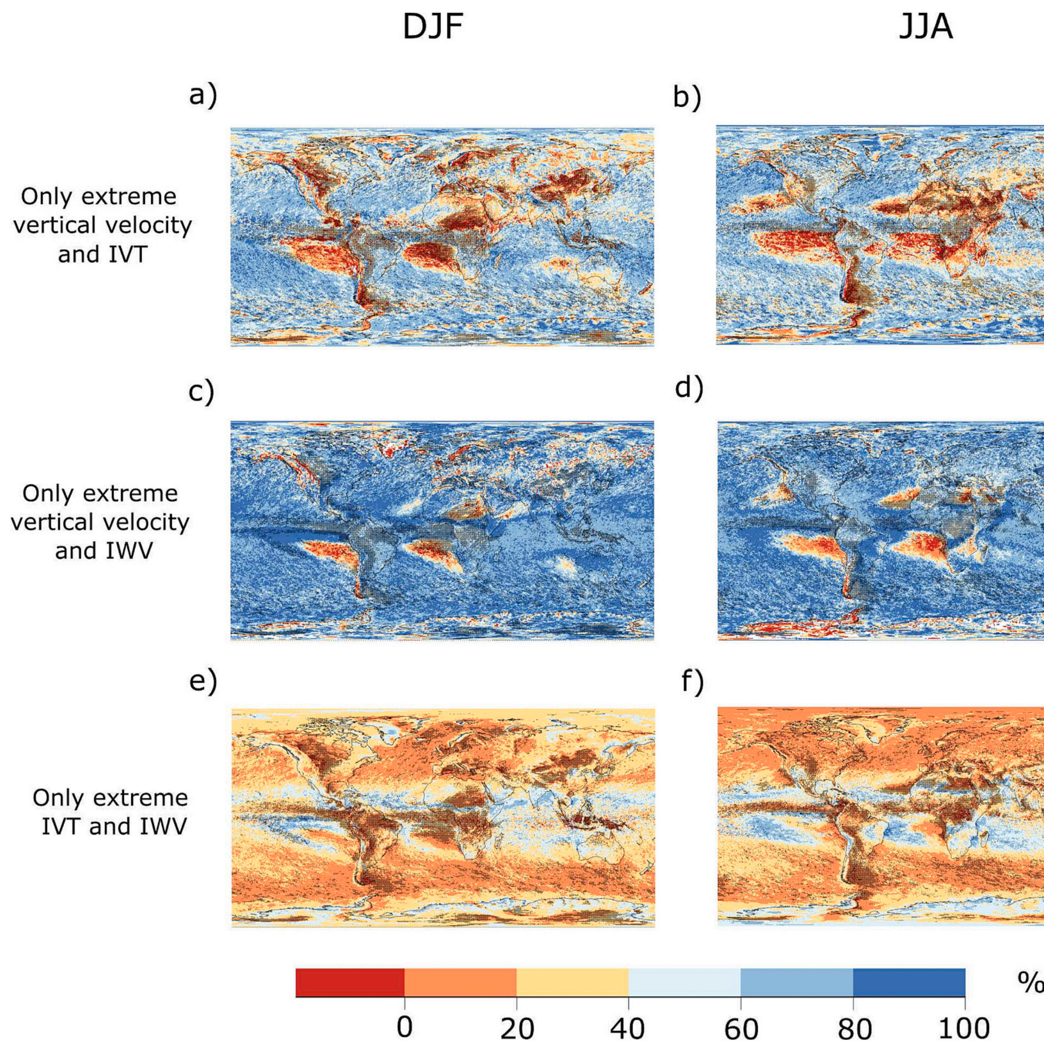

Fig. 4. Difference between the conditional probabilities of extreme precipitation for the combinations of two extreme drivers and the conditional probability in the reference case, i.e. when the three drivers are not extreme. Grid points without stippling are those whose values are significantly different from 0 at 95% confidence level. a), b) Refer to the combination of only extreme vertical velocity and IVT; c), d) only extreme vertical velocity and IWV; and e), f) only extreme IVT and IWV, for December–February and June–August, respectively.

velocity (see Subsection 3.3), with probability values between 80% and 100% in those regions.

3.3. Three extreme drivers

When the three drivers, that is, vertical velocity, IWV, and IVT, are simultaneously extreme (Figs. 5 and S3), probabilities of occurrence of extreme daily precipitation are generally between 80% and 100%. Probabilities are not statistically different from the case of no extremes only over the subtropical anticyclonic areas (areas with very low precipitation) and some regions in north-western North America, south-western South America, Scandinavia, the Mediterranean and continental areas of Eurasia.

3.4. The most relevant combination of drivers

We inspect which is the combination among all of those investigated so far that maximises the probability of precipitation extremes. Fig. 6 shows the dominant combination and how it varies as a function of latitude over landmasses. Two dominant combinations exist: (1) extreme vertical velocity and IWV (under non-extreme IVT) and (2) the three extreme drivers. Both combinations dominate over about 45% of landmasses, both in DJF and JJA. In general, the combination of the three drivers dominates in the subtropics and the combination of vertical velocity and IWV dominates elsewhere (Fig. 6b,d). This is in line with the fact that adding extreme IVT to the combination of extreme vertical velocity and IWV results in higher values of both IWV and vertical velocity in subtropics, thus increasing the chances of precipitation extremes, but not in a large part of extratropics (mainly the regions of inner American and Asian continental areas) (Fig. S4). This is in agreement with what was explained in Subsection 3.2: in the subtropics, extreme atmospheric instability is associated with low-level winds convergence, which added to extreme IVT implies an enhancement of the moisture flux convergence. Consequently, in the subtropics, under extreme IVT there is an increase in IWV and even in atmospheric instability by the thermodynamics/dynamics interplay (a higher low-level moisture is associated with higher thermodynamical instability and higher vertical velocity) (Kunkel et al., 2020a). Therefore, the combination of the three extreme drivers maximises the probability of extreme precipitation in subtropics. Regarding the regions where the combination of vertical velocity and IWV dominates (e.g. inner continental areas), they coincide with areas where it is not necessary to have extreme values of advected moisture (extreme values of IVT) for extreme precipitation to take place, as moisture comes from the soil by terrestrial sources (Gimeno et al., 2020), mainly from evapotranspiration (Miralles et al., 2016). Furthermore, in these extratropical regions atmospheric

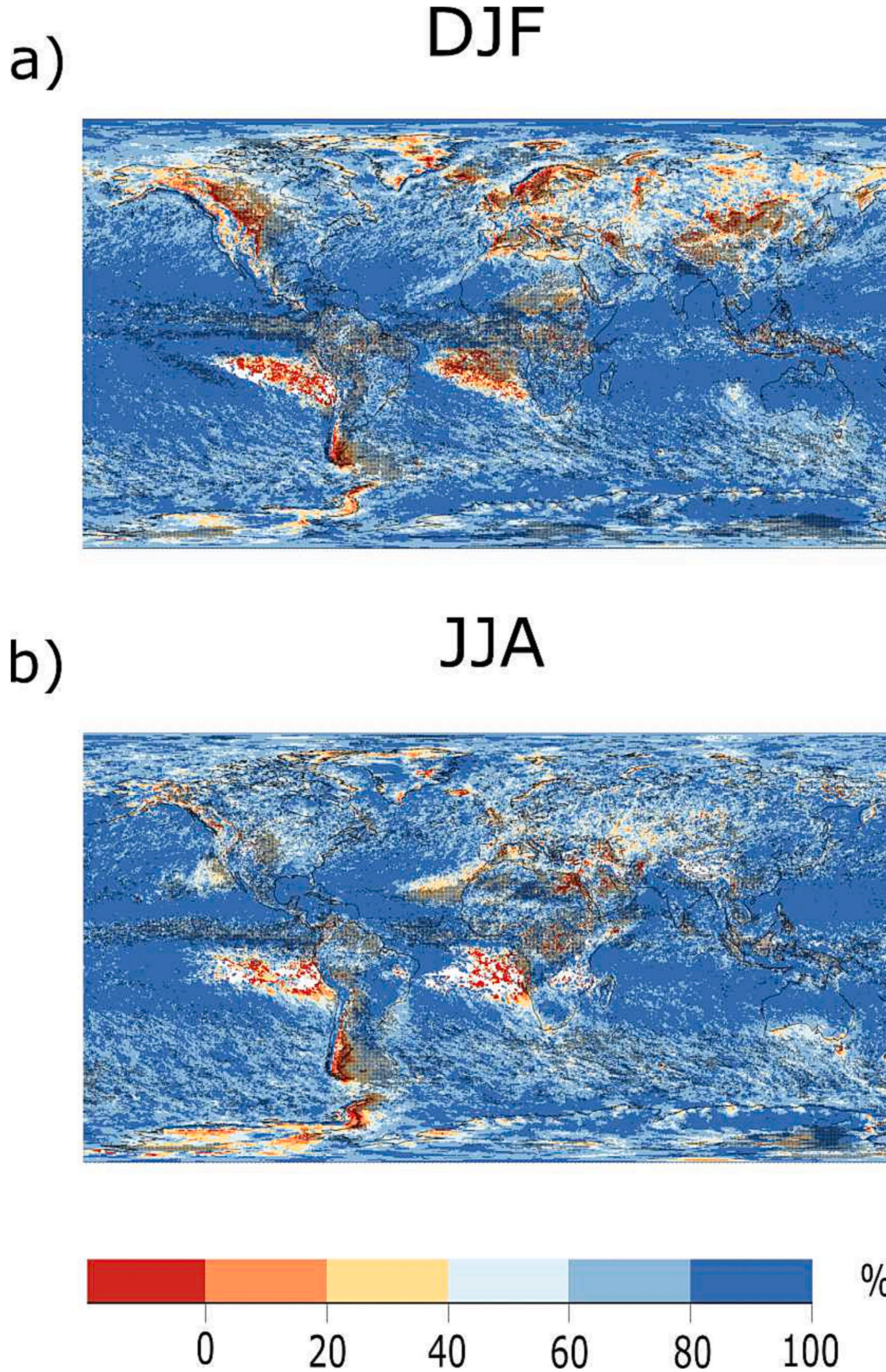

Fig. 5. Difference between the conditional probability of extreme precipitation for the case of the three extreme drivers and the conditional probability in the reference case, i.e. when the three drivers are not extreme, for a) December–February and b) June–August. Grid points without stippling are those whose values are significantly different from 0 at 95% confidence level.

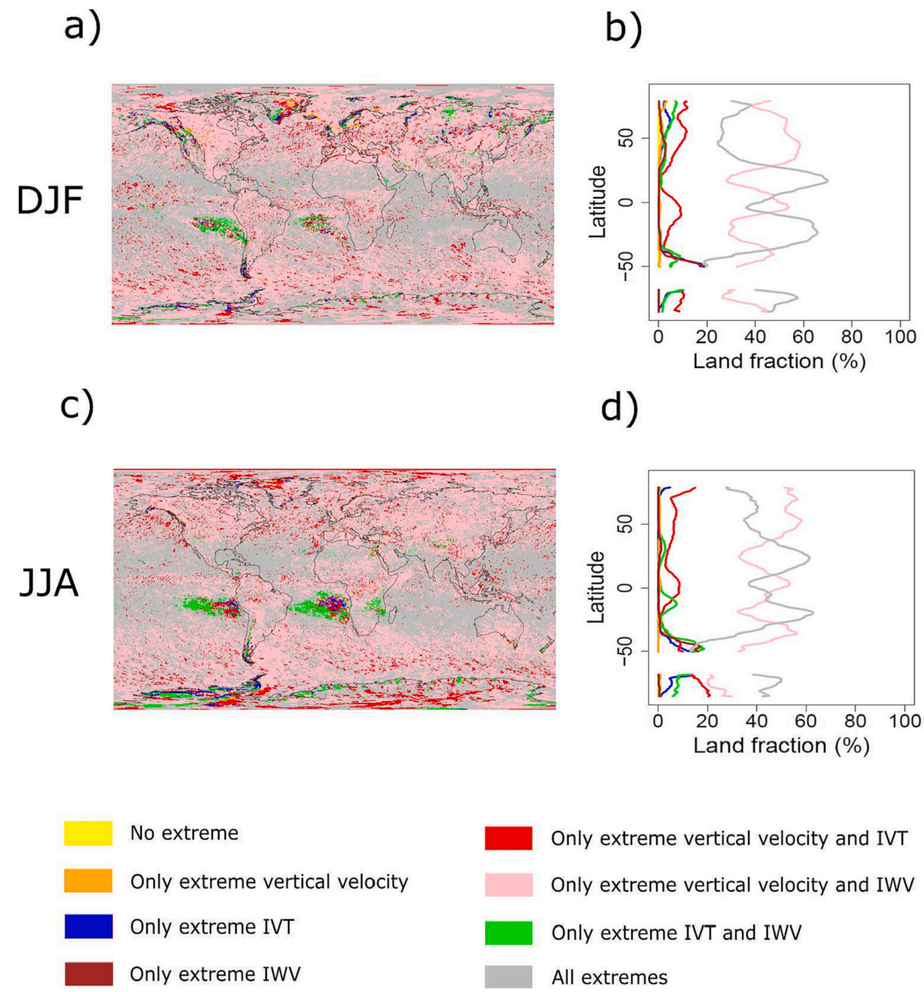

Fig. 6. a) Spatial pattern of the combination of drivers (with either one, two or three drivers in extreme conditions) associated with the highest extreme precipitation probability and b) associated latitudinal variation of the land fraction dominated by each of the combinations, for December–February. c-d) As a-b), but for June–August.

instability is dominated by baroclinic instability in which the link atmospheric instability-convergence of low-level winds is not so strong as for low latitudes, and the thermodynamics/dynamics interplay (stronger moisture-stronger atmospheric instability) is minimized because of the low moisture values. As such, there are many American and Eurasian continental regions where the combination of extreme vertical velocity and IWV (under non-extreme IVT) results in a higher probability of extreme precipitation than the combination of the three extreme drivers (Fig. 6a,c), as being evident in the values of fraction of landmasses dominated by that two-driver combination in extratropical regions of the Northern Hemisphere (Fig. 6b,d). The influence of atmospheric rivers on extreme precipitation is also observable in the predominant combination of extreme vertical velocity and IVT (and non-extreme IWV) in some coastal regions in Europe and North America in DJF, and in the dominance of the combination of the three drivers in Antarctica.

The average extreme precipitation probability under each of the conditions considered in this study is shown in Fig. S5, for the globe and for land and oceanic areas separately. Regarding landmasses, the combination of extreme vertical velocity and IWV (under non-extreme IVT) and that of the three extreme drivers are those that lead to the highest values (69% in DJF and 70% in JJA for the two-driver combination, and 67% in DJF and 72% in JJA for the three-driver one). This result highlights that focusing only on extreme vertical velocity and IWV is at least as adequate as considering the three extreme drivers (or even better in the case of DJF) when studying the drivers of extreme precipitation over land areas. The third combination in importance is the one of extreme vertical velocity and IVT (under non-extreme IWV), producing values that are substantially lower than in the previous two cases (42% of average probability over landmasses in DJF and 44% in JJA). Regarding the combinations of only one extreme driver, the case of only extreme vertical velocity clearly outperforms the other two cases, reaching an average probability of 29% over landmasses in DJF and 32% in JJA.

A further analysis was performed at the regional level, focusing on the IPCC land subregions (Fig. S6). For each subregion, we identified the dominant (second-dominant) combination as the one with the highest (second-highest) regionally averaged conditional probability of extreme precipitation (Figs. 7 and S7). The resulting dominant and second-dominant combinations are everywhere either the combination of extreme vertical velocity and IWV (under non-extreme IVT) or that of the three extreme drivers. We find that the spatial pattern of the dominant combination is the same in DJF and JJA and, in line with Fig. 6, the combination of extreme vertical velocity and IWV (under non-extreme IVT) is dominant in most extratropical regions. The three-driver combination is dominant in all the IPCC subregions included in the monsoon precipitation domain (Wang and Ding, 2008), which extends the traditional monsoon domain from Asian-Australian-west African monsoon to the North and South American monsoons and the southern African monsoon and that is related to the concept of global monsoon (Wang et al., 2023). Moreover, the three-driver combination also

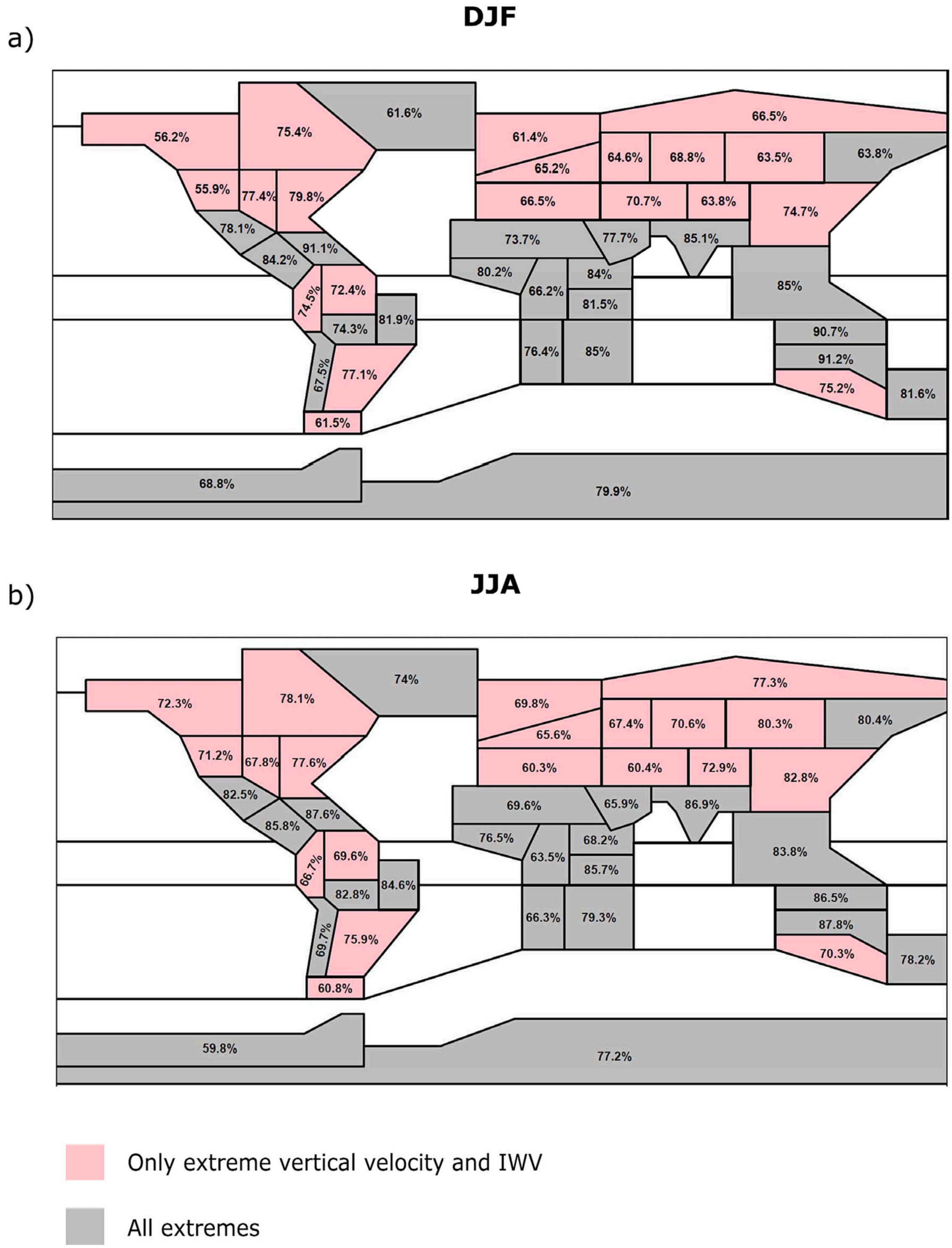

Fig. 7. Spatial pattern of the combination of drivers (with either one, two or three drivers in extreme conditions) associated with the highest average probability of extreme precipitation for each of the IPCC subregions used in this study, for a) December–February and b) June–August. For each subregion, the value of the average probability (in percentage) can be found inside its corresponding polygon.

dominates in polar regions, where extreme values of advected moisture (extreme values of IVT) are necessary for extreme precipitation to take place, as the moisture content in the air column is low because of the low temperatures. This analysis based on IPCC regions was also performed using other thresholds to define the extreme values (90th percentile and 98th percentile) and also considering two subperiods separately (1981–2000 and 2001–2020), obtaining the same spatial pattern for the dominant combination to that presented here.

4. Conclusions

In this study, the combinations of extremes of vertical velocity, total column water vapor, and horizontal moisture transport that most favor the occurrence of extreme daily precipitation on a global scale were studied. This study has some limitations associated with the quality of precipitation and water vapor column data from the reanalysis and the metric used to estimate atmospheric instability. Reanalyses are products built from a data assimilation scheme and global circulation models that ingest all available observations; however, despite the fact that ERA-5 is one of the most modern and best quality products, the quality of the precipitation data is generally low for regions with sparse observations, small-scale convective processes, and very complex orography. In this study atmospheric instability has been estimated as "-ω" at 500 hPa from the ERA5 reanalysis. This metric captures movements very well at a synoptic scale (100 to 1000 km), which includes precipitating systems linked to baroclinic instability (e.g. extratropical cyclones, fronts), but does not do so well for systems that occur on the mesoscale (10 to 100 km), in which thermodynamical instability (e.g. storms) is very relevant. For both reasons, the results of this study have greater confidence in the extratropical regions than in the tropical and main tropical rainforest regions.

These are the main conclusions of this study:

- If none of these drivers is extreme, there is virtually no chance of extreme daily precipitation. Hence, extreme values of at least one of them are required for extreme daily precipitation.
- Vertical velocity extremes alone have a greater influence on extreme daily precipitation, being associated with an average probability of 29% over landmasses in December–February and 32% in June–August. However, there are some exceptions, such as the subtropics or the regions with strong atmospheric river activity, where extreme total column water vapor alone or extreme horizontal moisture transport alone, respectively, is more advantageous for precipitation extremes.
- The combination of two extreme drivers that most influences extreme daily precipitation is that of extreme vertical velocity and total column water vapor (and non-extreme horizontal moisture transport). It leads to probabilities of extreme daily precipitation which are comparable to or even higher than those associated with the three drivers in extreme conditions (69% of average probability over landmasses in December–February and 70% in June–August for that two-driver combination; and 67% in December–February and 72% in June–August for the three-driver one). Focusing on continental regions, the combination of extreme vertical velocity and total column water vapor (and non-extreme horizontal moisture transport) is dominant in most extratropical areas, whereas that of extreme values of the three drivers is dominant in those regions included in the monsoon precipitation domain as well as in polar areas.

This study has implications for the design of process-oriented diagnostics (POD) for evaluating climate models. When designing a POD for extreme daily precipitation, it was found that the most convenient drivers to consider were vertical velocity and total column water vapor, except for some regions with high horizontal moisture transport activity. The use of only two drivers, one representing dynamic factors (vertical velocity) and the other thermodynamical factors (total column water vapor) could be useful to study the relative importance of these two factors in the current and projected extreme precipitation.

Author contributions

Luis Gimeno-Sotelo performed the analysis and generated the figures. All the authors contributed to the conceptualization, interpretation, discussions, writing and reviewing of the manuscript.

CRediT authorship contribution statement

Luis Gimeno-Sotelo: Conceptualization, Methodology, Software, Formal analysis, Writing – original draft, Writing – review & editing, Visualization. **Emanuele Bevacqua:** Conceptualization, Methodology, Writing – original draft, Writing – review & editing, Visualization, Supervision. **Luis Gimeno:** Conceptualization, Methodology, Writing – original draft, Writing – review & editing, Visualization, Supervision, Funding acquisition, Resources.

Declaration of Competing Interest

The authors declare that they have no known competing financial interests or personal relationships that could have appeared to influence the work reported in this paper.

Data availability

ERA5 reanalysis data are publicly available and can be obtained from https://cds.climate.copernicus.eu.

Acknowledgments

Luis Gimeno-Sotelo and Luis Gimeno acknowledge support from the SETESTRELO project (grant no. PID2021-122314OB-I00) funded by the Ministerio de Ciencia e Innovación, Spain. The EPhysLab group was co-funded by Xunta de Galicia, Consellería de Cultura, Educación e Universidade, under project ED431C 2021/44 "Programa de Consolidación e Estructuración de Unidades de Investigación Competitivas". Luis Gimeno-Sotelo was supported by a UVigo PhD grant ("Axudas para contratos predoutorais da Universidade de Vigo"). Emanuele Bevacqua has received funding from the European Union's Horizon 2020 research and innovation programme under grant agreement No 101003469. Luis Gimeno-Sotelo and Emanuele Bevacqua acknowledge the European COST Action DAMOCLES (CA17109). In addition, this work has been possible thanks to the computing resources and technical support provided by CESGA (Centro de Supercomputación de Galicia). Funding for open access charge: Universidade de Vigo/CISUG

Appendix A. Supplementary data

Supplementary data to this article can be found online at https://doi.org/10.1016/j.atmosres.2023.106959.

References

Allen, M.R., Ingram, W.J., 2002. Constraints on future changes in climate and the hydrologic cycle. Nature 419 (6903), 228–232. https://doi.org/10.1038/nature01092.

Bao, J., Sherwood, S.C., Alexander, L.V., Evans, J.P., 2017. Future increases in extreme precipitation exceed observed scaling rates. Nat. Clim. Chang. 7 (2), 128–132. https://doi.org/10.1038/nclimate3201.

Caretta, M.A., et al., 2022. Water. In: Pörtner, H.O., et al. (Eds.), Climate Change 2022: Impacts, Adaptation, and Vulnerability. Contribution of Working Group II to the Sixth Assessment Report of the Intergovernmental Panel on Climate Change. Cambridge University Press. In Press.

Donat, M.G., Lowry, A.L., Alexander, L.V., O'Gorman, P.A., Maher, N., 2016. More extreme precipitation in the world's dry and wet regions. Nat. Clim. Chang. 6 (5), 508–513. https://doi.org/10.1038/nclimate2941.

Douville, H., et al., 2021. Water Cycle Changes. In Climate Change 2021: The Physical Science Basis. Contribution of Working Group I to the Sixth Assessment Report of the Intergovernmental Panel on Climate Change [Masson-Delmotte, V., Et al.]. Cambridge University Press. In Press.

Emori, S., Brown, S.J., 2005. Dynamic and thermodynamic changes in mean and extreme precipitation under changed climate. Geophys. Res. Lett. 32 https://doi.org/10.1029/2005GL023272. L17706.

Gimeno, L., Nieto, R., Trigo, R.M., Vicente-Serrano, S.M., López-Moreno, J.I., 2010. Where does the Iberian Peninsula Moisture come from? An answer based on a Lagrangian approach. J. Hydrometeorol. 11 (2), 421–436. https://doi.org/10.1175/2009JHM1182.1.

Gimeno, L., Stohl, A., Trigo, R.M., Dominguez, F., Yoshimura, K., Yu, L., Drumond, A., Durán-Quesada, A.M., Nieto, R., 2012. Oceanic and terrestrial sources of continental precipitation. Rev. Geophys. 50 (4).

Gimeno, L., Nieto, R., Vázquez, M., Lavers, D.A., 2014. Atmospheric rivers: a mini-review. Front. Earth Sci. 2, 2. https://doi.org/10.3389/feart.2014.00002.

Gimeno, L., Dominguez, F., Nieto, R., Trigo, R., Drumond, A., Reason, C.J., Taschetto, A. S., Ramos, A.M., Kumar, R., Marengo, J., 2016. Major mechanisms of atmospheric moisture transport and their role in extreme precipitation events. Annu. Rev. Environ. Resour. 41, 117–141.

Gimeno, L., Nieto, R., Sorí, R., 2020. The growing importance of oceanic moisture sources for continental precipitation. Npj climate and Atmospheric. Science 3 (1), 27.

Gimeno-Sotelo, L., Gimeno, L., 2022. Concurrent extreme events of atmospheric moisture transport and continental precipitation: the role of landfalling atmospheric rivers. Atmos. Res. 278, 106356 https://doi.org/10.1016/j.atmosres.2022.106356.

Gimeno-Sotelo, L., Gimeno, L., 2023. Where does the link between atmospheric moisture transport and extreme precipitation matter? Weather Clim. Extremes 39, 100536.

Gimeno-Sotelo, L., de Zea Bermudez, P., Algarra, I., Gimeno, L., 2022. Modelling hydrometeorological extremes associated to the moisture transport driven by the Great Plains low-level jet. Stoch. Env. Res. Risk A. 1–25.

Hagos, S.M., Leung, L.R., Garuba, O.A., Demott, C., Harrop, B., Lu, J., Ahn, M., 2021. The Relationship between Precipitation and Precipitable Water in CMIP6 Simulations and Implications for Tropical Climatology and Change. J. Clim. 34 (5), 1587–1600. https://doi.org/10.1175/JCLI-D-20-0211.1.

Hersbach, H., Bell, B., Berrisford, P., Hirahara, S., Horányi, A., Muñoz-Sabater, J., Thépaut, J.N., 2020. The ERA5 global reanalysis. Q. J. R. Meteorol. Soc. 146 (730), 1999–2049.

Holton, J.R., 1973. An introduction to dynamic meteorology. Am. J. Phys. 41 (5), 752–754.

Insua-Costa, D., Senande-Rivera, M., Llasat, M.C., Miguez-Macho, G., 2022. A global perspective on western Mediterranean precipitation extremes. npj Clim. Atmos. Sci. 5, 1, 1–7. https://doi.org/10.1038/s41612-022-00234-w.

Kim, S., Sharma, A., Wasko, C., Nathan, R., 2022. Linking total precipitable water to precipitation extremes globally. Earth's. Future 10. https://doi.org/10.1029/2021EF002473 e2021EF002473.

Kunkel, K.E., Easterling, D.R., Kristovich, D.A.R., Gleason, B., Stoecker, L., Smith, R., 2012. Meteorological causes of the secular variations in observed extreme precipitation events for the conterminous United States. J. Hydrometeorol. 13 (3), 1131–1141. http://www.jstor.org/stable/24914694.

Kunkel, K.E., Stevens, S.E., Stevens, L.E., Karl, T.R., 2020a. Observed climatological relationships of extreme daily precipitation events with precipitable water and vertical velocity in the contiguous United States. Geophys. Res. Lett. 47 https://doi.org/10.1029/2019GL086721 e2019GL086721.

Kunkel, K.E., Karl, T.R., Squires, M.F., Yin, X., Stegall, S.T., Easterling, D.R., 2020b. Precipitation Extremes: Trends and Relationships with Average Precipitation and Precipitable Water in the Contiguous United States. J. Appl. Meteorol. Climatol. 59 (1), 125–142. https://doi.org/10.1175/JAMC-D-19-0185.1.

Miralles, D.G., Nieto, R., McDowell, N.G., Dorigo, W.A., Verhoest, N.E., Liu, Y.Y., Teuling, A.J., Dolman, A.J., Good, S.P., Gimeno, L., 2016. Contribution of water-limited ecoregions to their own supply of rainfall. Environ. Res. Lett. 11 (12), 124007.

Mo, R., So, R., Brugman, M.M., Mooney, C., Liu, A.Q., Jakob, M., Castellan, A., Vingarzan, R., 2021. Column relative humidity and primary condensation rate as two useful supplements to atmospheric river analysis. Water Resour. Res. 57 (11) e2021WR029678.

Neelin, J.D., Martinez-Villalobos, C., Stechmann, S.N., Ahmed, F., Chen, G., Norris, J.M., Kuo, Y.H., Lenderink, G., 2022. Precipitation Extremes and Water Vapor. Curr. Clim. Chang. Rep. 1 (8), 17–33, 2022 8.

Newcombe, R.G., 1998. Interval estimation for the difference between independent proportions: comparison of eleven methods. Stat. Med. 17 (8), 873–890.

Nie, J., Sobel, A.H., Shaevitz, D.A., Wang, S., 2018. Dynamic amplification of extreme precipitation sensitivity. Proc. Natl. Acad. Sci. 115, 9467–9472.

O'Gorman, P.A., 2015. Precipitation extremes under climate change. Curr. Clim. Change Rep. 1 (2), 49–59. https://doi.org/10.1007/s40641-015-0009-3.

Payne, A.E., Demory, M.E., Leung, L.R., Ramos, A.M., Shields, C.A., Rutz, J.J., Ralph, F. M., 2020. Responses and impacts of atmospheric rivers to climate change. Nat. Rev. Earth Environ. 1 (3), 143–157.

Pfahl, S., O'Gorman, P., Fischer, E., 2017. Understanding the regional pattern of projected future changes in extreme precipitation. Nat. Clim. Chang. 7, 423–427. https://doi.org/10.1038/nclimate3287.

R Core Team, 2022. R: A Language and Environment for Statistical Computing. R Foundation for Statistical Computing, Vienna, Austria. https://www.R-project.org/.

Roderick, T.P., Wasko, C., Sharma, A., 2019. Atmospheric moisture measurements explain increases in tropical rainfall extremes. Geophys. Res. Lett. 46, 1375–1382. https://doi.org/10.1029/2018GL080833.

Roderick, T.P., Wasko, C., Sharma, A., 2020. An improved covariate for projecting future rainfall extremes. Water Resour. Res. 56 https://doi.org/10.1029/2019WR026924 e2019WR026924.

Seneviratne, S.I., et al., 2021. Weather and climate Extreme events in a changing climate. In: Masson-Delmotte, V., et al. (Eds.), Climate Change 2021: The Physical Science Basis. Contribution of Working Group I to the Sixth Assessment Report of the Intergovernmental Panel on Climate Change. Cambridge University Press (In Press).

Soden, B.J., Held, I.M., 2006. An assessment of climate feedbacks in coupled ocean-atmosphere models. J. Clim. 19 (23) https://doi.org/10.1175/JCLI9028.1, 6263–3360.

Sun, Q., Zhang, X., Zwiers, F., Westra, S., Alexander, L.V., 2021. A global, continental, and regional analysis of changes in extreme precipitation. J. Clim. 34 (1), 243–258. https://doi.org/10.1175/jcli-d-19-0892.1.

Trenberth, K.E., Dai, A., Rasmussen, R.M., Parsons, D.B., 2003. The changing character of precipitation. Bull. Am. Meteorol. Soc. 84 (9), 1205–1218.

Wang, B., Ding, Q., 2008. Global monsoon: Dominant mode of annual variation in the tropics. Dyn. Atmos. Oceans 44 (3–4), 165–183.

Wang, B., Jin, C., Liu, J., 2023. Global monsoon: Concept and dynamic response to anthropogenic warming. MAUSAM 74 (2), 493–502.

Westra, S., Fowler, H.J., Evans, J.P., Alexander, L.V., Berg, P., Johnson, F., et al., 2014. Future changes to the intensity and frequency of short-duration extreme rainfall. Rev. Geophys. 52, 522–555. https://doi.org/10.1002/2014RG000464.

Zhu, Y., Newell, R.E., 1998. A proposed algorithm for moisture fluxes from atmospheric rivers. Mon. Weather Rev. 126 (3), 725–735.

4.4 The influence of contribution deficits from oceanic and terrestrial origin and major global moisture sources on drought occurrence

The fourth article of this chapter is entitled "**Unravelling the origin of the atmospheric moisture deficit that leads to droughts**" by **Gimeno-Sotelo, L.**, Sorí, R., Nieto, R., Vicente-Serrano, S. M., & Gimeno, L., and was published in the journal *Nature Water* in 2024.

nature water

Article

https://doi.org/10.1038/s44221-023-00192-4

Unravelling the origin of the atmospheric moisture deficit that leads to droughts

Received: 11 May 2023

Accepted: 21 December 2023

Published online: 6 February 2024

Check for updates

Luis Gimeno-Sotelo [1], Rogert Sorí [1], Raquel Nieto [1], Sergio M. Vicente-Serrano [2] & Luis Gimeno [1]

Drought is one of the most catastrophic natural hazards, and precipitation plays a major role in the development and intensification of drought events. The amount of precipitation resulting from humidity transported from a given moisture source can be key in revealing the origin of the atmospheric moisture deficit underlying drought occurrence. Here this study demonstrates, for the first time, the predominant role of moisture transport deficit in drought genesis. In most land areas, the estimated conditional probability of drought given an equivalent moisture deficit received either from the ocean or from the continents is higher than 10%. This probability is over 15% in the regions where the main atmospheric moisture transport mechanisms are active and over 20% in some hotspot regions, such as central-east North America, south-east South America and east Europe, where lower incoming moisture is almost synonymous with drought occurrence. Our results indicated that the contribution deficit of the dominant moisture source to the precipitation of a region could improve the predictability of droughts, with enormous hydrological, socioeconomic and environmental implications.

Droughts are the main natural hazard on a planetary scale, responsible for 650,000 deaths from 1970 to 2019[1], billion-dollar economic losses[2] and ecosystem impacts[3]. Despite being very complex phenomena that involve several aspects of the hydrological cycle, with several connections to ecosystem processes and water management[4–8], the main driving factor of droughts is a precipitation deficit compared with normal conditions[9,10]. This deficit can essentially occur for three reasons: because there is less moisture available for precipitation, because there is less atmospheric instability that forces air to rise, or a simultaneous occurrence of both. The relationship with moisture content may vary between different locations and seasons depending on the horizontal and temporal scale analysed, with the importance of instability usually being greater than the importance of moisture content, with the exception of its influence on extreme precipitation[11,12], where the humidity content is more important than instability. This is why, traditionally, there have been studies on meteorological and climatic conditions that do not favour instability mechanisms and therefore favour the occurrence of droughts (for example, Trenberth et al.[13]).

One major reason for the lower influence of the moisture content than the instability is the fact that it is not possible to determine how much water vapour is involved in precipitation simply from the amount of water vapour in an air column at any given time. The local humidity existing in an air column is mostly insufficient for generating precipitation[14], and lower humidity levels available for precipitation (local and advected) generally imply a deficit in the moisture that reaches the site in question. Therefore, moisture transport deficits generally lead to drought occurrence[15]. In this Article, this physical dependence between moisture transport and precipitation is the baseline for studying the statistical relationships between droughts and moisture source contribution deficits.

Atmospheric humidity that causes precipitation in a region can have two origins: (1) direct transport from the ocean or (2) subsequent recycling from the continents themselves[16–18]. The processes that control evaporation over oceans or continents and moisture transport are very different; additionally, there is a variable relationship between the oceanic and terrestrial origins of precipitation, both globally and

[1]Centro de Investigación Mariña, Environmental Physics Laboratory, Universidade de Vigo, Ourense, Spain. [2]Instituto Pirenaico de Ecología, Consejo Superior de Investigaciones Científicas, Zaragoza, Spain. e-mail: l.gimeno@uvigo.es

regionally[19]. The main sources of humidity are those regions where evaporation greatly exceeds precipitation, which mainly occurs in subtropical oceans, some quasi-inland seas (Mediterranean and Red seas), and the two terrestrial areas known as green oceans—the Amazon and Congo river basins[20].

The locations where the humidity coming from the entire ocean or continent precipitates have been previously reported[19], as well as the sinks of the humidity that originates from these large individual sources[20]. The effects of anomalous moisture transport on droughts in specific regions (for example, Drumond et al.[21])—even in those that are very remote from moisture sources—have also been studied[22], as well as the effect of variables closely related to the balance of evaporation and precipitation such as the sea surface salinity (for example, Rathore et al.[23]). However, the probability of drought occurrence under a given deficit in moisture transported from global oceanic and terrestrial areas and each of these major sources has not been fully evaluated globally. Understanding the relationship between drought and moisture deficit propagation in the atmosphere would provide a window of opportunity to predict precipitation deficits that has not been explored yet. Lagrangian approaches[19,24] that analyse moisture transport are highly promising for assessing this issue because they may estimate how much precipitation can be attributed to moisture arriving from a source and reveal the origin of the atmospheric moisture deficit underlying the occurrence of droughts. Applying this approach, we have quantified the extent to which moisture transport affects droughts on a global scale, considering both the entire oceanic and terrestrial areas as moisture sources as well as the major individual sources on the planet. Moreover, we have found that, in some world regions, the contribution deficit of the dominant moisture source may have predictive potential for drought occurrence.

Moisture deficit from ocean versus land triggering droughts

Using monthly values of precipitation and moisture source contributions to precipitation from a given source region, we apply techniques from copula theory to estimate the conditional probability of drought occurrence given an equivalent moisture source contribution deficit, that is, using the same threshold in standardized units for the definition of both phenomena (see Methods for details). A moisture source contribution deficit refers to a deficit of the moisture in the sink region as a consequence of a moisture transport deficit from a given source, understood as a transport of humidity from a given source to a given sink of a lower value than the usual (climatological). The moisture source contributions were estimated by Lagrangian techniques on the basis of tracking the positions and changes of specific humidity of all the particles that reach a given grid element and is in line with a set of different methodologies with similar Lagrangian foundations, very successfully used in the last two decades (for example, Stohl and James[25], van der Ent et al.[17], Tuinenburg et al.[26] and Dey et al.[27]).

If we account for the contribution of the whole oceanic global area and the whole terrestrial global area, we find that the conditional probability of drought occurrence given a moisture deficit from oceanic or terrestrial origin can be substantially different (Fig. 1 and Supplementary Figs. 1 and 2). It can reach values over two ($P \times 2$), three ($P \times 3$), four ($P \times 4$) or five ($P \times 5$) times greater than 5%, which is the conditional probability that indicates that drought occurrence and moisture transport deficit are independent, meaning that in that situation a moisture source contribution deficit does not have any influence on drought occurrence. Figure 1 is the representation of those spatial patterns ($P \times 2$, $P \times 3$, $P \times 4$ and $P \times 5$), which show the regions where a moisture deficit from oceanic or terrestrial origin is strongly associated with drought occurrence on an annual scale.

The $P \times 2$ pattern is very similar to that of the percentage contribution to precipitation of oceanic and terrestrial origins (see Fig. 2c in Gimeno et al.[19]). Regions where the oceanic origin of precipitation is dominant experience higher drought probabilities given a moisture contribution deficit from the global oceanic area (Fig. 1a,c); similarly, in regions where the terrestrial component dominates, moisture contribution deficits from the global terrestrial area lead to higher drought probabilities (Fig. 1b,d). When analysing the terrestrial origin of precipitation, it is observed that the continental area where drought occurrence is influenced by the moisture deficit from terrestrial origin is very large, including almost the whole Eurasian continent, America and a large part of Africa and Australia. This highlights the importance of recycling processes in drought occurrence[28] given the high level of land evapotranspiration in continental regions[29,30]. The spatial pattern is very similar, regardless of whether drought is defined with monthly or seasonal Standardized Precipitation Index (SPI1 or SPI3, respectively) values. Moreover, a similar spatial pattern between time scales can also be identified when the threshold is changed according to the higher probabilities $P \times 3$, $P \times 4$ and $P \times 5$.

As the conditional probability of drought increases ($P \times 3$ and $P \times 4$), the areas become more restricted, and the patterns reveal the regions where the main activity of moisture transport mechanisms takes place at a planetary scale[15,31]. For instance, the role of atmospheric rivers (ARs) in the oceanic origin of drought can be observed in areas in which precipitation is dominated by this phenomenon (for example, western coasts of North America and Europe)[32]. Moreover, the roles of tropical cyclones (TCs) in the oceanic origin of drought (for example, the eastern coast of North America) and that of low-level jets (LLJs) in the oceanic origin of drought in northern South America or in the terrestrial origin in the La Plata basin, whose main moisture source is the Amazon basin, are visible[33,34]. In regions with no major moisture transport mechanisms, such as the interior of the Eurasian continent, the influence of recycling and propagation between terrestrial sources and sinks has been observed in drought development[35]. Terrestrial evapotranspiration changes are expected as a consequence of anthropogenic forcing[36]. Further, key variations in the position and intensity of moisture transport mechanisms, including an increase in the intensity and poleward displacement of ARs[37], changes in the frequency, intensity and position of some LLJs[38] and a reduction in the frequency of TCs[39] is also expected. These changes have implications for the future occurrence and intensity of droughts in the regions indicated by $P \times 3$ and $P \times 4$.

There are some hotspot regions where the conditional probability of drought occurrence, given an equivalent deficit in moisture transported from oceanic or terrestrial sources, is considerably high, with values in the $P \times 5$ category. Considering a SPI at a time scale of 1 month, these areas can be identified in the Pacific and Atlantic coasts of North America, Western Europe and south-eastern China, with a moisture deficit of oceanic origin, and the interior of Eurasia and La Plata basin in South America when the origin is terrestrial. When the drought time scale is increased to 3 months, for the moisture deficit of terrestrial origin, the hotspot regions also include the north American Great Plains and some areas of inner China, southern Africa and Australia.

This influence of the oceanic or terrestrial origin of moisture on the genesis of droughts can be altered by changes in the atmospheric general circulation. Since a global estimate is difficult to achieve with the methodology used in this work, we can get closer to knowing if these are very relevant by quantifying the changes associated with two modes of climate variability that generate important changes in global circulation, namely the El Niño/Southern Oscillation, due to its global effect, and the North Atlantic Oscillation for its regional effects in the North Atlantic. The obtained patterns for the different mode phases (Supplementary Figs. 3 and 4) are not very different except for some slight displacements of the regions where the highest probability values occur and some intensifications of the probabilities in known regions of influence of these modes on precipitation occurrence[40,41]. As such, a greater extent of the importance of both oceanic and terrestrial sources in the genesis of drought is generally observed for the negative

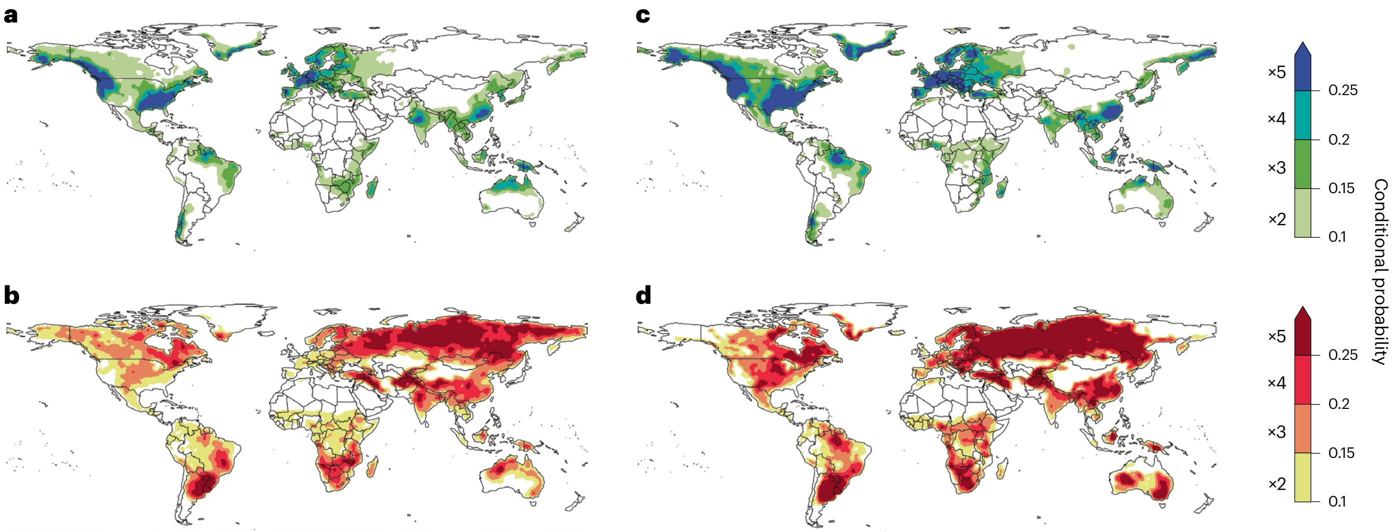

Fig. 1 | Conditional probability of drought occurrence given an equivalent moisture deficit from oceanic or terrestrial origin on an annual scale. **a**–**d**, Moisture deficit from oceanic origin for SPI time scales of 1 month (**a**) and 3 months (**c**) and from terrestrial origin for SPI time scales of 1 month (**b**) and 3 months (**d**). Probability is expressed as how many times greater it is than that of the independence case (5%), together with the corresponding values. Statistical method I was applied to the contribution to precipitation of oceanic and terrestrial origins (see Methods for details). A Gaussian filter was used to remove the spatial random noise (original values can be found in Supplementary Figs. 1a,d and 2a,d).

phase of El Niño/Southern Oscillation in comparison with the positive one, and of the oceanic source in the positive phase of North Atlantic Oscillation compared with the negative one.

Moisture deficit from major sources leading to droughts

Once the oceanic or terrestrial origin of the moisture deficit that generates drought is revealed, it is also possible to know the major planetary moisture source responsible for this deficit. Considering the conditional probability of drought given an equivalent moisture deficit from the major planetary moisture sources on an annual scale (Fig. 2), the spatial pattern of the regions where each moisture source is most influential in terms of droughts is similar to that regarding precipitation occurrence (see Fig. 4 in Gimeno et al.[20]) and extreme precipitation (see Fig. 5a in Vázquez et al.[24]). A detailed analysis of the conditional probability of drought given a deficit from each of these major moisture sources shows noticeable spatial differences and well-delineated regions of influence, as well as some seasonal differences mainly evidenced in the extension of the sinks (Supplementary Figs. 5–17).

Overall, there is a good match between relevant continental areas identified in Figs. 1 and 2, with the main discrepancies observed in southern Africa and large sectors of Asia. That is so because Fig. 1 accounts for the whole oceanic source and the whole terrestrial source, whereas Fig. 2 only accounts for major oceanic sources and the two major terrestrial ones, the Amazon and Congo basins. It does not include other minor oceanic sources and all terrestrial sources except for the two major ones, which implies the non-inclusion of recycling in all regions with the exception of the Amazon and Congo basins. The North Pacific source has the greatest influence on drought occurrence in the western half of North America and the eastern Asian coast, the Caribbean and Gulf of Mexico sources in the eastern half of North America, the North Atlantic source in Western Europe and northeastern South America, the Mediterranean source holds the main influence over the inner Eurasian continent, while the South Pacific and South Atlantic sources hold moderate influence over some coastal regions of South America, South East Asia and Southern Africa. Finally, the Indian sources are the main influence on drought occurrence in continental monsoon regions (Fig. 2). Thus, drought occurrence in most regions of the Indian subcontinent is mainly influenced by moisture deficits from the northwestern Indian source region; called in these works the Zanzibar Current and Arabian Sea. Additionally, droughts in Australia are mainly affected by a moisture deficit from the central-eastern Indian source. The two terrestrial sources have influence over their own basins and surrounding areas, which are very extended and intense for the Amazon and less extended for the Congo. In general, the extent and magnitude of the influence of the moisture deficit from major moisture sources is greater under a 3 month time scale than under a 1 month time scale.

This general pattern and the probability values could be altered by a very diverse set of factors, such as changes in the extent and position of the sources or changes in the temperature contrast between the continental sink and the oceanic source with variations in the relative humidity in the continental sink. The first of these effects cannot be appreciated in this paper since the methodology used implies the use of the main climatological sources (Methods), but the influence of the second one can be estimated to a certain extent. The land–ocean temperature contrast may play a role since the ocean temperature sets the saturation specific humidity such that it is not able to maintain relative humidity levels when supplying much warmer land (for example, Byrne and O'Gorman[42] and Wainwright et al.[43]). For each oceanic moisture source, we have calculated the conditional probability of drought in the continental area where it is dominant, according to Fig. 2a, given an equivalent moisture transport deficit from that source for two subsamples: high land–ocean temperature contrast and low land relative humidity versus low land–ocean temperature contrast and high land relative humidity (Supplementary Table 1). It is expected that, in the case of high temperature contrast between the continental sink and the oceanic source occurring together with low relative humidity in the continental sink, the role of the oceanic source in the precipitation of the land sink decreases. Thus, in that situation, the contribution of moisture from the continental sink region itself by evapotranspiration due to the high evaporative demand would have a greater relevance[35], and it can be expected that the probability of drought given a moisture transport deficit from the source will be lower than in the case of low temperature contrast and high relative humidity. Among the 11 oceanic moisture sources considered in this study, the results confirmed what

https://doi.org/10.1038/s44221-023-00192-4

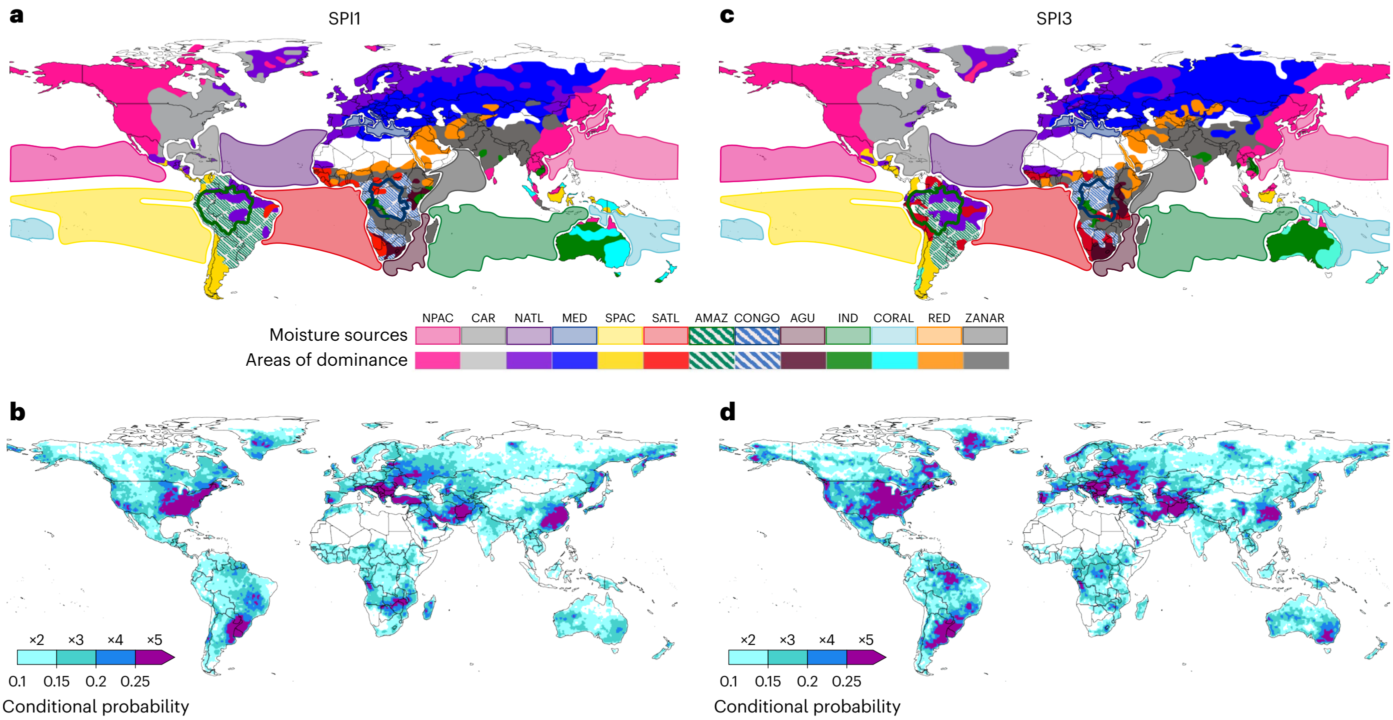

Fig. 2 | Moisture source with the highest associated conditional probability of drought given an equivalent moisture deficit from the major planetary moisture sources (both oceanic and terrestrial), together with the associated probability, on an annual scale. a–**d**, The spatial pattern of the dominant moisture source for SPI at 1 month (**a**) and 3 month (**c**) time scales and the associated probability for SPI at 1 month (**b**) and 3 month (**d**) time scales. Probability is expressed as how many times greater it is than that of the independence case (5%), together with the corresponding values. Statistical method I was applied to the contribution to precipitation of each of the major moisture sources (see Methods for details). NPAC, North Pacific Ocean moisture source; CAR, Caribbean Sea and Gulf of Mexico; NATL, North Atlantic Ocean; MED, Mediterranean Sea; SPAC, South Pacific Ocean; SATL, South Atlantic Ocean; AMAZ, Amazon River basin; CONGO, Congo River basin; AGU, Agulhas Current region; IND, Indian Ocean; CORAL, Coral Sea; RED, Red Sea; ZANAR, Zanzibar Current and Arabian Sea region. Oceanic moisture source regions are coloured with a light shading, and the land areas where each moisture source is dominant are represented by a dark shading. For the Amazon and Congo river basins, they are delimited by solid green and blue lines, and their areas of dominance are represented by oblique lines of those colours, respectively. A Gaussian filter is used to facilitate visualization.

is stated above, finding significant differences in this sense for eight of the sink regions.

Figure 3 focuses on those regions with a high conditional probability ($P \times 3$ and $P \times 4$) of drought occurrence given an equivalent moisture deficit from those major moisture sources on an annual scale. Most areas with $P \times 3$, $P \times 4$ and $P \times 5$ found in Fig. 1 appear, and it is now possible to identify the moisture source regions responsible for the transport deficit. Occasionally, drought occurrence is influenced by the deficit from a single source, such as the North Pacific source for drought conditions in western North America. However, in other cases, multiple sources are responsible, as in the case of eastern North America, with up to three sources influencing droughts in that region: the North Atlantic, North Pacific and Caribbean/Mexican sources. The probability of suffering droughts at time scales of 1 and 3 months when there are deficits in a single moisture source is over four times greater than that of the independence case in three large continental areas (Fig. 3b,d): central-east North America (CENA), associated with a moisture deficit from the Caribbean/Mexican source, south-east South America (SESA), associated with the Amazon source and east Europe (EEur), associated with the Mediterranean source.

Potential of moisture transport in drought predictability

Even with the extraordinary advance of weather and climate models largely linked to the great advance in computing, and better observations and modelling abilities, droughts are very difficult to predict[44], mainly because of the limited predictability of precipitation over time spans longer than 15 days[45]. Thus, seasonal to annual precipitation deficit predictions, which are relevant for drought prediction, are highly uncertain, particularly at mid-latitudes[46,47]. Therefore, and based on the use of models, whether they are weather or climate ones, it could be more advantageous to use predicted moisture transport than predicted precipitation to estimate the predicted occurrence of droughts in the same given future period. The reason for this is that models are able to predict large-scale circulation much better than smaller-scale phenomena, and taking into account that moisture transport is related to larger-scale circulation, it can be assumed that its predictability will be better than in the case of precipitation, which is more conditioned to more complex and smaller-scale atmospheric processes[48]. For medium-range (submonthly) time scales, Lavers et al.[49] demonstrated that integrated vertical moisture transport (a measure of moisture transport) was more predictable than precipitation in northwestern Europe and the western US, and the results obtained by Gvoždíková and Müller[50] for Central Europe are in line with it. For seasonal time scales, Wang and Yuan[51] for China's Yangtze River basin and Gao et al.[52] for the Northern Hemisphere also show the greater predictability of moisture transport. In this study, we show that the moisture transport deficit may affect drought severity in large world regions. Therefore, in regions where moisture transport deficits are strongly related to precipitation deficits, droughts could be potentially predicted on the basis of moisture transport. Figure 4 shows the conditional probability of drought given the observed values of moisture contribution deficits from the main moisture source of each of the three hotspot regions previously discussed, that is, CENA, SESA and EEur. Each of these three

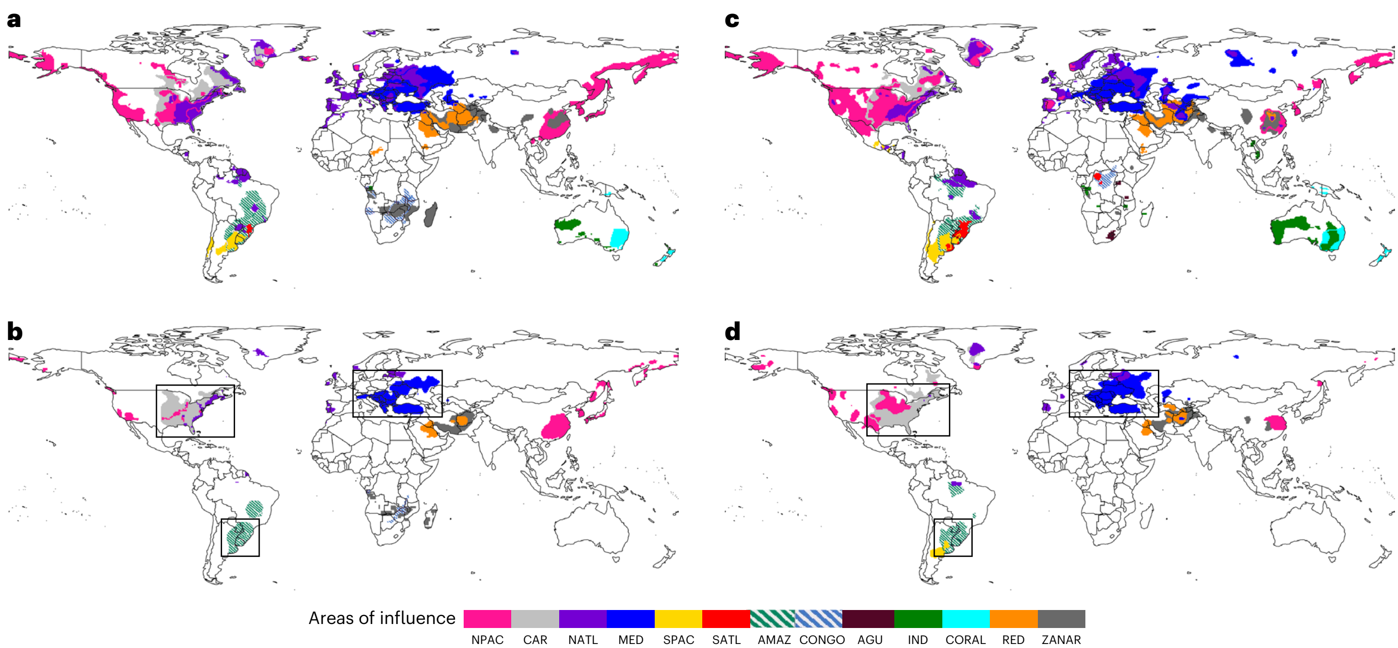

Fig. 3 | Regions where the conditional probability of drought occurrence given an equivalent moisture deficit from the major moisture sources of the planet is over three and four times greater than that of the independence case, respectively, on an annual scale. a–d, Patterns corresponding to a conditional probability over three times (**a** and **c**) or four times (**b** and **d**) greater than the independence case (5%) for SPI at 1 month (**a** and **b**) and 3 month (**c** and **d**) time scales. In **b** and **d**, the rectangles represent the boundaries of the three large continental areas influenced by a single moisture source with a conditional probability being more than four times greater than the independence case, namely CENA, SESA and EEur. Acronyms of moisture sources are the same as those used in Fig. 2. A Gaussian filter is used to facilitate visualization.

regions have a single dominant major moisture source: the Caribbean/Mexican source for CENA, Amazon source for SESA and Mediterranean source for EEur. Strong moisture source contribution deficits are associated with the highest drought probability values in all regions and time scales. Moreover, the observed cases with the highest values of drought probability corresponded to situations in which extreme and severe droughts took place. This means that the metric generated using moisture source contribution deficits reproduces droughts reasonably well in the analysed regions. Thus, considering a well-known drought event for each of those regions (Supplementary Table 2), the conditional probability of drought given the observed value of the moisture source contribution deficit at the peak of each event was estimated. The peak of the event was determined on the basis of the lowest SPI value. As such, it was found out that the probability of drought was higher than the independence case (5%) for all regions and both the 1 and 3 month SPI. Further, very high probabilities were obtained for CENA using the 1 and 3 month SPI (68.3% and 78.1%, respectively) and for EEur using the 1 month SPI (61.9%).

Conclusions

The results presented demonstrate the key role of the moisture transport deficit in drought genesis, especially in certain regions where drought is caused by a moisture deficit of oceanic or terrestrial origin, and in which drought severity is strongly determined by particular moisture sources. Our results suggest that the conditional probability of drought occurrence is at least two times greater than the independence case (5%) when there is an equivalent deficit of moisture received from either the ocean or continents in most regions. This indicates that moisture deficit plays a notable role in the development and/or intensification of drought events. Moreover, there exist certain hotspot regions in which this probability is three or more times greater than the independence case, owing to their low incoming moisture, as well as other regions in which this probability is much higher (CENA, SESA and EEur), where a moisture deficit from the major source (Caribbean, Amazon and Mediterranean, respectively) is almost synonymous with drought occurrence.

This work provides an opportunity to improve drought predictability in some world regions. The analysis of the three hotspot regions showed an agreement between the estimated drought probability based on the moisture deficit and the observed drought severity.

Further, this study could be a first step to studying the extent to which global climate change affects the relationship between moisture source contribution deficits and drought occurrence. It is expected that climate change can affect these relationships through shifts in circulation altering the source to sink patterns, mainly associated with changes in position and intensity of the Intertropical Convergence Zone and Hadley cells in tropical regions and the storm track in extratropics[53,54]. Additionally, these relationships could also be affected by the land–ocean warming contrasts with faster warming over land than the ocean and subsequent continental relative humidity decline, which have implications for current and future changes in moisture supply with impacts on the drought severity and likelihood (for example, Byrne and O'Gorman[42], Wainwright et al.[43] and Allan et al.[55]). In our current climate, this work already points to the direction that the relationship between droughts and moisture transport deficits may be slightly different when there are different conditions of relative humidity and land–ocean temperature contrast or changes in circulation associated with different phases of modes of climate variability.

The seasonal and climatic predictive power of the methodology used in this study opens new relevant topics to be explored, such as the role of the specific moisture sources of a given region in drought development, or the implications for the predictability of flash droughts[56] or rapid hydrological transitions or 'whiplash'[57]. These are phenomena that, when developed on smaller time scales than usual droughts, close to the submonthly scale, could benefit from the improved predictability of moisture transport versus precipitation.

https://doi.org/10.1038/s44221-023-00192-4

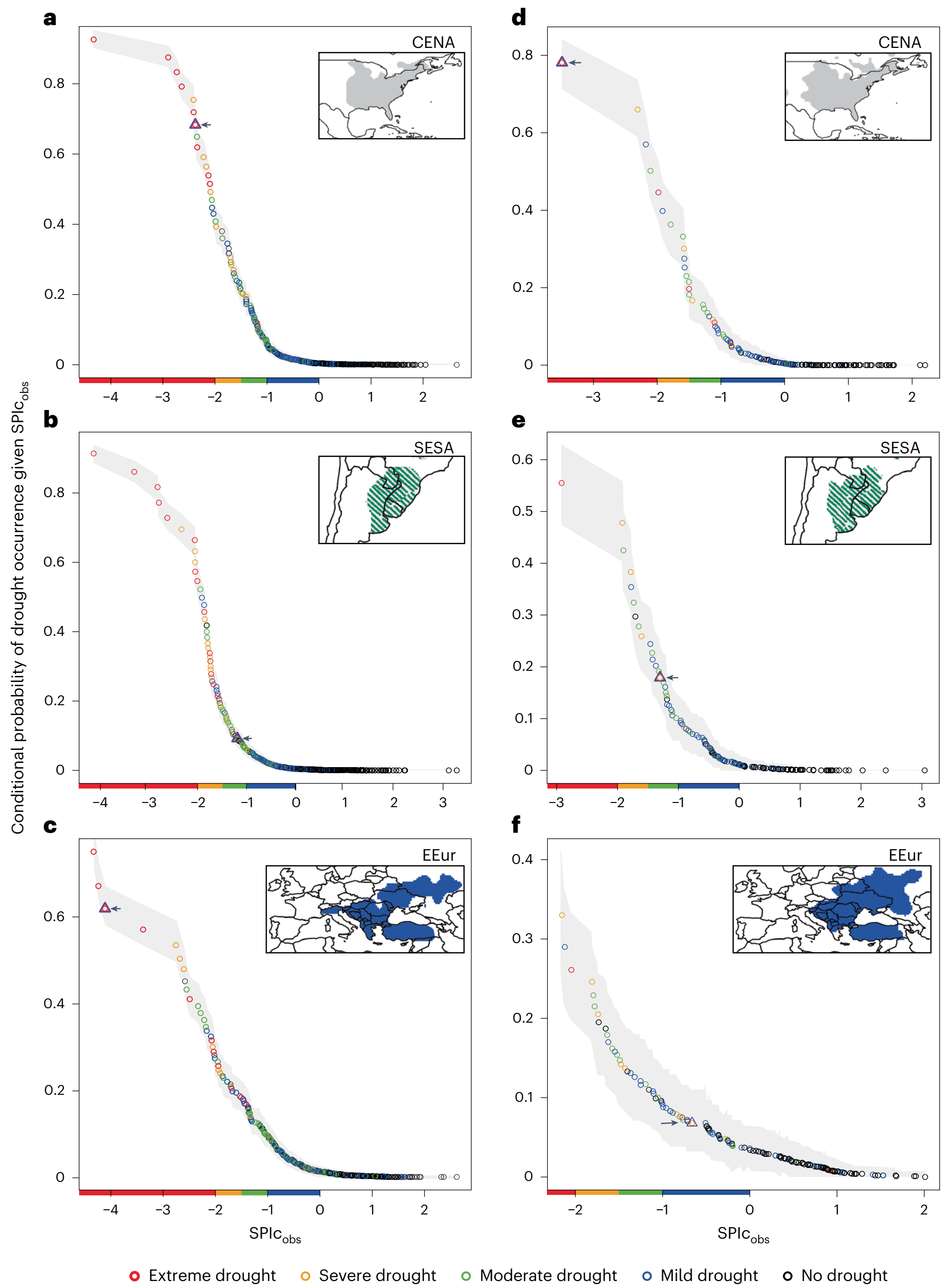

Fig. 4 | Conditional probability of drought occurrence given observed values of moisture contribution deficits from the main moisture source of CENA, SESA and EEur, respectively. a–f, Conditional probabilities for the CENA region using a SPI at the time scales of 1 month (**a**) and 3 months (**d**), the SESA region using a SPI at the time scales of 1 month (**b**) and 3 months (**e**) and the EEur region using a SPI at the time scales of 1 month (**c**) and 3 months (**f**). Statistical method II was applied to the contribution to precipitation series of the Caribbean/Mexican source for CENA, of the Amazon source for SESA and of the Mediterranean source for EEur (see Methods for details). Grey bands indicate 95% statistical confidence for the conditional probability (measure of centre for the error bands). Drought categories are taken according to the scale defined by McKee et al.[58], that is, the SPI thresholds of −2, −1.5, −1 and 0 refer to extreme droughts (red circles), severe (orange circles), moderate (green circles) and mild ones (blue circles), respectively. For each region and time scale, a purple triangle and an arrow are used to indicate the probability corresponding to the observed value of the moisture source contribution in the peak of the well-known drought event presented in Supplementary Table 2.

Methods

Calculation of drought indices

In this study, droughts were defined as monthly or cumulative precipitation deficits over 1 and 3 month periods obtained using the SPI[58], denoted as SPI1 and SPI3, respectively. The election of SPI instead of other indices that include temperature, such as the Standardized Precipitation–Evapotranspiration Index (SPEI)[59] or the evaporative demand[60] is twofold: (1) the study focuses on the short-term drought variability. In this case, the role of warming on drought severity is less relevant as the sensitivity of the SPEI to the increased atmospheric evaporative

https://doi.org/10.1038/s44221-023-00192-4

demand is mostly recorded on long time scales as a consequence of the high autocorrelation that characterises multi-scalar drought indices. Moreover, for the short-term variability, the SPEI is mostly driven by precipitation so the inclusion or not of the atmospheric evaporative demand is not going to produce a large impact on the obtained results, and (2) the study focuses on the role of moisture transport on drought severity so we try to isolate this influence, which is recorded on precipitation. Precipitation is driven by different dynamic and thermodynamic mechanisms but the availability of air moisture is a fundamental driver. On the contrary, the variability of the atmospheric evaporative demand is driven by other mechanisms, fundamentally thermodynamic, including radiative forcing as a consequence of enhanced emissions of greenhouse gases and also land–atmosphere feedbacks associated with the availability of soil moisture and the partition of sensible and latent heat fluxes. Although air humidity is a driver of the vapour pressure deficit, which has a role in the atmospheric evaporative demand, it has been observed that the main driver of changes in atmospheric evaporative demand is temperature. Thus, from a physical perspective, the inclusion of the atmospheric evaporative demand would include some noise in the analysis, as a component that is not expected to be related with air humidity transport would be included. The positive (negative) SPI values represent values that are higher (lower) than the mean precipitation, indicating wet (dry) conditions that can be spatio-temporally compared. Thus, the SPI1 reflects short-term precipitation conditions and the SPI3 short- and medium-term ones, providing a seasonal estimation of precipitation and reducing the influence of precipitation variability on a monthly scale. The SPI application can be closely related to meteorological types of drought along with short-term soil moisture and crop stress[61], but it is also useful for assessing hydrological and ecological drought impact[62,63].

The global gridded SPI was computed using the 0.5° × 0.5° monthly Multi-Source Weighted-Ensemble Precipitation (MSWEP) series for the 1980–2018 period. MSWEP dataset v2.8 (ref. 64) is a high-quality global product that takes advantage over other observed and estimated precipitation datasets because it merges gauge, satellite and re-analysis data. However, it has some limitations in the representation of precipitation in some regions, owing to variations in the number of daily observations and short periods with available data[64]. In some regions, such as Africa, the number of gauge observations is quite low, which might negatively impact the performance of the product, particularly affecting the identification of hydroclimate extremes[65]. Despite this, it has been shown that MSWEP performed better than other rainfall datasets (for example, Integrated Multi-satellitE Retrievals for GPM and Climate Hazards Group InfraRed Precipitation with Station data) at the daily time scale over the continent[66]. Another limitation of this product is that the climatology of the precipitation probability distribution in the latest version of MSWEP is based on the European Centre for Medium-Range Weather Forecasts re-analysis ERA5 (ref. 67), which leads to an underestimation of the maximum values, although it can generally capture their locations and patterns[68].

Calculation of the contribution to precipitation from the whole oceanic and terrestrial moisture sources

The moisture contribution to precipitation over land has two possible origins: the oceans and the continents. Nieto and Gimeno[69,70] proposed a methodology to obtain both contributions using an approach based on a Lagrangian technique for estimating the precipitation given the moisture transported from the two sources separately, which was already used by Gimeno et al.[19] to study changes in the ratio between them in the current climate. For this study, we used 0.5° × 0.5° monthly datasets for the 1980–2018 period of oceanic and terrestrial moisture contributions to precipitation.

These authors used the outputs of the Lagrangian particle dispersion model FLEXPART v9.0 (refs. 71,72) that moves approximately two million air parcels (of constant mass, m) in which the atmosphere was divided every 6 h for the period 1980–2018. The air parcels in the model were moved and have the meteorological characteristics given by the ERA-Interim[73] re-analysis from the European Centre for Medium-Range Weather Forecasts.

The air parcels residing over the whole ocean and the whole continents, separately, were tracked forwards in time to determine the changes in specific humidity every 6 h (dq/dt, dt = 6 h) along each trajectory for each of them. They were tracked by considering the optimum residence time of the water vapour in the atmosphere for each continental grid point, that is, the best Lagrangian time to match the precipitation data obtained from a reference re-analysis (ERA-Interim in this case) and the Lagrangian precipitation[70,74,75].

The individual increases (e) and decreases (p) of humidity were calculated as $(e - p) = m(dq/dt)$. The vertical integration of these individual $(e - p)$ values over each gridded area, from the surface to the top of the atmosphere, provided an estimation of the surface freshwater flux $(E - P)$, where E is the evaporation and P the precipitation rate per unit area. Values over zero indicate the prevalence of evaporation in the column, whereas negative values indicate moisture loss, which normally occurs by condensation and precipitation, so it was considered as a contribution to precipitation[25,76]. Hence, Nieto and Gimeno[70] computed those values of $(E - P) < 0$ over each grid point over the continents, which are considered as contributions to precipitation, for those air parcels with oceanic and terrestrial origin, respectively, being the both components of the total Lagrangian precipitation. The moduli of their final values were used for practical purposes.

To analyse the role of the oceanic and terrestrial moisture sources in drought events, we calculated analogous standardized indices to the SPI for every grid point using both the oceanic and terrestrial contributions to precipitation separately. Those standardized indices were denoted as SPIc.

Our approach only takes values in regions and times where the evaporation minus precipitation $(E - P)$ balance is negative to define precipitation, so the dataset used mainly shows the precipitation-deficit drought, although evaporation could be relevant for drought intensification under some conditions[77,78]. Nevertheless, the main role of precipitation on drought development and intensification is indisputable. Evapotranspiration could have a role on short time scales of precipitation deficits (for example, 1 month SPI). However, when moving to longer time scales (for example, 3 month SPI), which are representative of cumulative precipitation deficits, necessary to trigger a drought event, precipitation is the main variable controlling drought variability. Even using the atmospheric evaporative demand instead of evapotranspiration, precipitation is the main variable controlling variability of drought indices[79]. It is also important to warn on the use of $(P - E)$ to assess drought severity. This is a metric that is widely used to assess changes in the water availability for long periods (from annual to decadal) and it has shown changes for the long term[80]. Nevertheless, for the assessment of short-term droughts, the use of $(P - E)$ as a metric of drought severity is highly problematic, particularly during the dry season, in which E can be limited by the soil water availability, which can be determined by the precipitation over a long period. If E is suppressed given low soil moisture, this may produce situations in which under drought conditions, short time scales of $(P - E)$ may provide positive values (indicative of humid conditions), given reduced E. This was illustrated with the extreme drought that affected southwestern Europe and North Africa in 2005, in which drought severity was not identified using $(P - E)$ at short time scale[81]. For these reasons (and the existing uncertainties for a reliable estimation of E, including the important role of land cover changes), we consider it better to constrain our analysis to a drought metric based on precipitation, which is less uncertain, widely used for drought monitoring and early warning, and recommended by the World Meteorological Organization as the reference metric for drought quantification[82].

As the moisture transport data is based on the ERA-Interim, in a first approximation, the uncertainties of estimating moisture transport are those derived from the re-analysis uncertainties. For moisture transport estimation, uncertainties are mainly those linked to the correct estimation of atmospheric circulation and of the water vapour content. Owing to its construction process, based on a circulation model, one of the strong points of the re-analysis is the good reproduction of the large-scale general circulation of the atmosphere, so large uncertainties cannot be expected in this sense. Those linked to moisture content may be greater. In a very recent comparison between daily re-analysis data with the new Total Column Water Vapour Data Record (v2)—developed by the European Space Agency in coordination with the Satellite Application Facility on Climate Monitoring—Eiras-Barca et al.[83] showed low bias in most oceanic and continental areas, being generally less than ±2 kg m^{-2} in the main regions where moisture transport influences precipitation (regions of occurrence of ARs, LLJs and TCs). The temporal correlations between the re-analysis data and that new data record were above 0.8 in most areas of the world, finding the highest discrepancies in the main tropical rainforest regions.

Calculation of the contribution to precipitation from major moisture sources

Following the same methodology, we determined the individual moisture contributions to precipitation over the continents from 11 major climatological oceanic moisture sources[20] and two key terrestrial sources: the Amazon and Congo river basins[84,85], for the 1980–2018 period. In these regional forward experiments, the set of particles over each moisture source was selected.

As was done for the oceanic and terrestrial standardized indices, to analyse the role of the major moisture sources in drought events, we calculated analogous indices to the SPI for every grid point using their individual moisture contribution to precipitation. That is, we obtained the SPIc values corresponding to the contribution to precipitation from the major individual moisture sources. To analyse the three hotspot regions (CENA, SESA and EEur), the monthly MSWEP and each moisture source contribution series for the 1980–2018 period were spatially averaged over each studied region before obtaining the standardized indices.

The approach has some limitations linked to the definition of moisture source regions. Our analysis is based on a set of geographically fixed sources, namely all ocean versus all land in a first approximation and the 13 most important source regions at a global level estimated by climatological values (as revealed by the secular paper, Gimeno et al.[20]). Therefore, it does not allow to analyse changes in the positions of the sources, although it permits changes in the intensity of moisture transport from the source to any potential sink. This change in transport can be due to either a change in evaporation from the source, a change in the circulation from source to sink, or in both. Obviously, a given sink region can have specific source regions, which can vary both in position and intensity in current and future climates. But even analysing the specific sources of a given sink region, the use of source regions of variable extension over time does not allow the approximation used in this study, based on the probability of drought occurrence given a moisture source contribution deficit, since this requires the same source extension conditions. That is why the factor 'change in the position of the source' is not included in this study and the climatological positions were taken as a basis. However, and for specific target regions, other non-probabilistic approximations can be used based on extension and intensity anomalies of the source regions for drought events, widely used in previous studies (for example, the catalogue by Drumond et al.[21] for the Intergovernmental Panel on Climate Change reference regions).

Statistical method I: estimation of the conditional probability of drought occurrence given an equivalent moisture source contribution deficit

In this study, we relied on techniques from the copula theory[86] to estimate the probability of drought occurrence for a given moisture source contribution deficit. It is increasingly popular to model the dependence structure of a pair of variables by fitting a copula model, particularly in hydroclimatic applications[87]. Copulas offer a versatile framework for estimating conditional probabilities, as they enable the generation of synthetic data that preserves the observed dependence structure between the variables. It is a flexible methodology, as it is possible to choose a copula function that closely matches the observed dependence pattern. Whether relationships are linear, non-linear, symmetric or asymmetric, copula models can capture them effectively. Copulas excel in modelling tail dependence, which is crucial when studying extreme events such as droughts[88–90]. Although other statistical methods have been used in the context of compound extreme events, such as event coincidence analysis[91], multi-type point processes[92] or counting the simultaneous/consequential occurrences of multiple extremes[93], the singular properties of copulas permit a complete understanding of the dependence structure of the variables[90] and that is the reason why we opted for this methodology in this study.

We followed the semiparametric approach for model fitting by obtaining uniformly transformed values of the original variables (known as pseudo-observations) and applying the maximum likelihood estimation to obtain estimates of the copula parameters[94]. U_{SPI} and U_{SPIc} denoted the variables on a uniform scale. For each grid point, copula models were fitted to model the dependence structure of each (U_{SPI}, U_{SPIc}) pair for each moisture source contribution. For the 1 month temporal scale, all observations (monthly values) were used for model fitting. However, for the 3 month scale, only observations corresponding to March, June, September and December were considered, as they are the representative values of the corresponding seasons, that is, January–March, April–June, July–September and October–December, respectively.

We used R software[95], namely, the R package VineCopula[96]. Six different types of parametric copulas were used—Gaussian, Student *t*, Clayton, Gumbel, Frank and Joe copulas; their expressions can be found in Czado[97]. Using these copula models, it becomes possible to flexibly represent the dependence structure of the studied pair of variables. They provide a wide array of different radial asymmetry or symmetry shapes and tail dependence behaviour. Among the asymmetric models, the Clayton copula is used to model dependence in the lower tail, while the Gumbel and Joe can model upper tail dependence. Regarding the symmetric ones, the Gaussian and Frank copulas do not exhibit tail dependence, while the Student *t* copula can capture both lower and upper tail dependence. The independence copula (product copula) was also used, which corresponds to the case of both variables being independent.

Among the fitted copula models, the one with the lowest Akaike information criterion value was selected[98]. The statistical test by Huang and Prokhorov[99] based on White's[100] information matrix equality was applied to test the null hypothesis that the selected parametric copula model fits well to the data. Using the selected fitted copula model, we obtained 100,000 simulated values for the variables on a uniform scale. The large sample size allowed the estimation of the probability of the SPI being lower than its fifth percentile (approximately −1.64), conditional on the SPIc being lower than its corresponding fifth percentile (approximately −1.64), as follows:

1. Among the 100,000 simulated values of (U_{SPI}, U_{SPIc}), we selected the bivariate observations such that $U_{\mathrm{SPIc}} \leq u_{\mathrm{SPIc},5\%}$.
2. We constructed the empirical cumulative distribution function of U_{SPI} conditional on $U_{\mathrm{SPIc}} \leq u_{\mathrm{SPIc},5\%}$ and denoted this as $\hat{F}_{U_{\mathrm{SPI}}|U_{\mathrm{SPIc}} \leq u_{\mathrm{SPIc},5\%}}$.
3. We computed $\hat{F}_{U_{\mathrm{SPI}}|U_{\mathrm{SPIc}} \leq u_{\mathrm{SPIc},5\%}}(u_{\mathrm{SPI},5\%})$, which is an estimate of $P(U_{\mathrm{SPI}} \leq u_{\mathrm{SPI},5\%}|U_{\mathrm{SPIc}} \leq u_{\mathrm{SPIc},5\%})$

$$\sim P(\mathrm{SPI} \leq -1.64|\mathrm{SPIc} \leq -1.64),$$

where $u_{\mathrm{SPI},5\%}$ and $u_{\mathrm{SPIc},5\%}$ are the fifth percentile values of the uniformly transformed values for SPI and SPIc, respectively.

We used the same threshold (in standardized units) for both the SPI and SPIc when estimating the desired conditional probability (that is, we based our analysis on an 'equivalent moisture deficit') because our aim was to analyse droughts and moisture source contribution deficits defined under the same conditions.

Statistical method II: estimation of the conditional probability of drought occurrence given an observed value of moisture source contribution deficit

To estimate the conditional probability of drought occurrence given an observed value of moisture source contribution deficit for the three selected regions, the method was the same as that previously discussed in terms of model fitting. However, in this case, the 100,000 simulations were obtained from the conditional distribution function of SPI given an observed value of SPIc. That is, for an observed value of SPIc (let it be denoted as $\mathrm{SPIc}_{\mathrm{obs}}$, and let $u_{\mathrm{SPIc}_{\mathrm{obs}}}$ be the uniform-transformed value), the method is as follows:

1. We used 100,000 simulated values of $U_{\mathrm{SPI}}|U_{\mathrm{SPIc}} = u_{\mathrm{SPIc}_{\mathrm{obs}}}$ to construct its empirical cumulative distribution function, denoted as $\hat{F}_{U_{\mathrm{SPI}}|U_{\mathrm{SPIc}}=u_{\mathrm{SPIc}_{\mathrm{obs}}}}$.
2. We computed $\hat{F}_{U_{\mathrm{SPI}}|U_{\mathrm{SPIc}}=u_{\mathrm{SPIc}_{\mathrm{obs}}}}(u_{\mathrm{SPI},5\%})$, which is an estimate of $P(U_{\mathrm{SPI}} \leq u_{\mathrm{SPI},5\%}|U_{\mathrm{SPIc}} = u_{\mathrm{SPIc}_{\mathrm{obs}}})$

$$\sim P(\mathrm{SPI} \leq -1.64|\mathrm{SPIc} = \mathrm{SPIc}_{\mathrm{obs}}),$$

where $u_{\mathrm{SPI},5\%}$ is the fifth percentile value of the uniformly transformed values for SPI.

Uncertainties in the probability estimation were assessed using a repeated sampling procedure adapted from Ribeiro et al.[101], which enabled us to construct confidence intervals for the conditional probabilities. The procedure performed was the following: once the copula model was selected by means of the Akaike information criterion, we obtained a sample of 1,000 values for each conditional probability. Using that sample, we computed the 2.5% and 97.5% percentiles, corresponding to the lower and upper bounds of the 95% confidence interval for each conditional probability, respectively. Each of the 1,000 values of the sample was obtained by using n simulated values of $U_{\mathrm{SPI}}|U_{\mathrm{SPIc}} = u_{\mathrm{SPIc}_{\mathrm{obs}}}$, with n being the number of observations.

Reporting summary

Further information on research design is available in the Nature Portfolio Reporting Summary linked to this article.

Data availability

European Centre for Medium-Range Weather Forecasts Re-analysis dataset used to run FLEXPART and to calculate trajectories should be downloaded through the routine script available at https://www.flexpart.eu/downloads. Precipitation data used to calculate drought indices are taken from MSWEP, publicly available for download via https://www.gloh2o.org/mswep/.

Code availability

The FLEXPART model used to calculate trajectories is publicly available and can be downloaded from https://www.flexpart.eu/wiki/FpRoadmap. TROVA software used to calculate the contribution of the moisture sources is publicly available and can be downloaded from https://github.com/ElsevierSoftwareX/SOFTX-D-22-00100. For the calculation of the Standardized Precipitation Index (SPI) and the contribution indices obtained in an analogous way to SPI, the R package SPEI was used (available at https://cran.r-project.org/web/packages/SPEI/index.html). The conditional probability estimation was performed using the R package VineCopula (available at https://cran.r-project.org/web/packages/VineCopula/index.html).

References

1. *WMO Atlas of Mortality and Economic Losses from Weather, Climate and Water Extremes (1970–2019)* (World Meteorological Organization, 2021).
2. Smith, A. B. & Matthews, J. L. Quantifying uncertainty and variable sensitivity within the US billion-dollar weather and climate disaster cost estimates. *Nat. Hazards* **77**, 1829–1851 (2015).
3. Crausbay, S. D. et al. Defining ecological drought for the twenty-first century. *Bull. Am. Meteorol. Soc.* **98**, 2543–2550 (2017).
4. Douville, H. et al. in *Climate Change 2021: The Physical Science Basis* (eds Masson-Delmotte, V. et al.) 1055–1210 (Cambridge University Press, 2021).
5. Seneviratne, S. I. et al. in *Climate Change 2021: The Physical Science Basis* (eds. Masson-Delmotte, V. et al.) 1513–1766 (Cambridge University Press, 2021).
6. Ault, T. R. On the essentials of drought in a changing climate. *Science* **368**, 256–260 (2020).
7. AghaKouchak, A., Feldman, D., Hoerling, M., Huxman, T. & Lund, J. Water and climate: recognize anthropogenic drought. *Nature* **524**, 409–411 (2015).
8. Van Loon, A. F. et al. Drought in the Anthropocene. *Nat. Geosci.* **9**, 89–91 (2016).
9. Dai, A., Zhao, T. & Chen, J. Climate change and drought: a precipitation and evaporation perspective. *Curr. Clim. Change Rep.* **4**, 301–312 (2018).
10. Schubert, S. D. et al. Global meteorological drought: a synthesis of current understanding with a focus on SST drivers of precipitation deficits. *J. Clim.* **29**, 3989–4019 (2016).
11. Kunkel, K. E., Stevens, S. E., Stevens, L. E. & Karl, T. R. Observed climatological relationships of extreme daily precipitation events with precipitable water and vertical velocity in the contiguous United States. *Geophys. Res. Lett.* **47**, e2019GL086721 (2020).
12. Hagos, S. M. et al. The relationship between precipitation and precipitable water in CMIP6 simulations and implications for tropical climatology and change. *J. Clim.* **34**, 1587–1600 (2021).
13. Trenberth, K. E., Branstator, G. W. & Arkin, P. A. Origins of the 1988 North American drought. *Science* **242**, 1640–1645 (1988).
14. Trenberth, K. E., Dai, A., Rasmussen, R. M. & Parsons, D. B. The changing character of precipitation. *Bull. Am. Meteorol. Soc.* **84**, 1205–1218 (2003).
15. Gimeno, L. et al. Major mechanisms of atmospheric moisture transport and their role in extreme precipitation events. *Annu. Rev. Environ. Resources* **41**, 117–141 (2016).
16. Eltahir, E. A. B. & Bras, R. L. Precipitation recycling. *Rev. Geophys.* **34**, 367–378 (1996).
17. van der Ent, R. J., Savenije, H. H., Schaefli, B., & Steele-Dunne, S. C. Origin and fate of atmospheric moisture over continents. *Water Resour. Res.* https://doi.org/10.1029/2010WR009127 (2010).
18. Gimeno, L. et al. Oceanic and terrestrial sources of continental precipitation. *Rev. Geophys.* **50**, RG4003 (2012).
19. Gimeno, L., Nieto R., & Sorí R. The growing importance of oceanic moisture sources for continental precipitation. *NPJ Clim Atmos. Sci.* https://doi.org/10.1038/s41612-020-00133-y (2020).
20. Gimeno, L., Drumond A., Nieto R., Trigo R. M., & Stohl A. On the origin of continental precipitation. *Geophys. Res. Lett.* https://doi.org/10.1029/2010GL043712 (2010).
21. Drumond, A., Stojanovic, M., Nieto, R., Vicente-Serrano, S. M. & Gimeno, L. Linking anomalous moisture transport and drought episodes in the IPCC reference regions. *Bull. Amer. Meteor. Soc* **100**, 1481–1498 (2019).
22. Shen, Z. et al. Drying in the low-latitude Atlantic Ocean contributed to terrestrial water storage depletion across Eurasia. *Nat. Commun.* **13**, 1849 (2022).

23. Rathore, S., Bindoff, N. L., Ummenhofer, C. C., Phillips, H. E. & Feng, M. Near-surface salinity reveals the oceanic sources of moisture for Australian precipitation through atmospheric moisture transport. *J. Clim.* **33**, 6707–6730 (2020).
24. Vázquez, M., Nieto, R., Liberato, M. L. R. & Gimeno, L. Atmospheric moisture sources associated with extreme precipitation during the peak precipitation month. *Weather Clim. Extrem.* **30**, 100289 (2020).
25. Stohl, A. & James, P. A Lagrangian analysis of the atmospheric branch of the global water cycle. Part II: moisture transports between Earth's ocean basins and river catchments. *J. Hydrometeorol.* **6**, 961–984 (2005).
26. Tuinenburg, O. A., Theeuwen, J. J. E. & Staal, A. Highresolution global atmospheric moisture connections from evaporation to precipitation. *Earth Syst. Sci. Data* **12**, 3177–3188 (2020).
27. Dey, D., Aldama Campino, A. & Döös, K. Atmospheric water transport connectivity within and between ocean basins and land. *Hydrol. Earth Syst. Sci.* **27**, 481–493 (2023).
28. Herrera-Estrada, J. E., Satoh, Y. & Sheffield, J. Spatiotemporal dynamics of global drought. *Geophys. Res. Lett.* **44**, 2254–2263 (2017).
29. Dorigo, W., et al. Closing the water cycle from observations across scales: where do we stand? *Bull. Am. Meteorol. Soc.* https://doi.org/10.1175/BAMS-D-19-0316.1 (2021).
30. Oki, T. & Kanae, S. Global hydrological cycles and world water resourses. *Science* **313**, 1068–1072 (2006).
31. Gimeno-Sotelo, L. & Gimeno, L. Where does the link between atmospheric moisture transport and extreme precipitation matter? *Weather Clim. Extrem.* **39**, 100536 (2023).
32. Lavers, D. A. & Villarini, G. The contribution of atmospheric rivers to precipitation in Europe and the United States. *J. Hydrol.* **522**, 382–390 (2015).
33. Khouakhi, A., Villarini, G. & Vecchi, G. A. Contribution of tropical cyclones to rainfall at the global scale. *J. Clim.* **30**, 359–372 (2017).
34. Jones, C. Recent changes in the South America low-level jet. *NPJ Clim. Atmos. Sci.* **2**, 20 (2019).
35. Schumacher, D. L., Keune, J., Dirmeyer, P. & Miralles, D. G. Drought self-propagation in drylands due to land–atmosphere feedbacks. *Nat. Geosci.* **15**, 262–268 (2022).
36. Pan, S. et al. Responses of global terrestrial evapotranspiration to climate change and increasing atmospheric CO_2 in the 21st century. *Earths Future* **3**, 15–35 (2015).
37. Payne, A. E. et al. Responses and impacts of atmospheric rivers to climate change. *Nat. Rev. Earth Environ.* **1**, 143–157 (2020).
38. Torres-Alvarez, J. A. et al. Future projections in the climatology of global low-level jets from CORDEX-CORE simulations. *Clim. Dyn.* **57**, 1551–1569 (2021).
39. Knutson, T. et al. Tropical cyclones and climate change assessment: part II: projected response to anthropogenic warming. *Bull. Am. Meteorol. Soc.* **101**, E303–E322 (2020).
40. Ropelewski, C. F. & Halpert, M. S. Global and regional scale precipitation patterns associated with the El Niño/Southern Oscillation. *Mon. Wea. Rev.* **115**, 1606–1626 (1987).
41. Hurrell, J. Decadal trends in the North-Atlantic oscillation: regional temperatures and precipitation. *Science* **269**, 676–679 (1995).
42. Byrne, M. P. & O'Gorman, P. A. Trends in continental temperature and humidity directly linked to ocean warming. *Proc. Natl Acad. Sci. USA* **115**, 4863–4868 (2018).
43. Wainwright, C. M., Allan, R. P. & Black, E. Consistent trends in dry spell length in recent observations and future projections. *Geophys. Res. Lett.* **49**, e2021GL097231 (2022).
44. Hao, Z., Singh, V. P. & Xia, Y. Seasonal drought prediction: advances, challenges, and future prospects. *Rev. Geophys.* **56**, 108–141 (2018).
45. Doblas-Reyes, F. J., García-Serrano, J., Lienert, F., Biescas, A. P. & Rodrigues, L. R. L. Seasonal climate predictability and forecasting: status and prospects. *WIREs Clim. Change* **4**, 245–268 (2013).
46. Yuan, X. & Wood, E. F. Multimodel seasonal forecasting of global drought onset. *Geophys. Res. Lett.* **40**, 4900–4905 (2013).
47. Hoerling, M. et al. Causes and predictability of the 2012 Great Plains drought. *Bull. Am. Meteor. Soc.* https://doi.org/10.1175/BAMS-D-13-00055.1 (2014).
48. Lavers, D. A., Waliser, D. E., Ralph, F. M. & Dettinger, M. D. Predictability of horizontal water vapor transport relative to precipitation: enhancing situational awareness for forecasting western U.S. extreme precipitation and flooding. *Geophys. Res. Lett.* **43**, 2275–2282 (2016).
49. Lavers, D. A., Pappenberger, F. & Zsoter, E. Extending medium-range predictability of extreme hydrological events in Europe. *Nat. Commun.* **5**, 5382 (2014).
50. Gvoždíková, B. & Müller, M. Predictability of moisture flux anomalies indicating central European extreme precipitation events. *Q. J. R. Meteorol. Soc.* **147**, 3335–3348 (2021).
51. Wang, S. & Yuan, X. Extending seasonal predictability of Yangtze River summer floods. *Hydrol. Earth Syst. Sci.* **22**, 4201–4211 (2018).
52. Gao, S., Liu, P. & Lall, U. Seasonal precipitation predictability for the northern hemisphere using concurrent and preseason atmospheric water vapor transport and sea surface temperature. *J. Hydrometeorol.* **22**, 183–199 (2021).
53. Allan, R. P. et al. Advances in understanding large-scale responses of the water cycle to climate change. *Ann. NY Acad. Sci.* **1472**, 49–75 (2020).
54. Mamalakis, A. et al. Zonally contrasting shifts of the tropical rain belt in response to climate change. *Nat. Clim. Chang.* **11**, 143–151 (2021).
55. Allan, R. P., Willett, K. M., John, V. O. & Trent, T. Global changes in water vapor 1979–2020. *J. Geophys. Res. Atmos.* **127**, e2022JD036728 (2022).
56. Pendergrass, A. G. et al. Flash droughts present a new challenge for subseasonal-to-seasonal prediction. *Nat. Clim. Change* **10**, 191–199 (2020).
57. Tan, X. et al. Increasing global precipitation whiplash due to anthropogenic greenhouse gas emissions. *Nat. Commun.* **14**, 2796 (2023).
58. McKee, T. B., Doesken, N. J., & Kleist, J. The relationship of drought frequency and duration to time scales. In *Proceedings of the 8th Conference on Applied Climatology* Vol. 17, 179–183 (1993).
59. Vicente-Serrano, S. M., Beguería, S. & López-Moreno, J. I. A multiscalar drought index sensitive to global warming: the Standardized Precipitation Evapotranspiration Index. *J. Climate* **23**, 1696–1718 (2010).
60. Hobbins, M. T. et al. The evaporative demand drought index. Part I: linking drought evolution to variations in evaporative demand. *J. Hydrometeorol.* **17**, 1745–1761 (2016).
61. World Meteorological Organization. *Standardized Precipitation Index User Guide* https://library.wmo.int/records/item/39629-standardized-precipitation-index-user-guide (2012).
62. Barker, L. J., Hannaford, J., Chiverton, A. & Svensson, C. From meteorological to hydrological drought using standardised indicators. *Hydrol. Earth Syst. Sci.* **20**, 2483–2505 (2016).
63. Peña-Gallardo, M. et al. Complex influences of meteorological drought time-scales on hydrological droughts in natural basins of the contiguous Unites States. *J. Hydrol.* **568**, 611–625 (2019).
64. Beck, H. E. et al. MSWEP V2 global 3-hourly 0.1 precipitation: methodology and quantitative assessment. *Bull. Am. Meteorol. Soc.* **100**, 473–500 (2019).

65. Awange, J. L., Hu, K. X. & Khaki, M. The newly merged satellite remotely sensed, gauge and reanalysis-based Multi-Source Weighted-Ensemble Precipitation: evaluation over Australia and Africa (1981–2016). *Sci. Total Environ.* **670**, 448–465 (2019).
66. Mekonnen, K. et al. Accuracy of satellite and reanalysis rainfall estimates over Africa: a multi-scale assessment of eight products for continental applications. *J. Hydrol. Reg. Stud.* **49**, 101514 (2023).
67. Hersbach, H. et al. The ERA5 global reanalysis. *Q. J. R. Meteorol. Soc.* **146**, 1999–2049 (2020).
68. Lavers, D. A., Simmons, A., Vamborg, F. & Rodwell, M. J. An evaluation of ERA5 precipitation for climate monitoring. *Q. J. R. Meteorol. Soc.* **148**, 3124–3137 (2022).
69. Nieto, R. & Gimeno, L. A database of optimal integration times for Lagrangian studies of atmospheric moisture sources and sinks. *Sci. Data* **6**, 59 (2019).
70. Nieto, R. & Gimeno, L. Addendum: a database of optimal integration times for Lagrangian studies of atmospheric moisture sources and sinks. *Sci. Data* **8**, 130 (2021).
71. Stohl, A., Forster, C., Frank, A., Seibert, P. & Wotawa, G. The Lagrangian particle dispersion model FLEXPART version 6.2. *Atmos. Chem. Phys.* **5**, 2461–2474 (2005).
72. Pisso, I. et al. The Lagrangian particle dispersion model FLEXPART version 10.4. *Geosci. Model Dev.* **12**, 4955–4997 (2019).
73. Dee, D. P. et al. The ERA-Interim reanalysis: configuration and performance of the data assimilation system. *Q. J. R. Meteorol. Soc.* **137**, 553–597 (2011).
74. Nieto, R., & Gimeno, L. Optimal integration times for Lagrangian studies of atmospheric moisture sources and sinks. *Zenodo* https://doi.org/10.5281/zenodo.1453841 (2018).
75. Gimeno, L. et al. The residence time of water vapour in the atmosphere. *Nat. Rev. Earth Environ.* **2**, 558–569 (2021).
76. Stohl, A. & James, P. A Lagrangian analysis of the atmospheric branch of the global water cycle. Part I: method description, validation, and demonstration for the August 2002 flooding in central Europe. *J. Hydrometeorol.* **5**, 656–678 (2004).
77. Teuling, A. J. et al. Evapotranspiration amplifies European summer drought. *Geophys. Res. Lett.* **40**, 2071–2075 (2013).
78. Zhao, M., A, G., Liu, Y. & Konings, A. G. Evapotranspiration frequently increases during droughts. *Nat. Clim. Change* **12**, 1024–1030 (2022).
79. Tomas-Burguera, M. et al. Global characterization of the varying responses of the standardized precipitation evapotranspiration index to atmospheric evaporative demand. *J. Geophys. Res. Atmospheres* **125**, e2020JD033017 (2020).
80. Padrón, R. S. et al. Observed changes in dry-season water availability attributed to human-induced climate change. *Nat. Geosci.* **13**, 477–481 (2020).
81. Vicente-Serrano, S. M. et al. Global drought trends and future projections. *Philos. Trans. R. Soc. Math. Phys. Eng. Sci.* https://doi.org/10.1098/rsta.2021.0285 (2022).
82. Hayes, M., Svoboda, M., Wall, N. & Widhalm, M. The lincoln declaration on drought indices: universal meteorological drought index recommended. *Bull. Am. Meteorol. Soc.* **92**, 485–488 (2011).
83. Eiras-Barca, J. et al. Analysis of the main source regions of moisture transport events with the new ESA CCI/CM-SAF total column water vapour climate data record (v2). *Q. J. R. Meteorol. Soc.* **148**, 3244–3258 (2022).
84. Drumond, A. et al. The role of the Amazon Basin moisture in the atmospheric branch of the hydrological cycle: a Lagrangian analysis. *Hydrol. Earth Syst. Sci.* **18**, 2577–2598 (2014).
85. Sorí, R., Nieto, R., Vicente-Serrano, S. M., Drumond, A. & Gimeno, L. A Lagrangian perspective of the hydrological cycle in the Congo River basin. *Earth System Dynamics* **8**, 653–675 (2017).
86. Nelsen, R. B. *An Introduction to Copulas* (Springer, 2007).
87. Tootoonchi, F. et al. Copulas for hydroclimatic analysis: a practice-oriented overview. *Wiley Interdiscip. Rev. Water* **9**, e1579 (2022).
88. Brunner, M. I., Liechti, K. & Zappa, M. Extremeness of recent drought events in Switzerland: dependence on variable and return period choice. *Nat. Hazards Earth Syst. Sci.* **19**, 2311–2323 (2019).
89. Ribeiro, A. F., Russo, A., Gouveia, C. M. & Páscoa, P. Copula-based agricultural drought risk of rainfed cropping systems. *Agric. Water Manage.* **223**, 105689 (2019).
90. Ribeiro, A. F., Russo, A., Gouveia, C. M. & Pires, C. A. Drought-related hot summers: a joint probability analysis in the Iberian Peninsula. *Weather Clim. Extrem.* **30**, 100279 (2020).
91. Donges, J. F., Schleussner, C. F., Siegmund, J. F. & Donner, R. V. Event coincidence analysis for quantifying statistical interrelationships between event time series: on the role of flood events as triggers of epidemic outbreaks. *Eur. Phys. J. Spec. Top.* **225**, 471–487 (2016).
92. Toreti, A., Cronie, O. & Zampieri, M. Concurrent climate extremes in the key wheat producing regions of the world. *Sci. Rep.* **9**, 5493 (2019).
93. Wu, X., Hao, Z., Hao, F., Li, C., & Zhang, X. Spatial and temporal variations of compound droughts and hot extremes in China. *Atmosphere* https://doi.org/10.3390/atmos10020095 (2019).
94. Shemyakin, A., & Kniazev, A. *Introduction to Bayesian Estimation and Copula Models of Dependence* (Wiley, 2017).
95. R Core Team. R: a language and environment for statistical computing. *R Foundation for Statistical Computing* https://www.R-project.org/ (2022).
96. Nagler, T., et al. VineCopula: statistical inference of vine copulas, R package version 2.4.3. *R Project* https://CRAN.R-project.org/package=VineCopula (2021).
97. Czado, C. *Analyzing Dependent Data with Vine Copulas* (Springer, 2019).
98. Akaike, H. A new look at the statistical model identification. *IEEE Trans. Autom. Control* **19**, 716–723 (1974).
99. Huang, W. & Prokhorov, A. A goodness-of-fit test for copulas. *Econ. Rev.* **33**, 751–771 (2014).
100. White, H. Maximum likelihood estimation of misspecified models. *Econometrica* **50**, 1–25 (1982).
101. Ribeiro, A. F. S., Russo, A., Gouveia, C. M., Páscoa, P. & Zscheischler, J. Risk of crop failure due to compound dry and hot extremes estimated with nested copulas. *Biogeosciences* **17**, 4815–4830 (2020).

Acknowledgements

EPhysLab members were supported by SETESTRELO project (grant no. PID2021-122314OB-I00) funded by the Ministerio de Ciencia, Innovación y Universidades, Spain (MCIN/10.13039/501100011033), Xunta de Galicia (grant ED431C2021/44; Programa de Consolidación e Estructuración de Unidades de Investigación Competitivas (Grupos de Referencia Competitiva), Consellería de Cultura, Educación e Universidade) and 'ERDF A way of making Europe'. L.G.-S. was supported by a 'Ministerio de Ciencia, Innovación y Universidades' PhD grant (reference: PRE2022-101497) and R.S. by a 'Spanish Ministry Ramon y Cajal' grant. We thank M. Vázquez for providing necessary data for this study. In addition, this work was possible because of the computing resources and technical support provided by the Centro de Supercomputación de Galicia (CESGA). This study was also supported by the 'Unidad Asociada CSIC–Universidade de Vigo: Grupo de Física de la Atmósfera y del Océano'.

Author contributions

L.G.-S. designed the experiments and contributed to data analysis and the writing of the paper. R.S. performed the Lagrangian analysis and contributed to the writing of the paper. R.N. contributed to the creation of the final figures and the writing of the paper. S.M.V.-S. contributed to the discussion of results. L.G. conceived the idea of the study and contributed to the writing of the paper. All authors contributed to the review and editing of the paper.

Competing interests

The authors declare no competing interests.

Additional information

Supplementary information The online version contains supplementary material available at https://doi.org/10.1038/s44221-023-00192-4.

Correspondence and requests for materials should be addressed to Luis Gimeno.

Peer review information *Nature Water* thanks Richard Allan, Xuezhi Tan and Ricardo Trigo for their contribution to the peer review of this work.

nature portfolio

Corresponding author(s): Luis Gimeno

Last updated by author(s): Dec 21, 2023

Reporting Summary

Nature Portfolio wishes to improve the reproducibility of the work that we publish. This form provides structure for consistency and transparency in reporting. For further information on Nature Portfolio policies, see our Editorial Policies and the Editorial Policy Checklist.

Statistics

For all statistical analyses, confirm that the following items are present in the figure legend, table legend, main text, or Methods section.

n/a	Confirmed	
☐	☒	The exact sample size (n) for each experimental group/condition, given as a discrete number and unit of measurement
☒	☐	A statement on whether measurements were taken from distinct samples or whether the same sample was measured repeatedly
☐	☒	The statistical test(s) used AND whether they are one- or two-sided *Only common tests should be described solely by name; describe more complex techniques in the Methods section.*
☐	☒	A description of all covariates tested
☒	☐	A description of any assumptions or corrections, such as tests of normality and adjustment for multiple comparisons
☐	☒	A full description of the statistical parameters including central tendency (e.g. means) or other basic estimates (e.g. regression coefficient) AND variation (e.g. standard deviation) or associated estimates of uncertainty (e.g. confidence intervals)
☐	☒	For null hypothesis testing, the test statistic (e.g. F, t, r) with confidence intervals, effect sizes, degrees of freedom and P value noted *Give P values as exact values whenever suitable.*
☒	☐	For Bayesian analysis, information on the choice of priors and Markov chain Monte Carlo settings
☒	☐	For hierarchical and complex designs, identification of the appropriate level for tests and full reporting of outcomes
☐	☒	Estimates of effect sizes (e.g. Cohen's d, Pearson's r), indicating how they were calculated

Our web collection on statistics for biologists contains articles on many of the points above.

Software and code

Policy information about availability of computer code

Data collection	The FLEXPART model used to calculate trajectories is publicly available and can be downloaded from https://www.flexpart.eu/wiki/FpRoadmap. TROVA software used to calculate the contribution of the moisture sources is publicly available and can be downloaded from https://github.com/ElsevierSoftwareX/SOFTX-D-22-00100.
Data analysis	For the calculation of the Standardised Precipitation Index (SPI) and the contribution indices obtained in an analogous way to SPI, the R package SPEI was used (available at https://cran.r-project.org/web/packages/SPEI/index.html). The conditional probability estimation was performed using the R package VineCopula (available at https://cran.r-project.org/web/packages/VineCopula/index.html).

For manuscripts utilizing custom algorithms or software that are central to the research but not yet described in published literature, software must be made available to editors and reviewers. We strongly encourage code deposition in a community repository (e.g. GitHub). See the Nature Portfolio guidelines for submitting code & software for further information.

Data

Policy information about availability of data

All manuscripts must include a data availability statement. This statement should provide the following information, where applicable:

- Accession codes, unique identifiers, or web links for publicly available datasets
- A description of any restrictions on data availability
- For clinical datasets or third party data, please ensure that the statement adheres to our policy

European Centre for Medium-Range Weather Forecasts Reanalysis dataset used to run FLEXPART and to calculate trajectories should be downloaded through the routine script available at https://www.flexpart.eu/downloads
Precipitation data used to calculate drought indices are taken from MSWEP, publicly available for download via https://www.gloh2o.org/mswep/

Research involving human participants, their data, or biological material

Policy information about studies with human participants or human data. See also policy information about sex, gender (identity/presentation), and sexual orientation and race, ethnicity and racism.

Reporting on sex and gender	*Use the terms sex (biological attribute) and gender (shaped by social and cultural circumstances) carefully in order to avoid confusing both terms. Indicate if findings apply to only one sex or gender; describe whether sex and gender were considered in study design; whether sex and/or gender was determined based on self-reporting or assigned and methods used. Provide in the source data disaggregated sex and gender data, where this information has been collected, and if consent has been obtained for sharing of individual-level data; provide overall numbers in this Reporting Summary. Please state if this information has not been collected. Report sex- and gender-based analyses where performed, justify reasons for lack of sex- and gender-based analysis.*
Reporting on race, ethnicity, or other socially relevant groupings	*Please specify the socially constructed or socially relevant categorization variable(s) used in your manuscript and explain why they were used. Please note that such variables should not be used as proxies for other socially constructed/relevant variables (for example, race or ethnicity should not be used as a proxy for socioeconomic status). Provide clear definitions of the relevant terms used, how they were provided (by the participants/respondents, the researchers, or third parties), and the method(s) used to classify people into the different categories (e.g. self-report, census or administrative data, social media data, etc.) Please provide details about how you controlled for confounding variables in your analyses.*
Population characteristics	*Describe the covariate-relevant population characteristics of the human research participants (e.g. age, genotypic information, past and current diagnosis and treatment categories). If you filled out the behavioural & social sciences study design questions and have nothing to add here, write "See above."*
Recruitment	*Describe how participants were recruited. Outline any potential self-selection bias or other biases that may be present and how these are likely to impact results.*
Ethics oversight	*Identify the organization(s) that approved the study protocol.*

Note that full information on the approval of the study protocol must also be provided in the manuscript.

Field-specific reporting

Please select the one below that is the best fit for your research. If you are not sure, read the appropriate sections before making your selection.

☐ Life sciences ☐ Behavioural & social sciences ☒ Ecological, evolutionary & environmental sciences

For a reference copy of the document with all sections, see nature.com/documents/nr-reporting-summary-flat.pdf

Ecological, evolutionary & environmental sciences study design

All studies must disclose on these points even when the disclosure is negative.

Study description	The study is based on reanalysis data, a set of global climate data freely available with 6-hour temporal resolution
Research sample	As the study is based on reanalysis data we have not taken any measurement
Sampling strategy	As the study is based on reanalysis data we have not taken any measurement so there is no sampling strategy
Data collection	As the study is based on reanalysis data we have not taken any measurement
Timing and spatial scale	Reanalysis data are global with 6-hour temporal resolution

Data exclusions	No data exclusion
Reproducibility	Data and software is freely available so the study has full reproducibility
Randomization	There is no randomization
Blinding	There is no blinding

Did the study involve field work? ☐ Yes ☒ No

Reporting for specific materials, systems and methods

We require information from authors about some types of materials, experimental systems and methods used in many studies. Here, indicate whether each material, system or method listed is relevant to your study. If you are not sure if a list item applies to your research, read the appropriate section before selecting a response.

Materials & experimental systems

n/a	Involved in the study	
☒	☐	Antibodies
☒	☐	Eukaryotic cell lines
☒	☐	Palaeontology and archaeology
☒	☐	Animals and other organisms
☒	☐	Clinical data
☒	☐	Dual use research of concern
☒	☐	Plants

Methods

n/a	Involved in the study	
☒	☐	ChIP-seq
☒	☐	Flow cytometry
☒	☐	MRI-based neuroimaging

Plants

Seed stocks	*Report on the source of all seed stocks or other plant material used. If applicable, state the seed stock centre and catalogue number. If plant specimens were collected from the field, describe the collection location, date and sampling procedures.*
Novel plant genotypes	*Describe the methods by which all novel plant genotypes were produced. This includes those generated by transgenic approaches, gene editing, chemical/radiation-based mutagenesis and hybridization. For transgenic lines, describe the transformation method, the number of independent lines analyzed and the generation upon which experiments were performed. For gene-edited lines, describe the editor used, the endogenous sequence targeted for editing, the targeting guide RNA sequence (if applicable) and how the editor was applied.*
Authentication	*Describe any authentication procedures for each seed stock used or novel genotype generated. Describe any experiments used to assess the effect of a mutation and, where applicable, how potential secondary effects (e.g. second site T-DNA insertions, mosiacism, off-target gene editing) were examined.*

4.5 The importance of contribution deficits from specific moisture sources on drought occurrence

The fifth article of this chapter is entitled “**Nexus between the deficit in moisture transport and drought occurrence in regions with projected drought trends**” by **Gimeno-Sotelo, L.**, Stojanovic, M., Sorí, R., Nieto, R., Vicente-Serrano, S. M., & Gimeno, L., and was published in the journal *Environmental Research Letters* in 2024.

ENVIRONMENTAL RESEARCH
LETTERS

CrossMark

OPEN ACCESS

RECEIVED
8 February 2024

REVISED
24 May 2024

ACCEPTED FOR PUBLICATION
10 June 2024

PUBLISHED
21 June 2024

LETTER

Nexus between the deficit in moisture transport and drought occurrence in regions with projected drought trends

Luis Gimeno-Sotelo[1,*], Milica Stojanovic[1], Rogert Sorí[1], Raquel Nieto[1], Sergio M Vicente-Serrano[2] and Luis Gimeno[1]

[1] Centro de Investigación Mariña, Universidade de Vigo, Environmental Physics Laboratory (EPhysLab), Ourense, Spain
[2] Instituto Pirenaico de Ecología, Consejo Superior de Investigaciones Científicas (IPE–CSIC), Zaragoza, Spain
[*] Author to whom any correspondence should be addressed.

E-mail: luis.gimeno-sotelo@uvigo.es

Keywords: meteorological drought, moisture transport, moisture sources, FLEXPART, copulas

Supplementary material for this article is available online

Abstract

In this article, we focus on studying the nexus between moisture transport deficit and drought occurrence in nine key regions across the world where the magnitude of meteorological drought is projected to increase from 1850 to 2100 under a high anthropogenic emission scenario. These regions are central America, southwestern South America, northern Brazil, the Amazon, northeastern Brazil, the western Mediterranean, southern Africa, the eastern Mediterranean, and southwestern Australia. Using the Lagrangian particle dispersion model FLEXPART, we identify the specific moisture sources of the regions (the own region, the nearby continental source and the oceanic sources) and obtain their contributions to the precipitation in the regions for the period 1980–2018. For each region and specific moisture source, the conditional probability of meteorological drought occurrence given an equivalent contribution deficit from the source is estimated using copula models, a statistical methodology that allows us to capture complex relationships between variables. We identify the dominant moisture source in each region, which is the source for which the contribution deficit maximises drought probability. A variety of cases are found: in three regions, the dominant source is the region itself, in one region, it is the nearby terrestrial source, and in five regions, it is an oceanic source. In general, contribution deficits from specific moisture sources are associated with only slightly greater drought probabilities than those from major global moisture sources. We also reveal that the source that contributes the most to precipitation in a given region is not necessarily the dominant source of drought in the region. These results highlight the importance of understanding the role of dominant moisture sources and moisture transport deficits on meteorological drought occurrence at a regional scale.

1. Introduction

Drought is one of the main natural hazards at the global level and strongly impacts ecosystems and society through significant economic losses that lead to far-reaching humanitarian disasters (Erian *et al* 2021, IPCC 2022). To illustrate this in an easy-to-interpret-way, drought accounts for annual economic losses in the United States of America of approximately \$6.4 billion (NOAA-NCEI 2021) and €9 billion in the European Union (Cammalleri *et al* 2020, Naumann *et al* 2021). Although drought is a recurrent phenomenon that occurs in every region as a consequence of natural climate variability (Stine 1994, Woxodhouse *et al* 2010), the last IPCC report (Seneviratne *et al* 2021) concluded that there is medium confidence that climate change is responsible for the occurrence of more severe meteorological droughts in some regions of the world. Moreover, there is high confidence that more frequent and severe meteorological droughts will be recorded in some regions of the world under high global warming scenarios (Seneviratne *et al* 2021).

Despite the uncertainties associated with future emission scenarios, climate models, and the definition of drought, the use of multiple climate models together with multiple ways of identifying droughts allows us to find regions where there is greater agreement between models on the intensification of meteorological drought with climate change. Projections based on high warming scenarios in CMIP5 and CMIP6 show more frequent and severe droughts over great extensions of the world including in most of them southern North America, Central America, the Amazon region, the Mediterranean region, southern Africa, and southern Australia. The high agreement in the projections of different Earth System Models suggests that in these regions, there is high confidence that meteorological drought will intensify, particularly under high global warming scenarios.

Although drought has a multidimensional aspect and depends on different processes and interactions (Douville *et al* 2021), leading to different drought types and associated impacts (agricultural, hydrological and socioeconomic) (Wilhite *et al* 2007, Bachmair *et al* 2015), the main variable defining drought severity is indisputably the occurrence of a precipitation deficit relative to the mean climate. The dynamic and thermodynamic mechanisms that cause precipitation deficits are very complex, but to put it simply, precipitation depends on whether there is moisture in the air and whether it is forced to rise. With respect to moisture, the moisture contained in the atmospheric column at any given time is usually insufficient to produce the precipitation recorded at that location (Trenberth *et al* 2003), and deficiencies in moisture transport are essential to explain precipitation deficits (Gimeno *et al* 2012, 2016, Drumond *et al* 2019).

There is a series of published studies on moisture transport deficits and drought occurrence at the regional level based on different techniques, including sophisticated Lagrangian or semi-Lagrangian techniques, which can be used to accurately locate the main moisture sources responsible for precipitation in a region (see e.g. Salah *et al* 2018, Garcia-Herrera *et al* 2019, Herrera-Estrada *et al* 2019, Roy *et al* 2019, Wei and Dirmeyer 2019, Holgate *et al* 2020, Schumacher *et al* 2022). These works have been carried out for the present climate, given the enormous technical difficulties and the need for very intensive computations derived from using Lagrangian techniques in climate models. However, even when analysed in the present climate, these works are of interest in regions where changes are projected for the future since they locate the source regions where climate models should be focused, dealing with aspects such as the intensity of the source (evaporation–precipitation balance) or the source–sink circulation.

Recently, Gimeno-Sotelo *et al* (2024b) demonstrated that meteorological droughts are strongly connected with moisture transport deficits from major global moisture sources. Given the relevance of the processes driving drought severity, with implications for future climate scenarios, the main objectives of this work are (i) to analyse whether, given a moisture transport deficit, the probability of drought occurrence notably changes if, instead of using major global moisture sources, the specific moisture sources of the region are used and (ii) to determine whether the specific moisture source that most contributes to precipitation in a region is the dominant source for drought occurrence. Since these objectives essentially involve regional analyses, we are forced to choose a finite number of study regions. In this article, because of the relevance of drought to climate change, we focused on regions where there is the greatest confidence in drought intensification with global warming and where understanding drought mechanisms is a priority.

2. Materials and methods

2.1. Identification of key regions

To identify the regions in which increases in meteorological drought severity are projected, we used monthly precipitation data for the historical period (1850–2014) and the Shared Socioeconomic Pathway 5–8.5 (SSP5-8.5) from 2015 to 2100. These data were obtained from an ensemble of 18 CMIP6 models (Eyring *et al* 2016), namely, ACCESS-CM2, ACCESS-ESM1-5, CanESM5-CanOE, CanESM5, CMCC-ESM2, CNRM-CM6-1-HR, CNRM-CM6-1, CNRM-ESM2-1, FIO-ESM-2-0, GFDL-ESM4, GISS-E2-1-G, HadGEM3-GC31-LL, HadGEM3-GC31-MM, INM-CM4-8, IPSL-CM6A-LR, MIROC-ES2L, MIROC6, MRI-ESM2-0, and interpolated to a common resolution of $2.5^\circ \times 2.5^\circ$ using bilinear transformation. As in Gimeno-Sotelo *et al* (2024a), the analysis consisted of applying the run theory (Tallaksen *et al* 1997, Fleig *et al* 2006) to identify drought events. Trends were obtained by fitting a linear regression model to the annual series of magnitude values of drought events as a function of time, and significance was assessed using the Mann–Kendall test (1945, 1948) at a significance level of 0.05. The selection of key regions was based on high model agreement (at least 90%) in terms of a significant increase in the magnitude of drought events from 1850 to 2100.

The unfavourable SSP5-8.5 scenario was used because of the large socio-economic impacts that it may imply. The selection of other more favourable SSPs would not add more information to this paper than the analysis of different regions, most of which are similar to those in the SSP5-8.5, as is the case for North America, Central America, the Mediterranean, the Amazon, or southwestern Australia, where the difference is the severity of drought in the lower warming scenarios, which is significantly reduced (Cook *et al* 2020).

2.2. Identification of specific moisture sources in each region

The Lagrangian particle dispersion model FLEXPART v9.0 (Stohl *et al* 2005, Pisso *et al* 2019) was used to determine the sources and sinks of moisture by tracking water vapour trajectories. FLEXPART was constrained by 6-h specific humidity and 3D-wind data, among other data also used for internal model parameterisations (Pisso *et al* 2019), taken from the whole available period (1980–2018) of the ERA-Interim reanalysis (Dee *et al* 2011) from the European Centre for Medium-Range Weather Forecasts (ECMWF) at a 1° horizontal resolution (regridded from the original reduced Gaussian grid N128) and within 61 vertical levels of the atmosphere. We acknowledge the improvements of the latest ECMWF reanalysis, ERA5 (Hersbach *et al* 2020), over ERA-Interim; however, with these input data, FLEXPART has already been successfully and extensively used to identify the origin of precipitating moisture for different regions and synoptic weather systems (see e.g. Gimeno-Sotelo *et al* 2024b, and the review by Gimeno *et al* 2020). In addition, a recent paper by Fernández-Alvarez *et al* (2023) performed a comparison between the results of FLEXPART forced with ERA-Interim and ERA5 reanalyses and found no significant differences between the moisture source patterns.

The atmosphere was divided into approximately two million air particles that are moved by winds in a 3D space. The method was based on calculating the changes in the specific humidity of all particles (with constant mass, m) at 6 h intervals ($\frac{\mathrm{d}q}{\mathrm{d}t}$) along their trajectories and aggregating the net increases and decreases in humidity within the vertical atmospheric column over a given surface grid cell (of area A, 0.25° in this study, using linear interpolation; see Nieto and Gimeno 2019 for further details). This enabled the determination of the net flux of fresh water ($E - P = \frac{\sum m \frac{\mathrm{d}q}{\mathrm{d}t}}{A}$), which is the difference between evaporation (E) and precipitation (P). This approach has been used in several papers to calculate moisture sources and sinks in specific areas or meteorological systems (e.g. Gimeno *et al* 2010a; Algarra *et al* 2020, Vazquez *et al* 2020, Fernández-Alvarez *et al* 2023). A summary of the advantages and disadvantages of the method compared to other approaches for the calculation of moisture sources and sinks can be found in Gimeno *et al* (2012), (2020).

To identify the main specific climatological moisture sources of a given region, global outputs of the FLEXPART model were used for the period 1980–2018. The air masses that reach each independent region were backwards-tracked in time based on the mean optimal residence time of water vapour (Nieto and Gimeno 2019, 2021). Areas where air masses gain moisture along their pathway, i.e. where evaporation exceeds precipitation in the net moisture balance (E-P) > 0), were identified as moisture sources. To delimit the main individual moisture sources for each region, the 90% percentile threshold was applied to the annual climatological positive (E-P) values, encompassing areas where (E-P) is greater than that percentile. This technique has been previously applied for the same purpose in several papers (see Gimeno *et al* 2020).

2.3. Calculation of drought indices and moisture source contribution deficit indices

The standardised precipitation index (SPI) (McKee *et al* 1993) was used for the identification of meteorological droughts. This index was defined in standard deviations and was calculated from monthly precipitation series on different time scales, defined as the cumulative precipitation over a number of n months. The precipitation series accumulated on the chosen time scale was fitted to a gamma distribution according to the WMO recommendation (WMO 2012), and the cumulative probabilities were calculated and transformed into a standard normal distribution. Negative SPI values indicate less than median precipitation and consequently dry conditions, whereas positive values represent the opposite. The standardised nature of the SPI allows comparisons between regions with very different precipitation magnitude and seasonality. For the SPI calculation, the monthly gridded multi-source weighted-ensemble precipitation dataset (MSWEP) (Beck *et al* 2017) with a horizontal resolution of 0.1° was used for the period of 1980–2018.

Once the main moisture sources of each region were defined, to determine their contribution to the precipitation in the target region, the air masses were tracked forward in time. In forward tracking, the areas where the moisture is lost as precipitation are identified where negative values of the net moisture balance ((E-P) < 0) occur, which means where precipitation exceeds evaporation. That is, when there is an aggregated loss in specific humidity for all the air particles departing from the source and reaching each grid cell in the target region. The monthly sum of these negative values over the target region is assumed to indicate the precipitation coming for that month from the source involved in the analysis. The modulus of that quantity is used for practical reasons. Thus, for each region, a time series of the contribution to the precipitation in the region from its specific moisture sources could be constructed, and indices analogous to the

SPI could be computed (these indices are denoted as SPIc).

2.4. Estimation of conditional probabilities through copulas

As in Gimeno-Sotelo *et al* (2024b), we relied on copula models to estimate the conditional probability of drought (SPI lower than a certain threshold) given an equivalent moisture deficit from a source (SPIc lower than the same threshold) because this methodology allowed us to produce large amounts of synthetic data that reproduced the complex relationships between variables. The methodology consisted of transforming the original data to uniform-scale values and applying the maximum likelihood estimation to fit several copula models, namely, the Gaussian, Student-t, Clayton, Gumbel, Frank and Joe copulas (see Czado 2019), which have different features in terms of symmetry/asymmetry and tail dependence. A model was selected according to the Akaike information criterion (1974), and the goodness of fit was assessed by means of a test described by Huang and Prokhorov (2014) based on White´s (1982) information matrix equality. A total of 100 000 simulated values for the variables on a uniform scale were obtained from the selected copula model. Using the simulated values, it was possible to construct the empirical cumulative distribution function of the uniformly transformed SPI given the uniformly transformed SPIc being lower than a certain threshold (Gimeno-Sotelo *et al* 2024b). The value that this function takes at the 5th percentile of the uniformly transformed values for the SPI is an estimation of the conditional probability of interest, i.e. $P(SPI \leqslant -1.64|SPIc \leqslant -1.64)$.

3. Results and discussion

3.1. Sources of moisture for precipitation in regions with projected drought trends

We identified the hotspot regions where precipitation-based drought is projected to increase in a warming climate (based on the SSP5-8.5 scenario) according to the CMIP6 models used in this study. We specifically selected regions where at least 90% of the models agreed on a significant increase in the magnitude of drought events from 1850 to 2100. We found nine regions satisfying the required condition (figure 1(a)), which are consistent with the results of meteorological drought projections from previous studies (Gimeno-Sotelo *et al* 2024a, Spinoni 2020, Cook *et al* 2020, Ukkola *et al* 2020, Zhao and Dai 2022). These regions were central America (region 1), southwestern South America (region 2), northern Brazil (region 3), the Amazon (region 4), northeastern Brazil (region 5), the western Mediterranean (region 6), southern Africa (region 7), the eastern Mediterranean (region 8), and southwestern Australia (region 9).

We first analysed the main climatological moisture sources in the nine regions. The moisture sources are inextricably linked to the moisture fluxes associated with the general atmospheric circulation patterns. The picture of the seasonal vertically integrated moisture flux (figures 1(b) and (c)) gives an idea of the general pattern throughout the year, which is mainly dominated by air movement around the extended areas of high- and low-pressure centres, with important regional features such as monsoons, tropical cyclones, atmospheric rivers (ARs) and low-level jets (LLJs) (figure 1(a)). The southern branch of the subtropical high-pressure belts near 30° N and 30° S causes the trade winds to blow westward and equatorward at the Earth's surface. They merge and rise in the Intertropical Convergence Zone (ITCZ) near the equator carrying large amounts of moisture. The northern branch of the subtropical high-pressure belts flows poleward and eastward in the mid-latitudes, a movement also followed by extratropical cyclones and their associated ARs, which are the most effective systems for transporting moisture from the subtropics to the mid-latitudes, especially in winter. Seasonal differences are due to the intensification and expansion of the high-pressure belts and the poleward shift of the ITCZ during the hemispheric summer. In particular, over the northern Indian Ocean, the monsoon regime dominates the moisture flux, with moisture reaching the continent during its wet phase (northern hemisphere summer).

A schematic representation of the nine target regions (shaded in green) and their terrestrial (C1–C9) and oceanic (O1–O9) sources (shaded in orange and blue, respectively) is shown in figure 2. The moisture sources were detected using Lagrangian forward tracking during the optimal residence time of water vapour for each of the nine regions and delimited by the 90% threshold (table S1). A study region could gain moisture from more than one oceanic or terrestrial source of moisture, including its own region, through recycling processes (hereafter indicated as R). The moisture source areas detected for each region of interest are ordered in figure 2 based on the highest to lowest annual percentage contribution and are listed alphabetically. The oceanic and terrestrial sources are labelled independently. The total monthly contribution to precipitation from these specific moisture sources for each region is shown in figure 3.

For Central America (region 1), the own region acted as the most contributing moisture source (R1, 47.5%), followed by the North Atlantic source (O1A, 26%), which included the Caribbean Sea. Two oceanic sources contributed from the Pacific Ocean, with a slightly greater contribution from the North basin (10% vs. 7.9%). All the sources exhibited the same seasonal cycle (higher values during boreal summer), with a relative minimum occurring from both Pacific sources in July. Similar results were previously suggested by Durán-Quesada *et al* (2012). In

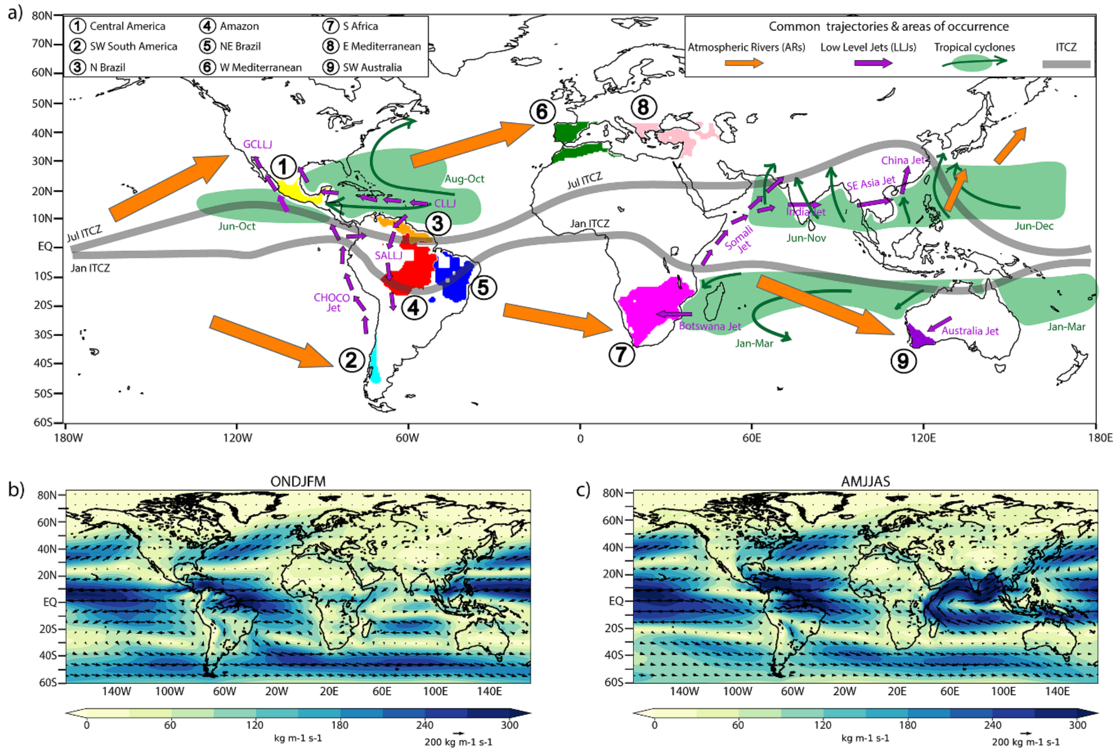

Figure 1. (a) Regions where at least 90% of the CMIP6 models used in this study agreed on a significant increase in precipitation-based drought magnitude from 1850 to 2100, together with the main moisture transport mechanisms affecting those regions (atmospheric rivers, low-level jets, and tropical cyclones). ITCZ: Intertropical Convergence Zone, GCLLJ: Gulf of California low-level jet, CLLJ: Caribbean low-level jet, SALLJ: South American low-level jet. (b), (c) Seasonally averaged vertically integrated moisture flux for October-March (ONDJFM) and April–September (AMJJAS), respectively, using ERA-Interim data for the period 1980–2018.

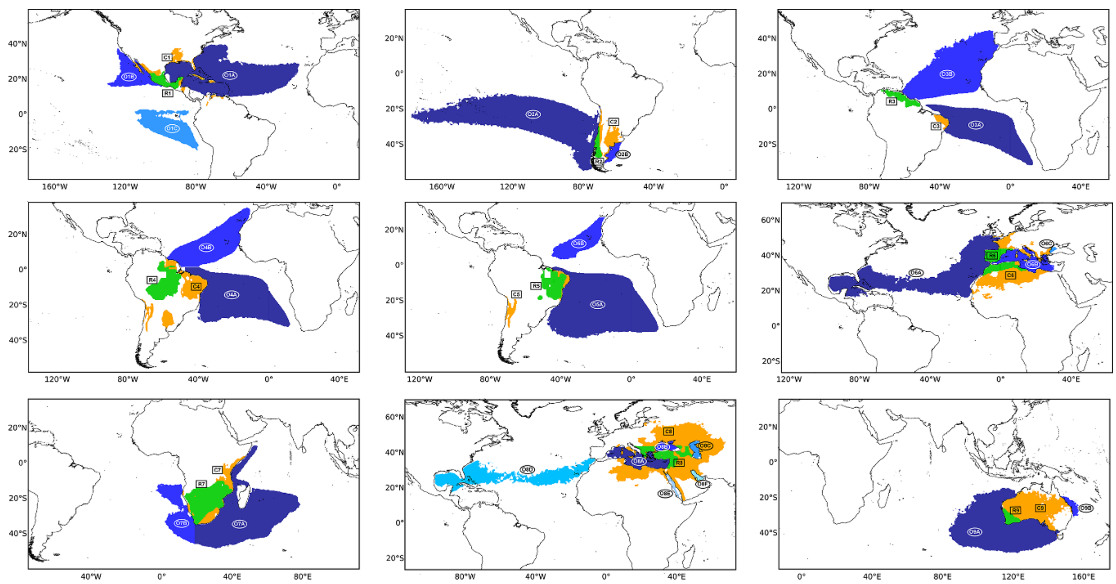

Figure 2. Schematic representation of the climatological moisture sources for the nine studied regions using ERA-Interim data: terrestrial moisture sources surrounding the region (C1–C9), the own region (R1–R9), and the different oceanic moisture source regions (the highest percentage of moisture contribution, OiA; the next, OiB; etc, where *i* is the number of the region).

general, moisture transport in the direction of central and northeastern South America is associated with the regional Caribbean LLJ from the Atlantic, the CHOCO LLJ from the South Pacific (Poveda *et al* 2014), and the Gulf of California summer coastal LLJ from the North Pacific (Parish 2000, Ordoñez *et al* 2019).

Three extratropical regions of the Southern Hemisphere were analysed: southwestern South America (region 2), southern Africa (region 7) and

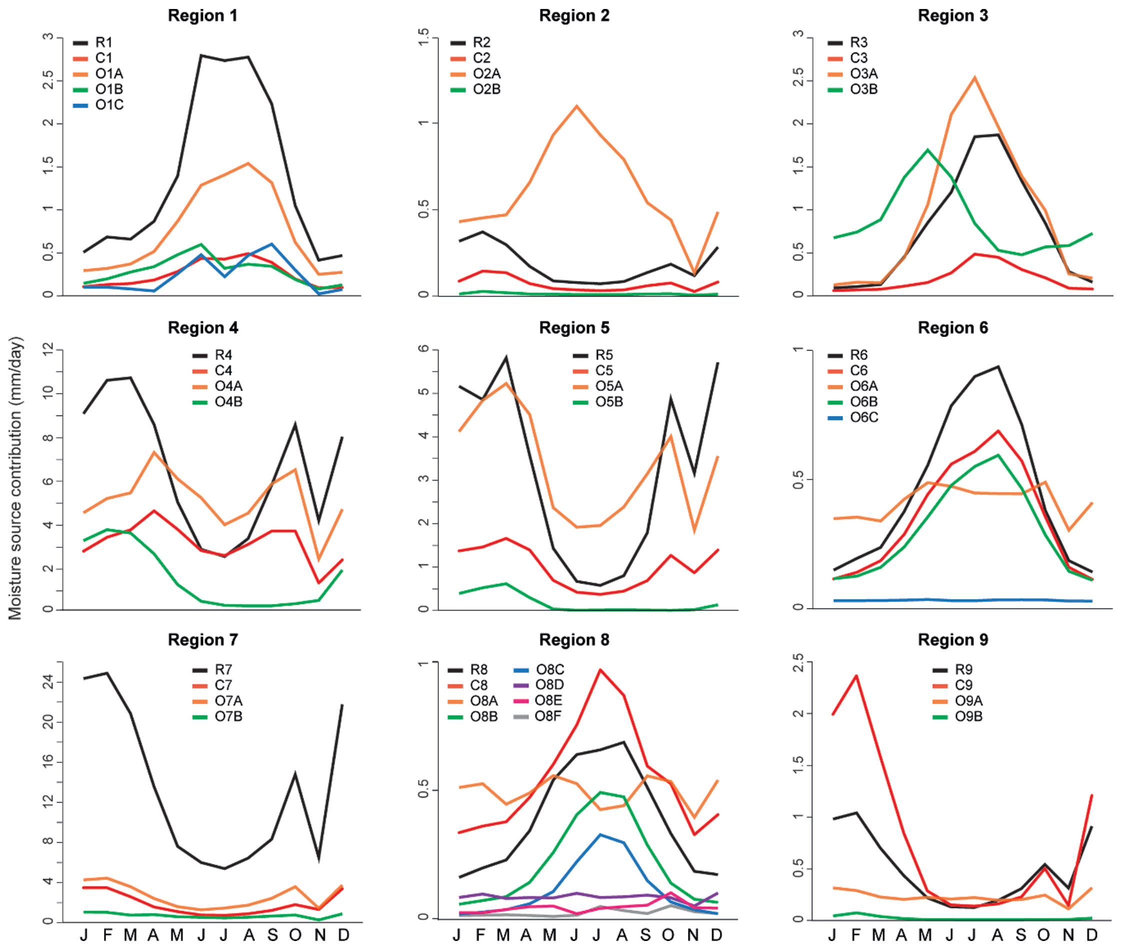

Figure 3. Monthly total contribution to precipitation from the specific moisture sources of each region for the period 1980–2018, using ERA-Interim data.

southwestern Australia (region 9). For region 2, along Chile, the most important source is the South Pacific basin (O2A, 69.8%), which supports the greatest amount of moisture throughout the year (Nieto *et al* 2014), with a marked peak in the austral winter. This maximum is linked with the ARs reaching the region (Valenzuela and Garreaud 2019, Algarra *et al* 2020) associated with extratropical cyclones, when the South Pacific high is weaker (Barret and Hameed 2017). The remaining sources, mainly the own terrestrial area (R2, 20.9%, the second source in importance) increased in relative importance, with considerable amounts occurring during the austral summer (when precipitation is often convective, Viale and Garreaud 2014) and when the South Pacific high is northwards positioned and closer to South America (Barrett and Hameed 2017). For regions 7 and 9 (southern Africa and southwestern Australia), the terrestrial sources are the most contributing ones, with R7 accounting for 72% in the former region and C9 accounting for 52.2% in the latter region. During the austral summer, high terrestrial moisture occurs due to a heat low over the interior of South Africa (Tyson and Preston-White 2000), which generates convective precipitation (Reason 2017) and is a consequence of the stronger easterlies associated with the local LLJs that inhibit moisture transport from the oceans located to their west (the Atlantic Ocean for region 7 and the Indian Ocean for region 9, Cheng and Lu 2023). The oceanic sources are spatially extensive, but they do not contribute more than 18% of the moisture to the sink regions in either case. For region 7 in winter, the Atlantic oceanic source (O7B) is associated with the passage of cyclone systems moving with westerlies and associated fronts and ARs (Reason 2017, Algarra *et al* 2020), and the Indian oceanic source (O7A) is positioned over the Agulhas Current System (Imbol Nkwinkwa *et al* 2021, Tim *et al* 2023).

For the two regions located in South America in the southern tropical band (regions 4 and 5), the main moisture source is terrestrial, with the regions themselves (R4 and R5) being the main contributors (40.35% and 41.6%, respectively), as recycling processes are relevant across these regions (Satyamurty *et al* 2013, Drumond *et al* 2019). Two oceanic moisture sources were detected for both regions, one over each basin of the Atlantic Ocean; the South Atlantic sources (O4A and O5A) provided more moisture (31.4% for region 4 and 43.1% for region 5) than did the North Atlantic sources (O4B and O5B). The overall contribution from all these sources shows a marked seasonal cycle (see figures 1(b) and (c)), in accordance with Drumond *et al* (2019), with lower contributions occurring during June-August (austral winter, with a more easterly zonal flow) and greater contributions occurring during October–March (austral summer, when R4 and R5 support more). Region 3, positioned in the northern tropical band, is fed mainly by oceanic moisture from both Atlantic basins at a similar percentage (34.1% from the south, i.e. O3A, and 31.6% from the north, i.e. O3B), as shown by Nieto *et al* (2008) and Sorí *et al* (2023). The highest moisture contribution from its sources, except O3B, occurred during the boreal summer (Nieto *et al* 2008). These patterns of moisture transport from the Atlantic Ocean in regions 3, 4 and 5 are consistent with the easterly winds on either side of the ITCZ along the southern and northern branches of the atmospheric circulation of the North and South Atlantic subtropical high-pressure systems, respectively (Gimeno *et al* 2020, and references therein).

In the eastern façade of the North Atlantic Ocean, for regions 6 and 8, which are west and east of the Mediterranean Sea, respectively, the moisture sources contributing most are the terrestrial ones, being more important the own region for the western Mediterranean region (R6, 30.5%) and the continental surrounding areas for the eastern Mediterranean region (C8, 28.8%). The closest ocean or sea positioned west of each region is the oceanic source with the greatest contribution; that is, the North Atlantic (O6A, 27%) for region 6, and the Mediterranean Sea (O8A, 26%) for region 8. Moisture is carried by the prevailing westerly winds at these latitudes and the usual synoptic meteorological systems (cyclones and ARs). All the sources for both regions present similar seasonal behaviours, with maximum values occurring in the boreal summer and minimum values occurring in the winter. However, during summer, terrestrial sources are more important, and in winter, the major contributor is the main oceanic source. These sources and variabilities were reported in early studies (e.g. Gómez-Hernández *et al* 2013, Schicker *et al* 2010 or Batibeniz *et al* 2020).

3.2. Origin of the moisture deficit responsible for droughts

Having identified the specific moisture sources of the nine studied regions, we computed the conditional probability of drought occurrence for each region given an equivalent moisture deficit from each source using standardised indices computed at the 1 month time scale (figure 4). This time scale enables to study short-duration droughts and it is the most relevant one to unravel the influence of moisture transport deficits, considering that the typical residence time of water vapour in the atmosphere is between 3 and 10 d (Gimeno *et al* 2021). Information about the selected copula models for each region and its specific moisture sources can be found in tables S2–S10. The results showed that for five out of the eight regions, the dominant moisture source (the one for which the deficit is associated with the highest drought probability) is the specific oceanic moisture source that contributes most to precipitation in that region (regions 1, 2, 6, 8 and 9, i.e. central America, southwestern South America, the western Mediterranean, the eastern Mediterranean and southwestern Australia). For regions 4, 5 and 7 (the Amazon, northeastern Brazil and southern Africa), the dominant source is its own region and for region 3 (northern Brazil), the nearby terrestrial source is the dominant source.

In general, for all the regions where drought is dominated by specific oceanic moisture sources, our results indicate that the probability of drought occurrence given a moisture deficit from those sources is only slightly greater than that considering the dominant global moisture source (figure 2(b) in Gimeno-Sotelo *et al* 2024b). For Central America, given a moisture deficit from the dominant specific source (located in the Atlantic Ocean), the conditional probability of drought is greater than 0.30, whereas considering the dominant major moisture source in that region (the North Atlantic moisture source), the probability is between 0.10 and 0.20. For southwestern South America, for a deficit from the dominant specific source (located in the Pacific Ocean), we found a drought probability greater than 0.25, while in most of the region, considering the dominant major moisture source (South Pacific source), the probabilities are lower than that value. For the western Mediterranean, a deficit from the specific moisture source corresponding to the North Atlantic Ocean implies a drought probability close to 0.35; however, for only a small subregion in the southwestern Iberian Peninsula, the probabilities are greater than 0.25 when the dominant major moisture source (the North Atlantic) is considered. For the eastern Mediterranean, a deficit from the specific moisture source (in the Mediterranean Sea) implies a drought probability of more than 0.40 (the major moisture source, the Mediterranean Sea; in this case, it is almost coincident with the specific one, so a deficit from the major source is also associated with very high probabilities in that region). For southwestern Australia, the specific dominant moisture source is located in the Indian Ocean, and given a deficit from that source, a drought probability of more than 0.20 is found; considering the dominant general moisture source (Indian Ocean), the probability is slightly lower (between 0.10 and 0.20).

For the regions where droughts are dominated by deficits from their own region, the deficits imply very high drought probabilities in the cases of the Amazon

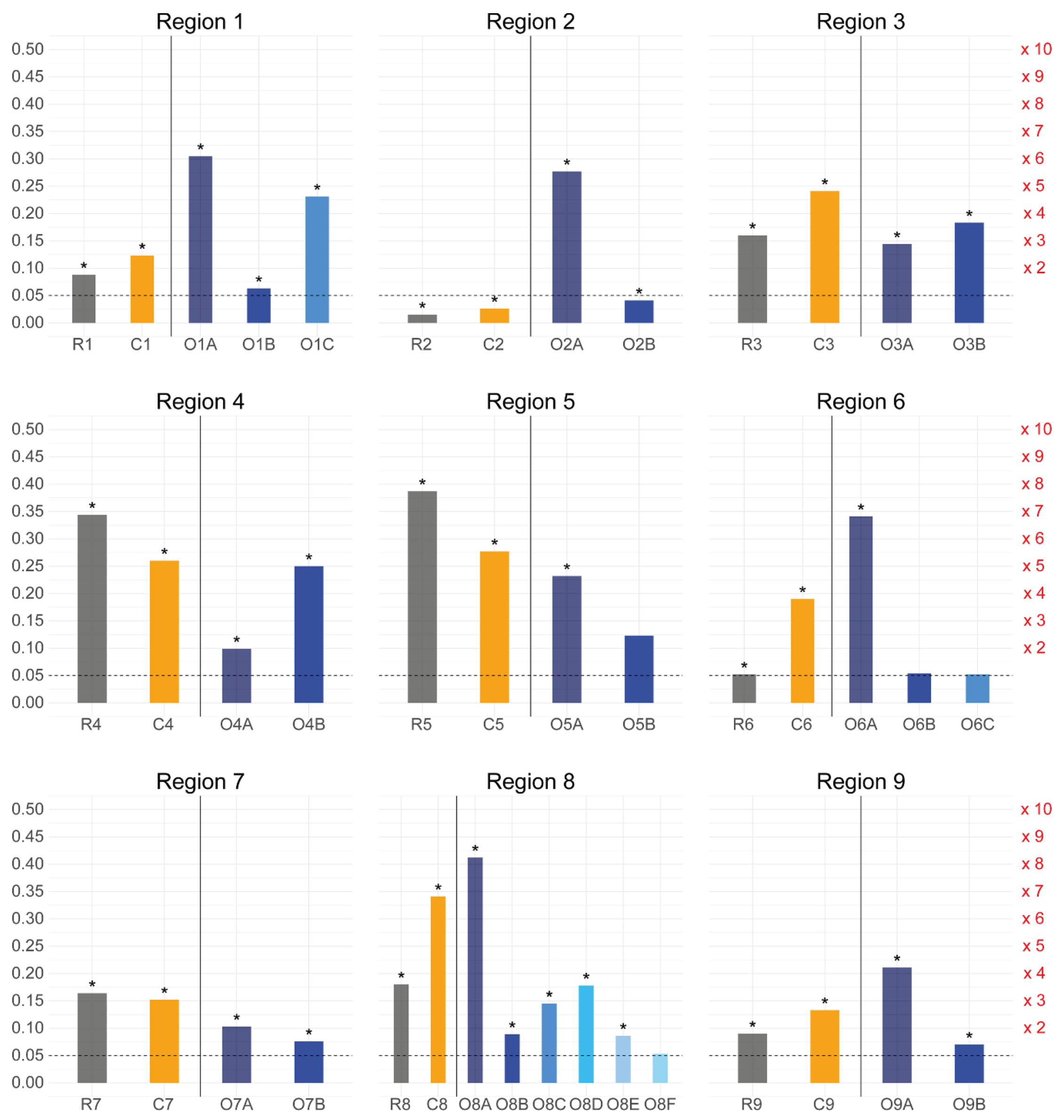

Figure 4. Conditional probability of drought occurrence given an equivalent moisture deficit from each of the specific moisture sources of each of the nine analysed regions for the standardised indices computed at the 1-month time scale. The left axis refers to the values of the probability, and the right axis indicates how many times the values are greater than the independence case (0.05). Asterisks indicate that the selected copula model fits well to the data at a significance level of 0.01.

and northeastern Brazil (close to 0.35 and close to 0.40, respectively) and a more moderate value in the case of southern Africa (slightly higher than 0.15). For northern Brazil, the deficit from the nearby terrestrial source, which is its dominant source, implies a fairly high drought probability (close to 0.25).

A relevant result is that the source that contributes the most to precipitation is not consistently the dominant source for the occurrence of droughts. Agreement occurs in four of the nine regions. In some cases, the source with the greatest contribution is the region itself for regions in areas with very strong evapotranspiration, such as the Amazon or southern Africa (region 4, region 5 and region 7). Another possibility is that the most contributing source is a remote oceanic source for a very narrow coastal area such as the Pacific coastal strip of South America (region 2).

Nonagreement takes place in five out of nine regions. This can occur when the moisture transport deficit from the oceanic source, despite not being the source contributing the most on average, is more effective in causing drought than the moisture transport deficit from the nearby continental source or the region itself (region 1, region 6, region 8 and region 9). In this case, the cascading connections between different moisture sources play a significant role. For example, there are regions where the terrestrial sources are the most contributing ones but their precipitation and enhanced moisture inputs mainly depend on remote oceanic moisture sources (figures 1(b) and (c) for a general view of the atmospheric circulation, which influences moisture transport; Gimeno *et al* 2012 for a review on the link moisture sources-sinks; and Gimeno *et al* 2016 for moisture transport mechanisms). A low contribution from the terrestrial sources (either the own region or the nearby continental source) does not necessarily imply a low contribution from the remote oceanic sources. However, and given cascading effects, a low contribution from the remote oceanic sources would imply a low contribution from the terrestrial sources with a greater or lesser delay as moisture availability decreases. This cascading effect is possible even on the one-month timescale used to analyse droughts, because moisture transport has a timescale linked to the residence time of water vapour in the atmosphere, typically between 3 and 10 d (Gimeno *et al* 2021), which is shorter than the timescale used in this article and therefore allows cascading effects. The difference between target regions where the most contributing terrestrial source dominates drought occurrence (regions 4, 5, and 7, mostly tropical) and target regions where the most contributing terrestrial source does not dominate (regions 1, 6, 8 and 9, mostly extratropical) would be explained by the fact that land evapotranspiration is more intense in tropical humid regions due to high atmospheric evaporative demand, so that recycling processes would dominate drought occurrence in the short term (Wang and Dickinson 2012, Singer *et al* 2021). All these processes, which are characterised by strong spatial variability, would explain why the deficit in the moisture contribution from oceanic moisture sources takes longer to produce a deficit in the contribution from the terrestrial sources of regions in tropical humid areas than in extratropical ones. For example, the probability that the contribution from the most contributing terrestrial source is lower than its 5% percentile, conditional on the contribution from the most contributing oceanic one being lower than its 5% percentile, is only 0.10 for region 4 (the Amazon), while it is as high as 0.39 for region 6 (western Mediterranean), i.e. almost four times higher. It is explained by the higher evapotranspiration values in the former (a tropical region) than in the latter one (an extratropical region). Thus, in extratropical target regions, a deficit in the contribution from distant oceanic sources has a more direct impact on drought occurrence than in tropical target regions. Nonagreement may also occur when the dominant source for drought occurrence is placed in the path of the moisture transported from both the most contributing remote oceanic source and another secondary remote oceanic source (region 3).

Although the results reported in this study refer to the present climate and source extents and intensities and drought probability values may vary in the future, they are highly relevant regarding climate change implications. The dominant moisture sources of regions 1, 2, 6, 8 and 9, which are oceanic, and the one corresponding to region 4, which is terrestrial (its own region) are located in areas where the balance between evaporation and precipitation is projected to increase strongly according to CMIP6 climate models (figure 5 in Allan 2023). Furthermore, a large proportion of the dominant sources are located in areas that are likely to experience changes in atmospheric circulation (Allan *et al* 2020), such as the narrowing and intensification of the ITCZ (which would affect the dominant source of regions such as 3 or 4) or the expansion to higher latitudes of the storm track and associated moisture transport mechanisms such as ARs (which would affect the dominant source of regions such as 1, 2, 6 and 8).

4. Concluding remarks

In this paper, we focused on regions for which climate models show the greatest agreement in increases in drought magnitude in the future climate. We identified the main climatological moisture sources of these regions and analysed the influence of moisture transport deficits from these sources on drought occurrence in the regions. We reached three important conclusions:

For the nine identified regions, there are a variety of situations for the dominant sources for drought; with three regions where it is the region itself (the Amazon, northeastern Brazil and southern Africa), highlighting the role of recycling; one region where it is the nearby terrestrial source (northern Brazil), and five regions where it is an oceanic source (central America, southwestern South America, both western and eastern Mediterranean and southwestern Australia).

The probability of drought occurrence given an equivalent contribution deficit from the dominant specific moisture source of a given region is generally high. In some cases, the drought probability is as high as 0.40, a value that is eight times greater than the one corresponding to the independence case (i.e. in which contribution deficit and drought are unrelated). However, in general, considering the moisture deficit from specific moisture sources instead of the deficit from major global moisture sources (Gimeno-Sotelo *et al* 2024b) provides only slightly higher drought probabilities.

The source that dominates drought occurrence in a region, i.e. the one associated with the highest probability, does not consistently coincide with the source that contributes the most to the precipitation in each region. This should be understood in terms of the cascading connections between different moisture sources, which explain why, in some regions, droughts predominantly depend on oceanic moisture sources despite the fact that the terrestrial sources are the most contributing ones. In those cases, low contributions from the oceanic sources imply low contributions from the terrestrial ones, especially in extratropical target regions, where land evapotranspiration is less intense than in tropical humid ones. This result is especially remarkable when contextualising the importance of the results, since we should focus on what will happen in these dominant moisture sources to correctly interpret how moisture transport deficits affect droughts at the regional scale. It should be noted that we analysed the moisture sources and their importance in drought occurrence in the present climate and did not evaluate how these sources may vary in the future, which would undoubtedly merit future studies.

Data availability statement

The data that support the findings of this study are openly available at the following URLs: https://esgf-node.llnl.gov/search/cmip6/; www.flexpart.eu/downloads; www.gloh2o.org/mswep/.

Acknowledgments

EPhysLab members are supported by the PID2021-122314OB-I00 and TED2021-129152B-C41/TED2021-129152B-C43 projects funded by the Ministerio de Ciencia, Innovación y Universidades, Spain (MICIU/AEI/10.13039/501100011033), Xunta de Galicia under the Project ED431C2021/44 (Programa de Consolidación e Estructuración de Unidades de Investigación Competitivas (Grupos de Referencia Competitiva) and Consellería de Cultura, Educación e Universidade), and by the European Union 'ERDF A way of making Europe' 'NextGenerationEU'/PRTR. Luis Gimeno-Sotelo was supported by a 'Ministerio de Ciencia,Innovación y Universidades' PhD Grant (reference: PRE2022-101497). Milica Stojanovic acknowledges the Grant No. ED481B-2021/134 from the Xunta of Galicia (regional government), and Rogert Sorí the grant RYC2021-034044-I funded by Ministerio de Ciencia, Innovación y Universidades, Spain (MICIU/ AEI/10.13039/501100011033) and the European Union Next Generation EU/PRTR. This work has also been possible thanks to the computing resources and technical support provided by CESGA (Centro de Supercomputación de Galicia) and RES (Red Española de Supercomputación). This study was also supported by the 'Unidad Asociada CSIC–Universidade de Vigo: Grupo de Física de la Atmósfera y del Océano'.

Author contributions

Luis Gimeno-Sotelo designed the experiments and contributed to data analysis and paper writing. Milica Stojanovic and Rogert Sorí performed the Lagrangian analysis and contributed to paper writing. Raquel Nieto contributed to the creation of the final figures and paper writing. Sergio M Vicente-Serrano contributed to the discussion of the results. Luis Gimeno conceived the idea for the study and contributed to the writing of the paper. All the authors contributed to the review and editing of the manuscript.

ORCID iDs

Luis Gimeno-Sotelo https://orcid.org/0000-0001-9305-2325
Milica Stojanovic https://orcid.org/0000-0002-6783-9025
Luis Gimeno https://orcid.org/0000-0002-0778-3605

References

Akaike H 1974 A new look at the statistical model identification *IEEE Trans. Autom. Control* **19** 716–23

Algarra I, Nieto R, Ramos A M, Eiras-Barca J, Trigo R M and Gimeno L 2020 Significant increase of global anomalous moisture uptake feeding landfalling atmospheric rivers *Nat. Commun.* **11** 5082

Allan R P *et al* 2020 Advances in understanding large-scale responses of the water cycle to climate change *Ann. New York Acad. Sci.* **1472** 49–75

Allan R P 2023 Amplified seasonal range in precipitation minus evaporation *Environ. Res. Lett.* **18** 094004

Bachmair S, Kohn I and Stahl K 2015 Exploring the link between drought indicators and impacts *Nat. Hazards Earth Syst. Sci.* **15** 1381–97

Barrett B S and Hameed S 2017 Seasonal variability in precipitation in Central and Southern Chile: modulation by the South Pacific high *J. Clim.* **30** 55–69

Batibeniz F, Ashfaq M, Önol B, Turuncoglu U U, Mehmood S and Evans K J 2020 Identification of major moisture sources across the Mediterranean Basin *Clim. Dyn.* **54** 4109–27

Beck H E, van Dijk A I J M, Levizzani V, Schellekens J, Miralles D G, Martens B and de Roo A 2017 MSWEP: 3-hourly 0.25° global gridded precipitation (1979–2015) by merging gauge, satellite, and reanalysis data *Hydrol. Earth Syst. Sci.* **21** 589–615

Cammalleri C *et al* 2020 *Global warming and drought impacts in the EU* (Publications Office of the European Union) (https://doi.org/10.1016/j.ejrh.2020.100723)

Cheng T F and Lu M 2023 Global Lagrangian tracking of continental precipitation recycling, footprints, and cascades *J. Clim.* **36** 1923–41

Cook B I, Mankin J S, Marvel K, Williams A P, Smerdon J E and Anchukaitis K J 2020 Twenty-first century drought projections in the CMIP6 forcing scenarios *Earth's Future* **8** e2019EF001461

Czado C 2019 *Analyzing Dependent Data with Vine Copulas (Lecture Notes in Statistics)* (Springer) p 222

Dee D P *et al* 2011 The ERA-Interim reanalysis: configuration and performance of the data assimilation system *Q. J. R. Meteorol. Soc.* **137** 553–97

Douville H *et al* 2021 Water cycle changes *Climate Change 2021: The Physical Science Basis. Contribution of Working Group I to the Sixth Assessment Report of the Intergovernmental Panel on Climate Change* ed V Masson-Delmotte (Cambridge University Press) pp 1055–210

Drumond A, Stojanovic M, Nieto R, Vicente-Serrano S M and Gimeno L 2019 Linking anomalous moisture transport and drought episodes in the IPCC reference regions *Bull. Am. Meteorol. Soc.* **100** 1481–98

Durán-Quesada A M, Reboita M and Gimeno L 2012 Precipitation in tropical America and the associated sources of moisture: a short review *Hydrol. Sci. J.* **57** 612–24

Erian W, Pulwarty R, Vogt J V, AbuZeid K, Bert F, Bruntrup M and Zougmore R B 2021 *GAR special report on drought 2021* (United Nations Office for Disaster Risk Reduction (UNDRR))
Eyring V, Bony S, Meehl G A, Senior C A, Stevens B, Stouffer R J and Taylor K E 2016 Overview of the coupled model intercomparison project phase 6 (CMIP6) experimental design and organization *Geosci. Model Dev.* **9** 1937–58
Fernández-Álvarez J C, Pérez-Alarcón A, Eiras-Barca J, Rahimi S, Nieto R and Gimeno L 2023 Projected changes in atmospheric moisture transport contributions associated with climate warming in the North Atlantic *Nat. Commun.* **14** 6476
Fernández-Alvarez J C, Vázquez M, Pérez-Alarcón A, Nieto R and Gimeno L 2023 Comparison of moisture sources and sinks estimated with different versions of FLEXPART and FLEXPART-WRF models forced with ECMWF reanalysis data *J. Hydrometeorol.* **24** 221–39
Fleig A K, Tallaksen L M, Hisdal H and Demuth S 2006 A global evaluation of streamflow drought characteristics *Hydrol. Earth Syst. Sci.* **10** 535–52
Garcia-Herrera R, Garrido-Perez J M, Barriopedro D, Ordóñez C, Vicente-Serrano S M, Nieto R, Gimeno L, Sorí R and Yiou P 2019 The European 2016/2017 drought *J. Clim.* **32** 3169–87
Gimeno L, Dominguez F, Nieto R, Trigo R, Drumond A, Reason C J, Taschetto A S, Ramos A M, Kumar R and Marengo J 2016 Major mechanisms of atmospheric moisture transport and their role in extreme precipitation events *Annu. Rev. Environ. Resour.* **41** 117–41
Gimeno L, Drumond A, Nieto R, Trigo R M and Stohl A 2010a On the origin of continental precipitation *Geophys. Res. Lett.* **37** L13804
Gimeno L, Eiras-Barca J, Durán-Quesada A M, Dominguez F, van der Ent R, Sodemann H, Sánchez-Murillo R, Nieto R and Kirchner J W 2021 The residence time of water vapour in the atmosphere *Nat. Rev. Earth Environ.* **2** 558–69
Gimeno L, Nieto R, Trigo R M, Vicente S and Lopez-Moreno J I 2010b Where does the Iberian Peninsula moisture come from? An answer based on a Lagrangian approach *J. Hydrometeorol.* **11** 421–36
Gimeno L, Stohl A, Trigo R M, Domínguez F, Yoshimura K, Yu L, Drumond A, Durán-Quesada A M and Nieto R 2012 Oceanic and terrestrial sources of continental precipitation *Rev. Geophys.* **50** RG4003
Gimeno L, Vázquez M, Eiras-Barca J, Sorí R, Stojanovic M, Algarra I, Nieto R, Ramos A M, Durán-Quesada A M and Dominguez F 2020 Recent progress on the sources of continental precipitation as revealed by moisture transport analysis *Earth Sci. Rev.* **201** 103070
Gimeno-Sotelo L, Sorí R, Nieto R, Vicente-Serrano S M and Gimeno L 2024b Unravelling the origin of the atmospheric moisture deficit that leads to droughts *Nat. Water* **2** 242–53
Gimeno-Sotelo L *et al* 2024a Assessment of the global relationship of different types of droughts in model simulations under high anthropogenic emissions *Earth's Future* **12** e2023EF003629
Gómez-Hernández M, Drumond A, Gimeno L and Garcia-Herrera R 2013 Variability of moisture sources in the Mediterranean region during the period 1980–2000 *Water Resour. Res.* **49** 6781–94
Herrera-Estrada J E, Martinez J A, Dominguez F, Findell K L, Wood E F and Sheffield J 2019 Reduced moisture transport linked to drought propagation across North America *Geophys. Res. Lett.* **46** 5243–53
Hersbach H *et al* 2020 The ERA5 global reanalysis *Q. J. R. Meteorol. Soc.* **146** 1999–2049
Holgate C M, Van Dijk A I J M, Evans J P and Pitman A J 2020 Local and remote drivers of southeast Australian drought *Geophys. Res. Lett.* **47** e2020GL090238
Huang W and Prokhorov A 2014 A goodness-of-fit test for copulas *Econ. Rev.* **33** 751–71
Imbol Nkwinkwa A S N, Rouault M, Keenlyside N and Koseki S 2021 Impact of the Agulhas current on Southern Africa precipitation: a modeling study *J. Clim.* **34** 9973–88
IPCC 2022 Climate change 2022: impacts, adaptation and vulnerability *Contribution of Working Group II to the Sixth Assessment Report of the Intergovernmental Panel on Climate Change* ed H-O Pörtner *et al* (Cambridge University Press) p 3056
Kendall M G 1948 Rank correlation methods
Mann H B 1945 Nonparametric tests against trend *Econometrica* **13** 245–59
McKee T B, Doesken N J and Kleist J 1993 The relationship of drought frequency and duration to time scales *Proc. 8th Conf. on Applied Climatology* vol 17 pp 179–83
Naumann G, Camalleri C, Mentaschi L and Feyen L 2021 Increased economic drought impacts in Europe with anthropogenic warming *Nat. Clim. Change* **11** 485–91
Nieto R, Castillo R, Drumond A and Gimeno L 2014 A catalog of moisture sources for continental climatic regions *Water Resour. Res.* **50** 5322–8
Nieto R, Gallego D, Trigo R, Ribera P and Gimeno L 2008 Dynamic identification of moisture sources in the Orinoco basin in equatorial South America *Hydrol. Sci. J.* **53** 602–17
Nieto R and Gimeno L 2019 A database of optimal integration times for Lagrangian studies of atmospheric moisture sources and sinks *Sci. Data* **6** 59
Nieto R and Gimeno L 2021 Addendum: a database of optimal integration times for Lagrangian studies of atmospheric moisture sources and sinks *Sci. Data* **8** 130
NOAA-NCEI (National Oceanic and Atmospheric Administration National Centers for Environmental Information) 2021 U.S. billion-dollar weather and climate disasters: overview (available at: www.ncdc.noaa.gov/billions/)
Ordoñez P, Nieto R, Gimeno L, Ribera P, Gallego D, Ochoa-Moya C A and Quintanar A I 2019 Climatological moisture sources for the Western North American Monsoon through a Lagrangian approach: their influence on precipitation intensity *Earth Syst. Dyn.* **10** 59–72
Parish T R 2000 Forcing of the summertime low-level jet along the California coast *J. Appl. Meteorol.* **39** 2421–33
Pisso I *et al* 2019 The Lagrangian particle dispersion model FLEXPART version 10.4 *Geosci. Model Dev.* **12** 4955–97
Poveda G, Jaramillo L and Vallejo L F 2014 Seasonal precipitation patterns along pathways of South American low-level jets and aerial rivers *Water Resour. Res.* **50** 98–118
Reason C J C 2017 Climate of southern Africa *Oxford Research Encyclopedia of Climate Science* p 450
Roy T, Martinez J A, Herrera-Estrada J E, Zhang Y, Dominguez F, Berg A, Ek M and Wood E F 2019 Role of moisture transport and recycling in characterizing droughts: perspectives from two recent U.S. droughts and the CFSv2 system *J. Hydrometeorol.* **20** 139–54
Salah Z, Nieto R, Drumond A, Gimeno L and Vicente-Serrano S 2018 A Lagrangian analysis of the moisture budget over the fertile crescent during two intense drought episodes *J. Hydrol.* **560** 382–95
Satyamurty P, da Costa C P W and Manzi A O 2013 Moisture source for the Amazon Basin: a study of contrasting years *Theor. Appl. Climatol.* **111** 195–209
Schicker I, Radanovics S and Seibert P 2010 Origin and transport of Mediterranean moisture and air *Atmos. Chem. Phys.* **10** 5089–105
Schumacher D L, Keune J, Dirmeyer P and Miralles D G 2022 Drought self-propagation in drylands due to land–atmosphere feedbacks *Nat. Geosci.* **15** 262–8
Seneviratne S I *et al* 2021 Weather and climate extreme events in a changing climate *Climate Change 2021: The Physical Science Basis. Contribution of Working Group I to the Sixth Assessment Report of the Intergovernmental Panel on Climate Change V* Masson-Delmotte ed (Cambridge University Press) pp 1513–766
Singer M B, Asfaw D T, Rosolem R, Cuthbert M O, Miralles D G, MacLeod D, Quichimbo E A and Michaelides K 2021

Hourly potential evapotranspiration at 0.1° resolution for the global land surface from 1981-present *Sci. Data* **8** 224
Sorí R, Gimeno-Sotelo L, Nieto R, Liberato M L, Stojanovic M, Pérez-Alarcón A, Gimeno L and Gimeno L 2023 Oceanic and terrestrial origin of precipitation over 50 major world river basins: implications for the occurrence of drought *Sci. Total Environ.* **859** 160288
Spinoni J *et al* 2020 Future global meteorological drought hot spots: a study based on CORDEX data *J. Clim.* **33** 3635–61
Stine S 1994 Extreme and persistent drought in California and Patagonia during mediaeval time *Nature* **369** 546–9
Stohl A, Forster C, Frank A, Seibert P and Wotawa G 2005 The Lagrangian particle dispersion model FLEXPART version 6.2 *Atmos. Chem. Phys.* **5** 2461–74
Tallaksen L M, Madsen H and Clausen B 1997 On the definition and modelling of streamflow drought duration and deficit volume *Hydrol. Sci. J.* **42** 15–33
Tim N, Zorita E, Hünicke B and Ivanciu I 2023 The impact of the Agulhas current system on precipitation in Southern Africa in regional climate simulations covering the recent past and future *Weather Clim. Dyn.* **4** 381–97
Trenberth K E, Dai A, Rasmussen R M and Parsons D B 2003 The changing character of precipitation *Bull. Am. Meteorol. Soc.* **84** 1205–18
Tyson D and Preston-White R A 2000 *The Weather and Climate of Southern Africa* (Oxford University Press)
Ukkola A, De Kauwe M, Roderick M, Abramowitz G and Pitman A J 2020 Robust future changes in meteorological drought in CMIP6 projections despite uncertainty in precipitation *Geophys. Res. Lett.* **47** e2020GL087820
Valenzuela R A and Garreaud R D 2019 Extreme daily rainfall in central-southern Chile and its relationship with low-level horizontal water vapor fluxes *J. Hydrometeorol.* **20** 1829–50
Vázquez M, Nieto R, Liberato M L R and Gimeno L 2020 Atmospheric moisture sources associated with extreme precipitation during the peak precipitation month *Weather Clim. Extremes* **30** 100289
Viale M and Garreaud R 2014 Summer precipitation events over the western slope of the subtropical Andes *Mon. Weather Rev.* **142** 1074–92
Wang K and Dickinson R E 2012 A review of global terrestrial evapotranspiration: observation, modeling, climatology, and climatic variability *Rev. Geophys.* **50** RG2005
Wei J and Dirmeyer P A 2019 Sensitivity of land precipitation to surface evapotranspiration: a nonlocal perspective based on water vapor transport *Geophys. Res. Lett.* **46** 12588–97
White H 1982 Maximum likelihood estimation of misspecified models *Econometrica* **50** 1–25
Wilhite D A, Svoboda M D and Hayes M J 2007 Understanding the complex impacts of drought: a key to enhancing drought mitigation and preparedness *Water Resour. Manage.* **21** 763–74
World Meteorological Organization. Standardized Precipitation Index User Guide 2012 (available at: https://library.wmo.int/records/item/39629-standardized-precipitation-index-user-guide)
Woxodhouse C A, Meko D M, MacDonald G M, Stahle D W and Cook E R 2010 A 1,200-year perspective of 21st century drought in Southwester North America *Proc. Natl Acad. Sci. USA* **107** 21283–8
Zhao T and Dai A 2022 CMIP6 model-projected hydroclimatic and drought changes and their causes in the twenty-first century *J. Clim.* **35** 897–921

4.6 Projected changes in the role of moisture transport in the occurrence of hydrometeorological extremes in the Euromediterranean region

This section is made up of a manuscript that was submitted in 2024, entitled "**The increasing influence of atmospheric moisture transport on hydrometeorological extremes in the Euromediterranean region with global warming**", by **Gimeno-Sotelo, L.**, Fernández-Alvarez, J. C., Nieto, R., Vicente-Serrano, S. M., & Gimeno, L.

The increasing influence of atmospheric moisture transport on hydrometeorological extremes in the Euromediterranean region with global warming

Luis Gimeno-Sotelo[1], José Carlos Fernández-Alvarez[1], Raquel Nieto[1], Sergio M. Vicente-Serrano[2], Luis Gimeno[1,*]

[1]Centro de Investigación Mariña, Environmental Physics Laboratory, Universidade de Vigo, Ourense, Spain

[2]Instituto Pirenaico de Ecología, Consejo Superior de Investigaciones Científicas, Zaragoza, Spain

*(Corresponding author: l.gimeno@uvigo.es)

Abstract

The Euromediterranean area is a key region in which the link between atmospheric moisture transport and hydrometeorological extremes concerns. Atmospheric rivers, one of the main moisture transport mechanisms, play a notable role in extreme precipitation there, subsequently associated with flood occurrence. Moreover, contribution deficits from two of the major oceanic moisture sources of the planet, the North Atlantic Ocean and the Mediterranean Sea, are strongly related to drought occurrence in that region. Here, we deeply examine the projected changes in these relationships with global warming. Our results show that, for the mid-21st century, a moderate increase in the influence of moisture transport on winter precipitation maxima is projected, in line with its increasing concurrence with atmospheric rivers. A stronger increase is estimated for the relationship between moisture source contribution deficits and drought occurrence, for which probabilities between two and three times greater than those observed in the present climate are obtained for the mid- and end-21st century. This highlights the increasing importance of moisture transport from the ocean in future droughts in the region, especially in the context of reduced local moisture inputs from terrestrial evaporation as a consequence of drier soil.

Introduction

Hydrometeorological extremes, including those associated with precipitation excesses or deficits, lead to floods and droughts, which cause great socioeconomic and environmental impacts (*IPCC, 2022*). Theoretical physics and numerical models provide strong evidence that extreme precipitation events and meteorological droughts are highly sensitive to global warming (*Seneviratne et al., 2021*).

Recent assessments suggest that extreme precipitation has increased over land areas and will continue to increase under global warming scenarios (*Douville et al., 2021; Seneviratne et al., 2021*), given the constraints imposed by increasing temperature because, according to the Clausius–Clapeyron relationship, humidity increases at a rate of 6-7% for each degree of temperature increase (*Soden and Held, 2006; Allen and Ingram, 2002*). This increase will be regionally modulated by dynamic mechanisms, as changes in atmospheric circulation will lead to modifications in the convergence of atmospheric humidity, affecting the rates of humidity change (*Pfahl et al., 2017*) and ultimately regional extreme precipitation (*O'Gorman, 2015; Bao et al., 2017; Gimeno-Sotelo et al., 2024c*). Similarly, the severity of meteorological droughts has increased in some regions (*Seneviratne et al., 2021*), and it is projected to increase, among other regions, in the Mediterranean, central Asia, northern South America, Southwest Australia, etc. (*Ukkola et al., 2020; Gimeno-Sotelo et al., 2024a*).

Behind extreme precipitation and meteorological drought, excesses or deficits in moisture transport to the region are frequent (*Gimeno et al., 2012; Liu et al., 2020*) since the available humidity at a given time and place is usually not sufficient to generate precipitation (*Trenberth et al., 2003*), and important moisture contributions from other regions are required for precipitation after its convergence *(Mo et al., 2021*). Nevertheless, the control of extreme precipitation and meteorological drought by moisture transport is not spatially or seasonally homogeneous; the main influence is recorded in regions dominated by the main mechanisms of moisture transport, such as atmospheric rivers, low-level jets or tropical cyclones (*Gimeno et al., 2016*), indicating that in some regions, moisture transport strongly controls extreme precipitation and meteorological drought (*Gimeno-Sotelo and Gimeno, 2023, Gimeno-Sotelo et al., 2024b*).

One of the regions where the relationships between moisture transport and precipitation excesses and deficits are most pronounced is the Euromediterranean area. It is affected by the strongest moisture transport mechanisms that affect both average and, above all, extreme precipitation: the atmospheric rivers (ARs) on the European Atlantic coast (*Lavers and Villarini, 2013a,b*), as well as on the northern coasts of the Mediterranean (*Lorente-Plazas et al., 2020*). Therefore, it is not surprising that around the Mediterranean, there are large continental regions where both extreme daily precipitation and meteorological droughts are strongly affected by anomalously high or low moisture transport. In particular, the influence of moisture transport on extreme daily precipitation bears the signature of the AR track (*Gimeno-Sotelo and Gimeno, 2023, Konstali et al., 2024*). Moreover, meteorological droughts are highly likely to occur in the region in response to deficits in moisture transport from the Atlantic Ocean or the

Mediterranean Sea (*Gimeno-Sotelo et al., 2024b*). These major moisture transport mechanisms are projected to change significantly with global warming (*Payne et al, 2020*), which could dramatically alter the frequency and severity of extreme precipitation and meteorological drought in the Euromediterranean region.

Moisture transport is expected to increase with global warming to values close to the Clausius–Clapeyron relation (*O'Gorman and Muller 2010*) but is modulated regionally by changes in atmospheric circulation (*Allan, et al. 2020*). This behaviour could have important consequences for the occurrence and intensity of extreme precipitation and meteorological drought in the future since it could i) alter the relative contribution of moisture transport against other mechanisms in the occurrence of these extreme events and ii) modify the amplitude of the seasons and regions in which moisture transport shows crucial importance in explaining extreme precipitation and meteorological drought. In the Euromediterranean region, these hypothetical modifications in moisture transport could have dramatic consequences given the limited water resources of the region (*García-Ruiz et al., 2011*) and the frequent occurrence of droughts (*Cook et al., 2016*) and extreme precipitation events (*Mastrantonas et al., 2021*).

Given the priority of solving this knowledge gap, here, we investigate the relationship between moisture transport and extreme precipitation and meteorological droughts in the Euromediterranean region in a scenario of high greenhouse gas emissions. For this purpose, we used advanced statistical methods for extreme value analysis and dependence modelling based on high-resolution simulations by the Weather Research and Forecast (WRF) Eulerian mesoscale model using the ERA5 reanalysis (*Hersbach et al., 2020*) and the Community Earth System Model Version 2 CESM2 climate model (*Danabasoglu, 2020*) for the shared socioeconomic pathway SSP5-8.5 of CMIP6 (*O'Neill, 2016*). Our results indicate a greater influence of moisture transport on these hydrometeorological extremes under the analysed scenario, which is particularly relevant for meteorological droughts.

Results and discussion

Changes in the relationship between moisture transport and extreme precipitation under a high greenhouse gas scenario

Using a Eulerian approach and Extreme Value Theory (EVT) methods, we calculated the dependence of extreme precipitation quantified at the daily scale on moisture transport quantified as integrated vertical moisture transport (IVT). This approach should be understood in the context of the influence of atmospheric rivers on extreme precipitation (see Methods section for details, and Figure S1 for information about the satisfactory goodness-of-fit assessment of the statistical models). Since the influence of moisture transport on extreme precipitation is much greater in winter than in summer in the Euromediterranean area (*Gimeno-Sotelo and Gimeno, 2023*), the main focus of our analysis is on the cold season (January-March), with a brief reference to the summer season (July-September).

CESM2 satisfactorily reproduces the average spatial patterns of extreme precipitation at a high resolution (Fig. 1a, b), as well as the associated IVT (Fig. 1e, f) and the percentage of days of extreme precipitation coinciding with atmospheric rivers (Fig. 1i, j). As expected, regions where the concurrence of ARs and extreme precipitation is high agree with those with the highest associated IVT values. However, this is not the case for the highest extreme precipitation values, which occur where there is also notable orography upwind of the dominant westerly and southerly flows from the Atlantic Ocean and the Mediterranean Sea, respectively (see Figure S2a). For example, atmospheric rivers are responsible for most of the extreme precipitation days recorded on both the French Atlantic coast and the western Iberian Peninsula, but extreme precipitation values are lower in the former case.

An increase in the projected extreme precipitation (based on the maximum daily values) is recorded in most of the region (Fig. 1c, d) but is characterized by a north–south gradient (*Zittis et al., 2021; Lionello and Scarascia, 2020*). A general increase of 40% and 80% is recorded in the northern part of the region in the mid- and end-century, respectively. In contrast, in southern Spain, Italy and Greece, a small decrease is recorded for the middle (up to 20%) and end (up to 40%) of the century, and in North Africa, the projected decrease is stronger (approximately 40% in the mid-century period and 60% in the end-century period). Nevertheless, independent of the north–south gradient of the projected extreme precipitation, there is a widespread increase in the importance of moisture transport on extreme precipitation (Fig. 1g, h), but regional differences are particularly visible in the Pyrenees, central Italy and Greece, and northern Africa. In contrast, the pattern of the percentage of atmospheric river occurrence on the maximum precipitation days is well reproduced by the CESM2 model with respect to the ERA5 pattern (Fig. 1i,j). The spatial distribution of the pattern is relatively stable, although with a general increasing value in the future (Fig. 1k,l), with the areas with the highest values on the western coast of the Iberian Peninsula and France (80 to 100%) and moderate to high values (50 to 70%) in the interior of the Iberian Peninsula and on the western coasts of Italy, the Balkans and Turkey.

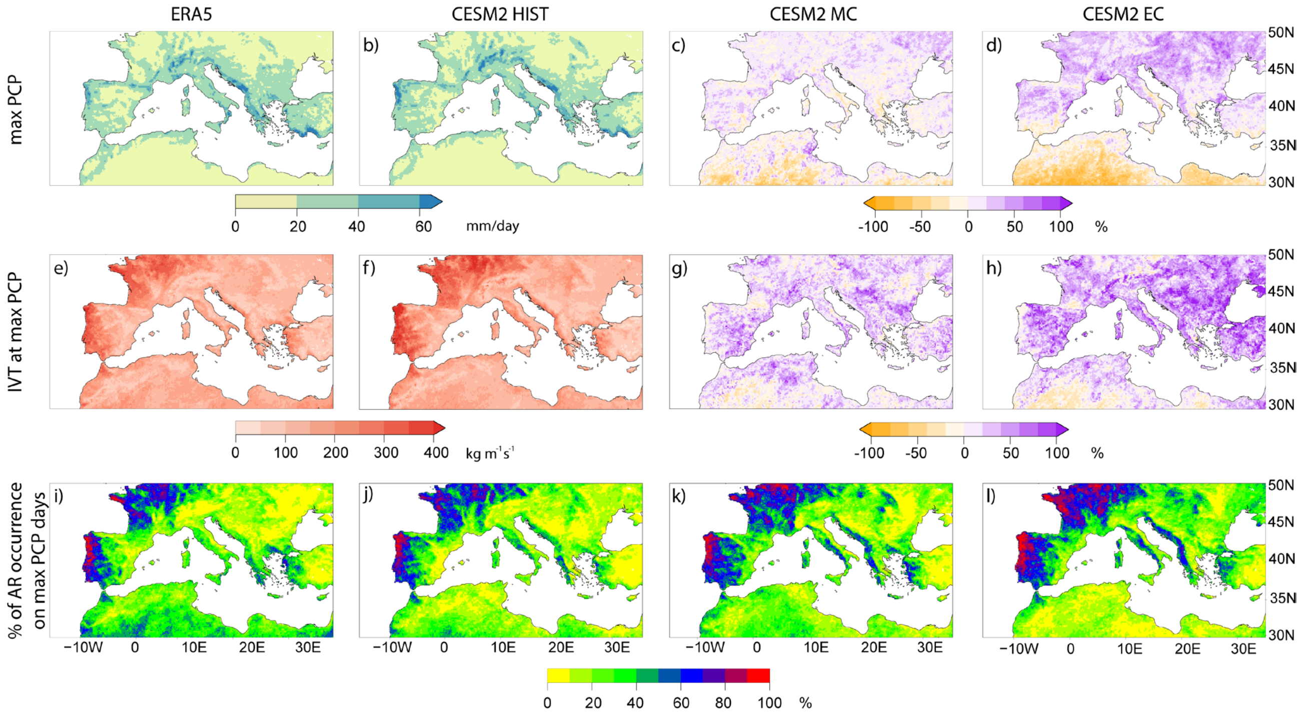

Figure 1. Precipitation maxima in the present and future periods, together with the associated moisture transport and atmospheric river occurrence, for the winter season. a), b) Median of the maximum precipitation values and e) f) median IVT on the maximum precipitation days for ERA5 and CESM2 in the historical period, respectively. c) d) variation percentage of the median of the maximum precipitation values; and g) h) median IVT on the maximum precipitation days for the mid-century and end-century periods, respectively. i) j) k) l) Percentage of atmospheric river occurrence on the maximum precipitation days for ERA5 and CESM2 in the historical, mid-century and end-century periods, respectively.

Therefore, the pattern of change in extreme precipitation substantially differs from the changes in the role of the IVT associated with extreme precipitation. This suggests that the dependence between these two variables will change in the future climate relative to the present climate, stressing the need to identify the spatial pattern and intensity of these changes.

The CESM2 accurately reproduces the spatial pattern of the influence of IVT on extreme precipitation (Fig. 2a, b). The areas of strong dependence between IVT and extreme precipitation coincide with the areas with the highest values of extreme precipitation. They also coincide with the areas of high AR–extreme precipitation concurrence in the presence of high orography upwind of the westerly moisture flow from the ocean. There is no strong dependence in regions with high concurrence but without notable orography, such as the French Atlantic coast. This pattern intensifies in the middle of the century and returns to values similar to those of the present climate by the end of the century (Fig. 2c, d, e, f). We now focus individually on the Iberian Peninsula, a region where there is longitudinal asymmetry both in the influence of IVT on extreme daily precipitation and in the coincidence of AR occurrence and extreme daily precipitation (very high in the western part and low in the central and eastern parts). As in the whole Euromediterranean area, there is a marked increase in the influence of moisture transport on extreme precipitation in the mid-century period with respect to the historical climate, with a decrease at the end of the century with respect to the mid-century (Fig. 2e). The increases at mid-century (variation changes on the order of 40%) are slightly greater than those for the whole Euromediterranean area. Additionally, on the Iberian Peninsula, there is still a slight projected increase of the end-century values on the order of 20% with respect to the historical climate values (Fig. 2f). It could be presumed that the increase in dependence at mid-century is due to the increase in the percentage of extreme precipitation days associated with ARs, from approximately 40% in the historical period to approximately 55% at mid-century (Fig. 2g). However, the decrease at the end of the century compared to the mid-century period is not supported by a decrease in the percentage of extreme precipitation days associated with atmospheric rivers, as this percentage remains relatively constant.

To understand the relationship between an increase in the percentage of extreme precipitation days coinciding with ARs and a stronger dependence between IVT and extreme precipitation, the concept of an atmospheric river, which is a structure of high moisture transport and therefore high IVT, should be considered *(Ralph et al, 2018*). The IVT of an extreme precipitation day that coincides with an atmospheric river is high. This indicates that the increase in these coinciding days implies a greater dependence between extreme precipitation and IVT. ARs are usually associated with extratropical cyclones *(Ralph et al, 2018; Gimeno et al., 2021a*), which, when affected by orography or incorporated into an extratropical cyclone that provides atmospheric instability, increase and produce heavy precipitation (*Patricola et al., 2022; Gimeno-Sotelo et al., 2023*). This makes ARs responsible for most extreme precipitation events in the region (*Lavers and Villarini, 2013a,b; Lorente-Plazas et al., 2020*). The decreased influence of IVT on extreme precipitation from the middle to the end of the century, a period in which the association between ARs and extreme precipitation does not decrease, must be related to the instability mechanisms involved in the associated extratropical cyclones. This hypothesis is reinforced by the fact that practically all simulations based on the SSP5-8.5 scenario project an increase in the frequency and intensity of ARs *(Payne et al, 2020*), but a decoupling between ARs and extratropical cyclones has been found in a warmer climate (*Wang et al., 2023*). ARs would occur with extratropical cyclones of low intensity given the enhanced moisture content in the future, which indicates that ARs with large IVT values can exist without the large wind values related to extratropical cyclones, confirming the dominant role of thermodynamic versus dynamic effects on ARs in a warmer climate (*Zhang et al., 2024*). In addition, the faster poleward migration of extratropical cyclones than that of ARs means that future ARs will tend to move further away from the centres of extratropical cyclones (*Wang et al., 2023*).

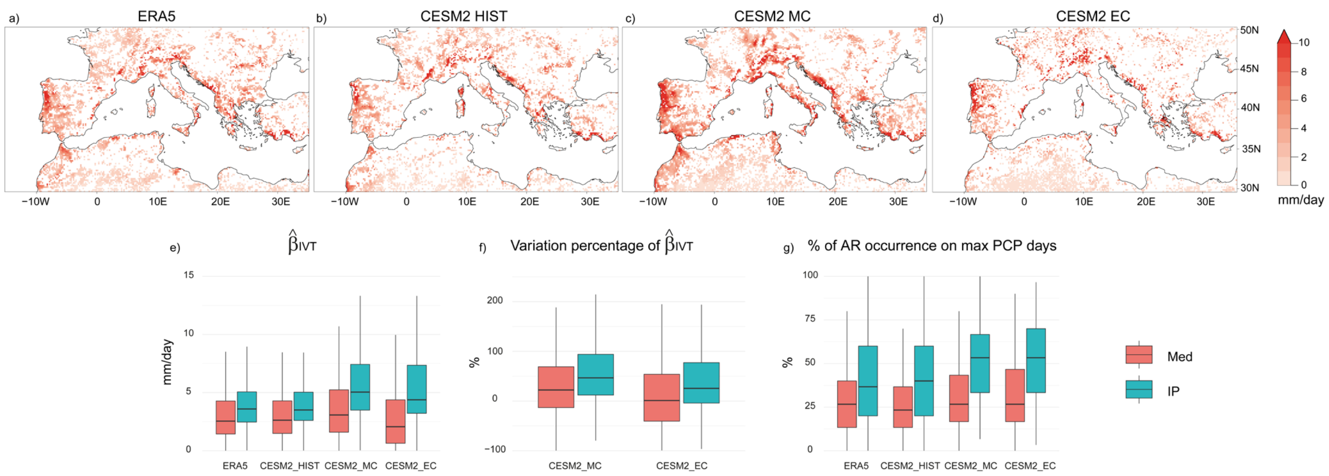

Figure 2. Dependence of precipitation maxima on moisture transport in historical and future periods for the winter season and projected changes in that relationship. a) b) c) d) Influence of IVT on extreme precipitation magnitude (measured as $\hat{\beta}_{IVT}$; see Methods) for ERA5 and CESM2 in the historical, mid-century and end-century periods, respectively; e) boxplots of $\hat{\beta}_{IVT}$ for the whole Euromediterranean area (Med) and the Iberian Peninsula (IP) for ERA5 and CESM2 in the historical, mid-century and end-century periods; f) boxplots of the variation percentage of $\hat{\beta}_{IVT}$ for Med and IP for the mid-century and end-century periods with respect to the historical period (CESM2 data); and g) boxplots of the percentage of atmospheric river occurrence on the maximum precipitation days for Med and IP for ERA5 and CESM2 in the historical, mid-century and end-century periods. In a) b) c) d) e) f), only statistically significant positive values of $\hat{\beta}_{IVT}$ are considered (at the 5% significance level).

The influence of moisture transport on extreme precipitation given the role of ARs is even more evident in the summer season (Figures S3 and S4). Extreme precipitation in summer is more strongly associated with convective processes than with dynamic mechanisms related to winds and moisture transport. The lower AR–extreme precipitation concurrence in summer than in winter translates into lower values of the dependence between extreme precipitation and IVT. Moreover, for the end of the century, the projected decrease in that concurrence in summer is linked to a greater decrease in the influence of moisture transport on extreme precipitation than in winter.

Changes in the influence of deficits in moisture transport on drought occurrence

It is well known that the North Atlantic Ocean and the Mediterranean Sea are the *dominant* moisture sources for drought occurrence in the Euromediterranean region in the present climate (*Gimeno-Sotelo et al., 2024b*). We understand as the *dominant* moisture source in a given region as the moisture source for which a deficit in the contribution to the precipitation in that region maximizes drought probability. Our aim is to improve our understanding of the changes in the influence of moisture deficits from these sources with global warming. For this purpose, we estimated the conditional probabilities of drought occurrence given equivalent contribution deficits from the North Atlantic Ocean and the Mediterranean Sea using copulas, a versatile statistical methodology for dependence modelling (see Methods, and Figure S5 for information about the selected copulas and satisfactory goodness-of-fit assessment).

Droughts in the western Euromediterranean region are mostly dominated by moisture deficits from the North Atlantic source, and the central and eastern regions are fundamentally affected by deficits from the Mediterranean Sea, a pattern well reproduced by the CESM2 model (Fig. 3a,b). Although the spatial patterns of the dominant moisture sources do not show substantial changes in the future scenarios (Fig. 3c, d), there is a considerable increase in the influence of moisture transport deficits from the dominant moisture source on drought occurrence everywhere in the Euromediterranean region (Figure 3g, h, i). Thus, under the current climate (Fig. 3e, f), there are moderate probabilities (from 0.05 to 0.20), but these values reach 0.30 in practically all regions in the Euromediterranean areas and 0.60 on the Iberian Peninsula, the Balkans and Turkey. Moreover, while the precipitation threshold that defines drought occurrence (see Methods) shows a slight decrease in the future, the equivalent contribution threshold from the dominant source is projected to increase considerably, with several areas affected by increases of 50%-150% with respect to the present climate (Figure S6).

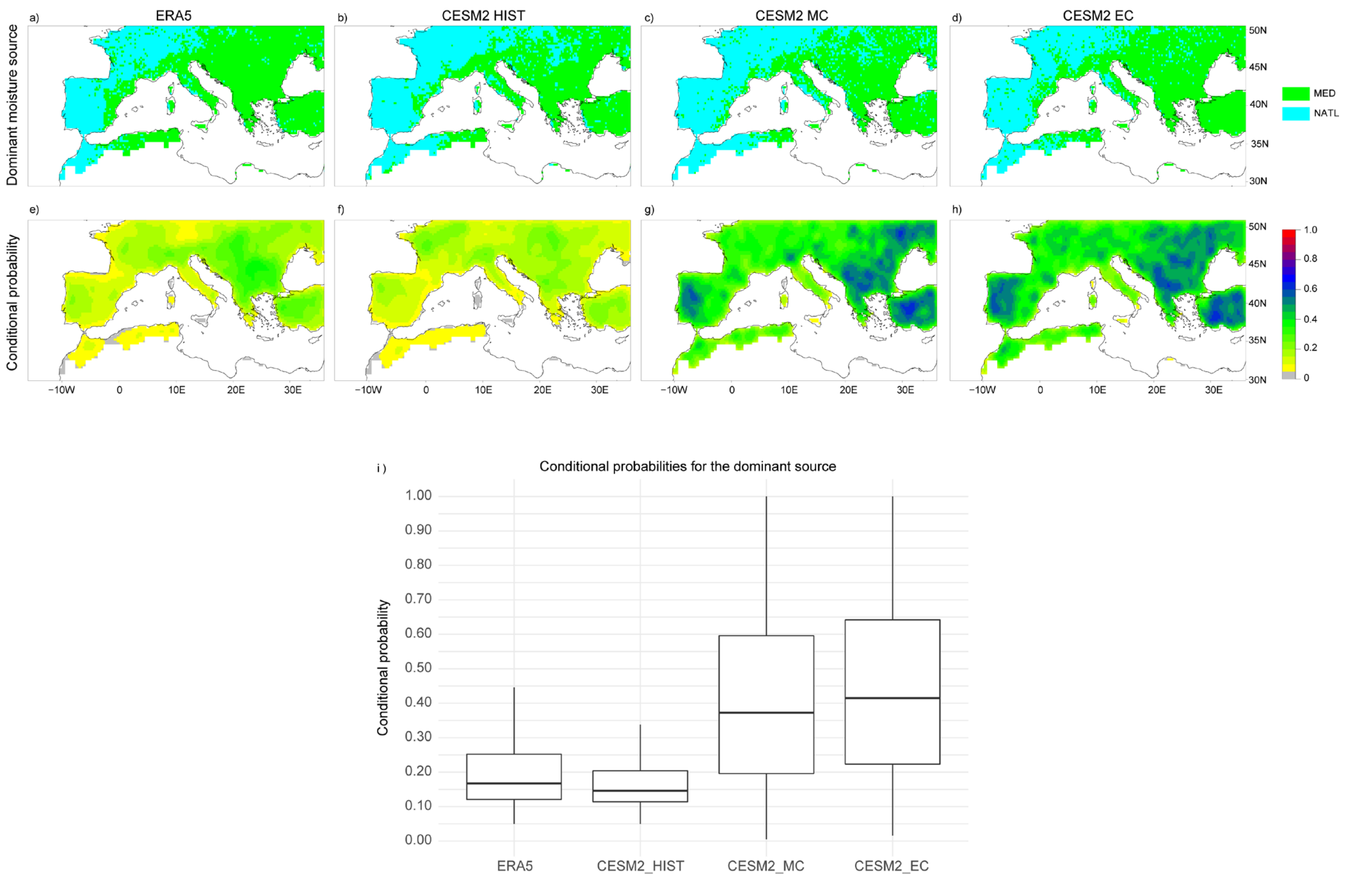

Figure 3. Conditional probability of drought occurrence given an equivalent moisture contribution deficit from the dominant oceanic moisture source in the Euromediterranean region. a) b) c) d) Spatial pattern of the dominant moisture source

(NATL: North Atlantic Ocean; and MED: Mediterranean Sea); e) f) g) h) values of the conditional probability for the ERA5 reanalysis and the CESM2 model in the historical, mid-century and end-century periods, respectively; and i) the corresponding boxplots of conditional probabilities for each period.

We analysed a specific hotspot region to study the role of contribution deficits from a wider range of moisture sources in an individual way. The chosen region is the Iberian Peninsula (Figure 4), which has known oceanic moisture sources: the North Atlantic Ocean, the Mediterranean Sea, and the Gulf of Mexico and Caribbean Sea. The climate model correctly reproduces the probability patterns and areas of influence associated with each moisture source (Fig. 4a, b, e, f, i, j). Deficits from the North Atlantic Ocean are related to higher drought probabilities, especially in the western half of the peninsula, which will increase from approximately 0.2 to approximately 0.6 in future climates (Fig. 4a, b, c, d). There is a considerable increase in the median values, from 0.10-0.15 in the present climate to 0.35-0.45 in the future periods, i.e., approximately three times greater (Fig. 4m). The other moisture sources show similar patterns of changes in their respective areas of influence, i.e., the eastern part of the Iberian Peninsula for the Mediterranean Sea (Fig. 4e, f, g, h) and the western part of the Gulf of Mexico and Caribbean Sea (Fig. 4i, j, k, l). The probability values in these areas of influence range from 0.10-0.20 in the present climate to 0.40-0.50 in the future climate. The median values increase from 0.05-0.10 to 0.20-0.35 (Fig. 4m). Thus, our results suggest a general increase of approximately three times with respect to the present climate in the median drought probability associated with moisture transport deficits in the future on the Iberian Peninsula, based on its main oceanic moisture sources.

The increased importance of moisture transport from the ocean on the occurrence of future droughts in the Euromediterranean region is linked to the projected decrease in terrestrial water storage levels (*Pokhrel et al, 2021*), which has been widely modelled using soil moisture (*e.g., Cook. et al. 2020; Gimeno-Sotelo et al, 2024a*). Soil moisture decline in the Mediterranean is projected by the majority of CMIP6 models (*IPCC, 2021*) and by the WRF-downscaled version of the CESM2 model (Figure S7). Although the soil–atmosphere coupling and its role in the hydrological cycle is a complex issue (*Seneviratne et al, 2010; Miralles et al., 2019*), in “water-limited” regions such as the Mediterranean, the projected reduction in soil moisture could have a significant impact on the hydrological cycle given the limitation of evapotranspiration and reduced moisture recycling for precipitation (*Zhou et al., 2021*). Under a projected decrease in soil moisture, it will be more challenging for terrestrial evaporation to compensate for a deficit of moisture from oceanic sources. Consequently, the probability of drought occurrence associated with contribution deficits from the ocean will be notably greater than that in the present climate.

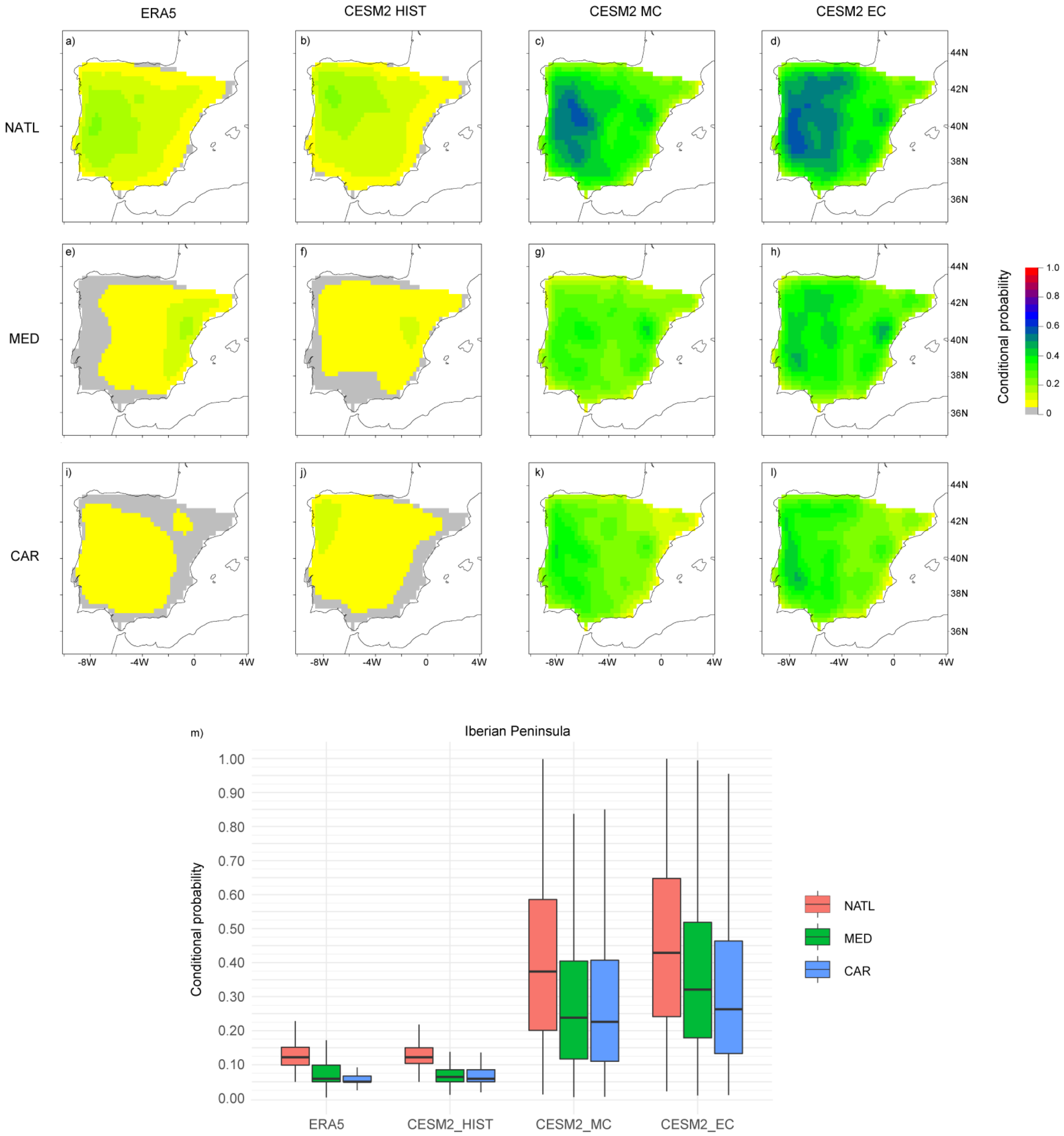

Figure 4. Conditional probability of drought occurrence given an equivalent moisture contribution deficit from each of the oceanic moisture sources of the Iberian Peninsula. a) b) c) d) Values of the conditional probability, for a contribution deficit from the North Atlantic Ocean (NATL), e) f) g) h) for a contribution deficit from the Mediterranean Sea (MED), and i) j) k) l) for a contribution deficit from the Gulf of Mexico and Caribbean Sea (CAR), for the ERA5 reanalysis and the CESM2 model in the historical, mid-century and end-century periods, respectively. m) Boxplots of conditional probabilities for contribution deficits from each source for each period.

Conclusions

Moisture transport will have a greater influence on Euromediterranean hydrometeorological extremes for the middle and end of the 21st century under a high greenhouse gas emission scenario (SSP5-8.5) than under the present climate. Nevertheless, the relative importance of this influence differs for precipitation extremes and droughts.

For extreme precipitation, the influence of moisture transport is expected to be only slightly greater than that observed in the present in winter and summer for the mid-century period. However, this is not expected to be the case for the end of the century in summer, in which its importance is projected to decrease. Furthermore, the increase in importance during winter is expected to be greater by mid-century than by the end of the century. This influence is contingent upon the occurrence of atmospheric rivers. The greater the percentage of concurrence is, the greater the influence. This is observed both spatially and temporally in the present and future climates. Nevertheless, this behaviour appears to undergo a transformation in the cold season by the end of the century. A comparable concurrence of ARs and extreme precipitation days during the end-century period with respect to the mid-century period corresponds to a reduction in the influence of moisture transport on extreme precipitation. This phenomenon is likely associated with a slight decoupling of atmospheric rivers from extratropical cyclones, the primary weather system responsible for the atmospheric instability necessary to generate extreme precipitation in the region.

For drought occurrence, moisture transport exerts a notably greater influence on future climates than on the present climate since there is a very high increase in the probability of drought occurrence associated with moisture transport deficits from the dominant oceanic moisture source. The median values are projected to be on the order of 40%, i.e., between two and three times greater in the future periods than in the present ones. This increase is also projected when all oceanic moisture sources in a particular region are analysed, as illustrated by the case of the Iberian Peninsula. This striking increase in the impact of moisture transport on drought probability could be attributed to the projected decline in terrestrial water storage levels across the Euromediterranean region. This would reduce the role of local moisture sources in generating precipitation, increasing the role of moisture transport from the ocean in the occurrence of Euromediterranean droughts.

These findings, although confined to the Euromediterranean region, highlight two overarching concerns. First, it is necessary to consider the changing relationship between extreme precipitation and high-moisture transport associated with atmospheric rivers. Second, it is necessary to consider the intensification of the influence of advected moisture from the ocean on regions that will experience drier conditions in the future, as the potential for local moisture inputs from terrestrial evaporation will likely decrease. These findings stress the importance of considering projected changes in moisture transport from oceanic areas in future climates to explain the changes in extreme precipitation and drought.

Methods

Data employed

A problem in the study of hydrometeorological extremes in the present and future climates is the low resolution of the reanalyses and models used, which do not reproduce well the orography and some physical processes, such as small-scale convective processes, which are very influential in the occurrence of extreme precipitation. It is therefore very useful to dynamically downscale reanalyses and models to improve their representativeness (*Iles et al, 2020*; *Zscheischler et al, 2021*).

This article is based on dynamically downscaled data from the ERA5 reanalysis (*Hersbach et al, 2020*) and the Community Earth System Model Version 2 (CESM2; *Danabasoglu, 2020*) climate model, obtained by applying the Weather Research and Forecast (WRF-ARW) Eulerian mesoscale model, Version 3.8.1 (*Skamarock et al., 2008*). Three periods of interest are considered: historical (HIST: 1985-2014), mid-century (MC: 2036-2065) and end-century (EC: 2071-2100). Reanalysis data are used with the aim of validating the results obtained for the climate model in the historical period.

The ERA5 reanalysis, from the European Centre for Medium-Range Weather Forecasts, excels in representing the hydrological cycle (*Nogueira, 2020*) and shows generally good agreement in precipitation patterns with respect to satellite (*Rivoire et al., 2020*) and gauge-based observational data (*Lavers et al., 2022*), being more skilful in extratropical areas than in tropical areas.

The CESM2 is a climate model from the Coupled Model Intercomparison Project Phase 6 (CMIP6) experiment (*Eyring et al., 2016*). This model has been evaluated successfully in terms of the most relevant climatic phenomena that characterize atmospheric circulation in the Northern Hemisphere (*Simpson et al., 2020*). The shared socioeconomic pathway SSP5-8.5 is used, a high-emission scenario for which a radiative forcing of 8.5 W m^{-2} is assumed to be reached in 2100. The reason for using this scenario is that stronger patterns of changes are expected, enhancing signal detection.

Extensive information about the simulation scheme, including the advantages of using this climate model with respect to other models available in the CMIP6 experiment, can be found in *Fernández-Alvarez et al. (2023)*.

In this study, we use data at a spatial resolution of 20 km and a daily (and monthly) frequency to study the projected changes in the influence of moisture transport on extreme precipitation (and droughts) in the Euromediterranean region. It is defined as a spatial domain encompassing latitudes from 30°N to 50°N and longitudes from 15°W to 35°E (Figure S2a).

Calculation of vertically integrated horizontal moisture transport and atmospheric rivers

To analyse the influence of moisture transport on extreme daily precipitation, we use daily vertically integrated water vapour transport (IVT), a Eulerian metric that quantifies moisture transport at each grid point. It has been the most prevalent among the various methods used for quantifying moisture transport (see *Gimeno et al., 2012* for a review) in extreme precipitation analysis. IVT is defined as the length of the vector that represents the water vapour flux at each grid point, i.e.,

$$IVT = \sqrt{IVT_u{}^2 + IVT_v{}^2},$$

where $IVT_u = \frac{1}{g}\int_{p_s}^{p_t} q\ u\ dp$, and $IVT_v = \frac{1}{g}\int_{p_s}^{p_t} q\ v\ dp$.

In the expressions above, q refers to specific humidity, g to gravitational acceleration, u and v to the eastwards and northwards components of wind, respectively; and $\mathrm{p_s}$ and $\mathrm{p_t}$ to pressure at the surface and top of the column considered (in our case, $\mathrm{p_s} = 1000\ \mathrm{hPa}$ and $\mathrm{p_t} = 300\mathrm{hPa}$). Pressure levels above 300 hPa have a minimal impact on the IVT calculation, as demonstrated by *Ratna et al. (2016)*.

Atmospheric rivers (ARs) are defined as long and narrow corridors of water vapour in the lower troposphere (*Zhu and Newell, 1998; Gimeno et al., 2014, Gimeno et al., 2021a*). Here, our aim is to analyse the percentage of AR occurrence on maximum precipitation days and to relate this concurrence with the influence of moisture transport on extreme precipitation. For atmospheric river detection, the Image-Processing-based Atmospheric River Tracking (IPART) method is applied (*Xu et al., 2020*). This technique was successfully used for detecting ARs arriving on the Iberian Peninsula (*Fernández-Alvarez et al., 2023b*) under the same simulation scheme as that used in our study.

Calculation of drought indices and contributions to precipitation from moisture sources

Droughts usually occur on longer timescales than extreme precipitation. For this reason, to determine the effect of moisture transport deficits on drought development and intensification, the Lagrangian approximation, which calculates the moisture transport deficit from the moisture sources of a given region, is widely used (*Drumond et al., 2019*, *Gimeno-Sotelo et al., 2024b*).

Dynamically downscaled monthly precipitation data from the ERA5 reanalysis and the CESM2 model are used for calculating the Standardised Precipitation Index (SPI) (*Mckee et al., 1993*). For the SPI calculation, accumulated precipitation series are obtained (for an m-month time scale, the accumulation is performed over m months). For each month of the year in an independent way, a gamma distribution is fitted to the series corresponding to each month of the year, and the data are subsequently transformed to a standard normal distribution. Thus, SPI values higher (lower) than zero are considered wet (dry) months.

The SPI is used in this study because it is exclusively based on precipitation data, and considering that the influence of moisture transport on meteorological droughts is mainly due to its relationship with precipitation, our aim is to isolate that effect. The 1-month time scale is selected because the residence time of water vapour in the atmosphere is typically between 3 and 10 days (*Gimeno et al., 2021b*); consequently, the influence of moisture transport deficits on meteorological droughts should be more clearly identified on a 1-month basis.

In this article, we study the influence of the contribution to precipitation deficits from the major oceanic moisture sources of the Euromediterranean region on the occurrence of meteorological droughts. It is well known that those major moisture sources are the North Atlantic Ocean and the Mediterranean Sea (*Gimeno et al., 2010a; Gimeno-Sotelo et al., 2024b*); see Figure S2b. To calculate the contribution to precipitation in the Euromediterranean region from a given moisture source, the FLEXPART-WRF methodology is applied (*Brioude et al., 2013*). This Lagrangian method consists of tracking the changes in specific humidity every 6 hours $\left(\frac{dq}{dt}\right)$ of the air parcels departing from a given source region and arriving at each grid point in a target region (*Stohl and James, 2005*). For each parcel of constant mass m, the individual balance between evaporation (e) and precipitation (p) can be computed: $(e-p)=m\left(\frac{dq}{dt}\right)$. By aggregating all the individual values of $(e-p)$ for the parcels arriving at each grid point of the target region, the balance between total evaporation (E) and total precipitation (P) at that point (of area A) can be estimated as follows: $(E-P)=\frac{\sum_{i=1}^{N}(e-p)_i}{A}$. A negative value of this quantity indicates moisture loss, and its modulus refers to the contribution to precipitation from the moisture source to that grid point in the target region. Following this methodology, using the dynamically downscaled data from the ERA5 reanalysis and the CESM2 model, it is possible to obtain the contribution to precipitation from the North Atlantic Ocean and Mediterranean Sea for every grid point in the Euromediterranean region. Additionally, the contribution to precipitation from the Caribbean Sea and Gulf of Mexico moisture source (Figure S2b), which is also a relevant oceanic moisture source for the Iberian Peninsula (*Gimeno et al., 2010b*), is obtained for that region in an analogous way.

Using monthly data of the contribution to precipitation from a given moisture source, an analogous standardization to that performed on the precipitation data is carried out, obtaining indices analogous to the SPI, denoted as SPIc, where "c" denotes "contribution" (to precipitation).

Extreme value analysis of precipitation as a function of its drivers

For the three periods of interest, i.e., the historical (1985-2014), mid-century (2036-2065) and end-century (2071-2100) and the winter and summer seasons (January-March and July-September), we independently fit non-stationary Generalised Extreme

Value (GEV) models for the annual precipitation maxima as a function of IVT, in line with the methodology presented in *Gimeno-Sotelo and Gimeno (2023)*. Following the statistical background from the Extreme Value Theory (see, e.g., *Coles, 2001*, and *Beirlant et al., 2004*), we use a GEV model for the distribution of the annual precipitation maxima for each grid point:

$$G(y;\ \mu,\sigma,\gamma) = \exp\left\{-[1+\gamma\frac{y-\mu}{\sigma}]^{-1/\gamma}\right\} \text{, with } 1+\gamma\frac{y-\mu}{\sigma} > 0,$$

where y is a value of Y, the variable representing the annual precipitation maxima, and $\mu \in \mathbb{R}$, $\sigma > 0$, and $\gamma \in \mathbb{R}$ are the parameters of the distribution (location, scale, and shape, respectively). To assess the influence that IVT has on the precipitation maxima, the location and scale parameters are expressed as linear functions of IVT: $\mu(IVT) = \beta_0 + \beta_1 IVT$ and $\sigma(IVT) = \theta_0 + \theta_1 IVT$.

Here, we pay special attention to the β_1 coefficient, which represents the influence that IVT has on the magnitude of the precipitation maxima. We obtain the maximum likelihood estimate for that coefficient, and its significance is assessed by means of a 95% confidence interval (if the value 0 is outside the interval, the coefficient is statistically significant from 0 at the 5% significance level).

For notational simplicity, the estimated β_1 coefficient is denoted as $\hat{\beta}_{IVT}$.

The goodness of fit of the non-stationary GEV models is assessed, as indicated by *Coles (2001)*, using diagnostic plots. We construct probability plots and determine our models appropriate if a linearity of points in the plots is observed. For each plot, the R^2 of the associated linear regression model provides that information, and we use that quantity as a goodness-of-fit metric for gridded data (as in *Gimeno-Sotelo and Gimeno, 2023*).

Drought occurrence given moisture source contribution deficits

In this article, we follow the methodology presented in *Gimeno-Sotelo et al. (2024b),* with the aim of assessing the influence that a moisture contribution deficit from a source has on the occurrence of droughts in the Euromediterranean region. We estimate conditional probabilities of drought occurrence given equivalent moisture source contribution deficits by means of copulas, which are statistical models for the dependence structure of a pair of variables (*Nelsen, 2006; Tootoonchi et al., 2022*). In our case, for each grid point, there is a pair (SPI, SPIc). Six different copula types are fitted, namely, the Gaussian, Student-t, Clayton, Gumbel, Frank and Joe types (see *Czado, 2019*), which provide a wide range of shapes in terms of symmetries and tail behaviour. Among those models, we utilize the one providing the best value in terms of the selection criterion (we use the Akaike information criterion; *Akaike, 1974*). To determine whether the copula is well fitted to the data, a goodness-of-fit statistical test is performed (*Huang and Prokhorov, 2014; White, 1982*). Obtaining 100,000 simulations from that selected copula model, it is possible to have a large enough sample to estimate the desired conditional probability, i.e., the conditional probability of the SPI being lower than the 5%-percentile threshold conditional on the SPIc being lower than the same threshold in standardized units: $P(SPI \leq\ -1.64 \mid SPIc\ \leq\ -1.64)$.

Uncertainties

The results presented in this research have some acceptable limitations, as already discussed by *Fernandez-Alvarez et al. (2023a)*. First, they are related to the use of a single climate model, CESM2, which is slightly warm. However, the authors found that a comparison of the results of their simulation of moisture sources obtained using CESM2 with another one based on an ensemble of models gave very similar results for a period of five years. Another limitation is the use of a single shared socioeconomic pathway (SSP5-8.5), which is the most pessimistic of those considered in CMIP6, although this approach is appropriate for this study because it enhances signal detection, as explained before. There is also a certain degree of subjectivity in the configuration of the WRF-ARW model used in the downscaling, despite the fact that the authors selected the most suitable parameterizations based on the literature.

Data availability

ERA5 reanalysis data can be obtained from https://cds.climate.copernicus.eu and CESM2 data is available at the World Climate Research Programme (WCRP, https://esgf-node.llnl.gov/search/cmip6/). The WRF-ARW outputs are available upon request to the corresponding author due to the large volume they occupy, which makes it impossible to store them in an online repository.

Code availability

Code is available on request from the corresponding author.

References

Akaike, H. (1974). A new look at the statistical model identification. IEEE transactions on automatic control, 19(6), 716-723.

Allan, R. P., Barlow, M., Byrne, M. P., Cherchi, A., Douville, H., Fowler, H. J., ... & Zolina, O. (2020). Advances in understanding large-scale responses of the water cycle to climate change. Annals of the New York Academy of Sciences, 1472(1), 49-75.

Allen, M. R., & Ingram, W. J. (2002). Constraints on future changes in climate and the hydrologic cycle. Nature, 419(6903), 228–232. https://doi.org/10.1038/nature01092.

Bao, J., Sherwood, S.C., Alexander, L.V., Evans, J.P. (2017). Future increases in extreme precipitation exceed observed scaling rates. Nature Climate Change 7, , 128-132. https://doi.org/10.1038/nclimate3201.

Beirlant, J., Goegebeur, Y., Segers, J., & Teugels, J. L. (2006). Statistics of extremes: theory and applications. John Wiley & Sons.

Brioude, J., Arnold, D., Stohl, A., Cassiani, M., Morton, D., Seibert, P., ... & Wotawa, G. (2013). The Lagrangian particle dispersion model FLEXPART-WRF version 3.1. Geoscientific Model Development, 6(6), 1889-1904.

Coles, S. (2001). An introduction to statistical modeling of extreme values. Springer, London.

Cook, B. I., Anchukaitis, K. J., Touchan, R., Meko, D. M., & Cook, E. R. (2016). Spatiotemporal drought variability in the Mediterranean over the last 900 years. Journal of Geophysical Research: Atmospheres, 121(5), 2060-2074.

Cook, B. I., Mankin, J. S., Marvel, K., Williams, A. P., Smerdon, J. E., & Anchukaitis, K. J. (2020). Twenty-first century drought projections in the CMIP6 forcing scenarios. Earth's Future, 8(6), e2019EF001461.

Czado, C. (2019). Analyzing dependent data with vine copulas. Lecture Notes in Statistics, Springer, 222.

Danabasoglu, G., Lamarque, J. F., Bacmeister, J., Bailey, D. A., DuVivier, A. K., Edwards, J., ... & Strand, W. G. (2020). The community Earth system model version 2 (CESM2). Journal of Advances in Modeling Earth Systems, 12(2), e2019MS001916. https://doi.org/10.1029/2019MS001916

Douville, H., Raghavan, K., Renwick, J., Allan, R. P., Arias, P. A., Barlow, M., Cerezo-Mota, R., Cherchi, A., Gan, T. Y., Gergis, J., Jiang, D., Khan, A., Pokam Mba, W., Rosenfeld, D., Tierney, J., & Zolina, O. (2021). Water Cycle Changes. In V. Masson-Delmotte, P. Zhai, A.

Pirani, S. L. Connors, C. Péan, S. Berger, N. Caud, Y. Chen, L. Goldfarb, M. I. Gomis, M. Huang, K. Leitzell, E. Lonnoy, J. B. R. Matthews, T. K. Maycock, T. Waterfield, O. Yelekçi, R. Yu, & B. Zhou (Eds.), Climate Change 2021: The Physical Science Basis. Contribution of Working Group I to the Sixth Assessment Report of the Intergovernmental Panel on Climate Change (pp. 1055–1210). Cambridge University Press. https://doi.org/10.1017/9781009157896.010

Drumond, A., M. Stojanovic, R. Nieto, S.M. Vicente-Serrano and Gimeno, L. (2019) Linking Anomalous Moisture Transport and Drought Episodes in the IPCC Reference Regions. Bull. Amer. Meteor. Soc, Vol 100, 8, 1481–1498 doi: https://doi.org/10.1175/BAMS-D-18-0111.1

Eyring, V., Bony, S., Meehl, G. A., Senior, C. A., Stevens, B., Stouffer, R. J., & Taylor, K. E. (2016). Overview of the Coupled Model Intercomparison Project Phase 6 (CMIP6) experimental design and organization. Geoscientific Model Development, 9(5), 1937-1958.

Fernández-Alvarez, J. C., Pérez-Alarcón, A., Eiras-Barca, J., Rahimi, S., Nieto, R., & Gimeno, L. (2023a). Projected changes in atmospheric moisture transport contributions associated with climate warming in the North Atlantic. Nature Communications, 14(1), 6476.

Fernández-Alvarez, J. C., Pérez-Alarcón, A., Eiras-Barca, J., Ramos, A. M., Rahimi-Esfarjani, S., Nieto, R., & Gimeno, L. (2023b). Changes in Moisture Sources of Atmospheric Rivers Landfalling the Iberian Peninsula With WRF-FLEXPART. Journal of Geophysical Research: Atmospheres, 128(8), e2022JD037612.

García-Ruiz, J. M., López-Moreno, J. I., Vicente-Serrano, S. M., Lasanta–Martínez, T., & Beguería, S. (2011). Mediterranean water resources in a global change scenario. Earth-Science Reviews, 105(3-4), 121-139.

Gimeno, L., Algarra, I., Eiras-Barca, J., Ramos, A. M., & Nieto, R. (2021a). Atmospheric river, a term encompassing different meteorological patterns. Wiley Interdisciplinary Reviews: Water, 8(6), e1558. https://doi.org/10.1002/wat2.1558

Gimeno, L., Dominguez, F., Nieto, R., Trigo, R., Drumond, A., Reason, C.J., Taschetto, A.S., Ramos, A.M., Kumar, R. and Marengo, J., (2016). Major mechanisms of atmospheric moisture transport and their role in extreme precipitation events. Annual Review of Environment and Resources, 41, pp.117-141.

Gimeno, L., Drumond, A., Nieto, R., Trigo, R. M., & Stohl, A. (2010a). On the origin of continental precipitation. Geophysical Research Letters, 37(13).

Gimeno, L., Eiras-Barca, J., Durán-Quesada, A. M., Dominguez, F., van der Ent, R., Sodemann, H., ... & Kirchner, J. W. (2021b). The residence time of water vapour in the atmosphere. Nature Reviews Earth & Environment, 2(8), 558-569.

Gimeno, L., Nieto, R., Trigo, R. M., Vicente-Serrano, S. M., & López-Moreno, J. I. (2010b). Where does the Iberian Peninsula moisture come from? An answer based on a Lagrangian approach. Journal of Hydrometeorology, 11(2), 421-436.

Gimeno, L., Nieto, R., Vázquez, M., & Lavers, D. A. (2014). Atmospheric rivers: A mini-review. Frontiers in Earth Science, 2, 2. https://doi.org/10.3389/feart.2014.00002.

Gimeno, L., Stohl A., Trigo R.M., Domínguez F., Yoshimura K., Yu L., Drumond A., Durán-Quesada A.M., Nieto R. (2012) Oceanic and Terrestrial Sources of Continental Precipitation, Reviews of Geophysics, 50, RG4003, doi:10.1029/2012RG000389

Gimeno-Sotelo, L. and L. Gimeno (2022) Concurrent extreme events of atmospheric moisture transport and continental precipitation: The role of landfalling atmospheric rivers, Atmospheric Research, Vol. 278, 106356: DOI: 10.1016/j.atmosres.2022.106356

Gimeno-Sotelo, L., Bevacqua, E., & Gimeno, L. (2023). Combinations of drivers that most favor the occurrence of daily precipitation extremes. Atmospheric Research, 294, 106959.

Gimeno-Sotelo, L., & Gimeno, L. (2023). Where does the link between atmospheric moisture transport and extreme precipitation matter?. Weather and Climate Extremes, 39, 100536. https://doi.org/10.1016/j.wace.2022.100536

Gimeno-Sotelo, L., El Kenawy, A., Franquesa, M., Noguera, I., Fernández-Duque, B., Domínguez-Castro, F., ... & Vicente-Serrano, S. M. (2024a). Assessment of the global relationship of different types of droughts in model simulations under high anthropogenic emissions. Earth's Future, 12(4), e2023EF003629.

Gimeno-Sotelo, L., Sorí, R., Nieto, R., Vicente-Serrano, S. M., & Gimeno, L. (2024b). Unravelling the origin of the atmospheric moisture deficit that leads to droughts. Nature Water, 1-12, https://doi.org/10.1038/s44221-023-00192-4.

Gimeno-Sotelo, L., Bevacqua, E., Fernández-Alvarez, J. C., Barriopedro, D., Zscheischler, J., & Gimeno, L. (2024c). Projected changes in extreme daily precipitation linked to changes in precipitable water and vertical velocity in CMIP6 models. Atmospheric Research, 304, 107413.

Hersbach, H, Bell, B, Berrisford, P, et al. (2020) The ERA5 global reanalysis. Q J R Meteorol Soc., 146: 1999–2049. https://doi.org/10.1002/qj.3803

Huang, W., & Prokhorov, A. (2014). A goodness-of-fit test for copulas. Econometric Reviews, 33(7), 751-771.

Iles, C. E., Vautard, R., Strachan, J., Joussaume, S., Eggen, B. R., and Hewitt, C. D.: (2020) The benefits of increasing resolution in global and regional climate simulations for European climate extremes, Geosci. Model Dev., 13, 5583–5607, https://doi.org/10.5194/gmd-13-5583-2020.

IPCC, 2021: Climate Change 2021: The Physical Science Basis. Contribution of Working Group I to the Sixth Assessment Report of the Intergovernmental Panel on Climate Change[Masson-Delmotte, V., P. Zhai, A. Pirani, S.L. Connors, C. Péan, S. Berger, N. Caud, Y. Chen, L. Goldfarb, M.I. Gomis, M. Huang, K. Leitzell, E. Lonnoy, J.B.R. Matthews, T.K. Maycock, T. Waterfield, O. Yelekçi, R. Yu, and B. Zhou (eds.)]. Cambridge University Press, Cambridge, United Kingdom and New York, NY, USA.

IPCC, 2022: Climate Change 2022: Impacts, Adaptation and Vulnerability. Contribution of Working Group II to the Sixth Assessment Report of the Intergovernmental Panel on Climate Change [H.-O. Pörtner, D.C. Roberts, M. Tignor, E.S. Poloczanska, K. Mintenbeck, A. Alegría, M. Craig, S. Langsdorf, S. Löschke, V. Möller, A. Okem, B. Rama (eds.)]. Cambridge University Press. Cambridge University Press, Cambridge, UK and New York, NY, USA, 3056 pp., doi:10.1017/9781009325844.

Konstali, K., Spensberger, C., Spengler, T., & Sorteberg, A. (2024). Global Attribution of Precipitation to Weather Features. Journal of Climate, 37(4), 1181-1196.

Knight, D. B., and Davis, R. E. (2009), Contribution of tropical cyclones to extreme rainfall events in the southeastern United States, J. Geophys. Res., 114, D23102, doi:10.1029/2009JD012511.

Lavers, D.A., Villarini, G., (2013a). The nexus between atmospheric rivers and extreme precipitation across Europe. Geophys. Res. Lett. 40 (12), 3259–3264. https://doi.org/10.1002/grl.50636

Lavers, D. A., and G. Villarini, (2013b) Atmospheric Rivers and Flooding over the Central United States. J. Climate, 26, 7829–7836, https://doi.org/10.1175/JCLI-D-13-00212.1.

Lavers, D. A., Simmons, A., Vamborg, F., & Rodwell, M. J. (2022). An evaluation of ERA5 precipitation for climate monitoring. Quarterly Journal of the Royal Meteorological Society, 148(748), 3152-3165.

Lionello, P., & Scarascia, L. (2020). The relation of climate extremes with global warming in the Mediterranean region and its north versus south contrast. Regional Environmental Change, 20(1), 31.

Liu, B, Tan, X, Gan, TY, et al. (2020) Global atmospheric moisture transport associated with precipitation extremes: Mechanisms and climate change impacts. WIREs Water. 7:e1412. https://doi.org/10.1002/wat2.1412.

Lorente-Plazas, R., Montavez, J. P., Ramos, A. M., Jerez, S., Trigo, R. M., & Jimenez-Guerrero, P. (2020). Unusual atmospheric-river-like structures coming from Africa induce extreme precipitation over the western Mediterranean Sea. Journal of Geophysical Research: Atmospheres, 125(2), e2019JD031280.

Mastrantonas, N., Herrera-Lormendez, P., Magnusson, L., Pappenberger, F., & Matschullat, J. (2021). Extreme precipitation events in the Mediterranean: Spatiotemporal characteristics and connection to large-scale atmospheric flow patterns. International Journal of Climatology, 41(4), 2710-2728.

McKee, T. B., Doesken, N. J., & Kleist, J. (1993, January). The relationship of drought frequency and duration to time scales. In Proceedings of the 8th Conference on Applied Climatology (Vol. 17, No. 22, pp. 179-183).

Miralles, D.G., Gentine, P., Seneviratne, S.I. and Teuling, A.J. (2019), Land–atmospheric feedbacks during droughts and heatwaves: state of the science and current challenges. Ann. N.Y. Acad. Sci., 1436: 19-35. https://doi.org/10.1111/nyas.13912

Mo, R., So, R., Brugman, M. M., Mooney, C., Liu, A. Q., Jakob, M., ... & Vingarzan, R. (2021). Column relative humidity and primary condensation rate as two useful supplements to atmospheric river analysis. Water Resources Research, 57(11), e2021WR029678.

Nelsen, R. B. (2006). An introduction to copulas. Springer.

Nogueira, M. (2020). Inter-comparison of ERA-5, ERA-interim and GPCP rainfall over the last 40 years: Process-based analysis of systematic and random differences. Journal of Hydrology, 583, 124632.

O’Gorman, P. A. & Muller, C. J. (2010) How closely do changes in surface and column water vapor follow Clausius-Clapeyron scaling in climate change simulations? Environ. Res. Lett. 5, 025207.

O’Gorman, P. A. (2015). Precipitation extremes under climate change. Current climate change reports 1, 2, 49-59. https://doi.org/10.1007/s40641-015-0009-3.

O'Neill, B. C., Tebaldi, C., Van Vuuren, D. P., Eyring, V., Friedlingstein, P., Hurtt, G., ... & Sanderson, B. M. (2016). The scenario model intercomparison project (ScenarioMIP) for CMIP6. Geoscientific Model Development, 9(9), 3461-3482.

Patricola, C. M., Wehner, M. F., Bercos-Hickey, E., Maciel, F. V., May, C., Mak, M., ... & Leal, S. (2022). Future changes in extreme precipitation over the San Francisco Bay Area: Dependence on atmospheric river and extratropical cyclone events. Weather and Climate Extremes, 36, 100440.

Payne, A. E., Demory, M. E., Leung, L. R., Ramos, A. M., Shields, C. A., Rutz, J. J., ... & Ralph, F. M. (2020). Responses and impacts of atmospheric rivers to climate change. Nature Reviews Earth & Environment, 1(3), 143-157.

Pfahl, S., O'Gorman, P. & Fischer, E. (2017). Understanding the regional pattern of projected future changes in extreme precipitation. Nature Clim Change 7, 423–427. https://doi.org/10.1038/nclimate3287.

Pokhrel, Y., Felfelani, F., Satoh, Y., Boulange, J., Burek, P., Gädeke, A., ... & Wada, Y. (2021). Global terrestrial water storage and drought severity under climate change. Nature Climate Change, 11(3), 226-233.

Ralph, F. M., Dettinger, M. D., Cairns, M. M., Galarneau, T. J., & Eylander, J. (2018). Defining "atmospheric river": How the glossary of meteorology helped resolve a debate. Bulletin of the American Meteorological Society, 99, 837–839. https://doi.org/10.1175/BAMS-D-17-0157.1

Ratna, S. B., Cherchi, A., Joseph, P. V., Behera, S. K., Abish, B., & Masina, S. (2016). Moisture variability over the Indo-Pacific region and its influence on the Indian summer monsoon rainfall. Climate dynamics, 46, 949-965.

Rivoire, P., Martius, O., & Naveau, P. (2021). A comparison of moderate and extreme ERA-5 daily precipitation with two observational data sets. Earth and Space Science, 8(4), e2020EA001633.

Seneviratne, S. I., Corti, T., Davin, E. L., Hirschi, M., Jaeger, E. B., Lehner, I., ... & Teuling, A. J. (2010). Investigating soil moisture–climate interactions in a changing climate: A review. Earth-Science Reviews, 99(3-4), 125-161.

Seneviratne, S. I., Zhang, X., Adnan, M., Badi, W., Dereczynski, C., Di Luca, A., Ghosh, S., Iskandar, I., Kossin, J., Lewis, S., Otto, F., Pinto, I., Satoh, M., Vicente-Serrano, S. M., Wehner, M., & Zhou, B. (2021). Weather and Climate Extreme Events in a Changing Climate. In V. Masson-Delmotte, P. Zhai, A. Pirani, S. L. Connors, C. Péan, S. Berger, N. Caud, Y. Chen, L. Goldfarb, M. I. Gomis, M. Huang, K. Leitzell, E. Lonnoy, J. B. R. Matthews, T. K. Maycock, T. Waterfield, O. Yelekçi, R. Yu, & B. Zhou (Eds.), Climate Change 2021: The Physical Science Basis. Contribution of Working Group I to the Sixth Assessment Report of the Intergovernmental Panel on Climate Change (pp. 1513–1766). Cambridge University Press. https://doi.org/10.1017/9781009157896.013

Simpson, I. R., Bacmeister, J., Neale, R. B., Hannay, C., Gettelman, A., Garcia, R. R., ... & Richter, J. H. (2020). An evaluation of the large-scale atmospheric circulation and its variability in CESM2 and other CMIP models. Journal of Geophysical Research: Atmospheres, 125(13), e2020JD032835.

Skamarock, W. C., Klemp, J. B., Dudhia, J., Gill, D. O., Barker, D., Duda, M. G., … Powers, J. G. (2008). A Description of the Advanced Research WRF Version 3 (No. NCAR/TN-475+STR). University Corporation for Atmospheric Research. doi:10.5065/D68S4MVH

Soden, B. J., & Held, I. M. (2006). An assessment of climate feedbacks in coupled ocean-atmosphere models. Journal of Climate, 19(23), 6263–3360. https://doi.org/10.1175/JCLI9028.1.

Stohl, A., & James, P. (2005). A Lagrangian analysis of the atmospheric branch of the global water cycle. Part II: Moisture transports between Earth's ocean basins and river catchments. Journal of Hydrometeorology, 6(6), 961-984.

Tootoonchi, F., Sadegh, M., Haerter, J. O., Räty, O., Grabs, T., & Teutschbein, C. (2022). Copulas for hydroclimatic analysis: A practice-oriented overview. Wiley Interdisciplinary Reviews: Water, 9(2), e1579.

Trenberth, K.E., Dai, A., Rasmussen, R.M., Parsons, D.B., (2003) The changing character of precipitation. Bull. Am. Meteorol. Soc. 84 (9), 1205–1218. https://doi.org/ 10.1175/BAMS-84-9-1205.

Ukkola, A. M., De Kauwe, M. G., Roderick, M. L., Abramowitz, G., & Pitman, A. J. (2020). Robust future changes in meteorological drought in CMIP6 projections despite uncertainty in precipitation. Geophysical Research Letters, 47(11), e2020GL087820.

Wang, S., Ma, X., Zhou, S., Wu, L., Wang, H., Tang, Z., ... & Gan, B. (2023). Extreme atmospheric rivers in a warming climate. Nature Communications, 14(1), 3219.

White, H. (1982). Maximum likelihood estimation of misspecified models. Econometrica: Journal of the econometric society, 1-25.

Xu, G., Ma, X., Chang, P., & Wang, L. (2020). Image-processing-based atmospheric river tracking method version 1 (ipart-1) [software]. Geoscientific Model Development, 13(10), 4639–4662. https://doi.org/10.5194/GMD-13-4639-2020

Zhang, L., Zhao, Y., Cheng, T. F., & Lu, M. (2024). Future changes in global atmospheric rivers projected by CMIP6 models. Journal of Geophysical Research: Atmospheres, 129, e2023JD039359. https://doi.org/10.1029/2023JD039359

Zhou, S., Williams, A. P., Lintner, B. R., Berg, A. M., Zhang, Y., Keenan, T. F., ... & Gentine, P. (2021). Soil moisture–atmosphere feedbacks mitigate declining water availability in drylands. Nature Climate Change, 11(1), 38-44.

Zhu, Y., & Newell, R. E. (1998). A proposed algorithm for moisture fluxes from atmospheric rivers. Monthly weather review, 126(3), 725-735.

Zittis, G., Bruggeman, A., and J. Lelieveld (2021) Revisiting future extreme precipitation trends in the Mediterranean. Weather and Climate Extremes, Volume 34, 10038,. https://doi.org/10.1016/j.wace.2021.100380.

Zscheischler, J., Naveau, P., Martius, O., Engelke, S., and Raible, C. C.: (2021) Evaluating the dependence structure of compound precipitation and wind speed extremes, Earth Syst. Dynam., 12, 1–16, https://doi.org/10.5194/esd-12-1-2021.

Acknowledgements

EPhysLab members are supported by the following projects: PID2021-122314OB-I00 and TED2021-129152B-C43, funded by the Ministerio de Ciencia, Innovación y Universidades, Spain (MICIU/AEI/10.13039/501100011033), Xunta de Galicia under the Project ED431C2021/44 (Programa de Consolidación e Estructuración de Unidades de Investigación Competitivas (Grupos de Referencia Competitiva) and Consellería de Cultura, Educación e Universidade), and by the European Union 'ERDF A way of making Europe' "NextGenerationEU"/PRTR. Luis Gimeno-Sotelo was supported by a 'Ministerio de Ciencia,Innovación y Universidades' PhD grant (reference: PRE2022-101497). We would like to express our gratitude to Rogert Sorí for providing help with issues related to the first steps of the design of the experiments. This work has also been possible thanks to the computing resources and technical support provided by CESGA (Centro de Supercomputación de Galicia) and RES (Red Española de Supercomputación). This study was also supported by the 'Unidad Asociada CSIC–Universidade de Vigo: Grupo de Física de la Atmósfera y del Océano'.

Contributions

L.G.-S. was responsible for the design of the experiments and contributed to the data analysis, creation of figures and writing of the paper. JC.F.-A. performed the modelling work and contributed to the creation of figures and discussion of the results. R.N. was involved in the creation of the final figures and discussion of the results. S.M.V.-S. contributed to the discussion of the results. L.G. contributed to the conceptualization of the study and writing of the paper. All authors participated in the review and editing of the paper.

5
Discussion

This thesis provides new insights into the analysis of the role of moisture transport in the occurrence of extreme precipitation and meteorological droughts, both for the present and the future climate. This chapter discusses some of the results described in Chapter 4.

On the regions where atmospheric moisture transport influences extreme precipitation

Moisture transport has been reported to show greater predictability than extreme precipitation in some world regions such as northwestern Europe (*Lavers et al., 2014*), the western US (*Lavers et al., 2016*), or China's Yangtze River basin (*Wang and Yuan, 2018*). Thus, the regions in which the relationship between moisture transport and extreme precipitation is strong, as identified in Section 4.1 for the present climate, should be those where the predictability of extreme precipitation may benefit the most from that relationship. It was found out that moisture transport exerts a weak influence on tropical regions, where a large amount of moisture already exists and moisture contributions from outside regions are not necessary for extreme precipitation occurrence. Instead, in those regions, the water vapour content has a higher importance (*Kim et al., 2022*). However, in subtropical and extratropical areas, moisture transport has a stronger influence on extreme precipitation, mainly linked to the patterns of the major moisture transport mechanisms (*Gimeno et al., 2016*). LLJs are highly relevant in subtropical areas, especially during the wet season in the Indian subcontinent, linked to the monsoon circulation, and along the area of occurrence of the SALLJ (*Jones, 2019*). The influence of ARs is particularly evident in extratropical coastal areas, namely the Pacific and Atlantic coasts of North America, the Atlantic European coast, the Pacific Asian coast, the Pacific coast of South America, southern Africa and Australia (*Algarra et al., 2020*). Tropical cyclones, which are other moisture-transporting structures, are also relevant in their areas of occurrence in the summer season, such as the Gulf of Mexico and the Caribbean Sea region and southeast Asia (*Khouakhi et al., 2017*). In fact, the regions where the major moisture transport mechanisms occur closely correspond to the areas of influence of the dynamic component of moisture transport on extreme precipitation. The dynamic component, linked to moisture-transporting winds, is intimately connected with the atmospheric circulation (*O'Brien et al., 2022*). This component should be key in understanding the changes in the relationship between moisture transport and extreme precipitation in a global warming context, considering that the changes in humidity (thermodynamic component) should affect moisture transport and extreme precipitation in a similar and well understood way.

On the role of ARs in linking atmospheric moisture transport and extreme precipitation

The simultaneous occurrence of extreme values of moisture transport and precipitation is clearly influenced by ARs in their regions of occurrence (Section 4.2). Analysing the number of precipitation days, the values of the thresholds used to define the extremes (the 90th percentiles of moisture transport and precipitation) and the estimated probability of a concurrent extreme of both variables, it is found out that high probabilities of concurrent extremes, together with reasonably high values of moisture transport and precipitation mainly occur in the regions where ARs make landfall (*Gimeno et al., 2016*). A specific analysis of these regions showed higher probabilities of concurrent extremes in the Northern than in the Southern Hemisphere, being especially high on the Pacific coast of North America. Additionally, the highest percentages of AR occurrence on the days of concurrent extremes of moisture transport and precipitation were found in those regions of atmospheric river occurrence (higher than 90%). Downwind of those areas, the fingerprint of the AR penetration on inland areas is clearly visible (with percentages higher than 75%). However, in most tropical regions (including monsoonal areas), the percentages of AR occurrence on the days of simultaneous extremes of moisture transport and precipitation do not exceed 50%, reflecting a low relationship of ARs with the occurrence of concurrent extremes there. Although Section 4.2 focused only on the present climate (1981-2017), the studied period was divided into two sub-periods of 15 years, an earlier and a later one, after removing the effects of El Niño-Southern Oscillation (ENSO), in order to see the effects of warming on the percentages of AR occurrence on the days of concurrent extremes of moisture transport and precipitation. Although other factors could also play a role in the changes in these percentages, such as the Atlantic Multidecadal Oscillation (AMO) or the Pacific Decadal Oscillation (PDO), a slight decrease in the percentages is generally found, being particularly strong on the North American coasts (both Atlantic and Pacific) in winter. This weakened relationship is also consistent with the detailed analysis of the regions of occurrence of landfalling ARs. To explain the possible decrease of AR importance in the occurrence of concurrent extremes of moisture transport and precipitation with warming, it should be considered that the IVT associated with ARs may increase more slowly with warming than the water vapour content associated with this moisture transport mechanism (*McClenny et al., 2020*). Thus, taking into account that extreme precipitation and the water vapour content may respond similarly to warming (*Emori and Brown, 2005*), extreme precipitation may increase faster than the moisture transport associated to ARs. Consequently, a decrease in the importance of this mechanism in the simultaneous occurrence of extreme values of moisture transport and precipitation may be expected.

On the relative importance of atmospheric moisture transport in extreme precipitation compared to other drivers

The importance of extreme moisture transport in the occurrence of extreme precipitation is analysed in terms of other two fundamental drivers of extreme precipitation (Section 4.3). These additional drivers are precipitable water (the water vapour content) and vertical velocity, which represent thermodynamic and dynamic factors affecting extreme precipitation, respectively. The conditional probability of extreme precipitation for all the combinations of extreme and non-extreme values of the three drivers is computed for the present climate. First, it is found out that at least one of the drivers should be extreme for extreme precipitation to occur. On a global scale, vertical velocity is the driver that, when being extreme, most favours the occurrence of extreme precipitation. However, precipitable water is the most relevant one for extreme precipitation in subtropical regions, and moisture transport in the regions of occurrence of ARs. Regarding the combinations of two drivers being extreme, the most favourable one is that of extreme values of vertical velocity and precipitable water, with non-extreme moisture transport. In fact, this two-driver combination is associated with extreme precipitation probabilities that are similar or even greater than that of the three drivers being extreme. There are clear latitudinal differences regarding the dominant combination for extreme precipitation occurrence. In the majority of extratropical areas, especially in regions located in the interior of the continents, the combination of precipitable water and vertical velocity is dominant. In these areas moisture transport is not so necessary for extreme precipitation occurrence, taking into account the greater influence of local moisture sources, fundamentally through evapotranspiration processes (*Miralles et al., 2016*). However, in subtropical areas, where moisture fluxes climatologically diverge (*Gimeno et al., 2010a*), the three-driver combination is dominant. In these regions, the presence of extreme values of horizontal moisture transport together with extreme water vapour content in the atmospheric column implies enhanced instability due to low-level moisture flux convergence (the opposite of the climatological conditions), consequently favouring extreme precipitation. This relationship between moisture flux convergence and atmospheric instability is weaker in extratropical regions, where instability is mainly caused by baroclinic activity. The combination of the three drivers in extreme conditions is also the most advantageous one in Antarctica, where moisture transport is necessary due to the low values of local moisture owing to the low temperatures there. To a lesser extent, the combination of extreme vertical velocity and moisture transport, under non-extreme precipitable water, is the most relevant one in some areas on the coast of North America and Europe in winter, which can be interpreted in terms of the role of ARs in the occurrence of extreme precipitation in those regions. The identification of the dominant combination of extreme precipitation drivers makes it possible to focus on the most relevant variables when studying the projected changes in extreme precipitation with global warming. For example, if the combination of two specific drivers reasonably represents extreme precipitation, extreme precipitation projections may be exclusively studied in terms of the changes in those drivers. This approximation, based on vertical velocity (representing dynamic factors) and precipitable water (accounting for thermodynamic factors) was adopted in Paper S2.

On the influence of contribution to precipitation deficits from the whole oceanic and terrestrial areas and the major global moisture sources on the occurrence of meteorological droughts

The contribution to precipitation from the whole global oceanic and terrestrial areas and the 13 major climatological moisture sources of the planet has a strong relationship with the occurrence of meteorological droughts (Section 4.4). In the majority of world regions, the conditional probability of drought occurrence given a contribution to precipitation deficit from either the whole global oceanic or terrestrial areas was estimated to be greater than 10%, that is, at least two times greater than in the situation of independence between moisture transport deficits and drought occurrence. The probability pattern shows a consistent spatial pattern with that of the climatological percentage contributions from those areas (*Gimeno et al., 2020a*). The fingerprint of the main moisture transport mechanisms is evident in the regions displaying higher drought probabilities (greater than 15%, 20% or 25%). Thus, for example, the influence of the AR frequency on drought occurrence of oceanic origin is visible in the western North American and European coasts (*Lavers and Villarini, 2015*), and the role of LLJs in land-origin droughts is notable in La Plata basin (an area which receives moisture from the Amazon region), and in oceanic-origin droughts in northern South America (*Jones, 2019*). The influence of tropical cyclones can also be observed in droughts of oceanic origin (*Khouakhi et al., 2017*), for instance, in southeastern North America. Many inner continental areas of the world (especially in Asia, North America, Africa and Australia) show a strong relationship between contribution deficits from terrestrial origin and the occurrence of meteorological droughts, which is associated with an outstanding role of recycling (*Van der Ent, 2010*) and drought propagation processes (*Schumacher et al., 2022*). Regarding the analysis of the 13 major global moisture sources, the spatial pattern of the areas of dominance of each source (understood as the areas in which the drought probability given a contribution deficit from that source is the highest one) resembles the patterns of precipitation and extreme precipitation occurrences associated with each source (*Gimeno et al., 2010a*; *Vázquez et al., 2020*). Three hotspots regions are found as those in which the contribution deficit from a single moisture source is highly related with drought occurrence at the 1 and 3-month time scales (drought probability greater than 20%): central-east North America (deficit from the Caribbean Sea and Gulf of Mexico source), south-east South America (Amazon source), and eastern Europe (Mediterranean source). In these regions, where the relationship between moisture transport deficits and drought occurrence is strong, the drought probability associated with specific values of contribution deficits agrees reasonably well with the severity of the observed droughts. This may serve as a starting point for improving drought predictability in those regions, considering that moisture transport, highly linked to large-scale atmospheric circulation, may be more predictable by models than precipitation, more associated with small-to-synoptic scale processes (*Lavers et al., 2014, 2016*; *Gvoždíková and Müller, 2021*; *Wang and Yuan, 2018*; *Gao et al., 2021*). Thus, in order to predict future droughts, it may be more helpful to use predicted moisture transport than predicted precipitation in those regions where moisture transport deficits are highly related with droughts. This predictive potential may be especially useful for improving the predictability of flash droughts, which is a type of drought that develops in a shorter time scale than the usual ones, near the submonthly scale (*Pendergrass et al., 2020*), or the predictability of sudden hydrological shifts (known as 'whiplash'; *Tan et al., 2023*). The results obtained in Section 4.4 are focused on the present climate, serving as a climatological basis. However, considering climate variability and global warming, there may be changes in the atmospheric circulation that may affect the obtained results (*Allan et al., 2020*). This possible effect was analysed in the present climate by means of the changes between the different phases of two modes of variability: a global one, ENSO, and a regional one affecting the North Atlantic area, the North Atlantic Oscillation (NAO). Only slight changes were found, related to the known effect of these modes on precipitation patterns (*Ropelewski and Halpert, 1987*; *Hurrell, 1995*). There may be additional effects from possible changes in the land-ocean temperature contrast, which may also have an influence on future droughts due to a decrease in the relative humidity of terrestrial areas (*Byrne and O'Gorman, 2018*; *Wainwright et al., 2022*).

On the importance of contribution to precipitation deficits from specific moisture sources on the occurrence of meteorological droughts

For nine key world regions of future drought aggravation, there is a strong relationship between contribution to precipitation deficits from their dominant specific moisture sources and drought occurrence (Section 4.5). In most cases, the obtained drought probabilities were only slightly higher than those considering the major moisture sources of the planet (Section 4.4). For each of the nine studied regions, which were identified as those where drought magnitude is projected to increase in the future under the SSP5-8.5 scenario, the dominant moisture source in terms of meteorological droughts may be the own region, the nearby continental source, or an oceanic one. The dominant moisture source of each region is identified as the source for which the drought probability associated with a contribution deficit is the highest. However, for a given region, the dominant source for drought occurrence does not always coincide with the source with the highest percentage contribution to precipitation. In some of the regions where the dominant and the most contributing source coincide (the Amazon, northeastern Brazil and southern Africa) this source is the own region, as they are areas with high values of evapotranspiration and key importance of recycling processes (*Drumond et al., 2019*). In another region (southwestern South America), which refers to a small area on the Pacific coast, the dominant source is oceanic (located in the Pacific Ocean), associated with regional ARs (*Valenzuela and Garreaud, 2019*). However, in the other regions, the dominant and the most contributing sources do not agree. The most contributing source is terrestrial in central America (*Durán-Quesada et al., 2012*), both the western and eastern Mediterranean (*Batibeniz et al., 2020*) and southwestern Australia (*Cheng and Lu, 2023*): the own region for central America and the western Mediterranean, and the nearby continental source for the eastern Mediterranean and southwestern Australia. Instead, the dominant moisture source for drought occurrence in those regions is oceanic (located in the North Atlantic Ocean for central America and the western Mediterranean, and in the Mediterranean Sea and the Indian Ocean, for the eastern Mediterranean and southwestern Australia, respectively). In those regions, which are mostly extratropical, a low contribution from the oceanic source implies a low contribution from the terrestrial source at a faster rate than in humid areas in the tropics, where there is a strong evapotranspiration, and recycling processes are highly relevant in short time scales (*Wang and Dickinson, 2012*). Thus, in those areas, due to that fast cascading effect from a deficit from the oceanic source to that of the terrestrial source, the oceanic sources have a stronger influence on drought occurrence than the terrestrial sources, in spite of being the most contributing ones. In another case (northern Brazil) the most contributing source is located in the South Atlantic Ocean (*Nieto et al., 2008*), while the dominant moisture source is the nearby terrestrial source, which is located within the pathways of the moisture transported from the two oceanic sources of the region. Consequently, a contribution deficit from that nearby continental source implies contribution deficits from the oceanic sources, that is, no incoming moisture transport in the region, favouring drought occurrence. The dominant moisture sources of many of the analysed regions are projected to undergo changes in their intensity with global warming (*Allan, 2023*), such as the dominant moisture sources of central America, southwestern South America, both the western and eastern Mediterranean, southwestern Australia (oceanic moisture sources), and the Amazon (the own region). In other regions, the dominant moisture sources are located in regions that may be affected by the projected changes in the atmospheric circulation (*Allan et al., 2020*), such as changes in the ITCZ (northern Brazil and the Amazon) or the storm track (central America, southwestern South America and both the western and eastern Mediterranean). Thus, the analysis carried out in Section 4.5 has meaningful climate change implications, arising from the selection of the analysed regions according to the projected drought trends.

On the analysis of the projected changes in the role of moisture transport in the occurrence of extreme precipitation and meteorological droughts over the Euromediterranean region

The influence of moisture transport on the occurrence of extreme precipitation and meteorological droughts is projected to increase in the Euromediterranean region, more strongly for droughts (Section 4.6). Concerning extreme precipitation, the concurrence of ARs and extreme precipitation highly conditions the relationship between moisture transport and extreme precipitation in the region (*Lavers and Villarini, 2013*; *Lorente-Plazas et al., 2020*). Indeed, the areas with the highest percentages of AR-extreme precipitation concurrence coincide with those with the strongest dependence between moisture transport and extreme precipitation, but only in the context of elevated terrain upwind of the moisture fluxes from the Atlantic Ocean or the Mediterranean Sea. An enhanced AR-extreme precipitation concurrence would explain the projected increase in the dependence between moisture transport and extreme precipitation that is found for the mid-21st century in the winter season. However, the AR-extreme precipitation concurrence is stable for the end-21st century in winter, indicating that changes in other mechanisms related to atmospheric instability should be considered. The projected decoupling between ARs and extratropical cyclones with global warming (*Wang et al., 2023*) would imply that atmospheric instability would not be associated with the occurrence of future ARs in the same terms as in the current climate, with a consequent decrease in the dependence between moisture transport and extreme precipitation at the end of the century. The decoupling between ARs and extratropical cyclones would occur due to the increased values of atmospheric moisture in a warmer climate, which would imply that high enough values of moisture transport would exist without the presence of strong winds associated to extratropical cyclones (*Zhang et al., 2024*). It is also projected that the location of ARs will move to the poles at a slower rate than that of the extratropical cyclones, with a consequent increase in the distance between them (*Wang et al., 2023*).

Focusing on the Iberian Peninsula, the results are, in general, similar to those obtained for the Euromediterranean region. In the Iberian Peninsula in winter, the AR-extreme precipitation concurrence is projected to increase in the mid-century period and remain approximately constant at the end of the century, which would explain the increase in the dependence between moisture transport and extreme precipitation in the mid-century (a greater increase than for the whole Euromediterranean region) and the subsequent decrease at the end of the century (although a slight increase with respect to the historical climate was still found). Regarding the summer season, less important in terms of the relationship between moisture transport and extreme precipitation in the region (Section 4.1), a strong connection between the AR-extreme precipitation concurrence and the dependence between moisture transport and extreme precipitation was also found for both the whole Euromediterranean region and the Iberian Peninsula. It is especially relevant when explaining the projected decrease in the influence of moisture transport on extreme precipitation in the end-century period in summer, which may be related to the projected decrease in the AR-extreme precipitation concurrence.

Regarding Euromediterranean meteorological droughts, there is a remarkable increase in the relationship between the contribution to precipitation deficits from the major oceanic moisture sources of the Euromediterranean region and the occurrence of meteorological droughts. The pattern of the dominant moisture source (the one whose contribution deficit maximises the drought probability) is projected to be fairly stable in the future climate, with the North Atlantic Ocean moisture source being dominant in the western part of the region, and the Mediterranean Sea in the central and eastern parts, consistently with the present climate pattern (Section 4.4). Considering the contribution deficit from the dominant moisture source at each grid point in the Euromediterranean region, the drought probabilities considerably increased from percentages between 5% and 20% in the present climate to percentages of 30% almost everywhere in the region, and 60% in hotspot areas such as Turkey, the Balkans and the Iberian Peninsula. In order to determine the influence of the contribution deficits from individual oceanic moisture sources on drought occurrence, a special focus was given to the Iberian Peninsula. For the three analysed moisture sources, a strong increase (of about three times compared to the present climate) in the median drought probability given contribution deficits from each source is projected for the future climates. The North Atlantic Ocean moisture source, which exerts a stronger influence on the western part of the peninsula, is projected to have drought probabilities on the order of 60% in the future climates, that is, about three times higher than in the present climate, which are on the order of 20%. The influence of the deficits from the Mediterranean Sea and the Caribbean Sea and Gulf of Mexico moisture sources, which are especially relevant on the eastern and western halves of the peninsula, respectively, undergo similar changes in the future. As a consequence, drought probabilities are projected to increase from ~10%-20% in the current climate to ~40%-50% in the future. This general increase in the influence of moisture transport from the ocean on drought occurrence should be understood in the context of a marked decline in the terrestrial water storage levels (*Pokhrel et al., 2021*). In line with the projections obtained for most CMIP6 models (*IPCC, 2021*), a decrease in soil moisture (representative of the terrestrial water storage levels) is projected in the Euromediterranean area (see Section 4.6). Consequently, it may be expected that evapotranspiration will diminish in the future, with a reduction in the importance of local moisture sources for the precipitation in the region (*Zhou et al., 2021*). Thus, deficits in the contribution to precipitation from the oceanic moisture sources of the Euromediterranean region are expected to play a more notable role in drought occurrence there in the future.

Limitations

The results obtained in this thesis should be understood within the context of different sources of uncertainties. One of the primary limitations lies in the use of reanalysis data, which tends to be less reliable in regions with limited observations, complex terrain, or where localised convective activity is relevant (*Rivoire et al., 2021*; *Lavers et al., 2022*; *Eiras-Barca et al., 2022*). Thus, comparing the results of this thesis with those obtained using high-resolution models is recommendable (*Zscheischler et al., 2021*), as it was done in Section 4.6 for the Euromediterranean region. Another important source of uncertainty is the sample size (*Li et al., 2019*), especially in those studies where, for each season, annual precipitation maxima are used in order to fit the extreme value models (Sections 4.1 and 4.6), or in Section 4.2 for using two sub-periods of 15 years for a first approach to study changes associated with global warming.

The definition of a concurrent extreme is also another limitation of this thesis. In order to have a sample size that is large enough, the 90th percentile of each variable is employed in Section 4.2 as the threshold for defining an extreme value, which is relatively low with respect to other more usual extreme value thresholds such as the 95th or 99th percentiles. Another limitation is the use of "-ω" at 500 hPa to analyse atmospheric instability in Section 4.3. This approximation is reasonably reliable for studying vertical motion related to synoptic meteorological systems such as extratropical cyclones or fronts but not so much for smaller-scale systems such as storms (*O'Gorman and Schneider, 2009*).

In Sections 4.4 and 4.5, the contribution to precipitation data from the studied moisture sources was obtained using data from the ERA-Interim reanalysis (*Dee et al., 2011*), the predecessor reanalysis of the state-of-the-art ERA5 (*Hersbach et al., 2020*) from the ECMWF. Global Lagrangian simulations based on ERA5 data were not available at the time when this research was performed due to the high computational effort they involve. However, a large number of studies that analysed moisture transport following the Lagrangian approach used in this thesis were based on ERA-Interim data (see *Gimeno et al., 2020b* for a review), and a comparison analysis of both reanalysis by *Fernández-Alvarez et al. (2023c)* showed that the obtained results were not significantly different between them.

Additionally, in Sections 4.4, 4.5 and 4.6, the use of moisture sources with fixed locations may be seen as another limitation. The location and/or extension of the specific moisture sources of a given target region may experience changes over time, but the probabilistic approach followed in Sections 4.4, 4.5 and 4.6 required the use of the same moisture sources for the entire studied period. Similarly, the results obtained in Section 4.6 have some uncertainties related to the model data used, already explained in *Fernández-Alvarez et al. (2023a)*. One of its main limitations is the use of a single CMIP6 model, the CESM2. However, *Fernández-Alvarez et al. (2023a)* found strong similarities between the results obtained using data from the CESM2 model and those using an ensemble of models, for a five-year period. The selected parameterisations of the WRF-ARW downscaling model, although based on the existing literature, represent another source of uncertainty (*Fernández-Alvarez et al., 2023a*). Finally, future projections rely on a single high-emission scenario, the SSP5-8.5, which facilitates the identification of anthropogenic signals. Future studies are encouraged to quantify the degree of scenario-related uncertainty in projections of moisture transport influence on hydrometeorological extremes.

6
Conclusions

The aim of this final chapter is to provide the general conclusions reached in this thesis, as well as future steps for continuing with the research topics presented here.

6.1 General conclusions

These are the general conclusions that can be drawn from this thesis:

1) The influence of moisture transport on extreme daily precipitation is stronger in subtropical and extratropical areas than in tropical ones, and the associated pattern reflects the fingerprints of the major moisture transport mechanisms. This pattern is similar to that of its dynamic component, key in a climate change context because of the uncertain changes in atmospheric circulation.
2) Atmospheric rivers (ARs) play an outstanding role in the occurrence of concurrent extremes of moisture transport and precipitation in the areas where they make landfall. These are also regions with fairly high values of both the probabilities of concurrent extremes and the thresholds used to define the extremes. However, a possible decline in the influence of ARs on the concurrent extremes in the current warming climate is found out.
3) Moisture transport is a key driver of extreme precipitation, but its influence is enhanced when combined with extreme values of precipitable water and vertical velocity. However, the importance of moisture transport is not geographically uniform, being more relevant in the subtropics, extratropical coastal regions and Antarctica than in inner continental areas, where there is a predominant role of

evapotranspiration processes. In continental inland areas, extreme values of precipitable water and vertical velocity may be sufficient for extreme precipitation to occur without extreme moisture transport.

4) Meteorological droughts are highly influenced by contribution to precipitation deficits from the whole global oceanic and terrestrial areas and the major climatological moisture sources of the planet. Strong relationships are obtained in the areas of influence of the main moisture transport mechanisms and those where recycling processes are especially relevant. Drought predictability may take advantage of these connections in some hotspot regions where meteorological droughts strongly depend on deficits from a single moisture source.
5) The influence of specific moisture sources on the occurrence of meteorological droughts is, in general, only slightly stronger than that found for the major planetary moisture sources. The dominant moisture source for drought occurrence in a given region does not always coincide with the source with the highest percentage contribution to precipitation. This disagreement is particularly evident in extratropical regions where the most contributing source is terrestrial but the dominant one for droughts is oceanic, in line with fast cascading effects from contribution deficits of oceanic origin to those of terrestrial origin.
6) The influence of moisture transport on extreme precipitation and meteorological droughts over the Euromediterranean region is projected to increase with global warming. Changes in the link between moisture transport and extreme precipitation are generally consistent with changes in the role of ARs in extreme precipitation occurrence, but not for the end of the 21st century in winter, when a decline in the influence of moisture transport on extreme precipitation is projected. The role of moisture transport deficits from the major oceanic moisture

sources in the occurrence of meteorological droughts is projected to undergo a pronounced increase in the future, linked to a decrease in soil moisture that may lead to a reduced importance of local moisture sources.

6.2 Future work

This thesis has tackled many aspects connected with the relationship between moisture transport and the occurrence of extreme precipitation and meteorological droughts. The following future studies may be carried out based on the framework presented in the thesis:

- The extreme value analysis employs a non-stationary GEV methodology based on annual precipitation maxima for each season (Sections 4.1 and 4.6). Under this methodology, only one value per year (the highest one) is used for the model fitting. This method is selected because of its simplicity, further considering that the analysis is performed at grid point level. However, there are other extreme value methods that take advantage of a larger amount of information. The non-stationary peaks-over-threshold methodology is a useful alternative, accounting for the observations above a specified threshold (see, for example, *Beguería et al., 2011*), but the selection of the threshold, especially when dealing with large gridded data, represents an issue (*Beguería, 2005*). There are other methodologies that use all the information available (all the values of the studied variable) for model fitting, avoiding the decision of selecting a threshold (*Naveau et al., 2016*). This approach may be an interesting upgrade for the variables studied in this thesis.

- In this thesis, the use of copulas for probability estimation has only been performed for bivariate data (Section 4.2, 4.4, 4.5 and 4.6). However, there are other alternatives for dealing with multivariate data, such as the so-called *vine copulas* (*Czado, 2019*). This kind of copula makes it possible to study complex interactions between more than two variables, which may be a useful approach for multivariate topics addressed in this thesis. For example, in Section 4.3 the probability of extreme precipitation for a given combination of drivers is estimated empirically, but the relationships between extreme precipitation and its drivers may be analysed in more detail by means of *vine copulas*, which merits future research. In Sections 4.4, 4.5 and 4.6, the drought probability associated with a contribution to precipitation deficit is estimated for each moisture source separately, but it would be interesting to use *vine copulas* to deal with contribution deficits from more than one source.
- To assess the robustness of the findings of this thesis, it would be interesting to compare the results in Sections 4.4 and 4.5 with those obtained with global Lagrangian simulations based on data from the ERA5 reanalysis (*Hersbach et al., 2020*).
- Studying the influence of the contribution to precipitation from given moisture sources on the occurrence of flash droughts, a kind of drought characterised by a short-term development (*Pendergrass et al., 2020*), or on the sudden changes from wet to dry events and vice versa, known as precipitation 'whiplash' (*Tan et al., 2023*), is a highly relevant topic for further research. This is so, particularly in the context of drought

predictability, considering that moisture transport may be more predictable than precipitation.

- The analysis based on future projections (Section 4.6) can be extended in several ways. First, it can be applied to other regions where moisture transport is known to play an important role in the occurrence of extreme precipitation and meteorological droughts. In order to compare with the results obtained for the Euromediterranean region, the extreme precipitation analysis would be especially interesting in regions of landfalling ARs, and the meteorological drought analysis in regions with projected soil moisture decline. Second, extending the analysis carried out in this thesis by using several climate models is highly recommended (*Bevacqua et al., 2023*) and a very interesting task to assess the robustness of the results of this thesis. Finally, the use of the high-end emission climate change scenario, the SSP5-8.5, could be unrealistic (*Hausfather and Peters, 2020*), and future research should be devoted to compare the results with other SSPs, such as the SSP2-4.5 or the SSP3-7.0 (*O'Neill et al., 2016*).

Supplementary material

This supplementary material contains three scientific papers (see Tables S1 and S2 for information about them and the journals where they were published) and the supplementary material of all the articles included in this thesis, as well as the one corresponding to the submitted manuscript.

Table S1. Information about the three supplementary articles of this thesis.

	Title	Authors	Year	Journal
PAPER S1	"Extreme precipitation events"	Gimeno, L., Sorí, R., Vázquez, M., Stojanovic, M., Algarra, I., Eiras-Barca, J., **Gimeno-Sotelo, L.**, & Nieto, R.	2022	*Wiley Interdisciplinary Reviews-Water* (*WIREs Water*)
PAPER S2	"Projected changes in extreme daily precipitation linked to changes in precipitable water and vertical velocity in CMIP6 models"	**Gimeno-Sotelo, L.**, Bevacqua, E., Fernández-Alvarez, J. C., Barriopedro, D., Zscheischler, J., & Gimeno, L.	2024	*Atmospheric Research*
PAPER S3	"Assessment of the global relationship of different types of droughts in model simulations under high anthropogenic emissions"	**Gimeno-Sotelo, L.**, El Kenawy, A., Franquesa, M., Noguera, I., Fernández-Duque, B., Domínguez-Castro, F., Peña-Angulo, D., Reig, F., Sorí, R., Gimeno, L., Nieto, R. & Vicente-Serrano, S. M.	2024	*Earth's Future*

Table S2. Information about the journals where the supplementary articles of this thesis were published, for those journals included in the Journal Citation Reports of the year 2023.

Journal	*Wiley Interdisciplinary Reviews-Water (WIREs Water)*	*Atmospheric Research*	*Earth's Future*
ISSN	2049-1948	0169-8095	2328-4277 (Electronic ISSN)
Region	USA	NETHERLANDS	USA
Publisher	WILEY	ELSEVIER SCIENCE INC	AMERICAN GEOPHYSICAL UNION
Impact Factor	6.8	4.5	7.3
Quartile (Category)	Q1 (WATER RESOURCES)	Q1 (METEOROLOGY & ATMOSPHERIC SCIENCES)	Q1 (GEOSCIENCES, MULTIDISCIPLINARY)

PAPER S1

Received: 3 April 2022 | Revised: 20 June 2022 | Accepted: 22 July 2022

DOI: 10.1002/wat2.1611

ADVANCED REVIEW

WIREs WATER WILEY

Extreme precipitation events

Luis Gimeno[1] | **Rogert Sorí**[1] | **Marta Vázquez**[1] | **Milica Stojanovic**[1,2] | **Iago Algarra**[1] | **Jorge Eiras-Barca**[1,3] | **Luis Gimeno-Sotelo**[1] | **Raquel Nieto**[1]

[1]Centro de Investigación Mariña, Environmental Physics Laboratory (EPhysLab), Universidade de Vigo, Ourense, Spain

[2]Department of Meteorology and Geophysics, Faculty of Physics, Sofia University "St. Kliment Ohridski", Sofia, Bulgaria

[3]Defense University Center, The Spanish Naval Academy, Marín, Spain

Correspondence

Luis Gimeno, Centro de Investigación Mariña, Environmental Physics Laboratory (EPhysLab), Universidade de Vigo, Campus As Lagoas S/N, 32004 Ourense, Spain.
Email: l.gimeno@uvigo.es

Funding information

Ministerio de Ciencia, Innovación y Universidades, Grant/Award Number: RTI2018-095772-B-I00; Xunta de Galicia, Consellería de Cultura, Educación e Universidade, Grant/Award Number: ED431C 2021/44

Edited by: Thom Bogaard, Associate Editor, Jan Seibert and Wendy Jepson, Co-Editors-in-Chief

Abstract

The effect of increased populations concentrated in urban areas, coupled with the ongoing threat of climate change, means that society is becoming increasingly vulnerable to the effects of extreme precipitation. The study of these events is therefore a key topic in climate research, in their physical basis, in the study of their impacts, and in our adaptation to them. From a meteorological perspective, the main questions are related to the definition of extreme events, changes in their distribution and intensity both globally and regionally, the dependence on large-scale phenomena including the role of moisture transport, and changes in their behavior due to anthropogenic pressures. In this review article, we address all these points and propose a set of challenges for future research.

This article is categorized under:

Science of Water > Water Extremes

Science of Water > Hydrological Processes

KEYWORDS

extreme precipitation, extreme threshold definition, global moisture transport, observed and future changes

1 | INTRODUCTION

Over the last few decades, the study of extreme events has become a focus of interest for society due to their social, economic, and environmental impacts (Ackerman, 2017; Alimonti et al., 2022; Lugo, 2018; Wernberg et al., 2013). Whether related to higher population densities in specific areas (United Nations Department of Economic and Social Affairs, 2019), or an increased dependence on critical infrastructure (for telecommunications, healthcare, or other services; Turoff et al., 2016) some societies are now particularly vulnerable to the impact of extreme events. Extreme events caused by natural hazards or/and human actions may in turn trigger natural and technological disasters (Girgin et al., 2019; Haddow et al., 2020). The cascading impacts of multi-hazard types have been described for historical catastrophic events such as the impact of Hurricane Irma on the Caribbean and the southeast of United States (Emrich et al., 2019) or the 2004 Indian Ocean Tsunami and 2011 great East Japan earthquake and tsunami (Suppasri et al., 2021).

Extreme events are investigated in a number of different fields such as social sciences, ecology, and engineering; however, weather and climate extremes—specifically precipitation—have attracted the most interest in the recent literature (McPhillips et al., 2018). Variations in the distribution and intensity of precipitation patterns have attracted a great deal of scientific interest due to the particular threat to human activities posed by extreme hydrological events such as extreme precipitation, and floods. Among the most recent catastrophic events, there are some worth mentioning; eastern China in June 2015 (Wang & Gu, 2016), western Europe in July 2019 (Science, 2021), or southeast Brazil in 2020 (Dalagnol et al., 2022); all of them causing catastrophic socio-economic and environmental impacts. Climate extremes demand preparedness and emergency response strategies that go beyond the emergency response services, including health and social care providers (Curtis et al., 2017). A recent study also confirmed that extreme rainfall reduces worldwide macroeconomic growth rates and slows the global economy rise (Liang, 2022).

There is growing evidence that anthropogenic activity affects the climate in numerous ways, and the effects of extreme conditions are likely to become stronger due to changes in their intensity and frequency. In particular, the intensity of extreme rainfall is expected to increase in regions with high moisture availability, particularly in wet moths. This will cause more frequent and severe flooding under global warming (e.g., Min et al., 2011; Pall et al., 2011; Tabari, 2020). Despite the current observational uncertainties of extreme rainfall (Herold et al., 2017), increasingly extreme rainfall has been reported in a large number of locations, even in regions where the average rainfall has decreased (e.g., Asadieh & Krakauer, 2015; Kharin et al., 2007; Kharin & Zwiers, 2005). The precipitation budget will be therefore affected, becoming a challenge to water resources management (Zittis et al., 2021). It is therefore of great interest to understand the changing characteristics and impacts of extreme precipitation events as part of attempts to design adaptation and mitigation policies that could allow improvements to be made in terms of the ability of society to adapt to potential changes caused by global warming (IPCC, 2013, 2021). However, modeling precipitation and detecting extreme events in future scenarios is challenging today; models still simulate varying magnitudes of precipitation response to anthropogenic forcing. This is mostly due to the use of different schemes for parameterizing processes at the subgrid-scale (Madakumbura et al., 2021). Uncertainties also arise regarding the future behavior of major mechanisms of atmospheric moisture transport and their role in the occurrence of extreme precipitation events under global warming (Gimeno et al., 2016).

In this review, we intend to address the phenomenon of extreme precipitation from several aspects, including its definition, the physical fundaments, generating mechanisms, spatiotemporal evolution, and future challenges. First, when approaching the study of extreme precipitation events it is important to clarify the definition of "extreme", a term that can have different meanings related to causes as fundamental as moisture transport mechanisms to effects such as natural hazards. The definition must also acknowledge different statistical techniques, from the very simple (such as the use of fixed precipitation thresholds) to more sophisticated (such as those derived from the application of the Extreme Value Theory). Sections 2 and 3 are therefore devoted to these aspects of the definition. Leaving aside some of the more detailed theoretical considerations; in Section 4, we will address the essential physical basis that underpins how the extremes of precipitation have changed over the last few decades and should change in the decades that follow, as a consequence of increased global temperatures. These observed and predicted changes will form the content of Section 5. In Section 6, we will address the intriguing role of moisture transport and its major mechanisms related to the extremes of precipitation, and finally, in the last section, we will formulate some of the main challenges for future research.

2 | THE PROBLEM OF DEFINING EXTREMES

As addressed in the introduction, the definition of "extreme" is not unique. Despite the increased use of the term, a unified definition of the word has never been achieved, either in an interdisciplinary sense or in specific research fields (McPhillips et al., 2018; Brosca et al., 2020). This section will address this issue from two different approaches. On the one hand, the perspective related to the disaster aspects. On the other hand, the perspective is based on the statistical approach to the amount of precipitation. In the latter, parametric and nonparametric—including indices used by Expert Team on Climate Change Detection and Indices (ETCCDI)—statistic methods will be introduced. Moreover, some alternatives to these methods will be discussed.

In general terms, and related to the disaster aspects, extreme events can be considered in terms of either their nature or their impacts. Despite the general use of impacts (economic losses, social effect) to define extreme events in some disciplines, in the climatological sciences extreme events are usually defined in terms of the anomaly of their occurrence and specifically by their characteristics (McPhillips et al., 2018). Despite the common association of "unusually rare" events (in terms of magnitude) with more severe impacts, in the last few decades, many important economic losses and environmental impacts have also been associated with nonextreme events. A number of factors can be attributed to these losses, and in many cases, unusually extreme impacts have been attributed to a combination of different types of events in different regions. For example, precipitation in combination with storm surges is expected to produce important coastal flooding in the future (Bevacqua et al., 2019; Ridder et al., 2018). The increased occurrence of this kind of damage has increased levels of interest in so-called "compound events", defined as the combination of variables or events that lead to an extreme impact (Leonard et al., 2014), even though the individual events may not necessarily be extreme in themselves.

Among the many different statistical techniques available for the definition of extreme precipitation, the easiest and probably the most widely used in literature are nonparametric methods based on the use of fixed values or percentiles to select a threshold for extreme events (Anagnostopoulou & Tolika, 2012). Following this methodology, the Expert Team on Climate Change Detection and Indices (ETCCDI) developed a set of 27 indices based on daily temperature and precipitation, which are used extensively to detect and monitor climate change (e.g., Alexander & Arblaster, 2017; Cooley & Chang, 2020; Yin & Sun, 2018). From this list, 10 indices are linked specifically to precipitation as presented in Table 1. Some of the precipitation indices are defined in terms of a specific value (such as 10 mm, 20 mm, or a user-defined threshold), with the index based on the number of days on which the threshold is exceeded over a given period. This type of index can be useful for specific purposes or for particular areas, although a percentile-based method is in general more suitable for allowing comparisons to be made between regions. For this reason, most authors use a percentile-based index, with the percentile ranging between 90 and 99 (McPhillips et al., 2018). While most ETCCDI indices are based on the analysis of precipitation on single days, the definition of extreme events can also be expressed in terms of the duration of a particular characteristic of precipitation, by defining extreme precipitation events as a number of consecutive days with precipitation above a threshold (She et al., 2015). For the definition of threshold-based extreme events, an important consideration is the sensitivity of the results to the selection of the threshold, which can lead to misinterpretation of results in some cases (Pendergrass, 2018; Schär et al., 2016). While it is clearly not possible to define a single fixed threshold for extreme precipitation for different regions, it is also clear that percentile-based thresholds are not always able to characterize extreme events fully. In both cases, the results depend strongly on the selection of the threshold; in most cases, this is determined arbitrarily. For example, almost 90% of the precipitation falls above the 95th precipitation percentile in some regions if all days are taken into consideration in the computation (Pendergrass, 2018). However, usually only precipitation days (with precipitation higher than 1 mm) are considered in

TABLE 1 Precipitation indices defined by the ETCCDI

Index	Definition
R10mm	Annual count of days when precipitation (PRCP) ≥ 10 mm
R20mm	Annual count of days when PRCP ≥ 20 mm
Rnnmm	Annual count of days when PRCP ≥ nn mm, nn is a user-defined threshold
RX1day	Maximum 1-day precipitation
RX5day	Maximum of consecutive 5-day precipitation mm
SDII	Ratio of annual total precipitation to the number of wet days (≥1 mm).
R95p	Amount of precipitation from days >95th percentile
R99p	Amount of precipitation from days >99th percentile
CWD	Maximum number of consecutive days with RR ≥1 mm
PRCPTOT	Annual total precipitation on wet days

the percentile computation according to Schär et al. (2016), but this methodology can also lead to artifacts and misleading results if significant variations in wet-day frequency are not taken into account.

The limitations of nonparametric techniques have led to increased interest in the use of different methods to investigate extreme events, including the parametric methodologies that have seen widespread use over the last few decades. The most common parametric method is the extreme value distribution fitting method, which is based on the use of probabilistic statistical techniques and precipitation data, in order to establish a threshold for the occurrence of extreme events (Liu et al., 2013). Several distribution functions can be applied in these methodologies, including the generalized Pareto distribution and the generalized extreme value distribution (Lazoglou et al., 2019), which will be discussed in Section 3.

Different authors have pointed to the better accuracy of parametric compared with nonparametric methods to define extreme precipitation (e.g., Anagnostopoulou & Tolika, 2012), although these methodologies also have limitations, such as the sensitivity to the size of the data series in the nonparametric percentile method or the discrepancies in the return periods between different parametric techniques (Lazoglou et al., 2019; Liu et al., 2013). For this reason, other methods have also received consideration, including detrended fluctuation analysis, which is the most popular alternative to both parametric and nonparametric methods. Detrended fluctuation analysis is an attempt to define objectively the threshold for extreme events by filtering the short-range dependence and any other trends of non-stationary time-series, thereby allowing detection of any long-range dependence in the data (Liu et al., 2013). The robustness of this methodology has been shown for different regions such as the Pearl River Basin (Liu et al., 2013) and the Loess Plateau of China (Zhang et al., 2020). However, the complexity of the calculation and the need for long series of rainfall (Liu et al., 2013) make this method less popular than others.

Despite an increased attention to extreme precipitation, there is no consensus on which methodology is the best for defining extreme events. The existence of many different methodologies with their advantages and disadvantages means that the proper understanding of the basis behind each of them is critical. A better understanding of each methodology could allow us to select the most suitable one for each case in order to allow the proper interpretation of results.

3 | EXTREME VALUE STATISTICS: FUNDAMENTALS AND APPLICATIONS

In climate science, extreme phenomena are of great interest; however, in most cases, there are few observations or none at all. In order to estimate the tail of the distribution of the relevant environmental random variable (e.g., precipitation, wind speed, etc.), a number of statistical techniques are available, which are derived from the so-called Extreme Value Theory (EVT). In this section, we will introduce some of the basic concepts that are widely used across many fields of knowledge.

We consider $X_1, X_2, ..., X_n$ as independent random variables, identically distributed to X, with distribution function F. Although our focus is on maxima, it is not restrictive because equivalent results for minima can easily be found by taking into account the fact that $\min(X_1, ..., X_n) = -\max(-X_1, ..., -X_n)$.

It is well known that the suitably normalized maximum converges to a distribution G that is not degenerate and is of the same type as one of these distributions ("the same type" means that the only differences are in location or scale):

- Type 1: (Gumbel): $G(x) = \Lambda(x) = \exp(-\exp(-x))$, for $x \in \mathbb{R}$.
- Type 2: (Fréchet): $G(x) = \Phi_\alpha(x) = \begin{cases} 0, x \le 0 \\ \exp(-x^{-\alpha}), x > 0, \alpha > 0 \end{cases}$
- Type 3: (Weibull): $G(x) = \Psi_\alpha(x) = \begin{cases} \exp(-(-x)^{\alpha}), x < 0, \alpha > 0 \\ 1, x \ge 0 \end{cases}$

Von Mises (1954) and Jenkinson (1955) unified the three families into the Generalized Extreme Value (GEV) distribution, with distribution function:

$$G_\gamma(x;\mu,\sigma) = \begin{cases} \exp\left(-\left(1+\gamma\frac{x-\mu}{\sigma}\right)^{-\frac{1}{\gamma}}\right), & (\gamma \neq 0), \\ \exp\left(-\exp\left(-\frac{x-\mu}{\sigma}\right)\right), & (\gamma = 0), \end{cases}$$

where $1+\frac{\gamma(x-\mu)}{\sigma}>0, \mu \in \mathbb{R}$, $\sigma>0$ and $\gamma \in \mathbb{R}$; μ is the location parameter, σ is the scale parameter, and γ is the shape parameter. If $\gamma<0$, the tail of the distribution of X is lighter than that corresponding to the exponential distribution (and F is of the Weibull type); if $\gamma=0$, the tail is exponential (and F is of the Gumbel type); and if $\gamma>0$, the tail is heavier than exponential (and F is of the Fréchet type).

By denoting $Y := \max(X_1, ..., X_n)$, it is possible to approximate its distribution using a $GEV(\gamma;\mu,\sigma)$. We can partition the observations X_i into blocks; for example, if our data consist of 30 years of daily observations of precipitation, we will have 30 blocks of 365 observations each. Therefore, we will be considering $Y_1, Y_2, ..., Y_{30}$ as a sample Y of dimension 30. This statistical approach is usually termed "block maxima."

At this point, there are some important concepts to mention:

- *Exceedance probability*: This is simply the probability that Y is greater than a predefined large value q, that is, $P(Y>q) \approx 1-G_\gamma(q;\mu,\sigma)$.
- *Return level*: For a given T, the return level is $U(T)$ such that $P(Y>U(T))=\frac{1}{T}$. For example, by taking Y as the annual maximum of precipitation, the 100-year return level, or $U(100)$, is such that, on average, Y is greater than that quantity once every 100 years. $U(T)$ can be expressed in terms of the GEV distribution: $U(T) \approx \overleftarrow{G_\gamma}\left(1-\frac{1}{T};\mu,\sigma\right)$, where $\overleftarrow{G_\gamma}(y;\mu,\sigma)$ denotes the inverse of the GEV distribution function.
- *Return period*: For a given y_T, the return period is $T=\frac{1}{P(Y>y_T)} \approx 1/\left(1-G_\gamma(y_T;\mu,\sigma)\right)$. In our example, the annual maximum of precipitation is, on average, greater than y_T once every T years.

We can obtain estimates of these quantities by substituting the unknown parameters of the GEV distribution with their corresponding estimates (the most common estimation methods are maximum likelihood and probability weighted moments).

In another statistical approach known as Peaks-Over-Threshold (POT), observations greater than a large threshold u are analyzed and the differences are calculated between each of these observations and u. If we denote $W := X-U$, we are studying the distribution of the random variable $W \mid W>0$, which can be approximated quite well by a Generalized Pareto (GP) distribution. Taking F_u as the distribution function of W and $H_\gamma(w;\sigma)$ as the distribution function of a GP distribution with shape parameter $\gamma \in \mathbb{R}$ and scale parameter >0 we have:

$$F_u(w) \approx H_\gamma(w;\sigma) = \begin{cases} 1-\left(1+\frac{\gamma w}{\sigma}\right)^{-\frac{1}{\gamma}}, w \in (0,\infty), \gamma>0 \\ 1-\exp\left(-\frac{w}{\sigma}\right), w \in (0,\infty), \gamma=0 \\ 1-\left(1+\frac{\gamma w}{\sigma}\right)^{-\frac{1}{\gamma}}, w \quad \left(0,-\frac{\sigma}{\gamma}\right), \gamma<0 \end{cases}$$

This approximation was first described by Pickands (1975) and Balkema and de Haan (1974). An interesting example of its use is as follows.

Taking the random variable X as the "amount of precipitation", we extract a sample of X of dimension n. For instance, our data may consist of n daily observations of precipitation. We can calculate the (approximate) probability that X is greater than the largest observation recorded over these n days, denoted $x_{(n)}$. Let N_u be the number of observations of the sample that exceed; with $w_{(N_u)}$ as the largest observation of the variable W we can write:

$$P\left(X>x_{(n)}\right) = \{1-F(u)\}\left[1-F_u\left(w_{(N_u)}\right)\right] \approx \frac{N_u}{n}\left(1-H_\gamma\left(w_{(N_u)};\sigma\right)\right),$$

we also note that $1-F(u) \approx \frac{N_u}{n}$.

In order to obtain an estimate of this probability, γ and σ must be substituted by their corresponding estimates (as for the "block maxima" approach, maximum likelihood and probability weighted moments are the most popular methods of estimation).

The problem of choosing the value of the threshold u is open and controversial. Davison and Smith (1990) proposed the study of the mean excess function, which in the case of the GP distribution, takes the form:

$$e(t) := E(X - t \mid X > t) = \frac{\sigma + \gamma t}{1 - \gamma}, \text{ if } \gamma < 1$$

In practice, it consists of choosing u such that the plot of $\widehat{e}_n(t)$ is approximately linear to the right of that value. $\widehat{e}_n(t)$ is the empirical version of $e(t)$ and can be expressed as:

$$\widehat{e}_n(t) := \frac{\sum_{i=1}^{n} x_i \mathbf{1}_{(t,+\infty)}(x_i)}{\sum_{i=1}^{n} \mathbf{1}_{(t,+\infty)}(x_i)} - t, \text{ where } \mathbf{1}_{(t,+\infty)}(x_i) = \begin{cases} 0, & x_i \leq t \\ 1, x_i > t \end{cases}.$$

Further information about threshold selection can be found in Beguería (2005).

Finally, it is important to note that throughout this section we have been considering that the parameters of the distributions are constant over time. However, in the context of climate change, they may be time-dependent (this is called "nonstationarity"). One way of solving this problem is by reformulating the parameters of the distributions, for example, in the case of the *GEV* model, we can write:

$$\mu(T) = \alpha_0 + \alpha_1 T,$$

$$\sigma(T) = \exp(\beta_0 + \beta_1 T),$$

$$\gamma(T) = \delta_0 + \delta_1 T.$$

Likewise, it is also possible to write the parameters of the *GP* distribution as $\sigma(T)$ and $\gamma(T)$, according to the same functional relationships indicated in the case of the *GEV* model, for example. The approach that consists of fitting a *GP* distribution with parameters that are allowed to vary with time is called "nonstationary POT", which is also very useful to model extreme precipitation (see, for instance, Beguería et al., 2011).

Aside from some technical limitations (it is difficult to maximize the log-likelihood function), the linear equations above may not be sufficiently accurate to express the true time dependence of the parameters (this difficulty is especially acute for long series). In order to cope with nonstationarity without dealing with the limitations of the linear forms, an alternative approach is the use of an inhomogeneous Poisson process, which incorporates a time-dependent occurrence rate $\lambda(T)$.

Last but not least, it is important to mention that extreme value analyses of precipitation tend to have a spatial dimension, in the sense that it is usually interesting to study the precipitation over large regions. Taking into account that the parameters of the distributions do not change so much when moving from one location to another one that is close to it, the purpose of the regional extreme-value analysis is to find a model (with a common shape parameter) that is valid for a homogeneous region. Nevertheless, it is possible to use spatial interpolation techniques to produce continuous maps of the parameters, making it easier to estimate spatially the extreme quantiles (see, e.g., Beguería & Vicente-Serrano, 2006; Beguería et al., 2009).

4 | RESPONSE OF PRECIPITATION EXTREMES TO WARMING

One of the main signs of climate change is the relentless rise in global average temperature. From a thermodynamic perspective, a warmer atmosphere leads to an increase in moisture content and to changes in the hydrological cycle, which include an intensification of precipitation. The increase in global mean precipitation is estimated to scale from 1% to 3% per degree of global mean temperature, limited by the atmospheric energy balance (e.g., Held & Soden, 2006; O'Gorman & Schneider, 2009). This increase is well below the Clausius–Clapeyron rate, where the global mean water vapor increases at a rate of 7% for each degree of increase in surface temperature (e.g., Held & Soden, 2006; O'Gorman & Muller, 2010). Additionally, the estimate of an increase in mean precipitation is not always supported by observations (Gu & Adler, 2015). The reason may be that the cloud radiative feedback is not properly represented by climate models or that the expected increase in global average precipitation due to increased emissions has been masked by aerosol drying, as suggested by different authors (Mauritsen & Stevens, 2015; Salzmann, 2016).

In any case, it is not expected that the increase in precipitation extremes will keep pace with the overall increase in mean precipitation. Some authors noted in the past that the intensity of the extremes of precipitation should increase in proportion to the average content of the atmospheric water vapor or at least at a similar rate as the climate warms (e.g., Allen & Ingram, 2002; Trenberth et al., 2003). Nevertheless, the intensity of the extreme precipitation is not limited by the global energy balance because this relates to the mean precipitation on a global scale, thus the rate of increase may be greater with global warming (Myhre et al., 2019; O'Gorman et al., 2012). The relationship between temperature and extreme rainfall is more complex than that suggested by the Clausius–Clapeyron equation. In fact, several regional studies have shown how the intensity of extreme rainfall increases more markedly at higher temperatures, especially for extreme rainfall events of short duration (Hardwick-Jones et al., 2010; Lenderink et al., 2011; Lenderink & Van Meijgaard, 2008).

O'Gorman and Schneider (2009) indicate a latitudinal effect where the extremes of extratropical precipitation may scale more slowly than the atmospheric water vapor content; extremes of tropical precipitation may not be simulated reliably due to highly variable changes in convection. In fact, extreme tropical precipitation events are mostly linked to long-term convective systems (Roca & Fiolleau, 2020), therefore the rate of increase of extreme precipitation could be higher if there is an increase in convective upward vertical flows. O'Gorman et al. (2012) showed an increase in extreme tropical precipitation events close to 10% for each degree of surface temperature, higher than that estimated for extratropical latitudes. Kharin et al. (2013) showed how the current simulated precipitation extremes according to return values determined as the quantiles of a Generalized Extreme Value (GEV) are suitable for the extratropics, but the uncertainty is greater for tropical precipitation extremes in both models and observations. The GEV approach was already described in Section 3, and it is characterized by providing a probabilistic framework for analyzing extremes in the tails of the distributions. This feature contrasts with the one provided by the ETCCSI, based on total values or predefined thresholds.

The intensity and frequency of extreme precipitation events have increased in most regions (Alexander et al., 2006). Sun et al. (2007) showed a consistent shift toward more intense and extreme rainfall on a global scale and in several different regions. Their results indicate an increase in the frequency of extreme rainfall, which is much greater than the increase in its intensity. Therefore, in a warmer climate, extreme precipitation events are expected to be more frequent than in the current conditions, reaching an unprecedented magnitude throughout the 21st century (Giorgi et al., 2019). There is some consensus that under a warmer climate, extreme precipitation events will experience an amplification similar to that predicted by Clasius–Clapeyron for the saturation vapor pressure although slight variations will occur under different circumstances. It is important to bear in mind that dynamic and thermodynamic contributions may also play an important role. Emori and Brown (2005) examined the role played by thermodynamic and dynamic changes related to increases in extreme precipitation. Their results generally show that thermodynamic changes—increases in atmospheric moisture content linked with global warming—play a major role in the changes observed in extreme precipitation patterns in many parts of the world, while the effect of atmospheric dynamics (atmospheric circulation) has only a minor effect that is limited to lower latitudes. An equivalent study has been carried out more recently by Norris et al. (2019), showing that in mid-latitudes the thermodynamic trend dominates, resulting in a similar increase to the Clausius–Clapeyron rate. At (sub)tropical latitudes, however, the dynamic effect and hence the increase are higher. In overall terms, Tabari et al. (2020) have shown that a good classification of the increase in extreme precipitation events can be given as a function of water availability. Thus, he has shown that in humid areas the increase is similar to the Clausius–Clapeyron rate. For semi-humid regions the increase is significantly lower, not reaching 6% K^{-1}. In the water-limited regions, the increase drops to 5.62 and 5.45% K^{-1} for semi-arid and arid regions, respectively.

In recent decades, a great deal of progress has been made in understanding the response of extreme precipitation to global warming. However, it is necessary to consider the relationship between thermodynamic effects at the local scale, and the dynamic contribution. Without this deeper understanding, the dominant processes related to potential changes in extreme rainfall patterns will not be properly understood.

5 | TRENDS IN OBSERVED AND MODELED PRECIPITATION EXTREMES

Increases in both the frequency and intensity of extreme precipitation have been identified in observations (Ali & Mishra, 2018; Donat et al., 2019; Easterling et al., 2017; Ghosh et al., 2012; Hegerl et al., 2015; Lochbihler et al., 2017; Min et al., 2011; Solomon et al., 2007) and climate model simulations (Donat, Alexander, et al., 2016; Donat, Lowry, et al. (2016); Fischer & Knutti, 2016; Kendon et al., 2018; Kharin et al., 2013; Pendergrass & Hartmann, 2014; Scoccimarro et al., 2013; Toreti et al., 2013; Wang et al., 2017; Westra et al., 2014; Zobel et al., 2018). Assessment of the trends has been undertaken for different periods and regions using different datasets, which makes it difficult to establish clear comparisons and conclusions. Nevertheless, in this section, our aim is to summarize the latest findings in order to provide some worldwide essential conclusions.

On a global scale, observations of annual maximum daily precipitation have shown an increase of an average of 5.73 mm over 110 years (1901–2010), which corresponds to an increase of 10% K^{-1} in global warming since 1901 (Asadieh & Krakauer, 2015). For a shorter period (1979–2010), Chou et al. (2013) revealed that global mean precipitation tends to increase during the rainy season and decrease during the dry season. However, when the period of analysis was extended to include previous years (1950–2009), no change was found in the total rainy-season precipitation, while the total dry-season precipitation showed an increase (Murray-Tortarolo et al., 2017). Papalexiou and Montanari (2019) used high-quality daily precipitation records from all over the globe to identify and compare changes in the frequency and magnitude of daily extremes over the period 1964–2013. They found that large parts of Eurasia (Europe, western Russia, most of China), North Australia, and the mid-western United States of America showed positive trends in frequency, whereas regions with positive trends in magnitude were in Asia (Vietnam, Cambodia, and Thailand), Central Russia (North of Mongolia), and western Europe (from Portugal to northern Norway). For a longer period (1901–2010), Donat et al. (2013) found that most of the precipitation indices showed (partly significant) changes towards more intense precipitation over the eastern half of North America as well as over large parts of eastern Europe, Asia, and South America. Areas with trends showing less frequent and intense precipitation were observed around the Mediterranean, in Southeast Asia, and in the northwestern part of North America. These changes in extreme precipitation were found for the number of heavy precipitation days (R10mm) and for the contribution from very wet days (R95PTOT). Similar patterns of change were also found for the average intensity, frequency, and duration of extreme precipitation. In a separate study, Donat et al. (2016) analyzed long-term changes and interannual variability of precipitation extremes using the global land-based gridded fields of the ETCCDI indices (e.g., R10mm) for the entire 20th century, finding global tendencies of more intense rainfall during most of the period, with a major agreement between datasets after 1950. Analysis of annual daily maxima and precipitation on very wet days (defined as days with annual total precipitation >95th percentile) show positive changes in South America, Asia, and Africa (e.g., Donat et al., 2016). The assessment of Carvalho (2019), which used instrumental records and a review of previous findings, revealed evidence of upward trends in extreme precipitation (amount, intensity, and frequency) in many parts of the world, but these were particularly evident over the mid-latitudes of North America and the subtropics of South America.

In order to provide a global historical overview of extreme precipitation trends over the continents, indices of gridded land-based temperature and precipitation extremes were established in HadEX3 gridded land surface extreme indices (Dunn et al., 2020). This database offers 12 precipitation indices derived from daily, in situ observations at 17,000 stations across the world, with the results being recommended by the World Meteorological Organization (WMO) ETCCDI. This database extends from 1901 to 2018; however, here we discuss the indices R95PTOT, R99PTOT, CED, and PRCTOT for the period 1970–2018, considering the period 1961–1990 as a reference. Trend maps are shown in Figure 1. As illustrated, positive statistically significant trends ($p < 0.10$) of PRCTOT are observed in North America, Central America, Central Amazonia, and the La Plata region in South America, West Africa, northern Europe, parts of the Middle East, and Southeast Asia, northeast Russia, and the western half of Australia. Negative trends are less common, but are generally seen to cover part of Greenland, northeast Brazil, Peru, southern South America, the Southwest part of West Africa, the eastern half of the Iberian Peninsula, the northern part of the Indian Peninsula, part of Southeast Asia, and parts of Oceania and Papua New Guinea. The pattern of trends for consecutive wet days (CWD) is very similar to that described above, although in this case, negative trends seem to be more widespread. Trends in extreme values according to R95PTOT and R99PTOT show clear increases over major parts of North and South America, West Africa, Europe, and South East Asia. In contrast, regions with negative anomalies cover smaller regions in northeast Brazil, and some parts of Canada, Russia, Asia, and central Australia.

According to Pendergrass et al. (2017), the variability of precipitation in most climate models increases over a majority of global land areas in response to warming (66% of land shows a clear increase in the variability of seasonal mean precipitation). Furthermore, global and regional climate simulations driven by future scenarios of increasing CO_2 concentrations agree on the increase of precipitation intensity and extremes for continued warming in the future (Ali & Mishra, 2018; Hegerl et al., 2004; Kharin et al., 2007, 2013; Min et al., 2011; Wang et al., 2017; Wentz et al., 2007; Zobel et al., 2018), which could almost double for each degree of further global warming (Myhre et al., 2019). Regional climate models from the Coupled Model Intercomparison Project phase 5 (CMIP5) and the Coordinated Regional

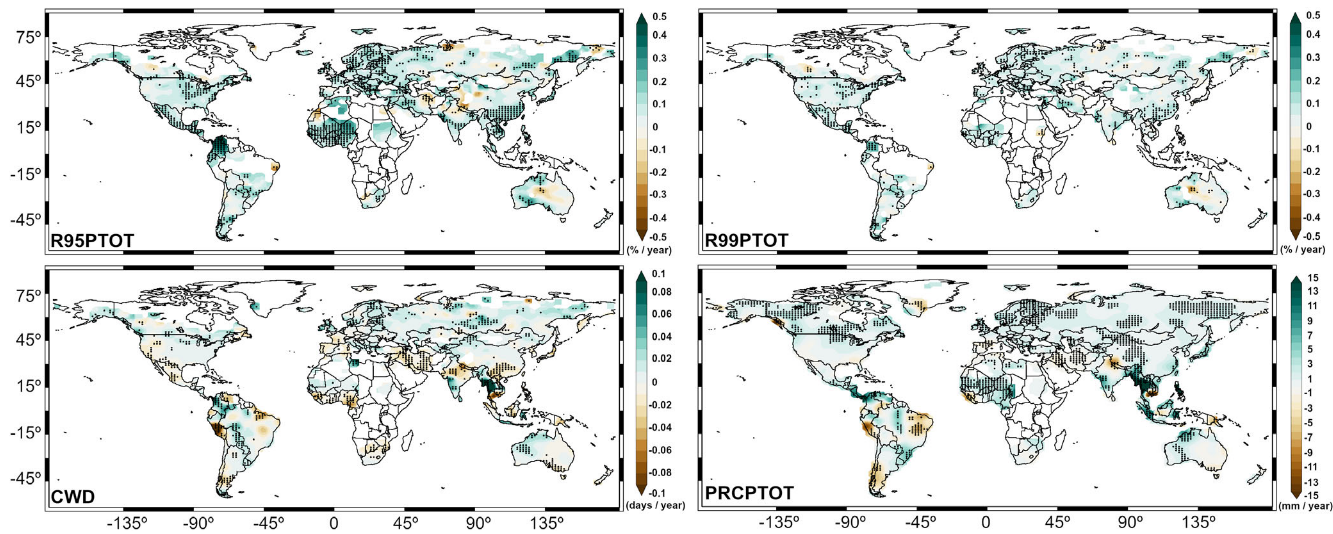

FIGURE 1 Linear trends in total daily precipitation exceeding the 95% (R95PTOT) and 99% (R99PTOT) percentile thresholds (top), and consecutive wet days (CWD) and total precipitation (PRCTOT) (bottom) for the period 1970–2018. Black dots represent statistically significant trends. Data from HadEX3: Peaks-Over-Threshold (Dunn et al., 2020)

Downscaling Experiment for 2071–2100 under the future emission scenario (Representative Concentration Pathways 8.5 W/m^2, RCP8.5) reveal that extreme precipitation could change substantially later in the year in most regions from summer toward autumn and winter (Marelle et al., 2018). However, this shift is not regionally homogeneous, and for the regions analyzed, it is strongest in northern Europe and northeastern North America (+12 and + 17 days, respectively), though local changes of more than a month are also likely. Despite the consensus, several differences exist regarding the spatial extent and intensity of increases or decreases in extreme daily precipitation, which depend also on the models and scenarios, but also on the statistical methods used. The uncertainty is significantly higher in dry regions than in wet regions (Kim et al., 2020).

According to Donat et al. (2016), despite uncertainties in the changes in total precipitation, extreme daily precipitation averaged over both dry and wet regimes shows robust increases in climate model projections for the rest of the 21st century. In addition, extreme precipitation according to r1X values under RCP8.5 are expected to increase over most continents by the last 30 years of the century, while decreasing in the subtropics, particularly the eastern ocean basins, extending to adjacent land areas, but representing just 1.5% of the total area (Pendergrass et al., 2017); the probability of flooding events would thus be increased in general terms (Fischer & Knutti, 2015; Fowler et al., 2021; IPCC, 2013; Kirchmeier-Young & Zhang, 2020; Mukherjee et al., 2018; Pall et al., 2011; Tabari et al., 2020). The general agreement regarding the increase in extreme precipitation this century is consistent with the Clausius–Clapeyron equation. An analysis based on precipitation for the CMIP5 outputs for the period 2006–2100 and considering the RCP8.5 scenarios as performed by Pfahl et al. (2017) revealed that thermodynamics alone would lead to a spatially homogeneous fractional increase, with different regional responses showing amplified increases in the Asian monsoon region, but weaker responses across the Mediterranean, South Africa, and Australia. In addition, over subtropical oceans, an appreciable regional decrease is predicted in extreme precipitation, which may partly result from a poleward shift in circulation (Hu et al., 2013; Nazarenko et al., 2015). Regional studies based on future simulations are thus crucial for identifying differences and making accurate comparisons to allow consideration of regional and local adaptation measures. Supporting Information includes a detailed description of the changes observed in Africa, the Americas, Europe, Asia, and Australia separately.

6 | ATMOSPHERIC MOISTURE TRANSPORT AND EXTREME PRECIPITATION

6.1 | Major moisture sources and extreme precipitation

The global transport of moisture is an important factor in the occurrence of extreme precipitation. Despite the generally local scales considered, the sources of moisture are diverse, and at the global scale, some regions are expected to contribute more to precipitation and hence to affect extreme precipitation events. Gimeno et al. (2010) defined the main global oceanic and terrestrial sources of continental precipitation as regions with higher values of divergence of vertical integrated moisture flux. By taking this into account, a total of 14 sources can be considered, shown in Figure 2 in annual terms. Most of the sources (11) are oceanic, and include some parts of the main Oceans (Atlantic, Pacific, or Indian Ocean) but also some enclosed Seas (Mediterranean or Red Sea). In addition to the oceanic regions, some continental sources are considered, such as Amazonia, the Sahel, or parts of southern Africa. Continental sources are especially relevant during the hemispheric winter. Update and revision of the effect of this moisture source on climatological and extreme precipitation over the continental areas in the peak precipitation month were undertaken by Nieto et al. (2019) and Vázquez et al. (2020), respectively. According to these authors, the contribution of these sources to continental precipitation shows contrasting behavior for mean precipitation compared with extreme events. Despite good agreement in terms of the primary source affecting most of the climatological and extreme precipitation over the continental areas, some differences in the extent of the influence may be observed. For extreme precipitation events (those with precipitation above the 95th percentile from monthly precipitation), transport from western oceanic areas seems to be favored. For example, the North and South Pacific increase their influence over eastern North and South America, respectively. The same phenomenon can also be seen in the Mediterranean and North Atlantic sources in Europe. Despite the increased area of contribution for some of the main global moisture sources, the results presented by Vázquez et al. (2020) suggest than for extreme precipitation events, the influence of local or other sources

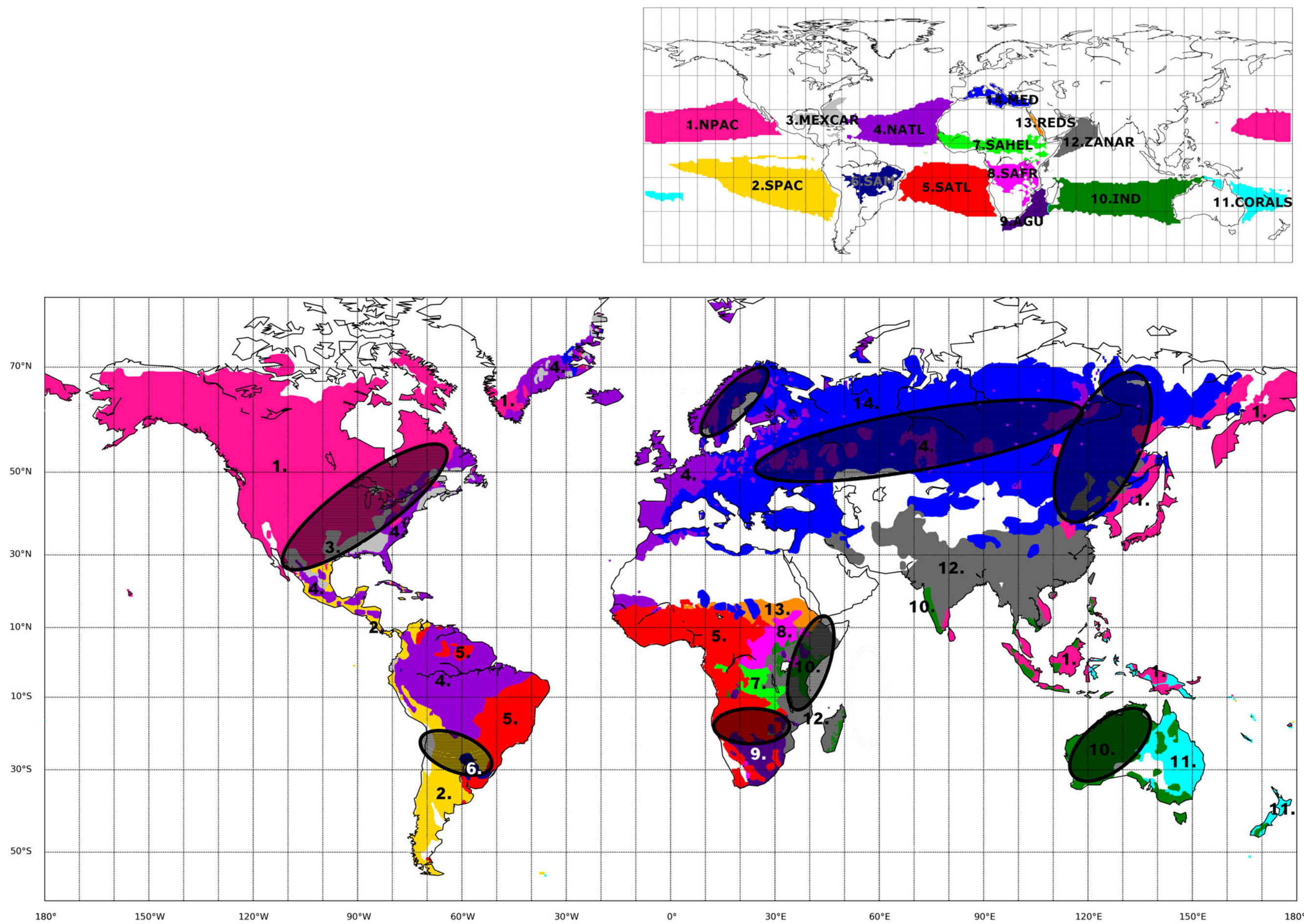

FIGURE 2 Main oceanic and terrestrial moisture sources and their area of higher moisture contribution associated with extreme precipitation events. The rounded areas represent the regions where the source of higher contribution changed compared with climatological mean precipitation. The sources defined are North and South Atlantic Ocean (NATL and SATL), North and South Pacific Ocean (NPAC and SPAC), Mediterranean and Red Seas (MED and REDS), Gulf of Mexico and Caribbean Sea (MEXCAR), Indian Ocean and Zanzibar Current and Arabian Sea (IND and ZANAR), Agulhas Current (AGU), South America (SAM), Sahel Region (SAHEL), and South Africa (SAFR).

different from the global climatological ones could be critical in the occurrence of precipitation. This is somewhat at odds with the decrease in precipitation as explained by the main global sources in extreme precipitation events compared with the climatological precipitation, the reduction being greater than 10% over most continental areas.

Considering the findings of Vázquez et al. (2020), individual analysis of extreme precipitation events over the different areas of the world would seem crucial in order to understand the local processes that occur. As an illustration, the Mediterranean and Atlantic moisture sources experience a redistribution of their influence over western Europe when extreme events occur. Vázquez et al. (2020) found penetration of moisture from the North Atlantic further east over the continent during extreme precipitation events in winter. This is in contrast to the stronger influence of this ocean during the western Mediterranean floods of 1982 as found by Insua-Costa et al. (2019) in comparison with the western Mediterranean (which shows a stronger influence over this area from a climatological point of view).

In this context, perhaps the most important challenge of the next few decades is to explore the specific characteristics of moisture transport associated with extreme precipitation and to understand more fully the mechanisms involved, especially in view of the importance of these events for the populations affected by them.

6.2 | Major mechanisms of moisture transport and extreme precipitation events

Different mechanisms are responsible from the moisture transport that produce extreme precipitation. Tropical and extratropical cyclones are linked to the occurrence of extreme precipitation events over several regions. For example, between 35% and 50% of the extreme 24 h precipitation over eastern North America, eastern Asia, or Japan is associated with tropical cyclones (Utsumi et al., 2017). Another mechanism of moisture transport causing extreme precipitation events is linked to the monsoonal circulations. This mechanism has important consequences over the regions that affects, and it is expected to be increased under global warming conditions (e.g., Lee et al., 2018; Zhang & Zhou, 2019). At local scale, land-atmospheric feedbacks are also critical in the occurrence of extreme precipitation. The convection associated with land-atmospheric feedbacks can highly influence the occurrence of extreme events (Diro et al., 2014; Guo et al., 2006; Lorenz et al., 2016). For example, at local scale, impacts of soil moisture on rainfall are relevant, especially in the transition zones between dry and wet areas (Guo et al., 2006).

Despite the variety of the mechanism involved in the occurrence of extreme precipitation, two of them are considered as the most important in terms of moisture transport, namely, Atmospheric Rivers (ARs) and Low-Level Jets (LLJs). In quantitative terms, the global transport of moisture is dominated mainly by these two meteorological phenomena (Gimeno et al., 2016). ARs are defined as elongated and narrow corridors through which large amounts of moisture are advected to extratropical latitudes mostly from (sub)tropical regions, whereas LLJs are wind corridors in which the maximum speed is found within the first km nearest the ground. LLJs are located mainly in tropical latitudes and are more localized than ARs in terms of their behavior than ARs. The two mechanisms are responsible for a significant portion of the meridional transport of moisture in the atmosphere, modulating regional and global patterns of precipitation on the continents. They thus play an important role in the availability of water resources, as well as in the maintenance of the current characteristics of the hydrological cycle. In fact, it is estimated that the transport of moisture from ARs alone represents more than 90% of the transport of the total flow of water vapor towards the poles at extratropical latitudes (Zhu & Newell, 1998).

LLJs cause maximum wind speeds in the lower troposphere, which is precisely where the maximum concentrations of water vapor are found. This explains why together with ARs LLJs are considered key drivers in the transport of vast amounts of water. These meteorological structures are well known to lead to precipitation events that could become "extreme" depending on the amount of water transported and their persistence. The link between LLJs and anomalous rainfall is documented in different regions such as the Great Plains (e.g., Harding & Snyder, 2015), South America (e.g., Vera et al., 2006), India (Viswanadhapalli et al., 2020), Africa (Vizy & Cook, 2019), or China (Du & Chen, 2019).

One of the best-documented LLJs on the Planet is the Great Plains Low-Level Jet (GPLLJ), which is responsible for the strong advection of moisture from the Gulf of Mexico and the Caribbean Sea to the eastern central United States (Algarra et al., 2019). It is estimated that one-third of the moisture that reaches landfall on the United States is carried by the GPLLJ (Helfand & Schubert, 1995; Higgins et al., 1997). Although the GPLLJ occurs throughout the year, it is more frequent and intense in the summer months and especially at night (Whiteman et al., 1997). Thus, any intensification of the GPLLJ is expected to be linked to increased precipitation in the western central United States. In fact, strong recurrent floods in this region are known to be linked with higher moisture transport as a consequence of the intensification of the GPLLJ (Barandiaran et al., 2013; Moore et al., 2012).

The South American LLJ (SALLJ) plays a major role in the distribution of rainfall in the South American continent. In general, the SALLJ penetrates the eastern margin of the South American continent, crossing the Amazon and diverting southwards through the Andes, transporting large amounts of moisture into the La Plata basin. Intensifications of the SALLJ have been linked to rainfall in this region (do Nascimento et al., 2016). Other relevant LLJs, although of secondary importance on the South American continent, are the Caribbean and Choco LLJs. The convergence of the two structures over western Colombia is well known in this region to contribute to the explanation of world-record rainfall (Poveda et al., 2014).

Monaghan et al. (2010) show a significant connection between the activity of NigthLLJs and nocturnal precipitation extremes in at least 10 regions of the world, including the Great Plains of the United States, Tibet, Northwest China, India, Southeast Asia, southeastern China, Argentina, Namibia, Botswana, and Ethiopia. Therefore, from the perspective of regional precipitation, LLJs are a focus of attention as a consequence of their importance for net moisture advection, and consequently for precipitation. Algarra (2019) identified the source and sink regions of moisture associated with LLJs on a global scale, showing enhanced evaporation in source regions when LLJs occur. Associated with global warming at a regional scale, enhanced peaks of rainfall and increased frequencies of GPLLJs are projected due to, among other factors, strengthening and westward displacements of the Atlantic subtropical anticyclone (Cook et al., 2008; Tang et al., 2017).

ARs are transient filamentary structures associated with enhanced transport of moisture from tropical and subtropical regions to extratropical latitudes. They feed warm conveyor belts, ahead of the cold front of extratropical cyclones, through enhanced water vapor transport in the lower troposphere (Ralph et al., 2018). The impact of ARs as precursors to extreme precipitation events and major floods is widely documented such as for the west coast of the United States (e.g., Dettinger, 2013; Dettinger et al., 2011), Europe (e.g., Eiras-Barca et al., 2021; Lavers & Villarini, 2013), and Chile (e.g., Viale et al., 2018). These meteorological structures are identified as the primary triggers of extreme precipitation events in these regions during the winter months. For example, it is estimated that ARs contribute quantitatively up to 50% of the annual precipitation seen in California (Ralph et al., 2018; Ralph & Dettinger, 2011; Rutz et al., 2014). Lavers and Villarini (2015) showed that ARs account for between 20% and 30% of the total precipitation in parts of Europe and the United States. A graphical summary of these results is displayed in Figure 3.

More recent studies have shown the positive effects of ARs on the hydroclimatology of these regions. This is in part due to their role in ending droughts (Dettinger, 2013), and also because it has been shown that in their milder versions they convey large amounts of nonextreme precipitation, which is necessary for the maintenance of the normal hydrological cycle (Eiras-Barca et al., 2021; Ralph et al., 2019).

The "force"—and therefore the risk of damage—of ARs will increase with the amount of water vapor carried by them, and with the increasing persistence of AR events (Ralph et al., 2019). Notwithstanding the plethora of mechanisms that lead to extreme precipitation through ARs, it is clear that orographic forcing is the main triggering factor for AR-related precipitation (e.g., Ralph et al., 2006; Smith et al., 2010).

Recent studies point to the more significant role of ARs in future climates (e.g., Espinoza et al., 2018; Payne et al., 2020). Considering the Clausius–Clapeyron scale, global warming is likely to bring about a wetter atmosphere and therefore a greater availability of water vapor in near-saturation transport events, inducing a greater advection of moisture by ARs. Algarra et al. (2020) report an increase in moisture content close to 7% for the period 1980–2017 in the sources of anomalous moisture uptake for ARs. Thus, in the context of global warming, any intensification of ARs due to the increased moisture contained in the structure means that the importance of ARs and thus the attention focused on them will increase, due to both their role in the maintenance of the hydrological cycle and to their socioeconomic impact.

6.3 | Future challenges

The proper understanding of weather and climate extremes is considered to be among the great challenges facing world climate research programmers. We now summarize the most pressing topics for future research.

Challenge 1: In recent decades, substantial progress has been made in the study of how global warming may affect extreme precipitation events. Despite this, there is still scope for improving the contextualization of the thermodynamic effect within the dynamic circulation, particularly at a local scale. Precipitation patterns will result from the interaction of the two mechanisms, which could help to explain the changes that take place.

Challenge 2: There is still substantial uncertainty inherent in the modeling of tropical extremes, which is related mostly to convection mechanisms. Some studies have estimated that the rate of increase of extreme tropical rainfall is

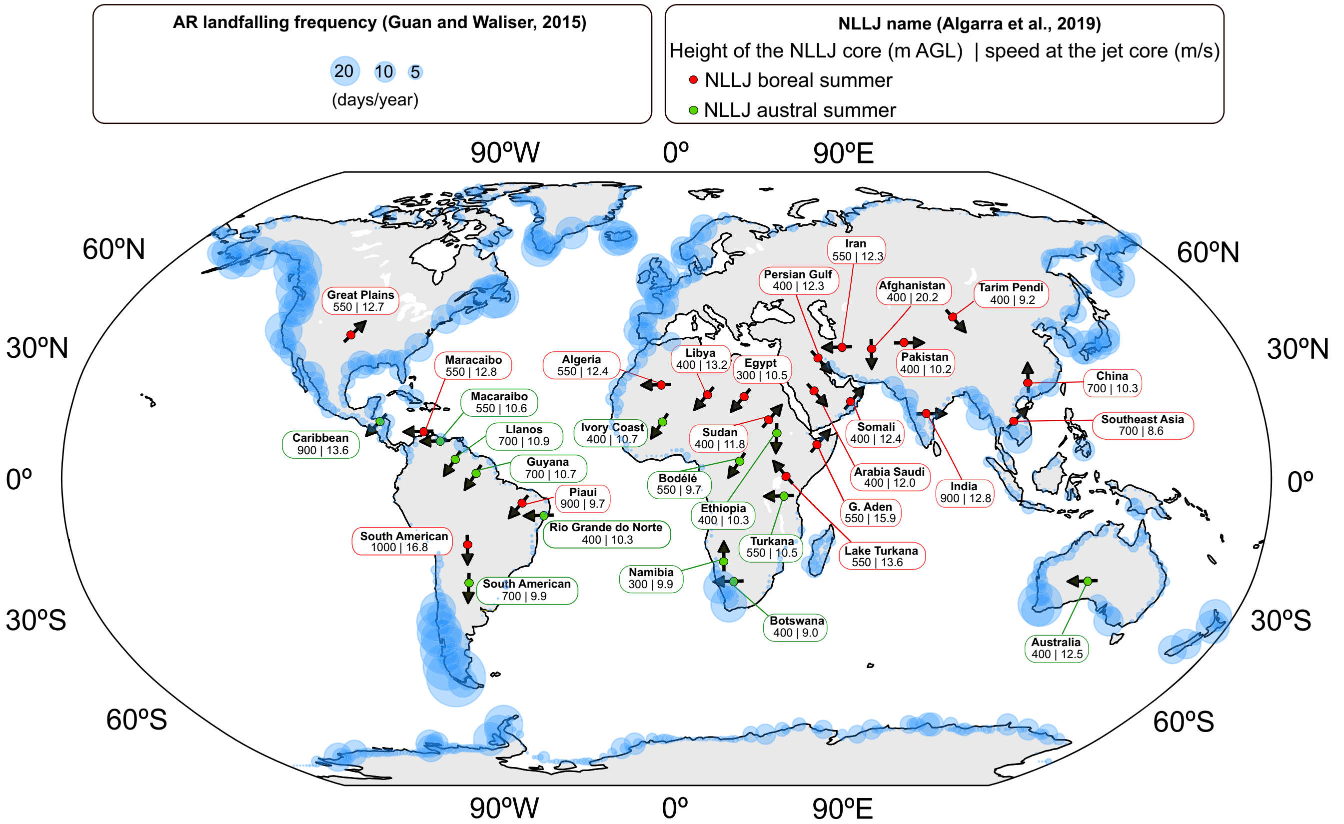

FIGURE 3 Location of the main moisture transport mechanisms at a global scale. The sizes of the blue circles reflect the landfall frequency of ARs (data from Guan & Waliser, 2015). The arrows indicate the direction of the Night LLJs (NLLJs) identified in Algarra (2019). The name of each NLLJ, height (in mgl) and speed (in mm/s) appears inside the colored boxes: Boreal summer NLLJs are in red and austral summer NLLJs are in green

increasing by around 10% per Kelvin (O'Gorman, 2012). Attempts to establish a clearer mechanistic understanding should therefore be a key focus for climate scientists.

Challenge 3: The estimated increase in the amount of expected atmospheric moisture content also suggests some kind of increase in precipitation. Moisture transport mechanisms will certainly play a major role in these potential changes in precipitation patterns. In particular, ARs and LLJs seem to have great potential in modulating these changes, as well as in the future availability of water resources. Despite significant improvements in the understanding of these mechanisms, substantial research is still required to improve the prediction of the behavior of the ARs and LLJs in the medium term. Understanding the changing characteristics essential to design mitigation and adaptation policies.

Challenge 4: The prediction of short- and long-term variability in time and space of extreme precipitation is a challenge of great interest in climate modeling and for studies of risk, both under current conditions and under projected continuous global warming. Models still simulate varying magnitudes of precipitation response to anthropogenic forcing, mostly due to the use of different schemes to parameterize at the subgrid scale. Not all parameterizations are appropriate in different contexts, and a consensus is needed to unify criteria and choose the most appropriate schemes.

Challenge 5: A better understanding and representation of the physical processes behind the convective mechanisms is needed, such as via the assimilation of water vapor flux data in model simulations, and enhanced resolutions and/or larger domain sizes are crucial to improve the simulation of extreme precipitation and its impacts (Guichard & Couvreux, 2017; Muller & Takayabu, 2020).

Challenge 6: A consensus, at least at regional scale, is required to achieve the best definition of the term "extreme" in order to establish the most accurate analysis of precipitation in this respect. There is a need to explore the different definitions of extremes and to establish the best procedures to use. This will allow more precise analysis and promote easier comparison between methods, as well as allowing an understanding of what is implied by the better characterization of these kinds of events.

Challenge 7: It is important to identify whether extreme events occur concurrently with other events (compound events), or whether intensification may be preceded by some additional factor that could help in their prediction (Zscheischler et al., 2018). A better understanding of compound events could improve the prediction of potentially high impact events.

Challenge 8: Given that a warmer environment could exacerbate extreme precipitation events, there is a clear need to improve robust techniques for the attribution of these changes to anthropogenic forcing, especially when they differ by region (Stott et al., 2016), and to minimize the uncertainties, with the aim of devising better predictive products to help society and decision-makers in the management of the risks associated with reducing vulnerability to extreme hydroclimatic events.

AUTHOR CONTRIBUTIONS

Luis Gimeno: Conceptualization (lead); funding acquisition (lead); supervision (equal); writing – original draft (equal); writing – review and editing (equal). **Rogert Sorí:** Methodology (equal); visualization (equal); writing – original draft (equal); writing – review and editing (equal). **Marta Vázquez:** Methodology (equal); visualization (equal); writing – original draft (equal); writing – review and editing (equal). **Milica Stojanovic:** Methodology (equal); visualization (equal); writing – original draft (equal); writing – review and editing (equal). **Iago Algarra:** Methodology (equal); visualization (equal); writing – original draft (equal). **Jorge Eiras-Barca:** Methodology (equal); visualization (equal); writing – original draft (equal); writing – review and editing (equal). **Luis Gimeno-Sotelo:** Methodology (equal); visualization (equal); writing – original draft (equal); writing – review and editing (equal). **Raquel Nieto:** Funding acquisition (lead); methodology (lead); supervision (equal); writing – original draft (equal); writing – review and editing (equal).

ACKNOWLEDGMENTS

Rogert Sorí, Marta Vázquez, and Milica Stojanovic were supported by the Xunta of Galicia under grants ED481B/2019/070, ED481B/2021/134, and ED481D/2022/020 respectively. Luis Gimeno-Sotelo was supported by a UVIGO PhD grant. Jorge Eiras-Barca thanks the Defense University Center at the Spanish Naval (CUD-ENM) for all the support provided for this research.

FUNDING INFORMATION

This work is part of the LAGRIMA project (grant no. RTI2018-095772-B-I00) funded by the Ministerio de Ciencia, Innovación y Universidades, Spain. The EPhysLab group was cofunded by Xunta de Galicia, Consellería de Cultura, Educación e Universidade, under project ED431C 2021/44 "Programa de Consolidación e Estructuración de Unidades de Investigación Competitivas."

CONFLICT OF INTEREST

The authors have declared no conflicts of interest for this article.

DATA AVAILABILITY STATEMENT

Data sharing is not applicable to this article as no new data were created or analyzed in this study.

ORCID

Luis Gimeno https://orcid.org/0000-0002-0778-3605
Rogert Sorí https://orcid.org/0000-0001-6699-4595
Marta Vázquez https://orcid.org/0000-0003-0505-1918
Milica Stojanovic https://orcid.org/0000-0002-6783-9025
Iago Algarra https://orcid.org/0000-0001-6916-7739
Jorge Eiras-Barca https://orcid.org/0000-0003-4401-5944
Luis Gimeno-Sotelo https://orcid.org/0000-0001-9305-2325
Raquel Nieto https://orcid.org/0000-0002-8984-0959

RELATED WIREs ARTICLES

Global atmospheric moisture transport associated with precipitation extremes: Mechanisms and climate change impacts

Atmospheric river, a term encompassing different meteorological patterns

FURTHER READING

Akinsanola, A. A., Kooperman, G. J., Reed, K. A., Pendergrass, A. G., & Hannah, W. M. (2020). Projected changes in seasonal precipitation extremes over the United States in CMIP6 simulations. *Environmental Research Letters*, *15*(10), 104078. https://doi.org/10.1088/1748-9326/abb397

Anderson, T. G., Anchukaitis, K. J., Pons, D., & Taylor, M. (2019). Multiscale trends and precipitation extremes in the central American midsummer drought. *Environmental Research Letters*, *14*(12), 124016. https://doi.org/10.1088/1748-9326/ab5023

Da Silva, P. E., Silva, C. M. S., Spyrides, M. H. C., & Andrade, L. M. B. (2019). Análise de Índices de Extremos Climáticos no Nordeste e Amazônia Brasileira para o Período entre 1980 a 2013. *Anuário do Instituto de Geociências - UFRJ*, *42*(2), 137–148. https://doi.org/10.11137/2019_2_137_148

de Souza, V. A. S., Medeiros Moreira, D., Rotunno Filho, O. C., & Rudke, A. P. (2020). Extreme rainfall events in Amazonia: The Madeira river basin. *Remote Sensing Applications: Society and Environment*, *18*, 100316. https://doi.org/10.1016/j.rsase.2020.100316

Dookie, N., Chadee, X. T., & Clarke, R. M. (2019). Trends in extreme temperature and precipitation indices for the Caribbean small islands: Trinidad and Tobago. *Theoretical and Applied Climatology*, *136*, 31–44. https://doi.org/10.1007/s00704-018-2463-z

Gallant, A. J., Karoly, D. J., & Gleason, K. L. (2014). Consistent trends in a modified climate extremes index in the United States, Europe, and Australia. *Journal of Climate*, *27*(4), 1379–1394. https://doi.org/10.1175/JCLI-D-12-00783.1

García-Ruiz, J. M., Arnáez, J., White, S., Lorente, A., & Beguería, S. (2000). Uncertainty assessment in the prediction of extreme rainfall events: An example from the central Spanish Pyrenees. *Hydrological Processes*, *14*, 887–898. https://doi.org/10.1002/(sici)1099-1085(20000415)14:5<887::aid-hyp976>3.0.co;2-0

Guerreiro, S. B., Fowler, H. J., Barbero, R., Westra, S., Lenderink, G., Blenkinsop, S., Lewis, E., & Li, X.-F. (2018). Detection of continental-scale intensification of hourly rainfall extremes. *Nature Climate Change*, *8*(9), 803–807. https://doi.org/10.1038/s41558-018-0245-3

Imbach, P., Chou, S. C., Lyra, A., Rodrigues, D., Rodriguez, D., Latinovic, D., Siqueira, G., Silva, A., Garofolo, L., & Georgiou, S. (2018). Future climate change scenarios in Central America at high spatial resolution. *PLoS One*, *13*(4), e0193570. https://doi.org/10.1371/journal.pone.0193570

Krishnamurthy, C. K. B., Lall, U., & Kwon, H.-H. (2009). Changing frequency and intensity of rainfall extremes over India from 1951 to 2003. *Journal of Climate*, *22*, 4737–4746. https://doi.org/10.1175/2009JCLI2896.1

MacKellar, N., New, M., & Jack, C. (2014). Observed and modelled trends in rainfall and temperature for South Africa: 1960–2010. *South African Journal of Science*, *110*(7/8), 1–13. https://doi.org/10.1590/sajs.2014/20130353

Marengo, J. A., Jones, R., Alves, L. M., & Valverde, M. C. (2009). Future change of temperature and precipitation extremes in South America as derived from the PRECIS regional climate modeling system. *International Journal of Climatology*, *29*, 2241–2255. https://doi.org/10.1002/joc.1863

Martel, J., Mailhot, A., & Brissette, F. (2020). Global and regional projected changes in 100-yr subdaily, daily, and multiday precipitation extremes estimated from three large ensembles of climate simulations. *Journal of Climate*, *33*(3), 1089–1103.

McLean, N. M., Stephenson, T. S., Taylor, M. A., & Campbell, J. D. (2015). Characterization of future Caribbean rainfall and temperature extremes across rainfall zones. *Advances in Meteorology*, *18*, 425987. https://doi.org/10.1155/2015/425987

Mohan, S., Clarke, R. M., & Chadee, X. T. (2020). Variations in extreme temperature and precipitation for a Caribbean Island: Barbados (1969–2017). *Theoretical and Applied Climatology*, *140*, 1277–1290. https://doi.org/10.1007/s00704-020-03157-9

Ortiz-Gómez, R., Muro-Hernández, L. J., & Flowers-Cano, R. S. (2020). Assessment of extreme precipitation through climate change indices in Zacatecas, Mexico. *Theoretical and Applied Climatology*, *141*, 1541–1557. https://doi.org/10.1007/s00704-020-03293-2

Ruiz-Alvarez, O., Singh, V. P., Enciso-Medina, J., Ontiveros–Capurata, R. E., & Santos, C. A. C. (2020). Observed trends in daily extreme precipitation indices in Aguascalientes. *Mexico. Meteorological Applications*, *27*(1), e1838. https://doi.org/10.1002/met.1838

Stephenson, T. S., Vincent, L. A., Allen, T., van Meerbeeck, C. J., McLean, N., Peterson, T. C., Taylor, M. A., Aaron-Morrison, A. P., Auguste, T., Bernard, D., Boekhoudt, J. R. I., Blenman, R. C., Braithwaite, G. C., Brown, G., Butler, M., Cumberbatch, C. J. M., Etienne-Leblanc, S., Lake, D. E., Martin, D. E., … Trotman, A. R. (2014). Changes in extreme temperature and precipitation in the Caribbean region, 1961–2010. *International Journal of Climatology*, *34*, 2957–2971. https://doi.org/10.1002/joc.3889

Sy, S., & Quesada, B. (2020). Anthropogenic land cover change impact on climate extremes during the 21st century. *Environmental Research Letters*, *15*, 034002.

REFERENCES

Ackerman, F. (2017). *Worst-case economics: Extreme events in climate and finance*. Anthem Press.

Alexander, L. V., & Arblaster, J. M. (2017). Historical and projected trends in temperature and precipitation extremes in Australia in observations and CMIP5. *Weather and Climate Extremes*, *15*, 34–56. https://doi.org/10.1016/j.wace.2017.02.001

Alexander, L. V., Zhang, X., Peterson, T. C., Caesar, J., Gleason, B., Klein Tank, A. M. G., Haylock, M., Collins, D., Trewin, B., Rahimzadeh, F., Tagipour, A., Rupa Kumar, K., Revadekar, J., Griffiths, G., Vincent, L., Stephenson, D. B., Burn, J., Aguilar, E., Brunet, M., … Vazquez-Aguirre, J. L. (2006). Global observed changes in daily climate extremes of temperature and precipitation. *Journal of Geophysical Research-Atmospheres*, *111*(5), D05109. https://doi.org/10.1029/2005JD006290

Algarra, I., Eiras-Barca, J., Miguez-Macho, G., Nieto, R., & Gimeno, L. (2019). On the assessment of the moisture transport by the Great Plains low-level jet. *Earth System Dynamics*, *10*(1), 107–119. https://doi.org/10.5194/esd-10-107-2019

Algarra, I., Eiras-Barca, J., Nieto, R., & Gimeno, L. (2019). Global climatology of nocturnal low-level jets and associated moisture sources and sinks. *Atmospheric Research*, *229*, 39–59. https://doi.org/10.1016/j.atmosres.2019.06.016

Algarra, I., Nieto, R., Ramos, A. M., Eiras-Barca, J., Trigo, R. M., & Gimeno, L. (2020). Significant increase of global anomalous moisture uptake feeding landfalling atmospheric Rivers. *Nature Communications*, *11*(1), 1–7. https://doi.org/10.1038/s41467-020-18876-w

Ali, H., & Mishra, V. (2018). Contributions of dynamic and thermodynamic scaling in subdaily precipitation extremes in India. *Geophysical Research Letters*, *45*, 2352–2361. https://doi.org/10.1002/2018GL077065

Alimonti, G., Mariani, L., Prodi, F., & Ricci, R. A. (2022). A critical assessment of extreme events trends in times of global warming. *European Physical Journal - Plus*, *137*, 112. https://doi.org/10.1140/epjp/s13360-021-02243-9

Allen, M. R., & Ingram, W. J. (2002). Constraints on future changes in climate and the hydrologic cycle. *Nature*, *419*, 228–232. https://doi.org/10.1038/nature01092

Anagnostopoulou, C., & Tolika, K. (2012). Extreme precipitation in Europe: Statistical threshold selection based on climatological criteria. *Theoretical and Applied Climatology*, *107*(3–4), 479–489. https://doi.org/10.1007/s00704-011-0487-8

Asadieh, B., & Krakauer, N. Y. (2015). Global trends in extreme precipitation: Climate models versus observations. *Hydrology and Earth System Sciences*, *19*, 877–891. https://doi.org/10.5194/hess-19-877-2015

Balkema, A., & de Haan, L. (1974). Residual life time at great age. *Annals of Probability*, *2*, 792–804.

Barandiaran, D., Wang, S.-Y., & Hilburn, K. (2013). Observed trends in the Great Plains low-level jet and associated precipitation changes in relation to recent droughts. *Geophysical Research Letters*, *40*(23), 6247–6251. https://doi.org/10.1002/2013GL058296

Beguería, S. (2005). Uncertainties in partial duration series modelling of extremes related to the choice of the threshold value. *Journal of Hydrology*, *303*(1–4), 215–230. https://doi.org/10.1016/j.jhydrol.2004.07.015

Beguería, S., Angulo-Martínez, M., Vicente-Serrano, S. M., López-Moreno, J. I., & el-Kenawy, A. (2011). Assessing trends in extreme precipitation events intensity and magnitude using non-stationary peaks-over-threshold analysis: A case study in Northeast Spain from 1930 to 2006. *International Journal of Climatology*, *31*(14), 2102–2114. https://doi.org/10.1002/joc.2218

Beguería, S., & Vicente-Serrano, S. M. (2006). Mapping the hazard of extreme rainfall by peaks over threshold extreme value analysis and spatial regression techniques. *Journal of Applied Meteorology and Climatology*, *45*(1), 108–124. https://doi.org/10.1175/JAM2324.1

Beguería, S., Vicente-Serrano, S. M., López-Moreno, J. I., & García-Ruiz, J. M. (2009). Annual and seasonal mapping of peak intensity, magnitude and duration of extreme precipitation events across a climatic gradient, Northeast Spain. *International Journal of Climatology: A Journal of the Royal Meteorological Society*, *29*(12), 1759–1779. https://doi.org/10.1002/joc.1808

Bevacqua, E., Maraun, D., Vousdoukas, M. I., Voukouvalas, E., Vrac, M., Mentaschi, L., & Widmann, M. (2019). Higher probability of compound flooding from precipitation and storm surge in Europe under anthropogenic climate change. Science. *Advances*, *5*(9), eaaw5531. https://doi.org/10.1126/sciadv.aaw5531

Brosca, L. H., Poganietz, W. R., & Vögelea, S. (2020). Extreme events defined—A conceptual discussion applying a complex systems approach. *Futures*, *115*, 102490. https://doi.org/10.1016/j.futures.2019.102490

Carvalho, L. M. V. (2019). Assessing precipitation trends in the Americas with historical data: A review. *WIREs Climate Change*, *11*(2), e627. https://doi.org/10.1002/wcc.627

Chou, C., Chiang, J. C. H., Lan, C.-W., Chung, C.-H., Liao, Y.-C., & Lee, C.-J. (2013). Increase in the range between wet and dry season precipitation. *Nature Geoscience*, *6*, 263–267. https://doi.org/10.1038/ngeo1744

Cook, K. H., Vizy, E. K., Launer, Z. S., & Patricola, C. M. (2008). Springtime intensification of the great plains low-level jet and Midwest precipitation in GCM simulations of the twenty-first century. *Journal of Climate*, *21*(23), 6321–6340. https://doi.org/10.1175/2008JCLI2355.1

Cooley, A. K., & Chang, H. (2020). Detecting change in precipitation indices using observed (1977–2016) and modeled future climate data in Portland, Oregon, USA. *Journal of Water and Climate Change*, *12*(4), 1135–1153. https://doi.org/10.2166/wcc.2020.043

Curtis, S., Fair, A., Wistow, J., Val, D. V., & Oven, K. (2017). Impact of extreme weather events and climate change for health and social care systems. *Environmental Health*, *16*, 128. https://doi.org/10.1186/s12940-017-0324-3

Dalagnol, R., Gramcianinov, C. B., Crespo, N. M., Luiz, R., Chiquetto, J. B., Marques, M. T. A., Neto, G. D., de Abreu, R. C., Li, S., Lott, F. C., Anderson, L. O., & Sparrow, S. (2022). Extreme rainfall and its impacts in the Brazilian Minas Gerais state in January 2020: Can we blame climate change? *Climate Resilience and Sustainability*, *1*, e15. https://doi.org/10.1002/cli2.15

Davison, A. C., & Smith, R. L. (1990). Models for exceedances over high thresholds. *Journal of the Royal Statistical Society: Series B*, *52*(3), 393–425.

Dettinger, M. D. (2013). Atmospheric rivers as drought busters on the U.S. west coast. *Journal of Hydrometeorology*, *14*(6), 1721–1732. https://doi.org/10.1175/JHM-D-13-02.1

Dettinger, M. D., Ralph, F. M., Das, T., Neiman, P. J., & Cayan, D. R. (2011). Atmospheric rivers, floods and the water resources of California. *Water (Switzerland)*, *3*(2), 445–478. https://doi.org/10.3390/w3020445

Diro, G. T., Sushama, L., Martynov, A., Jeong, D. I., Verseghy, D., & Winger, K. (2014). Land-atmosphere coupling over North America in CRCM5. *Journal of Geophysical Research – Atmospheres*, *119*, 11,955–11,972. https://doi.org/10.1002/2014JD021677

do Nascimento, M. G., Herdies, D. L., & de Souza, D. O. (2016). The south American water balance: The influence of low-level jets. *Journal of Climate*, *29*(4), 1429–1449. https://doi.org/10.1175/JCLI-D-15-0065.1

Donat, M. G., Alexander, L. V., Herold, N., & Dittus, A. J. (2016). Temperature and precipitation extremes in century-long gridded observations, reanalyses, and atmospheric model simulations. *Journal of Geophysical Research-Atmospheres*, *121*, 11174–11189. https://doi.org/10.1002/2016JD025480

Donat, M. G., Alexander, L. V., Yang, H., Durre, I., Vose, R., Dunn, R. J. H., Willett, K. M., Aguilar, E., Brunet, M., Caesar, J., Hewitson, B., Jack, C., Klein Tank, A. M. G., Kruger, A. C., Marengo, J., Peterson, T. C., Renom, M., Oria Rojas, C., Rusticucci, M., … Kitching, S. (2013). Updated analyses of temperature and precipitation extreme indices since the beginning of the twentieth century: The HadEX2 dataset. *Journal of Geophysical Research-Atmospheres*, *118*, 2098–2118. https://doi.org/10.1002/jgrd.50150

Donat, M. G., Angélil, O., & Ukkola, A. M. (2019). Intensifcation of precipitation extremes in the world's humid and water-limited regions. *Environmental Research Letters*, *14*(6), 065003. https://doi.org/10.1088/1748-9326/ab1c8e

Donat, M. G., Lowry, A. L., Alexander, L. V., O'Gorman, P. A., & Maher, N. (2016). More extreme precipitation in the world's dry and wet regions. *Nature Climate Change*, *6*(5), 508–513. https://doi.org/10.1038/nclimate2941

Du, Y., & Chen, G. (2019). Climatology of low-level jets and their impact on rainfall over southern China during the early-summer rainy season. *Journal of Climate*, *32*(24), 8813–8833. https://doi.org/10.1175/JCLI-D-19-0306.1

Dunn, R. J. H., Alexander, L. V., Donat, M. G., Zhang, X., Bador, M., Herold, N., Lippmann, T., Allan, R., Aguilar, E., Barry, A. A., Brunet, M., Caesar, J., Chagnaud, G., Cheng, V., Cinco, T., Durre, I., Guzman, R., Htay, T. M., Wan Ibadullah, W. M., … Bin Hj Yussof, M. N. A. (2020). Development of an updated global land in situ-based data set of temperature and precipitation extremes: HadEX3. *Journal of Geophysical Research-Atmospheres*, *125*(16), e2019JD032263. https://doi.org/10.1029/2019JD032263

Easterling, D. R., Kunkel, K. E., Arnold, J. R., Knutson, T., LeGrande, A. N., Leung, L. R., Vose, R. S., Waliser, D. E., & Wehner, M. F. (2017). Precipitation change in the United States. In D. J. Wuebbles, D. W. Fahey, K. A. Hibbard, D. J. Dokken, B. C. Stewart, & T. K. Maycock (Eds.), *Climate science special report: Fourth National Climate Assessment* (Vol. I, pp. 207–230). U.S. Global Change Research Program. https://doi.org/10.7930/J0H993CC

Eiras-Barca, J., Ramos, A. M., Algarra, I., Vázquez, M., Dominguez, F., Miguez-Macho, G., Nieto, R., Gimeno, L., Taboada, J., & Ralph, F. M. (2021). European west coast atmospheric Rivers: A scale to characterize strength and impacts. Weather and climate. *Extremes*, *31*, 100305.

Emori, S., & Brown, S. J. (2005). Dynamic and thermodynamic changes in mean and extreme precipitation under changed climate. *Geophysical Research Letters*, *32*(17), 1–5. https://doi.org/10.1029/2005GL023272

Emrich, C. T., Alvarez, S., Knox, C. C., Sadiq, A. A., & Zhou, Y. (2019). Hurricane Irma and Cascading impacts. In C. B. Rubin & S. L. Cutter (Eds.), *U.S. emergency management in the 21st century from disaster to catastrophe* (1st ed., p. 290). Routledge. https://doi.org/10.4324/9780429424670

Espinoza, V., Waliser, D. E., Guan, B., Lavers, D. A., & Ralph, F. M. (2018). Global analysis of climate change projection effects on atmospheric Rivers. *Geophysical Research Letters*, *45*(9), 4299–4308. https://doi.org/10.1029/2017GL076968

Fischer, E. M., & Knutti, R. (2015). Anthropogenic contribution to global occurrence of heavy-precipitation and high-temperature extremes. *Nature Climate Change*, *5*, 560–564. https://doi.org/10.1038/nclimate2617

Fischer, E. M., & Knutti, R. (2016). Observed heavy precipitation increase confirms theory and early models. *Nature Climate Change*, *6*, 986–991. https://doi.org/10.1038/nclimate3110

Fowler, H. J., Lenderink, G., Prein, A. F., Westra, S., Allan, R. P., Ban, N., Barbero, R., Berg, P., Blenkinsop, S., do, H. X., Guerreiro, S., Haerter, J. O., Kendon, E. J., Lewis, E., Schaer, C., Sharma, A., Villarini, G., Wasko, C., & Zhang, X. (2021). Anthropogenic intensification of short-duration rainfall extremes. *Nature Reviews Earth & Environment*, *2*, 107–122. https://doi.org/10.1038/s43017-020-00128-6

Ghosh, S., Das, D., Kao, S. C., & Ganguly, A. R. (2012). Lack of uniform trends but increasing spatial variability in observed Indian rainfall extremes. *Nature Climate Change*, *2*, 86–91. https://doi.org/10.1038/nclimate1327

Gimeno, L., Dominguez, F., Nieto, R., Trigo, R., Drumond, A., Reason, C. J. C., Taschetto, A. S., Ramos, A. M., Kumar, R., & Marengo, J. (2016). Major mechanisms of atmospheric moisture transport and their role in extreme precipitation events. *Annual Review of Environment and Resources*, *41*(1), 117–141. https://doi.org/10.1146/annurev-environ-110615-085558

Gimeno, L., Drumond, A., Nieto, R., Trigo, R. M., & Stohl, A. (2010). On the origin of continental precipitation. *Geophysical Research Letters*, *37*, L13804. https://doi.org/10.1029/2010GL043712

Giorgi, F., Raffaele, F., & Coppola, E. (2019). The response of precipitation characteristics to global warming from climate projections. *Earth System Dynamics*, *10*(1), 73–89. https://doi.org/10.5194/esd-10-73-2019

Girgin, S., Necci, A., & Krausmann, E. (2019). Dealing with cascading multi-hazard risks in national risk assessment: The case of Natech accidents Int. *International Journal of Disaster Risk Reduction*, *35*, 101072. https://doi.org/10.1016/j.ijdrr.2019.101072

Gu, G., & Adler, R. F. (2015). Spatial patterns of global precipitation change and variability during 1901–2010. *Journal of Climate*, *28*(11), 4431–4453.

Guan, B., & Waliser, D. E. (2015). Detection of atmospheric rivers: Evaluation and application of an algorithm for global studies. *Journal of Geophysical Research-Atmospheres*, *120*(24), 12514–12535. https://doi.org/10.1002/2015JD024257

Guichard, F., & Couvreux, F. (2017). A short review of numerical cloud-resolving models. *Tellus A*, *69*, 1373578. https://doi.org/10.1080/16000870.2017.1373578

Guo, Z., Dirmeyer, P. A., Koster, R. D., Bonan, G., Chan, E., Cox, P., Gordon, C. T., Kanae, S., Kowalczyk, E., Lawrence, D., Liu, P., Lu, C.-H., Malyshev, S., McAvaney, B., McGregor, J. L., Mitchell, K., Mocko, D., Oki, T., Oleson, K. W., … Yamada, T. (2006). GLACE: The global land–atmosphere coupling experiment. Part II: Analysis. *Journal of Hydrometeorology*, *7*(4), 611–625. https://doi.org/10.1175/JHM511.1

Haddow, G. D., Bullock, J. A., & Coppola, D. P. (2020). Chapter 2—Natural and technological hazards and risk assessment. In G. D. Haddow, J. A. Bullock, & D. P. Coppola (Eds.), *Introduction to emergency management* (7th ed., pp. 33–84). Butterworth-Heinemann. https://doi.org/10.1016/B978-0-12-817139-4.00002-6

Harding, K. J., & Snyder, P. K. (2015). The relationship between the Pacific-north American teleconnection pattern, the great plains low-level jet, and north central U.S. heavy rainfall events. *Journal of Climate*, *28*(17), 6729–6742. https://doi.org/10.1175/JCLI-D-14-00657.1

Hardwick-Jones, R., Westra, S., & Sharma, A. (2010). Observed relationships between extreme sub-daily precipitation, surface temperature, and relative humidity. *Geophysical Research Letters*, *37*(22), L22805. https://doi.org/10.1029/2010GL045081

Hegerl, G. C., Zwiers, F. W., Stott, P. A., & Kharin, V. V. (2004). Detectability of anthropogenic changes in temperature and precipitation extremes. *Journal of Climate*, *17*, 3683–3700. https://doi.org/10.1175/1520-0442(2004)017<3683:DOACIA>2.0.CO;2

Hegerl, G. E., Black, E., Allan, R. P., Ingram, W. J., Polson, D., Trenberth, K. E., Chadwick, R. S., Arkin, P. A., Sarojini, B. B., Becker, A., Dai, A., Durack, P. J., Easterling, D., Fowler, H. J., Kendon, E. J., Huffman, G. J., Liu, C., Marsh, R., New, M., … Zhang, X. (2015). Challenges in quantifying changes in the global water cycle. *Bulletin of the American Meteorological Society*, *96*, 1097–1115. https://doi.org/10.1175/BAMS-D-13-00212.1

Held, I. M., & Soden, B. J. (2006). Robust responses of the hydrological cycle to global warming. *Journal of Climate*, *19*(21), 5686–5699. https://doi.org/10.1175/JCLI3990.1

Helfand, H. M., & Schubert, S. D. (1995). Climatology of the simulated Great Plains low-level jet and its contribution to the continental moisture budget of the United States. *Journal of Climate*, *8*(4), 784–806. https://doi.org/10.1175/1520-0442(1995)008<0784:COTSGP>2.0.CO;2

Herold, N., Behrangi, A., & Alexander, L. V. (2017). Large uncertainties in observed daily precipitation extremes over land. *Journal of Geophysical Research – Atmospheres*, *122*, 668–681. https://doi.org/10.1002/2016JD025842

Higgins, R. W., Yao, Y., Yarosh, E. S., Janowiak, J. E., & Mo, K. C. (1997). Influence of the great plains low-level jet on summertime precipitation and moisture transport over the Central United States. *Journal of Climate*, *10*(3), 481–507. https://doi.org/10.1175/1520-0442(1997)010<0481:IOTGPL>2.0.CO;2

Hu, Y., Tao, L., & Liu, J. (2013). Poleward expansion of the hadley circulation in CMIP5 simulations. *Advances in Atmospheric Sciences*, *30*, 790–795. https://doi.org/10.1007/s00376-012-2187-4

Insua-Costa, D., Miguez-Macho, G., & Llasat, M. C. (2019). Local and remote moisture sources for extreme precipitation: A study of the two catastrophic 1982 western Mediterranean episode. *Hydrology and Earth System Sciences*, *23*, 3885–3900. https://doi.org/10.5194/hess-23-3885-2019

IPCC (2013). Climate change 2013: The physical science basis. In T. F. Stocker, D. Qin, G.-K. Plattner, M. Tignor, S. K. Allen, J. Boschung, A. Nauels, Y. Xia, V. Bex, & P. M. Midgley (Eds.), *Contribution of working group I to the fifth assessment report of the intergovernmental panel on climate change* (p. 1535 pp. Retrieved from). Cambridge University Press. https://www.ipcc.ch/site/assets/uploads/2018/02/WG1AR5_all_final.pdf

IPCC (2021). Summary for policymakers. In V. Masson-Delmotte, P. Zhai, A. Pirani, S. L. Connors, C. Péan, S. Berger, N. Caud, Y. Chen, L. Goldfarb, M. I. Gomis, M. Huang, K. Leitzell, E. Lonnoy, J. B. R. Matthews, T. K. Maycock, T. Waterfield, O. Yelekçi, R. Yu, & B. Zhou (Eds.), *Climate change 2021: The physical science basis. Contribution of working group I to the sixth assessment report of the intergovernmental panel on climate change* (pp. 3–32). Cambridge University Press. https://doi.org/10.1017/9781009157896.001

Jenkinson, A. F. (1955). The frequency distribution of the annual maximum (or minimum) values of meteorological events. *Quarterly Journal of the Royal Meteorological Society*, *81*, 158–172.

Kendon, E. J., Blenkinsop, S., & Fowler, H. J. (2018). When will we detect changes in short-duration precipitation extremes? *Journal of Climate*, *31*, 2945–2964. https://doi.org/10.1175/JCLI-D-17-0435.1

Kharin, V. V., & Zwiers, F. W. (2005). Estimating extremes in transient climate change simulations. *Journal of Climate*, *18*(8), 1156–1173. https://doi.org/10.1175/JCLI3320.1

Kharin, V. V., Zwiers, F. W., Zhang, X., & Hegerl, G. C. (2007). Changes in temperature and precipitation extremes in the IPCC ensemble of global coupled model simulations. *Journal of Climate*, *20*(8), 1419–1444. https://doi.org/10.1175/JCLI4066.1

Kharin, V. V., Zwiers, F. W., Zhang, X., & Wehner, M. (2013). Changes in the temperature and precipitation extremes in the CMIP5 ensemble. *Climatic Change*, *119*, 345–357. https://doi.org/10.1007/s10584-013-0705-8

Kim, S., Eghdamirad, S., Sharma, A., & Kim, J. H. (2020). Quantification of uncertainty in projections of extreme daily precipitation. *Earth and Space Science*, *7*, e2019EA001052. https://doi.org/10.1029/2019EA001052

Kirchmeier-Young, M. C., & Zhang, X. (2020). Human influence has intensified extreme precipitation in North America. *Proceedings of the National Academy of Sciences of the United States of America*, *117*(24), 13308–13313. https://doi.org/10.1073/pnas.1921628117

Lavers, D. A., & Villarini, G. (2013). The nexus between atmospheric rivers and extreme precipitation across Europe. *Geophysical Research Letters*, *40*(12), 3259–3264. https://doi.org/10.1002/grl.50636

Lavers, D. A., & Villarini, G. (2015). The contribution of atmospheric rivers to precipitation in Europe and the United States. *Journal of Hydrology*, *522*, 382–390. https://doi.org/10.1016/j.jhydrol.2014.12.010

Lazoglou, G., Anagnostopoulou, C., Tolika, K., & Kolyva-Machera, F. (2019). A review of statistical methods to analyze extreme precipitation and temperature events in the Mediterranean region. *Theoretical and Applied Climatology*, *136*(1–2), 99–117. https://doi.org/10.1007/s00704-018-2467-8

Lee, D., Min, S.-K., Fischer, E., Shiogama, H., Bethke, I., Lierhammer, L., & Scinocca, J. F. (2018). Impacts of half a degree additional warming on the Asian summer monsoon rainfall characteristics. *Environmental Research Letters*, *13*, 044033. https://doi.org/10.1088/1748-9326/aab55d

Lenderink, G., Mok, H. Y., Lee, T. C., & Van Oldenborgh, G. J. (2011). Scaling and trends of hourly precipitation extremes in two different climate zones - Hong Kong and The Netherlands. *Hydrology and Earth System Sciences*, *15*(9), 3033–3041. https://doi.org/10.5194/hess-15-3033-2011

Lenderink, G., & Van Meijgaard, E. (2008). Increase in hourly precipitation extremes beyond expectations from temperature changes. *Nature Geoscience*, *1*(8), 511–514. https://doi.org/10.1038/ngeo262

Leonard, M., Westra, S., Phatak, A., Lambert, M., van den Hurk, B., McInnes, K., Risbey, J., Schuster, S., Jakob, D., & Stafford-Smith, M. (2014). A compound event framework for understanding extreme impacts. *WIREs Climate Change*, *5*, 113–128. https://doi.org/10.1002/wcc.252

Liang, X.-Z. (2022). Extreme rainfall slows the global economy. *Nature*, *601*, 193–194.

Liu, B., Chen, J., Chen, X., Lian, Y., & Wu, L. (2013). Uncertainty in determining extreme precipitation thresholds. *Journal of Hydrology*, *503*, 233–245. https://doi.org/10.1016/j.jhydrol.2013.09.002

Lochbihler, K., Lenderink, G., & Siebesma, A. P. (2017). The spatial extent of rainfall events and its relation to precipitation scaling. *Geophysical Research Letters*, *44*, 8629–8636. https://doi.org/10.1002/2017GL074857

Lorenz, R., Argüeso, D., Donat, M. G., Pitman, A. J., van den Hurk, B., Berg, A., Lawrence, D. M., Chéruy, F., Ducharne, A., Hagemann, S., Meier, A., Milly, P. C. D., & Seneviratne, S. I. (2016). Influence of land-atmosphere feedbacks on temperature and precipitation extremes in the GLACE-CMIP5 ensemble. *Journal of Geophysical Research – Atmospheres*, *121*, 607–623. https://doi.org/10.1002/2015JD024053

Lugo, A. E. (2018). Characterization of ten extreme disturbance events in the context of social and ecological systems. *Biogeochemistry*, *141*, 385–400. https://doi.org/10.1007/s10533-018-0453-y

Madakumbura, G. D., Thackeray, C. W., Norris, J., Goldenson, N., & Hall, A. (2021). Anthropogenic influence on extreme precipitation over global land areas seen in multiple observational datasets. *Nature Communications*, *12*, 3944. https://doi.org/10.1038/s41467-021-24262-x

Marelle, L., Myhre, G., Hodnebrog, Ø., Sillmann, J., & Samset, B. H. (2018). The changing seasonality of extreme daily precipitation. *Geophysical Research Letters*, *45*(20), 11352–11360. https://doi.org/10.1029/2018GL079567

Mauritsen, T., & Stevens, B. (2015). Missing iris effect as a possible cause of muted hydrological change and high climate sensitivity in models. *Nature Geoscience*, *8*(5), 346–351.

McPhillips, L. E., Chang, H., Chester, M. V., Depietri, Y., Friedman, E., Grimm, N. B., Kominoski, J. S., McPhearson, T., Méndez-Lázaro, P., Rosi, E. J., & Shafiei Shiva, J. (2018). Defining extreme events: A cross-disciplinary review. *Earth's Future*, *6*, 441–455. https://doi.org/10.1002/2017EF000686

Min, S. K., Zhang, X., Zwiers, F. W., & Hegerl, G. C. (2011). Human contribution to more-intense precipitation extremes. *Nature*, *470*, 378–381. https://doi.org/10.1038/nature09763

Monaghan, A. J., Rife, D. L., Pinto, J. O., Davis, C. A., & Hannan, J. R. (2010). Global precipitation extremes associated with diurnally varying low-level jets. *Journal of Climate*, *23*(19), 5065–5084. https://doi.org/10.1175/2010JCLI3515.1

Moore, B. J., Neiman, P. J., Ralph, F. M., & Barthold, F. E. (2012). Physical processes associated with heavy flooding rainfall in Nashville, Tennessee, and vicinity during 1–2 may 2010: The role of an atmospheric river and mesoscale convective systems. *Monthly Weather Review*, *140*(2), 358–378. https://doi.org/10.1175/MWR-D-11-00126.1

Mukherjee, S., Aadhar, S., Stone, D., & Mishra, V. (2018). Increase in extreme precipitation events under anthropogenic warming in India. *Weather and Climate Extremes*, *20*, 45–53. https://doi.org/10.1016/j.wace.2018.03.005

Muller, C., & Takayabu, Y. (2020). Response of precipitation extremes to warming: what have we learned fromtheory and idealized cloud-resolving simulations, and what remains to belearned? *Environmental Research Letters*, *15*, 035001. https://doi.org/10.1088/1748-9326/ab7130

Murray-Tortarolo, G., Jaramillo, V. J., Maass, M., Friedlingstein, P., & Sitch, S. (2017). The decreasing range between dry- and wet- season precipitation over land and its effect on vegetation primary productivity. *PLoS One*, *12*, e0190304. https://doi.org/10.1371/journal.pone.0190304

Myhre, G., Alterskjær, K., Stjern, C. W., Hodnebrog, Ø., Marelle, L., Samset, B. H., Sillmann, J., Schaller, N., Fischer, E., Schulz, M., & Stohl, A. (2019). Frequency of extreme precipitation increases extensively with event rareness under global warming. *Scientific Reports*, *9*(1), 1–10. https://doi.org/10.1038/s41598-019-52277-4

Nazarenko, L., Schmidt, G. A., Miller, R. L., Tausnev, N., Kelley, M., Ruedy, R., Russell, G. L., Aleinov, I., Bauer, M., Bauer, S., Bleck, R., Canuto, V., Cheng, Y., Clune, T. L., del Genio, A. D., Faluvegi, G., Hansen, J. E., Healy, R. J., Kiang, N. Y., … Zhang, J. (2015). Future climate change under RCP emission scenarios with GISS ModelE2. *Journal of Advances in Modeling Earth Systems*, *7*, 244–267. https://doi.org/10.1002/2014MS000403

Nieto, R., Ciric, D., Vázquez, M., Liberato, M. L. R., & Gimeno, L. (2019). Contribution of the main moisture sources to precipitation during extreme peak precipitation months. *Advances in Water Resources*, *131*, 103385. https://doi.org/10.1016/j.advwatres.2019.103385

Norris, J., Chen, G., & Neelin, J. D. (2019). Thermodynamic versus dynamic controls on extreme precipitation in a warming climate from the community earth system model large ensemble. *Journal of Climate*, *32*(4), 1025–1045.

O'Gorman, P. A. (2012). Sensitivity of tropical precipitation extremes to climate change. *Nature Geoscience*, *5*(10), 697–700. https://doi.org/10.1038/ngeo1568

O'Gorman, P. A., Allan, R. P., Byrne, M. P., & Previdi, M. (2012). Energetic constraints on precipitation under climate change. *Surveys in Geophysics*, *33*(3–4), 585–608. https://doi.org/10.1007/s10712-011-9159-6

O'Gorman, P. A., & Muller, C. J. (2010). How closely do changes in surface and column water vapor follow Clausius-Clapeyron scaling in climate change simulations? *Environmental Research Letters*, *5*(2), 025207. https://doi.org/10.1088/1748-9326/5/2/025207

O'Gorman, P. A., & Schneider, T. (2009). The physical basis for increases in precipitation extremes in simulations of 21st-century climate change. *Proceedings of the National Academy of Sciences of the United States of America*, *106*(35), 14773–14777. https://doi.org/10.1073/pnas.0907610106

Pall, P., Aina, T., Stone, D. A., Stott, P. A., Nozawa, T., Hilberts, A. G. J., Lohmann, D., & Allen, M. R. (2011). Anthropogenic greenhouse gas contribution to flood risk in England and Wales in autumn 2000. *Nature*, *470*(7334), 382–385. https://doi.org/10.1038/nature09762

Papalexiou, S. M., & Montanari, A. (2019). Global and regional increase of precipitation extremes under global warming. *Water Resources Research*, *55*, 4901–4914. https://doi.org/10.1029/2018wr024067

Payne, A. E., Demory, M.-E., Leung, L. R., Ramos, A. M., Shields, C. A., Rutz, J. J., Siler, N., Villarini, G., Hall, A., & Ralph, F. M. (2020). Responses and impacts of atmospheric rivers to climate change. *Nature Reviews Earth & Environment*, *1*(3), 143–157. https://doi.org/10.1038/s43017-020-0030-5

Pendergrass, A. G. (2018). What precipitation is extreme? *Science*, *360*(6393), 1072–1073. https://doi.org/10.1126/science.aat1871

Pendergrass, A. G., & Hartmann, D. L. (2014). Changes in the distribution of rain frequency and intensity in response to global warming. *Journal of Climate*, *27*, 8372–8383. https://doi.org/10.1175/JCLI-D-14-00183.1

Pendergrass, A. G., Knutti, R., Lehner, F., Deser, C., & Sanderson, B. M. (2017). Precipitation variability increases in a warmer climate. *Scientific Reports*, *7*(1), 17966. https://doi.org/10.1038/s41598-017-17966-y

Pfahl, S., O'Gorman, P., & Fischer, E. (2017). Understanding the regional pattern of projected future changes in extreme precipitation. *Nature Climate Change*, *7*, 423–427. https://doi.org/10.1038/nclimate3287

Pickands, J. (1975). Statistical inference using extreme order statistics. *Annals of Statistics*, *3*, 119–131.

Poveda, G., Jaramillo, L., & Vallejo, L. F. (2014). Seasonal precipitation patterns along pathways of south American low-level jets and aerial rivers. *Water Resources Research*, *50*(1), 98–118. https://doi.org/10.1002/2013WR014087

Ralph, F. M., Dettinger, M. C. L. D., Cairns, M. M., Galarneau, T. J., & Eylander, J. (2018). Defining "Atmospheric river": How the glossary of meteorology helped resolve a debate. *Bulletin of the American Meteorological Society*, *99*(4), 837–839. https://doi.org/10.1175/BAMS-D-17-0157.1

Ralph, F. M., & Dettinger, M. D. (2011). Storms, floods, and the science of atmospheric rivers. *Eos*, *92*(32), 265–266. https://doi.org/10.1029/2011EO320001

Ralph, F. M., Neiman, P. J., Wick, G. A., Gutman, S. I., Dettinger, M. D., Cayan, D. R., & White, A. B. (2006). Flooding on California's Russian River: Role of atmospheric rivers. *Geophysical Research Letters*, *33*(13), L13801. https://doi.org/10.1029/2006GL026689

Ralph, F. M., Rutz, J. J., Cordeira, J. M., Dettinger, M., Anderson, M., Reynolds, D., Schick, L. J., & Smallcomb, C. (2019). A scale to characterize the strength and impacts of atmospheric rivers. *Bulletin of the American Meteorological Society*, *100*(2), 269–289. https://doi.org/10.1175/BAMS-D-18-0023.1

Ridder, N., de Vries, H., & Drijfhout, S. (2018). The role of atmospheric rivers in compound events consisting of heavy precipitation and high storm surges along the Dutch coast. *Natural Hazards and Earth System Sciences*, *18*, 3311–3326. https://doi.org/10.5194/nhess-18-3311-2018

Roca, R., & Fiolleau, T. (2020). Extreme precipitation in the tropics is closely associated with long-lived convective systems. *Communications Earth & Environment*, *1*(1), 1–6. https://doi.org/10.1038/s43247-020-00015-4

Rutz, J. J., James Steenburgh, W., & Martin Ralph, F. (2014). Climatological characteristics of atmospheric rivers and their inland penetration over the western United States. *Monthly Weather Review*, *142*(2), 905–921. https://doi.org/10.1175/MWR-D-13-00168.1

Salzmann, M. (2016). Global warming without global mean precipitation increase? *Science Advances*, *2*(6), e1501572.

Schär, C., Ban, N., Fischer, E. M., Rajczak, J., Schmidli, J., Frei, C., Giorgi, F., Karl, T. R., Kendon, E. J., Tank, A. M. G. K., O'Gorman, P. A., Sillmann, J., Zhang, X., & Zwiers, F. W. (2016). Percentile indices for assessing changes in heavy precipitation events. *Climatic Change*, *137*, 201–216. https://doi.org/10.1007/s10584-016-1669-2

Science. (2021). Europe's deadly floods leave scientists stunned. Retrieved from https://www.sciencemag.org/news/2021/07/europe-s-deadly-floods-leave-scientists-stunned.

Scoccimarro, E., Gualdi, S., Bellucci, A., Zampieri, M., & Navarra, A. (2013). Heavy precipitation events in a warmer climate: Results from CMIP5 models. *Journal of Climate*, *26*, 7902–7911. https://doi.org/10.1175/JCLI-D-12-00850.1

She, D., Shao, Q., Xia, J., Taylor, J. A., Zhang, Y., Zhang, L., Zhang, X., & Zou, L. (2015). Investigating the variation and non-stationarity in precipitation extremes based on the concept of event-based extreme precipitation. *Journal of Hydrology*, *530*, 785–798. https://doi.org/10.1016/j.jhydrol.2015.10.029

Smith, B. L., Yuter, S. E., Neiman, P. J., & Kingsmill, D. E. (2010). Water vapor fluxes and orographic precipitation over northern California associated with a landfalling atmospheric river. *Monthly Weather Review*, *138*(1), 74–100. https://doi.org/10.1175/2009MWR2939.1

Solomon, S., Qin, D., Manning, M., Marquis, M., Averyt, K., Tignor, M. M. B., Miller, H. L., & Chen, Z. (2007). *The physical science basis, contribution of working group I to the fourth assessment report of the IPCC* (Vol. 4). Cambridge University Press. Retrieved from. https://www.ipcc.ch/site/assets/uploads/2018/05/ar4_wg1_full_report-1.pdf

Stott, P. A., Christidis, N., Otto, F. E. L., Sun, Y., Vanderlinden, J. P., van Oldenborgh, G. J., Vautard, R., von Storch, H., Walton, P., Yiou, P., & Zwiers, F. W. (2016). Attribution of extreme weather and climate-related events. *WIREsClim Change*, *7*, 23–41. https://doi.org/10.1002/wcc.380

Sun, Y., Solomon, S., Dai, A., & Portmann, R. W. (2007). How often will it rain? *Journal of Climate*, *20*(19), 4801–4818. https://doi.org/10.1175/JCLI4263.1

Suppasri, A., Maly, E., Kitamura, M., Syamsidik, Pescaroli, G., Alexander, D., & Imamura, F. (2021). Cascading disasters triggered by tsunami hazards: A perspective for critical infrastructure resilience and disaster risk reduction. *International Journal of Disaster Risk Reduction*, *66*, 102597. https://doi.org/10.1016/j.ijdrr.2021.102597

Tabari, H. (2020). Climate change impact on flood and extreme precipitation increases with water availability. *Scientific Reports*, *10*(1), 1–10.

Tabari, H., Madani, K., & Willem, P. (2020). The contribution of anthropogenic influence to more anomalous extreme precipitation in Europe. *Environmental Research Letters*, *15*(10), 104077. https://doi.org/10.1088/1748-9326/abb268

Tang, Y., Winkler, J., Zhong, S., Bian, X., Doubler, D., Yu, L., & Walters, C. (2017). Future changes in the climatology of the Great Plains low-level jet derived from fine resolution multi-model simulations. *Scientific Reports*, *7*(1), 1–10. https://doi.org/10.1038/s41598-017-05135-0

Toreti, A., Naveau, P., Zampieri, M., Schindler, A., Scoccimarro, E., Xoplaki, E., Dijkstra, H. A., Gualdi, S., & Luterbacher, J. (2013). Projections of global changes in precipitation extremes from coupled model Intercomparison project phase 5 models. *Geophysical Research Letters*, *40*, 4887–4892. https://doi.org/10.1002/grl.50940

Trenberth, K. E., Dai, A., Rasmussen, R. M., & Parsons, D. B. (2003). The changing character of precipitation. *Bulletin of the American Meteorological Society*, *84*, 1205–1218. https://doi.org/10.1175/BAMS-84-9-1205

Turoff, M., Bañuls, V. A., Plotnick, L., Hiltz, S. R., & Ramírez de la Huerga, M. (2016). A collaborative dynamic scenario model for the interaction of critical infrastructures. *Futures*, *84*, 23–42.

United Nations Department of Economic and Social Affairs. (2019). *World urbanization prospects: The 2019 revision*. UNDESA. Retrieved from. https://population.un.org/wpp/Publications/Files/WPP2019_Highlights.pdf

Utsumi, N., Kim, H., Kanae, S., & Oki, T. (2017). Relative contributions of weather systems to mean and extreme global precipitation. *Journal of Geophysical Research – Atmospheres*, *122*, 152–167. https://doi.org/10.1002/2016JD025222

Vázquez, M., da Silva-Ferreira, F., Nieto, R., Liberato, M.L.R., & Gimeno, L. (2020). Moisture transport toward Europe and extreme precipitation events. In *Proceedings of The 3rd International Electronic Conference on Atmospheric Sciences (ECAS 2020)*. https://doi.org/10.3390/ecas2020-08137.

Vázquez, M., Nieto, R., Liberato, M. L. R., & Gimeno, L. (2020). Atmospheric moisture sources associated with extreme precipitation during the peak precipitation month. *Weather and Climate Extremes*, *30*, 100289. https://doi.org/10.1016/j.wace.2020.100289

Vera, C., Baez, J., Douglas, M., Emmanuel, C. B., Marengo, J., Meitin, J., Nicolini, M., Nogues-Paegle, J., Paegle, J., Penalba, O., Salio, P., Saulo, C., Silva Dias, M. A., Dias, P. S., & Zipser, E. (2006). The south American low-level jet experiment. *Bulletin of the American Meteorological Society*, *87*(1), 63–77. https://doi.org/10.1175/BAMS-87-1-63

Viale, M., Valenzuela, R., Garreaud, R. D., & Ralph, F. M. (2018). Impacts of atmospheric rivers on precipitation in southern South America. *Journal of Hydrometeorology*, *19*(10), 1671–1687. https://doi.org/10.1175/JHM-D-18-0006.1

Viswanadhapalli, Y., Dasari, H. P., Dwivedi, S., Madineni, V. R., Langodan, S., & Hoteit, I. (2020). Variability of monsoon low-level jet and associated rainfall over India. *International Journal of Climatology*, *40*(2), 1067–1089. https://doi.org/10.1002/joc.6256

Vizy, E. K., & Cook, K. H. (2019). Observed relationship between the Turkana low-level jet and boreal summer convection. *Climate Dynamics*, *53*(7–8), 4037–4058. https://doi.org/10.1007/s00382-019-04769-2

Von Mises, R. (1954). La distribution de la plus grande de n valeurs. In *Selected papers* (Vol. II, pp. 271–294). American Mathematical Society.

Wang, G., Wang, D., Trenberth, K. E., Erfanian, A., Yu, M., Bosilovich, M. G., & Parr, D. T. (2017). The peak structure and future changes of the relationships between extreme precipitation and temperature. *Nature Climate Change*, *7*(4), 268–274. https://doi.org/10.1038/nclimate3239

Wang, L., & Gu, W. (2016). The Eastern China flood of June 2015 and its causes. *Science Bulletin*, *61*(2), 178–184. https://doi.org/10.1007/s11434-015-0967-9

Wentz, F. J., Ricciardulli, L., Hilburn, K., & Mears, C. (2007). How much more rain will global warming bring? *Science*, *317*, 233–235. https://doi.org/10.1126/science.1140746

Wernberg, T., Smale, D., Tuya, F., Thomsen, M. S., Langlois, T. J., de Bettignies, T., Bennett, S., & Rousseaux, C. S. (2013). An extreme climatic event alters marine ecosystem structure in a global biodiversity hotspot. *Nature Climate Change*, *3*, 78–82. https://doi.org/10.1038/nclimate1627

Westra, S., Fowler, H. J., Evans, J. P., Alexander, L. V., Berg, P., Johnson, F., Kendon, E. J., Lenderink, G., & Roberts, N. M. (2014). Future changes to the intensity and frequency of short-duration extreme rainfall. *Reviews of Geophysics*, *52*, 522–555. https://doi.org/10.1002/2014RG000464

Whiteman, C. D., Bian, X., & Zhong, S. (1997). Low-level jet climatology from enhanced rawinsonde observations at a site in the southern Great Plains. *Journal of Applied Meteorology*, *36*(10), 1363–1376. https://doi.org/10.1175/1520-0450(1997)036<1363:LLJCFE>2.0.CO;2

Yin, H., & Sun, Y. (2018). Characteristics of extreme temperature and precipitation in China in 2017 based on ETCCDI indices. *Advances in Climate Change Research*, *9*(4), 218–226. https://doi.org/10.1016/j.accre.2019.01.001

Zhang, J., Gao, G., Fu, B., Wang, C., Gupta, H. V., Zhang, X., & Li, R. (2020). A universal multifractal approach to assessment of spatiotemporal extreme precipitation over the loess plateau of China. *Hydrology and Earth System Sciences*, *24*, 809–826. https://doi.org/10.5194/hess-24-809-2020

Zhang, W., & Zhou, T. (2019). Significant increases in extreme precipitation and the associations with global warming over the global land monsoon regions. *Journal of Climate*, *32*(24), 8465–8488. https://doi.org/10.1175/JCLI-D-18-0662.1

Zhu, Y., & Newell, R. E. (1998). A proposed algorithm for moisture fluxes from atmospheric rivers. *Monthly Weather Review*, *126*(3), 725–735. https://doi.org/10.1175/1520-0493(1998)126<0725:APAFMF>2.0.CO;2

Zittis, G., Bruggeman, A., & Lelieveld, J. (2021). Revisiting future extreme precipitation trends in the Mediterranean. *Weather and Climate Extremes.*, *34*, 100380. https://doi.org/10.1016/j.wace.2021.100380

Zobel, Z., Wang, J., Wuebbles, D. J., & Kotamarthi, V. R. (2018). Analyses for high-resolution projections through the end of the 21st century for precipitation extremes over the United States. *Earth's Future*, *6*(10), 1471–1490. https://doi.org/10.1029/2018EF000956

Zscheischler, J., Westra, S., van den Hurk, B. J. J. M. Seneviratne, S. I., Ward, P. J., Pitman, A., AghaKouchak, A., Bresch, D. N., Leonard, M., Wahl, T., & Zhang, X. (2018). Future climate risk from compoundevents. *Nature Climate Change*, *8*, 469–477. https://doi.org/10.1038/s41558-018-0156-3

SUPPORTING INFORMATION

Additional supporting information can be found online in the Supporting Information section at the end of this article.

How to cite this article: Gimeno, L., Sorí, R., Vázquez, M., Stojanovic, M., Algarra, I., Eiras-Barca, J., Gimeno-Sotelo, L., & Nieto, R. (2022). Extreme precipitation events. *WIREs Water*, *9*(6), e1611. https://doi.org/10.1002/wat2.1611

PAPER S2

Atmospheric Research 304 (2024) 107413

Contents lists available at ScienceDirect

Atmospheric Research

journal homepage: www.elsevier.com/locate/atmosres

Projected changes in extreme daily precipitation linked to changes in precipitable water and vertical velocity in CMIP6 models

Luis Gimeno-Sotelo [a,*], Emanuele Bevacqua [b], José Carlos Fernández-Alvarez [a,c], David Barriopedro [d], Jakob Zscheischler [b,e], Luis Gimeno [a]

[a] Centro de Investigación Mariña, Universidade de Vigo, Environmental Physics Laboratory (EPhysLab), Campus da Auga, 32004 Ourense, Spain
[b] Department of Compound Environmental Risks, Helmholtz Centre for Environmental Research – UFZ, Leipzig, Germany
[c] Departamento de Meteorología, Instituto Superior de Tecnologías y Ciencias Aplicadas, Universidad de La Habana, La Habana 10400, Cuba
[d] Instituto de Geociencias, IGEO, CSIC–UCM, Madrid, Spain
[e] Technische Universität Dresden, Dresden, Germany

ARTICLE INFO

Keywords:
CMIP6
Extreme precipitation
Precipitable water
Vertical velocity

ABSTRACT

Understanding the drivers of precipitation and their changes in a non-stationary climate is crucial for effective climate adaptation and water resource management, as it helps us anticipate and respond to shifting precipitation patterns and their impacts. Here, analysing simulations from the Coupled Model Intercomparison Project Phase 6 (CMIP6) we show that the conditional probability of extreme daily precipitation given joint extremes of two drivers (precipitable water and vertical velocity) will be stable in a 3 °C warmer future. Consistent with earlier work, we find that the near-global increase in precipitable water (thermodynamic influence) is the baseline for changes in extreme precipitation, which are modulated by changes in vertical velocity (dynamic influence). Thus, in regions where vertical velocity increases, the effect of the two drivers is additive and their changes contribute to an increase in extreme precipitation. The changes of the two drivers are opposite where vertical velocity decreases, resulting in only small increases in extreme precipitation or even a decrease. Furthermore, we reveal that there are moderate changes in the dependence between the drivers, which are larger over the ocean than over landmasses, but they contribute only little to the overall changes in extreme precipitation. We conclude that the use of two very simple drivers that are readily available from climate models can be of great utility for evaluating precipitation extremes in models and understanding their projected changes.

1. Introduction

Global warming has caused changes in precipitation extremes (e.g. Donat et al., 2016; Sun et al., 2021; Douville et al., 2021) and will do so with even greater intensity in the future (e.g. Westra et al., 2014; Bao et al., 2017; John et al., 2022). Behind these changes, there are robust thermodynamic causes linked to the increase in humidity with temperature given the Claussius-Clapeyron relationship (Soden and Held, 2006; Allen and Ingram, 2002; Neelin et al., 2022), which affect the globe as a whole, although with different intensities in tropical and extratropical regions (Neelin et al., 2022). There are also dynamic causes linked to changes in atmospheric circulation and therefore changes in the convergence of humidity, which modulate the changes in extreme precipitation (EP) at the regional level (O'Gorman, 2015; Bao et al., 2017; Pfahl et al., 2017; John et al., 2022). Although the relationship of precipitation with its main drivers is complex, in a first approximation, daily EP can be scaled with a measure of atmospheric instability and a measure of available water vapor content for precipitation (Emori and Brown, 2005; Nie et al., 2018).

At the daily time scale, the amount of moisture measured in the air column at any given time is always less than the amount of precipitation during actual EP events (Trenberth et al., 2003). One way of addressing EP is to also consider the moisture influx from the outside, that is, the horizontal moisture transport (Gimeno et al., 2012, 2016). However, in a recent work, Gimeno-Sotelo et al. (2023) concluded that the analysis of the joint extremes of vertical velocity and precipitable water provides a sound basis for evaluating EP in climate models and understanding projected changes. Specifically, they considered atmospheric instability, measured as vertical velocity at 500 hPa, the moisture content in the column, measured as the vertically-integrated water vapor (also known

* Corresponding author.
E-mail address: luis.gimeno-sotelo@uvigo.es (L. Gimeno-Sotelo).

https://doi.org/10.1016/j.atmosres.2024.107413
Received 19 December 2023; Received in revised form 4 March 2024; Accepted 9 April 2024
Available online 10 April 2024

as precipitable water), and horizontal moisture transport, measured as the vertically-integrated horizontal moisture transport (IVT) as major potential drivers of EP in ERA5 reanalysis (Hersbach et al., 2020). They found that in most of the extratropical land areas (mainly in inner continental areas), the combination of drivers leading to the highest probability of EP was the joint occurrence of extremes in vertical velocity and precipitable water (and non-extreme horizontal moisture transport). It was also the second most favorable combination for tropical regions, causing EP with sligthly lower probabilities than the simultaneous occurrence of extremes in the three drivers.

Scaling EP with these two variables allows us to study the thermodynamic response (represented by humidity) versus the dynamic (represented by vertical movement) of EP to global warming. This has been done previously using CMIP5 models (Pfahl et al., 2017) and very recently with CMIP6 models (Paik et al., 2023), obtaining similar general conclusions. The thermodynamic component is constrained by the relationship between humidity and temperature given by the Clausius-Clapeyron equation, being responsible for an increase in EP that scales approximately 6%/K in an almost spatially homogeneous manner. The dynamic component is responsible for most of the spatial variability, with responses at a planetary scale such as the amplification of increases in EP in the Intertropical Convergence Zone (ITCZ), or the decrease in the subtropical oceans, but also at a regional scale such as the weakening of increases in EP in the Mediterranean, South Africa, and Australia. Some studies have explored, using quasi-geostrophic (QG) diagnoses, the causes of the dynamic component (Li et al., 2020; Nie et al., 2018), for which they decompose the vertical movement into a dry component due to large-scale adiabatic perturbations and a moist component, driven by diabatic heating of moist convection, which implies a moisture-vertical movement feedback. They found that in the tropics the vertical ascent is dominated by the moist component, whereas in the extratropics the vertical motion is dominated by large-scale perturbations, i.e., the dry component. As such, the moisture-vertical motion feedback driven by the release of latent heat was found to be less important than in the tropics, although with regional differences.

Here, we analyse the output of CMIP6 models (Eyring et al., 2016) to investigate whether the relationship found by Gimeno-Sotelo et al. (2023) between vertical velocity, precipitable water, and daily EP in ERA5 is also observed in CMIP6 models. We explore projected changes in both intensity and extension of this relationship in a 3 °C-warmer climate than preindustrial conditions. Furthermore, we study which of the two terms, the dynamic, quantified by changes in vertical velocity, or the thermodynamic, quantified by changes in precipitable water, is the most important, and where it dominates the projected changes in daily EP. Unlike the previous works mentioned above, which used complex metrics for the dynamical and thermodynamical contributions based on mass-weighted vertical integral over the whole troposphere of both vertical velocity and changes in saturation-specific humidity, our analysis is based on two simpler and easier variables to obtain directly from climate models, such as the vertical velocity in the middle troposphere and the water vapor column, a variable that has also the advantage of having a strong relationship with air temperature, which is very valuable to interpret the response of EP to the increased temperature associated with climate change. Finally, we analyse the changes in the dependence between the drivers, and the contribution of these changes to those in extreme precipitation, with the aim of accounting for the influence of the moisture-vertical motion feedback processes associated with the diabatic heating of moist convection.

2. Data and methods

This article is based on the outputs of CMIP6 models. CMIP6 is the Sixth Phase of the Coupled Model Intercomparison Project (CMIP), organized by the World Climate Research Programme (WCRP) consisting of an intercomparison effort of climate models in a coordinated suite of model simulations that make it possible to give robustness to climate change projections (Eyring et al., 2016). Climate models are intercompared in individual Model Intercomparison Projects (MIPs), which include both simulations in future climate under different Shared Socioeconomic Pathways (SSPs) (Riahi et al., 2017), as well as historical climate simulations. CMIP6 ensures both the scientific knowledge and the correct use of model outputs in a wide range of climate change impact and adaptation studies, including the latest IPCC report (IPCC, 2021).

We only considered the CMIP6 models providing daily data of precipitation, precipitable water (PRW) and vertical velocity at 500 hPa ($\omega = \frac{dp}{dt}$, where p refers to atmospheric pressure) for the historical and the SSP5–8.5 experiments. These conditions were satisfied by 12 models of the CMIP6 archive (see Table S1).

Note that positive values of ω denote downward motion, often associated to stable weather. Therefore, herein we defined vertical velocity (VV) as ″ $-\omega$″, which corresponds to updrafts, thus providing a measure of atmospheric instability. 500 hPa is the level that represents the mid-troposphere and allows capturing weather systems related to extreme precipitation, including those that reach their greatest expression in the mid-lower troposphere (extratropical cyclones) and in the mid-upper troposphere (e.g. cut-off lows). It is also a level where other key precipitation-related phenomena are clearly marked (e.g. subtropical and polar jets; Woollings et al., 2010).

The data was interpolated at a common resolution of 1.5 degrees. As a reference historical climate we considered the 1985–2014 period of the historical simulation. The +3 °C world was computed for each model as the 30-year future period in which the global mean temperature is projected to be 3 °C higher than in the preindustrial (1850–1900) period, according to Hauser et al. (2021). We also performed the analysis for the +2 °C world with the aim of assessing the sensitivity of the obtained results.

For each of the CMIP6 models and for the historical and future periods separately, the conditional probability of EP under extreme PRW and extreme VV was estimated empirically, as the ratio between the number of days with simultaneous occurrence of EP, extreme PRW and extreme VV, and the number of days with both extreme PRW and extreme VV, that is:

$$\widehat{P}(EP|extreme\,PRW\,and\,extreme\,VV) = \frac{n(\{EP, extreme\,PRW\,and\,extreme\,VV\})}{n(\{extreme\,PRW\,and\,extreme\,VV\})}$$

where “$n(A)$” is the notation for the number of elements of a set A. Daily extremes in precipitation and its drivers (PRW and VV) are defined as values above the daily 95th percentile of the corresponding 30-year period.

Using the CMIP6 model, we computed the percentage change in extreme precipitation (EP) between the historical (HIST) and the future (FUT) periods, as follows:

$$\Delta EP = \frac{< EP^{FUT} > - < EP^{HIST} >}{< EP^{HIST} >} * 100$$

where $< EP^{HIST} >$and $< EP^{FUT} >$ refer to the mean of the EP for the historical and future periods, respectively.

The percentage changes in extreme precipitable water and vertical velocity (as ″ $-\omega$″) were computed analogously.

The changes in the dependence between the variables were assessed by means of the difference of Spearman’s correlations between the two studied periods.

For each CMIP6 model, using the historical data, a linear regression model was fitted to precipitation extremes, i.e., EP, as a function of the product of precipitable water and vertical velocity associated with the EP on the same day, in line with the relationship presented in Pfahl et al. (2017). The fitted regression model, which was evaluated by means of its coefficient of determination (R^2), allowed us to obtain precipitation predictions in terms of values of the product of those variables, as follows:

$$\widehat{Prec} = \widehat{a}*PRW*(-\omega) + \widehat{b}$$

Precipitation predictions were obtained for both the historical and future periods. Using the obtained predictions, it was possible to compute the estimated percentage change in EP between those periods, as follows:

$$\Delta\widehat{EP} = \frac{<\widehat{EP}^{FUT}> - <\widehat{EP}^{HIST}>}{<\widehat{EP}^{HIST}>}*100$$

where $<\widehat{EP}^{HIST}>$and $<\widehat{EP}^{FUT}>$refer to the mean of the EP predictions for the historical and future periods, respectively. Analogously to the case of the EP observations, EP predictions refer to precipitation predictions that are greater than the 95th percentile of the predictions in each period.

We computed the difference between the percentage change in predicted EP and that found using the CMIP6 outputs as a way of assessing the performance of the regression model regarding the obtained predictions.

In order to analyse the contribution of the change in precipitable water, vertical velocity and the dependence between them in the change in extreme precipitation, three "alternative futures" were obtained by means of the statistical transformations presented in Bevacqua et al. (2019). The "new" values for precipitable water and vertical velocity were obtained for a future scenario in which:

1) only the marginal distribution of precipitable water changes, but neither the marginal distribution of vertical velocity nor the dependence between them changes (ΔPRW).
2) only the marginal distribution of vertical velocity changes, but neither the marginal distribution of precipitable water nor the dependence between them changes ($\Delta(-\omega)$).
3) only the dependence between precipitable water and vertical velocity changes (Spearman's correlation and tail dependence, i.e., dependence at extreme values), but the marginal distribution of the variables does not change (ΔDep).

For each of these three scenarios, EP predictions were computed. As such, it was possible to estimate the percentage change in EP in a situation in which only the marginal distribution of precipitable water changes ($\Delta\widehat{EP}$ (ΔPRW)), only the marginal distribution of vertical velocity changes ($\Delta\widehat{EP}$ $(\Delta(-\omega))$) and only the dependence between them changes ($\Delta\widehat{EP}$ (ΔDep)), as follows:

$$\Delta\widehat{EP}(\Delta PRW) = \frac{<\widehat{EP}^{FUT,\Delta PRW}> - <\widehat{EP}^{HIST}>}{<\widehat{EP}^{HIST}>}*100$$

$$\Delta\widehat{EP}(\Delta(-\omega)) = \frac{<\widehat{EP}^{FUT,\Delta(-\omega)}> - <\widehat{EP}^{HIST}>}{<\widehat{EP}^{HIST}>}*100,$$

$$\Delta\widehat{EP}(\Delta Dep) = \frac{<\widehat{EP}^{FUT,\Delta Dep}> - <\widehat{EP}^{HIST}>}{<\widehat{EP}^{HIST}>}*100$$

where $<\widehat{EP}^{HIST}>$refers to the mean of the EP predictions for the historical period, and $<\widehat{EP}^{FUT,\Delta PRW}>$, $<\widehat{EP}^{FUT,\Delta(-\omega)}>$ and $<\widehat{EP}^{FUT,\Delta Dep}>$ to the mean of the EP predictions for the three "alternative futures".

3. Results

We begin by showing that the relationship between the EP and the two driving factors considered in this study, i.e., PRW and VV, is generally high and is stable between the historical period and a + 3 °C world.

For this purpose, the conditional probability of EP given joint extremes of PRW and VV was computed using the CMIP6 model data. The probability pattern for the historical period for December–February (DJF) and June–August (JJA) (Fig. 1a,b) is consistent with the results found for the combination of extreme PRW and VV (under non-extreme moisture transport) using the ERA5 reanalysis (Gimeno-Sotelo et al., 2023). We find very high conditional probabilities (over 0.8) in most areas, especially in inner continental ones, where moisture transport is not so relevant because most of the moisture comes from the soil by evapotranspiration (Miralles et al., 2016) and the simultaneous occurrence of extreme PRW and VV may be sufficient for EP to occur. Moderate probabilities (0.4 to 0.6) are obtained in regions of occurrence of moisture transport mechanisms such as atmospheric rivers (western coast of North America and European coast) because in those regions the total amount of water vapor in the air column at a given time may be insufficient to generate EP and moisture should be supplied from the outside (Trenberth et al., 2003). In subtropical anticyclonic areas, low probabilities are found (~0.2) because these regions are characterised by air descents (vertical velocity in the downward direction, i.e., negative values of VV following the definition in this article) and extreme values of VV may not be high enough for EP to take place.

The results point to a stable pattern between the historical period and a + 3 °C world (Fig. 1c,d). There is not an appreciable change in the conditional probabilities of EP, with the ratio between future and historical values being close to 1 almost everywhere (Fig. 1e,f). In DJF, there is only 1.1% of land areas where at least 90% of the models agree in the sign of the change of those probabilities, and only 0.8% in JJA. These robust results enable us to rely on PRW and VV as drivers of EP in this study.

We now proceed to analyse the projected changes in EP in a + 3 °C world. Fig. 2 shows the percentage change in EP between the historical and future periods in DJF and JJA (Fig. S1 for intermediate seasons). The results are in line with other studies analysing changes in EP in CMIP6 (see, e.g., John et al., 2022). The pattern shows the strongest increase (~50%) in the ITCZ in both DJF and JJA, with at least 90% model agreement. In subtropical anticyclonic areas, most models agree on a moderate decrease in EP of about 30%. In extratropical areas there are important seasonal differences. For example, in the extratropical continental regions of the Northern Hemisphere, models point to a moderate increase of about 30% in DJF, but, in general, they do not agree on the projected change in JJA. These changes are in overall agreement with an intensification of the hydrological cycle (Held and Soden, 2006).

We move to assessing changes in the drivers of EP, and in the dependence between those variables. As expected from the Claussius-Clapeyron relationship, models agree on an overall increase in extreme PRW of about 20% in a 3 °C warmer world with respect to the period 1850–1900 (Fig. 3a,b). Regional differences are linked to the availability of moisture, which are very notable in climatologically dry areas in the interior of the continents and in subtropical oceanic regions characterised by large-scale subsidence. Concerning changes in extreme VV (Fig. 3c,d), most models agree on an intensification of upward and downward motions in the ITCZ (of about 50%) and subtropical regions (of about 20–30%), respectively, being consistent with the expected response of the ITCZ and Hadley cells to climate change (Allan et al., 2020). We also found out modest changes in the dependence between PRW and VV (Fig. 3e,f), as models agree on an increase in the Spearman's correlation between them in the ITCZ (of about 0.2) and a decrease in several subtropical regions (of about 0.1). Changes in the dependencies are more pronounced over ocean than over land, with the areal extent of model agreement being also larger over oceanic areas. The percentage of area where at least 90% of models agreed in the sign of the change in the Spearman's correlation was 7.1% over land and 13% over ocean area in DJF. Those values were slightly higher in JJA (12.1% over land and 13.7% over ocean).

With the aim of analysing the contribution of the projected changes in PRW, VV and the dependence between them in the change in EP, a linear regression model was fitted (see the Data and Methods section). The results for the "slope" coefficient (i.e. the influence of the product of PRW and VV on EP), are shown in Fig. S2a,b. Positive values are

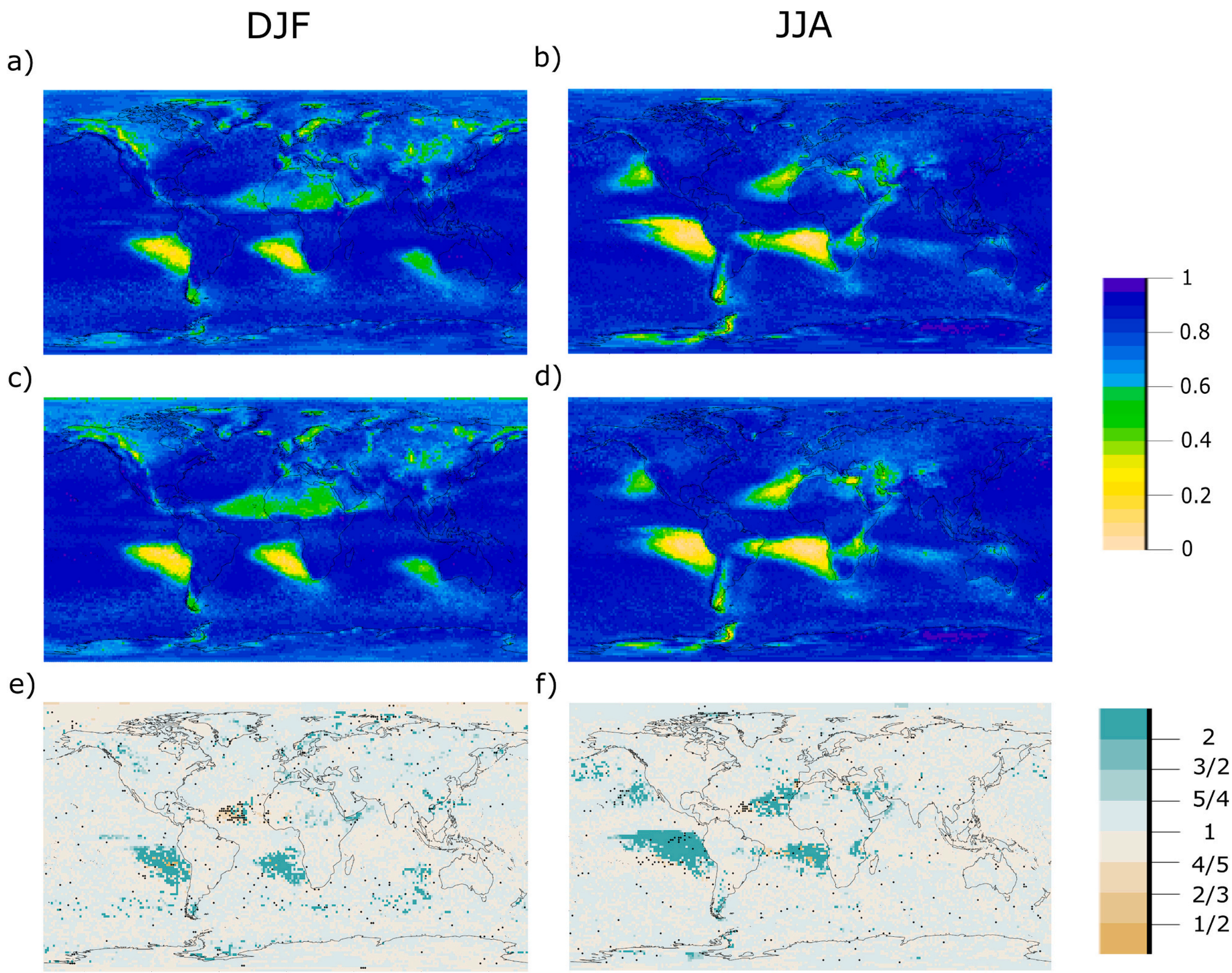

Fig. 1. Multimodel average of the conditional probability of daily extreme precipitation (EP) given the simultaneous occurrence of extreme precipitable water (PRW) and vertical velocity (VV, defined as $-\omega$), for a), b) historical period and c), d) +3 °C future period; e), f) average ratio between values for the +3 °C future and historical periods, for DJF and JJA, respectively. In e) and f), stippling refers to a model agreement of at least 90% in the sign of the change (greater/lower than 1).

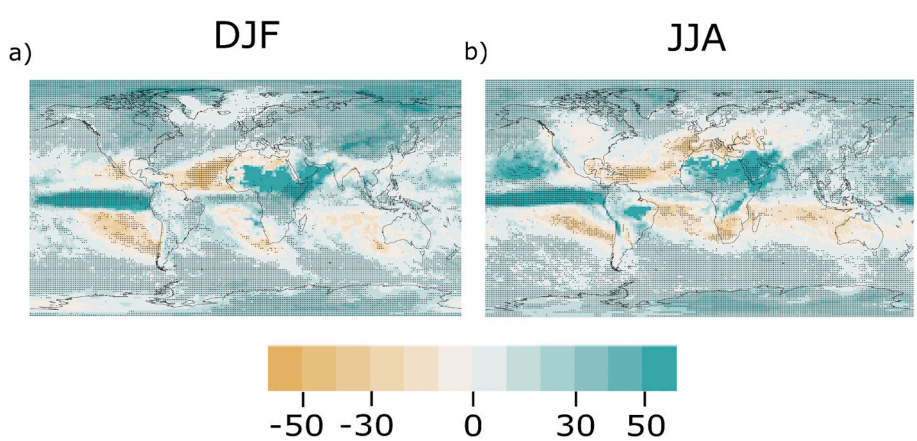

Fig. 2. Multimodel average of the percentage change in EP between the historical and + 3 °C future periods using the CMIP6 model data, for a) DJF and b) JJA. Stippling refers to model agreement of at least 90% in the sign of the change.

observed almost everywhere, implying that EP scales linearly with the product of PRW and VV. However, the influence is more intense in tropical regions and in extratropical inner continental areas of the Northern Hemisphere, the latter especially in DJF. The estimated "intercept" coefficient (Fig. S2c,d), which represents the value that is added to the product term in order to get the corresponding value of EP, indicates that the product is insufficient for EP to occur in some regions, such as those of atmospheric river occurrence (western and eastern coasts of North America, western Europe and eastern Asia; see Gimeno-Sotelo and Gimeno, 2023). The R^2 value (Fig. S1e,f) measures the

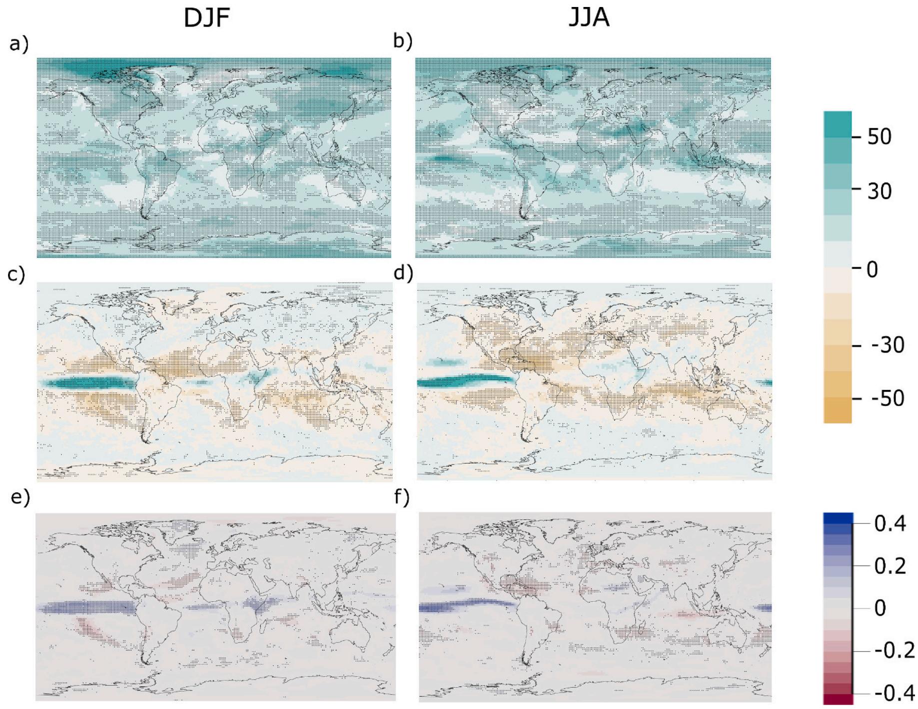

Fig. 3. Multimodel average of a), b) the percentage change in the 95th percentile of PRW; c), d) the same for VV; e), f) the difference of Spearman's correlations between PRW and VV (+3 °C future minus historical periods), for DJF and JJA, respectively. Stippling refers to model agreement of at least 90% in the sign of the change.

percentage of variance in EP that is explained by the product of PRW and VV, and it was used for model evaluation (Fig. S2e,f). The highest values were found in tropical regions (of about 0.8), indicating that in those areas the drivers explain EP variability very well. Moderate values (0.4–0.6) occurred in extratropical regions such as eastern Asia or eastern North America, the latter especially in DJF. Moderate-to-low values (0.2–0.4) were observed in extratropical inner continental areas, such as the interior of Eurasia, and low values (below 0.2) dominated in subtropical anticyclonic areas.

Using the daily precipitation predictions inferred from the regression model based on PRW and VV, we estimated the percentage change in predicted EP, $\widehat{EP}$, (Fig. 4a,b), and compared it with the true percentage change of EP found in CMIP6 (Fig. S3a,b). Although the general pattern of changes was well-represented by the precipitation predictions, there was an underestimation in some regions, predominantly in the ITCZ and the extratropical continental regions of the Northern Hemisphere, the latter especially in DJF. Differently, an overestimation was observed in subtropical anticyclonic areas. In order to test the effect of changing the fitting period, we also fitted the regression model to pooled data of historical and future periods, producing very similar results (Fig. S3c,d).

Finally, using the regression models, we obtained future precipitation predictions considering three scenarios in which only the marginal distribution of PRW, VV or the dependence between the variables changes (see the Data and Methods section). These predictions enabled us to compute the percentage change in extreme precipitation under each of these three "alternative futures". The corresponding percentage changes in predicted EP represent the contribution of the change in PRW, VV and the dependence between them to the change in EP. In a situation in which only PRW changed, EP would increase all over the world (Fig. 4c,d). If only VV changed, the most marked effects would be an increase in EP in the ITCZ and a decrease in the subtropics (Fig. 4e,f). A moderate decrease in EP was also found in extratropical continental areas of the Northern Hemisphere in JJA. Considering the case in which only the dependence between PRW and VV changed, EP would not change appreciably in the future, with the exception of small regions in the ITCZ and the subtropics (Fig. 4g,h). As such, our results indicate that the marginal distribution changes of PRW and VV are the most responsible ones for changes in EP, whereas changes in the dependence between those drivers do not play an important role. Intermediate patterns between the summer and winter ones are obtained for March–May (MAM) and September–November (SON) (Fig. S4).

The analysis was also performed for a 2 °C warming level, and the results indicate that the obtained patterns are the same as those obtained for a 3 °C warming level but with a lower magnitude (Figs. S5 and S6), which is consistent, as changes are more noticeable as the warming signal is stronger.

4. Discussion and conclusions

Here we studied the conditional probability of daily extreme precipitation (EP) given joint extremes of precipitable water (PRW) and vertical velocity (VV) using CMIP6 models. The multimodel average pattern of conditional probability of EP in the historical period is consistent with that observed in the ERA5 reanalysis for the combination of those drivers under non-extreme moisture transport (Gimeno-Sotelo et al., 2023) and does not change substantially in a 3 °C global warming scenario. It consists of very high probabilities of EP in tropical regions and inside the extratropical continents, moderate-to-high probabilities in those extratropical regions strongly affected by the major moisture transport mechanisms, especially atmospheric rivers (Gimeno et al., 2014; Gimeno-Sotelo and Gimeno, 2022, 2023), and low probabilities in subtropical regions. We have found modest changes in the dependence between PRW and VV, with an increase in the ITCZ, a region dominated by the humid component of the VV, driven by diabatic heating of moist convection (Nie et al., 2018), which may be due to a thermodynamic amplification factor (Kim et al., 2022) and the lightly stronger moist convection in a warmer climate (Del Genio et al., 2007). The limitations of $-\omega$ at 500 hPa to represent the smaller scales of the humid component of the VV prevent us from making solid conclusions on this and motivates further investigation.

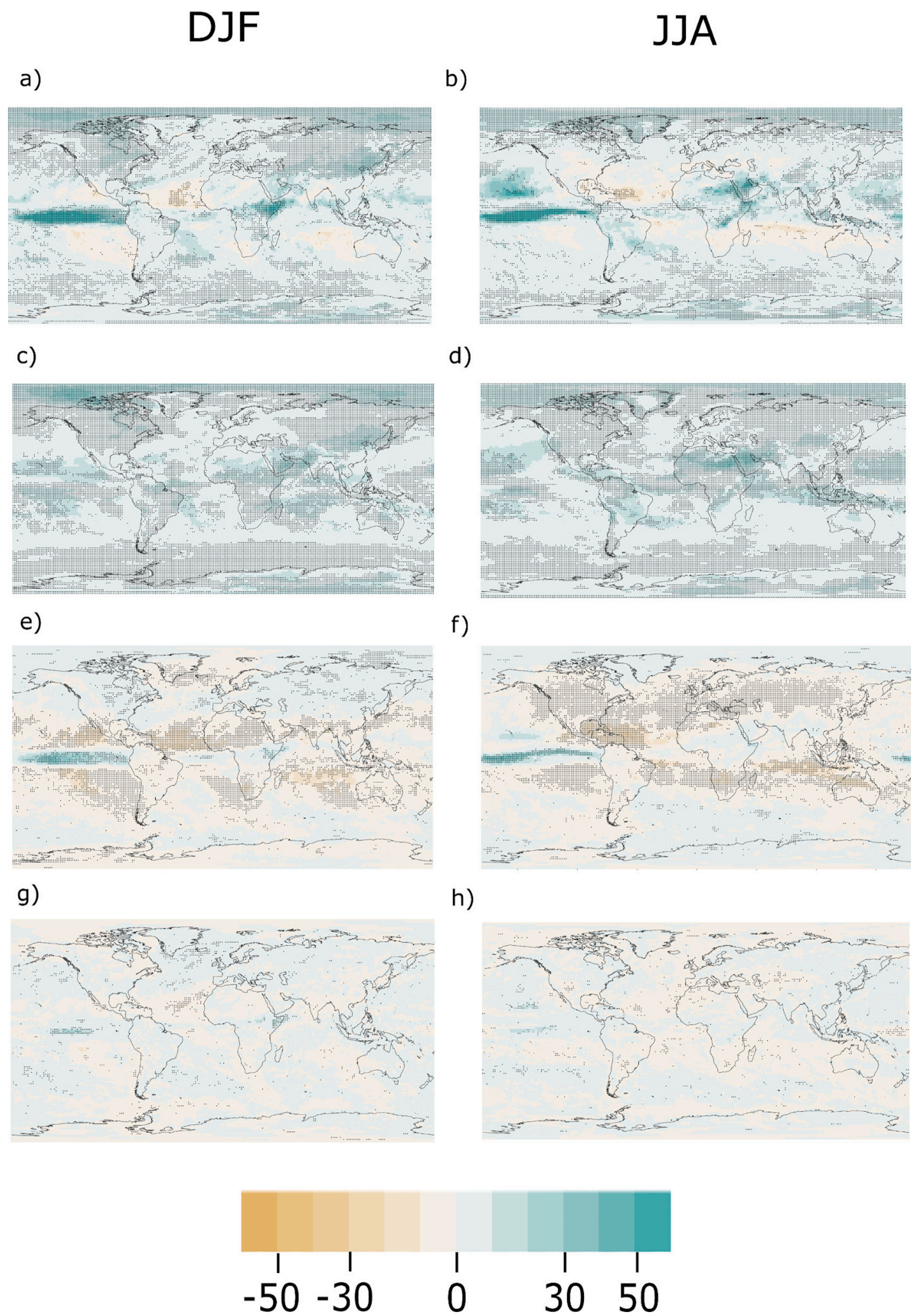

Fig. 4. Multimodel average of the estimated percentage change in EP between the historical and + 3 °C future periods, computed by means of the precipitation predictions obtained from the fitted regression model, using PRW and VV for the future period based on a),b) original data; c), d) the change in the marginal distribution of PRW; e), f) the change in the marginal distribution of VV; and g), h) the change in the dependence between PRW and VV, for DJF and JJA, respectively. Stippling refers to model agreement of at least 90% in the sign of the change.

As expected, CMIP6 projections indicate that EP will become more intense with global warming (Li et al., 2020; John et al., 2022), consistent with a baseline expectation given by the Claussius-Clapeyron based-relation increases in low-altitude moisture. However, this thermodynamic response is strongly modified by the moisture limitation in some continental regions and especially by dynamical responses (O'Gorman and Schneider, 2009; Pfahl et al., 2017), which are spatially and seasonally dependent. As shown herein, this dynamical response (represented by VV) results in a non-homogeneous change in EP, with areas experiencing large increases in EP, such as the ITCZ, and others reporting small increases or even decreases, such as the subtropical anticyclonic regions. The extratropics have a seasonally varying response in the Northern Hemisphere, with an increase in winter but not in summer.

We have found that the near-global increase in PRW is the baseline for the changes in EP, which are modulated by changes in VV. In those regions where VV increases, such as the ITCZ in both seasons, the effect of the two drivers is additive and their changes contribute to an increase in EP. In areas where VV does not change appreciably, such as the extratropical continental regions of the Northern Hemisphere in winter, the increase in EP is mainly due to the increase in PRW. However, in regions where VV decreases, the changes of the two drivers are opposite, resulting in non-appreciable changes (extratropical continental regions of the Northern Hemisphere in summer) or a decrease (subtropical areas) in EP. It was also shown that, in general, future changes in the dependence between the drivers do not have a noticeable effect on changes in EP, with an influence pattern resembling that of the humid component of the vertical velocity (Nie et al., 2018), due to the moisture-vertical velocity feedback mechanism driven by the released latent heating by convection.

Results are consistent with previous modelling studies (e.g. Emori and Brown, 2005; O'Gorman and Schneider, 2009), which showed that the dynamic component of the changes in EP (in our study due to changes in VV) plays a significant role over tropics, being the thermodynamic component (in our study due to changes in PRW) dominant in extratropics. The patterns of dynamic and thermodynamic influence are in clear agreement with those achieved for CMIP5 (e.g. Pfahl et al., 2017) and very recently for CMIP6 (Gu et al., 2023; Paik et al., 2023). However, in these two studies, changes are diagnosed by means of more complex metrics for the dynamical and thermodynamical contributions. In particular, EP was scaled with the mass-weighted vertical integral over the whole troposphere of both VV and changes in saturation-specific humidity. Instead, in our study, we made us of the VV at a single vertical level, representative of the middle troposphere, and of the total content of the water column. These two variables are much simpler to obtain and manage for the evaluation of models. The latter has the additional advantage of having a strong relationship with air temperature, which is very valuable to interpret the response of EP to the increased temperature associated with climate change.

Our results are also consistent with the expected response of the intensity of extratropical cyclones, the ITCZ and the Hadley cells to climate change. Extratropical cyclones are the main meteorological systems responsible for VV leading to extratropical precipitation, including EP in the Northern Hemisphere, where the percentage of EP directly related to extratropical cyclones can exceed 80% (Pfahl and Wernli, 2012). There is a consensus on the increase in the intensity of the most extreme cyclones in the future (Sinclair et al., 2020; Dolores-Tesillos et al., 2022), although with important regional and seasonal differences. Cyclones are projected to increase in intensity in the Southern Hemisphere with a likely decrease in the Northern Hemisphere (Chang et al., 2013; Colle et al., 2013; Priestley and Catto, 2022), much more marked during summertime (Lehmann et al., 2014). Changes in tropical circulation linked to precipitation are well-summarized by Byrne et al. (2018) from CMIP5 projections, for which most of the models agree that the ITCZ will narrow over the twenty-first century without a change of position, and there will be an expansion of the descending region of the Hadley circulation. Both phenomena will be strongly correlated, and the fractional changes predicted for ITCZ narrowing will be lower than those corresponding to the expansion of the descending Hadley cells. As a consequence, VV, moisture convergence and precipitation will increase in the ITCZ and decrease in the subtropics.

The results of this analysis are based on the outputs of a moderate number of CMIP6 models (12 models) and the validity of "$-\omega$" to represent VV both in reanalysis and in models, a metric which has some limitations, especially in tropical regions (O'Gorman and Schneider, 2009). However, the robustness of the results achieved in the multi-model ensemble and the coherence with the expected response of the hydrological cycle to global warming enables us to trust in the validity of the conclusions reached.

It is also important to point out that moisture transport is an important driver of EP in some world regions (Gimeno-Sotelo and Gimeno, 2023), such as the oceanic extratropical latitudes and the western coast of the continents. Changes in the moisture transported by atmospheric rivers feeding extratropical cyclones are expected (Payne et al., 2020; Algarra et al., 2020; Shields et al., 2023; Fernández-Alvarez et al., 2023). Studying the effect of the changes in moisture transport on the changes in EP is outside the scope of this article, but it is an interesting topic for further research.

CRediT authorship contribution statement

Luis Gimeno-Sotelo: Conceptualization, Formal analysis, Investigation, Methodology, Visualization, Writing – original draft, Writing – review & editing. **Emanuele Bevacqua:** Conceptualization, Methodology, Supervision, Visualization, Writing – original draft, Writing – review & editing. **José Carlos Fernández-Alvarez:** Formal analysis, Methodology, Writing – review & editing. **David Barriopedro:** Supervision, Writing – review & editing. **Jakob Zscheischler:** Conceptualization, Supervision, Writing – review & editing. **Luis Gimeno:** Conceptualization, Funding acquisition, Supervision, Writing – original draft, Writing – review & editing.

Declaration of competing interest

The authors declare that they have no known competing financial interests or personal relationships that could have appeared to influence the work reported in this paper.

Data availability

The data from the CMIP6 models is available at the World Climate Research Programme (WCRP, https://esgf-node.llnl.gov/search/cmip6/). From that page, it is possible to download the necessary data for this research.

Acknowledgments

EPhysLab members are supported by the SETESTRELO project (grant no. PID2021-122314OB-I00) funded by the Ministerio de Ciencia, Innovación y Universidades, Spain (MICIU/AEI/10.13039/501100011033), Xunta de Galicia under the Project ED431C2021/44 (Programa de Consolidación e Estructuración de Unidades de Investigación Competitivas (Grupos de Referencia Competitiva) and Consellería de Cultura, Educación e Universidade), and by the European Union 'ERDF A way of making Europe' "NextGenerationEU"/PRTR. Luis Gimeno-Sotelo was supported by a 'Ministerio de Ciencia,Innovación y Universidades' PhD grant (reference: PRE2022-101497) . Emanuele Bevacqua has received funding from the European Union's Horizon 2020 Research and Innovation Programme under grant agreement No 101003469. Luis Gimeno-Sotelo, Emanuele Bevacqua and Jakob Zscheischler acknowledge the European COST Action DAMOCLES (CA17109). This work has also been possible thanks to the computing resources and technical support provided by CESGA (Centro de Supercomputación de Galicia) and RES (Red Española de Supercomputación). Funding for open access charge: Universidade de Vigo/CISUG

Appendix A. Supplementary data

Supplementary data to this article can be found online at https://doi.org/10.1016/j.atmosres.2024.107413.

References

Algarra, I., Nieto, R., Ramos, A.M., Eiras-Barca, J., Trigo, R.M., Gimeno, L., 2020. Significant increase of global anomalous moisture uptake feeding landfalling atmospheric rivers. Nat. Commun. 11 (1), 1–7. https://doi.org/10.1038/s41467-020-18876-w.

Allan, R.P., Barlow, M., Byrne, M.P., Cherchi, A., Douville, H., Fowler, H.J., Gan, T.Y., Pendergrass, A.G., Rosenfeld, D., Swann, A.L.S., Wilcox, L.J., Zolina, O., 2020. Advances in understanding large-scale responses of the water cycle to climate change. Ann. N. Y. Acad. Sci. 1472 (1), 49–75. ISSN 1749-6632. https://doi.org/10.1111/nyas.14337.

Allen, M.R., Ingram, W.J., 2002. Constraints on future changes in climate and the hydrologic cycle. Nature 419 (6903), 228–232. https://doi.org/10.1038/nature01092.

Bao, J., Sherwood, S.C., Alexander, L.V., Evans, J.P., 2017. Future increases in extreme precipitation exceed observed scaling rates. Nat. Clim. Chang. 7 (2), 128–132. https://doi.org/10.1038/nclimate3201.

Bevacqua, E., Maraun, D., Vousdoukas, M.I., Voukouvalas, E., Vrac, M., Mentaschi, L., Widmann, M., 2019. Higher probability of compound flooding from precipitation and storm surge in Europe under anthropogenic climate change. Science. Advances 5 (9), eaaw5531.

Byrne, M.P., Pendergrass, A.G., Rapp, A.D., et al., 2018. Response of the Intertropical Convergence Zone to Climate Change: Location, Width, and Strength. Curr. Clim. Chang. Rep. 4, 355–370. https://doi.org/10.1007/s40641-018-0110-5.

Chang, E.K.M., Guo, Y., Xia, X., Zheng, M., 2013. Storm-Track activity in IPCC AR4/ CMIP3 Model Simulations. J. Clim. 26, 246–260. https://doi.org/10.1175/JCLI-D-11-00707.1.

Colle, B.A., Zhang, Z., Lombardo, K.A., Chang, E., Liu, P., Zhang, M., 2013. Historical Evaluation and Future Prediction of Eastern North American and Western Atlantic Extratropical Cyclones in the CMIP5 Models during the cool season. J. Clim. 26, 6882–6903. https://doi.org/10.1175/JCLI-D-12-00498.1.

Del Genio, A.D., Yao, M.-S., Jonas, J., 2007. Will moist convection be stronger in a warmer climate? Geophys. Res. Lett. 34, L16703. https://doi.org/10.1029/2007GL030525.

Dolores-Tesillos, E., Teubler, F., Pfahl, S., 2022. Future changes in North Atlantic winter cyclones in CESM-LE – Part 1: Cyclone intensity, potential vorticity anomalies, and horizontal wind speed. Weather Clim. Dynam. 3 (2), 429–448.

Donat, M.G., Lowry, A.L., Alexander, L.V., O'Gorman, P.A., Maher, N., 2016. More extreme precipitation in the world's dry and wet regions. Nat. Clim. Chang. 6 (5), 508–513.

Douville, H., Raghavan, K., Renwick, J., Allan, R.P., Arias, P.A., Barlow, M., Cerezo-Mota, R., Cherchi, A., Gan, T.Y., Gergis, J., Jiang, D., Khan, A., Mba, W.P., Rosenfeld, D., Tierney, J., Zolina, O., 2021. Water cycle changes. In: Masson-Delmotte, V.P., Zhai, P., Pirani, A., Connors, S.L., Péan, C., Berger, S., Caud, N., Chen, Y., Goldfarb, L., Gomis, M.I., Huang, M., Leitzell, K., Lonno, E., Matthews, J.B. R., Maycock, T.K., Waterfield, T., Yelekçi, O., Yu, R., Zhou, B. (Eds.), Climate Change 2021: The Physical Science Basis. Contribution of Working Group I to 45 the Sixth Assessment Report of the Intergovernmental Panel on Climate Change. Cambridge University Press, Cambridge, UK, pp. 1055–1210.

Emori, S., Brown, S.J., 2005. Dynamic and thermodynamic changes in mean and extreme precipitation under changed climate. Geophys. Res. Lett. 32, L17706. https://doi.org/10.1029/2005G L023272.

Eyring, V., Bony, S., Meehl, G.A., Senior, C.A., Stevens, B., Stouffer, R.J., Taylor, K.E., 2016. Overview of the coupled model intercomparison project phase 6 (CMIP6) experimental design and organization. Geosci. Model Dev. 9, 1937–1958. https://doi.org/10.5194/gmd-9-1937-2016.

Fernández-Alvarez, J.C., Pérez-Alarcón, A., Eiras-Barca, J., Ramos, A.M., Rahimi-Esfarjani, S., Nieto, R., Gimeno, L., 2023. Changes in moisture sources of atmospheric rivers landfalling the Iberian Peninsula with WRF-FLEXPART. J. Geophys. Res. Atmos. 128, e2022JD037612 https://doi.org/10.1029/2022JD037612.

Gimeno, L., Stohl, A., Trigo, R.M., Dominguez, F., Yoshimura, K., Yu, L., Drumond, A., Durán-Quesada, A.M., Nieto, R., 2012. Oceanic and terrestrial sources of continental precipitation. Rev. Geophys. 50 (4).

Gimeno, L., Nieto, R., Vázquez, M., Lavers, D.A., 2014. Atmospheric rivers: A mini-review. Front. Earth Sci. 2, 2. https://doi.org/10.3389/feart.2014.00002.

Gimeno, L., Dominguez, F., Nieto, R., Trigo, R., Drumond, A., Reason, C.J., Taschetto, A. S., Ramos, A.M., Kumar, R., Marengo, J., 2016. Major mechanisms of atmospheric moisture transport and their role in extreme precipitation events. Annu. Rev. Environ. Resour. 41, 117–141.

Gimeno-Sotelo, L., Gimeno, L., 2022. Concurrent extreme events of atmospheric moisture transport and continental precipitation: the role of landfalling atmospheric rivers. Atmos. Res. 278, 106356.

Gimeno-Sotelo, L., Gimeno, L., 2023. Where does the link between atmospheric moisture transport and extreme precipitation matter? Weather Clim. Extrem. 39, 100536.

Gimeno-Sotelo, L., Bevacqua, E., Gimeno, L., 2023. Combinations of drivers that most favor the occurrence of daily precipitation extremes. Atmos. Res. 294, 106959.

Gu, L., Yin, J., Gentine, P., Wang, H.M., Slater, L.J., Sullivan, S.C., Guo, S., 2023. Large anomalies in future extreme precipitation sensitivity driven by atmospheric dynamics. Nat. Commun. 14 (1), 3197.

Hauser, M., Engelbrecht, F., Fischer, E.M., 2021. Transient global warming levels for CMIP5 and CMIP6 (v0.2.0) [Data set]. Zenodo. https://doi.org/10.5281/zenodo.4600706.

Held, I.M., Soden, B.J., 2006. Robust responses of the hydrological cycle to global warming. J. Clim. 19 (21), 5686–5699.

Hersbach, H., Bell, B., Berrisford, P., Hirahara, S., Horányi, A., Muñoz-Sabater, J., Thépaut, J.N., 2020. The ERA5 global reanalysis. Q. J. R. Meteorol. Soc. 146 (730), 1999–2049.

IPCC, 2021. Annex II: Models [Gutiérrez, J M., A.-M. Tréguier (eds.)]. In: Masson-Delmotte, V., Zhai, P., Pirani, A., Connors, S.L., Péan, C., Berger, S., Caud, N., Chen, Y., Goldfarb, L., Gomis, M.I., Huang, M., Leitzell, K., Lonnoy, E., Matthews, J. B.R., Maycock, T.K., Waterfield, T., Yelekçi, O., Yu, R., Zhou, B. (Eds.), Climate Change 2021: The Physical Science Basis. Contribution of Working Group I to the Sixth Assessment Report of the Intergovernmental Panel on Climate Change. Cambridge University Press, Cambridge, United Kingdom and New York, NY, USA, pp. 2087–2138. https://doi.org/10.1017/9781009157896.016.

John, A., Douville, H., Ribes, A., Yiou, P., 2022. Quantifying CMIP6 model uncertainties in extreme precipitation projections. Weather Clim. Extrem. 36, 100435.

Kim, S., Sharma, A., Wasko, C., Nathan, R., 2022. Linking total precipitable water to precipitation extremes globally. Earth's Future 10, e2021EF002473. https://doi.org/10.1029/2021EF002473.

Lehmann, J., Coumou, D., Frieler, K., Eliseev, A.V., Levermann, A., 2014. Future changes in extratropical storm tracks and baroclinicity under climate change. Environ. Res. Lett. 9, 084002 https://doi.org/10.1088/1748-9326/9/8/084002.

Li, C., Zwiers, F., Zhang, X., Li, G., Sun, Y., Wehner, M., 2020. Changes in annual extremes of daily temperature and precipitation in cmip6 models. J. Clim. 1–61.

Miralles, D.G., Nieto, R., McDowell, N.G., Dorigo, W.A., Verhoest, N.E., Liu, Y.Y., Gimeno, L., 2016. Contribution of water-limited ecoregions to their own supply of rainfall. Environ. Res. Lett. 11 (12), 124007.

Neelin, J.D., Martinez-Villalobos, C., Stechmann, S.N., Ahmed, F., Chen, G., Norris, J.M., Lenderink, G., 2022. Precipitation extremes and water vapor: relationships in current climate and implications for climate change. Curr. Clim. Chang. Rep. 8 (1), 17–33.

Nie, J., Sobel, A.H., Shaevitz, D.A., Wang, S., 2018. Dynamic amplification of extreme precipitation sensitivity. Proc. Natl. Acad. Sci. 115 (38), 9467–9472.

O'Gorman, P.A., 2015. Precipitation extremes under climate change. Curr. Clim. Chang. Rep. 1 (2), 49–59. https://doi.org/10.1007/s40641-015-0009-3.

O'Gorman, P.A., Schneider, T., 2009. The physical basis for increases in precipitation extremes in simulations of 21st-century climate change. Proc. Natl. Acad. Sci. 106, 14773–14777.

Paik, S., An, S.I., Min, S.K., King, A.D., Kim, S.K., 2023. Emergent constraints on future extreme precipitation intensification: from global to continental scales. Weather Clim. Extrem. 100613.

Payne, A.E., Demory, M.E., Leung, L.R., et al., 2020. Responses and impacts of atmospheric rivers to climate change. Nat. Rev. Earth Environ. 1, 143–157. https://doi.org/10.1038/s43017-020-0030-5.

Pfahl, S., Wernli, H., 2012. Quantifying the Relevance of Cyclones for Precipitation Extremes. J. Clim. 25, 6770–6780.

Pfahl, S., O'Gorman, P.A., Fischer, E.M., 2017. Understanding the regional pattern of projected future changes in extreme precipitation. Nat. Clim. Chang. 7 (6), 423–427.

Priestley, M.D.K., Catto, J.L., 2022. Future changes in the extratropical storm tracks and cyclone intensity, wind speed, and structure. Weather Clim. Dynam. 3, 337–360. https://doi.org/10.5194/wcd-3-337-2022.

Riahi, K., Van Vuuren, D.P., Kriegler, E., Edmonds, J., O'neill, B.C., Fujimori, S., Tavoni, M., 2017. The Shared Socioeconomic Pathways and their energy, land use, and greenhouse gas emissions implications: An overview. Glob. Environ. Chang. 42, 153–168.

Shields, C.A., Payne, A.E., Shearer, E.J., Wehner, M.F., O'Brien, T.A., Rutz, J.J., et al., 2023. Future atmospheric rivers and impacts on precipitation: Overview of the ARTMIP Tier 2 high-resolution global warming experiment. Geophys. Res. Lett. 50, e2022GL102091 https://doi.org/10.1029/2022GL102091.

Sinclair, V.A., Rantanen, M., Haapanala, P., Räisänen, J., Järvinen, H., 2020. The characteristics and structure of extra-tropical cyclones in a warmer climate. Weather Clim. Dynam. 1, 1–25. https://doi.org/10.5194/wcd-1-1-2020.

Soden, B.J., Held, I.M., 2006. An assessment of climate feedbacks in coupled ocean-atmosphere models. J. Clim. 19 (23), 3360–6263. https://doi.org/10.1175/JCLI9028.1.

Sun, Q., Zhang, X., Zwiers, F., Westra, S., Alexander, L.V., 2021. A global, continental, and regional analysis of changes in extreme precipitation. J. Clim. 34 (1), 243–258. https://doi.org/10.1175/jcli-d-19-0892.1.

Trenberth, K.E., Dai, A., Rasmussen, R.M., Parsons, D.B., 2003. The changing character of precipitation. Bull. Am. Meteorol. Soc. 84 (9), 1205–1218.

Westra, S., Fowler, H.J., Evans, J.P., Alexander, L.V., Berg, P., Johnson, F., et al., 2014. Future changes to the intensity and frequency of short-duration extreme rainfall. Rev. Geophys. 52, 522–555. https://doi.org/10.1002/2014RG000464.

Woollings, T., Hannachi, A., Hoskins, B., 2010. Variability of the North Atlantic eddy-driven jet stream. Q. J. R. Meteorol. Soc. 136 (649), 856–868.

PAPER S3

Earth's Future

RESEARCH ARTICLE
10.1029/2023EF003629

Special Section:
CMIP6: Trends, Interactions, Evaluation, and Impacts

Key Points:
- Important differences in drought projections as a function of drought metrics
- The temporal relationship between the precipitation-based climatic metrics is high worldwide
- A weak relationship is found between climatic and ecological drought indices

Supporting Information:
Supporting Information may be found in the online version of this article.

Correspondence to:
L. Gimeno-Sotelo,
luis.gimeno-sotelo@uvigo.es

Citation:
Gimeno-Sotelo, L., El Kenawy, A., Franquesa, M., Noguera, I., Fernández-Duque, B., Domínguez-Castro, F., et al. (2024). Assessment of the global relationship of different types of droughts in model simulations under high anthropogenic emissions. *Earth's Future*, *12*, e2023EF003629. https://doi.org/10.1029/2023EF003629

Received 25 FEB 2023
Accepted 19 JAN 2024

Author Contributions:
Conceptualization: Luis Gimeno-Sotelo, Sergio M. Vicente-Serrano
Formal analysis: Luis Gimeno-Sotelo, Fergus Reig
Funding acquisition: Sergio M. Vicente-Serrano
Investigation: Luis Gimeno-Sotelo, Sergio M. Vicente-Serrano
Methodology: Luis Gimeno-Sotelo, Sergio M. Vicente-Serrano
Project administration: Sergio M. Vicente-Serrano

Assessment of the Global Relationship of Different Types of Droughts in Model Simulations Under High Anthropogenic Emissions

Luis Gimeno-Sotelo[1], Ahmed El Kenawy[2], Magí Franquesa[2], Iván Noguera[2], Beatriz Fernández-Duque[2], Fernando Domínguez-Castro[2], Dhais Peña-Angulo[3], Fergus Reig[2], Rogert Sorí[1], Luis Gimeno[1], Raquel Nieto[1], and Sergio M. Vicente-Serrano[2]

[1]Centro de Investigación Mariña, Universidade de Vigo, Environmental Physics Laboratory (EPhysLab), Ourense, Spain,
[2]Instituto Pirenaico de Ecología, Consejo Superior de Investigaciones Científicas (IPE–CSIC), Zaragoza, Spain,
[3]Department of Geography, University of Zaragoza, Zaragoza, Spain

Abstract This study provides a global analysis of the relationship between drought metrics obtained from several climatic, hydrologic and ecological variables in a climate change framework using CMIP6 model data. A comprehensive analysis of the evolution of drought severity on a global scale is carried out for the historical experiment (1850–2014) and for future simulations under a high emissions scenario (SSP5-8.5). This study focuses on comparing trends in the magnitude and duration of drought events according to different standardized indices over the world land-surface area. The spatial and temporal relationship between the different drought indices on a global scale was also evaluated. Overall, there is a fairly large consensus among models and drought metrics in pointing to drought increase in southern North America, Central America, the Amazon region, the Mediterranean, southern Africa and southern Australia. Our results show important spatial differences in drought projections, which are highly dependent on the drought metric employed. While a strong relationship between climatic indices was evident, climatic and ecological drought metrics showed less dependency over both space and time. Importantly, our study demonstrates uncertainties in future projections of drought trends and their interannual variability related to the relationship among indices, stressing the importance of coherent climatic, hydrological and plant physiological patterns when analyzing CMIP6 model simulations of droughts under a warming climate scenario.

Plain Language Summary Using climate change models, we perform a drought analysis in terms of climatic, hydrologic and ecological variables on a global scale, studying the projections under a high emission scenario. We analyze how drought events will evolve in the future with respect to their magnitude and duration, and if the different drought metrics agree in space and time. In general, models and metrics agree that there will be drought increase in southern North America, Central America, the Amazon region, the Mediterranean, southern Africa and southern Australia. However, results differ across the world and really depend on the metric used. We show that climatic indices are strongly connected with each other, but no so related to ecological ones. We also find that there are uncertainties in future projections of drought trends, highlighting that we should always take into account the spatial and temporal agreement between climatic, hydrological and plant physiological patterns when studying drought projections.

1. Introduction

Assessment of future drought projections is at the forefront of scientific debate in the current research on climate, hydrology, agriculture, and ecology. This is simply due to the multiple dimensions of droughts, which cause strong complexity for drought assessment and quantification (Douville et al., 2021; Lloyd-Hughes, 2014). In addition, the strong environmental and socioeconomic implications of drought changes in future climate scenarios adds more complexity to this debate (Naumann et al., 2021; Van Loon et al., 2016; Xu et al., 2019).

In order to robustly assess future changes in drought severity, we must refer to different types of drought. This is fundamental to properly evaluate the impacts associated with drought in future climates. Generally, the concepts of meteorological drought (precipitation deficits), agricultural droughts (crop failure or yield decrease), ecological droughts (damages in natural vegetation, reduced photosynthesis activity, and carbon uptake and increased plant mortality), and hydrological droughts (reductions in the availability of water in different sources

Earth's Future

10.1029/2023EF003629

Resources: Sergio M. Vicente-Serrano
Supervision: Luis Gimeno, Sergio M. Vicente-Serrano
Visualization: Luis Gimeno-Sotelo
Writing – original draft: Luis Gimeno-Sotelo, Ahmed El Kenawy, Magí Franquesa, Iván Noguera, Beatriz Fernández-Duque, Fernando Domínguez-Castro, Dhais Peña-Angulo, Rogert Sorí, Luis Gimeno, Raquel Nieto, Sergio M. Vicente-Serrano
Writing – review & editing: Luis Gimeno-Sotelo, Ahmed El Kenawy, Magí Franquesa, Iván Noguera, Beatriz Fernández-Duque, Fernando Domínguez-Castro, Dhais Peña-Angulo, Rogert Sorí, Luis Gimeno, Raquel Nieto, Sergio M. Vicente-Serrano

such as reservoir storages, streamflow and groundwater) are used commonly to refer to drought types. These types are largely impacted by different physical and ecological processes (Douville et al., 2021; Lobell, 2014; Vicente-Serrano, Quiring, et al., 2020; Wilhite & Buchanan-Smith, 2005).

In the literature, a wide spectrum of studies characterized drought projections on the global scale using model simulations of various climatic, hydrological, and vegetation variables under different future climates scenarios (e.g., Cook et al., 2014, 2020; Lu et al., 2019; Martin, 2018; Papalexiou et al., 2021; Ridder et al., 2022; Ukkola et al., 2020; Vicente-Serrano, Domínguez-Castro, et al., 2020; Zeng et al., 2022; Zhao & Dai, 2021; Zhu & Yang, 2021). Nonetheless, most of these studies focused on metrics directly simulated by different Coupled Model Intercomparison Projects (CMIP) since they allow to directly evaluate drought impacts on a variety of agricultural, ecological, and hydrological systems (Bachmair et al., 2016, 2018; Hlavinka et al., 2009; O'Connor et al., 2022; Quiring & Papakryiakou, 2003; Stagge, Kohn, et al., 2015; Vicente-Serrano et al., 2012).

In the literature, the most widely used drought metrics for drought monitoring and impact assessment are synthetic indices that combine precipitation and atmospheric evaporative demand (AED), allowing for a direct quantification of drought severity and drought extent (Dai, 2021; Tomas-Burguera et al., 2020; van der Schrier et al., 2013; Vicente-Serrano et al., 2010), as well as their impacts on ecosystems (Bachmair et al., 2015). For future simulations, different studies analyzed drought projections based on these indices, employing Earth System Models (ESMs) outputs under different future climate scenarios (Dai, 2012; Naumann et al., 2018; Spinoni et al., 2020; Vicente-Serrano, Domínguez-Castro, et al., 2020; Zhao & Dai, 2022). According to these scenarios, drought severity would increase, mainly as a consequence of the enhanced AED in a warming climate. Nonetheless, some studies suggest uncertainty of using these metrics (e.g., Berg & Sheffield, 2018; McColl et al., 2022). Specifically, the criticisms argue are that these indices are not necessarily representative of the metrics based on water storage (i.e., soil moisture), surface water generation (i.e., runoff) or vegetation activity (i.e., leaf area and net primary production (NPP)). These arguments would be supported by the notion that hydrological and ecological systems might show different dynamics and responses under future climates (Berg & Sheffield, 2018; Scheff, 2018). Furthermore, CMIP models generate simulations of hydrological and plant metrics, which would make it unnecessary to focus on climate metrics as proxies of drought impacts (McColl et al., 2022). Moreover, drought indices that include AED in their calculations might overestimate drought severity under high-emissions future climate scenarios. This is simply because future increase in AED is likely to be higher than the expected increase in land evapotranspiration (Et) (Milly & Dunne, 2016; Roderick et al., 2015; Scheff, 2018; Yang et al., 2019), which is also determined by water availability.

As such, a more complete spatio-temporal comparison of different drought metrics is necessary to provide a more robust picture of how drought responds to future climate and better assessment of the advantages and limitations of using drought indices based on simulations of climate variables versus the use of indices based on simulated hydrological and ecological variables. Although recent studies have analyzed global drought projections based on the latest model outputs from the CMIP6 using different drought metrics (e.g., Cook et al., 2020; Li et al., 2021; Meng et al., 2022; Papalexiou et al., 2021; Ukkola et al., 2020; Zeng et al., 2022; Zhao & Dai, 2022; Zhu and Yang, 2021), these studies lacked the opportunity to investigate some drought metrics that are important for assessing agricultural and ecological droughts. As such, a focus on these gaps may provide new evidence that provides more certainties about the use of different drought metrics to asses future trends in drought severity. On the other hand, it is necessary to test the spatial and temporal relationship among the different drought metrics, which can give indications on the reliability of drought projections. In the pursuit of this background, the objectives of this study are to:

1. know the differences in the future drought projections based on a wide set of climatic, ecological and hydrological drought metrics, providing an assessment of the regional and global coherence and uncertainty in the projections.
2. determine the spatial and temporal relationship among the different drought metrics in replicating drought severity based on the comparison of the spatial and temporal agreement of drought conditions at the annual scale.

Accordingly, the current global assessment can contribute to the arising debate on the robustness of the different drought metrics, and the existing uncertainties for agricultural, ecological, and hydrological drought projections under a high-emission climate scenario.

10.1029/2023EF003629

2. Data and Methods

We employed monthly data of a set of hydroclimatic variables from the CMIP6 experiment (Eyring et al., 2016). These variables included precipitation, runoff, total column soil moisture, leaf area index (LAI) and NPP. Data were provided for the historical period (1850–2014) and for the Shared Socioeconomic Pathway (SSP; 5–8.5) from 2015 to 2100. All CMIP6 individuals that secure data for the necessary variables, as well as the period 1850–2100, were considered in our analysis (see Table S1 in Supporting Information S1). Recalling that the CMIP6 outputs are provided in different native spatial resolutions, we interpolated data to a common resolution of $2.5° \times 2.5°$ by means of a bilinear transformation. We used this low spatial resolution in order to be conservative to avoid that the models are resampled to a higher spatial resolution than the original simulations. In general, bilinear transformation provides excellent results to convert CMIP models to a comparable spatial resolution, and it has been used for the data analysis in the IPCC reports (Gutiérrez et al., 2021; Stocker et al., 2013), being a usual procedure in climate studies (Almazroui et al., 2020; Rettie et al., 2023; Thorarinsdottir et al., 2020; Wu et al., 2022). To assess future projections in drought severity, our decision was made to consider the SSP5-8.5 scenario, which represents the worst possible scenario compared to the historical experiment, thereby accentuating the most pronounced differences among various climatic, hydrological, and ecological metrics.

The standardized drought indices were computed based on the common data inputs (e.g., precipitation, runoff, total column soil moisture, LAI and NPP). Nonetheless, other indices were computed using a combination of new variables. For example, maximum and minimum air temperatures, relative humidity, wind speed and solar radiation, were used to calculate AED following the Penman-Monteith FAO-56 equation (Pereira et al., 2015). Overall, based on these data and data of Evapotranspiration (Et), we calculated different indices using: (a) the difference between precipitation and AED (P-AED), which is a metric that has been widely used for drought assessment since it summarizes the balance between the water available in the form of precipitation and the existing AED (Tomas-Burguera et al., 2020; Vicente-Serrano et al., 2010), (b) precipitation minus land evapotranspiration (P-Et), which is considered a long-term water budget and has been accordingly used to assess drought severity in several works (e.g., Padrón et al., 2020), and (c) the difference between Et and AED (Et-AED), which compares the difference between the available water to evaporate and the water demand by the atmosphere (Kim & Rhee, 2016; Vicente-Serrano et al., 2018) and is highly related to plant water stress (Stephenson, 1990). All these drought metrics were transformed into the same standardized units to make robust spatial and temporal comparisons. To fit data distribution, a log-logistic distribution was used, which is capable of standardizing different climate and hydrological records under different climate conditions, as being evidenced in earlier works (e.g., Vicente-Serrano & Beguería, 2016; Vicente-Serrano, Domínguez-Castro, et al., 2020). The only exception was for precipitation, which was fitted to a Gamma distribution (Stagge, Tallaksen, et al., 2015). We tested the goodness of fit of the standardized indices using the Kolmogorov-Smirnov test (Kolmogorov, 1933; Smirnov, 1948), which was used to assess if they followed a normal distribution. It compares the cumulative distribution function of a data set to the theoretical normal distribution, quantifying the maximum difference (the KS statistic). The p-value represents the probability of obtaining a KS statistic as extreme as the one observed, assuming that the data follows a normal distribution (null hypothesis). A smaller p-value reveals stronger evidence against the normality assumption, while a larger p-value indicates weaker evidence. The obtained results suggest that, for the majority of world regions, the multimodel median p-value is above 0.01 and therefore we can assume that the indices that were constructed fit well to a normal distribution (Figure S1 in Supporting Information S1). Afterward, a second standardization procedure was carried out independently for each of the 12 monthly series of the indices. To make this standardization, both the mean and the standard deviation were computed for the reference period 1850–2014. This procedure minimizes the possible impacts of strong trends presented in the analyzed variables for future scenarios in the possibility of calculating the drought indices (Vicente-Serrano, Domínguez-Castro, et al., 2020). Furthermore, this standardization allows for a robust spatial and temporal comparability between the different metrics. Accordingly, drought duration and magnitude can be quantified for each time series and for the different indices. Drought events were identified using the run theory (Fleig et al., 2006; Tallaksen et al., 1997), considering a threshold of $z = -1.28$, which corresponds to a 10% probability of a standard normal observation being below that value. For drought event identification, all indices were computed at the 3-month time scale. To analyze the trends in the duration and magnitude of drought events, we used the annual values summarizing the drought conditions recorded during the different months of the year. A linear regression model was fitted as a function of time, and the estimated slope was used to quantify the amount

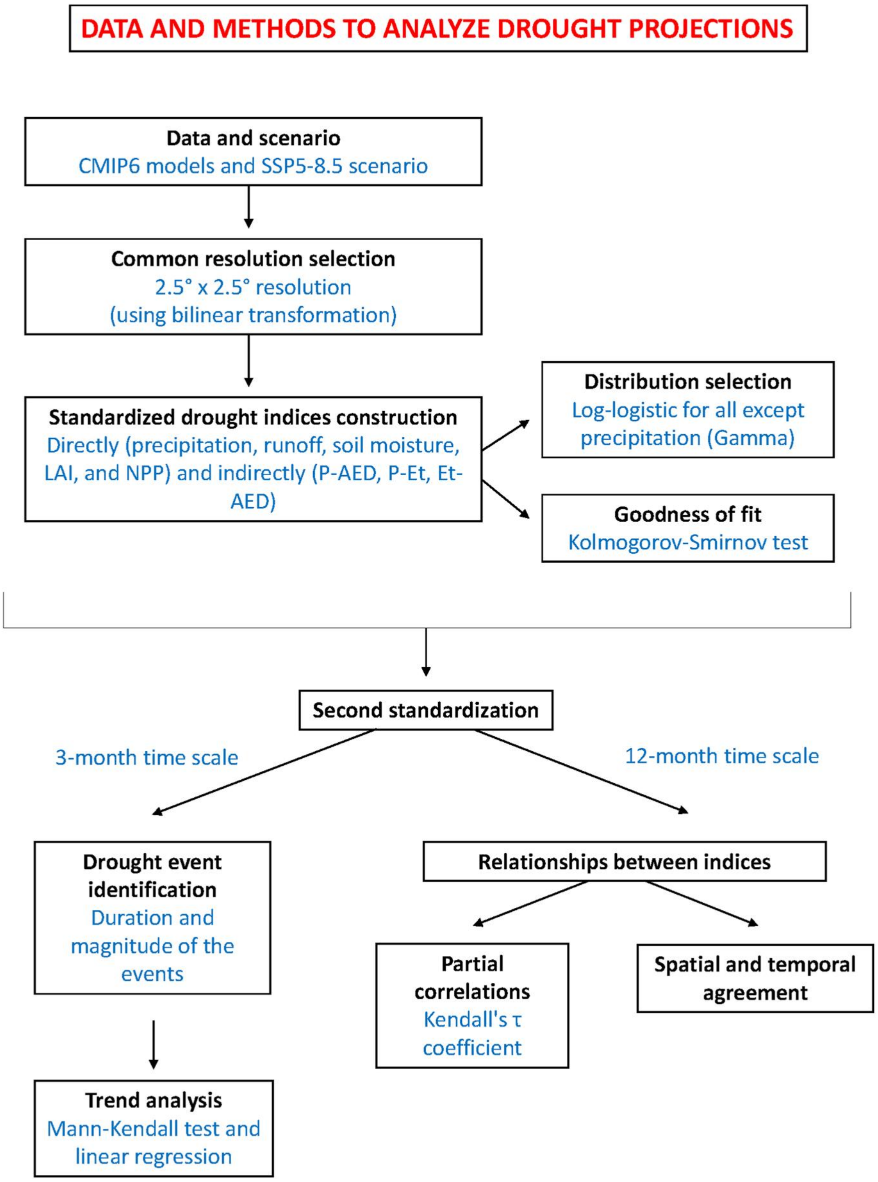

Figure 1. Workflow chart that summarizes the methodology followed in this study.

of change over time. The significance of these changes was assessed using the Mann–Kendall test (Kendall, 1948; Mann, 1945), at a significance level of $\alpha = 0.05$.

We also analyzed the relationship between the annual indices (computed at 12-month time scale) using partial correlations, which enabled us to understand the unique association between each pair of variables, while controlling for the effects of the other variables (Kim, 2015). They were computed using the Kendall's rank correlation coefficient, that is, Kendall's τ coefficient (Kendall, 1938). This coefficient is a nonparametric measure of rank correlation that is more suitable than parametric statistics (e.g., Pearson's linear correlation coefficient) because it accounts for the non-linear relationships between variables.

For each grid point, the temporal agreement between the indices (computed at 12-month scale) was assessed by obtaining the percentage of simultaneous occurrence of years in which a pair of indices were below $z = -1.28$, thus producing a 2-dimensional representation of the results. Also, we computed the percentage of grid points where each pair of indices showed z-value below -1.28, resulting in a time series.

A workflow chart that summarizes the methodology followed in this study can be found in Figure 1.

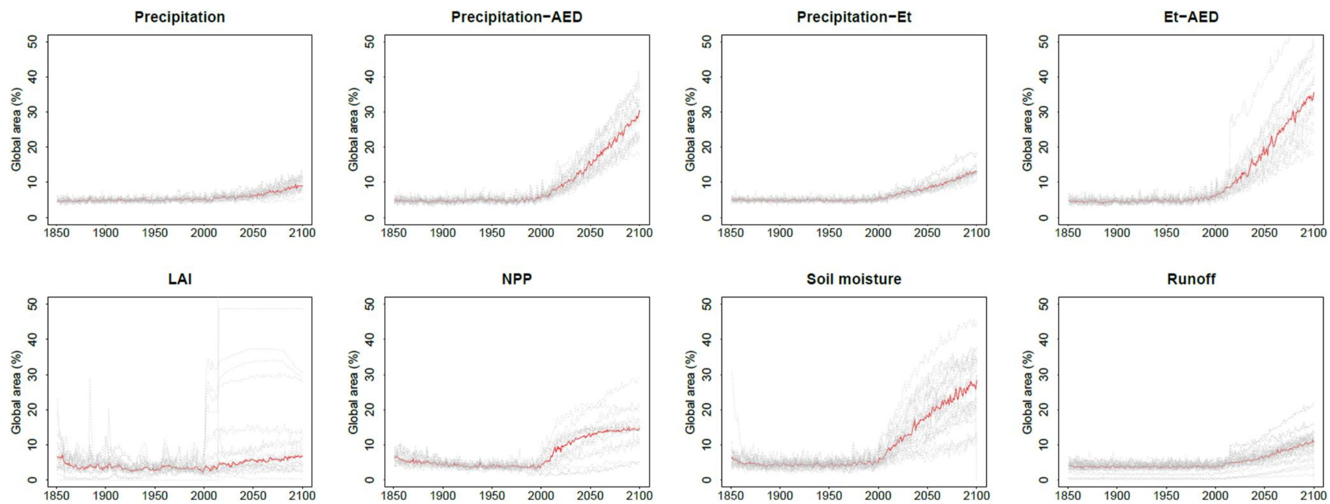

Figure 2. Evolution of the annual average percentage of global land area affected by extreme dry conditions (5%) from 1850 to 2100. Gray lines represent the value for the different independent models and red lines refer to the median.

3. Results

3.1. Evolution of Drought Severity Based on Different Metrics

Figure 2 shows the evolution of the world land surface affected by drought between 1850 and 2100. It is computed as the percentage of land grid points below the fifth percentile of each raw (non-standardized) variable. This percentile is computed independently for each month, considering the 1850–2014 reference period. For all the variables, we found an increase in the world land surface impacted by dry conditions from 1850 to 2010, albeit with some considerable spatial differences. Results demonstrate that precipitation, leaf area, and runoff would likely show a small increase of drought severity in the future. For precipitation-Et and NPP, the increase is mostly intermediate, although a sharp increase in NPP is noted between 2010 and 2030, followed by a constant behavior to the end of the twenty-first century. The possible mechanisms of this sharp increase are not well determined but probably this would be caused by discontinuities in the radiative forcing of the historical and the SSP 5–8.5 scenarios. It can be a feature of certain problem for the temporal comparability of the model outputs considering periods covered by different forcing experiments. For precipitation-AED, Et-AED and soil moisture, a remarkable increase is noted at the end of the twenty-first century. As illustrated in Figures S2 and S3 in Supporting Information S1, some variables exhibited important seasonal and regional differences. For example, during the boreal winter season, drought based on NPP, soil moisture, and Et-AED increase. Rather, for precipitation and runoff, irrelevant drought increase is noted from 1850 to 2100. On the contrary, in the boreal summer season, the main drought increase is recorded for precipitation-AED, Et-AED, and soil moisture, with little increase for other variables (e.g., precipitation, runoff, and precipitation-Et).

Overall, we noted an increase in the magnitude of drought events that affects large areas of the world in terms of precipitation-AED, Et-AED, and soil moisture, albeit with significant spatial differences (Figure 3). Interestingly, these three drought metrics showed a high agreement in terms of the areas that are likely to exhibit the highest increase in the magnitude of drought periods, including the Mediterranean region, Central America, northern South America and western South America, West Africa and South Africa. Nevertheless, it can be noted that the areas affected are much larger using Et-AED metric, with almost the entire land showing an increase in drought severity. Meteorological droughts, based on precipitation, show an increase in drought magnitude in areas of Central and South America, West Africa, South Australia and the Mediterranean region, although this increase is not as high as suggested by other drought indices (i.e., Et-AED, and soil moisture). This pattern is almost similar when considering precipitation-Et, although some areas of South America did not show an increase in drought severity, suggesting that—in specific regions-the increase in drought magnitude can be reduced if Et is included in the calculations. Drought magnitude trends based on runoff show smaller changes than considering exclusively precipitation, suggesting that CMIP6 models project a less increase in the magnitude of hydrological droughts than in the magnitude of meteorological (precipitation) droughts in a high emissions scenario. LAI did not show

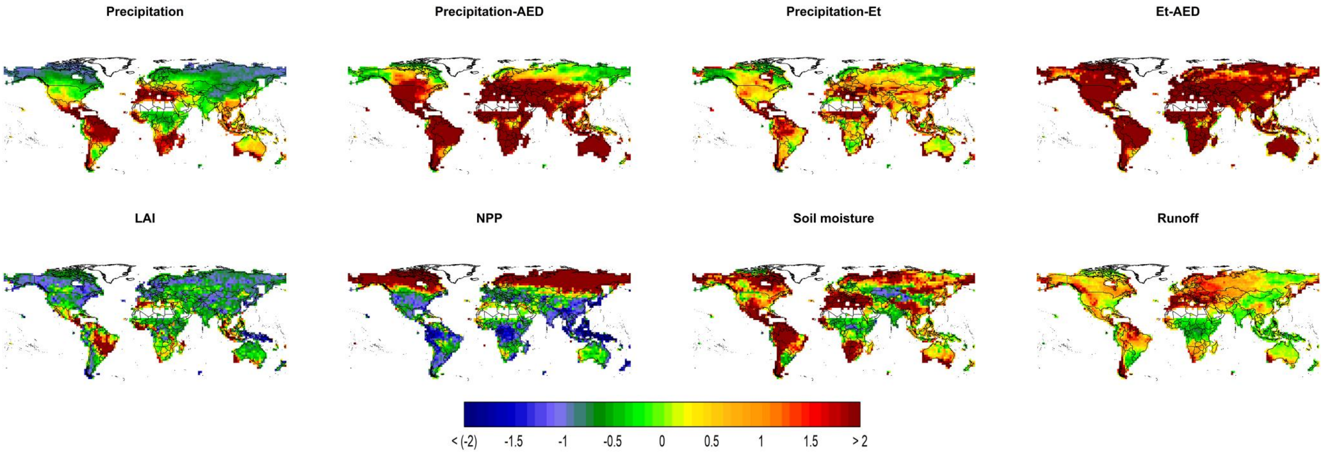

Figure 3. Spatial distribution of the median trend in the magnitude of drought events between 1850 and 2100 (Factor: 100).

an increase in the magnitude of drought events in large areas of the world, except for parts of East Brazil. Thus, the spatial pattern was sparse on the global scale, with strong regional variability and a dominance of no changes or decrease in the magnitude of drought events in some regions (e.g., South America, Southeast Asia, Central Europe, and North America). Notably, the NPP-based assessment showed a strong reinforcement of drought magnitude in the high latitudes of the Northern Hemisphere. Rather, in some areas of Africa, South America and Southeast Asia, a decrease in the magnitude of the drought episodes, based on the NPP, was noted. Changes in the duration of drought events were almost similar to those of drought magnitude, particularly in terms of spatial patterns and the behavior of the different drought metrics (Figure S4 in Supporting Information S1).

Some drought metrics show high consistency in identifying positive trends in drought magnitude among the different models. Figure 4 shows the percentage of models showing positive and statistically significant trends in drought magnitude between 1850 and 2100. As depicted, almost all models defined the same the regions with strong increase in drought magnitude considering precipitation-AED and Et-AED. This agreement was much lower for soil moisture, even in large regions where the multimodel median values showed an increase in drought magnitude. A representative example is found in southern North America and South Africa, where multimodel medians showed a large increase in drought magnitude, while less than 40% of the models showed a positive and significant trend. In other regions whereas decline in drought magnitude was observed like northern South America or the Mediterranean, the percentage of models showing significant declining trends was roughly 50%, suggesting a strong uncertainty in model projections. Notably, although precipitation, precipitation-Et and runoff showed a drought increase in fewer regions than soil moisture, the consistency of this increase among models seems to be greater. More than 50% of the models suggest a positive and statistically significant increase in drought magnitude in northern South America and Central America, the Mediterranean and southern Africa for

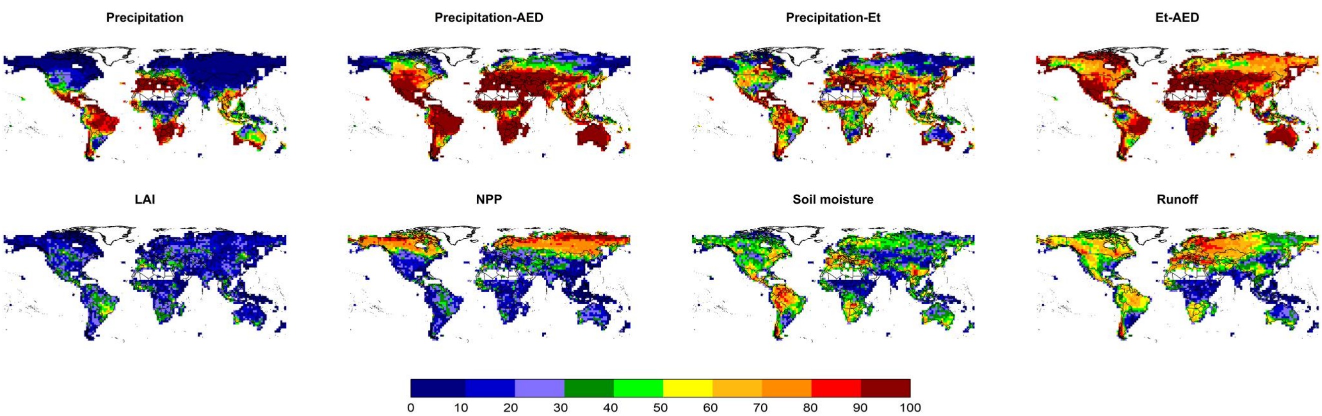

Figure 4. Percentage of models showing positive and statistically significant trends in drought magnitude from 1850 to 2100.

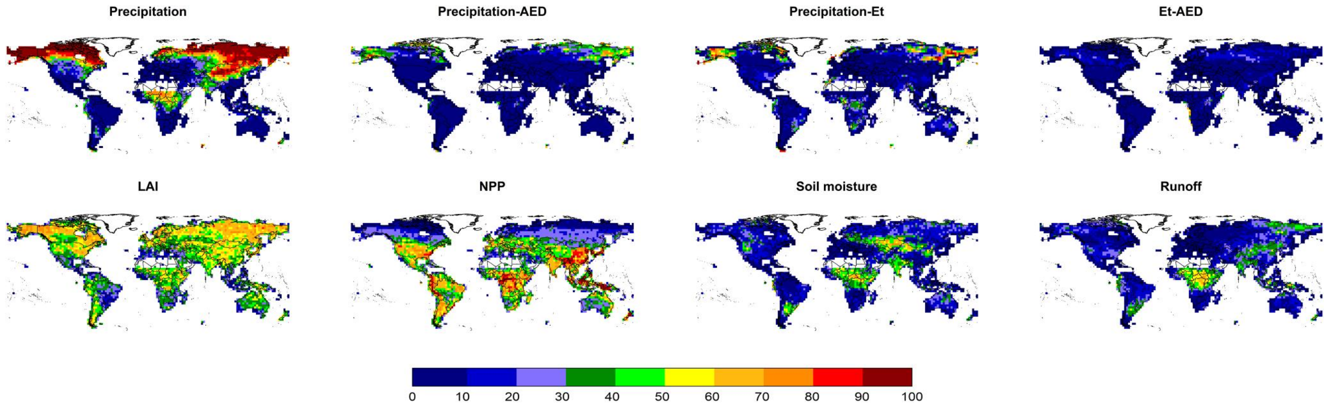

Figure 5. Percentage of models showing negative and statistically significant trends in drought magnitude from 1850 to 2100.

precipitation. A similar pattern was evident for vast areas in North and South America, Central Africa, and Central and South Asia when considering P-Et. This suggests that Et projections suppress the trend toward higher drought magnitudes in Southern Africa in comparison to precipitation-based projections, with only few models showing a positive and statistically significant trend. Interestingly, for runoff almost 50% of the models suggested a significant increase in drought magnitude in large regions of the Northern Hemisphere (e.g., Alaska, Labrador, Scandinavia, West Russia), while they did not witness a relevant increase in drought magnitude based on precipitation and precipitation-Et metrics. In the same context, apart from the high latitudes of the Northern Hemisphere, there were no regions where more than 30% of models showed an increase in drought magnitude for the NPP. Interestingly, results demonstrate that drought magnitude based on LAI will not change anywhere worldwide, with almost no model suggests significant changes.

Like drought magnitude, similar patterns of drought duration changes were observed globally (Figure S5 in Supporting Information S1), with majority of the models suggesting no significant changes in ecological and agricultural droughts across majority of the world regions under scenarios of high greenhouse gas emissions.

The negative trends in drought magnitude (Figure 5) and duration (Figure S6 in Supporting Information S1) indicated few regions and metrics in which the models agree on a decrease in drought severity, mainly for precipitation in the high latitudes of the Northern Hemisphere. Even for LAI and NPP, the percentage of models that showed a decrease in drought magnitude is low. As depicted, although some areas, based on some metrics, showed a projected decrease in drought duration and magnitude with multimodel medians (e.g., Southeast Asia with LAI, Central Africa with the NPP, West Russia with soil moisture), there is still large inconsistency among the models. In the same context, while a steady increase in drought duration and magnitude was projected for some regions and variables, only few areas witnessed a decrease in drought duration and magnitude, irrespective of drought metric used. Thus, although there are important uncertainties between drought metrics and models related to the increase of drought duration and magnitude, there is a high consistency between models and metrics concerning drought decrease since drought magnitude and duration are not expected to decrease under a scenario of high greenhouse gasses emissions.

3.2. Spatio-Temporal Relationships Among Drought Metrics

In addition to knowing the consistency of trends between different drought metrics and models, it is also relevant to analyze the consistency of the temporal relationship in the drought severity based on these metrics (Figure S7 in Supporting Information S1). As illustrated, we found strong annual relationships between some pairs of drought indices in the historical period. For example, the correlation was higher than 0.8 between precipitation and precipitation-AED and between precipitation and precipitation-Et in most areas of the world. Also, a high correlation was observed between precipitation-AED and precipitation-Et, with few exceptions, mainly in arid and semiarid regions where correlations decreased. Other pairs of drought metrics showed lower relationships on global scale, with important spatial differences. For example, the relationship between precipitation and Et-AED was only high in water-limited regions, where Et is mostly determined by water availability. It is worth mentioning that the relationship between precipitation (and also between the other climatic metrics) and soil moisture was low in most regions. Thus, the correlation with soil moisture was higher considering precipitation-AED and particularly Et-AED in regions like South America, Africa, and South Asia. LAI and NPP showed high correlations particularly in water-limited and cold regions. Nevertheless, these two ecological variables showed low correlations with the different meteorological drought metrics, suggesting that the interannual variability of agricultural and ecological droughts simulated by models is independent from those of climatic droughts in most regions of the world. This pattern was also observed considering soil moisture, with low correlations found between the interannual variability of soil moisture and the NPP and LAI in most regions, irrespective of biome types and bioclimatic conditions. The relationship between precipitation and runoff was high in most regions of the world, except for North America and most of Eurasia. In contrast, the relationship between interannual variability of runoff and soil moisture tended to be low globally, apart from the Mediterranean, northern South America, and Africa. Similarly, ecological metrics (i.e., NPP and LAI) showed low correlations with runoff worldwide.

Overall, these results suggest that, except for the high relationship between different climate metrics and their corresponding spatial differences that are mainly determined by the average water availability and temperature, the temporal relationship between different drought metrics was generally low in most regions of the world. This relationship was particularly low between climatic and vegetation metrics, as well as between soil moisture and other drought metrics.

The spatial pattern and the magnitude of the temporal relationships between the different variables, analyzed by means of partial correlations, did not show important changes considering future simulations (2015–2100), as compared with historical simulations (Figure S8 in Supporting Information S1), albeit with some important exceptions (Figure 6). For example, the relationship between the interannual variability of precipitation and other climatic drought metrics generally decreased, which is quite relevant in some areas of Central Asia considering precipitation-AED, but also in the Sahel and high latitudes of the Northern Hemisphere considering Et-AED. On the contrary, the relationship between precipitation and precipitation-Et remained stable for both the historical period and future. Also, we found a decrease in the relationship between precipitation-AED and precipitation-Et in some regions of Europe, South America, and Africa. The relationship between LAI and NPP was stable for the historical period and future simulations in most regions, albeit with a trend to reinforce in some regions. In addition, the relationship between precipitation and LAI tended to reinforce in the high latitudes of the Northern Hemisphere. This was also observed with the NPP, although a decline in the correlation between precipitation and NPP was observed in the Mediterranean, southern North America and northern South America. While the relationship between NPP and precipitation-AED was low during the historical period, this relationship was projected to decline further in the future, particularly in arid regions, the Amazon basin, and some wet areas of Africa. The decrease in the relationship with the NPP was even more severe when considering Et-AED, with an overall global decline. In addition, the relationship between NPP and soil moisture is likely to decline over large areas (e.g., the Mediterranean, northern South America, southern Africa, and Australia). Finally, the relationship of the runoff to other drought metrics tended to be stable between the historical period and the future high emission scenario, although a decreasing correlation with precipitation was observed in Scandinavia, and particularly with precipitation-AED and Et-AED in most Africa and the Amazon basin.

The temporal agreement in drought conditions among the different metrics is small in most regions during the historical period (Figure S9 in Supporting Information S1), suggesting that the annual drought conditions tend to differ noticeably between metrics. There was some agreement in the identified drought periods between precipitation and precipitation-AED, except in arid lands. A similar pattern was also noted between precipitation and precipitation-Et in wet regions and between precipitation-AED and Et-AED in arid lands. Nevertheless, the agreement in the occurrence of droughts between climatic, ecologic, and hydrologic metrics was small. Herein, it is worth to note that while our analysis is restricted to annual droughts to reduce the role of seasonality and the lags in the response of hydrological, agricultural and ecological drought conditions to meteorological droughts and irrespective of the physical consistency among models, drought periods mostly do not coincide in time among the different metrics. For the projected scenario, the temporal agreement between metrics shows some increase (Figure S10 in Supporting Information S1). This is particularly relevant in some regions, such as the Mediterranean region, southern Africa, the Amazon basin, and Central America when comparing drought episodes recorded with precipitation and precipitation-AED, precipitation-Et, Et-AED and soil moisture and also between precipitation-AED and precipitation-Et and between Et-AED and soil moisture, particularly in water-limited regions. The agreement in the temporal identification of drought conditions also increases when comparing

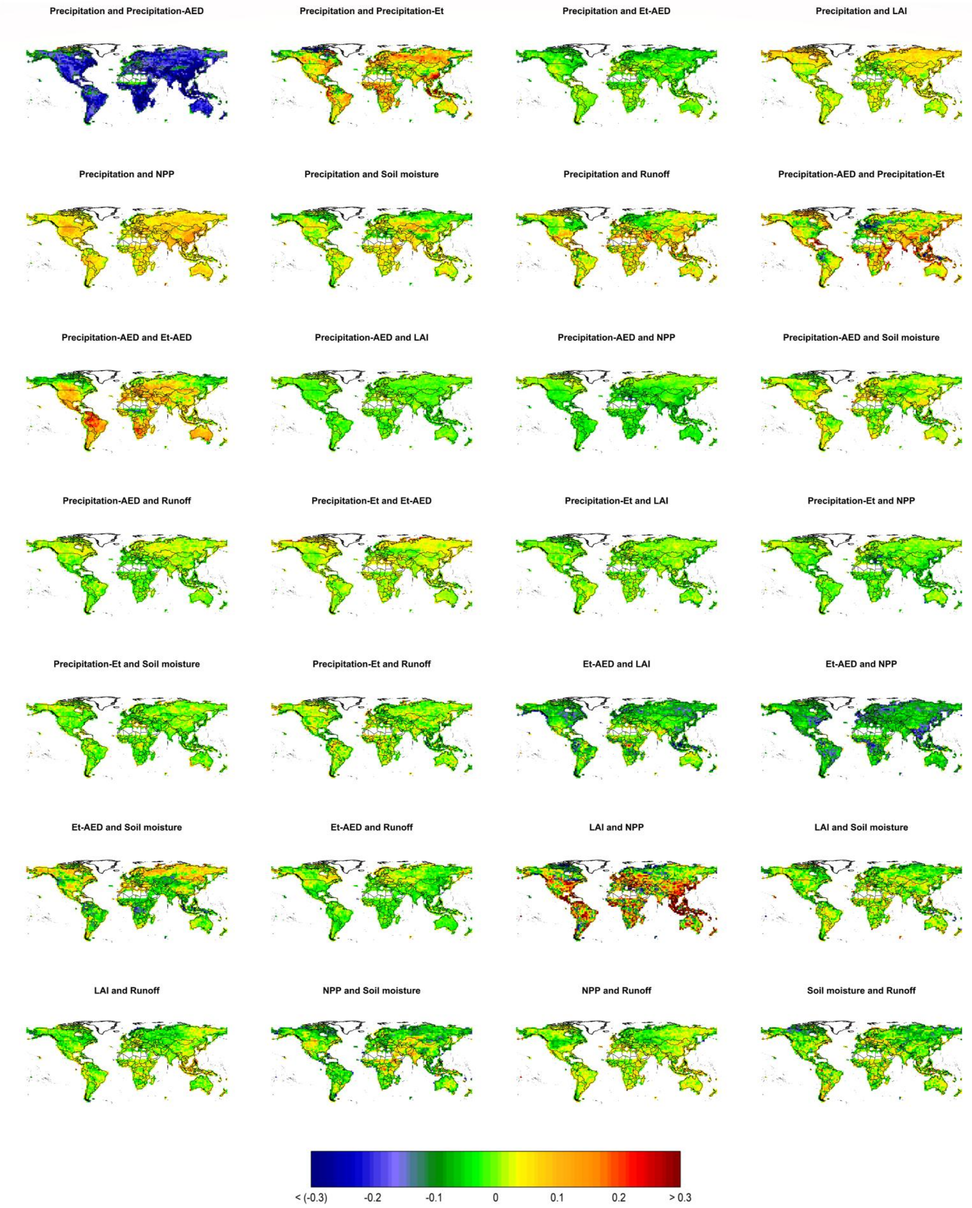

Figure 6. Differences in the median Kendall's τ partial correlations between the projected (2015–2100) and historical period (1850–2014) for the different models.

the climatic indices and the runoff in some areas, particularly in the Amazon and the humid regions of Africa, suggesting an agreement in annual droughts between some pairs of drought metrics, especially in water-limited or humid regions (Figure 7).

The temporal agreement between annual droughts was low during the historical period between the different metrics, and also with low spatial agreement, suggesting that the global spatial patterns of annual drought severity usually did not agree between drought metrics obtained from CMIP6 simulations (Figure 8). The spatial agreement of drought conditions tends to increase under future climate change, in particular for some metrics (e.g., precipitation-AED and precipitation-Et, precipitation-AED and Et-AED, precipitation-AED and soil moisture). Nevertheless, the spatial agreement between droughts on the annual scale between climatic indices, runoff, and ecological droughts was low in both the historical experiment and the projected scenario, indicating spatial differences in replicating annual droughts among the different drought metrics obtained from ESMs.

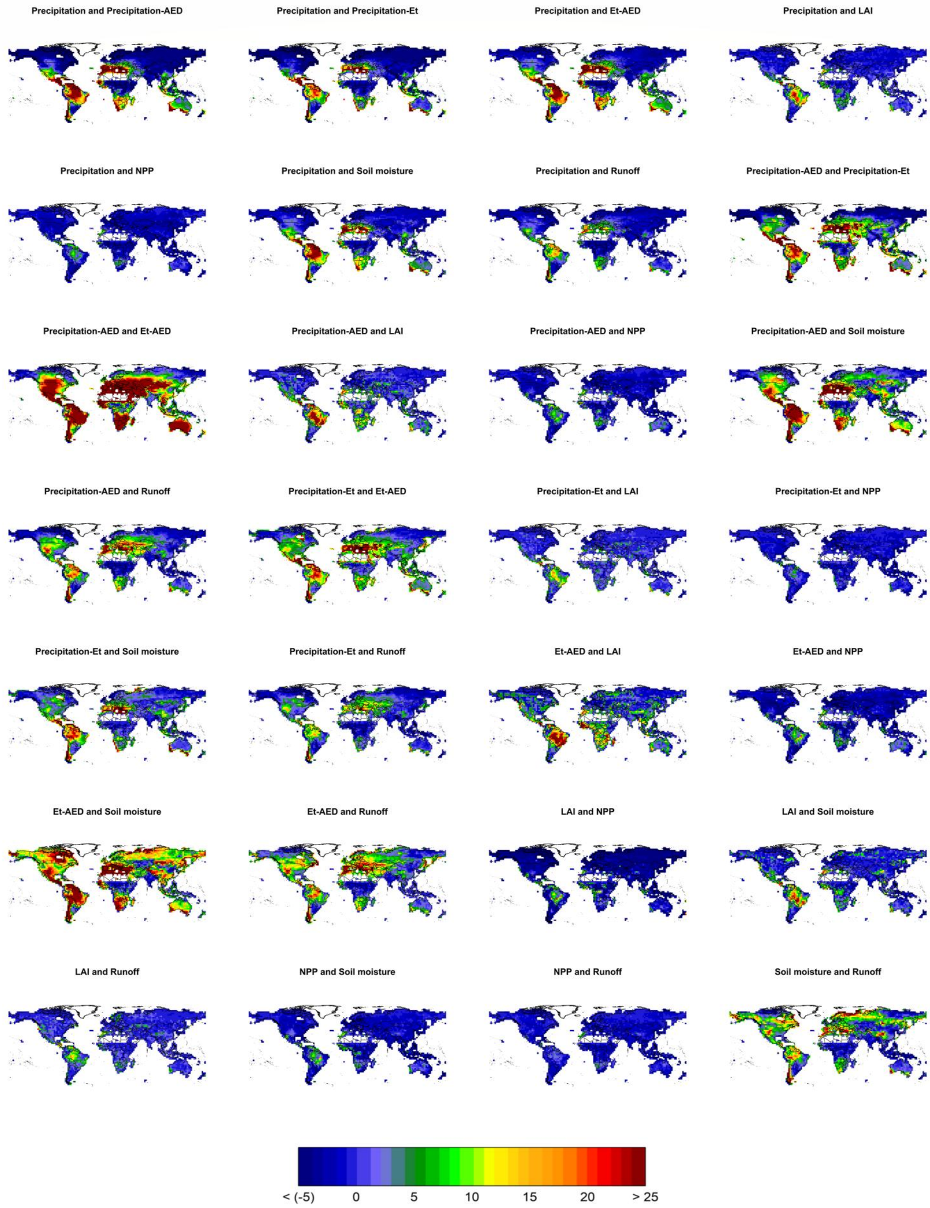

Figure 7. Differences in the average percentage of temporal agreement among the different metrics between the projected (2015–2100) and the historical period (1850–2014) for the different models.

4. Discussion

This study analyzed long-term evolution of different drought metrics on a global scale using CMIP6 models from 1850 to 2100. These metrics represent different climatic, hydrologic, and ecological variables. Results were presented for the historical experiment (1850–2014) and future projections (2015–2100) under a high-emission scenario (SSP5-8.5). While numerous studies assessed drought severity for future climate using CMIP6 models (e.g., Cook et al., 2020; Guo et al., 2022; Papalexiou et al., 2021; Ukkola et al., 2020; Wang et al., 2021; Zhao & Dai, 2022), our assessment employed a larger number of drought metrics, including climate-based (precipitation, precipitation-AED, precipitation-Et, Et-AED), hydrological-based (soil moisture and runoff) and plant physiology-based metrics (LAI and NPP). An evaluation of this variety of different metrics is essential to assess different drought types (meteorological, agricultural/ecological and hydrological) and to determine their consistency in terms of projected drought severity.

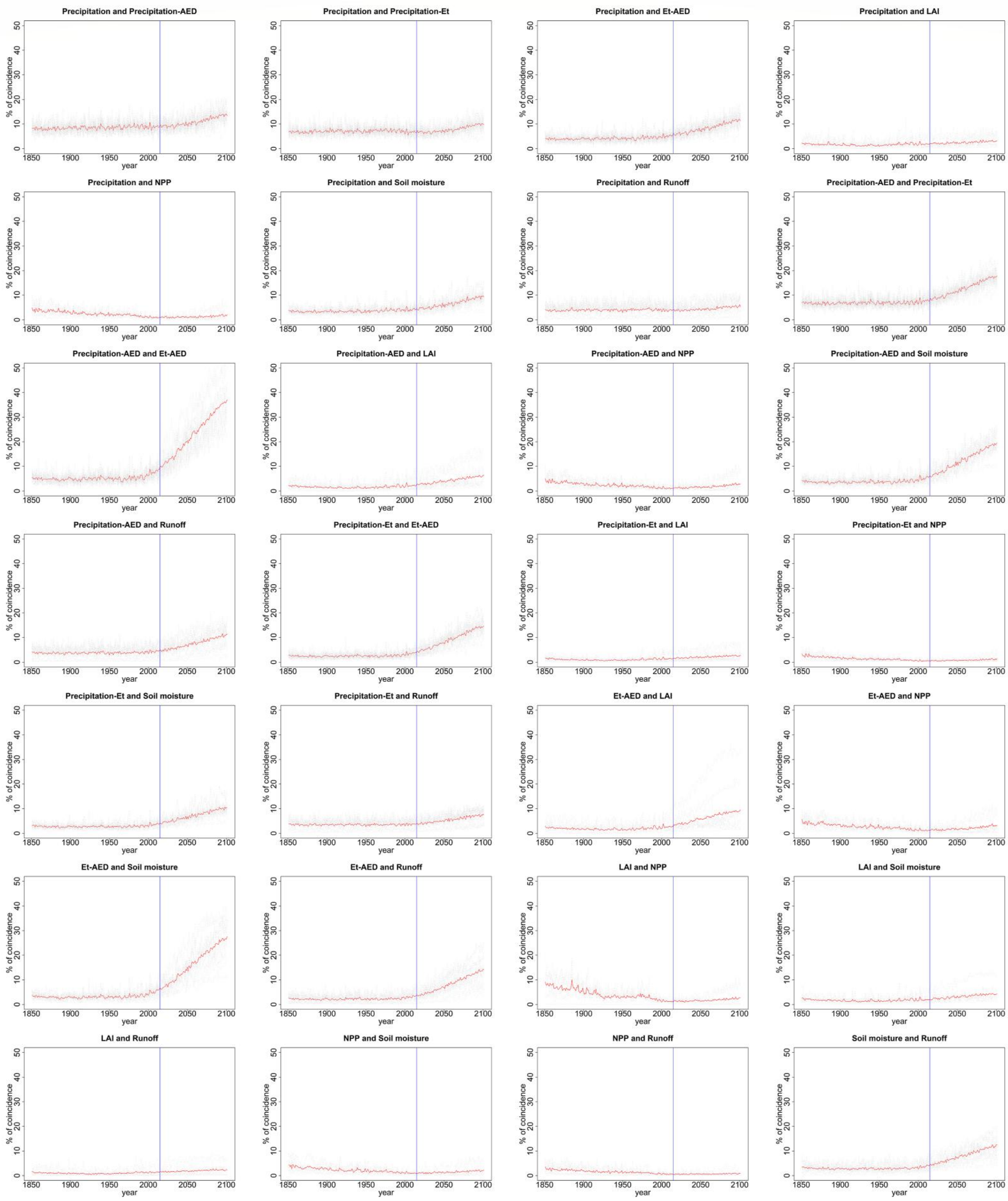

Figure 8. Evolution of the spatial agreement of dry conditions between the different drought metrics.

4.1. Global Drought Projections Based on Different Metrics

Our results, as suggested by most models and drought metrics, suggest that in a high emissions scenario drought would increase in southern North America, Central America, the Amazon region, the Mediterranean, southern Africa, and southern Australia, which agrees with earlier studies (e.g., Cook et al., 2020; Seneviratne et al., 2021; Ukkola et al., 2020; Wang et al., 2021; Zhao & Dai, 2022). These projections must be considered carefully since the models are affected by substantial biases (Adeyeri et al., 2022, 2023), strong differences with the trends in observations during the historical period (Vicente-Serrano, Miralles, et al., 2022b) and limitations to consider key ecohydrological processes (e.g., the interactions between plant root systems, soil moisture and runoff generation with groundwater) (Miguez-Macho & Fan, 2021; Ndehedehe et al., 2023).

In accordance with previous studies (Cook et al., 2020; Scheff et al., 2021), our results showed important differences in drought projections as a function of drought metrics. For example, the use of AED-based drought metrics (e.g., the Standardized Precipitation Evapotranspiration Index (SPEI)) revealed that drought severity is likely to enhanced in future, as compared to those metrics based on precipitation, precipitation-Et, and runoff. This finding agrees with some investigations based on CMIP6 (e.g., Zeng et al., 2022), and CMIP5 outputs (e.g., Cook et al., 2014) and also by studies that employed other metrics like the Palmer Drought Severity Index (PDSI) (e.g., Scheff et al., 2021; Yang et al., 2021; Zhao & Dai, 2022). The different magnitude of drought projections as simulated based on hydrological (i.e., runoff) and climatic drought indices (which use AED in the calculations) is behind the suggested overestimation of drought severity based on climatic indices under high emissions climate change scenarios (Berg & McColl, 2021; Berg & Sheffield, 2018; Greve et al., 2019; Scheff, 2018).

While it can be argued that focusing on the metrics directly indicative of impacts in agricultural, ecological and hydrological systems (i.e., soil moisture, runoff, NPP, and LAI) instead of climatic proxies of drought severity can be a more practical approach (McColl et al., 2022), it is necessary to note that models show higher uncertainties in simulating complex hydrological and plant physiology processes than climate variables, irrespective of the existing uncertainties related to the simulation of different meteorological processes and also the possible coupling mechanisms between the land and the atmosphere. For example, the spatial and temporal variability in soil moisture involves several processes, some of them are unknown, while others are difficult to simulate (Lu et al., 2019; van den Hurk et al., 2011). This may explain poor agreement between soil moisture observations and model simulations (Ford & Quiring, 2019; Yuan & Quiring, 2017). Streamflow generation is also very complex and models usually fail to simulate hydrological droughts (Barella-Ortiz & Quintana-Seguí, 2018; Tallaksen & Stahl, 2014). Plant physiology is also a key factor controlling both hydrological, agricultural and ecological droughts, and models show strong limitations and uncertainties in simulating plant physiological processes and water interchanges with soil and atmosphere (Liu et al., 2020). These problems are even more important for future climate projections (Gentine et al., 2019) in which the models show strong uncertainties when simulating plant physiological processes (Padrón et al., 2022), and other processes may introduce other sources of uncertainty (e.g., the role of atmospheric CO_2 concentrations) (De Kauwe et al., 2021; Vicente-Serrano, Miralles, et al., 2022). For example, Li et al. (2023) have showed very difficult to separate the radiative and physiological effect of the CO_2 concentrations on hydrological and ecological simulations. These authors showed that the increase of the water use efficiency by plants associated to CO_2 is limited by the increase of the temperature and the vapor pressure deficit. This mechanisms could enhance vapotranspiration and plant water stress under scenarios characterized by a high warming (as the SSP5-8.5 used here). In fact, these mechanisms seem to be incompatible with the limited increase of drought severity based on runoff and soil moisture projections. For these reasons, although some studies argue that ecological and hydrological drought metrics obtained from model simulations may be more accurate than AED-based climatic indices, we should consider that these metrics are affected by stronger biophysical and hydrological uncertainties. On the contrary, the drought indices based on climate variables, although simpler conceptually, would be less constrained by these problems.

One of the novelties of our study is the use of diverse metrics, which is fundamental to address drought characteristics and impacts. In particular, we employed the Standardized Evapotranspiration Deficit Index (SEDI), based on the difference between Et and AED, which is informative on plant water stress (Alsafadi et al., 2022; Jiang et al., 2022; Kim & Rhee, 2016; Li et al., 2019, 2020; Vicente-Serrano et al., 2018; Zhang et al., 2019) with several biogeographic implications (Stephenson, 1990). Changes in the SEDI, both in spatial patterns and drought severity, were almost similar, or even stronger than those obtained by the SPEI, and are characterized by an increase in drought severity under future scenarios of high anthropogenic emissions. In addition, we used two eco-physiological metrics, LAI and NPP, which have been considered by few studies as metrics of drought severity in model simulations (e.g., Scheff et al., 2021). As opposed to the SEDI, our assessment based on the LAI and NPP did not suggest an increase in agricultural and ecological drought severity, except for the high latitudes of the Northern Hemisphere. This regional pattern may be explained by the role of snow and permafrost melt processes that could affect water availability (Chen et al., 2021).

4.2. Uncertainties in Ecological Drought Projections

The picture provided by the eight drought metrics showed some paradoxical projections that are difficult to explain by plant physiological processes. In particular, different studies focusing on plant physiology have highlighted that plant mortality could strongly increase in the future as a consequence of increased plant water stress and air temperature (e.g., Brodribb et al., 2020; McDowell & Allen, 2015; Williams et al., 2013; Xu et al., 2019). This assessment is consistent with observations of ecological and agricultural impacts of droughts, which have reinforced by the observed increase in AED (Allen et al., 2010; Asseng et al., 2015; Breshears et al., 2005, 2013; Carnicer et al., 2011; Lobell et al., 2011; Sánchez-Salguero et al., 2017). In opposition to this empirical evidence and also to the strong increase of drought severity as suggested by some climatic indices, LAI-based drought projections suggest small changes in drought severity in the future high-emissions scenario.

This limited increase in drought severity based on ecological metrics is difficult to be supported according to the widely known response of plants to water availability (Vicente-Serrano, Quiring, et al., 2020) and atmospheric water demand (Breshears et al., 2013; Grossiord et al., 2020), particularly in water-limited regions where meteorological droughts (e.g., southern Africa, southern North America, and the Mediterranean), and AED are projected to increase (Scheff & Frierson, 2015; Vicente-Serrano, McVicar, et al., 2020). These conditions would lead to a remarkable increase in plant water stress incompatible with increases in LAI and NPP. Thus, the unique explanation of limited increase in ecological droughts in water-limited regions, where climate aridity is projected to increase, is related to the physiological effects of the atmospheric CO_2 concentrations (Gonsamo et al., 2021; Mankin et al., 2017; Scheff et al., 2022). Several studies have showed a reduction in the leaf stomatal conductance and plant resistance to water stress in response to enhanced atmospheric CO_2 concentrations (e.g., Ainsworth & Long, 2005; Ceulemans & Mousseau, 1994; Donohue et al., 2013; Green et al., 2020). However, the effects of increasing CO_2 concentrations on ecological and agricultural drought severity are very complex (Allen et al., 2015; De Kauwe et al., 2021), and there are still several uncertainties in the assessment of these effects based on ESMs (De Kauwe et al., 2021; Gentine et al., 2019), which tend to overestimate the effects of increasing CO_2 concentrations on plant physiology (Kolby Smith et al., 2015; Marchand et al., 2020; Zhao et al., 2020). Moreover, CO_2 effects would not ameliorate plant stress during periods of water deficit, given that leaf stomatal conductance would not be controlled by CO_2 concentrations, but mostly by soil moisture content (Menezes-Silva et al., 2019; Morgan et al., 2004; Xu et al., 2019). Therefore, the assessment of future agricultural and ecological droughts based on model simulations should be considered highly uncertain given the current evidence of the responses of plants to enhanced water stress and AED and the several sources of uncertainty in the modeling of the carbon cycle by the ESMs (Padrón et al., 2022). Thus, it is difficult to support that ecological droughts will not increase in areas in which models show a strong decrease in precipitation and a remarkable increase in AED.

4.3. Uncertainties in Hydrological Drought Projections

Our results indicate that future projections of droughts quantified with soil moisture tend to resemble the pattern of the projections of drought severity using precipitation-AED. This seems to disagree with some previous studies that had suggested less increase in soil moisture deficits than the decrease in meteorological indices including AED in future drought projections (Berg & Sheffield, 2018; Milly & Dunne, 2016). This disagreement can be basically explained by the different statistical methods used to assess the future projections of these metrics. The assessment is strongly affected by the autocorrelation of some of the drought metrics (e.g., the PDSI), as well as by focusing on changes in the average values versus the tails of the complete set of the distribution values (Vicente-Serrano, Domínguez-Castro, et al., 2020). Thus, the last IPCC report has showed a strong increase in drought severity worldwide based on extreme events of the total column soil moisture, particularly during the boreal summer season (Seneviratne et al., 2021). This increase in the duration and magnitude of soil moisture deficits would be coherent with an increase in agricultural and ecological drought severity, even more considering the strong increase in AED, as projected by the CMIP models (Scheff & Frierson, 2015; Vicente-Serrano, McVicar, et al., 2020d), which would cause enhanced plant stress. Also, uncertainties in the projected Et are noticeably affect drought projections based on precipitation-Et, which is usually considered a metric of water availability. Thus, the projections of precipitation showed a stronger increase in drought duration and magnitude than projections based on precipitation-Et and runoff, which seems to introduce some incoherence regarding to what would be expected with Et in a warming world. It would be expected that hydrological droughts will not increase at similar rates of agricultural and ecological droughts, in response to increased AED. This is basically because the response of streamflow to enhanced AED is expected to be lower than to precipitation, as observed with streamflow data (Ficklin et al., 2018; Vicente-Serrano et al., 2019; Yang et al., 2018). This issue has been well-established based on the ESMs, as runoff simulations mostly respond to precipitation at short time scales (Scheff et al., 2022). However, even responding more to precipitation than to AED, it is difficult to support a smaller increase in drought severity by runoff than by precipitation under scenarios of a high increase in AED. Probably, this behavior would be explained by the suppression of Et as a consequence of the decreased leaf stomatal conductance given the enhanced atmospheric CO_2 concentrations, which would reduce the severity of hydrological droughts (Milly & Dunne, 2016; Roderick et al., 2015; Yang et al., 2019). However, a main constrain of this assessment is that the influence of this mechanism on future Et is highly uncertain in ESMs (Vicente-Serrano, García-Herrera, et al., 2022). Moreover, Et is also observed to increase during dry periods (Zhao et al., 2022) and evaporation in surface water bodies is expected to increase in future scenarios (Wang et al., 2018). For these reasons, we find uncertain to support that hydrological droughts quantified using precipitation-Et and runoff would increase less than meteorological droughts, based on precipitation.

4.4. Relationship Among Drought Metrics

In addition to the comparative assessment of drought trends based on different drought metrics, another aspect of novelty in our study is that it assesses the spatial and temporal relationship between different drought metrics under the historical experiment and future SSP5-8.5 scenario. Specifically, we found that the temporal relationship between the precipitation-based climatic metrics (i.e., precipitation, precipitation-AED, and P-Et) is high worldwide, with some spatial exceptions (e.g., in water-limited regions for P-Et). This behavior is expected given that precipitation is a main controller of the interannual variability of climate drought indices (Tomas-Burguera et al., 2020; Vicente-Serrano et al., 2015). For example, in the case of precipitation-AED, precipitation explains more than 90% of the variability of this metric, while AED is only relevant during periods of precipitation deficit, particularly in water-limited regions (Tomas-Burguera et al., 2020). This main role of precipitation is also observed in other drought indices such as the PDSI (van der Schrier et al., 2013; Vicente-Serrano et al., 2015). On the other hand, under the SSP5-8.5 scenario, the correlation between precipitation and AED-based drought indices is expected to decrease, suggesting a greater role of AED. Nevertheless, this temporal relationship remains high in most world regions.

The close relationship found between climate drought indices in historical and future simulations contrasts with the low correlations found between climatic and ecological drought indices, given the low percentage of years when drought conditions coincide following meteorological and ecological metrics. The interannual variability of LAI and NPP showed high agreement in both the historical period and in the future scenario. This is in agreement with observations recorded in the last decades using vegetation activity from satellites (as a surrogate of the leaf area) and tree-ring growth (as a surrogate of NPP) (Vicente-Serrano et al., 2016, 2020c). Nevertheless, unexpectedly, we noted a poor relationship between the temporal evolution of both LAI and NPP and the climatic drought indices, albeit with the use of a wide set of metrics used here that highly represent plant water stress conditions (e.g., Et-AED). Moreover, this low relationship is also found between the ecological variables and soil moisture, which is one of the main factors controlling vegetation activity and carbon uptake worldwide (Green et al., 2019). This low relationship between climatic indices (and soil moisture) and ecological metrics could be explained by the uncoupling between water availability and plant water requirements as a consequence of the physiological effects of atmospheric CO_2 concentrations (as discussed above). Nevertheless, low interannual correlations were also found in the historical experiment. We consider that the low relationship between ecological drought metrics and climatic and soil moisture metrics introduces another important source of uncertainty in the assessment of the drought severity under future climate scenarios. It is expected that the agreement between NPP, LAI, and the different climatic metrics and soil moisture should be high, given the climate forcings used in the historical experiment. Thus, based on different vegetation metrics, numerous studies found strong temporal correlations between climate drought indices and soil moisture and different ecological measurements in the past decades, including satellite metrics (e.g., Bachmair et al., 2018; Vicente-Serrano et al., 2013), and tree ring growth (e.g., Orwig & Abrams, 1997; Vicente-Serrano et al., 2014). This unexpectedly low correlation between climatic drought metrics, soil moisture deficits and agricultural and ecological metrics during the historical experiment suggests that the temporal decoupling between these metrics is not related to the possible physiological effects of the enhanced CO_2 concentrations. Rather, it can probably be due to the existing limitations of the models in reproducing the real physiological response of vegetation to water deficits. Moreover, in addition to the low temporal agreement, there is a general spatial disconnection between the occurrence of climatic and ecological droughts in different regions worldwide, which introduce an additional uncertainty.

The temporal agreement between climatic drought metrics, soil moisture, precipitation-Et, and runoff is also low, both in the historical experiment and the SSP5-8.5 scenario. With the exception of the tropical and subtropical regions in the case of runoff, the remaining world showed low correlations with climatic metrics. Thus, the temporal correlations were low between the interannual variability of soil moisture and runoff in most regions of the world. This suggests that, considering climatic and hydrological drought metrics, the consistency of ESMs simulations on long temporal scales (i.e., annual) may be also affected by uncertainties. Thus, as opposed to

CMIP6 outputs, the interannual variability of observed streamflow is highly consistent with climate variables in most basins of the world (Dai, 2021).

5. Conclusions

This study provided new evidence on the interannual relationships and long-term trends between drought types based on different drought metrics obtained from ESM simulations. In the existing debate related to the assessment of drought severity in future climate projections based on different metrics from CMIP models, this study stresses some uncertainties of this assessment and the limited spatial and temporal consistency among different types of drought metrics that usually show agreement with observations, particularly with the use of hydrological (runoff and soil moisture) and ecological (LAI and NPP) drought metrics that are directly generated from model outputs. The main conclusion of this study is that the coherence of the trends and the interannual relationships between drought metrics suggest uncertainties that can largely impact any robust assessment of drought projections under scenarios of high emissions of greenhouse gases. Although some previous studies have suggested that the use of climatic drought indices could overestimate drought severity under future scenarios, this study indicates that projections based on hydrological (i.e., soil moisture and runoff) and ecological drought metrics (i.e., NPP and LAI) can be affected by important inconsistencies, particularly for the projected interannual relationship between drought metrics. We believe that still there are several sources of uncertainty, particularly linked to the plant processes and the physiological influences of the enhanced CO_2 atmospheric concentrations, which have important implications for the assessment of both ecological and hydrological droughts in future scenarios. Recent evidence highlights increased drought effects on crop systems and natural environments in response to drought events characterized by warmer conditions (Breshears et al., 2013; Fontes et al., 2018; Williams et al., 2013), but also hydrological implications given enhanced evaporation from crops, natural vegetation, and water bodies (Althoff et al., 2020; Friedrich et al., 2018; Vicente-Serrano et al., 2017). Although the response of plant physiology and hydrological processes could change in the future, with more adaptive strategies to much warmer conditions leading to a reduction in the severity of hydrological, agricultural, and ecological droughts compared to climatic droughts conditions, uncertainties persist in the assessment of processes related to elevated CO_2 concentrations, primarily due to the intricate challenge of distinguishing between radiative and physiological effects.

Drought severity projections are an extremely relevant topic with several environmental and socioeconomic implications, which deserves robust studies. Nevertheless, we must be aware that assessments based on model projections may be affected by considerable uncertainties. Indeed, improving the knowledge and modeling of the complex processes involved could reduce these uncertainties, but we are probably still far from finding this solution. A focus on simple, but robust models, as suggested by McColl et al. (2022), could be a better approach to improve the assessment of future drought severity. However, this assessment may actually be simpler, as in future periods of precipitation deficits (anthropogenic or naturally induced), the projected increased warming will undoubtedly cause more stress on hydrological and environmental systems as observed in near-present climate.

Data Availability Statement

The data from the CMIP6 models is available at the World Climate Research Programme (WCRP, https://esgf-node.llnl.gov/search/cmip6/). From that page, it is possible to download the necessary data for this research. For each CMIP6 model, which is selected in Source ID, it consists of selecting Experiment ID equal to “historical” and “ssp585”, Frequency equal to “mon” and Variable ID equal to “pr” (Precipitation), “evspsbl” (Evaporation Including Sublimation and Transpiration), “mrros” (Surface Runoff), “mrso” (Total Soil Moisture Content), “lai” (Leaf Area Index) and “npp” (Net Primary Production on Land as Carbon Mass Flux) and those necessary to compute the atmospheric evaporative demand, that is, “hurs” (Near-Surface Relative Humidity), “rsds” (Surface Downwelling Shortwave Radiation), “tasmax” (Daily Maximum Near-Surface Air Temperature), “tasmin” (Daily Minimum Near-Surface Air Temperature) and “tran” (Transpiration).

Acknowledgments
This work was supported by projects PCI2019-103631, PID2019-108589RA-I00, PID2021-122314OB-I00, SPIP2022-02857, TED2021-129152B-C41 and TED2021-129152B-C43, financed by the Ministerio de Ciencia, Innovación y Universidades, Spain (MCIN/10.13039/501100011033) and “ERDF A way of making Europe”; LINKB20080 of the programme i-LINK 2021 of CSIC and CROSSDRO financed by AXIS (Assessment of Cross(X) - sectoral climate Impacts and pathways for Sustainable transformation), JPI-Climate co-funded call of the European Commission. This study was also supported by the “Unidad Asociada CSIC–Universidade de Vigo: Grupo de Física de la Atmósfera y del Océano.” The work of Luis Gimeno-Sotelo was financially supported by CSIC Programa JAE and a “Ministerio de Ciencia, Innovación y Universidades” PhD grant (reference: PRE2022-101497). The EPhysLab group was also funded by Xunta de Galicia and ERDF, under project ED431C 2021/44 “Programa de Consolidación e Estructuración de Unidades de Investigación Competitivas.”

References

Adeyeri, O. E., Zhou, W., Laux, P., Ndehedehe, C. E., Wang, X., Usman, M., & Akinsanola, A. A. (2023). Multivariate drought monitoring, propagation, and projection using bias-corrected general circulation models. *Earth's Future*, *11*(4), e2022EF003303. https://doi.org/10.1029/2022ef003303

Adeyeri, O. E., Zhou, W., Wang, X., Zhang, R., Laux, P., Ishola, K. A., & Usman, M. (2022). The trend and spatial spread of multisectoral climate extremes in CMIP6 models. *Scientific Reports*, *12*(1), 21000. https://doi.org/10.1038/s41598-022-25265-4

Ainsworth, E. A., & Long, S. P. (2005). What have we learned from 15 years of free-air CO2 enrichment (FACE)? A meta-analytic review of the responses of photosynthesis, canopy properties and plant production to rising CO2. *New Phytologist*, *165*(2), 351–372. https://doi.org/10.1111/j.1469-8137.2004.01224.x

Allen, C. D. C. D., Breshears, D. D. D., & McDowell, N. G. N. G. (2015). On underestimation of global vulnerability to tree mortality and forest die-off from hotter drought in the Anthropocene. *Ecosphere*, *6*(8), art129–55. https://doi.org/10.1890/ES15-00203.1

Allen, C. D. C. D., Macalady, A. K. A. K., Chenchouni, H., Bachelet, D., McDowell, N., Vennetier, M., et al. (2010). A global overview of drought and heat-induced tree mortality reveals emerging climate change risks for forests. *Forest Ecology and Management*, *259*(4), 660–684. https://doi.org/10.1016/j.foreco.2009.09.001

Almazroui, M., Saeed, S., Saeed, F., Islam, M. N., & Ismail, M. (2020). Projections of precipitation and temperature over the South Asian countries in CMIP6. *Earth Systems and Environment*, *4*(2), 297–320. https://doi.org/10.1007/s41748-020-00157-7

Alsafadi, K., Al-Ansari, N., Mokhtar, A., Mohammed, S., Elbeltagi, A., Sh Sammen, S., & Bi, S. (2022). An evapotranspiration deficit-based drought index to detect variability of terrestrial carbon productivity in the Middle East. *Environmental Research Letters*, *17*(1), 014051. https://doi.org/10.1088/1748-9326/ac4765

Althoff, D., Rodrigues, L. N., & da Silva, D. D. (2020). Impacts of climate change on the evaporation and availability of water in small reservoirs in the Brazilian savannah. *Climatic Change*, *159*(2), 215–232. https://doi.org/10.1007/s10584-020-02656-y

Asseng, S., Ewert, F., Martre, P., Rötter, R. P., Lobell, D. B., Cammarano, D., et al. (2015). Rising temperatures reduce global wheat production. *Nature Climate Change*, *5*(2), 143–147. https://doi.org/10.1038/nclimate2470

Bachmair, S., Kohn, I., & Stahl, K. (2015). Exploring the link between drought indicators and impacts. *Natural Hazards and Earth System Sciences*, *15*(6), 1381–1397. https://doi.org/10.5194/nhess-15-1381-2015

Bachmair, S., Svensson, C., Hannaford, J., Barker, L. J., & Stahl, K. (2016). A quantitative analysis to objectively appraise drought indicators and model drought impacts. *Hydrology and Earth System Sciences*, *20*(7), 2589–2609. https://doi.org/10.5194/hess-20-2589-2016

Bachmair, S., Tanguy, M., Hannaford, J., & Stahl, K. (2018). How well do meteorological indicators represent agricultural and forest drought across Europe? *Environmental Research Letters*, *13*(3), 034042. https://doi.org/10.1088/1748-9326/aaafda

Barella-Ortiz, A., & Quintana-Seguí, P. (2018). Evaluation of drought representation and propagation in Regional Climate Model simulations over Spain. *Hydrology and Earth System Sciences Discussions*, 1–32. https://doi.org/10.5194/hess-2018-603

Berg, A., & McColl, K. A. (2021). No projected global drylands expansion under greenhouse warming. *Nature Climate Change*, *11*(4), 331–337. https://doi.org/10.1038/s41558-021-01007-8

Berg, A., & Sheffield, J. (2018). Climate change and drought: The soil moisture perspective. *Current Climate Change Reports*, *4*(2), 180–191. https://doi.org/10.1007/s40641-018-0095-0

Breshears, D. D., Adams, H. D., Eamus, D., Mcdowell, N. G., Law, D. J., Will, R. E., et al. (2013). The critical amplifying role of increasing atmospheric moisture demand on tree mortality and associated regional die-off. *Frontiers in Plant Science*, *4*(AUG). https://doi.org/10.3389/fpls.2013.00266

Breshears, D. D., Cobb, N. S., Rich, P. M., Price, K. P., Allen, C. D., Balice, R. G., et al. (2005). Regional vegetation die-off in response to global-change-type drought. *Proceedings of the National Academy of Sciences of the United States of America*, *102*(42), 15144–15148. https://doi.org/10.1073/pnas.0505734102

Brodribb, T. J., Powers, J., Cochard, H., & Choat, B. (2020). Hanging by a thread? Forests and drought. *Science*, *368*(6488), 261–266. American Association for the Advancement of Science. https://doi.org/10.1126/science.aat7631

Carnicer, J., Coll, M., Ninyerola, M., Pons, X., Sánchez, G., & Peñuelas, J. (2011). Widespread crown condition decline, food web disruption, and amplified tree mortality with increased climate change-type drought. *Proceedings of the National Academy of Sciences of the United States of America*, *108*(4), 1474–1478. https://doi.org/10.1073/pnas.1010070108

Ceulemans, R., & Mousseau, M. (1994). Tansley review No. 71. Effects of elevated atmospheric CO_2 on woody plants. *New Phytologist*, *127*(3), 425–446. [Wiley, New Phytologist Trust]. https://doi.org/10.1111/j.1469-8137.1994.tb03961.x

Chen, Y., Romps, D. M., Seeley, J. T., Veraverbeke, S., Riley, W. J., Mekonnen, Z. A., & Randerson, J. T. (2021). Future increases in Arctic lightning and fire risk for permafrost carbon. *Nature Climate Change*, *11*(5), 404–410. https://doi.org/10.1038/s41558-021-01011-y

Cook, B. I., Mankin, J. S., Marvel, K., Williams, A. P., Smerdon, J. E., & Anchukaitis, K. J. (2020). Twenty-first century drought projections in the CMIP6 forcing scenarios. *Earth's Future*, *8*(6), e2019EF001461. John Wiley & Sons, Ltd. https://doi.org/10.1029/2019EF001461

Cook, B. I., Smerdon, J. E., Seager, R., & Coats, S. (2014). Global warming and 21st century drying. *Climate Dynamics*, *43*(9), 2607–2627. https://doi.org/10.1007/s00382-014-2075-y

Dai, A. (2012). Increasing drought under global warming in observations and models. *Nature Climate Change*, *3*(1), 52–58. Nature Publishing Group. https://doi.org/10.1038/nclimate1633

Dai, A. (2021). Hydroclimatic trends during 1950–2018 over global land. *Climate Dynamics*, *56*(11), 4027–4049. https://doi.org/10.1007/s00382-021-05684-1

De Kauwe, M. G., Medlyn, B. E., & Tissue, D. T. (2021). To what extent can rising [CO2] ameliorate plant drought stress? *New Phytologist*, *231*(6), 2118–2124. John Wiley & Sons, Ltd. https://doi.org/10.1111/nph.17540

Donohue, R. J., Roderick, M. L., McVicar, T. R., & Farquhar, G. D. (2013). Impact of CO_2 fertilization on maximum foliage cover across the globe's warm, arid environments. *Geophysical Research Letters*, *40*(12), 3031–3035. https://doi.org/10.1002/grl.50563

Douville, H., Raghavan, K., & Renwick, J. (2021). Water cycle changes. In *Climate change 2021: The physical climate, basis. Contribution of working group I to the sixth assessment report of the intergovernmental panel on climate change*.

Eyring, V., Bony, S., Meehl, G. A., Senior, C. A., Stevens, B., Stouffer, R. J., & Taylor, K. E. (2016). Overview of the Coupled Model Intercomparison Project Phase 6 (CMIP6) experimental design and organization. *Geoscientific Model Development*, *9*(5), 1937–1958. https://doi.org/10.5194/gmd-9-1937-2016

Ficklin, D. L., Abatzoglou, J. T., Robeson, S. M., Null, S. E., & Knouft, J. H. (2018). Natural and managed watersheds show similar responses to recent climate change. *Proceedings of the National Academy of Sciences of the United States of America*, *115*(34), 201801026–8557. National Academy of Sciences. https://doi.org/10.1073/PNAS.1801026115

Fleig, A. K., Tallaksen, L. M., Hisdal, H., & Demuth, S. (2006). A global evaluation of streamflow drought characteristics. *Hydrology and Earth System Sciences*, *10*(4), 535–552. https://doi.org/10.5194/hess-10-535-2006

Fontes, C. G., Dawson, T. E., Jardine, K., McDowell, N., Gimenez, B. O., Anderegg, L., et al. (2018). Dry and hot: The hydraulic consequences of a climate change–type drought for Amazonian trees. *Philosophical Transactions of the Royal Society B: Biological Sciences*, *373*(1760), 20180209. https://doi.org/10.1098/rstb.2018.0209

Ford, T. W., & Quiring, S. M. (2019). *Comparison of contemporary in situ, model, and satellite remote sensing soil moisture with a focus on drought monitoring*. Water Resources Research.

Friedrich, K., Grossman, R. L., Huntington, J., Blanken, P. D., Lenters, J., Holman, K. D., et al. (2018). Reservoir evaporation in the Western United States. *Bulletin of the American Meteorological Society*, *99*(1), 167–187. https://doi.org/10.1175/BAMS-D-15-00224.1

Gentine, P., Green, J., Guerin, M., Humphrey, V., Seneviratne, S., Zhang, Y., & Zhou, S. (2019). Coupling between the terrestrial carbon and water cycles – A review. *Environmental Research Letters*, *14*(8), 083003. https://doi.org/10.1088/1748-9326/ab22d6

Gonsamo, A., Ciais, P., Miralles, D. G., Sitch, S., Dorigo, W., Lombardozzi, D., et al. (2021). Greening drylands despite warming consistent with carbon dioxide fertilization effect. *Global Change Biology*. John Wiley & Sons, Ltd, *27*(14), 3336–3349. https://doi.org/10.1111/gcb.15658

Green, J. K., Berry, J., Ciais, P., Zhang, Y., & Gentine, P. (2020). Amazon rainforest photosynthesis increases in response to atmospheric dryness. *Science Advances*, *6*(47), eabb7232. https://doi.org/10.1126/sciadv.abb7232

Green, J. K., Seneviratne, S. I., Berg, A. M., Findell, K. L., Hagemann, S., Lawrence, D. M., & Gentine, P. (2019). Large influence of soil moisture on long-term terrestrial carbon uptake. *Nature*, *565*(7740), 476–479. https://doi.org/10.1038/s41586-018-0848-x

Greve, P., Roderick, M. L., Ukkola, A. M., & Wada, Y. (2019). The aridity Index under global warming. *Environmental Research Letters*, *14*(12), 124006. IOP Publishing. https://doi.org/10.1088/1748-9326/ab5046

Grossiord, C., Buckley, T. N., Cernusak, L. A., Novick, K. A., Poulter, B., Siegwolf, R. T. W., et al. (2020). Plant responses to rising vapor pressure deficit. *New Phytologist*, *226*(6), 1550–1566. John Wiley & Sons, Ltd. https://doi.org/10.1111/nph.16485

Guo, H., He, S., Li, M., Bao, A., Chen, T., Zheng, G., & De Maeyer, P. (2022). Future changes of drought characteristics in Coupled Model Intercomparison Project phase 6 Shared Socioeconomic Pathway scenarios over Central Asia. *International Journal of Climatology*, *42*(7), 3888–3908. https://doi.org/10.1002/joc.7450

Gutiérrez, J. M., Jones, R. G., Narisma, G. T., Alves, L. M., Amjad, M., Gorodetskaya, I. V., et al. (2021). Atlas. In V. Masson-Delmotte, P. Zhai, A. Pirani, S. L. Connors, C. Péan, S. Berger, et al. (Eds.), *Climate change 2021: The physical science basis. Contribution of working group I to the sixth assessment report of the intergovernmental panel on climate change* (pp. 1927–2058). Cambridge University Press. https://doi.org/10.1017/9781009157896.021

Hlavinka, P., Trnka, M., Semerádová, D., Dubrovský, M., Žalud, Z., & Možný, M. (2009). Effect of drought on yield variability of key crops in Czech Republic. *Agricultural and Forest Meteorology*, *149*(3), 431–442. https://doi.org/10.1016/j.agrformet.2008.09.004

Jiang, W., Niu, Z., Wang, L., Yao, R., Gui, X., Xiang, F., & Ji, Y. (2022). Impacts of drought and climatic factors on vegetation dynamics in the Yellow River Basin and Yangtze River Basin, China. *Remote Sensing*, *14*(4), 930. https://doi.org/10.3390/rs14040930

Kendall, M. G. (1938). A new measure of rank correlation. *Biometrika*, *30*(1/2), 81–93. https://doi.org/10.2307/2332226

Kendall, M. G. (1948). Rank correlation methods.

Kim, D., & Rhee, J. (2016). A drought index based on actual evapotranspiration from the Bouchet hypothesis. *Geophysical Research Letters*, *43*(19), 10277–10285. https://doi.org/10.1002/2016GL070302

Kim, S. (2015). ppcor: An R package for a fast calculation to semi-partial correlation coefficients. *Communications for Statistical Applications and Methods*, *22*(6), 665–674. https://doi.org/10.5351/csam.2015.22.6.665

Kolby Smith, W., Reed, S. C., Cleveland, C. C., Ballantyne, A. P., Anderegg, W. R. L., Wieder, W. R., et al. (2015). Large divergence of satellite and Earth system model estimates of global terrestrial CO2 fertilization. *Nature Climate Change*, *6*(3), 306–310. Nature Publishing Group. https://doi.org/10.1038/nclimate2879

Kolmogorov, A. N. (1933). Sulla determinazione empirica di una legge di distribuzione. *Giornale dell'Istituto Italiano Degli Attuari*, *4*, 83–91.

Li, F., Xiao, J., Chen, J., Ballantyne, A., Jin, K., Li, B., et al. (2023). Global water use efficiency saturation due to increased vapor pressure deficit. *Science*, *381*(6658), 672–677. https://doi.org/10.1126/science.adf5041

Li, G., Sun, S., Han, J., Yan, J., Liu, W., Wei, Y., et al. (2019). Impacts of Chinese Grain for Green program and climate change on vegetation in the Loess Plateau during 1982–2015. *Science of the Total Environment*, *660*, 177–187. https://doi.org/10.1016/j.scitotenv.2019.01.028

Li, H., Li, Z., Chen, Y., Xiang, Y., Liu, Y., Kayumba, P. M., & Li, X. (2021). Drylands face potential threat of robust drought in the CMIP6 SSPs scenarios. *Environmental Research Letters*, *16*(11), 114004. https://doi.org/10.1088/1748-9326/ac2bce

Li, J., Wang, Z., & Lai, C. (2020). Severe drought events inducing large decrease of net primary productivity in mainland China during 1982–2015. *Science of the Total Environment*, *703*, 703. https://doi.org/10.1016/j.scitotenv.2019.135541

Liu, Y., Kumar, M., Katul, G. G., Feng, X., & Konings, A. G. (2020). Plant hydraulics accentuates the effect of atmospheric moisture stress on transpiration. *Nature Climate Change*, *10*(7), 691–695. https://doi.org/10.1038/s41558-020-0781-5

Lloyd-Hughes, B. (2014). The impracticality of a universal drought definition. *Theoretical and Applied Climatology*, *117*(3–4), 607–611. https://doi.org/10.1007/s00704-013-1025-7

Lobell, D. B. (2014). Climate change adaptation in crop production: Beware of illusions. *Global Food Security*, *3*(2), 72–76. https://doi.org/10.1016/j.gfs.2014.05.002

Lobell, D. B., Schlenker, W., & Costa-Roberts, J. (2011). Climate trends and global crop production since 1980. *Science*, *333*(6042), 616–620. https://doi.org/10.1126/science.1204531

Lu, J., Carbone, G. J., & Grego, J. M. (2019). Uncertainty and hotspots in 21st century projections of agricultural drought from CMIP5 models. *Scientific Reports*, *9*(1), 4922. https://doi.org/10.1038/s41598-019-41196-z

Mankin, J. S., Smerdon, J. E., Cook, B. I., Williams, A. P., & Seager, R. (2017). The curious case of projected twenty-first-century drying but greening in the American west. *Journal of Climate*, *30*(21), 8689–8710. American Meteorological Society. https://doi.org/10.1175/JCLI-D-17-0213.1

Mann, H. B. (1945). Nonparametric tests against trend. *Econometrica: Journal of the Econometric Society*, *13*(3), 245–259. https://doi.org/10.2307/1907187

Marchand, W., Girardin, M. P., Hartmann, H., Depardieu, C., Isabel, N., Gauthier, S., et al. (2020). Strong overestimation of water-use efficiency responses to rising CO2 in tree-ring studies. *Global Change Biology*. John Wiley & Sons, Ltd, *26*(8), 4538–4558. https://doi.org/10.1111/gcb.15166

Martin, E. R. (2018). Future projections of global pluvial and drought event characteristics. *Geophysical Research Letters*, *45*(21). https://doi.org/10.1029/2018GL079807

McColl, K. A., Roderick, M. L., Berg, A., & Scheff, J. (2022). The terrestrial water cycle in a warming world. *Nature Climate Change*, *12*(7), 604–606. https://doi.org/10.1038/s41558-022-01412-7

McDowell, N. G., & Allen, C. D. (2015). Darcy's law predicts widespread forest mortality under climate warming. *Nature Climate Change*, *5*(7), 669–672. https://doi.org/10.1038/nclimate2641

Menezes-Silva, P. E., Loram-Lourenço, L., Alves, R. D. F. B., Sousa, L. F., Almeida, S. E. d. S., & Farnese, F. S. (2019). Different ways to die in a changing world: Consequences of climate change for tree species performance and survival through an ecophysiological perspective. *Ecology and Evolution*, *9*(20), 11979–11999. https://doi.org/10.1002/ece3.5663

Meng, Y., Hao, Z., Feng, S., Zhang, X., & Hao, F. (2022). Increase in compound dry-warm and wet-warm events under global warming in CMIP6 models. *Global and Planetary Change*, *210*, 103773. https://doi.org/10.1016/j.gloplacha.2022.103773

Miguez-Macho, G., & Fan, Y. (2021). Spatiotemporal origin of soil water taken up by vegetation. *Nature*, *598*(7882), 624–628. https://doi.org/10.1038/s41586-021-03958-6

Milly, P. C. D., & Dunne, K. A. (2016). Potential evapotranspiration and continental drying. *Nature Climate Change*, *6*(10), 946–949. https://doi.org/10.1038/nclimate3046

Morgan, J. A., Pataki, D. E., Körner, C., Clark, H., Del Grosso, S. J., & Grünzweig, J. M. (2004). Water relations in grassland and desert ecosystems exposed to elevated atmospheric CO2. *Oecologia*, *140*(1), 11–25. https://doi.org/10.1007/s00442-004-1550-2

Naumann, G., Alfieri, L., Wyser, K., Mentaschi, L., Betts, R. A., Carrao, H., et al. (2018). Global changes in drought conditions under different levels of warming. *Geophysical Research Letters*, *45*(7), 3285–3296. https://doi.org/10.1002/2017GL076521

Naumann, G., Cammalleri, C., Mentaschi, L., & Feyen, L. (2021). Increased economic drought impacts in Europe with anthropogenic warming. *Nature Climate Change*, *11*(6), 485–491. https://doi.org/10.1038/s41558-021-01044-3

Ndehedehe, C. E., Ferreira, V. G., Adeyeri, O. E., Correa, F. M., Usman, M., Oussou, F. E., et al. (2023). Global assessment of drought characteristics in the Anthropocene. *Resources, Environment and Sustainability*, *12*, 100105. https://doi.org/10.1016/j.resenv.2022.100105

O'Connor, P., Murphy, C., Matthews, T., & Wilby, R. (2022). Relating drought indices to impacts reported in newspaper articles. *International Journal of Climatology*, *43*(4), 1796–1816. https://doi.org/10.1002/joc.7946

Orwig, D. A., & Abrams, M. D. (1997). Variation in radial growth responses to drought among species, site, and canopy strata. *Trees: Structure and Function*, *11*(8), 474–484. https://doi.org/10.1007/s004680050110

Padrón, R. S., Gudmundsson, L., Decharme, B., Ducharne, A., Lawrence, D. M., Mao, J., et al. (2020). Observed changes in dry-season water availability attributed to human-induced climate change. *Nature Geoscience*, *13*(7), 477–481. https://doi.org/10.1038/s41561-020-0594-1

Padrón, R. S., Gudmundsson, L., Liu, L., Humphrey, V., & Seneviratne, S. I. (2022). Drivers of intermodel uncertainty in land carbon sink projections. *Biogeosciences*, *19*(23), 5435–5448. https://doi.org/10.5194/bg-19-5435-2022

Papalexiou, S. M., Rajulapati, C. R., Andreadis, K. M., Foufoula-Georgiou, E., Clark, M. P., & Trenberth, K. E. (2021). Probabilistic evaluation of drought in CMIP6 simulations. *Earth's Future*. John Wiley & Sons, Ltd, *9*(10), e2021EF002150. https://doi.org/10.1029/2021EF002150

Pereira, L. S., Allen, R. G., Smith, M., & Raes, D. (2015). Crop evapotranspiration estimation with FAO56: Past and future. *Agricultural Water Management*, *147*, 4–20. https://doi.org/10.1016/j.agwat.2014.07.031

Quiring, S. M., & Papakryiakou, T. N. (2003). An evaluation of agricultural drought indices for the Canadian prairies. *Agricultural and Forest Meteorology*, *118*(1), 49–62. https://doi.org/10.1016/S0168-1923(03)00072-8

Rettie, F. M., Gayler, S., Weber, T. K., Tesfaye, K., & Streck, T. (2023). High-resolution CMIP6 climate projections for Ethiopia using the gridded statistical downscaling method. *Scientific Data*, *10*(1), 442. https://doi.org/10.1038/s41597-023-02337-2

Ridder, N. N., Ukkola, A. M., Pitman, A. J., & Perkins-Kirkpatrick, S. E. (2022). Increased occurrence of high impact compound events under climate change. *npj Climate and Atmospheric Science*, *5*(1), 3. https://doi.org/10.1038/s41612-021-00224-4

Roderick, M. L., Greve, P., & Farquhar, G. D. (2015a). On the assessment of aridity with changes in atmospheric CO2. *Water Resources Research*, *51*(7), 5450–5463. https://doi.org/10.1002/2015WR017031

Sánchez-Salguero, R., Camarero, J. J., Carrer, M., Gutiérrez, E., Alla, A. Q., Andreu-Hayles, L., et al. (2017). Climate extremes and predicted warming threaten Mediterranean Holocene firs forests refugia. *Proceedings of the National Academy of Sciences of the United States of America*, *114*(47), E10142–E10150. https://doi.org/10.1073/pnas.1708109114

Scheff, J. (2018). Drought indices, drought impacts, CO2, and warming: A historical and geologic perspective. *Current Climate Change Reports*, *4*(2), 202–209. https://doi.org/10.1007/s40641-018-0094-1

Scheff, J., Coats, S., & Laguë, M. M. (2022). Why do the global warming responses of land-surface models and climatic dryness metrics disagree? *Earth's Future*, *10*(8). https://doi.org/10.1029/2022EF002814

Scheff, J., & Frierson, D. M. W. (2015). Terrestrial aridity and its response to greenhouse warming across CMIP5 climate models. *Journal of Climate*, *28*(14), 5583–5600. https://doi.org/10.1175/JCLI-D-14-00480.1

Scheff, J., Mankin, J. S., Coats, S., & Liu, H. (2021). CO2-plant effects do not account for the gap between dryness indices and projected dryness impacts in CMIP6 or CMIP5. *Environmental Research Letters*, *16*(3), 034018. IOP Publishing. https://doi.org/10.1088/1748-9326/abd8fd

Seneviratne, S., Zhang, X., Adnan, M., Badi, W., Dereczynski, C., Di Luca, A., et al. (2021). Weather and climate extreme events in a changing climate. In V. MassonDelmotte & E. Al (Eds.), *Climate change 2021: The physical science basis. Contribution of working group I to the sixth assessment report of the intergovernmental panel on climate change*. Cambridge University Press.

Smirnov, N. (1948). Table for estimating the goodness of fit of empirical distributions. *The Annals of Mathematical Statistics*, *19*(2), 279–281. https://doi.org/10.1214/aoms/1177730256

Spinoni, J., Barbosa, P., Bucchignani, E., Cassano, J., Cavazos, T., Christensen, J. H., & Dosio, A. (2020). Future global meteorological drought hot spots: A study based on CORDEX data. *Journal of Climate*, *33*(9), 3635–3661. American Meteorological Society. https://doi.org/10.1175/JCLI-D-19-0084.1

Stagge, J. H., Kohn, I., Tallaksen, L. M., & Stahl, K. (2015). Modeling drought impact occurrence based on meteorological drought indices in Europe. *Journal of Hydrology*, *530*, 37–50. https://doi.org/10.1016/j.jhydrol.2015.09.039

Stagge, J. H., Tallaksen, L. M., Gudmundsson, L., Van Loon, A. F., & Stahl, K. (2015). Candidate distributions for climatological drought indices (SPI and SPEI). *International Journal of Climatology*, *35*(13), 4027–4040. John Wiley and Sons Ltd. https://doi.org/10.1002/joc.4267

Stephenson, N. L. (1990). Climatic control of vegetation distribution: The role of the water balance. *The American Naturalist*, *135*(5), 649–670. https://doi.org/10.1086/285067

Stocker, T. F., Qin, D., Plattner, G.-K., Alexander, L. V., Allen, S. K., Bindoff, N. L., & Xie, S.-P. (2013). Technical summary. In *Climate change 2013: The physical science basis*.

Tallaksen, L. M., Madsen, H., & Clausen, B. (1997). On the definition and modelling of streamflow drought duration and deficit volume. *Hydrological Sciences Journal*, *42*(1), 15–33. Taylor & Francis Group. https://doi.org/10.1080/02626669709492003

Tallaksen, L. M., & Stahl, K. (2014). Spatial and temporal patterns of large-scale droughts in Europe: Model dispersion and performance. *Geophysical Research Letters*, *41*(2), 429–434. https://doi.org/10.1002/2013GL058573

Thorarinsdottir, T. L., Sillmann, J., Haugen, M., Gissibl, N., & Sandstad, M. (2020). Evaluation of CMIP5 and CMIP6 simulations of historical surface air temperature extremes using proper evaluation methods. *Environmental Research Letters*, *15*(12), 124041. https://doi.org/10.1088/1748-9326/abc778

Tomas-Burguera, M., Vicente-Serrano, S. M., Peña-Angulo, D., Domínguez-Castro, F., Noguera, I., & El Kenawy, A. (2020a). Global characterization of the varying responses of the standardized precipitation evapotranspiration index to atmospheric evaporative demand. *Journal of Geophysical Research: Atmospheres*, *125*(17). Blackwell Publishing Ltd. https://doi.org/10.1029/2020JD033017

Ukkola, A. M., De Kauwe, M. G., Roderick, M. L., Abramowitz, G., & Pitman, A. J. (2020). Robust future changes in meteorological drought in CMIP6 projections despite uncertainty in precipitation. *Geophysical Research Letters*, *47*(11), e2020GL087820. John Wiley & Sons, Ltd. https://doi.org/10.1029/2020GL087820

van den Hurk, B., Best, M., Dirmeyer, P., Pitman, A., Polcher, J., & Santanello, J. (2011). Acceleration of land surface model development over a decade of glass. *Bulletin of the American Meteorological Society*, *92*(12), 1593–1600. American Meteorological Society. https://doi.org/10.1175/BAMS-D-11-00007.1

van der Schrier, G., Barichivich, J., Briffa, K. R., & Jones, P. D. (2013). A scPDSI-based global data set of dry and wet spells for 1901–2009. *Journal of Geophysical Research: Atmospheres*, *118*(10), 4025–4048. https://doi.org/10.1002/jgrd.50355

Van Loon, A. F., Gleeson, T., Clark, J., Van Dijk, A. I. J. M., Stahl, K., Hannaford, J., et al. (2016). Drought in the anthropocene. *Nature Geoscience*, *9*(2), 89–91. https://doi.org/10.1038/ngeo2646

Vicente-Serrano, S. M., & Beguería, S. (2016). Comment on "Candidate distributions for climatological drought indices (SPI and SPEI)" by James H. Stagge et al. *International Journal of Climatology*, *36*(4), 2120–2131. https://doi.org/10.1002/joc.4474

Vicente-Serrano, S. M., Beguería, S., & López-Moreno, J. I. (2010). A multiscalar drought index sensitive to global warming: The standardized precipitation evapotranspiration index. *Journal of Climate*, *23*(7), 1696–1718. https://doi.org/10.1175/2009JCLI2909.1

Vicente-Serrano, S. M., Beguería, S., Lorenzo-Lacruz, J., Camarero, J. J., López-Moreno, J. I., Azorin-Molina, C., et al. (2012). Performance of drought indices for ecological, agricultural, and hydrological applications. *Earth Interactions*, *16*(10), 1–27. https://doi.org/10.1175/2012EI000434.1

Vicente-Serrano, S. M., Camarero, J. J., & Azorin-Molina, C. (2014). Diverse responses of forest growth to drought time-scales in the Northern Hemisphere. *Global Ecology and Biogeography*, *23*(9), 1019–1030. https://doi.org/10.1111/geb.12183

Vicente-Serrano, S. M., Camarero, J. J., Olano, J. M., Martín-Hernández, N., Peña-Gallardo, M., Tomás-Burguera, M., et al. (2016). Diverse relationships between forest growth and the Normalized Difference Vegetation Index at a global scale. *Remote Sensing of Environment*, *187*, 14–29. https://doi.org/10.1016/j.rse.2016.10.001

Vicente-Serrano, S. M., der Schrier, G., Beguería, S., Azorin-Molina, C., & Lopez-Moreno, J.-I. (2015). Contribution of precipitation and reference evapotranspiration to drought indices under different climates. *Journal of Hydrology*, *526*, 42–54. https://doi.org/10.1016/j.jhydrol.2014.11.025

Vicente-Serrano, S. M., Domínguez-Castro, F., McVicar, T. R., Tomas-Burguera, M., Peña-Gallardo, M., Noguera, I., et al. (2020). Global characterization of hydrological and meteorological droughts under future climate change: The importance of timescales, vegetation-CO_2 feedbacks and changes to distribution functions. *International Journal of Climatology*, *40*(5), 2557–2567. https://doi.org/10.1002/joc.6350

Vicente-Serrano, S. M., García-Herrera, R., Peña-Angulo, D., Tomas-Burguera, M., Domínguez-Castro, F., Noguera, I., et al. (2022). Do CMIP models capture long-term observed annual precipitation trends? *Climate Dynamics*, *58*(9–10), 2825–2842. https://doi.org/10.1007/s00382-021-06034-x

Vicente-Serrano, S. M., Gouveia, C., Camarero, J. J., Beguería, S., Trigo, R., López-Moreno, J. I., & Sanchez-Lorenzo, A. (2013). Response of vegetation to drought time-scales across global land biomes. *Proceedings of the National Academy of Sciences of the United States of America*, *110*(1), 52–57. National Academy of Sciences. https://doi.org/10.1073/pnas.1207068110

Vicente-Serrano, S. M., Martín-Hernández, N., Camarero, J. J. J., Gazol, A., Sánchez-Salguero, R., Peña-Gallardo, M., & Diego Galván, J. (2020). Linking tree-ring growth and satellite-derived gross primary growth in multiple forest biomes. Temporal-scale matters. *Ecological Indicators*, *108*, 105753. https://doi.org/10.1016/j.ecolind.2019.105753

Vicente-Serrano, S. M., McVicar, T. R., Miralles, D. G., Yang, Y., & Tomas-Burguera, M. (2020). Unraveling the influence of atmospheric evaporative demand on drought and its response to climate change. *Wiley Interdisciplinary Reviews: Climate Change*, *11*(2), e632. https://doi.org/10.1002/wcc.632

Vicente-Serrano, S. M., Miralles, D. G., Domínguez-Castro, F., Azorin-Molina, C., El Kenawy, A., McVicar, T. R., et al. (2018). Global assessment of the standardized evapotranspiration deficit index (SEDI) for drought analysis and monitoring. *Journal of Climate*, *31*(14), 5371–5393. https://doi.org/10.1175/jcli-d-17-0775.1

Vicente-Serrano, S. M., Miralles, D. G., McDowell, N., Brodribb, T., Domínguez-Castro, F., & Leung, R. (2022). The uncertain role of rising atmospheric CO2 on global plant transpiration. *Earth-Science Reviews*, *230*, 104055. https://doi.org/10.1016/j.earscirev.2022.104055

Vicente-Serrano, S. M., Peña-Gallardo, M., Hannaford, J., Murphy, C., Lorenzo-Lacruz, J., Dominguez-Castro, F., et al. (2019). Climate, irrigation, and land-cover change explain streamflow trends in countries bordering the Northeast Atlantic. *Geophysical Research Letters*, *46*(19), 10821–10833. https://doi.org/10.1029/2019gl084084

Vicente-Serrano, S. M., Quiring, S. M., Peña-Gallardo, M., Yuan, S., & Domínguez-Castro, F. (2020). A review of environmental droughts: Increased risk under global warming? *Earth-Science Reviews*, *201*, 102953. https://doi.org/10.1016/j.earscirev.2019.102953

Vicente-Serrano, S. M., Zabalza-Martínez, J., Borràs, G., López-Moreno, J. I., Pla, E., Pascual, D., et al. (2017). Effect of reservoirs on streamflow and river regimes in a heavily regulated river basin of Northeast Spain. *Catena*, *149*, 727–741. https://doi.org/10.1016/j.catena.2016.03.042

Wang, T., Tu, X., Singh, V. P., Chen, X., & Lin, K. (2021). Global data assessment and analysis of drought characteristics based on CMIP6. *Journal of Hydrology*, *596*, 126091. https://doi.org/10.1016/j.jhydrol.2021.126091

Wang, W., Lee, X., Xiao, W., Liu, S., Schultz, N., Wang, Y., et al. (2018). Global lake evaporation accelerated by changes in surface energy allocation in a warmer climate. *Nature Geoscience*, *11*(6), 410–414. https://doi.org/10.1038/s41561-018-0114-8

Wilhite, D. A., & Buchanan-Smith, M. (2005). Drought as hazard: Understanding the natural and social context. In *Drought and water crises: Science, technology, and management issues*.

Williams, A. P., Allen, C. D., Macalady, A. K., Griffin, D., Woodhouse, C. A., Meko, D. M., & Mcdowell, N. G. (2013). Temperature as a potent driver of regional forest drought stress and tree mortality. *Nature Climate Change*, *3*(3), 292–297. https://doi.org/10.1038/nclimate1693

Wu, H., Lei, H., Lu, W., & Liu, Z. (2022). Future changes in precipitation over the upper Yangtze River basin based on bias correction spatial downscaling of models from CMIP6. *Environmental Research Communications*, *4*(4), 045002. https://doi.org/10.1088/2515-7620/ac620e

Xu, C., McDowell, N. G., Fisher, R. A., Wei, L., Sevanto, S., Christoffersen, B. O., et al. (2019). Increasing impacts of extreme droughts on vegetation productivity under climate change. *Nature Climate Change*, *9*(12), 948–953. https://doi.org/10.1038/s41558-019-0630-6

Yang, Y., Roderick, M. L., Yang, D., Wang, Z., Ruan, F., McVicar, T. R., et al. (2021). Streamflow stationarity in a changing world. *Environmental Research Letters*, *16*(6), 064096. https://doi.org/10.1088/1748-9326/ac08c1

Yang, Y., Roderick, M. L., Zhang, S., McVicar, T. R., & Donohue, R. J. (2019). Hydrologic implications of vegetation response to elevated CO2 in climate projections. *Nature Climate Change*, *9*(1), 44–48. https://doi.org/10.1038/s41558-018-0361-0

Yang, Y., Zhang, S., McVicar, T. R., Beck, H. E., Zhang, Y., & Liu, B. (2018). Disconnection between trends of atmospheric drying and continental runoff. *Water Resources Research*, *54*(7), 4700–4713. https://doi.org/10.1029/2018WR022593

Yuan, S., & Quiring, S. M. (2017). Evaluation of soil moisture in CMIP5 simulations over the contiguous United States using in situ and satellite observations. *Hydrology and Earth System Sciences*, *21*(4), 2203–2218. https://doi.org/10.5194/hess-21-2203-2017

10.1029/2023EF003629

Zeng, J., Li, J., Lu, X., Wei, Z., Shangguan, W., Zhang, S., et al. (2022). Assessment of global meteorological, hydrological and agricultural drought under future warming based on CMIP6. *Atmospheric and Oceanic Science Letters*, *15*(1), 100143. https://doi.org/10.1016/j.aosl.2021.100143

Zhang, X., Li, M., Ma, Z., Yang, Q., Lv, M., & Clark, R. (2019). Assessment of an evapotranspiration deficit drought index in relation to impacts on ecosystems. *Advances in Atmospheric Sciences*, *36*(11), 1273–1287. https://doi.org/10.1007/s00376-019-9061-6

Zhao, M., Liu, Y., & Konings, A. G. (2022). Evapotranspiration frequently increases during droughts. *Nature Climate Change*, *12*(11), 1024–1030. https://doi.org/10.1038/s41558-022-01505-3

Zhao, Q., Zhu, Z., Zeng, H., Zhao, W., & Myneni, R. B. (2020). Future greening of the Earth may not be as large as previously predicted. *Agricultural and Forest Meteorology*, *292–293*, 108111. https://doi.org/10.1016/j.agrformet.2020.108111

Zhao, T., & Dai, A. (2021). CMIP6 model-projected hydroclimatic and drought changes and their causes in the 21st century. *Journal of Climate*, 1–58. American Meteorological Society. https://doi.org/10.1175/JCLI-D-21-0442.1

Zhao, T., & Dai, A. (2022). CMIP6 model-projected hydroclimatic and drought changes and their causes in the twenty-first century. *Journal of Climate*, *35*(3), 897–921. American Meteorological Society. https://doi.org/10.1175/JCLI-D-21-0442.1

Zhu, Y., & Yang, S. (2021). Interdecadal and interannual evolution characteristics of the global surface precipitation anomaly shown by CMIP5 and CMIP6 models. *International Journal of Climatology*, *41*(S1), E1100–E1118. https://doi.org/10.1002/joc.6756

COMPENDIUM OF SUPPLEMENTARY MATERIALS

SUPPLEMENTARY INFORMATION FOR:

Where does the link between atmospheric moisture transport and extreme precipitation matter?

Luis Gimeno-Sotelo[1] and Luis Gimeno[1*]

[1]Centro de Investigación Mariña, Universidade de Vigo, Environmental Physics Laboratory (EPhysLab), Ourense, Spain

(*) Corresponding author (l.gimeno@uvigo.es)

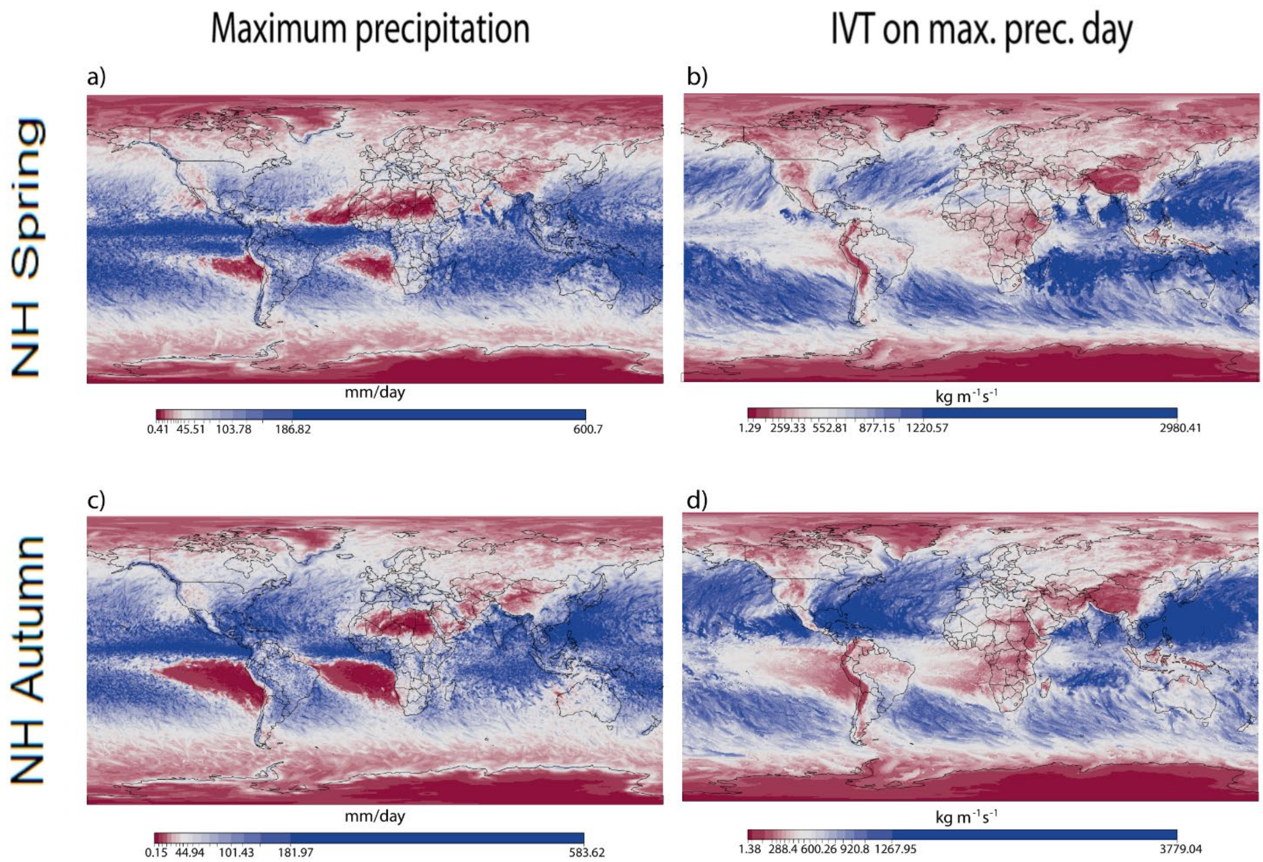

Supplementary Figure 1. Same as Figure 1 for intermediate seasons: a) and b) for Northern Hemisphere Spring (March-May) and c) and d) for Northern Hemisphere Autumn (September-November)

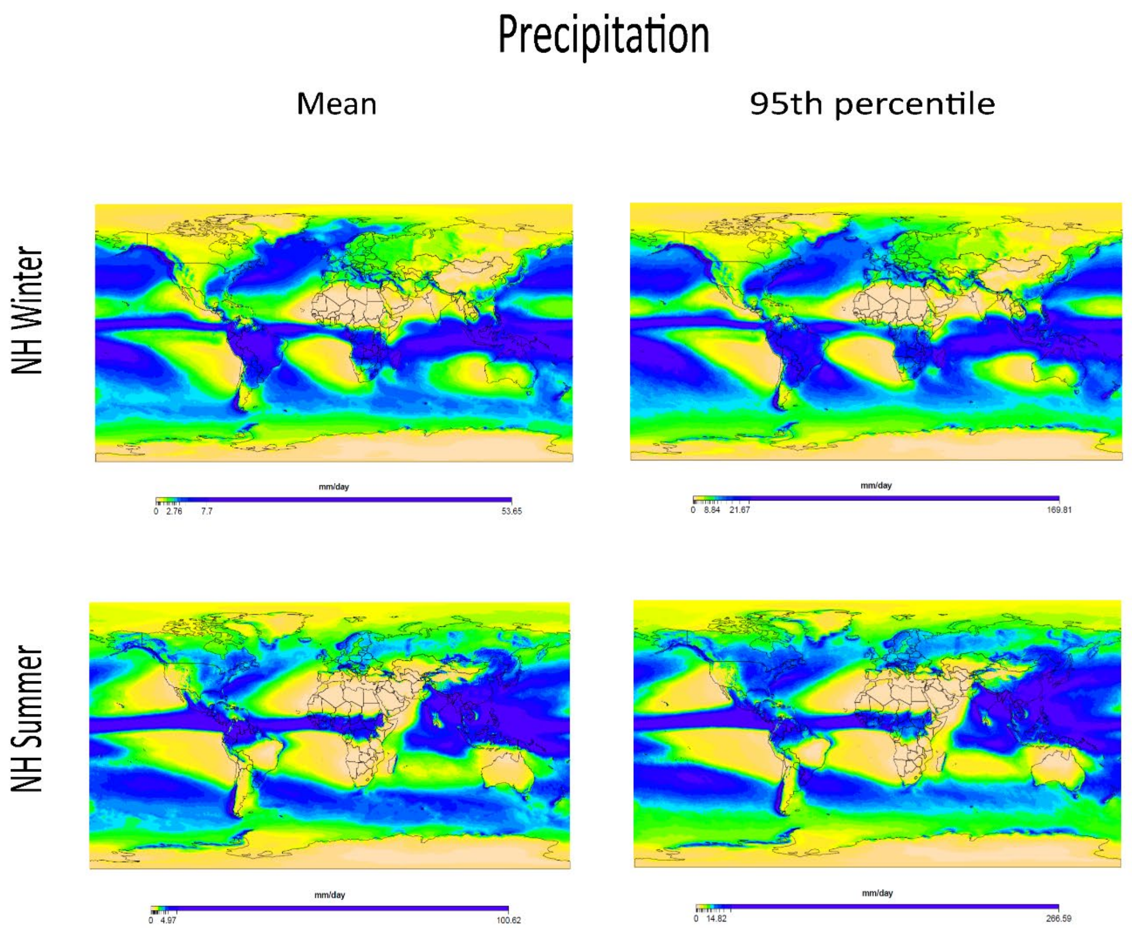
Precipitation
Mean
95th percentile
NH Winter
NH Summer
mm/day
0 2.76 7.7 53.65
mm/day
0 6.84 21.67 169.81
mm/day
0 4.97 100.62
mm/day
0 14.82 266.59

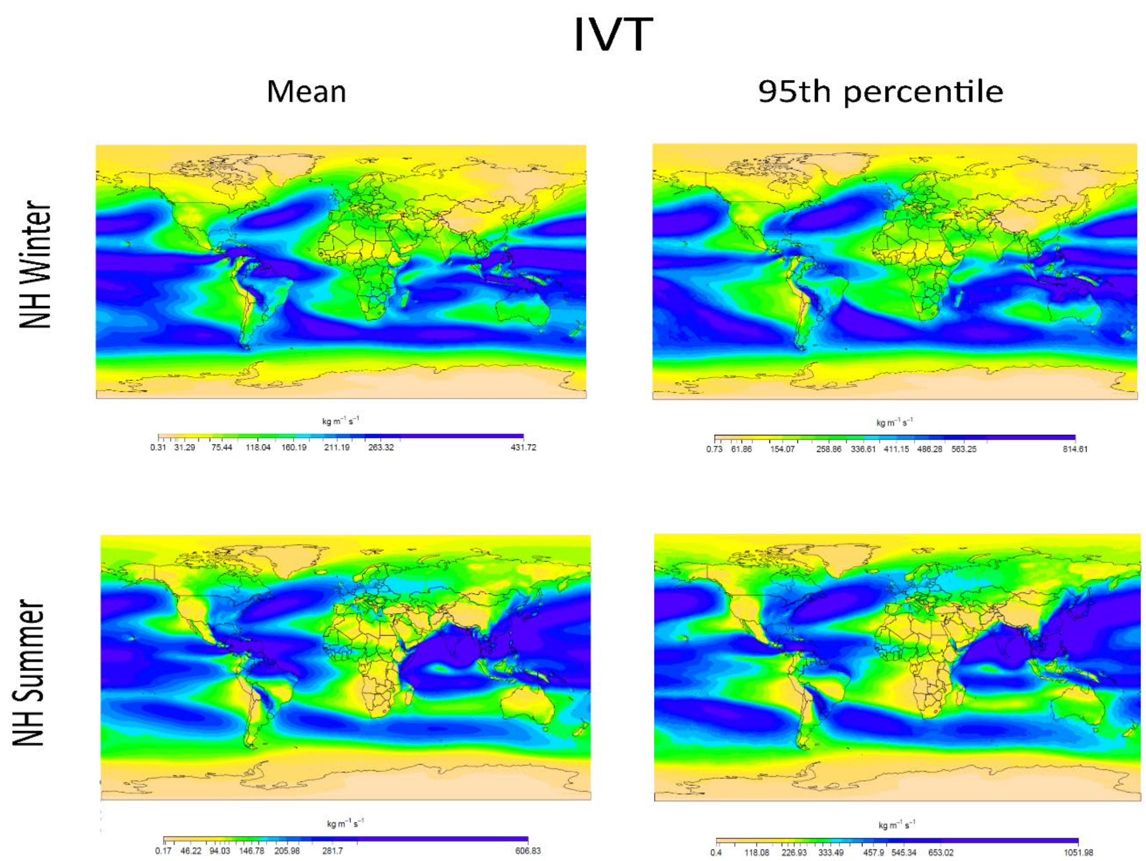
IVT
Mean
95th percentile
NH Winter
NH Summer
kg m⁻¹ s⁻¹
0.31 31.29 75.44 118.04 160.19 211.19 263.32 431.72
kg m⁻¹ s⁻¹
0.73 61.86 154.07 258.86 336.61 411.15 486.28 563.25 814.61
kg m⁻¹ s⁻¹
0.17 46.22 94.03 146.78 205.98 281.7 606.83
kg m⁻¹ s⁻¹
0.4 118.08 226.93 333.49 457.9 545.34 653.02 1051.98

Supplementary Figure 2. Spatial patterns of the mean and 95th percentile for precipitation (top panel) and IVT (bottom panel), for the Northern Hemisphere Winter (December–February) and the Northern Hemisphere Summer (June–August), for the period 1981–2020

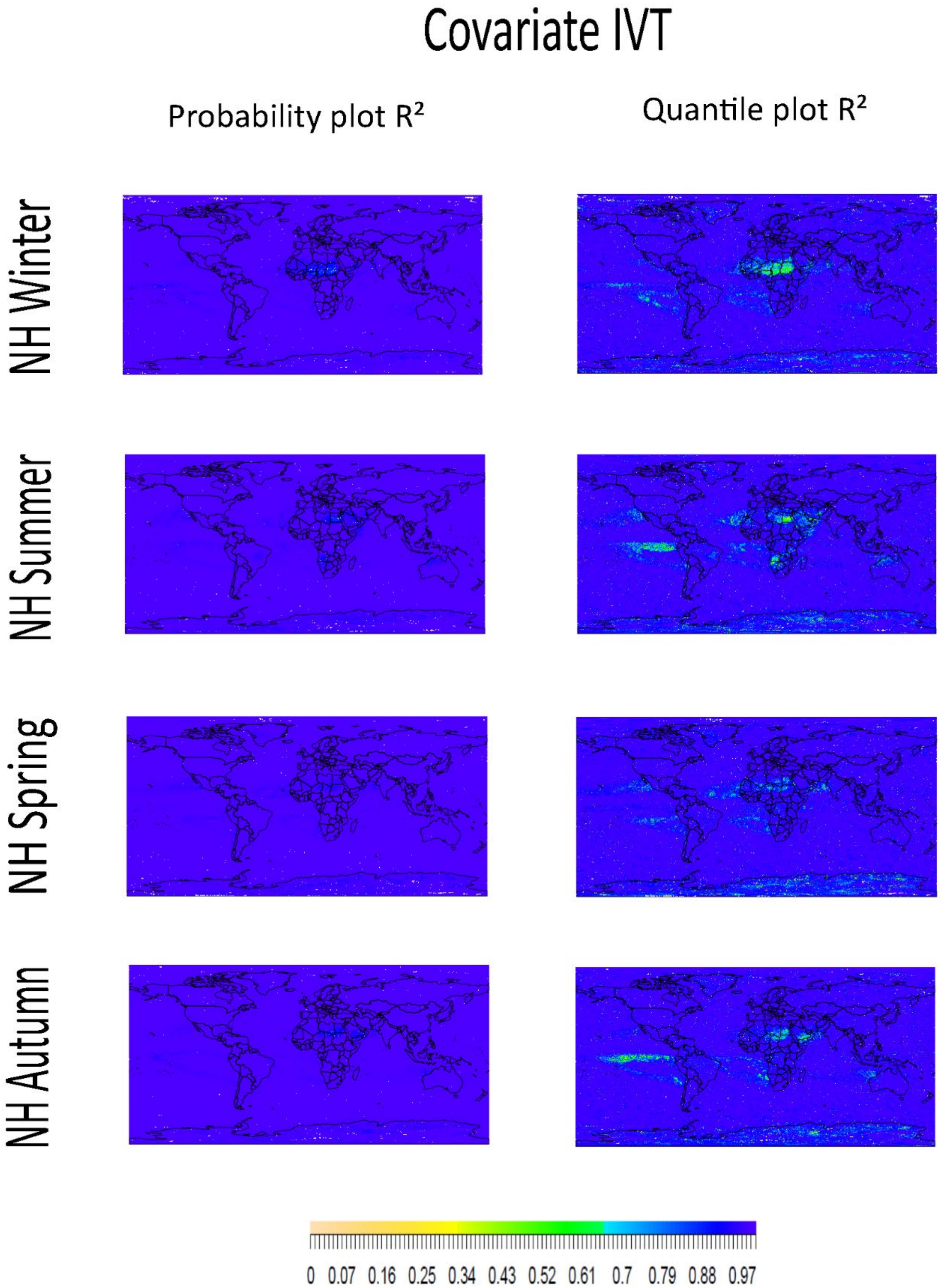

Supplementary Figure 3. Spatial patterns of the R^2 values for the linear models associated with the probability plots (first column) and quantile plots (second column) used for assessing the goodness-of-fit of the non-stationary GEV model with IVT as a covariate in both the location and the scale parameters, for the Northern Hemisphere Winter (December–February), Northern Hemisphere Spring (March-May), Northern Hemisphere Summer (June–August) and Northern Hemisphere Autumn (September-November), for the period 1981–2020

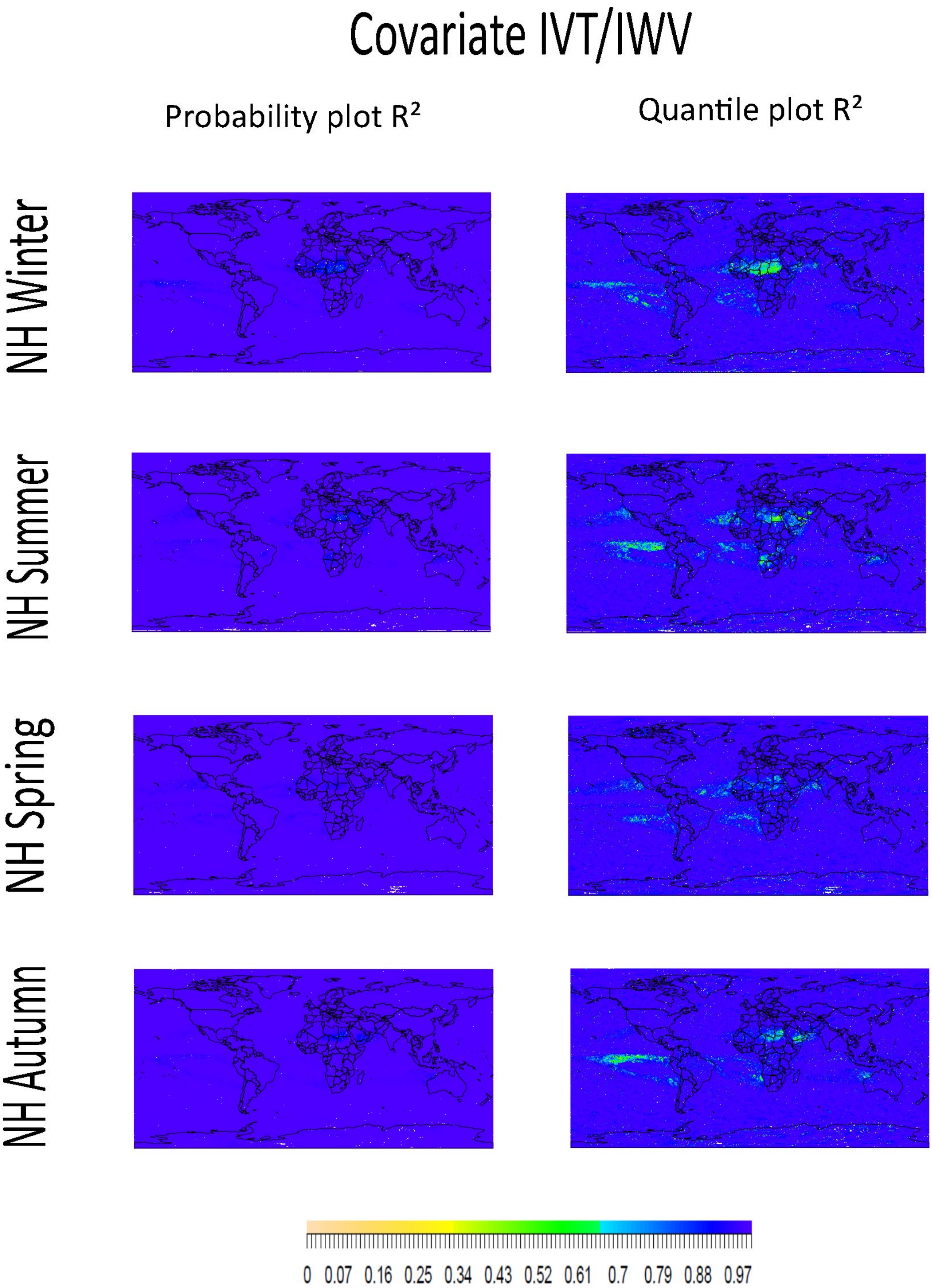

Covariate IVT/IWV
Probability plot R²
Quantile plot R²
NH Winter
NH Summer
NH Spring
NH Autumn
0
0.07
0.16
0.25
0.34
0.43
0.52
0.61
0.7
0.79
0.88
0.97

Supplementary Figure 4. Same as Supplementary Figure 3, but for the non-stationary GEV model with IVT/IWV as a covariate in both the location and the scale parameters

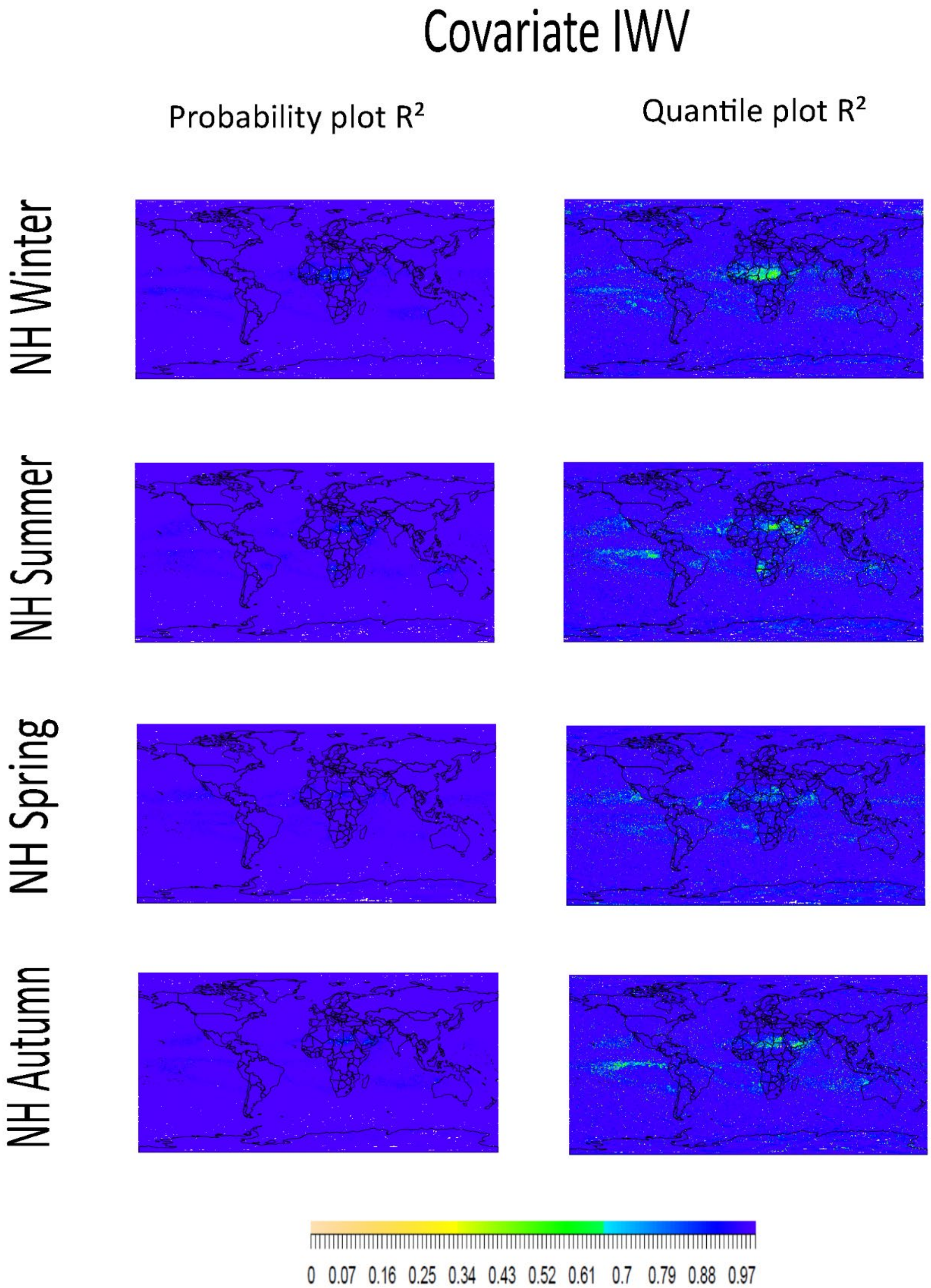

Supplementary Figure 5. Same as Supplementary Figure 3, but for the non-stationary GEV model with IWV as a covariate in both the location and the scale parameters

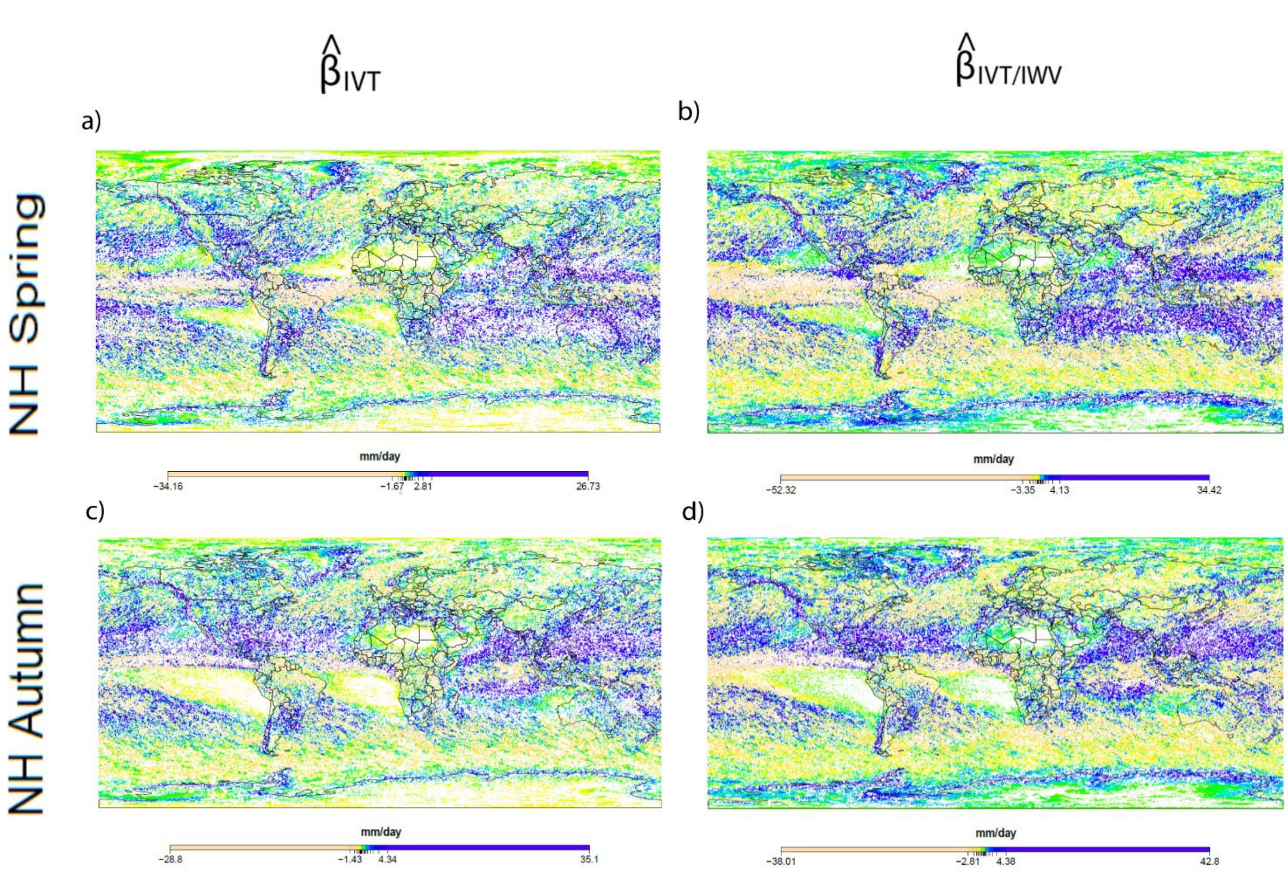

Supplementary Figure 6. Same as Figure 2 for intermediate seasons: a) and b) for Northern Hemisphere Spring (March-May) and c) and d) for Northern Hemisphere Autumn (September-November)

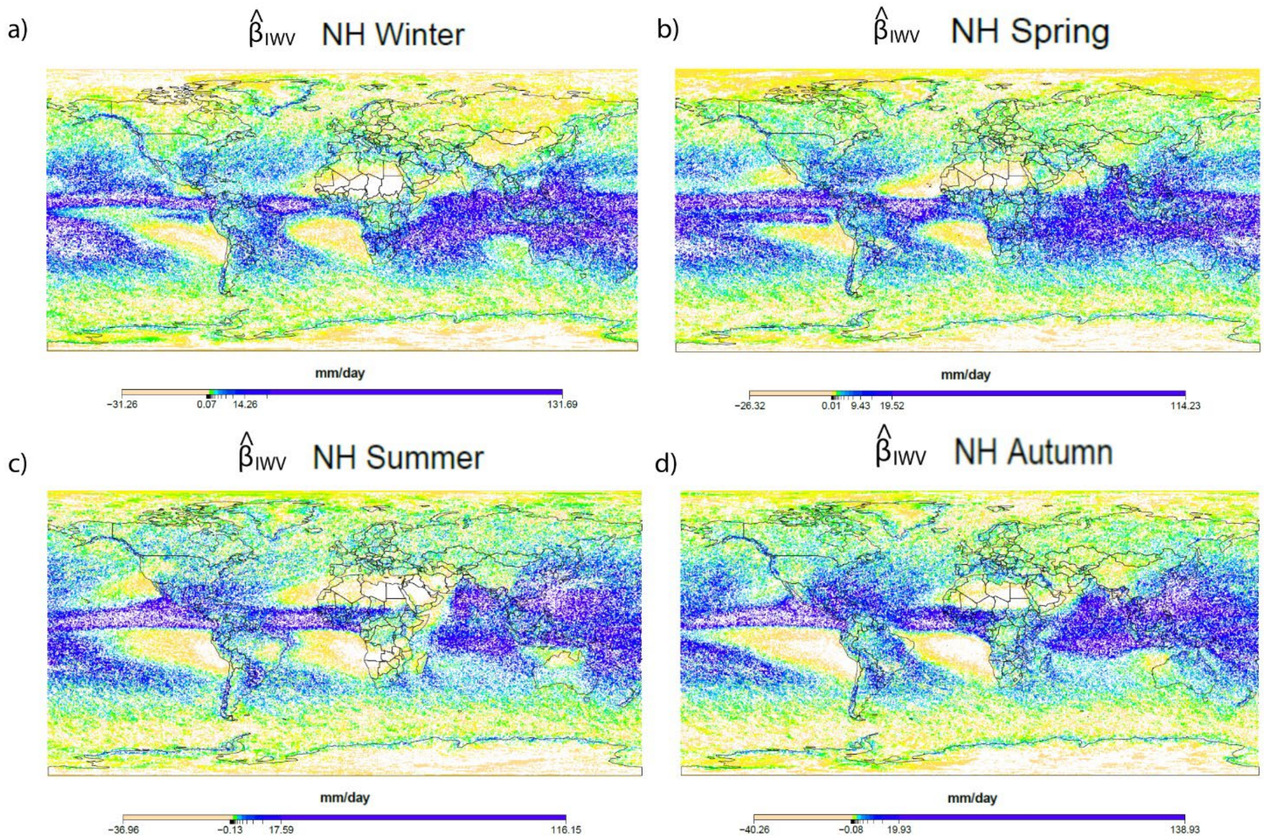

Supplementary Figure 7. Spatial patterns of the significant values of the estimated coefficient that represents the influence of IWV on maximum precipitation according to the GEV analysis (95% confidence level), for a) Northern Hemisphere Winter (December–February), b) Northern Hemisphere Spring (March-May), c) Northern Hemisphere Summer (June–August) and d) Northern Hemisphere Autumn (September-November), for the period 1981–2020

SUPPLEMENTAL MATERIAL FOR:

Concurrent extreme events of atmospheric moisture transport and continental precipitation: the role of landfalling atmospheric rivers

Luis Gimeno-Sotelo [a,*] , Luis Gimeno [a]

[a] *Centro de Investigación Mariña, Universidade de Vigo, Environmental Physics Laboratory (EPhysLab), Ourense, Spain*

[*] *Corresponding author (luis.gimeno-sotelo@uvigo.es)*

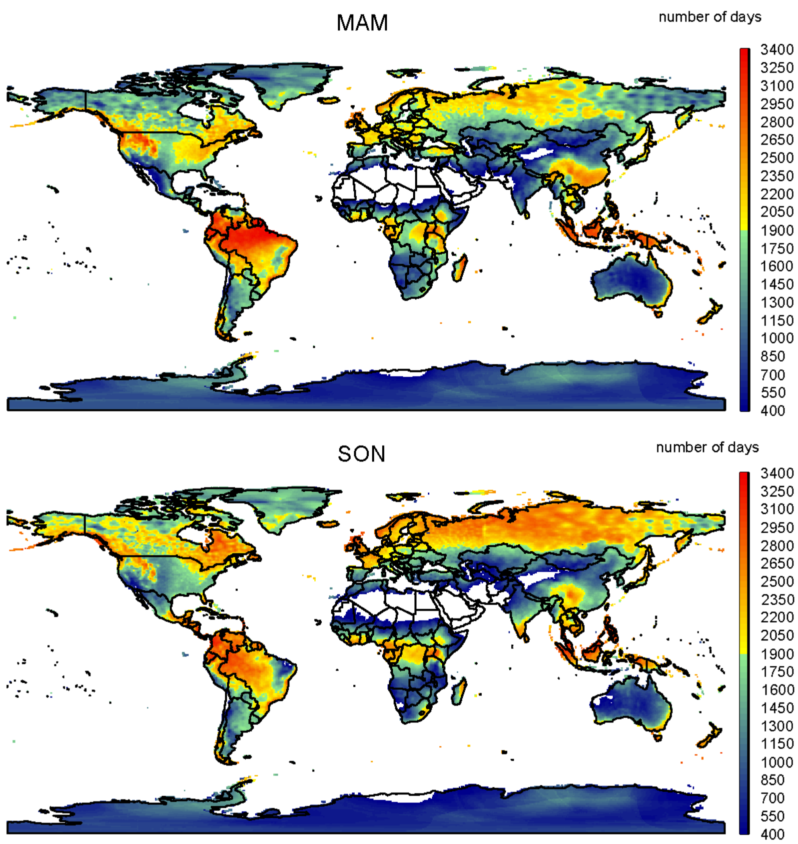

Figure S1: Total number of days for the period 1981-2017 with nonzero precipitation at each grid point for March-April-May (top) and September-October-November (bottom).

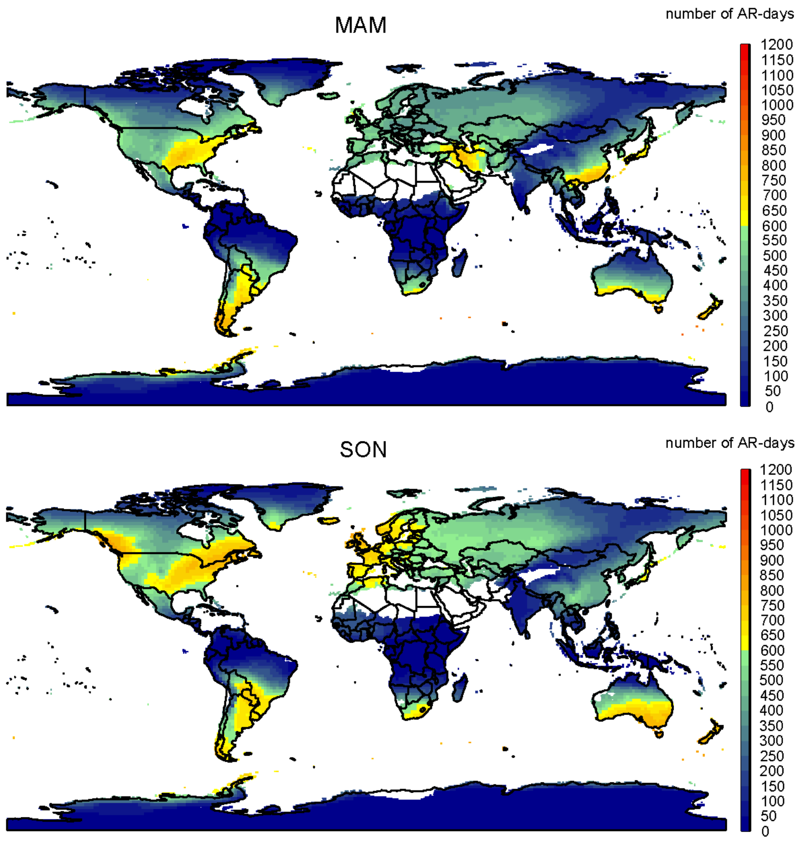

Figure S2: Number of days of occurrence of landfalling ARs for the period 1981-2017 at each grid point, for March-April-May (top) and September-October-November (bottom).

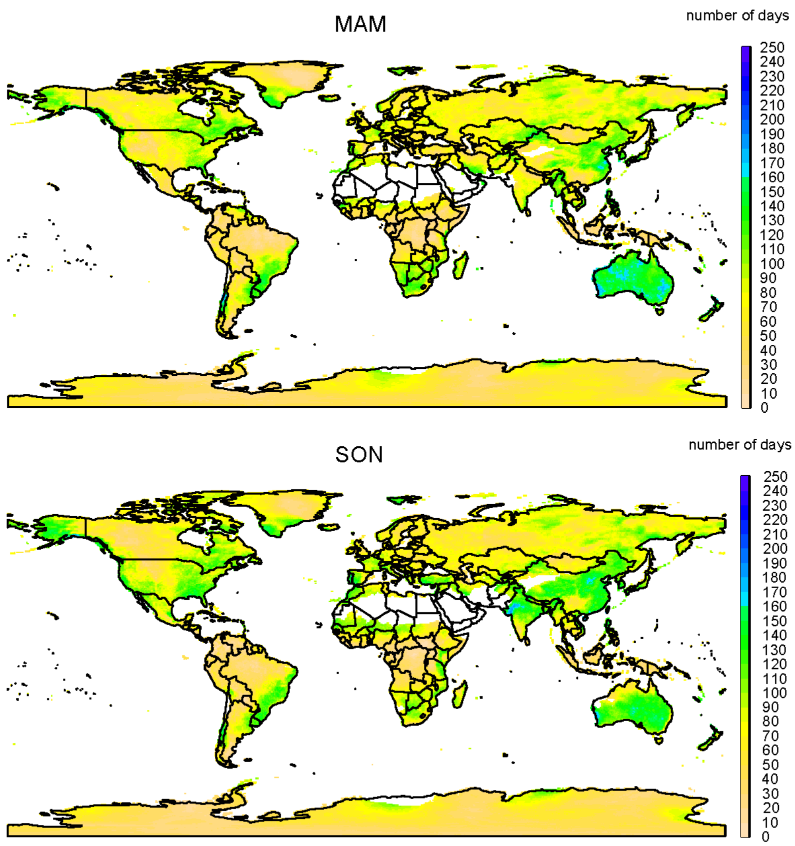

Figure S3: Number of days exceeding the bivariate threshold ($q90_{IVT}$, $q90_{prec}$) for March-April-May (top) and September-October-November (bottom) for the period 1981-2017. The quantiles were calculated including the days of zero precipitation.

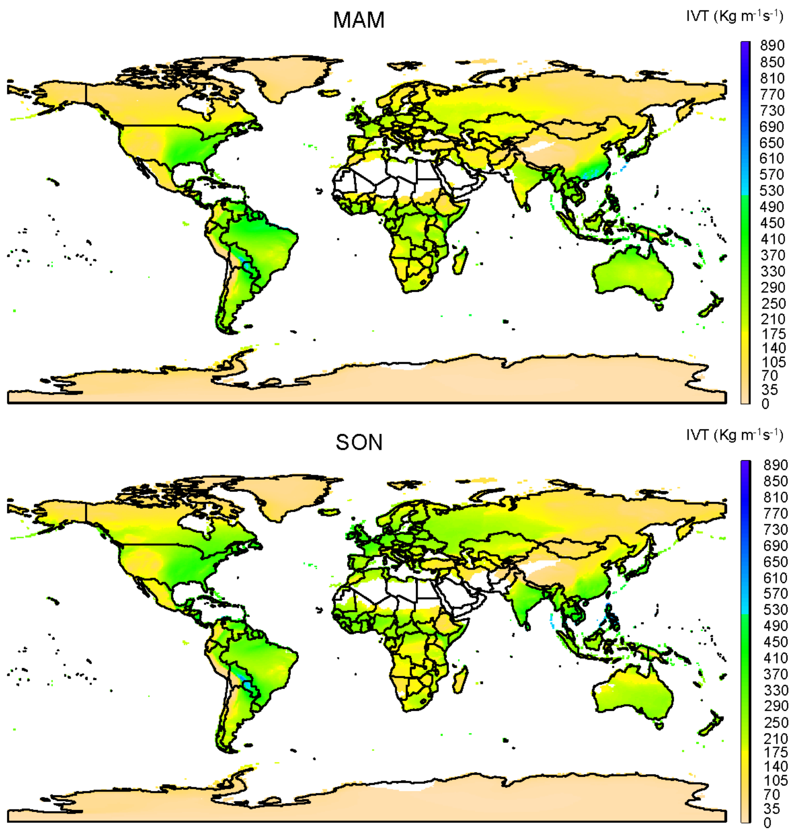

Figure S4: 90th percentile of IVT for March-April-May (top) and September-October-November (bottom) for the period 1981-2017. It was calculated including the days of zero precipitation.

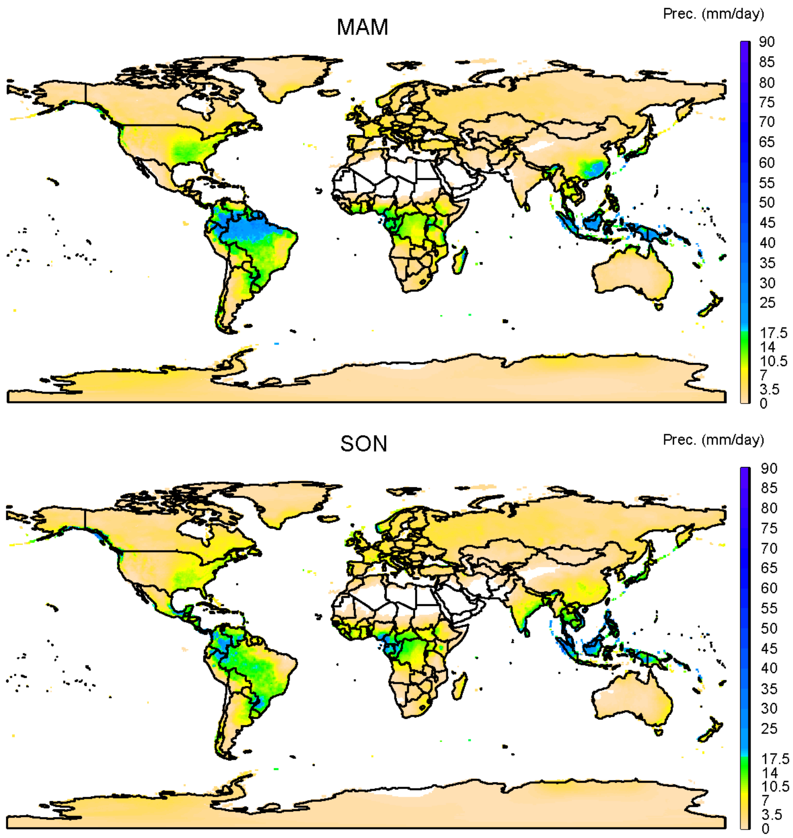

Figure S5: 90th percentile of continental precipitation for March-April-May (top) and September-October-November (bottom) for the period 1981-2017. It was calculated including the days of zero precipitation.

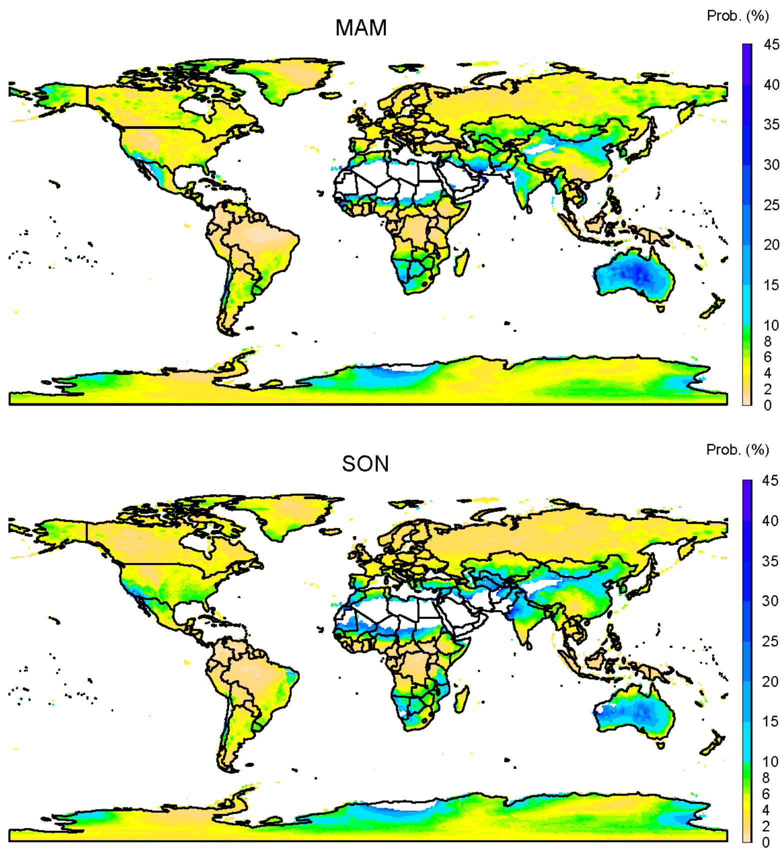

Figure S6: Estimated probability of achieving a concurrent extreme of IVT and continental precipitation (percent), for March-April-May and September-October-November for the period 1981-2017. It is computed using the copula model with the lowest AIC value for each grid point. The quantile-based thresholds were calculated including the days of zero precipitation.

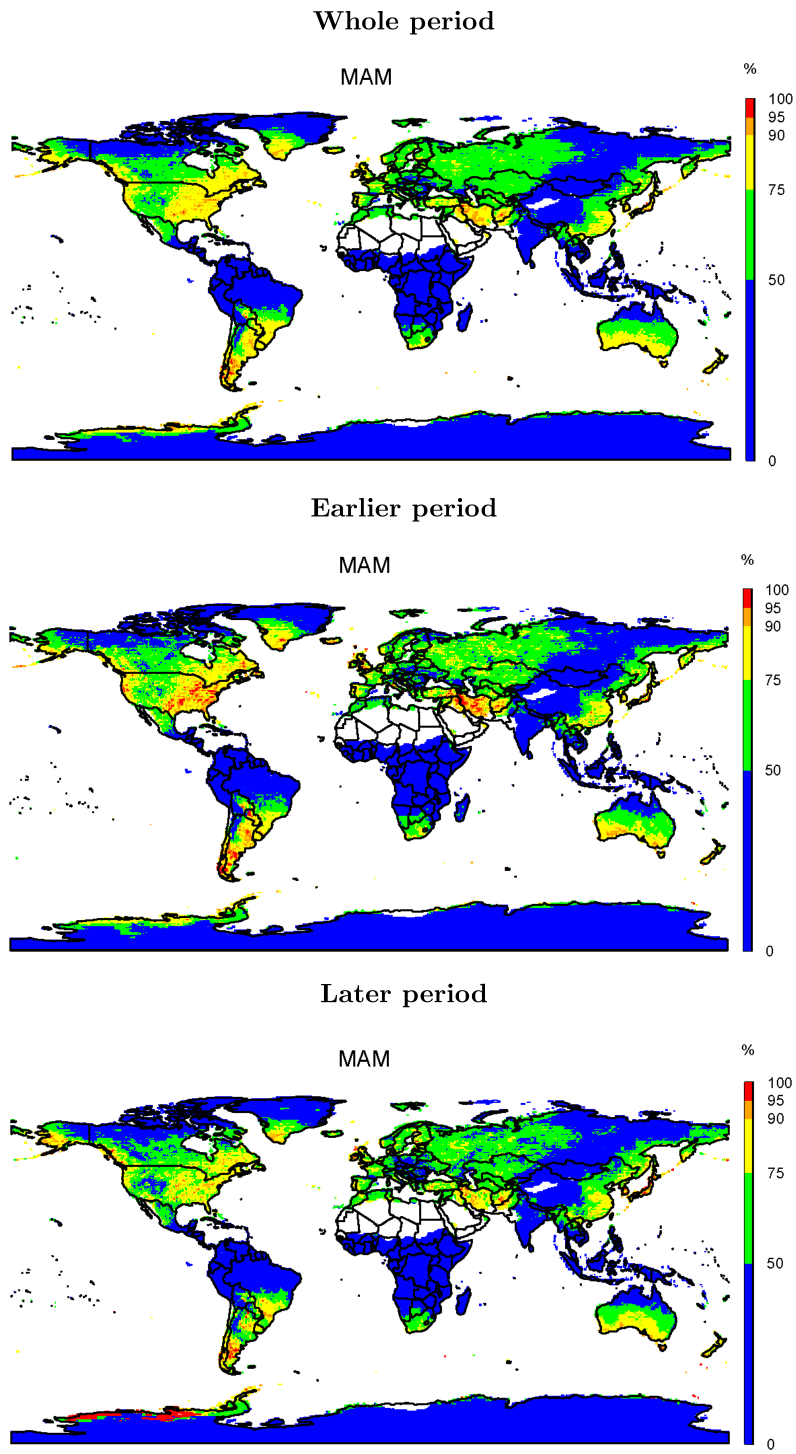

Figure S7: Percentage of concurrent extreme days of IVT and continental precipitation that coincide with the occurrence of landfalling ARs, for **March-April-May**, for the whole period 1981-2017, and the earlier and later studied periods.

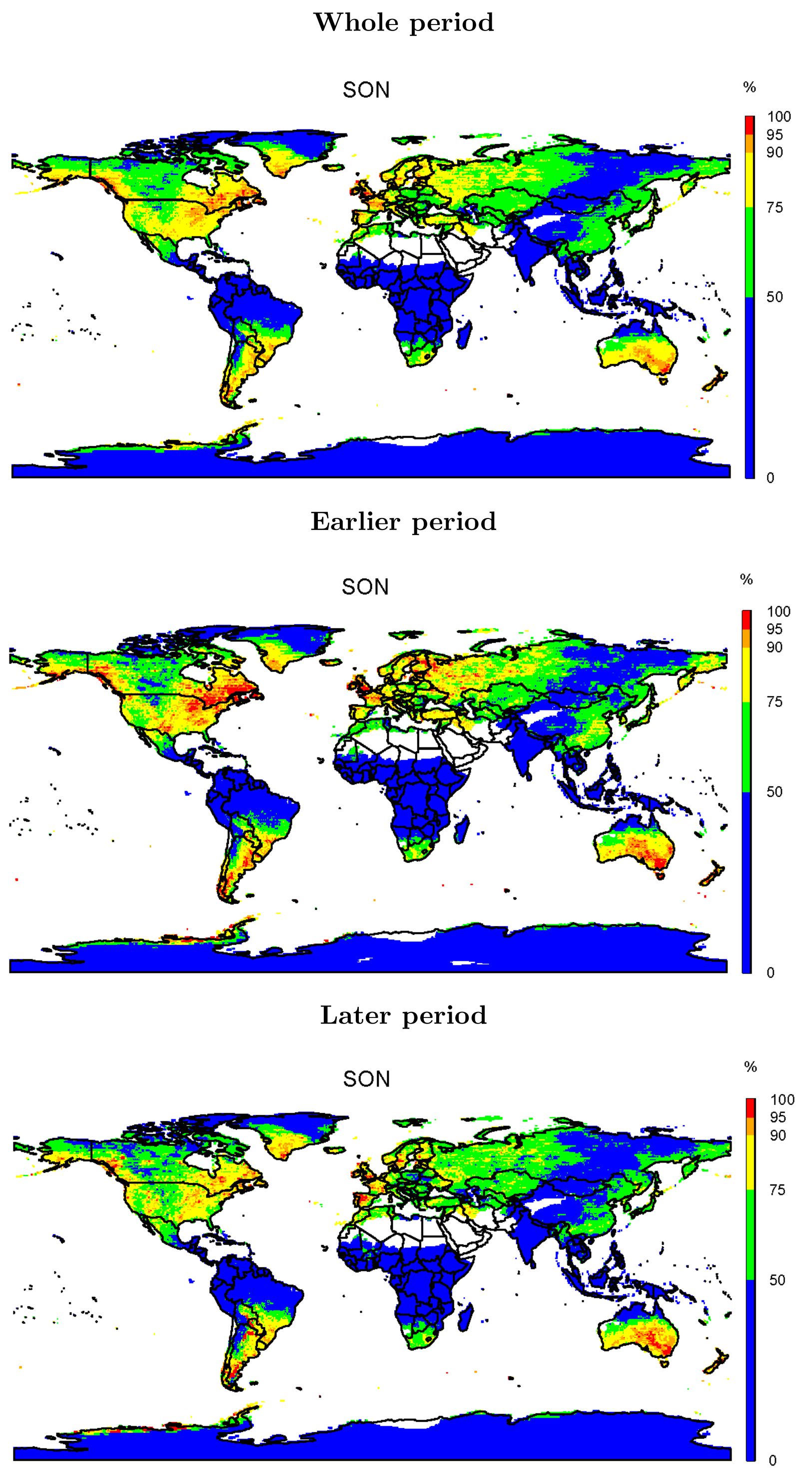

Figure S8: Percentage of concurrent extreme days of IVT and continental precipitation that coincide with the occurrence of landfalling ARs, for **September-October-November**, for the whole period 1981-2017, and the earlier and later studied periods.

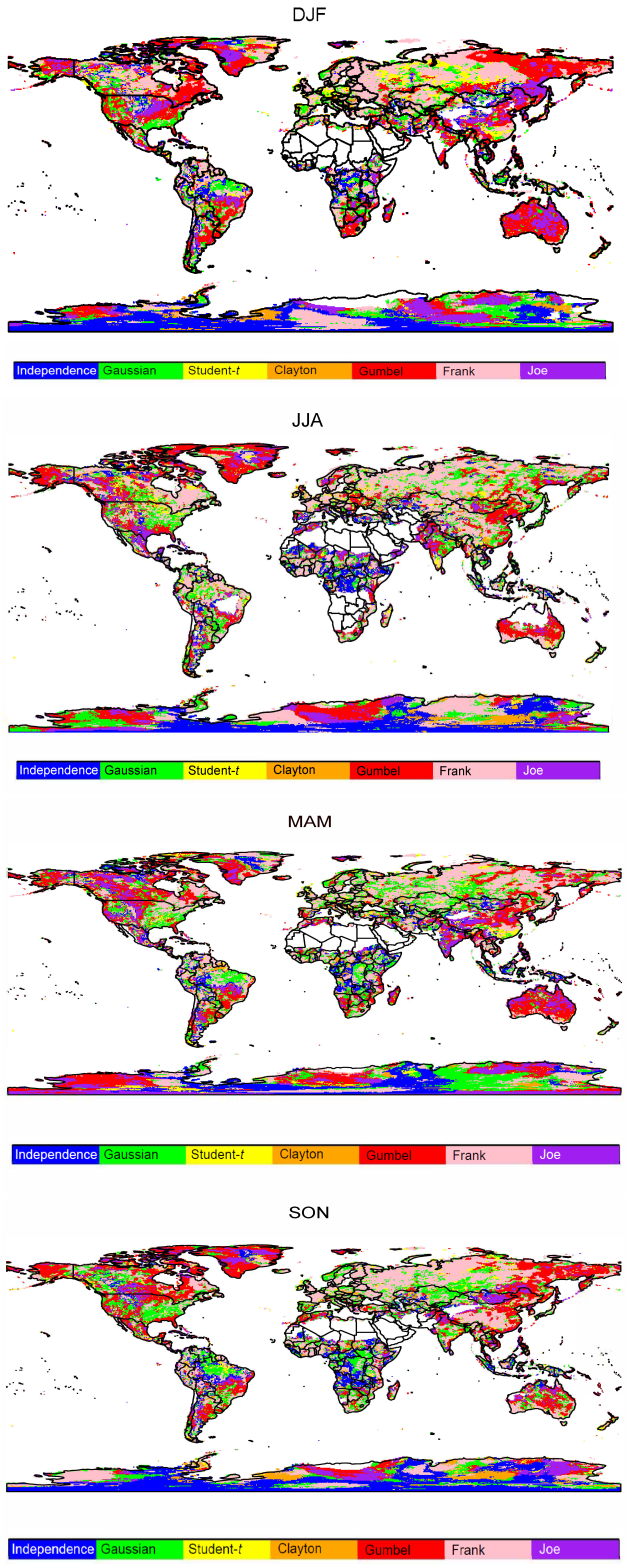

Figure S9: Fitted copula type with the lowest AIC value for each season for the period 1981-2017.

Table S1: Fitted copula type with the lowest AIC value for the IVT and continental precipitation averaged over the main AR landfalling regions, for the whole period 1981-2017 and the earlier and later studied periods.

REG.	**SEASON**	whole period	earlier period	later period
1	DJF	Student-t	Gaussian	Gaussian
2	DJF	Gaussian	Frank	Gumbel
3	DJF	Gaussian	Gumbel	Gaussian
4	DJF	Gumbel	Gumbel	Gumbel
	JJA	Student-t	Gaussian	Student-t
5	JJA	Student-t	Student-t	Student-t
6	DJF	Gaussian	Gaussian	Gaussian
	JJA	Gumbel	Student-t	Gumbel
7	DJF	Gumbel	Gumbel	Gaussian
8	DJF	Gumbel	Frank	Gumbel
9	DJF	Gumbel	Gumbel	Gumbel
10	DJF	Gaussian	Gaussian	Gaussian
11	DJF	Gaussian	Gaussian	Gaussian
12	DJF	Gaussian	Gaussian	Frank
13	DJF	Frank	Student-t	Frank
14	JJA	Frank	Frank	Gumbel
15	DJF	Gumbel	NA	NA
	JJA	Gumbel	Gaussian	Gumbel
16	DJF	Gumbel	Gaussian	Gumbel
	JJA	Gaussian	Gaussian	Gaussian
17	DJF	Gumbel	Gumbel	Gumbel
18	DJF	Gaussian	Gaussian	Gaussian
19	JJA	Frank	Frank	Frank
20	JJA	Frank	Frank	Frank
21	JJA	Student-t	Gaussian	Student-t
22	JJA	Frank	Gaussian	Frank
23	JJA	Joe	Frank	Independence
24	JJA	Gumbel	Gumbel	Gumbel

NA (Not Available): The number of days of nonzero precipitation in the corresponding period is lower or equal to 400.

SUPPLEMENTARY MATERIAL FOR:

Combinations of drivers that most favor the occurrence of daily precipitation extremes

Luis Gimeno-Sotelo[1,*], Emanuele Bevacqua[2], Luis Gimeno[1]

[1] Centro de Investigación Mariña, Universidade de Vigo, Environmental Physics Laboratory (EPhysLab), Campus da Auga, 32004, Ourense, Spain
[2] Department of Computational Hydrosystems, Helmholtz Centre for Environmental Research, 04318 Leipzig, Germany

[*]Corresponding author (luis.gimeno-sotelo@uvigo.es)

Supplementary Method:

Statistical test used to assess the significance of the difference between the probability associated with each of the combination of extreme drivers and the probability associated with the reference case under no extreme drivers (see Method 11 in Newcombe, 1998)

Statistical significance for those differences is assessed using a test based on continuity-corrected score intervals. They are constructed as follows: let *m* the number of cases corresponding to the reference combination of drivers and *n* the one corresponding to a different combination, and *A* and *B* the random variables that represent the number of cases of extreme precipitation within those samples, respectively. The observed values of *A* and *B* are denoted as *a* and *b*, respectively. The estimated conditional probability of extreme precipitation for the reference combination is therefore $p_1 = \frac{a}{m}$ and for the other combination it is $p_2 = \frac{b}{n}$. The confidence interval for the difference of estimated probabilities, i.e., $\hat{\theta} = p_1 - p_2$, has a lower bound $L = \hat{\theta} - \delta$ and an upper bound $U = \hat{\theta} + \varepsilon$, where $\delta = z\sqrt{\frac{l_1(1-l_1)}{m} + \frac{u_2(1-u_2)}{n}}$ and $\varepsilon = z\sqrt{\frac{u_1(1-u_1)}{m} + \frac{l_2(1-l_2)}{n}}$. In the previous expressions, z is the standard normal quantile of probability $1-\frac{\alpha}{2}$, which is equal to 1.96 for α=0.05 (confidence level=95%); l_1 and u_1 are the limits of the interval $\left\{\pi_1 \text{ such that } |\pi_1 - \frac{a}{m}| - \frac{1}{2m} \leq z\sqrt{\frac{\pi_1\,(1-\pi_1\,)}{m}}\right\}$ and l_2 and u_2 are the limits of the interval $\left\{\pi_2 \text{ such that } |\pi_2 - \frac{b}{n}| - \frac{1}{2n} \leq z\sqrt{\frac{\pi_2\,(1-\pi_2\,)}{n}}\right\}$, where π_1 and π_2 are the expected values of the random variables $\frac{A}{m}$ and $\frac{B}{n}$, respectively.

Newcombe, R. G. (1998). Interval estimation for the difference between independent proportions: comparison of eleven methods. Statistics in medicine, 17(8), 873-890.

Figures

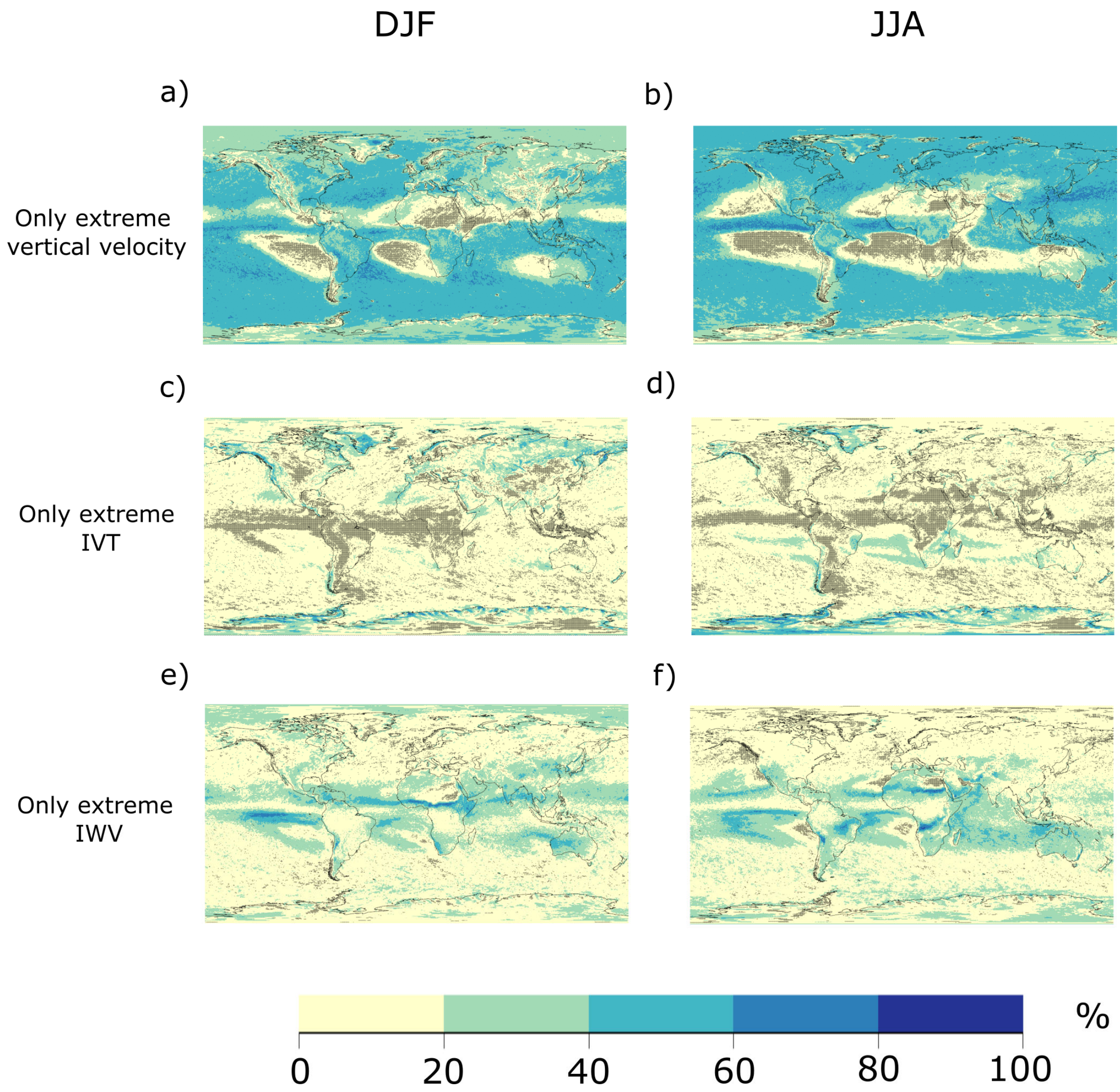

Figure S1. Estimated conditional probability of extreme precipitation for the combinations of one extreme driver (areas without stippling for values greater than 5%, i.e., the value expected under the independence of precipitation extreme occurrence from the drivers). a), b) refer to the combination of only extreme vertical velocity; c), d) to only extreme IVT; and e), f) to only extreme IWV, for December-February and June-August, respectively

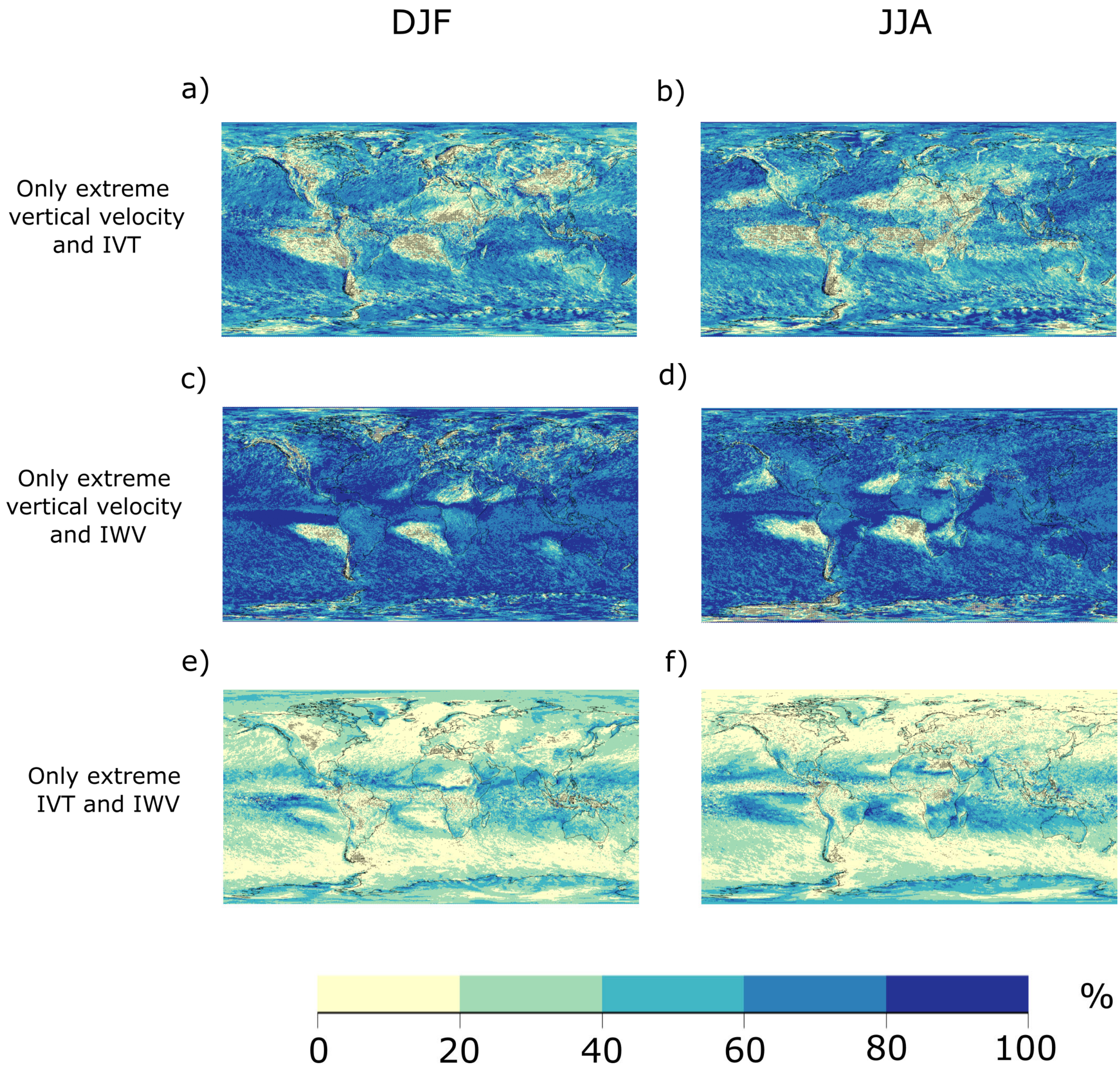

Figure S2. Estimated conditional probability of extreme precipitation for the combinations of two extreme drivers (areas without stippling for values greater than 5%, i.e., the value expected under the independence of precipitation extreme occurrence from the drivers). a), b) refer to the combination of only extreme vertical velocity and IVT; c), d) to only extreme vertical velocity and IWV; and e), f) to only extreme IVT and IWV, for December-February and June-August, respectively

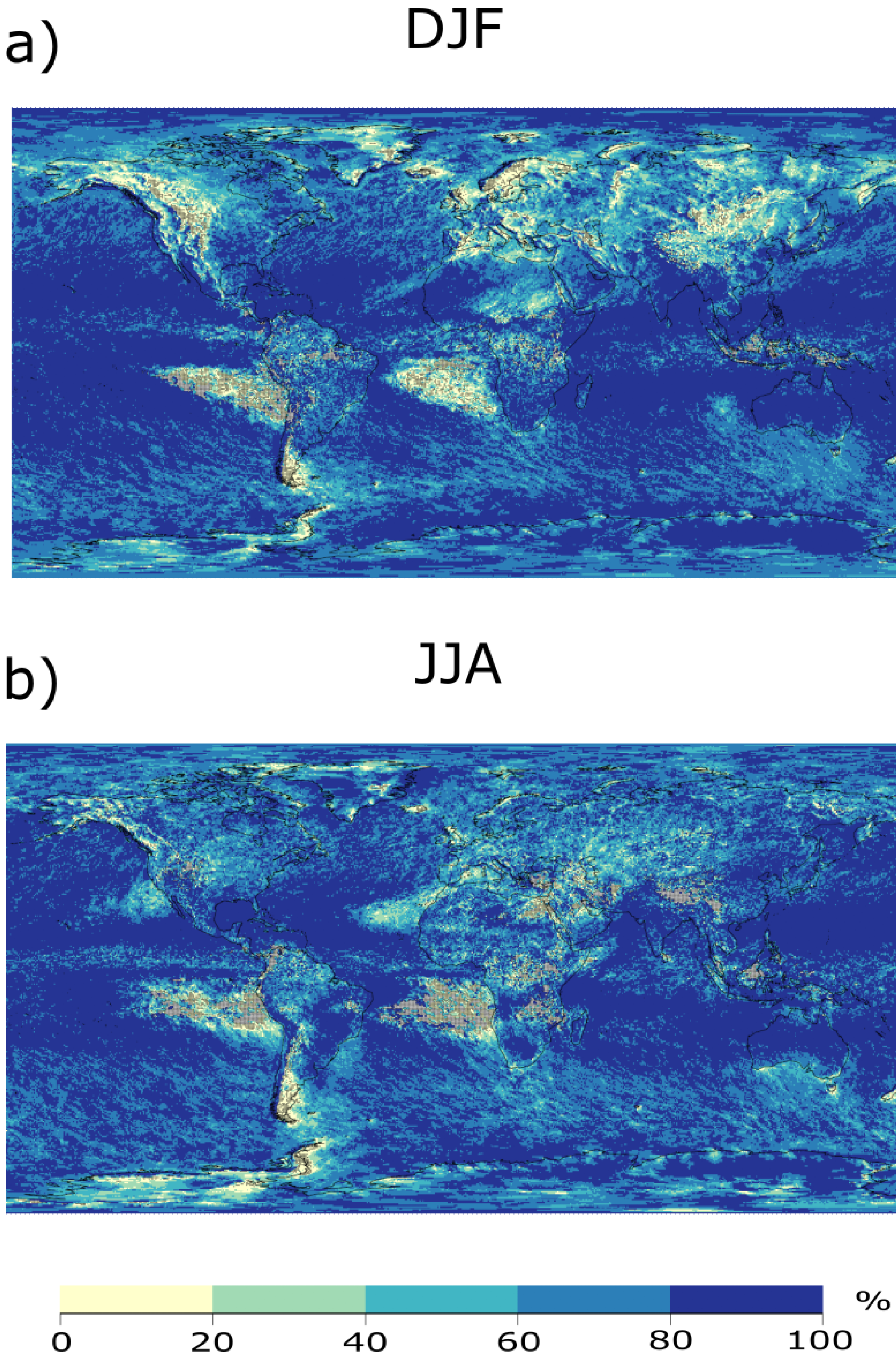
a)
DJF
b)
JJA
%
0
20
40
60
80
100

Figure S3. Estimated conditional probability of extreme precipitation for the combination of the three extreme drivers (areas without stippling for values greater than 5%, i.e., the value expected under the independence of precipitation extreme occurrence from the drivers), for a) December-February and b) June-August

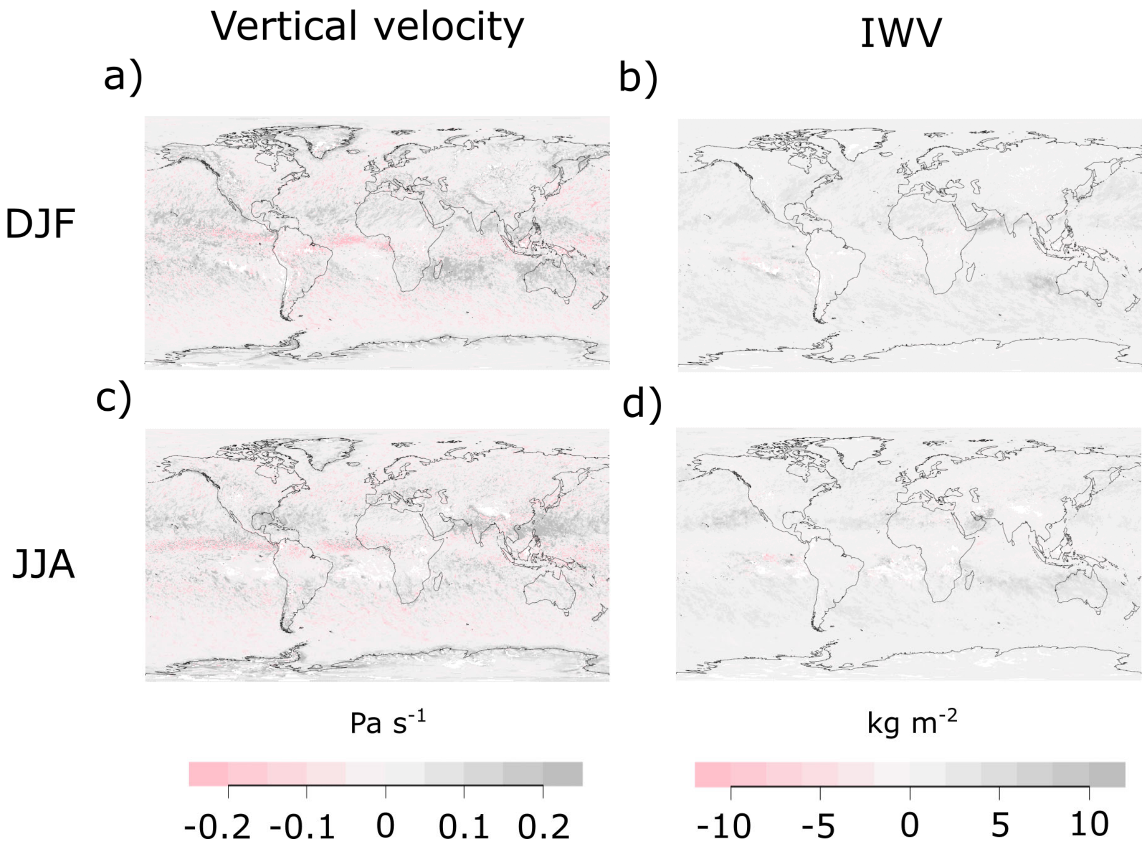

Figure S4. Difference between the mean values of vertical velocity and total column water vapor under the combination of the three extreme drivers and those under the combination of only extreme vertical velocity and IWV (and non-extreme IVT). a), c) Refer to the vertical velocity difference; b), d) IWV difference, for December-February and June-August, respectively

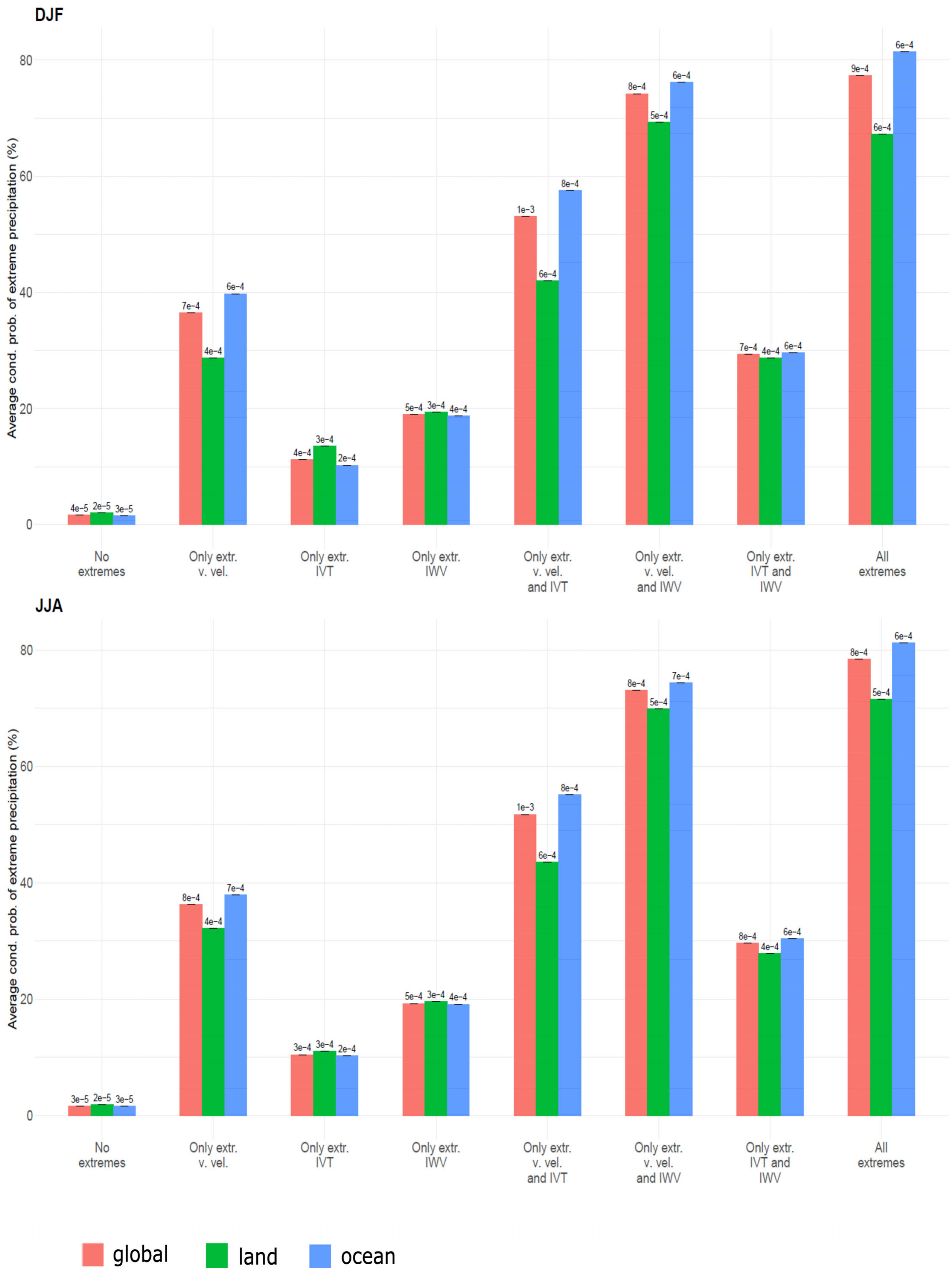

DJF
JJA
Average cond. prob. of extreme precipitation (%)
No extremes
Only extr. v. vel.
Only extr. IVT
Only extr. IWV
Only extr. v. vel. and IVT
Only extr. v. vel. and IWV
Only extr. IVT and IWV
All extremes
global
land
ocean

Figure S5. Average conditional probability of extreme precipitation for each combination of drivers, for all the globe and for land and oceanic areas separately, for December-February and June-August. The corresponding standard errors can be found above each bar

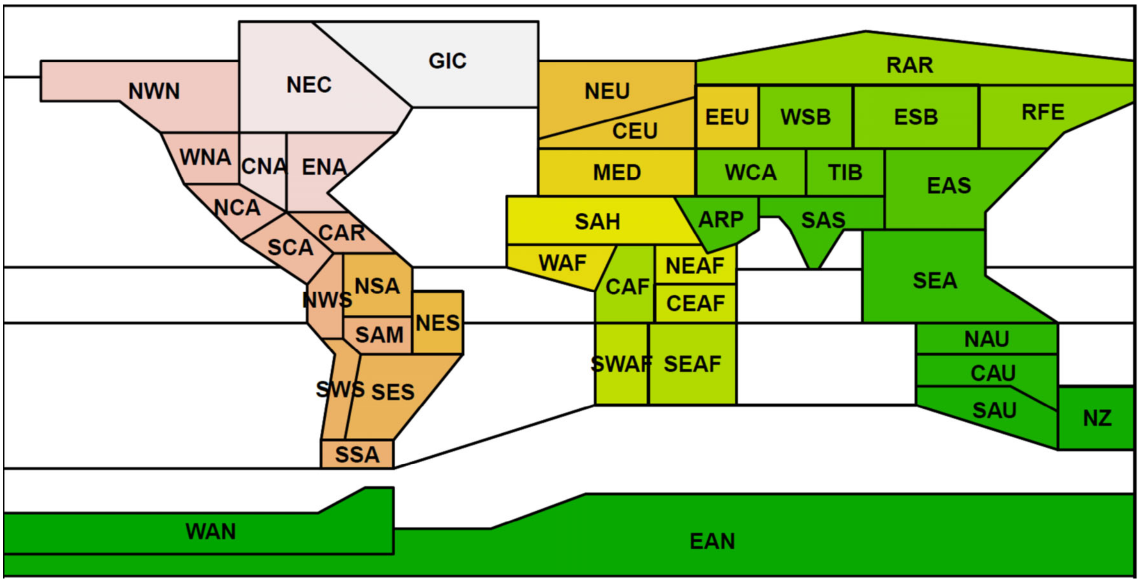

Figure S6. IPCC subregions used in this study. GIC: Greenland/Iceland, NEC: N.E.Canada, CNA: C.North-America, ENA: E.North-America, NWN: N.W.North-America, WNA: W.North-America, NCA: N.Central-America, SCA: S.Central-America, CAR: Caribbean, NWS: N.W.South-America, SAM: South-American-Monsoon, SSA: S.South-America, SWS: S.W.South-America, SES: S.E.South-America, NSA: N.South-America, NES: N.E.South-America, NEU: N.Europe, CEU: C.Europe, EEU: E.Europe, MED: Mediterranean, WAF: West-Africa, SAH: Sahara, NEAF: North-East-Africa, CEAF: Central-East-Africa, SWAF: South-West-Africa, SEAF: South-Eeast-Africa, CAF: Central-Africa, RAR: Russian-Arctic, RFE: Russian-Far-East, ESB: E.Siberia, WSB: W.Siberia, WCA: W.C.Asia, TIB: Tibetan-Plateau, EAS: E.Asia, ARP: Arabian-Peninsula, SAS: S.Asia, SEA: S.E.Asia, NAU: N.Australia, CAU: C.Australia, SAU: S.Australia, NZ: New-Zealand, EAN: E.Antarctica, WAN: W.Antarctica. IPCC subregions website: https://github.com/SantanderMetGroup/ATLAS/tree/v1.1

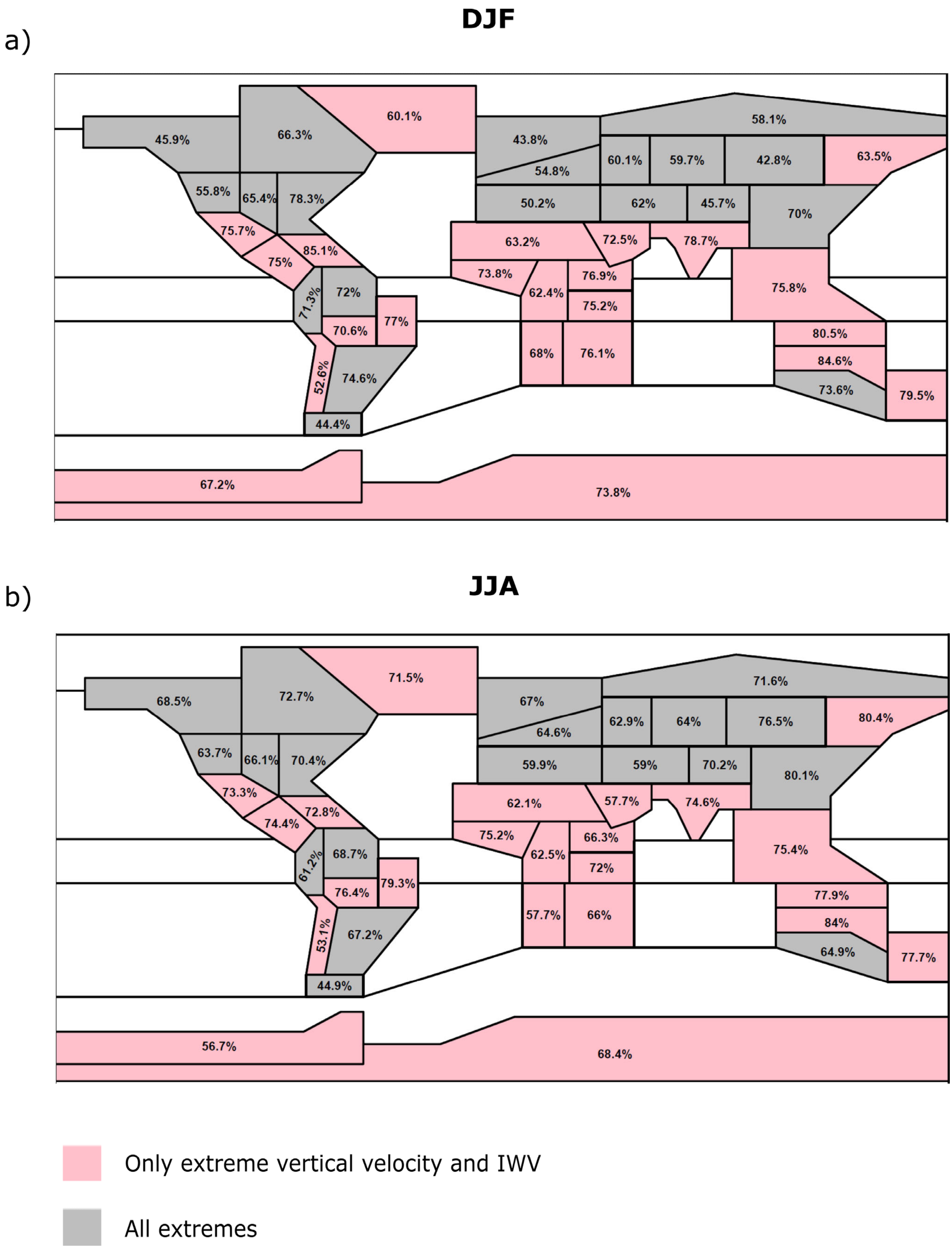

Figure S7. Same as Figure 7, but for the combination of drivers associated with the second-highest average probability of extreme precipitation for each of the IPCC subregions used in this study

nature water

Article https://doi.org/10.1038/s44221-023-00192-4

Unravelling the origin of the atmospheric moisture deficit that leads to droughts

In the format provided by the authors and unedited

Contents of this file

Supplementary Tables

Table S1: Average conditional probability of drought given an equivalent moisture transport deficit over the areas of dominance of the major oceanic moisture sources considered in this study, for two subsamples: 1) considering only months with high land-ocean temperature contrast and low land relative humidity, and 2) months with low land-ocean temperature contrast and high land relative humidity. For each moisture source, its acronym is the same as that used in Figure 2 and its area of dominance is shown in Figure 2a (SPI at one-month time scale was used as it enabled the subsamples to have a larger sample size). In this context, a month is considered to have high (low) temperature contrast or relative humidity if it is within the top (bottom) 50% values of that variable. In the table, a value appears in bold if the average probability for that subsample is greater and significantly different from that corresponding to the other subsample at 5% significance level, using a two-sample *t*-test for difference in means

	High land-ocean temperature contrast and low land relative humidity	Low land-ocean temperature contrast and high land relative humidity
NATL	0.139	**0.159**
MED	0.135	**0.172**
ZANAR	0.123	**0.162**
SPAC	0.143	0.142
SATL	**0.110**	0.091
RED	0.142	0.176
NPAC	0.145	**0.184**
IND	0.087	**0.201**
CORAL	0.128	**0.159**
AGU	0.104	**0.117**
CAR	0.177	**0.275**

Table S2: Results about the analysis of a well-known drought event in CENA (central-east North America), SESA (south-east South America) and EEur (east Europe), for SPI at the time scales of 1 and 3 months. For each time scale, the peak SPI value in each event is identified, and the probability of drought occurrence given the observed moisture source contribution deficit at the peak SPI date is estimated using a copula model (information about the copula family and goodness-of-fit test can also be found). For this analysis, the monthly MSWEP and each moisture source contribution series were first averaged over the studied regions before obtaining the standardized indexes

Region	CENA	SESA	EEur
Major moisture source	Caribbean/Mexican	Amazon	Mediterranean
Event	1988	1988	2011
Reference	Trenberth et al.[1], Cook et al.[2], Spinoni et al.[3]	Vargas et al.[4]	Spinoni et al.[5], Ionita and Nagavciuc[6]
1-month time scale			
Dates Episode SPI	01/1988 – 07/1988	02/1988 – 08/1988	08/2011 - 11/2011
Peak SPI value (Date)	-2.6 (05/1988)	-1.9 (07/1988)	-3.1(11/2011)
SPIc at peak SPI date	-2.4	-1.2	-4.1
Copula family (SPI , SPIc)	Student-t	Student-t	Student-t
Goodness-of-fit test p-value	0.63	0.51	0.07
Probability of drought given SPIc at peak SPI date	68.3 %	9.2 %	61.9 %
3-month time scale			
Dates Episode SPI	02/1988 – 08/1988	02/1988 – 07/1989	03/2011 - 01/2012
Peak SPI value (Date)	-3.6 (06/1988)	-1.6 (06/1988)	-1.6(03/2011)
SPIc at peak SPI date	-3.5	-1.3	-0.7
Copula family (SPI, SPIc)	Gaussian	Gumbel	Gumbel

Goodness-of-fit test p-value	0.20	0.95	0.85
Probability of drought given SPIc at peak SPI date	78.1 %	17.8 %	6.7 %

Supplementary Figures

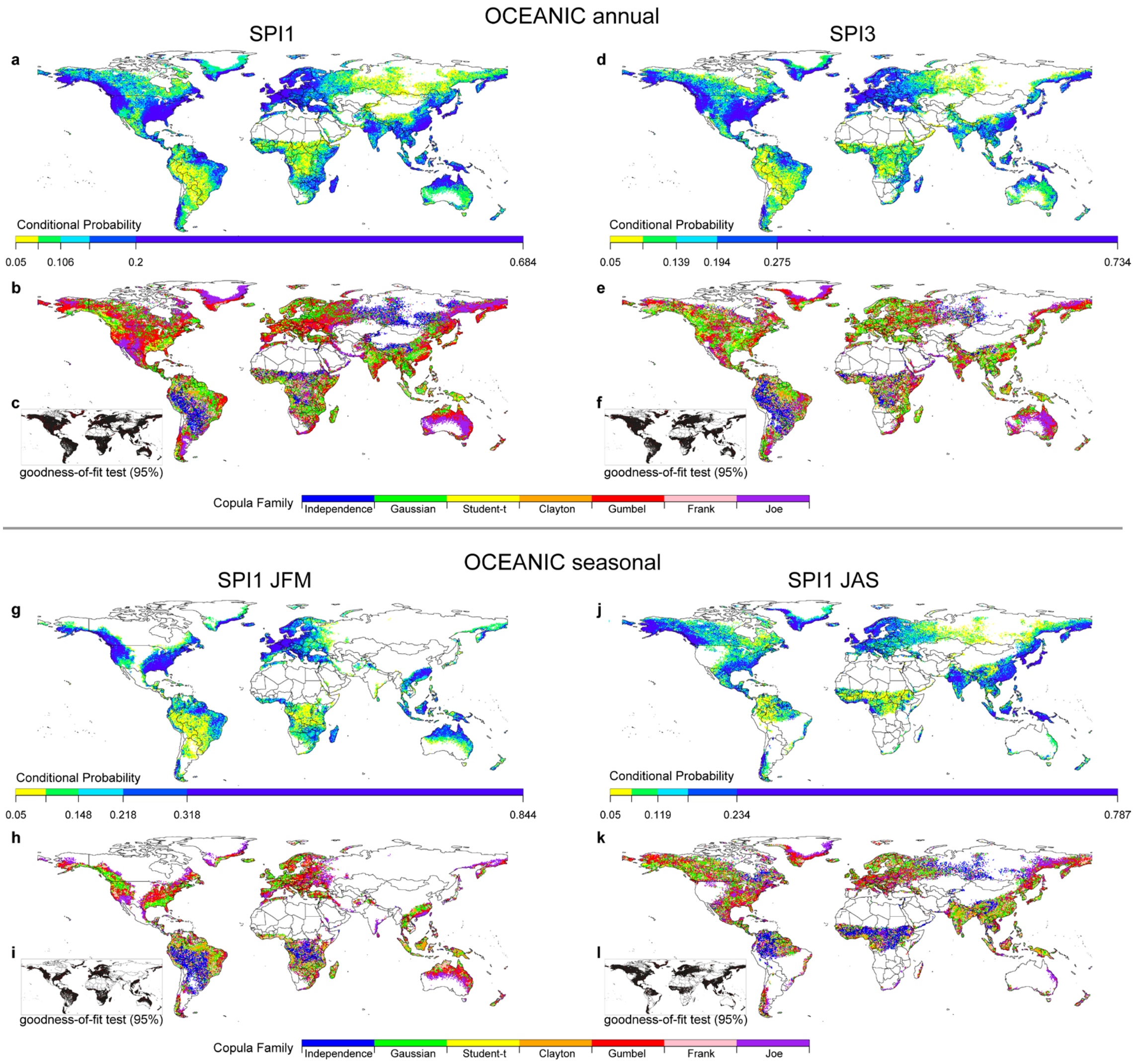

Figure S1: Values of the conditional probability of drought occurrence given an equivalent moisture deficit from oceanic origin, and information about the selected copula model at each grid point, for annual and seasonal scales. The Statistical method I was applied to the contribution to precipitation of oceanic origin (see Methods for details). a) and d) refer to the spatial pattern of the values of that conditional probability, b) and e) to the copula family of the selected model at each grid point, and c) and f) to the results of the goodness-of-fit test (a black dot indicates that the selected copula at that grid point fits well to the data at 95% confidence level; a red dot is used otherwise), for January-December and SPI at the time scales of 1 and 3 months, respectively. g) and j) are analogous to a), h) and k) are analogous to b), and i) and l) are analogous to c), but for January-March and July-September, respectively (SPI at one-month time scale was used as it enabled the subsamples to have a larger sample size)

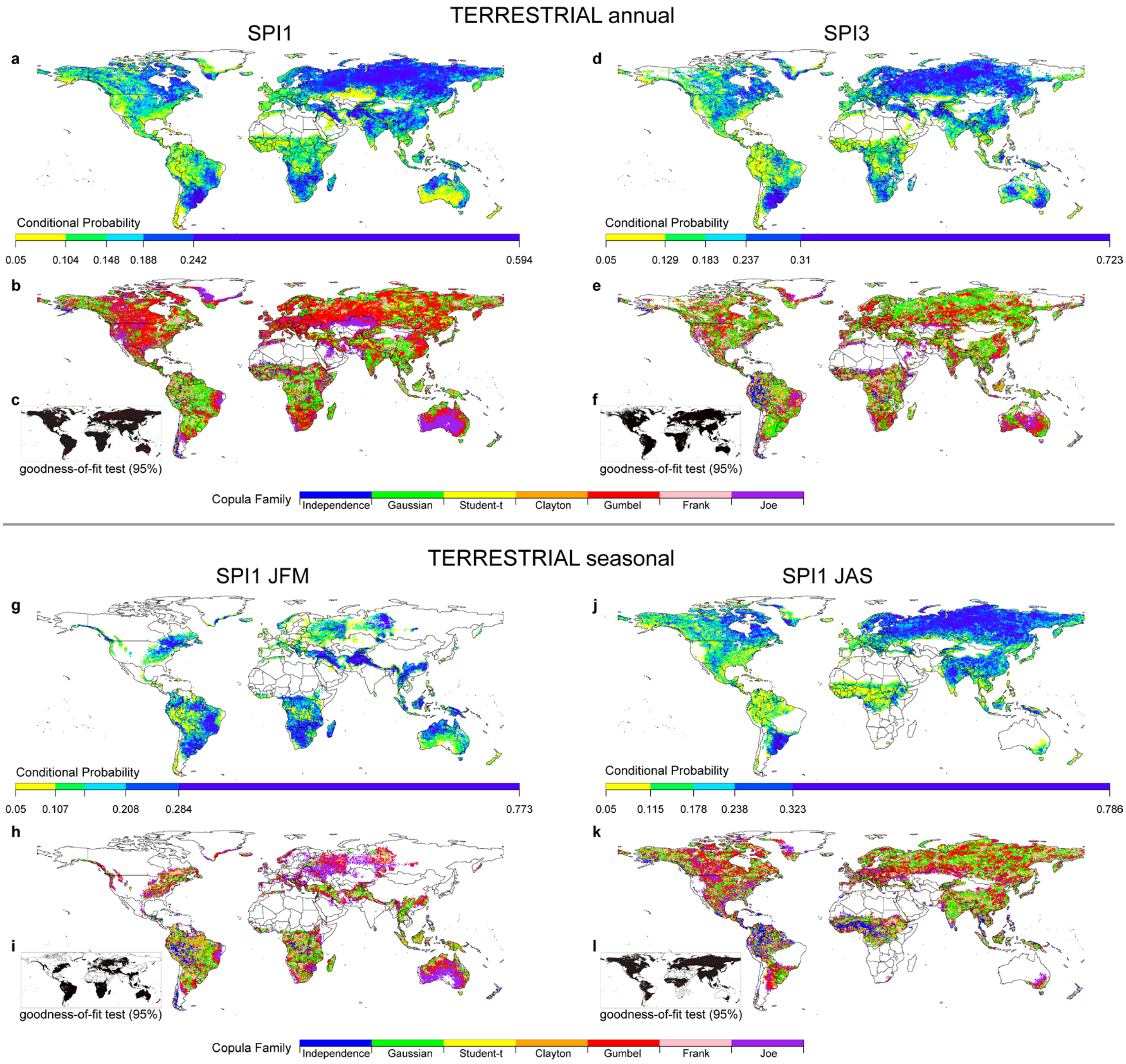

Figure S2: Same as Figure S1, but for the moisture deficit from terrestrial origin

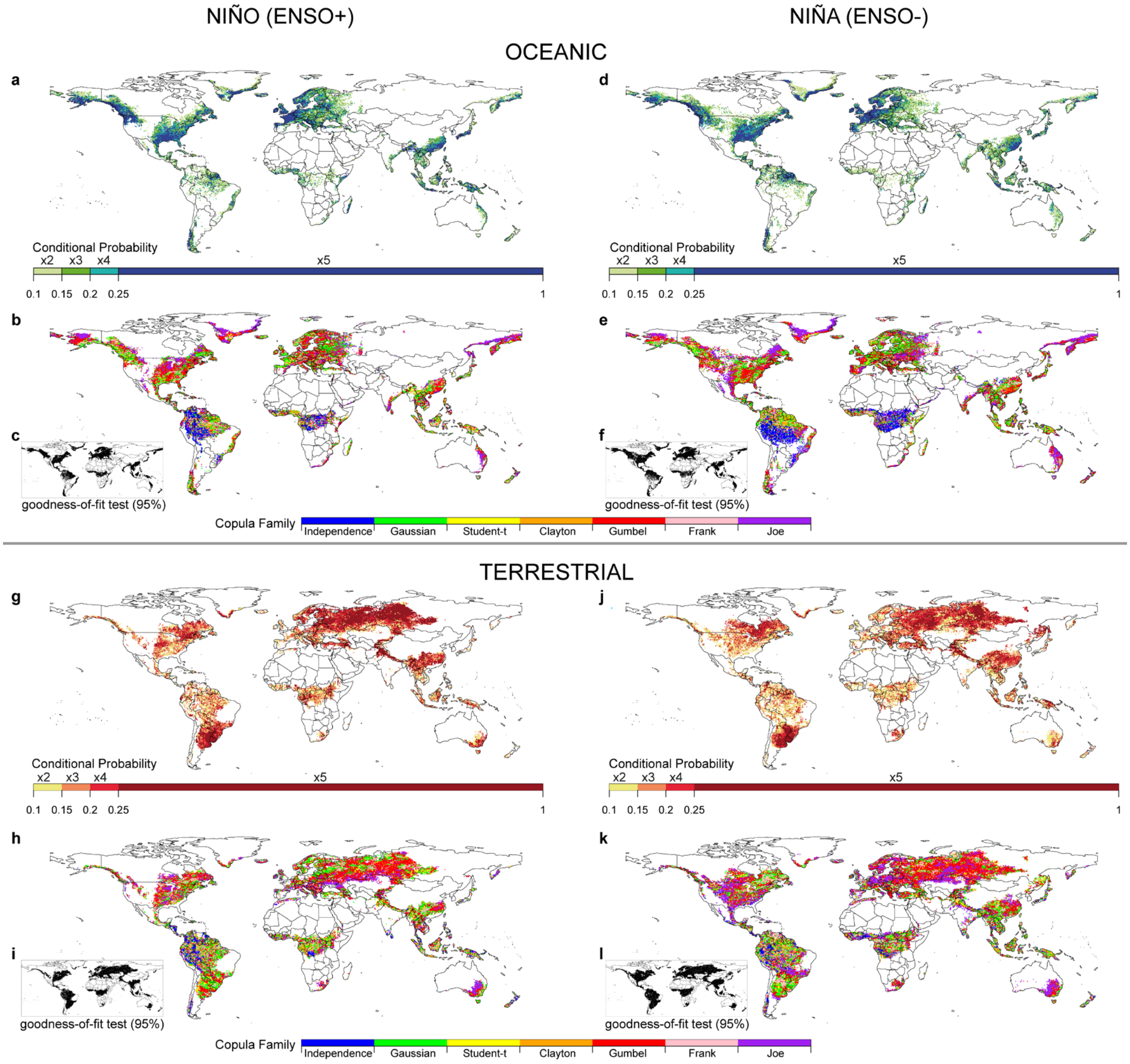

Figure S3: Conditional probability of drought occurrence given an equivalent moisture deficit from oceanic or terrestrial origin, for two subsamples: 1) considering only months in a positive El Niño/Southern Oscillation phase (ENSO+), and 2) months in a negative ENSO phase (ENSO-). a) and d) are analogous to Figure 1a, b) and e) are analogous to Figure S1b, c) and f) are analogous to Figure S1c, g) and j) are analogous to Figure 1b, h) and k) are analogous to Figure S2b, and i) and l) are analogous to Figure S2c, for ENSO+ and ENSO-, respectively (SPI at one-month time scale was used as it enabled the subsamples to have a larger sample size). In a), d), g) and j), unlike Figure 1a and 1b, no Gaussian filter is applied. Months in an ENSO+ phase are considered as those with an ENSO index higher or equal than 0.5, and those in a ENSO- phase are those with index lower or equal than -0.5. The MEI.v2 index is used (see https://psl.noaa.gov/enso/mei/)

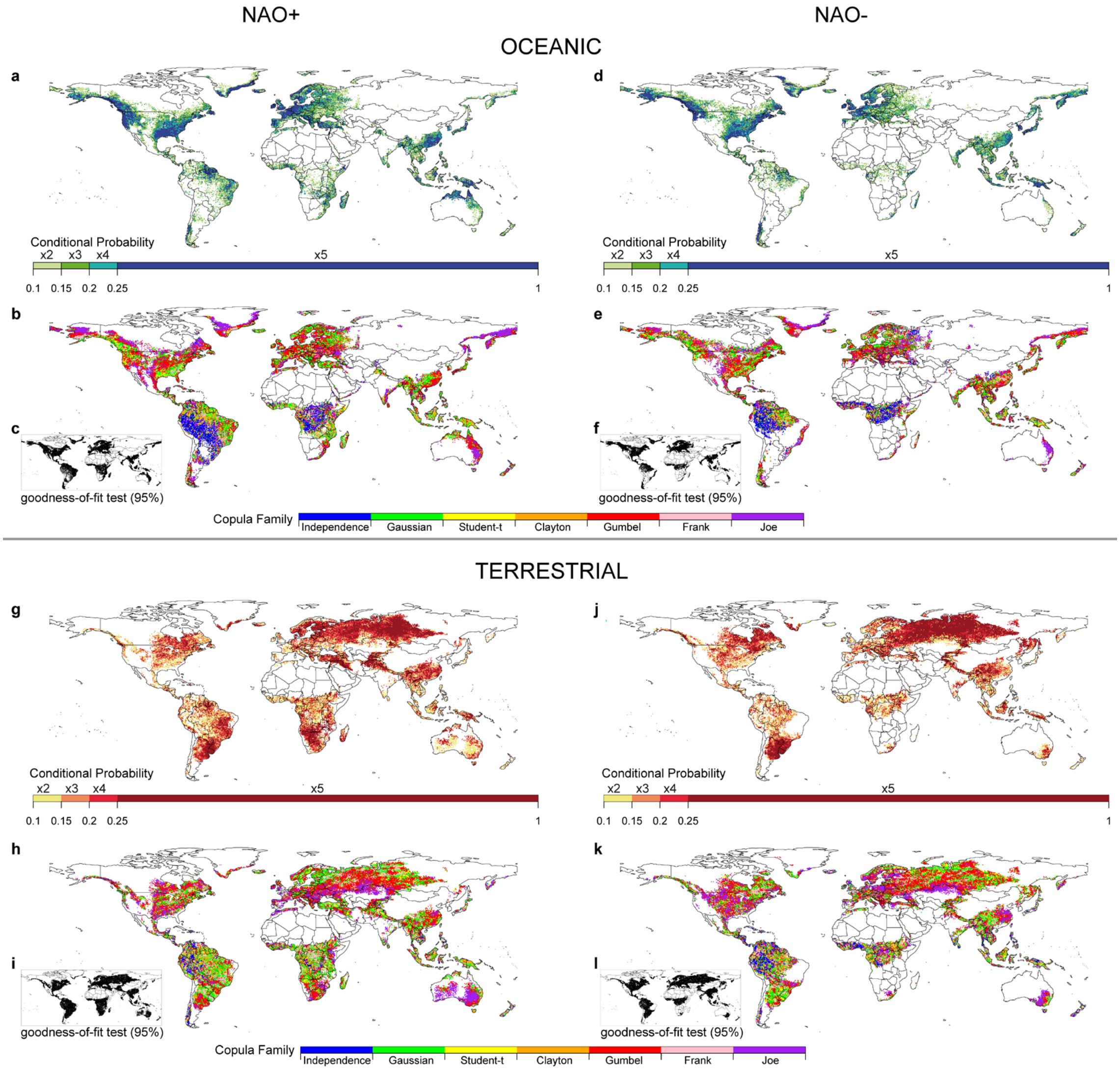

Figure S4. Same as Figure S3, but for the North Atlantic Oscillation (NAO). The 0.5/-0.5 threshold is also considered to determine the months in a positive/negative phase (NAO index values can be found here: https://www.cpc.ncep.noaa.gov/products/precip/CWlink/pna/nao.shtml). Only the results for the Northern Hemisphere are shown in the maps because this mode of variability mainly affects this hemisphere

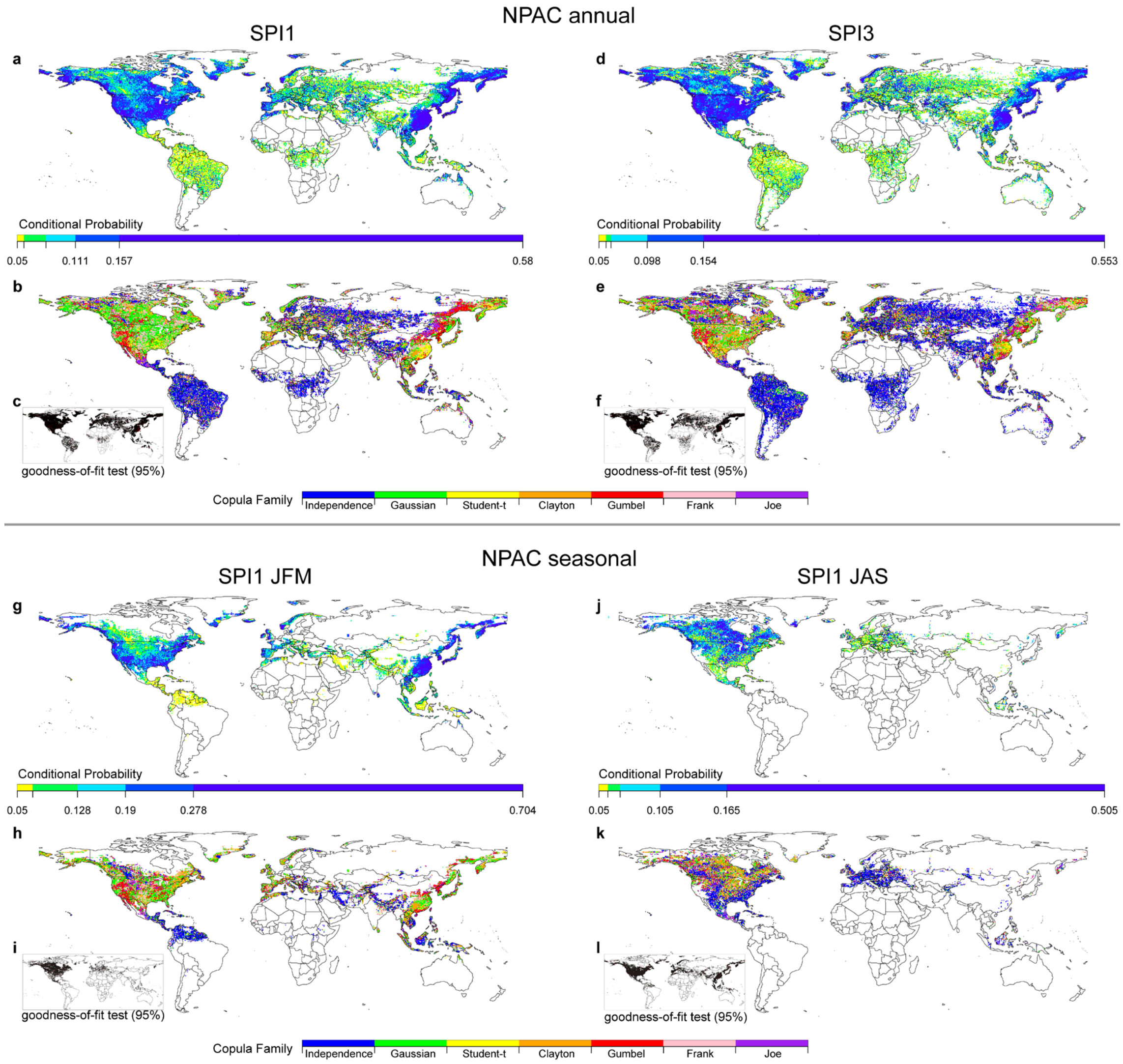

Figure S5: Same as Figure S1, but for the deficit from the North Pacific Ocean moisture source

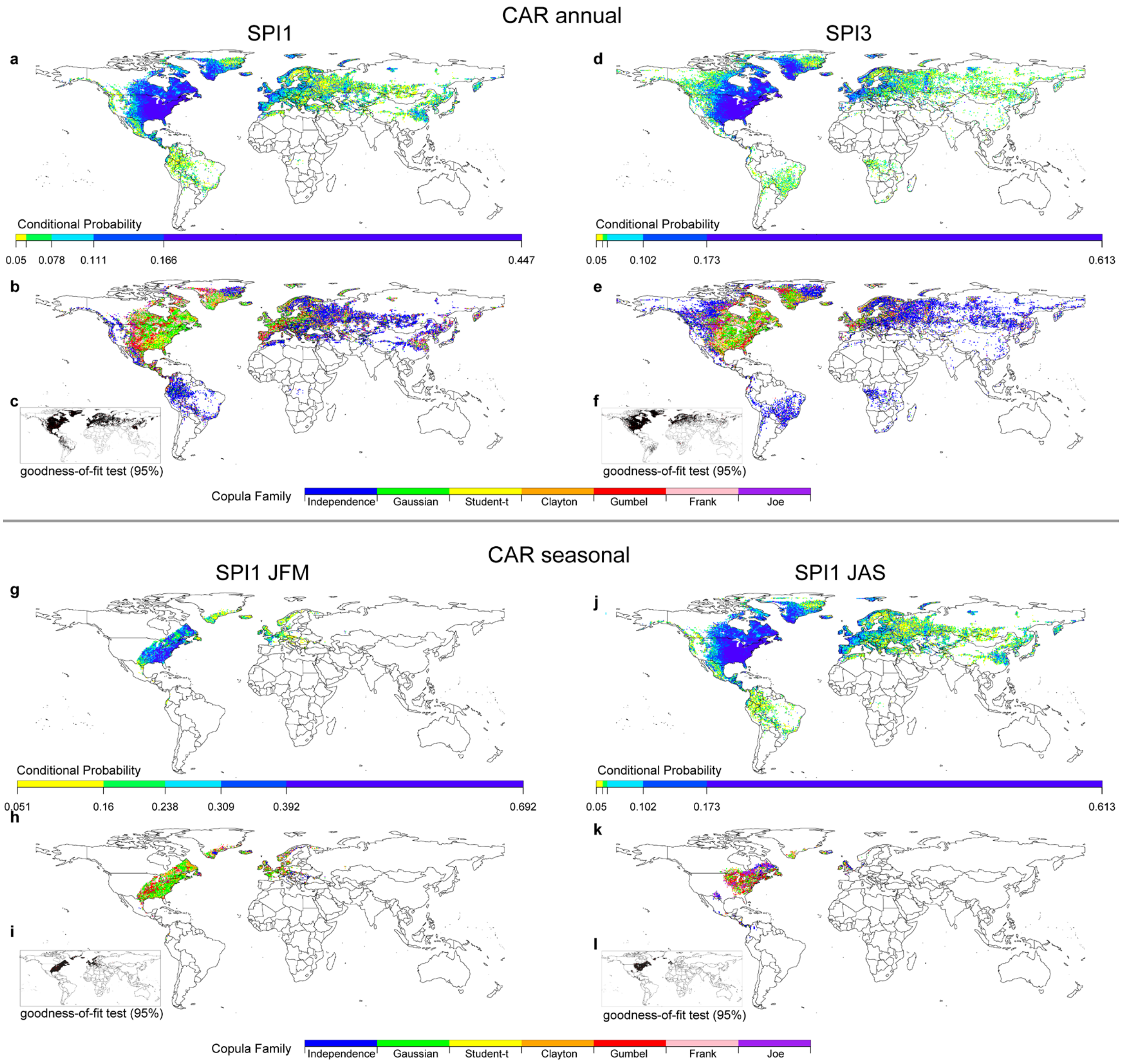

Figure S6: Same as Figure S1, but for the deficit from the Caribbean Sea and Gulf of Mexico moisture source

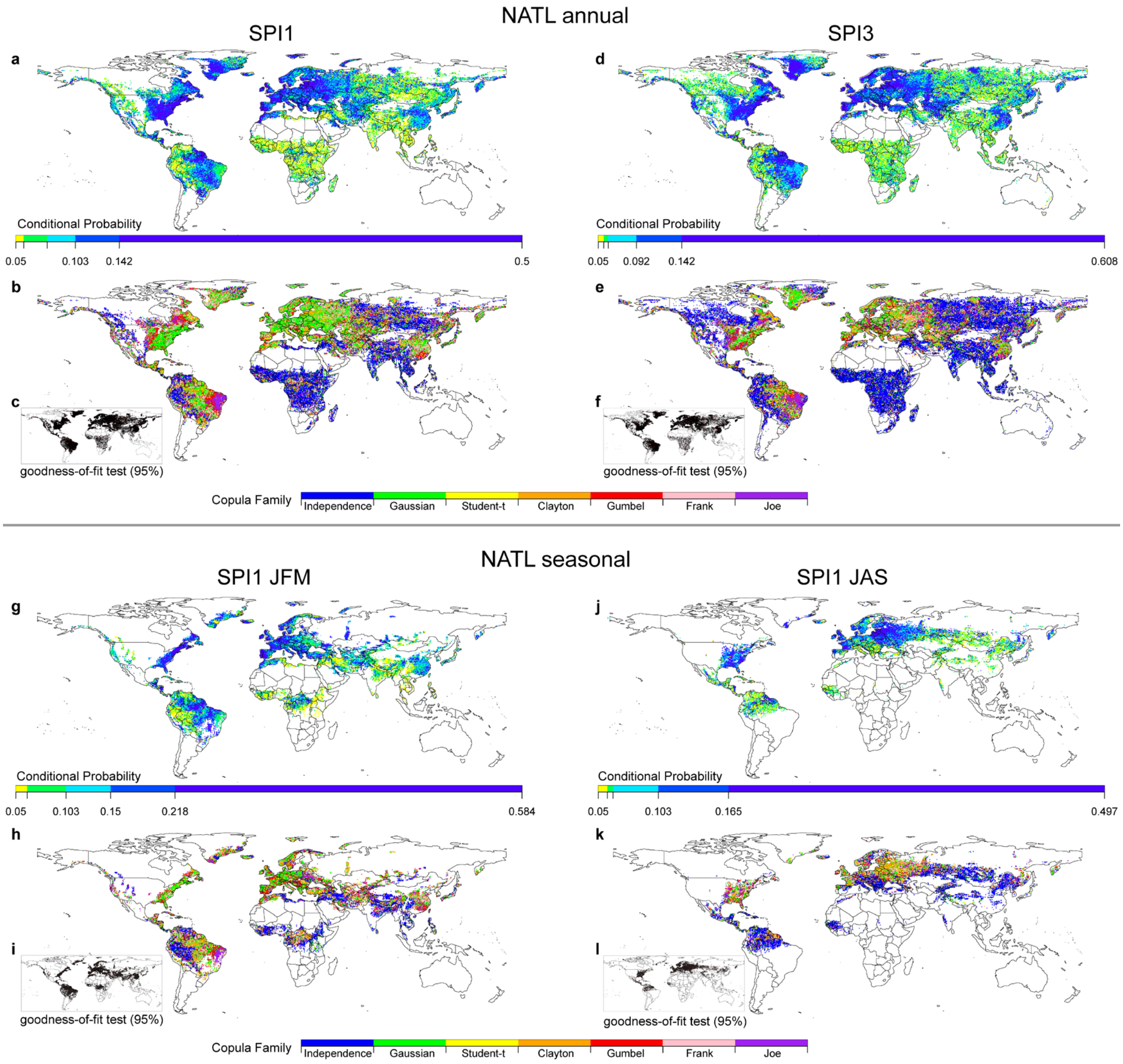

Figure S7: Same as Figure S1, but for the deficit from the North Atlantic Ocean moisture source

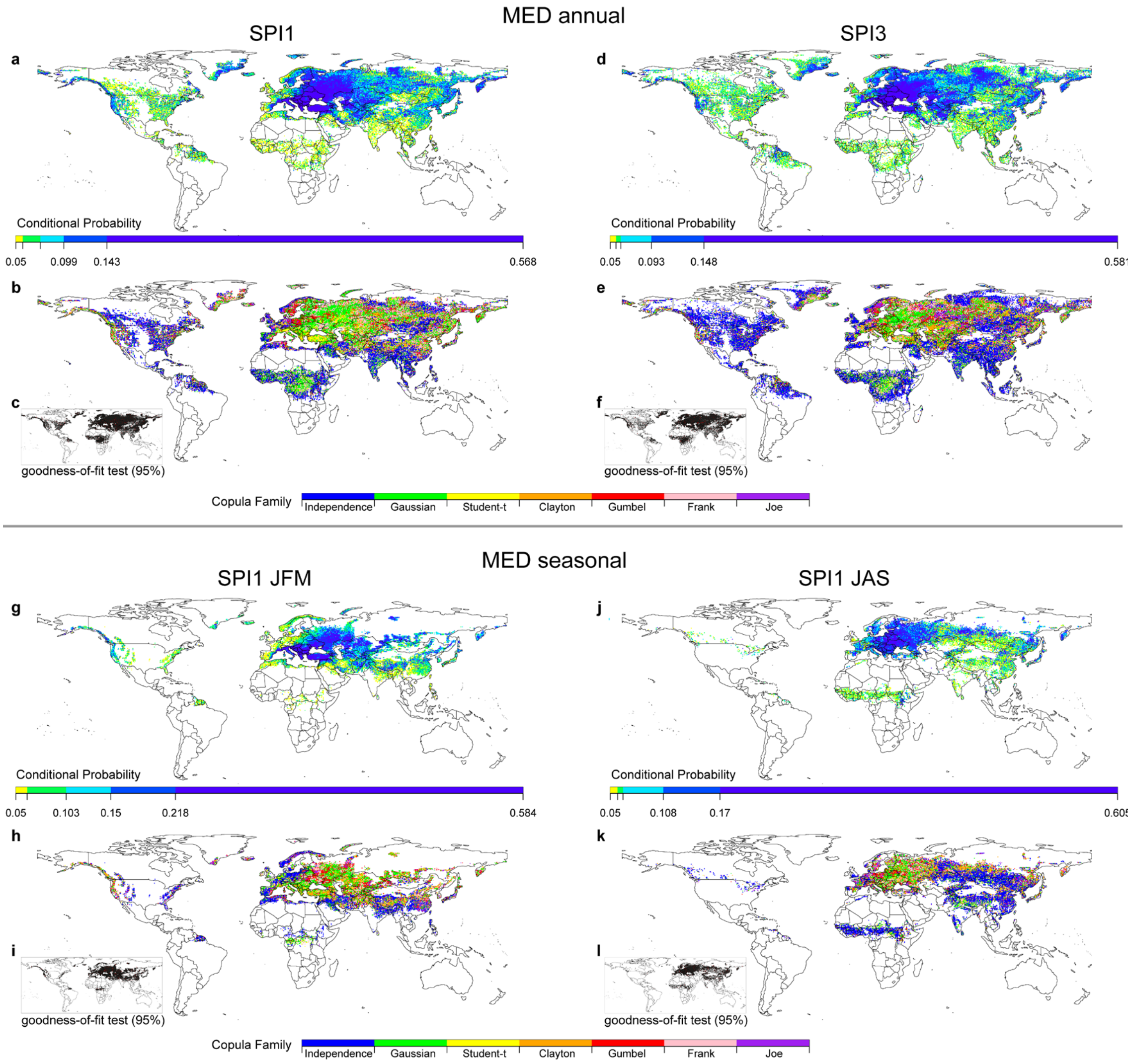

Figure S8: Same as Figure S1, but for the deficit from the Mediterranean Sea moisture source

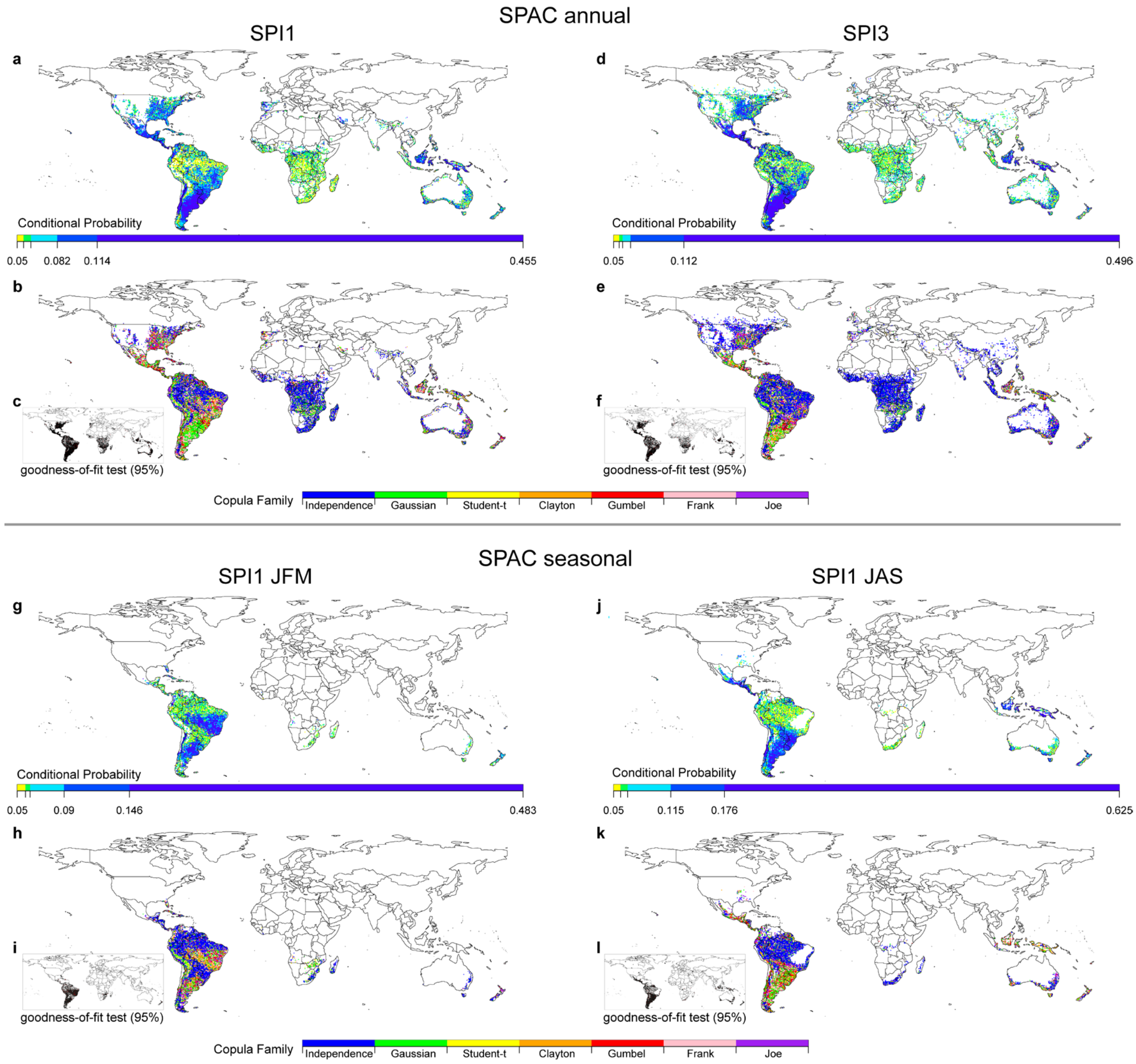

Figure S9: Same as Figure S1, but for the deficit from the South Pacific Ocean moisture source

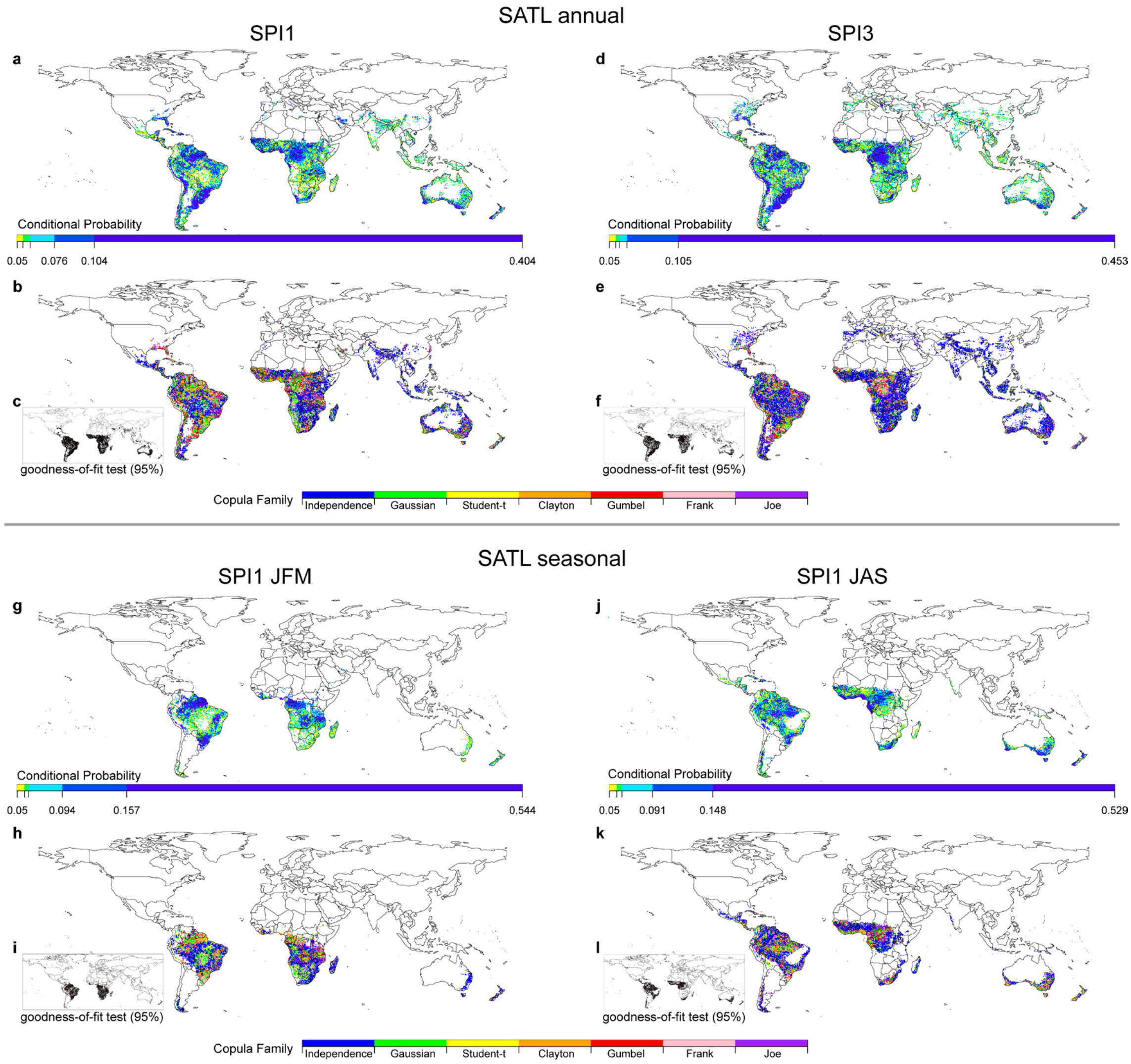

Figure S10: Same as Figure S1, but for the deficit from the South Atlantic Ocean moisture source

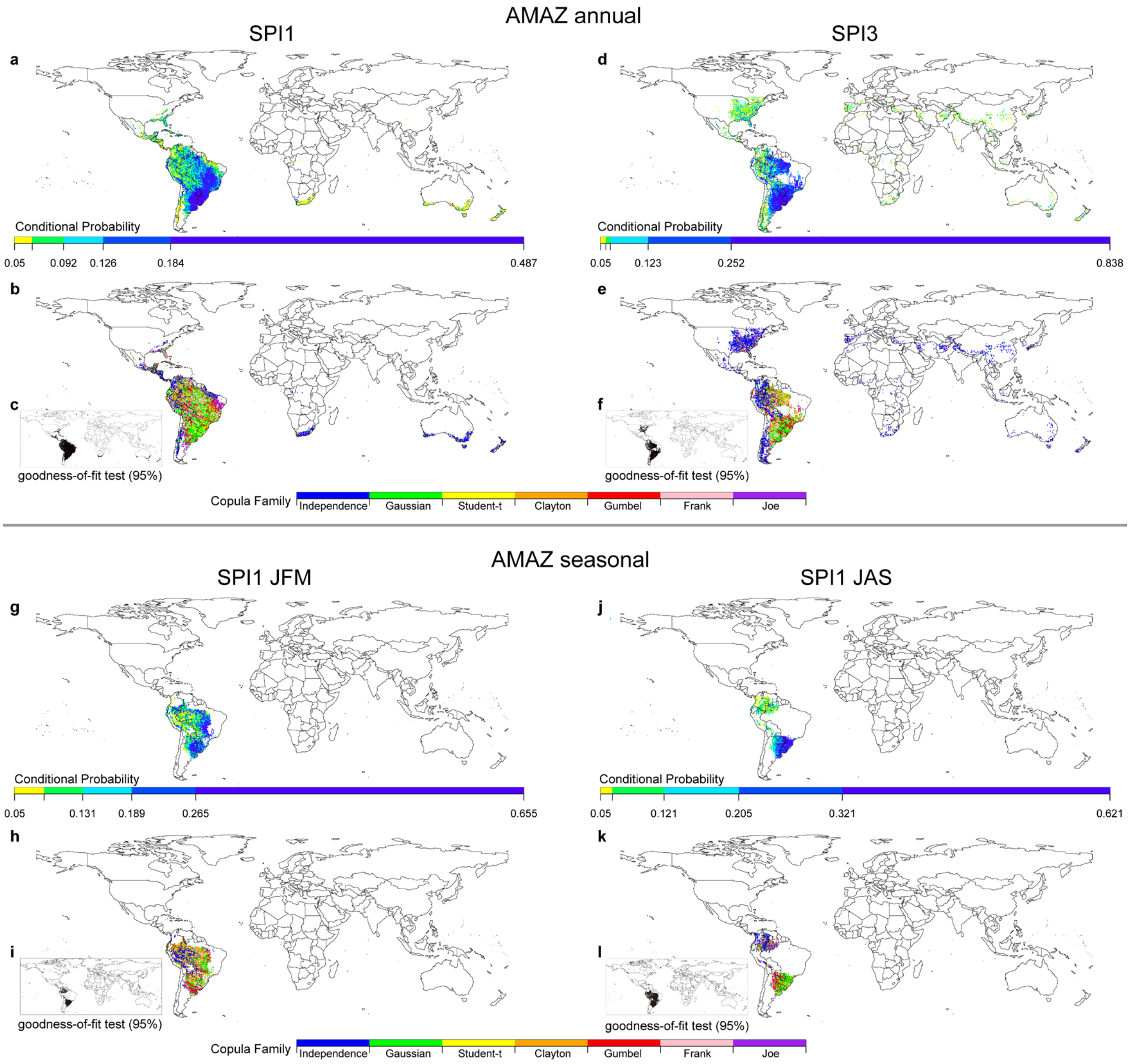

Figure S11: Same as Figure S1, but for the deficit from the Amazon river basin moisture source

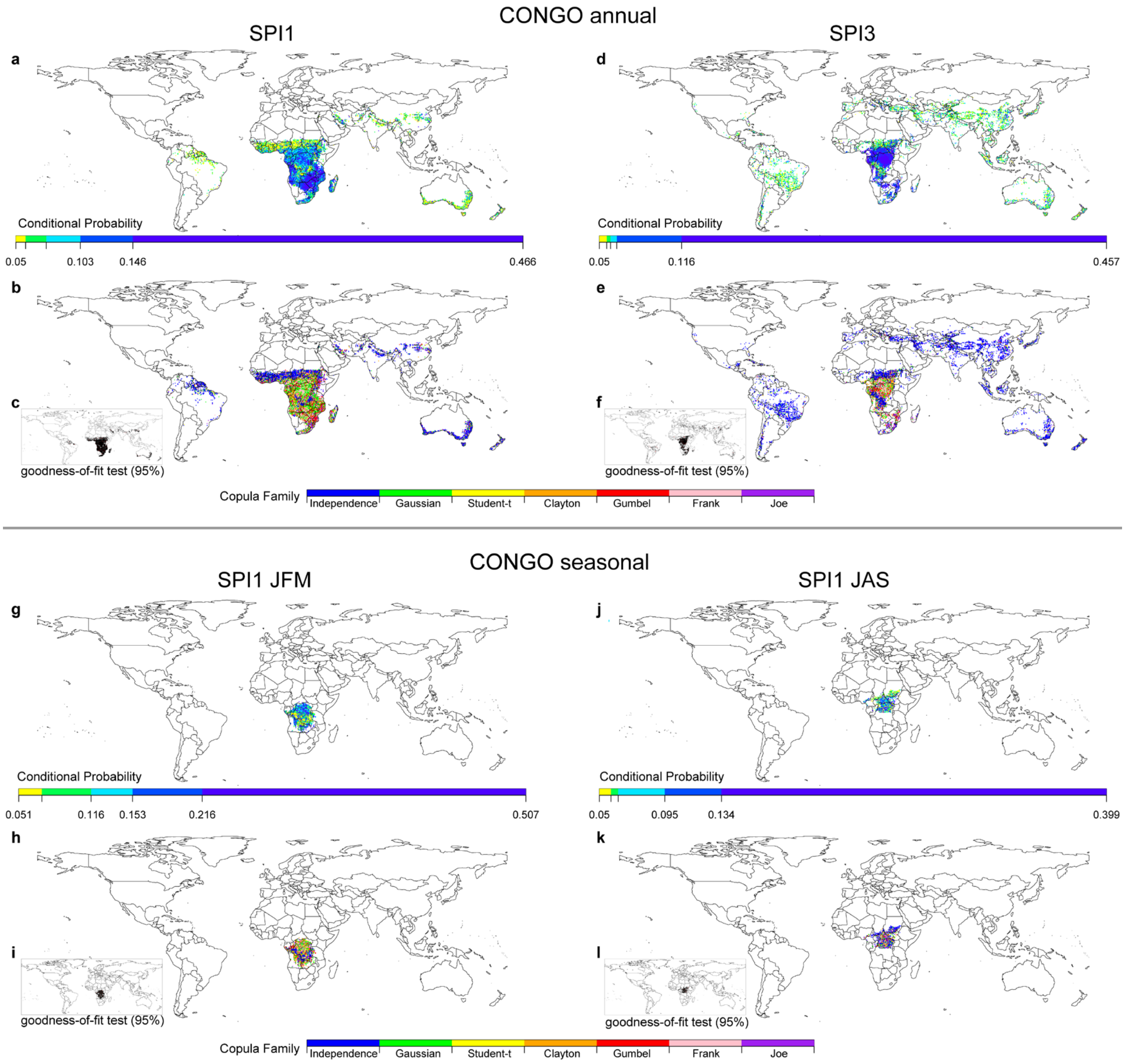

Figure S12: Same as Figure S1, but for the deficit from the Congo river basin moisture source

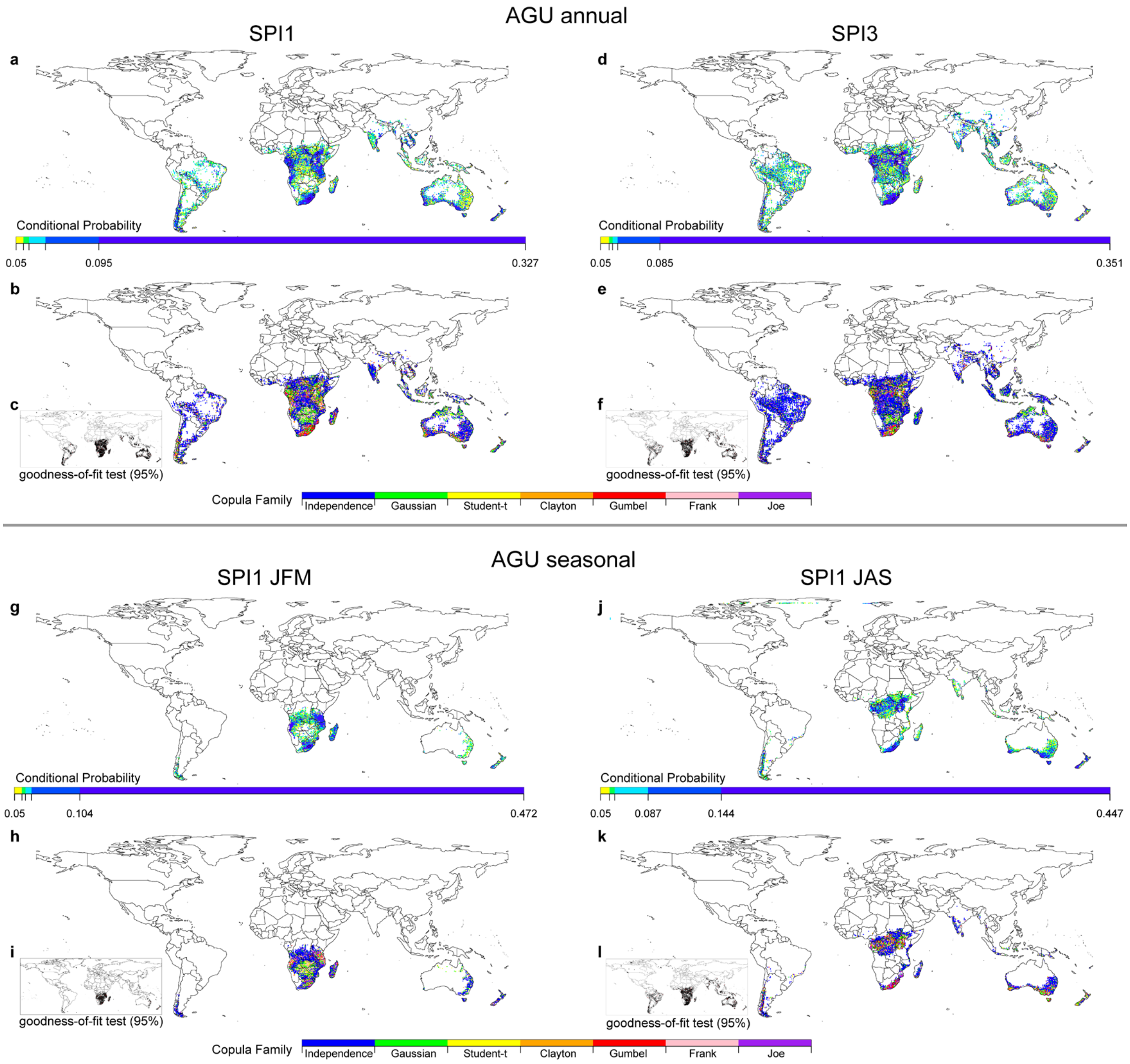

Figure S13: Same as Figure S1, but for the deficit from the Agulhas Current moisture source

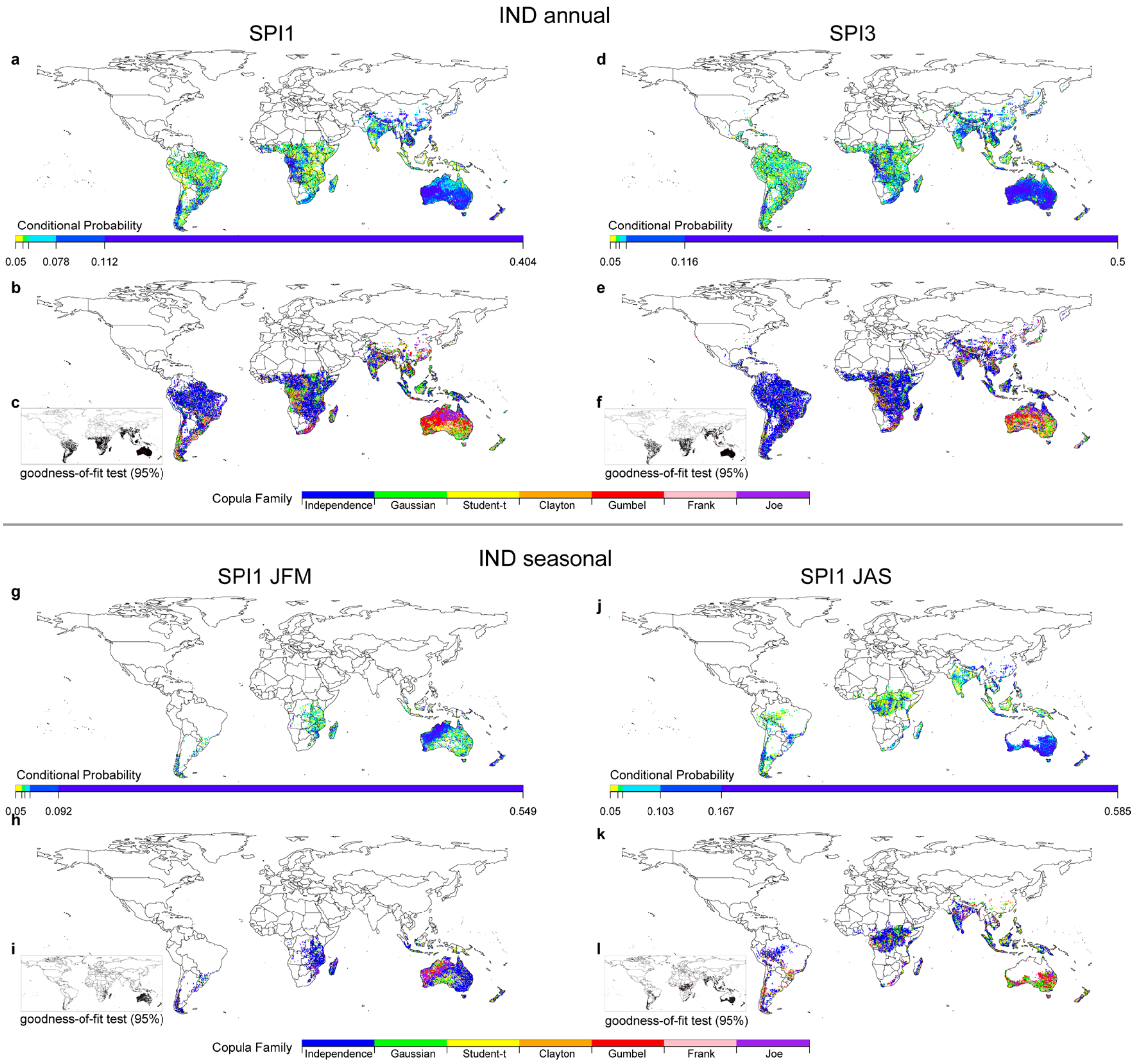

Figure S14: Same as Figure S1, but for the deficit from the Indian Ocean moisture source

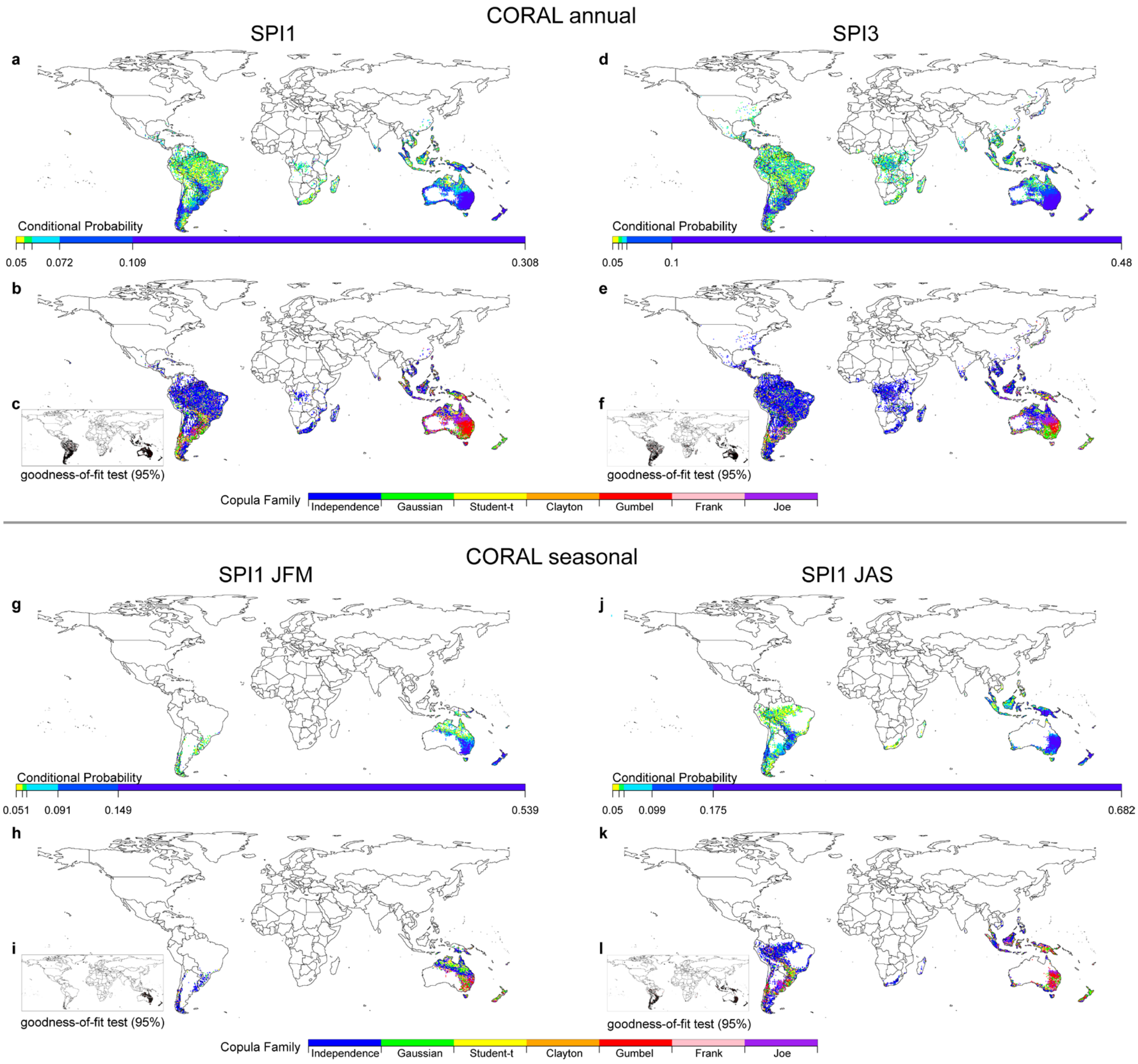

Figure S15: Same as Figure S1, but for the deficit from the Coral Sea moisture source

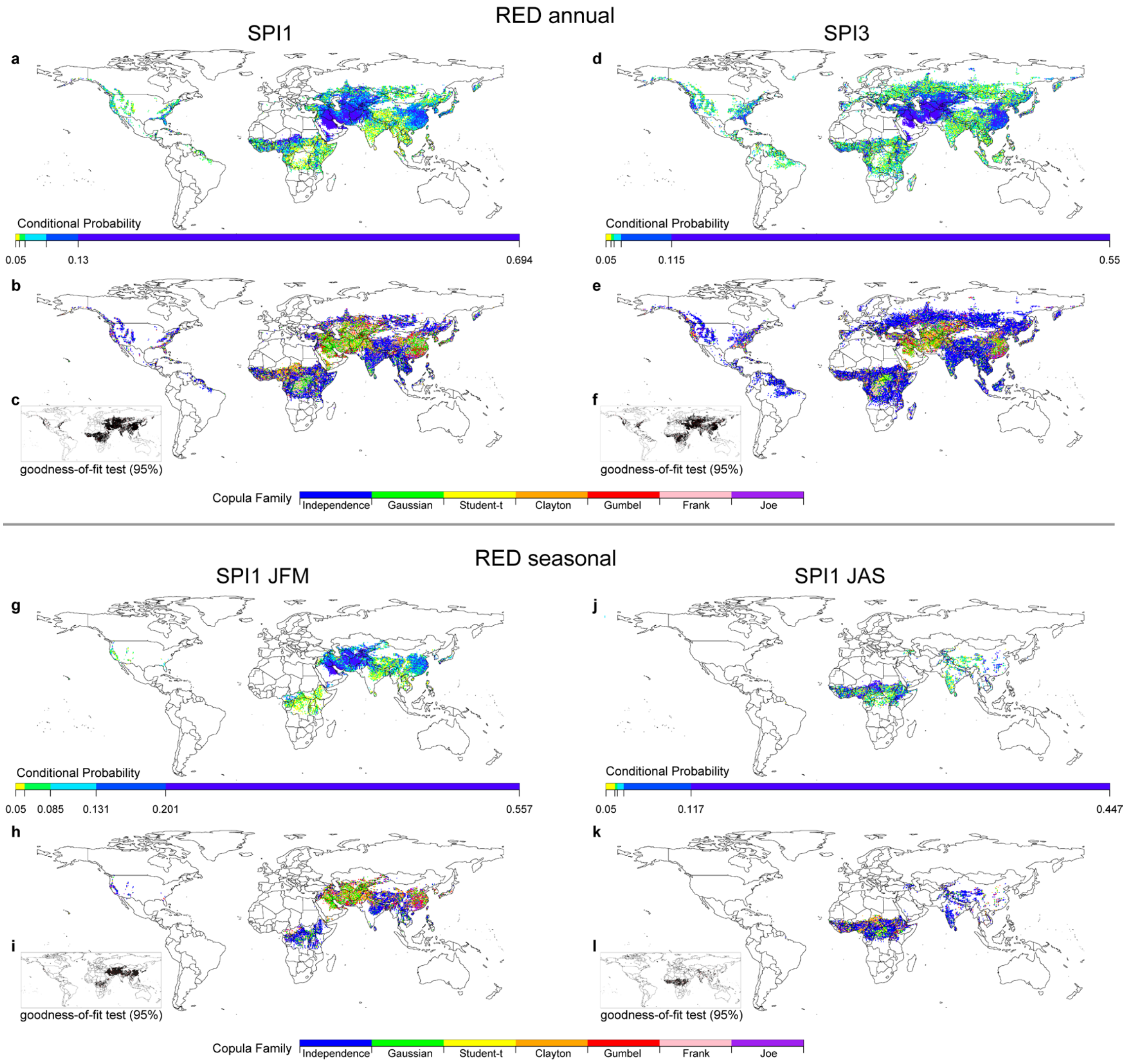

Figure S16: Same as Figure S1, but for the deficit from the Red Sea moisture source

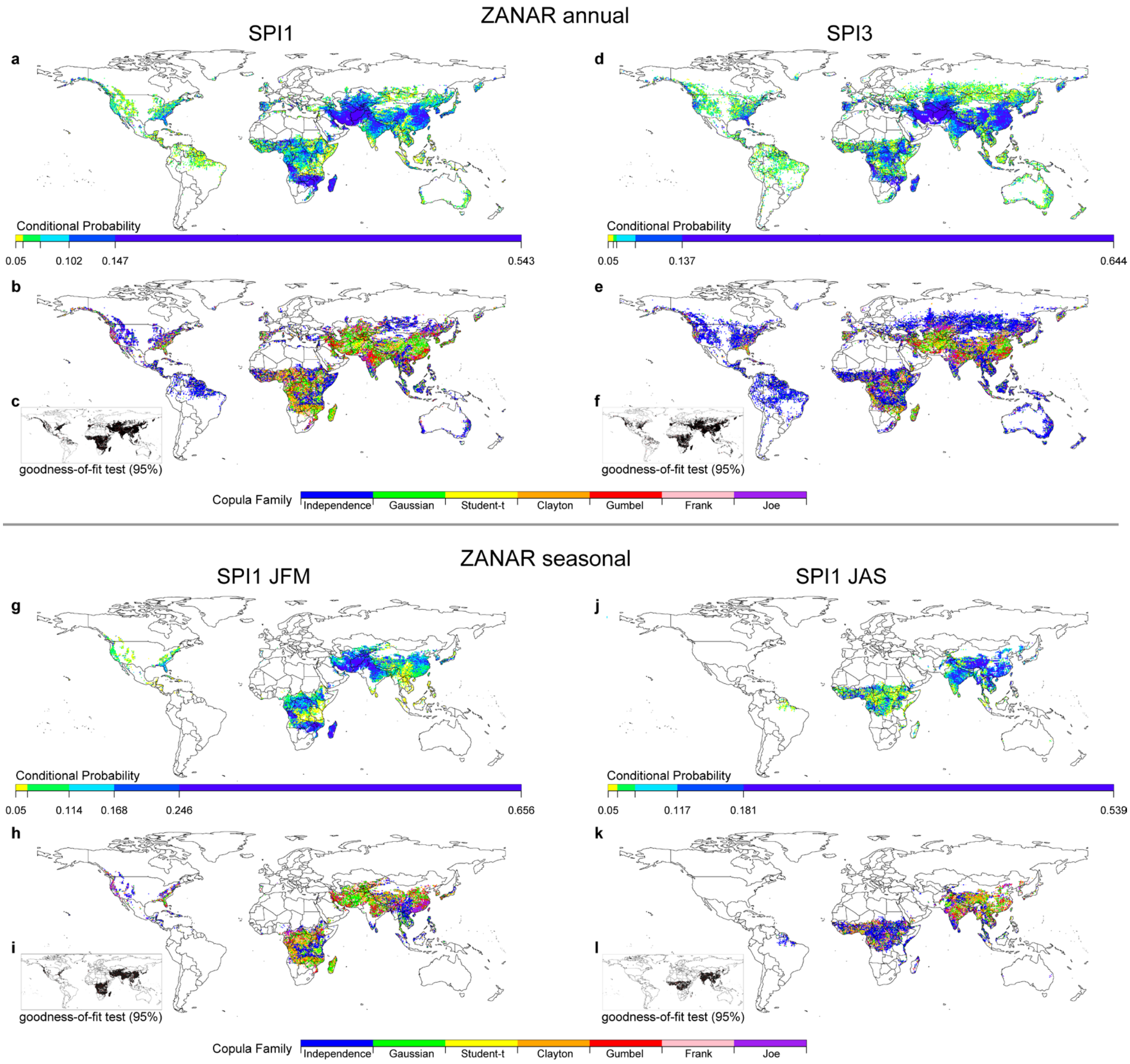

Figure S17: Same as Figure S1, but for the deficit from the Zanzibar Current and Arabian Sea moisture source

Supplementary Material References

1. Trenberth, K.E., Branstator, G.W. & Arkin, P.A. Origins of the 1988 North American Drought. *Science*, **242**, 1640-1645 (1988).
2. Cook, E.R., Seager, R., Cane, M.A. & Stahle, D.W. North American drought: Reconstructions, causes, and consequences. *Earth-Science Reviews*, **81**, 93-134 (2007).
3. Spinoni, J. et al. A new global database of meteorological drought events from 1951 to 2016, *Journal of Hydrology: Regional Studies*, **22**, 100593 (2019).
4. Vargas, W.M., Naumann, G. & Minetti, J.L. Dry spells in the River Plata Basin: an approximation of the diagnosis of droughts using daily data, *Theor. Appl. Climatol.*, **104**, 159–173 (2011).

5. Spinoni, J., Naumann, G., Vogt, J.V. & Barbosa, P. The biggest drought events in Europe from 1950 to 2012, *Journal of Hydrology: Regional Studies*, **3**, 509-524 (2015).
6. Ionita, M. & Nagavciuc, V. Changes in drought features at the European level over the last 120 years, *Nat. Hazards Earth Syst. Sci.*, **21**, 1685–1701 (2021).

SUPPLEMENTARY MATERIAL FOR:

Nexus between the deficit in moisture transport and drought occurrence in regions with projected drought trends

Luis Gimeno-Sotelo, Milica Stojanovic, Rogert Sorí, Raquel Nieto, Sergio M. Vicente-Serrano, Luis Gimeno

Table S1: Annual optimal integration time of water vapour and 90th percentile of the annual climatological positive values of the net moisture balance (E-P) for each of the nine studied regions

Regions	Annual optimal integration time (days)	90th Percentile (E − P > 0) (mm/day)
1	10	0.0059
2	11	0.0035
3	12	0.0127
4	11	0.0407
5	9	0.0101
6	8	0.0052
7	6	0.0065
8	9	0.0071
9	7	0.0023

Table S2: For region 1 and each of its specific moisture sources, information about the selected copula model, p-value of the goodness-of-fit test, and conditional probability of drought occurrence given an equivalent moisture contribution deficit

	R1	C1	O1A	O1B	O1C
Copula family	Gaussian	Gumbel	Student-t	Joe	Gaussian
Goodness-of-fit p-value	0.18	0.92	0.03	0.35	0.54
Conditional probability	0.088	0.123	0.305	0.063	0.231

Table S3: Same as Table S2, but for region 2

	R2	C2	O2A	O2B
Copula family	Gaussian	Frank	Gaussian	Frank
Goodness-of-fit p-value	0.52	0.62	0.26	0.72
Conditional probability	0.015	0.026	0.277	0.041

Table S4: Same as Table S2, but for region 3

	R3	C3	O3A	O3B
Copula family	Frank	Gaussian	Frank	Gaussian
Goodness-of-fit p-value	0.34	0.56	0.26	0.15
Conditional probability	0.16	0.241	0.144	0.183

Table S5: Same as Table S2, but for region 4

	R4	O4B	O4A	C4
Copula family	Student-t	Gaussian	Frank	Gaussian
Goodness-of-fit p-value	0.84	0.76	0.74	0.07
Conditional probability	0.344	0.25	0.099	0.26

Table S6: Same as Table S2, but for region 5

	R5	C5	O5A	O5B
Copula family	Student-t	Student-t	Student-t	Gumbel
Goodness-of-fit p-value	0.65	0.51	0.53	0
Conditional probability	0.387	0.277	0.232	0.123

Table S7: Same as Table S2, but for region 6

	R6	C6	O6A	O6B	O6C
Copula family	Joe	Student-t	Gaussian	Independence	Independence
Goodness-of-fit p-value	0.98	0.48	0.07	---	---
Conditional probability	0.052	0.19	0.341	0.054	0.052

Table S8: Same as Table S2, but for region 7

	R7	C7	O7A	O7B

Copula family	Gumbel	Gaussian	Gumbel	Gaussian
Goodness-of-fit p-value	0.56	0.87	0.8	0.82
Conditional probability	0.164	0.152	0.103	0.076

Table S9: Same as Table S2, but for region 8

	R8	C8	O8A	O8B	O8C	O8D	O8E	O8F
Copula family	Student-t	Gaussian	Student-t	Frank	Clayton	Gaussian	Student-t	Independence
Goodness-of-fit p-value	0.45	0.44	0.78	0.92	0.9	0.02	0.74	---
Conditional probability	0.18	0.341	0.412	0.089	0.145	0.178	0.086	0.053

Table S10: Same as Table S2, but for region 9

	R9	C9	O9A	O9B
Copula family	Gumbel	Gumbel	Gaussian	Gumbel
Goodness-of-fit p-value	0.54	0.66	0.73	0.33
Conditional probability	0.09	0.133	0.211	0.07

SUPPLEMENTARY MATERIAL FOR:

The increasing influence of atmospheric moisture transport on hydrometeorological extremes in the Euromediterranean region with global warming

Luis Gimeno-Sotelo, José Carlos Fernández-Alvarez, Raquel Nieto, Sergio M. Vicente-Serrano, Luis Gimeno

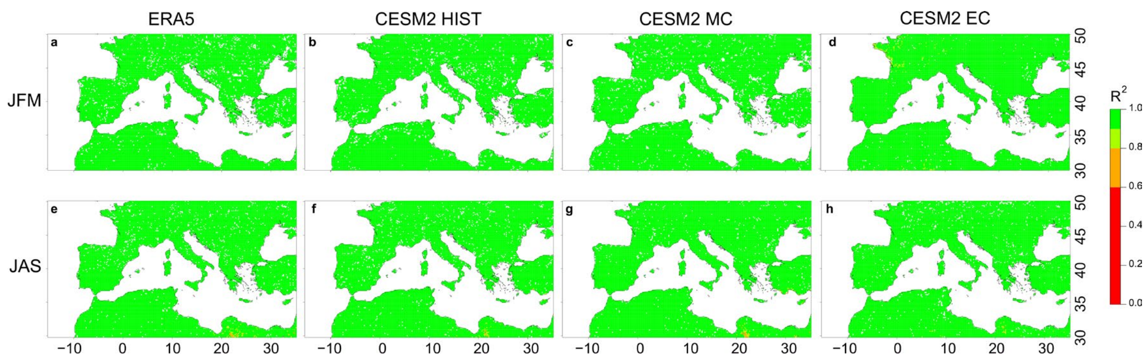

Figure S1: Goodness of fit assessment for the non-stationary GEV models used in this study. R^2 metric of the linear regression model associated with the probability plots corresponding to the non-stationary GEV models with the location and scale parameters expressed as linear functions of IVT, for a) e) ERA5 data, b) f) CESM2 data in the historical period, c) g) CESM2 data in the mid-century period, and d) h) CESM2 data in the end-century period, for the winter season (January-March) and the summer season (July-September), respectively.

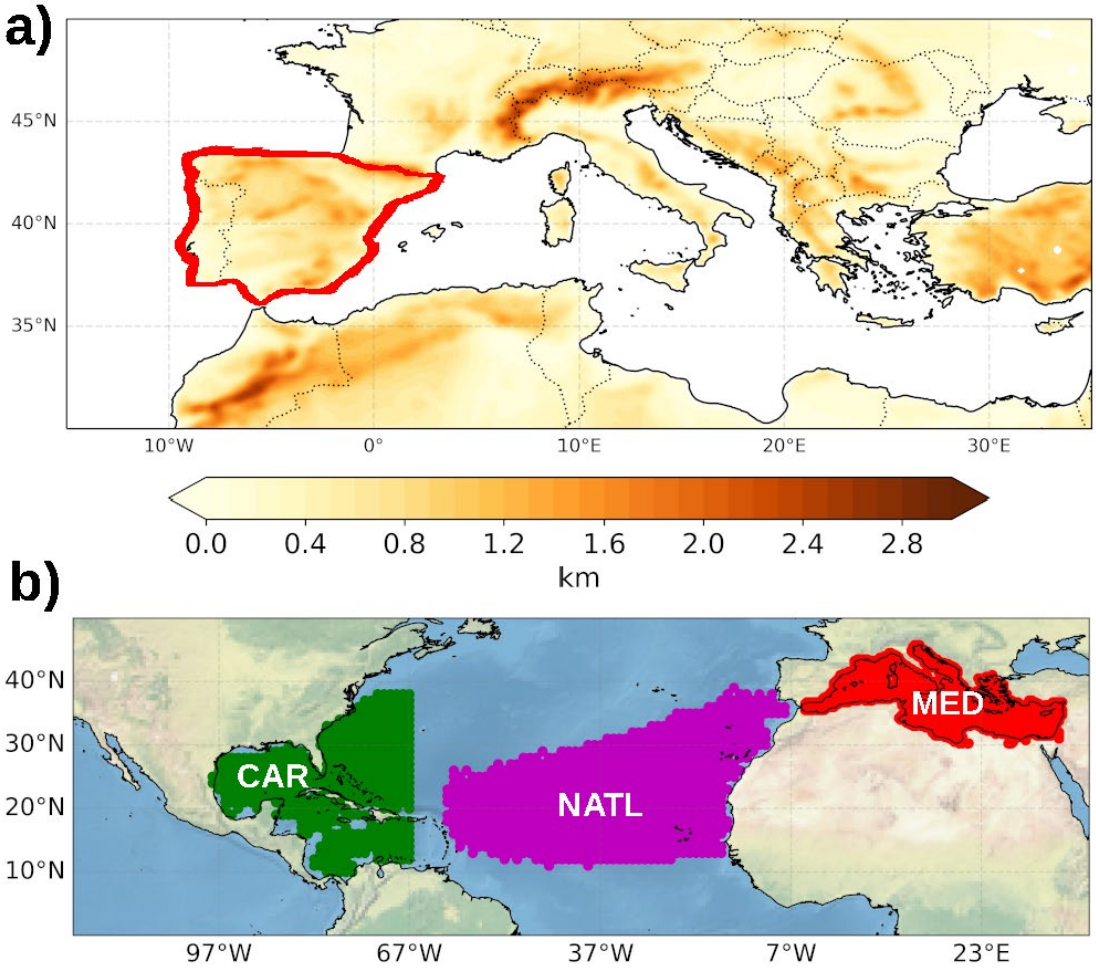

Figure S2: Spatial domain and orography of the Euromediterranean region, and major oceanic moisture sources considered in this study. a) Orography of the Euromediterranean region, considering a spatial domain which encompasses latitudes from 30ºN to 50ºN and longitudes from 15ºW to 35ºE. The red contour indicates the Iberian Peninsula, which is a hotspot region in this study. b) Major oceanic moisture sources of the Euromediterranean region: the North Atlantic Ocean (NATL, in magenta colour) and Mediterranean Sea (MED, in red colour); together with the Caribbean Sea and Gulf of Mexico (CAR, in green colour), which is also a major oceanic moisture source of the Iberian Peninsula.

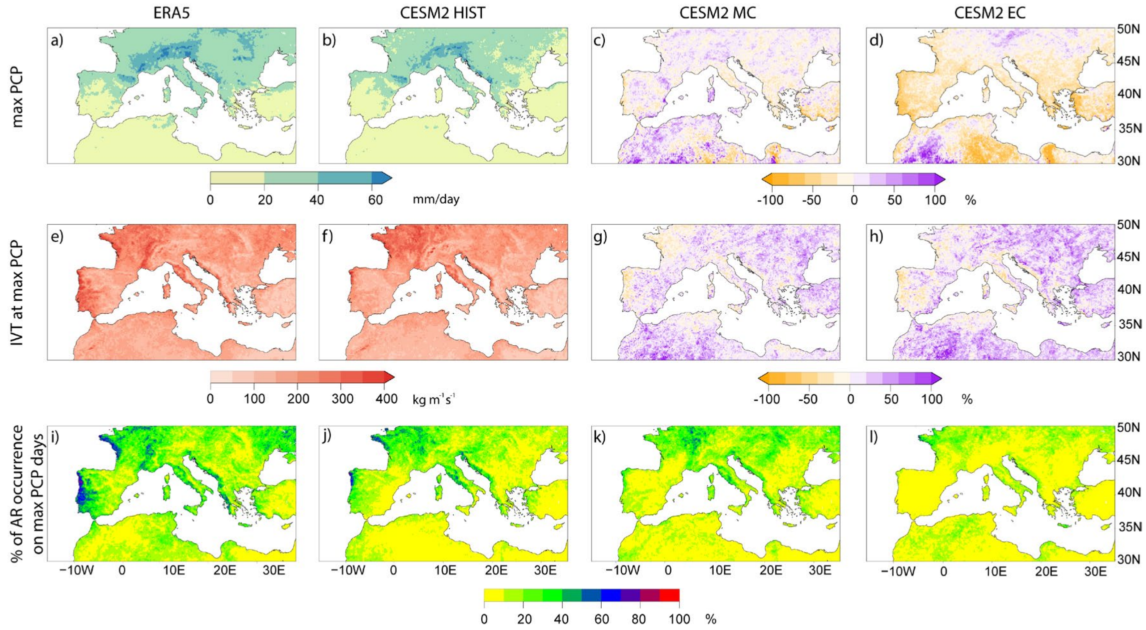

Figure S3: Same as Figure 1, but for the summer season (July-September).

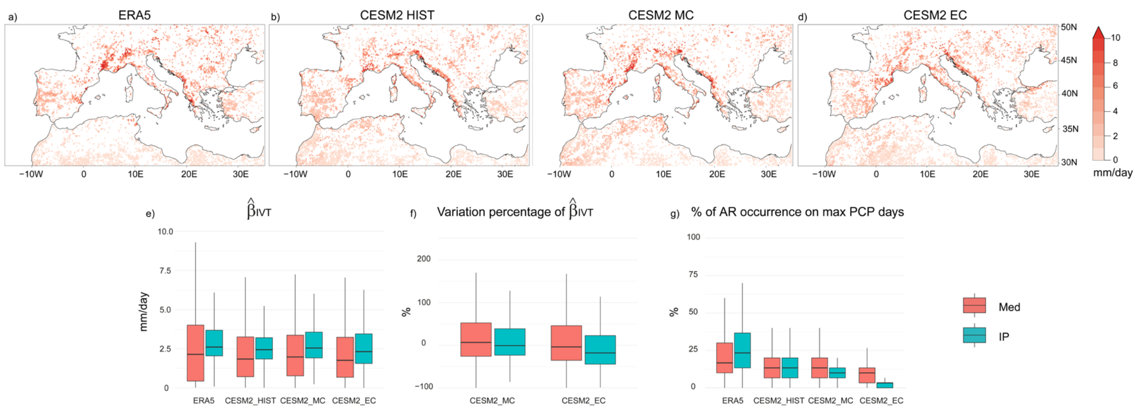

Figure S4: Same as Figure 2, but for the summer season (July-September).

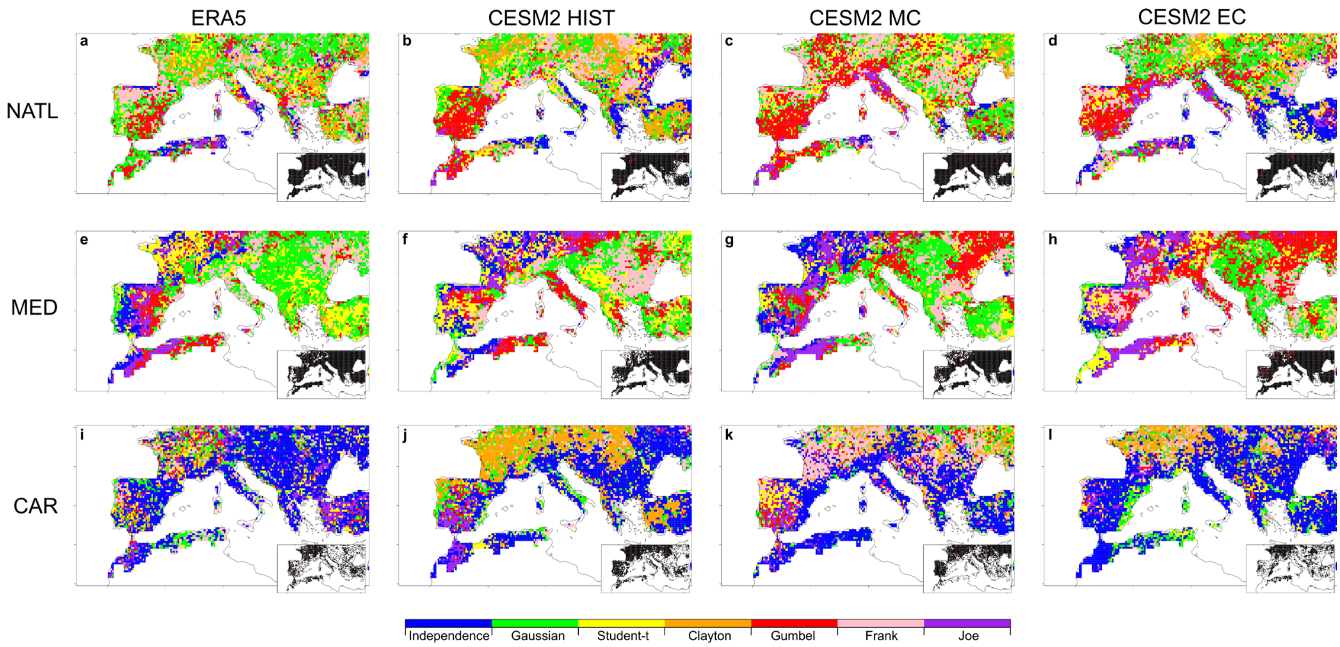

Figure S5: Information about the selected copulas used in this study. The main panels refer to the selected copula families (one among the Independence, Gaussian, Student-t, Clayton, Gumbel, Frank or Joe copulas), while the bottom-right ones provide information about the goodness of fit of each copula (points in black indicate that the selected copula fits well to the data at 5% significance level; and red points are used otherwise). a) b) c) d) Information about the selected copulas corresponding to the contribution to precipitation from the North Atlantic Ocean (NATL), e) f) g) h) the Mediterranean Sea (MED), and i) j) k) l) the Caribbean Sea and Gulf of Mexico (CAR), for the ERA5 reanalysis and the CESM2 model in the historical, mid-century and end-century periods, respectively.

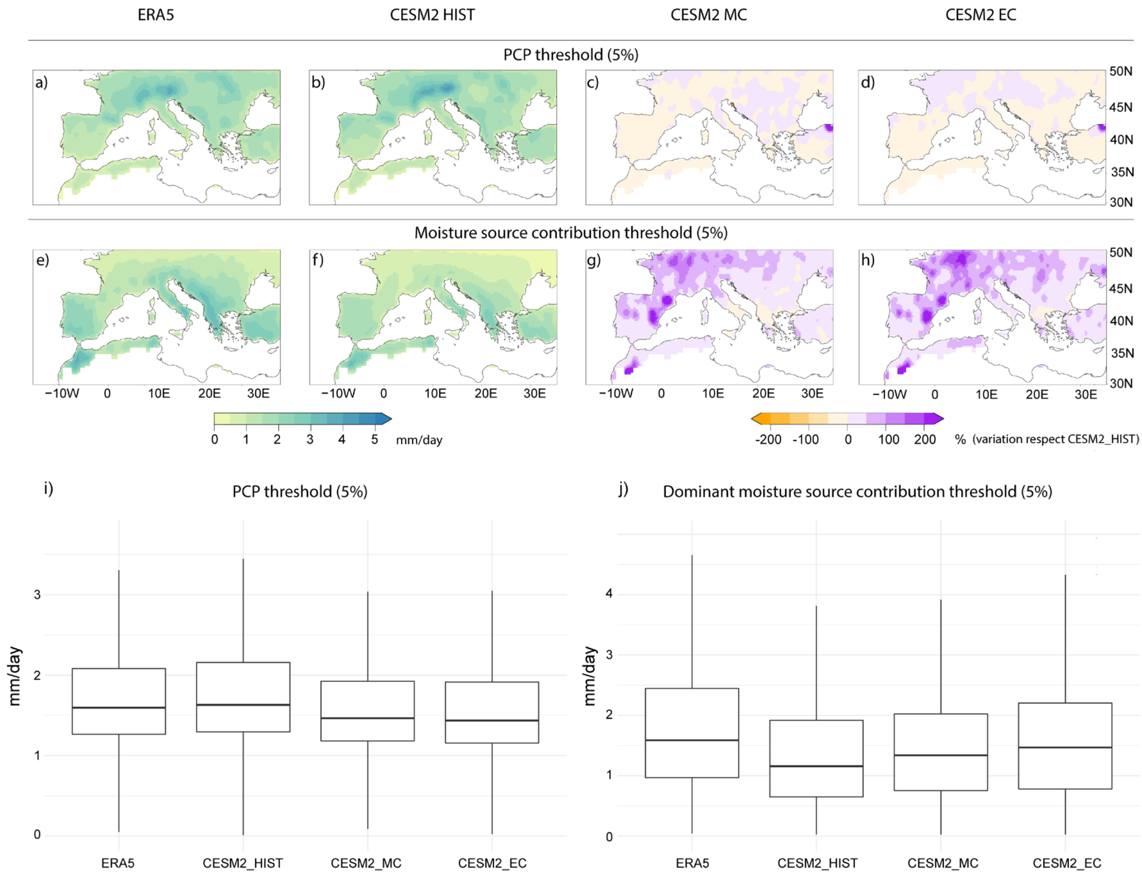

Figure S6: Precipitation and moisture source contribution values corresponding to the thresholds associated with the identification of drought and contribution deficit from the dominant oceanic moisture source, respectively. a) b) Precipitation threshold (associated with a 5% percentile drought definition), for ERA5 and CESM2 in the historical period, respectively. c) d) Variation percentage of the precipitation threshold, for the mid-century and end-century periods, respectively. e) f) Contribution threshold from the dominant oceanic moisture source (associated with a 5% percentile contribution deficit), for ERA5 and CESM2 in the historical period, respectively. g) h) Variation percentage of the moisture source contribution threshold, for the mid-century and end-century periods, respectively. i) j) Boxplots of the precipitation and moisture source contribution thresholds, respectively.

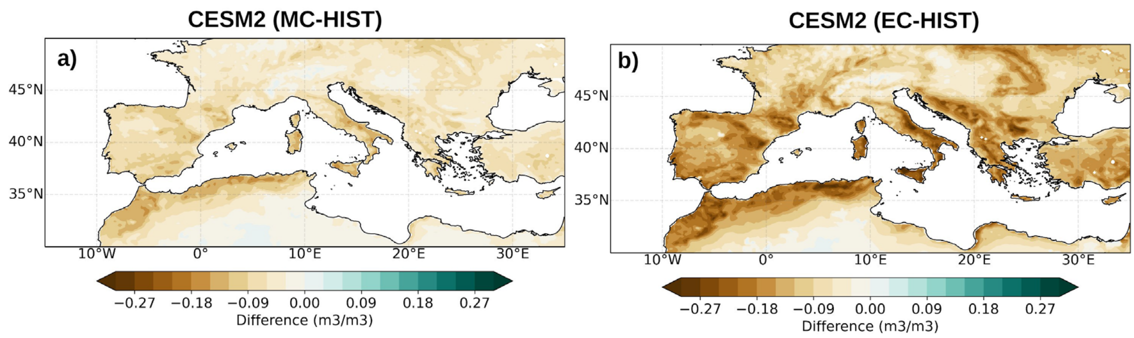

Figure S7: Projected changes in soil moisture in the Euromediterranean region, according to the simulations used in this study. a) Difference between the mid-century and the historical values of soil moisture and b) between the end-century and the historical ones, according to the dynamically downscaled data from the CESM2 model used in this study.

Supplementary Material

Extreme precipitation events

Luis Gimeno (1*), Rogert Sorí (1), Marta Vázquez (1), Milica Stojanovic (1), Iago Algarra (1), Jorge Eiras-Barca (1,2), Luis Gimeno-Sotelo (3) and Raquel Nieto (1).

1. REGIONAL TRENDS IN OBSERVED AND MODELLED PRECIPITATION EXTREMES

1.1 Africa

Various indices of extreme precipitation calculated using the reanalysis datasets 20CR and ERA-20C for 1901-2010 show different patterns of trends over Africa (Donat et al., 2016a). The 20CR dataset indicates a change towards less frequent heavy precipitation days in western central Africa over the past century, while ERA-20C shows slight increases in this region, but with a drying trend in southeast Africa. A more recent study found that one gauge and three satellite-gauge products agree in the occurrence of positive trends of the wet season PRCPTOT in the central and west Sahel, and South Africa, while it seemed to decrease over central equatorial Africa, and East Africa (Harrison et al., 2019). These regions have been a focus for trend analyses of extreme precipitation in Africa. Ly et al. (2013) described an overall decreasing trend in the maximum number of consecutive wet days from 1960 to the mid-1980s in the west African Sahel, but an increasing trend in some locations such as Niamey in Niger, Bamako in Mali, and Ouagadougou in Burkina Faso from the late 1980s to 2010. For a shorter but earlier study period (1998 – 2013), trends in the occurrence of extreme summer precipitation events indicate significant decreases over West Africa, although local increases are found in western Sahel (Odoulami and Akinsanola, 2017). By applying a POT approach, Panthou et al. (2014) argued that the proportion of annual rainfall associated with extreme rainfall increased from 17% in 1970–1990 to 19% in 1991–2000 and to 21% in 2001–2010 in Central Sahel. Moreover, Taylor et al. (2017) used satellite observations for 1982–2015 to show a persistent increase in the frequency of extreme storms over the Sahel region. This finding was confirmed by Salack et al. (2018), who highlighted an increase in the 99th percentile daily rainfall threshold in western Sahel. Furthermore, an analysis conducted by Panthou et al. (2018) revealed an increase in daily precipitation intensity over the Sahel since the 1980s, associated with an increase in extreme sub-daily intensities in southwest Niger since 1990. In agreement with this, over the period 1981–2015 trends of R95p and R99p values were significant over most parts of Ghana in West Africa, with negative trends dominating the northern parts and positive trends dominating the southern coast (Atiah et al., 2020). Furthermore, Diatta et al. (2020) used high resolution data from CHIRPS with 8 extreme precipitation indices for the period 1982-2016 to show an increased trend in wet indices over western and southern Sahel.

East Africa is one of the most vulnerable parts of the continent to extreme weather and climate events. Recently, Gebrechorkos et al. (2018) evaluated trends and variability of precipitation extremes (1981–2016) in some countries in this region (Ethiopia, Kenya, and Tanzania), using the ETCCDI Indices. Their results show an increasing trend in the number of very wet (R95p) and extremely wet (R99p) days in different parts of Kenya, southern Ethiopia, and the northern (around Arusha) and central parts of Tanzania. They also show significant decreasing trends in R95p and R99p in some parts of eastern Ethiopia and the southern part of Tanzania. Kruger and Nxumalo (2017) confirmed that very high daily rainfall (R95p, R99p) has generally increased in the southern and south-eastern interior, with some variations in the spatial extent of the significant trends for the period 1921 – 2015. This finding is in agreement with the results of other studies performed for shorter study periods (Donat et al., 2013; MacKellar et al., 2014).

An ensemble of CMIP5 models for the period 2006–2100 forced by the RCP8.5 scenario showed a tendency for less frequent but more intense rainfall, longer dry spells, and shorter wet spells over Central Africa (Dosio et al., 2019). Similarly, they observed a robust increase in both maximum daily intensity (RX1 day) and the frequency of extreme events (R10 mm) over the Horn of Africa. In agreement, a more recent study based on a multimodel ensemble of CMIP6 models for 2081 – 2100 found an increase (decrease) in CDD (CWD) over East Africa (Ayugi et al., 2021). In contrast, the West African domain is expected to experience more extreme precipitation events (RX5d and RX1d), which will increase according to climate simulations under RCP8.5 for 2075–2099 (Kitoh and Endo, 2016). Finally, for southern Africa multimodel climate simulations under the RCP4.5 and RCP8.5 scenarios point to significant decreases in annual PRCPTOT for the period 2069–2098 (Pinto et al., 2016). For a better interpretation of these results, Figure S1 shows a spatial representation as a summary of the trends in the historical and future periods across Africa.

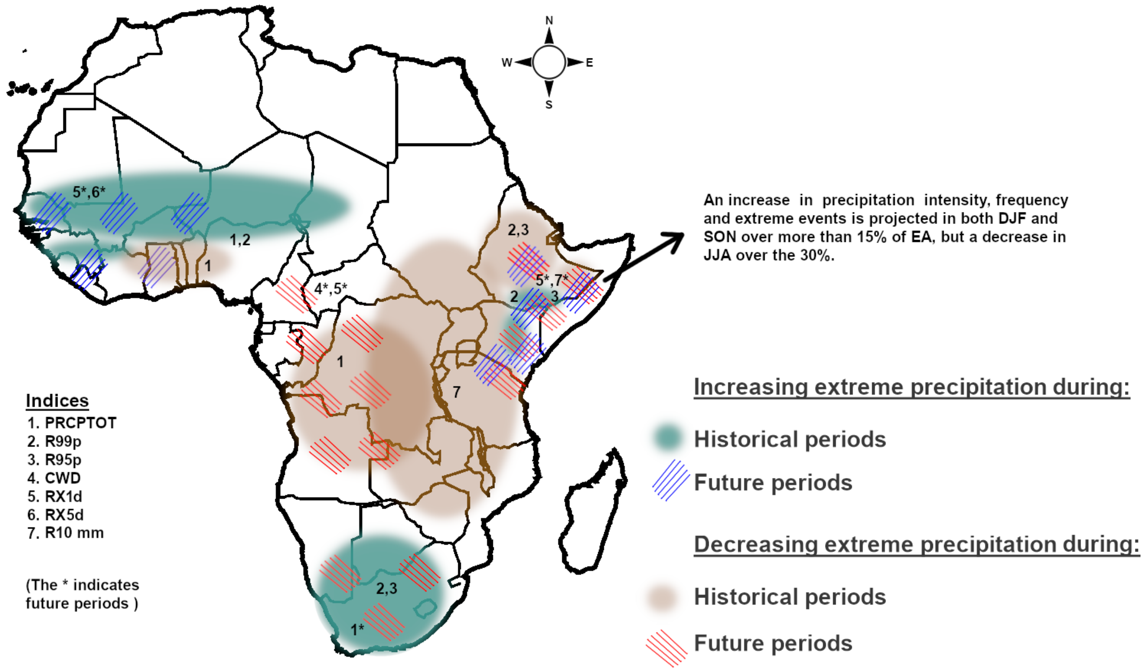

Figure S1. Schematic representation of observed and expected changes of extreme precipitation over Africa according with several indices shown in the figure.

1.2 America

1.2.1 North America

According to observations, over the period 1950 – 2010 most regions near the Pacific coast, central Boreal regions, and near the Atlantic coast in Canada showed an increase in annual maximum daily precipitation, while there was a decrease in the Canadian Prairies, Boreal regions over northern Manitoba, eastern Ontario and western Quebec, and northwestern Canada (Tan et al., 2017). A trend analysis of seasonal maximum daily precipitation performed by the same authors showed a mix of results, with more stations indicating a significant increase in spring, summer and autumn across most regions in Canada, while there was a significant decrease (increase) in winter over southern (northern) Canada. For the Artic region of Canada, the trend of extreme precipitation for the period 1950-2010 suggests an increasing frequency and variability over the Southern Arctic regions, but an inconclusive result over the northern Arctic (Chaudhuri and Robertson, 2019). Vincent et al. (2018) also investigated extreme precipitation trends but for two periods: 1948– 2016 for all stations in Canada, and 1900–2016 for stations in the south of Canada, revealing an increase in the number of days with extreme precipitation according to R90p (precipitation ≥ 90th percentile) in the southern regions.

Some studies have also found an increase in the frequency of extreme precipitation events over the United States since the first half of the 20th century (Kunkel, 2003), particularly over the Upper Mississippi, the Midwest, and the South; these increases were statistically significant for annual increases for very intense precipitation extremes (above the 99.7th percentiles) for 1908–2002 (Groisman et al., 2004), which was also confirmed by Groisman et al. (2012) for 1948-2009. Additionally, a positive trend of extreme daily precipitation from the gridded Climate Prediction Center (CPC) at a resolution of 0.25° × 0.25°, defined by the 95th percentile, revealed an increase during the months of June–August for the period 1981 – 2010 in the eastern, but particularly the north-eastern United States (Marquardt-Collow et al., 2016). For a longer period (1890 – 2013) the central United States also experienced a positive trend in precipitation extremes according to R95p and R5d (Rahmani and Harrington, 2019). In a recent study, Armal et al. (2018) used high quality precipitation data obtained from stations across the United States from the Global Historical Climatology Network for investigating extreme precipitation (95th percentile of the daily nonzero rainfall) over the period 1900-2014 (115 years). Their results show that while Colorado and Utah (Southwest climate region) show a negative trend, the trend over much of the country is positive. However, for the southeastern USA a trend analysis performed by Mahjabin and Abdul-Aziz (2020) was inconclusive, although the magnitude of the annual maximum rainfall, as well as the number of above-threshold events, generally showed a higher rate of change per year during more recent times.

From the Special Report on Emission Scenarios (SRES), significant increases in the fraction of extreme precipitation based on the average baseline 95th percentile of daily precipitation (R95p) for the period 2070–2099 considering the A1B scenario are mostly expected for the north and east of North America, while decreases are expected over the southwest (Singh et al., 2013). Swain et al. (2018) noted that a 25-100% increase in dry-to-wet events according to the 80th percentile of the accumulated annual precipitation (R80PTOT) is projected over California by the end of the 21st century as a result of anthropogenic forcing. The CMIP5 multi-model average shows the percentage changes in the mean seasonal maximum pentad total precipitation (Rx5 day) by the end of the 21st century (2080–2100) with respect to the period 1985–2005, revealing similar patterns in DJF and MAM (Barlow et al., 2019). Both are characterised by reductions over the southwestern United States and the north of Mexico, with increases over the rest of the USA and Canada. In JJA the reduction extends over northwest, central, and southeast USA, while in SON the reduction is only observed over the west coast. The 100-yr annual maximum precipitation is more frequent in future climates (2080–99) for most land grid points in North America than it is for historical periods (1980–99) (Martel et al., 2020). CMIP6 projections also reveal the amplification of heavy precipitation over the northern US during winter, while some inter-model spread is prevalent in the summer projections. Specially, heavy and very heavy winter precipitation days (R10mm and R20mm) show larger increases compared with other aspects of precipitation (Akinsanola et al., 2020). Figure S2 represents visually the most important findings on extreme precipitation in North America discussed in this section.

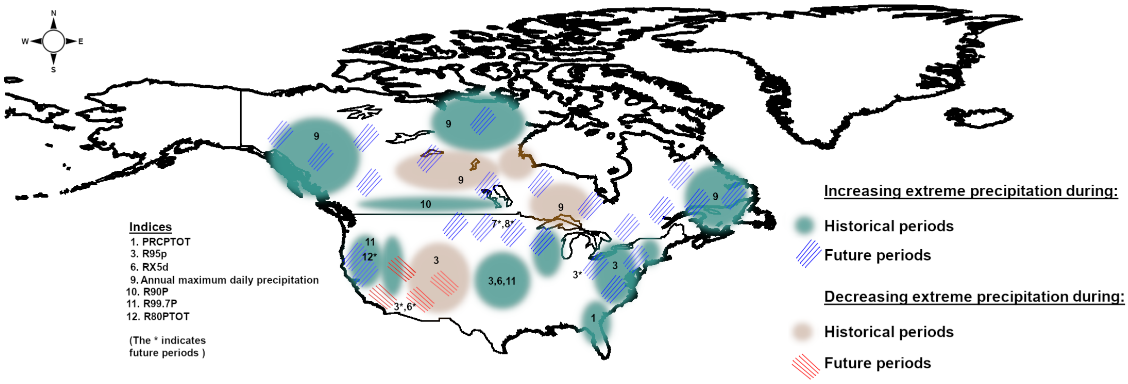

Figure S2. Schematic representation of observed and expected changes of extreme precipitation over North America, according with several indices shown in the figure.

1.2.2 Mexico, Central America and the Caribbean

The maximum 1-day and 5-day precipitation amounts, and the number of very heavy precipitation days showed a significant positive trend at 12% of the weather stations in Aguascalientes (central Mexico) over a period of 34 years (1980–2013) (Ruiz-Alvarez, et al., 2020). In contrast, also for central Mexico (Zacatecas), Ortiz-Gómez et al. (2020) revealed through observational datasets that precipitation events according to PRCPTOT, R99p, R95p decreased but became slightly more intense for the period 1961-2014. For the rainy season (May-October) of 1981 – 2018, the major part of southern Mexico and Guatemala experienced an increase in extreme daily precipitation (using the threshold of the 95th percentile), although mostly of these were not statistically significant (p>0.05) (Anderson et al., 2019). Trends in heavy rainfall events were also weak for the Caribbean region for the period 1960 – 2010, although small positive trends were found in annual total precipitation, daily intensity, maximum number of consecutive dry days, and heavy rainfall events, particularly for the period 1986–2010 (Stephenson et al., 2014). For Trinidad and Tobago, extreme wet days (R99p) also increased for the period 1985–2015 (Dookie et al., 2019) as well as for the period 1969-2017 on the island of Barbados (Mohan et al., 2020).

Projections of downscaling over Central America at an 8-km resolution using the Eta Regional Climate Model, driven by HadGEM2-ES simulations of RCP4.5 scenarios for 2021–2050 indicate positive trends in extreme precipitation, measured by R50mm and R90p, for the east coast around Costa Rica, with negative trends in the northern part of the continent (Imbach et al., 2018). For the Caribbean, McLean et al. (2015) revealed that the prevailing pattern of future projections from the ECHAM driven PRECIS RCM for 2071–2099 under A2 and B2 relative to the model baseline is a tendency towards more intense rainfall events over much of Cuba, Lamentin, Martinique and Barbados, i.e., in the northern and eastern zones, though with less consensus with respect to changes in the lengths of wet and dry spells. A CMIP5 multi-model average simulation of the percentage change in the mean seasonal maximum RX5d for the period 2080–2100 indicated an important reduction over Mexico and the Caribbean during JJA and MAM, and DJF, whereas for SON the same regions generally experiment an increase (Barlow et al., 2019). The main information from the studies consulted for this section appears in Figure S3.

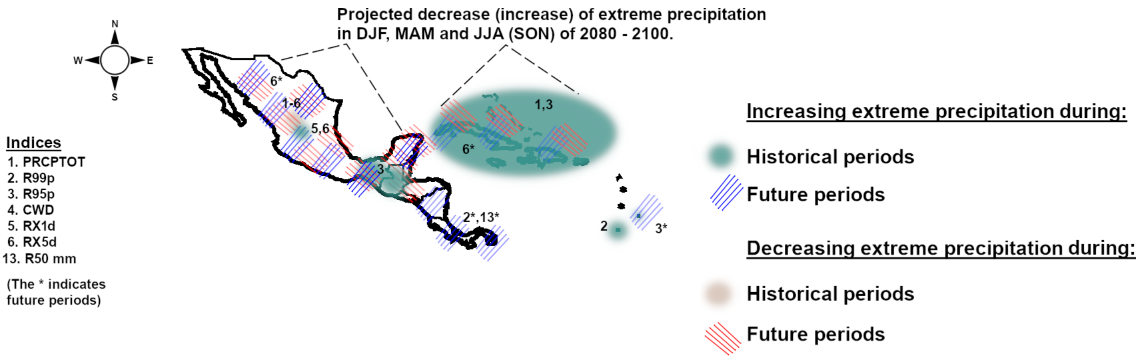

Figure S3. Schematic representation of observed and expected changes of extreme precipitation over Mexico, Central America and the Caribbean, according with several indices shown in the figure.

1.2.3 South America

With regard to South America, several authors have shown increasing trends in the frequency of heavy and extreme precipitation events (PRCPTOT, R99p, R95p, R20 mm, etc.) in south and south-eastern Brazil and the La Plata River Basin using rain-gauge and gridded precipitation data for various study periods including 1976-1999 (Liebmann et al., 2004); 1950–1999, 1990–1999 (Dufek and Ambrizzi, 2008); 1933-2010 (Silva Dias et al., 2013); 1961-2010 (Penalba and Robledo, 2010); 1960- 2014 (Teixeira and Satyamurty, 2011). By studying trends in total and extreme precipitation for the whole of South America for the period 1960–2000, Haylock et al. (2006) found upward trends in Ecuador, northern Peru, southern Brazil, Paraguay, Uruguay, and northern and central Argentina, but downward trends in precipitation over southern Peru and southern Chile. However, many of the studies of trends in extreme rainfall in South America have focused on river basins. According to datasets from the Climate Hazards Group InfraRed Precipitation with Stations (CHIRPS) for the period 1982 – 2018, the western part of the Amazon basin shows an increasing trend in the number of days with precipitation greater than 20 mm for both the dry and wet seasons, but all other regions show a decreasing trend in both seasons (Haghtalab et al., 2020). The Amazon basin is of course composed of several smaller river basins, the main one being the Madeira river basin. Trends in the maximum annual rainfall series composed from maximum daily precipitation and from CHIRPS for the Madeira basin for 1981 – 2017 show a number of regions with a reduction in the magnitude of extreme rainfall (de Souza et al., 2020). For a longer but earlier study period (1955-2004), de Barros Soares et al. (2017) found significant positive trends in precipitation using three observational precipitation datasets (CRU, UDEL, and GPCC) over a region that encompasses roughly the southern part of the La Plata Basin (southern Brazil, Uruguay, and northeastern Argentina). The same authors also described positive significant trends in parts of Colombia, Ecuador, a region between Brazil, Guyana, and Venezuela, and a region between Brazil, Peru, and Bolivia. Negative significant trends are observed in all data sets over southern Chile and French Guiana. These results are in agreement with those of Rao et al. (2015), who studied precipitation trends over Brazil for 1979–2011 and found significant negative trends over regions of southeast Brazil, as well as significant positive trends in western northern Brazil and the northern Amazon. A seasonal trend analysis of daily precipitation above the 95th and 99th percentile for the Brazilian Amazon over the period 1980-2013 revealed different signs apart from for the eastern region where the increase was significant (Da Silva et al., 2019), whereas in northeast Brazil the clearest result was the decrease in extreme precipitation along its northern coast. In the São Francisco River Basin, which is also located in eastern Brazil, the number of very and extremely wet days generally decreased over the period 1947 – 2012, apart from in the southern part of the basin, where the number mostly increased (Bezerra et al., 2019). In the central eastern part of South America, a significant increase in total annual rainfall in the northern central sector of the Paraná basin in 1986 – 2011 was related to higher rates of heavy rainfall, mainly above the 95th percentile, as well as to the highest numbers event of rainfall above 10 mm (Zandonadi et al., 2016). Another study was carried out over a longer study period (1938-2012) using records from two datasets: a daily gridded precipitation dataset from the Physical Sciences Division (PSD), Earth System Research Laboratory and data from individual stations operated by different Brazilian agencies. The results showed a decrease (increase) in the number of rainy days per decade in the northeast (southeast) of Brazil (Zilli et al., 2017). However, these authors also found that over great part of northeast Brazil has increased the number of daily extreme precipitation (R95p) per decade. For a shorter period covering from 1972 to 2002 Oliveira et al. (2016) found heterogeneous trend signs on the number of extreme precipitation events according to R95p values within Northeast Brazil, but a prevailing increase during JJA. Regional climate model simulations also showed an increase in the frequency of extremely wet days (R99p) per decade in the period 1965 – 2005 (Dereczynski et al., 2020). A trend analysis carried out on a daily precipitation series of 124 years (1889 – 2013) for Curitiba – Southern Brazil also showed an increase in the number of extreme values (Pedron et al., 2017).

An ensemble simulation with the global 20-km mesh AGCM at the end of the 21st century (2075–2099) under the RCP8.5 scenario revealed an increase the annual maximum 1- and 5-day total precipitation over South America (Kitoh and Endo, 2016). In agreement, other findings reveal that for 2071–2100 under RCP4.5, an increase in extreme precipitation events (R95p) over the subtropics of South America stands out as a strong signal among the models, whereas for tropical latitudes the dispersion among models is high, which reduces somewhat the level of confidence in the projections (Blázquez and Silvina, 2020). Other results confirm that the Tocantis and San Francisco rivers basins, that extend north south in central and central eastern Brazil, will experience a reduction of daily precipitation above the 95th percentile during the 2041- 2070 and 2071-2099 periods compared to 1961-1990 (Valverde and Marengo, 2014). Projected trends of RX5d for 2071 – 2100 under B2 scenarios relative do 1961 – 1990 indicates a significant decrease (Marengo et al., 2009) that has been also confirmed for RX5d and

PRCPTOT in North East Brazil considering land cover changes averaged over 2071 – 2100 under the RCP8.5 scenarios (Sy and Quesada, 2020). Figure S4 represent the results discussed in this section.

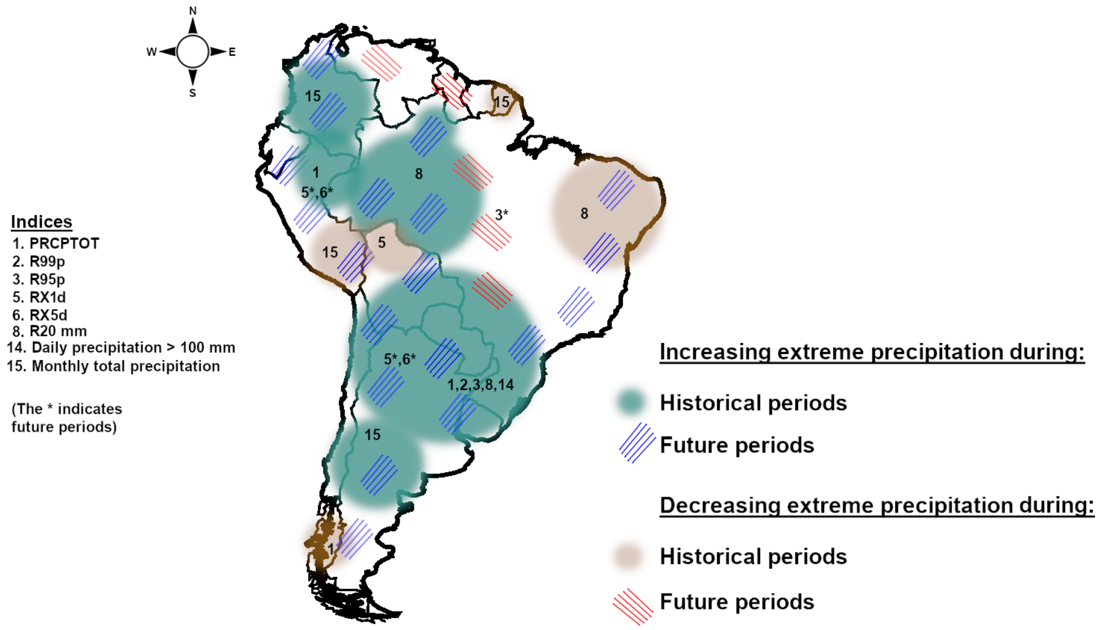

Figure S4. Schematic representation of observed and expected changes of extreme precipitation over Africa according to several indices shown in the figure.

1.3 Australia

From observational and modelling datasets, Alexander and Arblaster (2017) showed that the number of heavy precipitation days (R10mm) generally decreased during 1911 – 2010 over the north and west of Australia. Using a shorter period (1951 – 1980) the PRCPTOT was shown to have increased over the southwest and central part of Australia, while negative trends were seen over central Australia (Donat et al., 2016a). For an extended period (1950-2012), Gallant et al. (2014) found increasing areas where the proportion of annual total precipitation fell on heavy-rainfall days. This accords with the increasing magnitude of extreme daily rainfall for 1966–1989 and 1990–2013 over Australia (Guerreiro et al., 2018). At regional scales, Groisman et al. (2005) found that precipitation totals increased by 16% over 100 years in the southeast, but decreased by the same amount in the southwest during 1907–98 and 1913–98, respectively. Using data from 1976 to 2005 and considering two distinct clusters of observational sites in southeast Australia, Jakob et al. (2011) found precipitation to be on the increase in the southern cluster (north east of Melbourne) while decreasing in the northern cluster (near Sydney); these changes were persistent over timescales from 6 min to 72 h and for return periods from 2 to 50 years. In agreement, a recent study by Osburn et al. (2021) for Victoria (southeast Australia) found that precipitation events greater than 12 and 18 mm/h became more frequent from 1958 to 2014, particularly for the warm season (April – September).

Regional climate simulations at a 50 km spatial resolution over Australia for 2020–2039 and 2060–2079 under the SRES A2 scenario showed an increase of extreme precipitation (according to R95PTOT and R99PTOT over most of Australia; however, the maximum monthly number of consecutive wet days seems to increase for DJF and MAM, while decreasing for JJA and SON (Herold et al., 2018). Nevertheless, CMIP5 model simulations under RCP4.5 and RCP8.5 project increases in very wet and extremely wet days in Australia, with some evidence of scaling with emissions scenario in the multi-model mean from 2005 to 2100 (Alexander and Arblaster, 2017). Similar findings were also found for the end of the 21st century (Myhre et al., 2019). A schematic representation of these results was summarised in Figure S5.

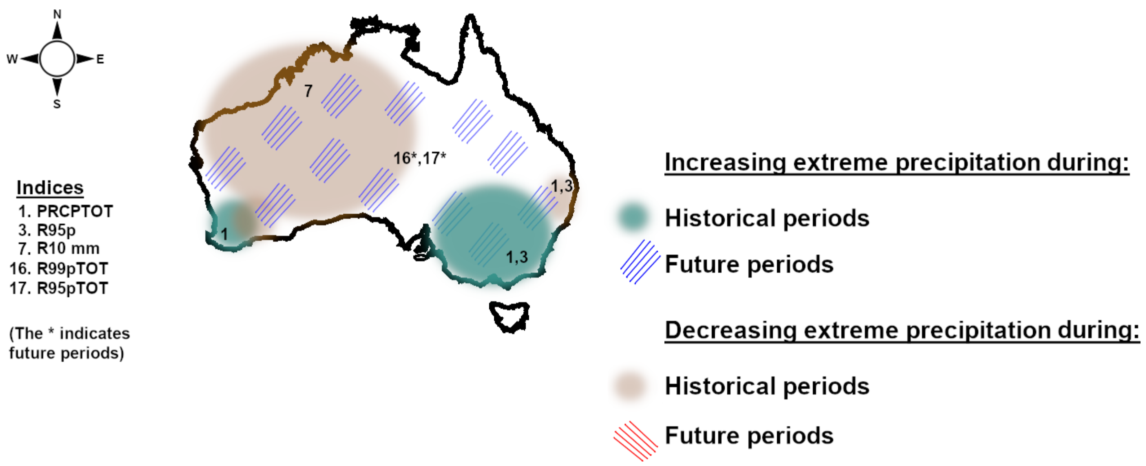

Figure S5. Schematic representation of observed and expected changes of extreme precipitation over Australia according to several indices shown in the figure.

1.4 Europe

A predominantly positive trend in R95p values for all seasons for the period 1950 – 2010 over Europe has been noted (Casanueva et al., 2014). According to Fischer and Knutti (2016), the number of days with very heavy precipitation over Europe has increased on average by about 45% according to observations (for 1981–2013 compared with 1951–1980). In agreement, Myhre et al. (2019) note observations that show that the amount of daily precipitation above the 99th percentile increased significantly over the period 1951 – 1980 and continuously for 1984 – 2013. Regional differences in extreme precipitation trends have been observed in Europe during the 20th century, showing that northern Europe became significantly wetter, and dryer conditions prevailed in the Mediterranean region (Kostopoulou and Jones 2005; IPCC, 2013; Stagge et al., 2017), in particular over Austria, Switzerland, Germany and the Netherlands (Zeder and Fisher, 2020). Historical simulations (1861–2014) from 26 CMIP6 and 25 CMIP5 Global Climate Models and E-OBS data (1950–2014) confirmed the temporal evolution and latitudinal pattern of anthropogenic influences on the 99th percentile of daily precipitation over Europe and its latitudinal dependency on fluctuations in extreme precipitation anomalies over Europe for all seasons, and the largest discrepancy of the trend in summer for southern Europe where/when extreme precipitation is mainly convective and represented poorly by large scale climate models (Tabari et al., 2020). Increasing sea surface temperatures in the Mediterranean have amplified the extreme summer precipitation in Central Europe for 2000-2012 (Volosciuk et al., 2016). Furthermore, a major part of the Iberian Peninsula, particularly the south, experienced a decreasing trend of extreme rainfall over the period 1951 – 2007 (Łupikasza, 2007).

Simulation of the Centro Euro-Mediterraneo sui Cambiamenti Climatici coupled atmosphere-ocean general circulation model (CMCC-CM; Scoccimarro et al. 2011; Bellucci et al. 2015) under RCP8.5 for the period 2081–2100 shows a tendency towards more extreme daily rainfall events (R90p) (Scoccimarro et al., 2015). Additional future projections (2070–2099) of precipitation extremes over Europe, provided by an extensive multimodel ensemble of 12 and 50 km resolution EURO-CORDEX Regional Climate Models (RCMs) forced by the RCP2.6, RCP4.5, and RCP8.5 scenarios reveal that for the majority of seasons and regions, simulated heavy precipitation events will intensify compared to present-day conditions, but changes in the overall character of precipitation are complex and depend on season and location, as the observed reduction of precipitation extremes over the Iberian Peninsula during summer (Rajczak and Schär, 2017). Even for a longer period of simulation (2099–2108), the extremes for daily maximum hourly precipitation and daily frequency increases are also concentrated over northern Europe, with larger areas of significant positive change over the UK, Norway, and around the Baltic Sea and Denmark (Chan et al., 2020). This finding is also in agreement with Huo et al. (2021), who showed that larger increases are shown for 100- and 200-yr return periods than for 5- and 10-yr precipitation in both RCP scenarios with respect to historical periods. Figure S6 represents the most important findings on extreme precipitation in Europe discussed in this section.

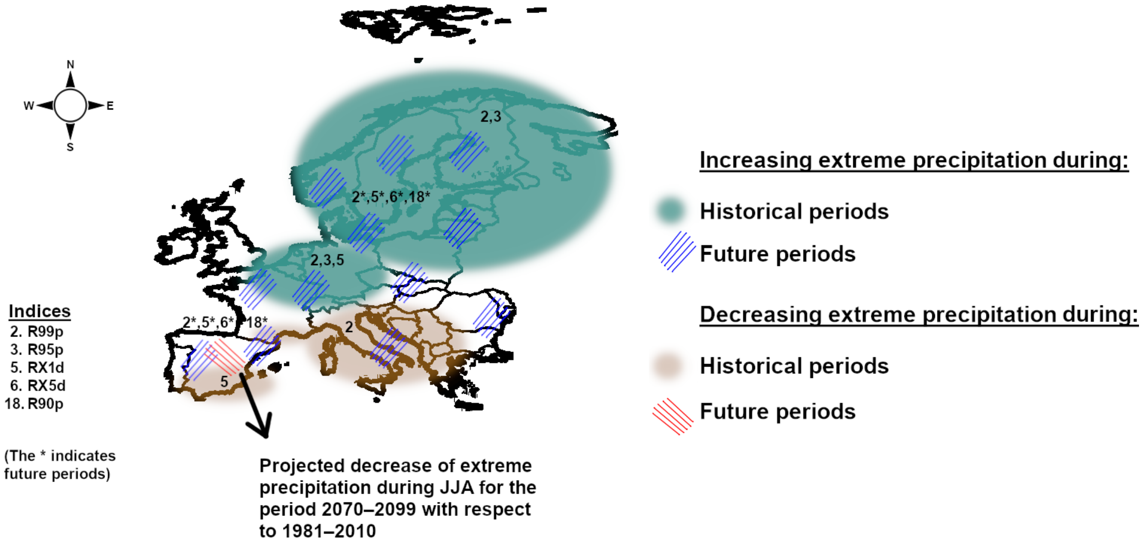

Figure S6. Schematic representation of observed and expected changes of extreme precipitation over Europe according to several indices shown in the figure.

1.5 Asia

With regard to the Asian continent, the recent study by Kim et al. (2019) contained a report on decadal trends in extreme precipitation using the R95p of the daily precipitation probability distribution function (PDF) for June-July-August of each year using rain gauge data (APHRODITE, CPC-UNI), satellite data (TRMM, GPCP1DD), and reanalysis (ERA-Interim, MERRA, and JRA55) for the period 1998–2007. Their results reveal that apart from APHRODITE, ERA-Interim, and JRA55, the remaining datasets indicate a remarkable increasing trend over central India, while decreasing trends are observed only in the northern part of the Himalayas. Over the Indian region, extreme precipitation events were on the increase during the 20th Century (Sen and Balling, 2004; Goswami et al. 2006; Rajeevan et al., 2008; Krishnan et al., 2016; Roxy et al. 2017) with an increase of up to 10–30% over India (Krishnan et al., 2016), at a rate of about 13 events per decade (more than one per year; Roxy et al., 2017). Roxy et al. (2017) also showed that the frequency of extreme precipitation events (daily precipitation ≥ 150 mm) over central India increased by about 75% from 1950 to 2015, and the extremes themselves are intensifying over time according to the increase in the 99.5th percentile (R99.5p) values. However, the overall increase in intensity and frequency of extreme events over the Indian region have been spatially non-uniform (Ghosh et al., 2009; Krishnamurthy et al., 2009; Ghosh et al., 2012; Ali et al., 2014; Mondal and Mujumdar 2015). In China, the frequency and intensity of extreme precipitation events have increased on average, showing also some spatial variation (Zhai et al., 2005; Wang and Zhou, 2005; Chen and Zhai, 2013; Yuan et al., 2017; Tao et al., 2018; Chen et al., 2019). The second half of the 20th century was characterised by a significant decrease in total annual precipitation and precipitation extremes in northern China and over the Sichuan Basin, and significant increases in western China, in the mid–lower reaches of the River Yangtze, and in parts of the coastal regions of southwest and southern China (Zhai et al., 2005). An analysis of maximum precipitation recorded at more than 2000 Chinese stations over the period January 1,1951, to July 31, 2012 revealed a positive trend in a region of southeast China, a positive trend in a region of northwest China, and a negative trend in a region of north China (Sun and Zhang, 2017). Confirmation was also provided of the positive trends in PRCPTOT and R95p during the summer monsoonal season of 1960 – 2014 over central-east China and southeast coastal regions (Gao et al., 2017). The Tibetan Plateau experienced a positive trend in extreme precipitation according to R95p and R99p for the period 1960 – 2012, which was particularly strong after 2000 (Cao and Pan, 2014), while at the same indices revealed a significant trend over the period 1961 – 2018 over northwest China (Hu et al., 2021). For the Russian Far East, strong positive trends of extreme precipitation (R95p) were observed for 1991- 2013 compared to the climate baseline conditions of 1961-1990 (Zolotokrylin and Cherenkova, 2017), particularly in winter and spring. An increasing number of days with precipitation above 95% percentile in winter was found at stations in European Russia and Western Siberia for 1977- 2006 (Bulygina et al. 2007).

Using the output of the Southeast Asia Regional Climate Downscaling/Coordinated Regional Climate Downscaling Experiment – Southeast Asia (SEACLID/CORDEX-SEA), projected precipitation extremes for 2081–2100 over Southeast Asia indicate a decrease in annual PRCPTOT over most of the region, except for Myanmar and Northern Thailand, with magnitudes of as much as 20% (30%) under RCP4.5 (RCP8.5) (Supari et al., 2020). A general increase is particularly expected this century over the Indian region (Suman and Maity, 2020). An assessment of changes in precipitation using a CMIP6 multi-model ensemble under the SSP has also confirmed the increase of PRCPTOT over most of southeast Asia under all SSP scenarios for 2071–2100 (Ge et al., 2021). However, these authors also argue that in agreement with previous results, other extreme indices also reveal a non-uniform occurrence of extremes, suggesting the intensification of both wet and dry conditions over Southeast Asia. Other findings also confirm the expected increase of the annual maximum 5-day precipitation total (RX5d) in parts of the Middle East for the period 2075–2099 under RCP8.5 (Kitoh and Endo, 2016). These findings appear summarised in Figure S7.

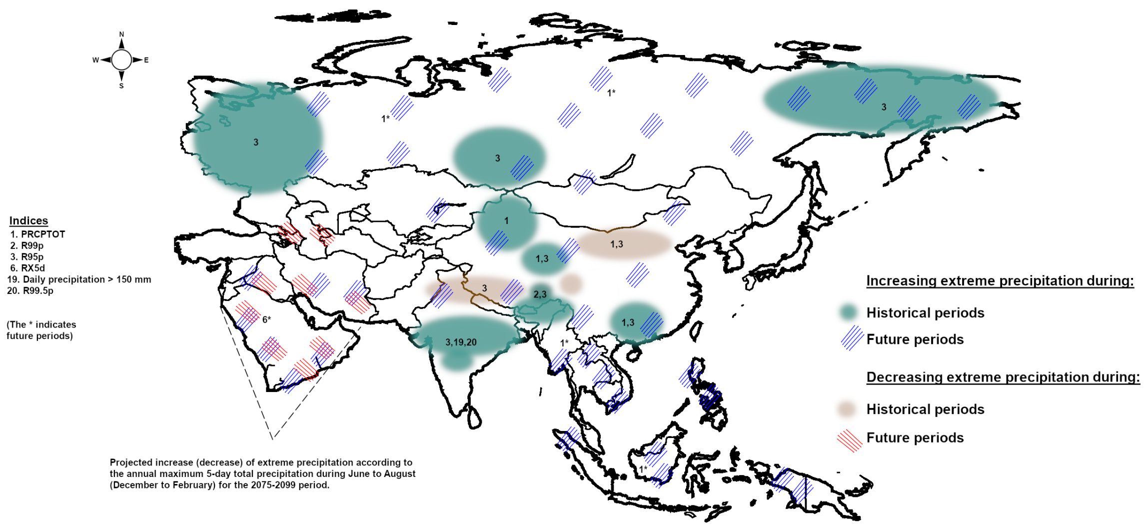

Figure S7. Schematic representation of observed and expected changes of extreme precipitation over Asia according to several indices shown in the figure.

References

Alexander, L.V., & Arblaster, J.M. (2017). Historical and projected trends in temperature and precipitation extremes in Australia in observations and CMIP5. Weather and Climate Extremes, 15, 34–56. https://doi.org/10.1016/j.wace.2017.02.001

Ali, H., Mishra, V. & Pai, D. (2014). Observed and projected urban extreme rainfall events in India. Journal of Geophysical Research: Atmospheres, 119, 12621-12641. https://doi.org/10.1002/2014JD022264

Armal, S., Devineni, N., & Khanbilvardi, R. (2018). Trends in Extreme Rainfall Frequency in the Contiguous United States: Attribution to Climate Change and Climate Variability Modes. Journal of Climate, 31(1), 369-385. https://doi.org/10.1175/JCLI-D-17-0106.1

Atiah, W.A., Mengistu Tsidu, G., Amekudzi, L.K. et al. (2020). Trends and interannual variability of extreme rainfall indices over Ghana, West Africa. Theoretical and Applied Climatology, 140, 1393–1407. https://doi.org/10.1007/s00704-020-03114-6

Ayugi, B., Dike, V., Ngoma, H., Babaousmail, H., & Ongoma, V. (2021) Future Changes in Precipitation Extremes Over East Africa Based on CMIP6 Projections. Preprints, 2021010112. https://doi.org/10.20944/preprints202101.0112.v1

Barlow, M., Gutowski, W.J., Gyakum, J.R. et al. (2019). North American extreme precipitation events and related large-scale meteorological patterns: a review of statistical methods, dynamics, modeling, and trends. Climate Dynamics, 53, 6835–6875. https://doi.org/10.1007/s00382-019-04958-z

Bellucci, A., Haarsma, R., Gualdi, S. et al. (2015). An assessment of a multi-model ensemble of decadal climate predictions. Climate Dynamics, 44, 2787–2806. https://doi.org/10.1007/s00382-014-2164-y

Bezerra, B.G., Silva, L.L., Santos e Silva, C.M. et al. (2019). Changes of precipitation extremes indices in São Francisco River Basin, Brazil from 1947 to 2012. Theoretical and Applied Climatology, 135, 565–576. https://doi.org/10.1007/s00704-018-2396-6

Blázquez, J., & Silvina, A.S. (2020). Multiscale precipitation variability and extremes over South America: analysis of future changes from a set of CORDEX regional climate model simulations. Climate Dynamics, 55, 2089–2106. https://doi.org/10.1007/s00382-020-05370-8

Bulygina, O., Razuvaev, V., Korshunova, N., & Groisman, P. (2007). Climate variations and changes in extreme climate events in Russia. Environmental Research Letters, 2(4), 045020. https://doi.org/10.1088/1748-9326/2/4/045020

Cao, L.G., & Pan, S.M. (2014). Changes in precipitation extremes over the “Three-River Headwaters” region, hinterland of the Tibetan Plateau, during 1960-2012. Quaternary International, 321,105–115. https://doi.org/10.1016/j.quaint.2013.12.041

Casanueva, A., Rodríguez-Puebla, C., Frías, M.D., & González-Reviriego, N. (2014). Variability of extreme precipitation over Europe and its relationships with teleconnection patterns. Hydrology and Earth System Sciences, 18, 709–725. https://doi.org/10.5194/hess-18-709-2014

Chan, S.C., Kendon, E.J., Berthou, S. et al. (2020). Europe-wide precipitation projections at convection permitting scale with the Unified Model. Climate Dynamics, 55, 409–428. https://doi.org/10.1007/s00382-020-05192-8

Chaudhuri, C., & Robertson, C. (2019). A novel method to analyze trends of extreme precipitation distribution-A case study over the Arctic regions of Canada. Spatial Knowledge and Information Canada, 7(2), 1.

Chen, Y., & Zhai, P.M. (2013). Persistent extreme precipitation events in China during 1951-2010. Climate Research, 57(2),143–155. https://doi.org/10.3354/cr01171

Chen, A.J., He, X.G., Guan, H.D., & Zhang, X.P. (2019). Variability of seasonal precipitation extremes over China and their associations with largescale ocean-atmosphere oscillations. International Journal of Climatology, 39, 613–628. https://doi.org/10.1002/joc.5830

da Silva, P.E., Santos e Silva, C.M., Constantino-Spyrides, M.H., Barbosa-Andrade, L de M. (2019). Análise de Índices de Extremos Climáticos no Nordeste e Amazônia Brasileira para o Período entre 1980 a 2013. Anuario do Instituto de Geociencias, 42, 2, p. 137-148.

de Barros Soares, D., Lee, H., Loikith, P.C., Barkhordarian, A., & Mechoso, C.R. (2017). Can significant trends be detected in surface air temperature and precipitation over South America in recent decades? International Journal of Climatology, 37, 1483–1493. https://doi.org/10.1002/joc.4792

Dereczynski, C. et al. (2020). Downscaling of climate extremes over South America – Part I: Model evaluation in the reference climate. Weather and Climate Extremes, 29, 100273. https://doi.org/10.1016/j.wace.2020.100273

Diatta, S., Diedhiou, C.W., Dione, D.M., & Sambou, S. (2020). Spatial Variation and Trend of Extreme Precipitation in West Africa and Teleconnections with Remote Indices. Atmosphere, 11(9), 999. https://doi.org/10.3390/atmos11090999

Donat, M.G., Alexander, L.V., Yang, H., Durre, I., Vose, R., Dunn, R.J.H., et al. (2013). Updated analyses of temperature and precipitation extreme indices since the beginning of the twentieth century: The HadEX2 dataset. Journal of Geophysical Research: Atmospheres, 118, 2098–2118. https://doi.org/10.1002/jgrd.50150

Donat, M.G., Alexander, L.V., Herold, N., & Dittus, A.J. (2016a). Temperature and precipitation extremes in century-long gridded observations, reanalyses, and atmospheric model simulations. Journal of Geophysical Research: Atmospheres, 121, 11,174–11,189, doi:10.1002/ 2016JD025480

Dosio, A., Jones, R.G., Jack, C. et al. (2019). What can we know about future precipitation in Africa? Robustness, significance and added value of projections from a large ensemble of regional climate models. Climate Dynamics, 53, 5833–5858. https://doi.org/10.1007/s00382-019-04900-3

Dufek, A.S., & Ambrizzi, T. (2008). Precipitation variability in Sao Paulo State, Brazil. Theoretical and Applied Climatology, 93, 167–178. https://doi.org/10.1007/s00704-007-0348-7

Fischer, E.M. & Knutti, R. (2016). Observed heavy precipitation increase confrms theory and early models. Nature Climate Change, 6, 986–991. https://doi.org/10.1038/nclimate3110

Gallant, A. J. E., Karoly, D. J., & Gleason, K. L. (2014). Consistent Trends in a Modified Climate Extremes Index in the United States, Europe, and Australia, Journal of Climate, 27(4), 1379-1394.

Gao, T., Wang, H.J., Zhou, T. (2017). Changes of extreme precipitation and nonlinear influence of climate variables over monsoon region in China. Atmospheric Research, 197, 379-389. https://doi.org/10.1016/j.atmosres.2017.07.017.

Ge, F., Zhu, S., Luo, H., Zhi, X., & Wang H. (2021). Future changes in precipitation extremes over Southeast Asia: insights from CMIP6 multi-model ensemble. Environmental Research Letters, 16(2), 024013. https://doi.org/10.1088/1748-9326/abd7ad

Gebrechorkos, S.H., Hülsmann, S., & Bernhofer, C. (2018). Changes in temperature and precipitation extremes in Ethiopia, Kenya, and Tanzania. International Journal of Climatology. 39, 18–30. https://doi.org/10.1002/joc.5777

Ghosh, S., Luniya, V. & Gupta, A. (2009). Trend analysis of Indian summer monsoon rainfall at different spatial scales. Atmospheric Science Letters, 10, 285–290. https://doi.org/10.1002/asl.235

Ghosh, S., Das, D., Kao, S.C., & Ganguly, A.R. (2012). Lack of uniform trends but increasing spatial variability in observed Indian rainfall extremes. Nature Climate Change, 2, 86–91. https://doi.org/10.1038/nclimate1327

Goswami, B.N., Venugopal, V., Sengupta, D., Madhusoodanan, M.S., & Xavier, P.K. (2006). Increasing trend of extreme rain events over India in a warming environment. Science, 314(5804), 1442–1445. https://doi.org/10.1126/science.1132027

Guerreiro, S.B., Fowler, H.J., Barbero, R., Westra, S., Lenderink, G., Blenkinsop, S., Lewis, E., & Li, X.-F. (2018). Detection of continental-scale intensification of hourly rainfall extremes. Nature Climate Change, 8(9), 803. https://doi.org/10.1038/s41558-018-0245-3

Groisman, P.Y, Knight, R.W., Karl, T.R., Easterling, D.R., Sun, B., & Lawrimore, J. M. (2004). Contemporary changes of the hydrological cycle over the contiguous United States: Trends derived from in situ observations. Journal of Hydrometeorology, 5, 64–85. https://doi.org/10.1175/1525-7541(2004)005<0064:CCOTHC>2.0.CO;2

Groisman, P.Y., Knight, R.W., Easterling, D.R., Karl, T.R., Hegerl, G.C., & Razuvaev, V.N. (2005). Trends in intense precipitation in the climate record. Journal of Climate, 18, 1326–1350. https://doi.org/10.1175/JCLI3339.1

Groisman, P.Y., Knight, R.W., & Karl, T.R. (2012). Changes in intense precipitation over the central United States. Journal of Hydrometeorology, 13(1), 47–66. https://doi.org/10.1175/JHM-D-11-039.1

Haghtalab, N., Moore, N., Heerspink, B.P. et al. (2020). Evaluating spatial patterns in precipitation trends across the Amazon basin driven by land cover and global scale forcings. Theoretical and Applied Climatology, 140, 411–427. https://doi.org/10.1007/s00704-019-03085-3

Harrison, L., Funk, C., & Peterson, P. (2019). Identifying changing precipitation extremes in Sub-Saharan Africa with gauge and satellite products. Environmental Research Letters, 14, 085007, https://doi.org/10.1088/1748-9326/ab2cae.

Haylock, M.R., Peterson, T.C., Alves, L.M., Ambrizzi, T., et al. (2006). Trends in total and extreme South American rainfall in 1960–2000 and links with sea surface temperature. Journal of Climate, 19, 1490–1512. https://doi.org/10.1175/JCLI3695.1

Herold, N., Ekström, M., Kala., J., Goldie, J., & Evans, J.P. (2018). Australian climate extremes in the 21st century according to a regional climate model ensemble: Implications for health and agriculture. Weather and Climate Extremes, 20, 54-68. https://doi.org/10.1016/j.wace.2018.01.001

Hu, W., Yao, J., He, Q., & Chen, J. (2021). Changes in precipitation amounts and extremes across Xinjiang (northwest China) and their connection to climate indices. PeerJ Environmental Science, 9, e10792. https://doi.org/10.7717/peerj.10792

Huo, R., Li, L., Chen, H., Xu, C., Chen, J., & Guo, S. (2021). Extreme Precipitation Changes in Europe from the Last Millennium to the End of the Twenty-First Century. Journal of Climate, 34(2), 567-588.

IPCC, 2013: Climate Change 2013: The Physical Science Basis. Contribution of Working Group I to the Fifth Assessment Report of the Intergovernmental Panel on Climate Change [Stocker, T.F., D. Qin, G.-K. Plattner, M. Tignor, S.K. Allen, J. Boschung, A. Nauels, Y. Xia, V. Bex and P.M. Midgley (eds.)]. Cambridge University Press, Cambridge, United Kingdom and New York, NY, USA, 1535 pp. https://www.ipcc.ch/site/assets/uploads/2018/02/WG1AR5_all_final.pdf

Jakob, D., Karoly, D., & Seed, A. (2011). Non-stationarity in daily and sub-daily intense rainfall–part 2: regional assessment for sites in south-east Australia. Natural Hazards and Earth System Sciences, 11(8), 2273-2284. https://doi.org/10.5194/nhess-11-2273-2011

Kim, I.W., Oh, J., Woo, S. et al. (2019). Evaluation of precipitation extremes over the Asian domain: observation and modelling studies. Climate Dynamics, 52, 1317–1342. https://doi.org/10.1007/s00382-018-4193-4

Kitoh, A., & Endo, H. (2016). Changes in precipitation extremes projected by a 20-km mesh global atmospheric model. Weather and Climate Extremes, 11, 41–52. https://doi.org/10.1016/j.wace.2015.09.001

Kostopoulou, E., & Jones, P.D. (2005). Assessment of climate extremes in the Eastern Mediterranean. Meteorology and Atmospheric Physics, 89, 69–85. http://dx.doi.org/10.1007/ s00703-005-0122-2.

Krishnan, R. et al. (2016). Deciphering the desiccation trend of the South Asian monsoon hydroclimate in a warming world. Climate Dynamics, 47, 1007-1027. https://doi.org/10.1007/s00382-015-2886-5

Kruger, A.C., & Nxumalo, M.P. (2017). Historical rainfall trends in South Africa: 1921–2015. Water SA, 43(2). https://doi.org/10.4314/wsa.v43i2.12

Kunkel, K.E. (2003). North American trends in extreme precipitation. Natural Hazards, 29(2), 291–305. https://doi.org/10.1023/ A:1023694115864

Liebmann, B., Vera, C.S., Carvalho, L.M.V., Camilloni, I. A., Hoerling, M. P., Allured, D., et al. (2004). An observed trend in central South American precipitation. Journal of Climate, 17, 4357–4367. https://doi.org/10.1175/3205.1

Łupikasza, E.B. (2017). Seasonal patterns and consistency of extreme precipitation trends in Europe, December 1950 to February 2008. Climate Research, 72, 217-237. https://doi.org/10.3354/cr01467

Ly, M., Traore, S.B., Alhassane, A., & Sarr, B. (2013). Evolution of some observed climate extremes in the West African Sahel. Weather and Climate Extremes, 1, 19–25. https://doi.org/10.1016/j.wace.2013.07.005

Mahjabin, T., & Abdul-Aziz, O.I. (2020). Trends in the Magnitude and Frequency of Extreme Rainfall Regimes in Florida. Water, 12(9), 2582. https://doi.org/10.3390/w12092582

Marquardt Collow, A.B., Bosilovich, M.G., & Koster, R.D. (2016). Large-Scale Influences on Summertime Extreme Precipitation in the Northeastern United States. Journal of Hydrometeorology, 17(12), 3045-3061. https://doi.org/10.1175/JHM-D-16-0091.1

Mondal, A., & Mujumdar, P.P. (2015). Modeling non-stationarity in intensity, duration and frequency of extreme rainfall over India. Journal of Hydrology, 521, 217–231. https://doi.org/10.1016/j.jhydrol.2014.11.071

Myhre, G., Alterskjær, K., Stjern, C.W., Hodnebrog, Marelle, L., Samset, B.H., … Stohl, A. (2019). Frequency of extreme precipitation increases extensively with event rareness under global warming. Scientific Reports, 9(1), 1–10. https://doi.org/10.1038/s41598-019-52277-4

Odoulami, R.C., & Akinsanola, A.A. (2017). Recent assessment of West African summer monsoon daily rainfall trends. Weather, 73, 283–287. https://doi.org/10.1002/wea.2965

Oliveira, P.T., Santos e Silva, C.M. & Lima, K.C. (2017). Climatology and trend analysis of extreme precipitation in subregions of Northeast Brazil. Theor Appl Climatol 130, 77–90, https://doi.org/10.1007/s00704-016-1865-z

Osburn, L., Hope, P., & Dowdy, A. (2021). Changes in hourly extreme precipitation in Victoria, Australia, from the observational record. Weather and Climate Extremes, 31, 100294. https://doi.org/10.1016/j.wace.2020.100294.

Panthou, G., Vischel, T., & Lebel, T. (2014). Recent trends in the regime of extreme rainfall in the Central Sahel. International Journal of Climatology, 34, 3998-4006. https://doi.org/10.1002/joc.3984

Panthou, G., Lebel, T., Vischel, T., & Quantin, G. (2018). Rainfall intensification in tropical semi-arid regions: The Sahelian case. Environmental Research Letters, 13, 064013. https://doi.org/10.1088/1748-9326/aac334

Pedron, I.T., Silva Dias, M.A.F., de Paula Dias, S., Carvalho, L.M.V., & Freitas, E.D. (2017). Trends and variability in extremes of precipitation in Curitiba – Southern Brazil. International Journal of Climatology, 37, 1250-1264. https://doi.org/10.1002/joc.4773

Penalba, O.C., & Robledo, F.A. (2010). Spatial and temporal variability of the frequency of extreme daily rainfall regime in the La Plata Basin during the 20th century. Climatic Change, 98, 531–550. https://doi.org/10.1007/s10584-009-9744-6

Pinto, I., Lennard, C., Tadross, M. et al. (2016). Evaluation and projections of extreme precipitation over southern Africa from two CORDEX models. Climatic Change, 135, 655–668. https://doi.org/10.1007/s10584-015-1573-1

Rahmani, V., Harrington, J. (2019). Assessment of climate change for extreme precipitation indices: A case study from the central United States. International Journal of Climatology, 39, 1013– 1025. https://doi.org/10.1002/joc.5858.

Rajczak, J., & Schär, C. (2017). Projections of future precipitation extremes over Europe: A multimodel assessment of climate simulations. Journal of Geophysical Research: Atmospheres, 122, 1 10,773-10,800. https://doi.org/10.1002/2017JD027176

Rajeevan, M., Bhate, J., & Jaswal, A. (2008). Analysis of variability and trends of extreme rainfall events over India using 104 years of gridded daily rainfall data. Geophysical Research Letters, 35, L18707. https://doi.org/10.1029/2008GL035143

Rao, V.B., Franchito, S.H., Santo, C.M.E., & Gan, M.A. (2015). An update on the rainfall characteristics of Brazil: seasonal variations and trends in 1979-2011. International Journal of Climatology, 36(1), 291–302. https://doi.org/10.1002/joc.4345

Roxy, M.K. et al. (2017). A threefold rise in widespread extreme rain events over central India. Nature Communications, 8, 708. https://doi.org/10.1038/s41467-017-00744-9

Salack, S., Saley, I.A., Lawson, N.Z., Zabré, I., & Daku, E.K. (2018). Scales for rating heavy rainfall events in the West African Sahel. Weather and Climate Extremes, 21, 36–42. https://doi.org/10.1016/j.wace.2018.05.004

Scoccimarro, E., Gualdi, S., Bellucci, A., Sanna, A., Fogli, P.G., Manzini, E., Vichi, M., Oddo, P., & Navarra, A. (2011). Effects of tropical cyclones on ocean heat transport in a high resolution coupled general circulation model. Journal of Climate, 24, 4368–4384, https://doi.org/10.1175/2011JCLI4104.1

Scoccimarro, E., Villarini, G., Vichi, M., Zampieri, M., Fogli, P.G., Bellucci, A., & Gualdi, S. (2015). Projected Changes in Intense Precipitation over Europe at the Daily and Subdaily Time Scales, Journal of Climate, 28(15), 6193-6203. https://doi.org/10.1175/JCLI-D-14-00779.1

Sen Roy, S., & Balling Jr, R.C. (2004). Trends in extreme daily precipitation indices in India. International Journal of Climatology, 24, 457–466. https://doi.org/10.1002/joc.995

Silva Dias, M.A.F., Dias, J., Carvalho, L.M.V., Freitas, E.D., & Dias, P.L.S. (2013). Changes in extreme daily rainfall for São Paulo, Brazil. Climatic Change, 116, 705–722. https://doi.org/10.1007/s10584-012-0504-7

Singh, D., Tsiang, M., Rajaratnam, B., and Diffenbaugh, N.S. (2013). Precipitation extremes over the continental United States in a transient, high-resolution, ensemble climate model experiment. Journal of Geophysical Research: Atmospheres, 118, 7063–7086. https://doi.org/10.1002/jgrd.50543

Stagge, J.H., Kingston, D.G., Tallaksen, L.M., & Hannah, D.M. (2017). Observed drought indices show increasing divergence across Europe. Scientific Reports, 7, 14045. https://doi.org/10.1038/s41598-017-14283-2

Suman, M., & Maity, R. (2020). Southward shift of precipitation extremes over south Asia: Evidences from CORDEX data. Scientific Reports, 10, 6452. https://doi.org/10.1038/s41598-020-63571-x

Sun, J., & Zhang, F. (2017). Daily extreme precipitation and trends over China. Science China Earth Sciences, 60, 2190–2203. https://doi.org/10.1007/s11430-016-9117-8

Supari, T.F., Juneng, L., Cruz, F., Chung, J.X., Ngai, S.T., & Salimun, E. (2020). Multi-model projections of precipitation extremes in Southeast Asia based on CORDEX-Southeast Asia simulations. Environmental Research, 184, 109350. https://doi.org/10.1016/j.envres.2020.109350

Swain, D.L., Langenbrunner, B., Neelin, J.D., & Hall., A. (2018). "Increasing precipitation volatility in twenty-first-century California." Nature Climate Change, 8, 427–433. https://doi.org/10.1038/s41558-018-0140-y

Sy, S., & Quesada, B. (2020). Anthropogenic land cover change impact on climate extremes during the 21st century. Environ. Res. Lett. 15 034002

Tabari, H., Madani, K., & Willem, P. (2020). The contribution of anthropogenic influence to more anomalous extreme precipitation in Europe. Environmental Research Letters, 15 (10), 104077. https://doi.org/10.1088/1748-9326/abb268

Tan, X., Gan, T.Y., Shao, D. (2017). Effects of persistence and large-scale climate anomalies on trends and change points in extreme precipitation of Canada. J. of Hydrology, 550, 453-465, https://doi.org/10.1016/j.jhydrol.2017.05.028.

Taylor, C.M., Belušic, D., Guichard, F., Parker, D.J., Vischel, T., Bock, O., Harris, P.P., Janicot, S., Klein, C., & Panthou, G. (2017). Frequency of extreme Sahelian storms tripled since 1982 in satellite observations. Nature, 544, 475–478. https://doi.org/10.1038/nature22069

Teixeira, M.D., & Satyamurty, P. (2011). Trends in the frequency of intense precipitation events in southern and southeastern Brazil during 1960–2004. Journal of Climate, 24, 1913–1921. https://doi.org/10.1175/2011JCLI3511.1

Tao, Y.Y., Wang, W., Song, S., & Ma, J. (2018). Spatial and Temporal Variations of Precipitation Extremes and Seasonality over China from 1961–2013. Water, 10(6), 719. https://doi.org/10.3390/w10060719

Valverde, M.C., & Marengo, J.A. (2014). Extreme rainfall indices in the hydrographic basins of Brazil. Open J Mod Hydrol, 04, 10–26. https://doi.org/10.4236/ojmh.2014.41002

Vincent, L., Zhang, X., Mekis, É., Wan, H., & Bush, E. (2018). Changes in Canada's climate: Trends in indices based on daily temperature and precipitation data. Atmosphere-Ocean, 56, 332–349. https://doi.org/10.1080/07055900.2018.1514579

Volosciuk, C., Maraun, D., Semenov, V.A., Tilinina, N., Gulev, S.K., & Latif, M. (2016). Rising Mediterranean Sea Surface Temperatures Amplify Extreme Summer Precipitation in Central Europe. Scientific Reports, 6, 32450. https://doi.org/10.1038/srep32450

Wang, Y., & Zhou, L. (2005). Observed trends in extreme precipitation events in China during 1961–2001 and the associated changes in large-scale circulation. Geophysical Research Letters, 32, L09707. https://doi.org/10.1029/2005GL022574

Yuan, Z., Yang, Z.Y., Yan, D.H., & Yin, J. (2017). Historical changes and future projection of extreme precipitation in China. Theoretical and Applied Climatology, 127, 393–407. https://doi.org/10.1007/s00704-015-1643-3

Zhai, P.M., Zhang, X.B., & Pan, X.H. (2005). Trends in total precipitation and frequency of daily precipitation extremes over China Journal of Climate, 18, 1096–108. https://doi.org/10.1175/JCLI-3318.1

Zandonadi, L., Acquaotta, F., Fratianni, S. et al. (2016). Changes in precipitation extremes in Brazil (Paraná River Basin). Theoretical and Applied Climatology, 123, 741–756. https://doi.org/10.1007/s00704-015-1391-4

Zeder, J., & Fisher, E.M. (2020). Observed extreme precipitation trends and scaling in Central Europe. Weather and Climate Extremes, 29, 100266. https://doi.org/10.1016/j.wace.2020.100266

Zilli, M.T., Carvalho, L.M., Liebmann, B., & Silva Dias, M.A. (2017). A comprehensive analysis of trends in extreme precipitation over southeastern coast of Brazil. International Journal of Climatology, 37, 2

Zolotokrylin, A.Í., & Cherenkova, E.À. (2017). Seasonal changes in precipitation extremes in Russia for the last several decades and their impact on vital activities of the human population. Geography, Environment, Sustainability. 4(10), 69-82. https://doi.org/10.24057/2071-9388-2017-10-4-69-82269–2279. https://doi.org/10.1002/joc.4840

SUPPLEMENTARY MATERIAL FOR:

Projected changes in extreme daily precipitation linked to changes in precipitable water and vertical velocity in CMIP6 models

Luis Gimeno-Sotelo, Emanuele Bevacqua, José Carlos Fernández-Alvarez, David Barriopedro, Jakob Zscheischler and Luis Gimeno

Tables

Table S1: Information about the CMIP6 models used in this article

CMIP6 MODEL (VARIANT)	NATIVE LATITUDE x LONGITUDE	30-YEAR 2ºC-WARMER PERIOD	30-YEAR 3ºC-WARMER PERIOD
CESM2 (r11i1p1f1)	0.94º x 1.25º	2024-2053	2042-2071
CESM2-WACCM (r1i1p1f1)	0.94º x 1.25º	2019-2048	2039-2068
CMCC-CM2-SR5 (r1i1p1f1)	0.9° x 1.25°	2019-2048	2038-2067
CMCC-ESM2 (r1i1p1f1)	0.9° × 1.25°	2025-2054	2041-2070
CNRM-CM6-1-HR (r1i1p1f2)	0.50° × 0.50°	2015-2044	2037-2066
GFDL-CM4 (r1i1p1f1)	1º x 1º	2027-2056	2045-2074
HadGEM3-GC31-LL (r1i1p1f3)	1.25º x 1.875º	2016-2045	2033-2062
HadGEM3-GC31-MM (r1i1p1f3)	0.56° × 0.83°	2020-2049	2035-2064
MIROC6 (r1i1p1f1)	1.41º x 1.41º	2039-2068	2062-2091
MPI-ESM1-2-LR (r11i1p1f1)	1.875º x 1.875º	2034-2063	2055-2084
NorESM2-LM (r1i1p1f1)	1.875º x 2.5º	2042-2071	2063-2092
NorESM2-MM (r1i1p1f1)	0.9º x 1.25º	2040-2069	2062-2091

Figures

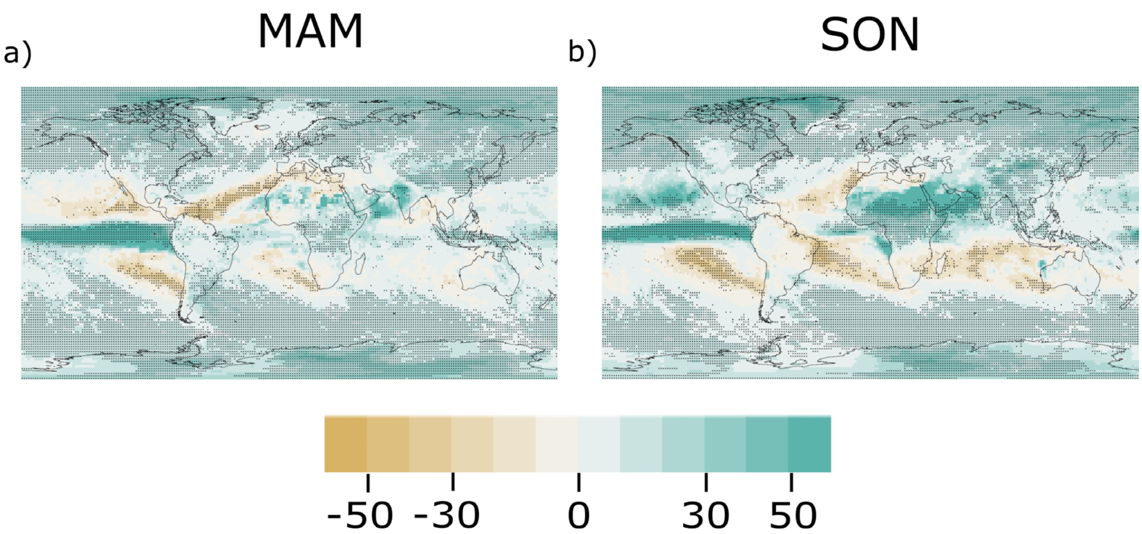

Figure S1: Same as Figure 2, but for a) March-May (MAM) and b) September-November (SON)

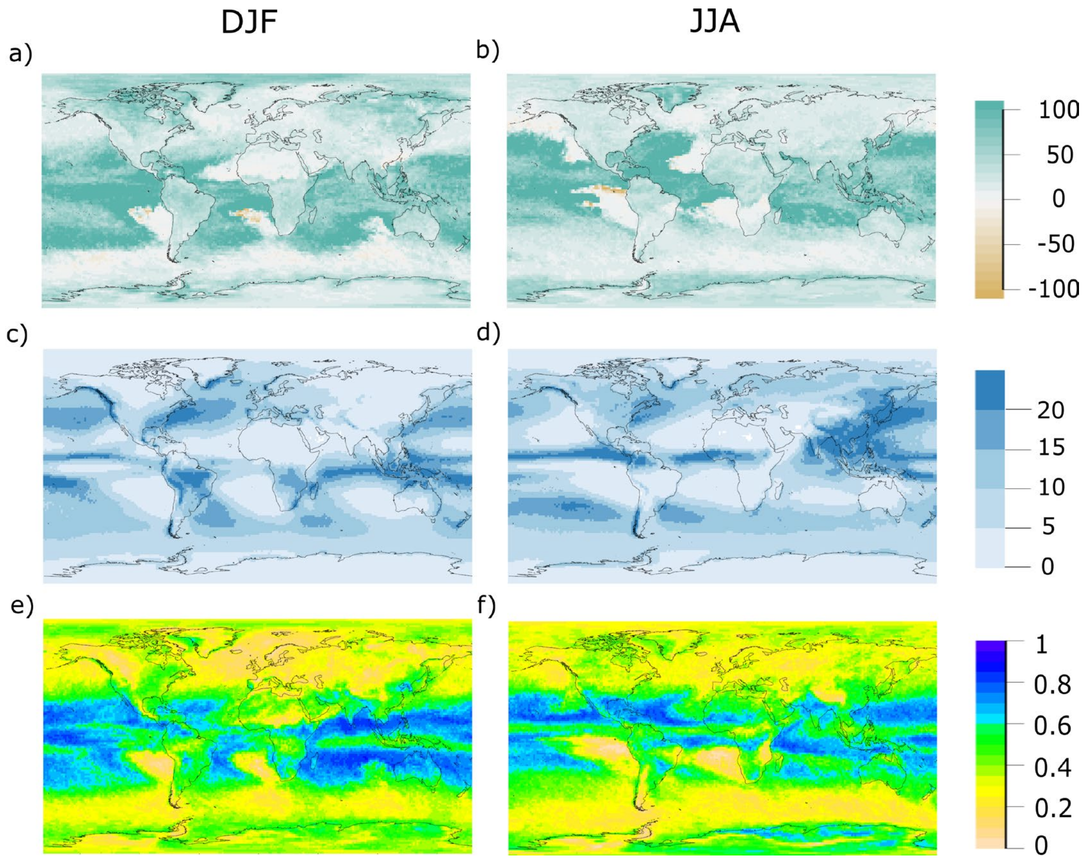

Figure S2: Multimodel average of a) and b) estimated slope, c) and d) estimated intercept, and e) and f) R^2 value, for the fitted regression model that enables to obtain precipitation predictions in terms of values of the product of precipitable water and vertical velocity, for DJF and JJA, respectively

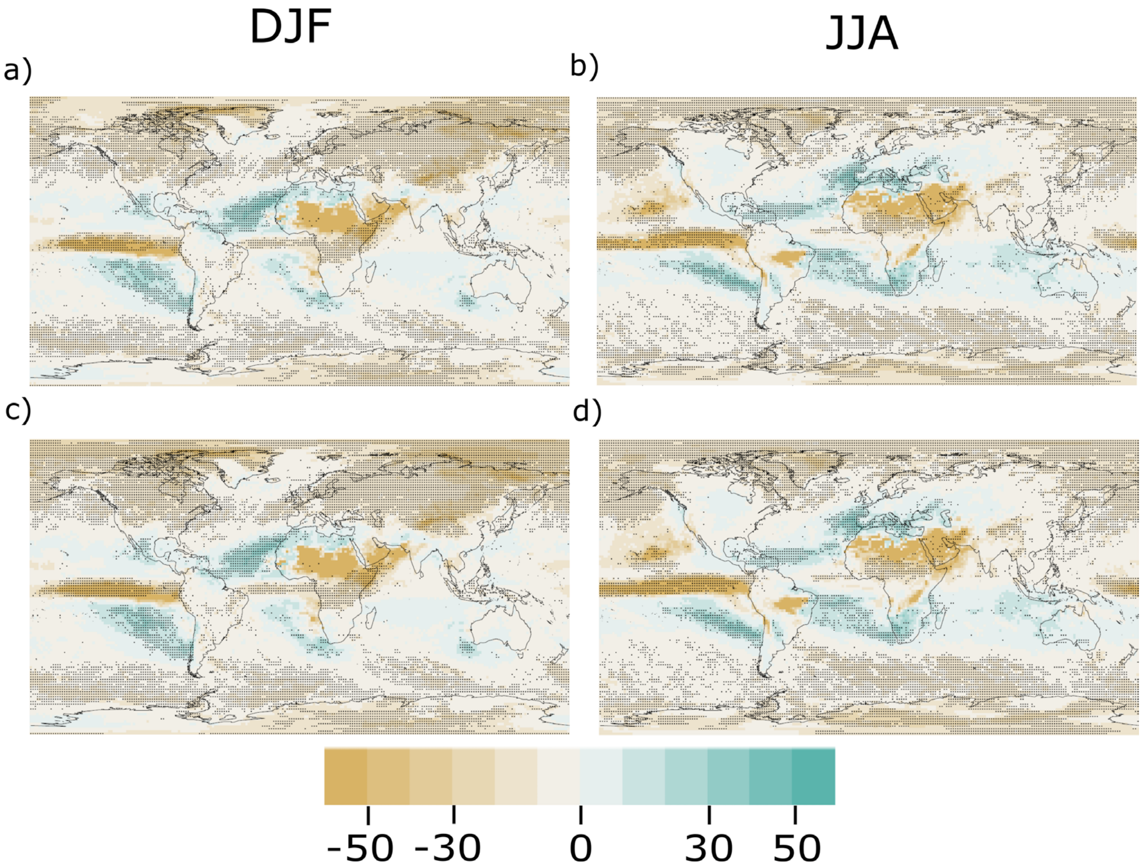

Figure S3: a),b) Multimodel average of the difference between the estimated percentage change in extreme precipitation using the precipitation predictions obtained from the regression model fitted using historical data and the percentage change in extreme precipitation using the CMIP6 model data, for DJF and JJA, respectively. c),d) Same as a) and b) but for the regression model fitted using pooled data of historical and future periods. Stippling refers to model agreement of at least 90% in the sign of the change

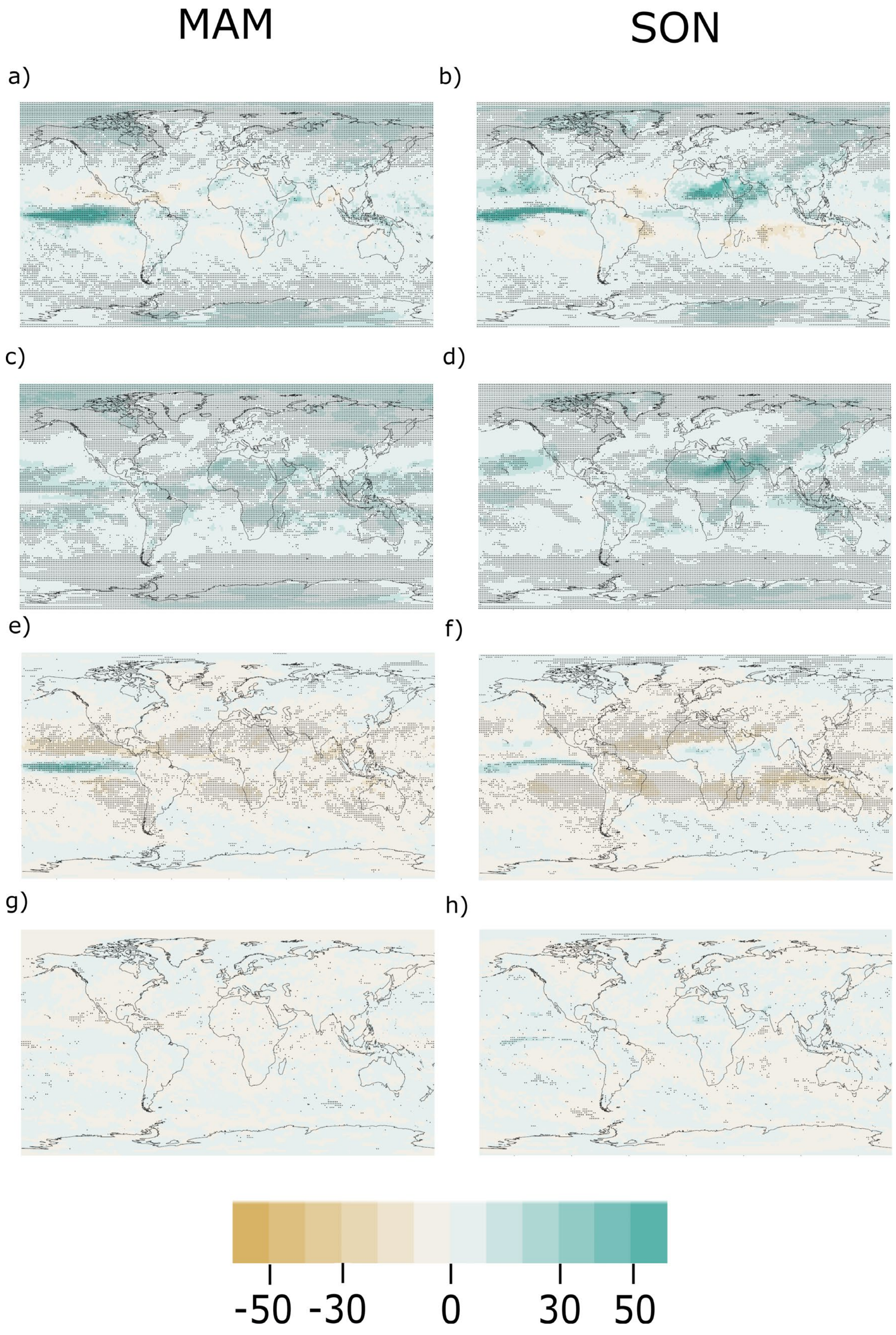
MAM
SON
a)
b)
c)
d)
e)
f)
g)
h)
-50
-30
0
30
50

Figure S4: Same as Figure 4, but for a),c),e),g) March-May (MAM) and b),d),f),h) September-November (SON)

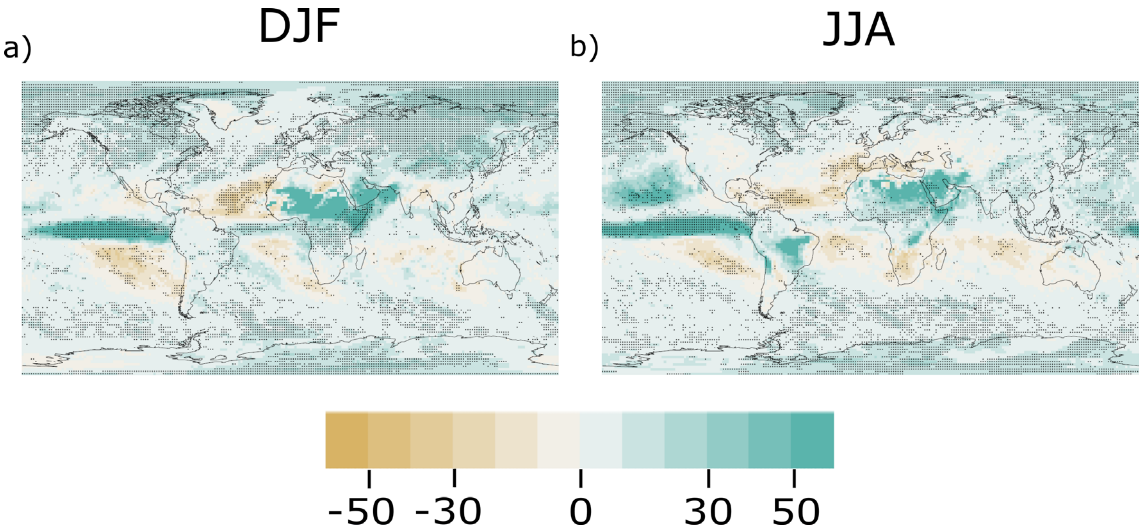

Figure S5: Same as Figure 2, but for the +2°C future period

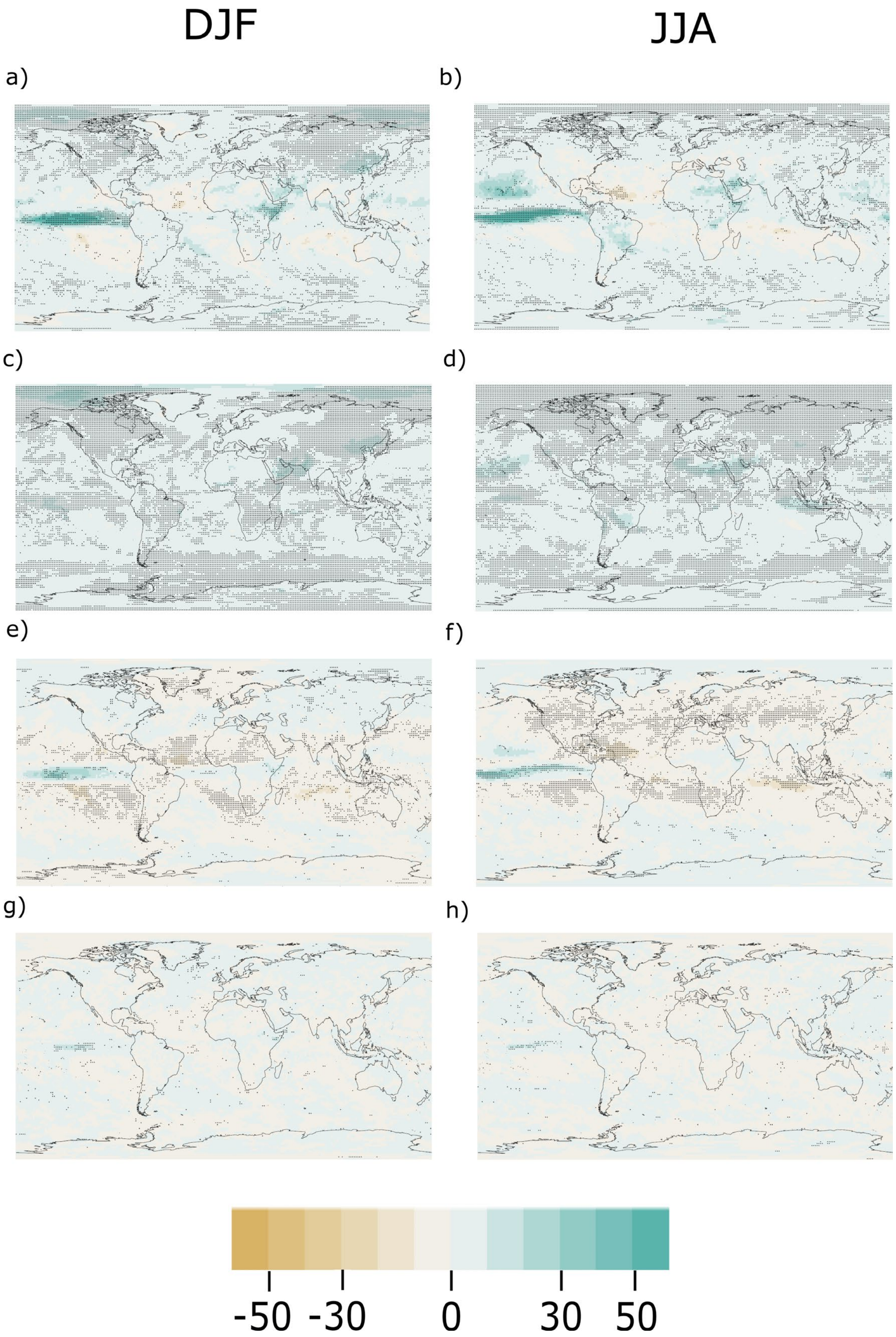
DJF
JJA
a)
b)
c)
d)
e)
f)
g)
h)
-50 -30 0 30 50

Figure S6: Same as Figure 4, but for the +2°C future period

Earth's Future

Supporting Information for

Assessment of the global relationship of different types of droughts in model simulations under high anthropogenic emissions

Luis Gimeno-Sotelo[1], Ahmed El Kenawy[2], Magí Franquesa[2], Iván Noguera[2], Beatriz Fernández-Duque[2], Fernando Domínguez-Castro[2], Dhais Peña-Angulo[3], Fergus Reig[2], Rogert Sorí[1], Luis Gimeno[1], Raquel Nieto[1], Sergio M. Vicente-Serrano[2]

[1]Centro de Investigación Mariña, Universidade de Vigo, Environmental Physics Laboratory (EPhysLab), Ourense, Spain,[2]Instituto Pirenaico de Ecología, Consejo Superior de Investigaciones Científicas (IPE–CSIC), Zaragoza, Spain,[3]Department of Geography, University of Zaragoza, Zaragoza, Spain

Contents of this file

Figures S1 to S10
Table S1

Introduction

This is a supplementary file that includes all figures and tables that complement the information provided in the manuscript.

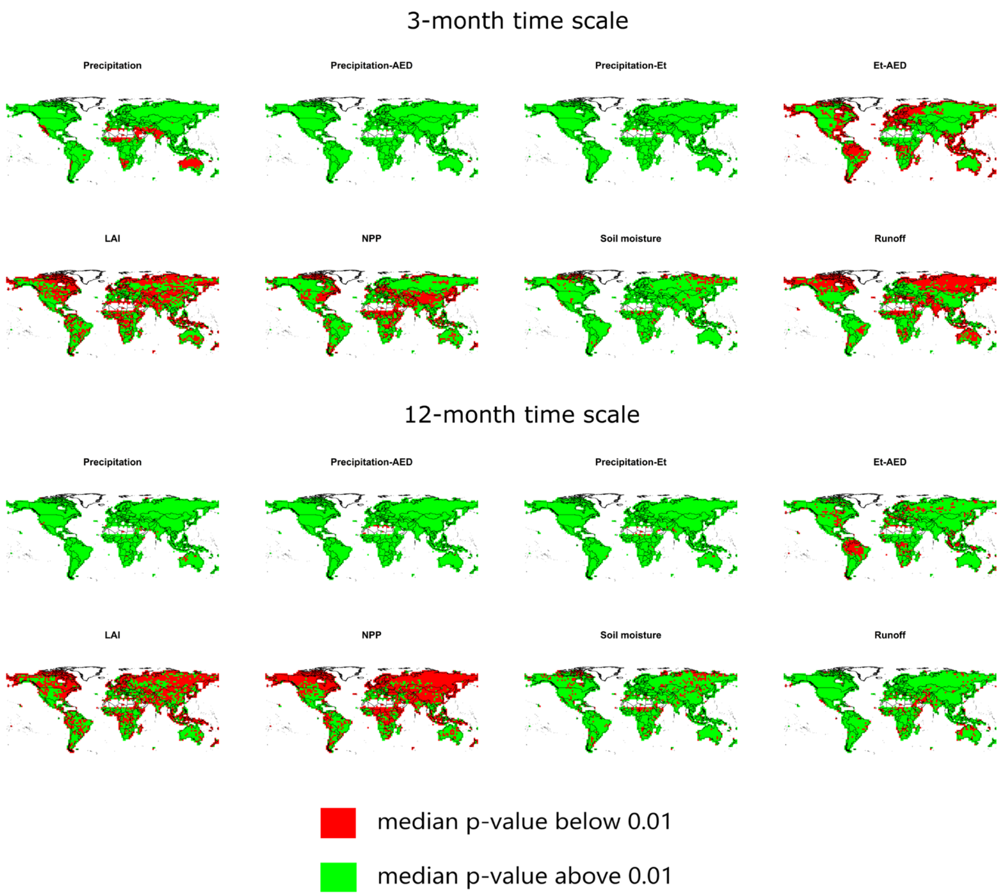

Figure S1. Multimodel median p-value of the Kolmogorov-Smirnov test used for assessing the normality of the index obtained by standardizing the studied variables by means of the log-logistic distribution (gamma distribution for precipitation)

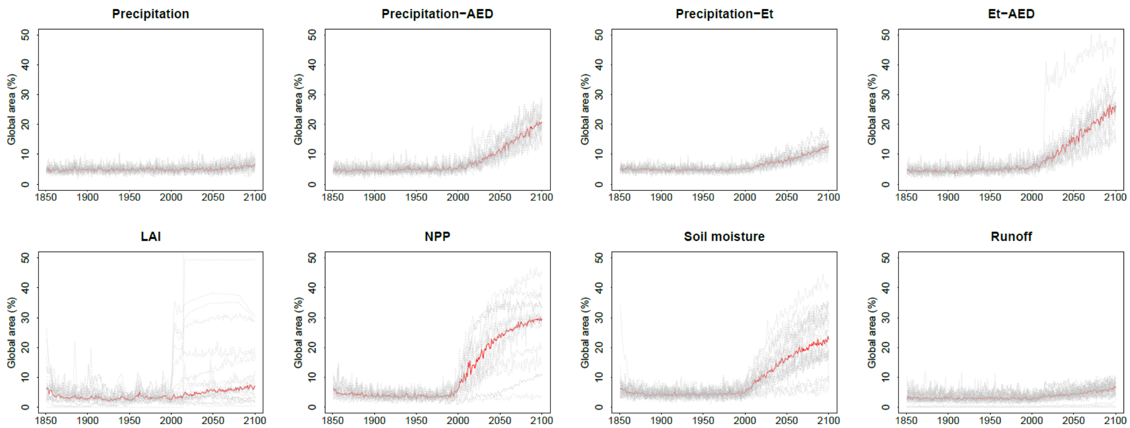

Figure S2. Average percentage of global land area affected by extreme dry conditions. Same as Fig. 2, but for the evolution of the Boreal winter season (DJF)

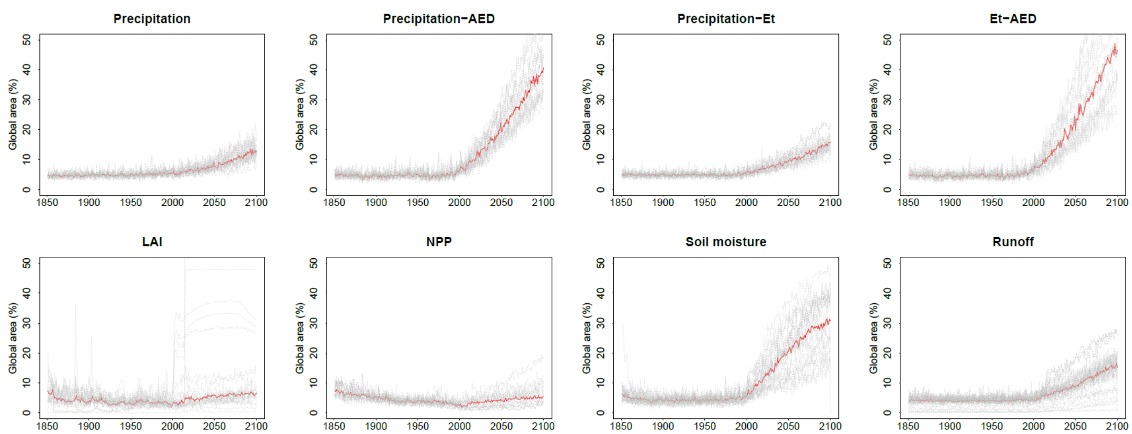

Figure S3. Average percentage of global land area affected by extreme dry conditions. Same as Fig. 2, but for the evolution of the Boreal summer season (JJA)

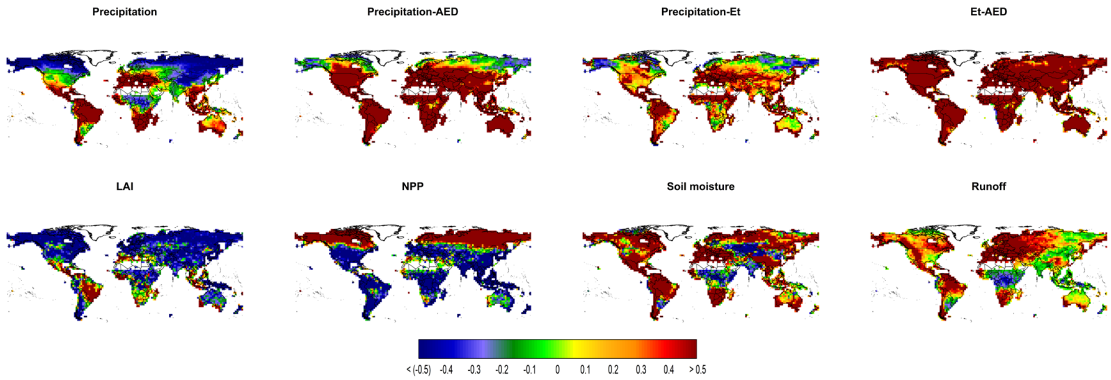

Figure S4. Spatial distribution of the median trend in the duration of drought events between 1850 and 2100 (Factor: 100)

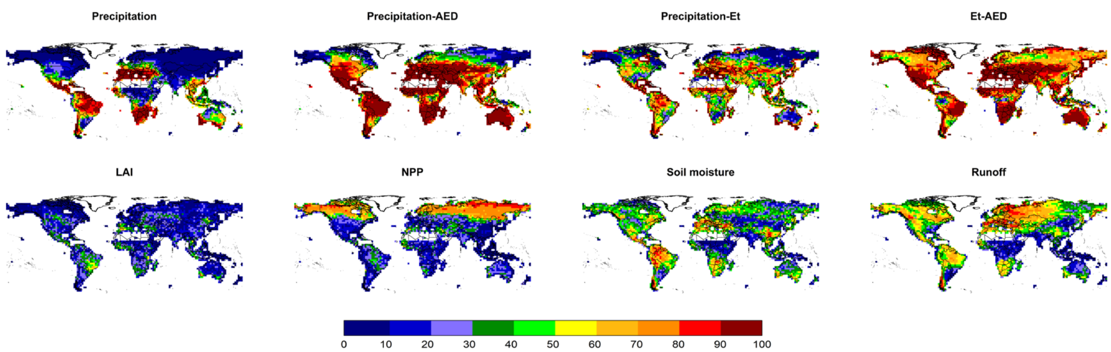

Figure S5. Percentage of models showing positive and statistically significant trends in drought duration from 1850 to 2100

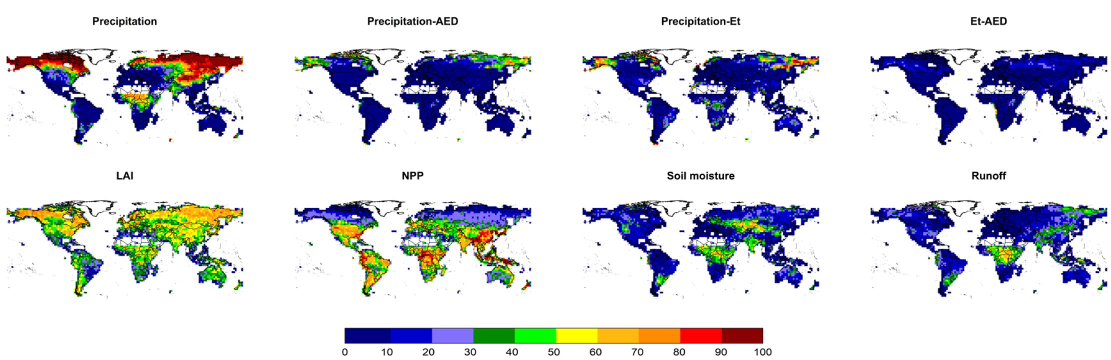

Figure S6. Percentage of models showing negative and statistically significant trends in drought duration from 1850 to 2100

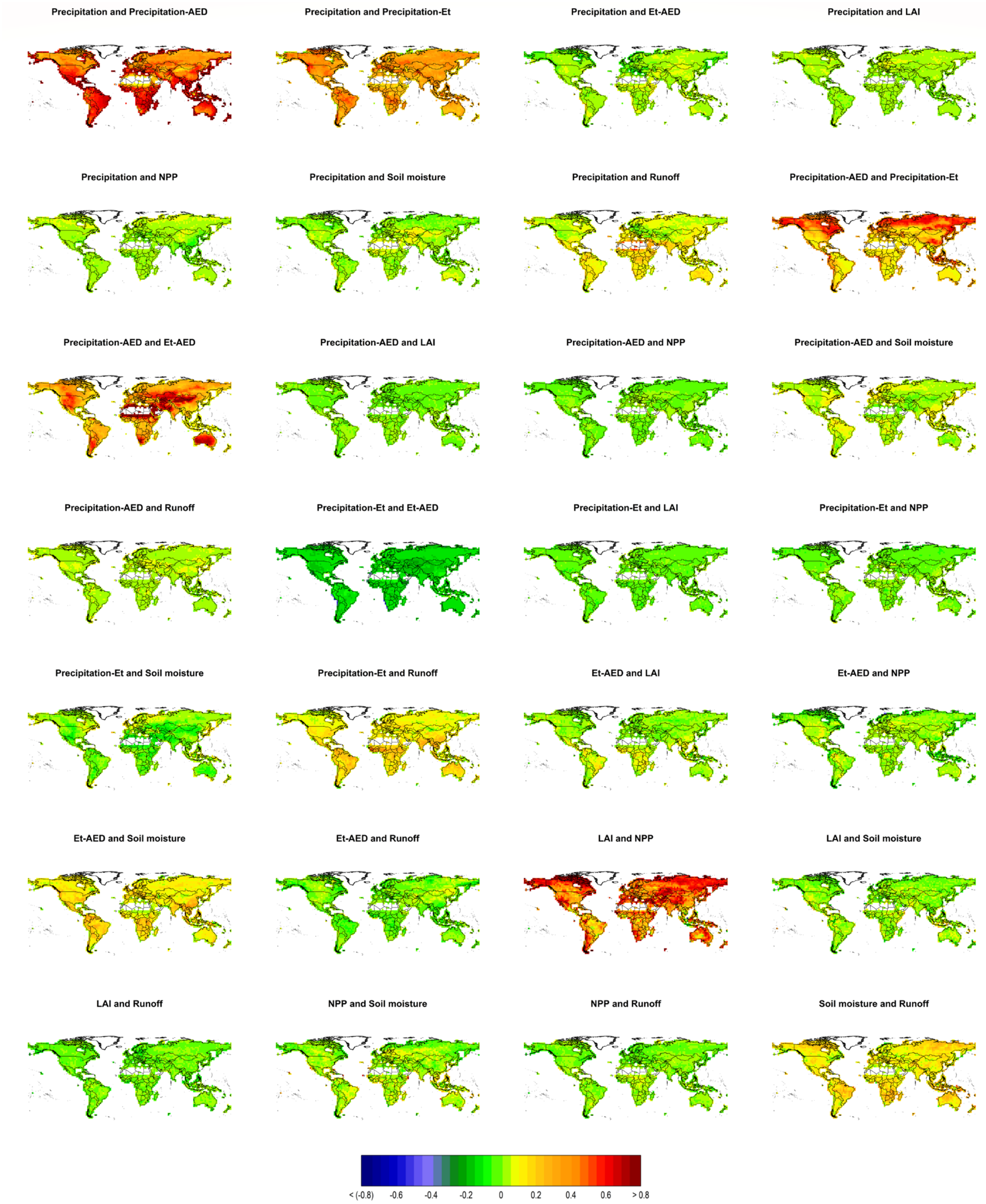

Figure S7. Median Kendall's τ partial correlation in the historical period (1850-2014) among the various metrics for the different models

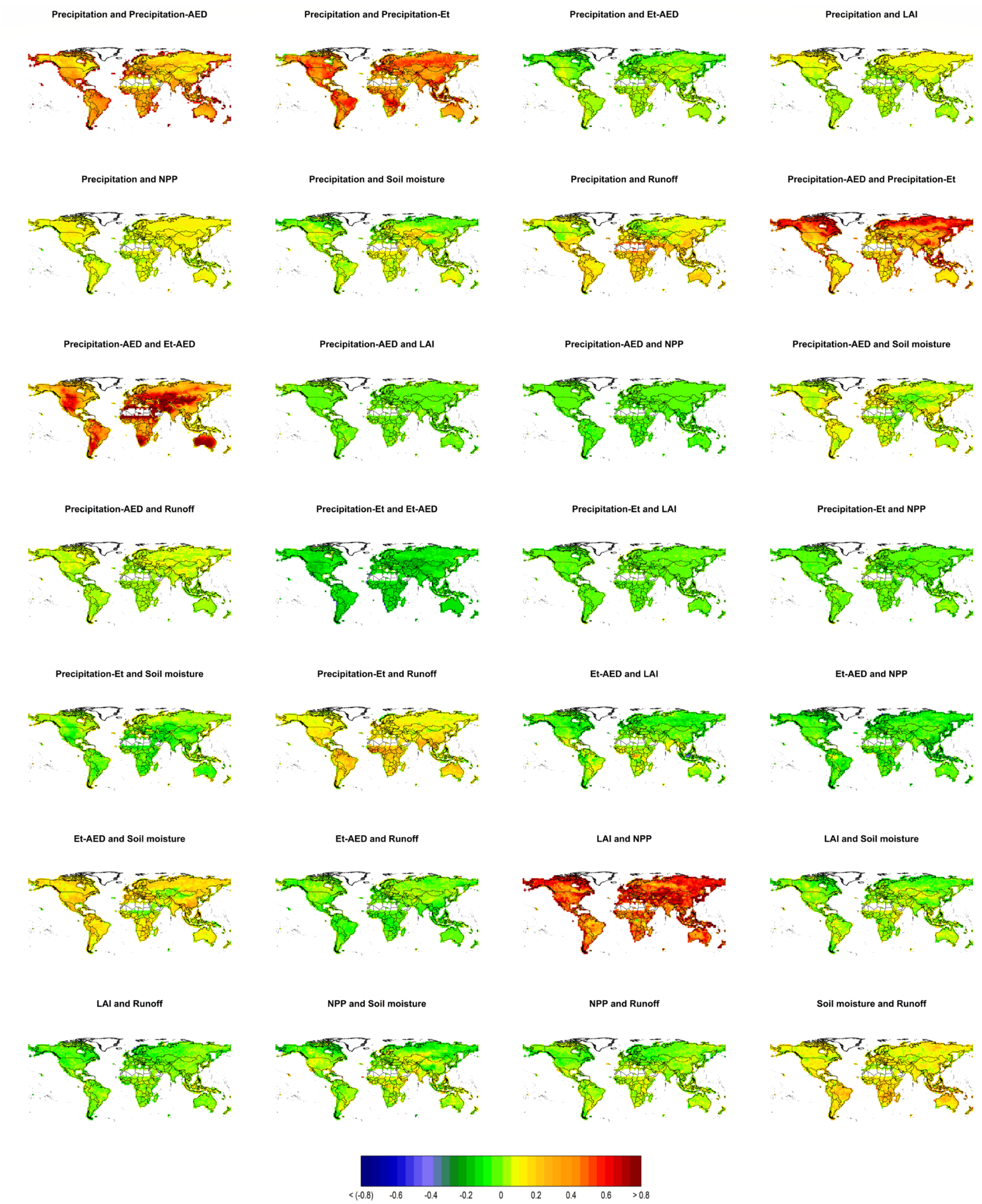

Figure S8. Median Kendall's τ partial correlation in the projected period (2015-2100) among the various metrics for the different models

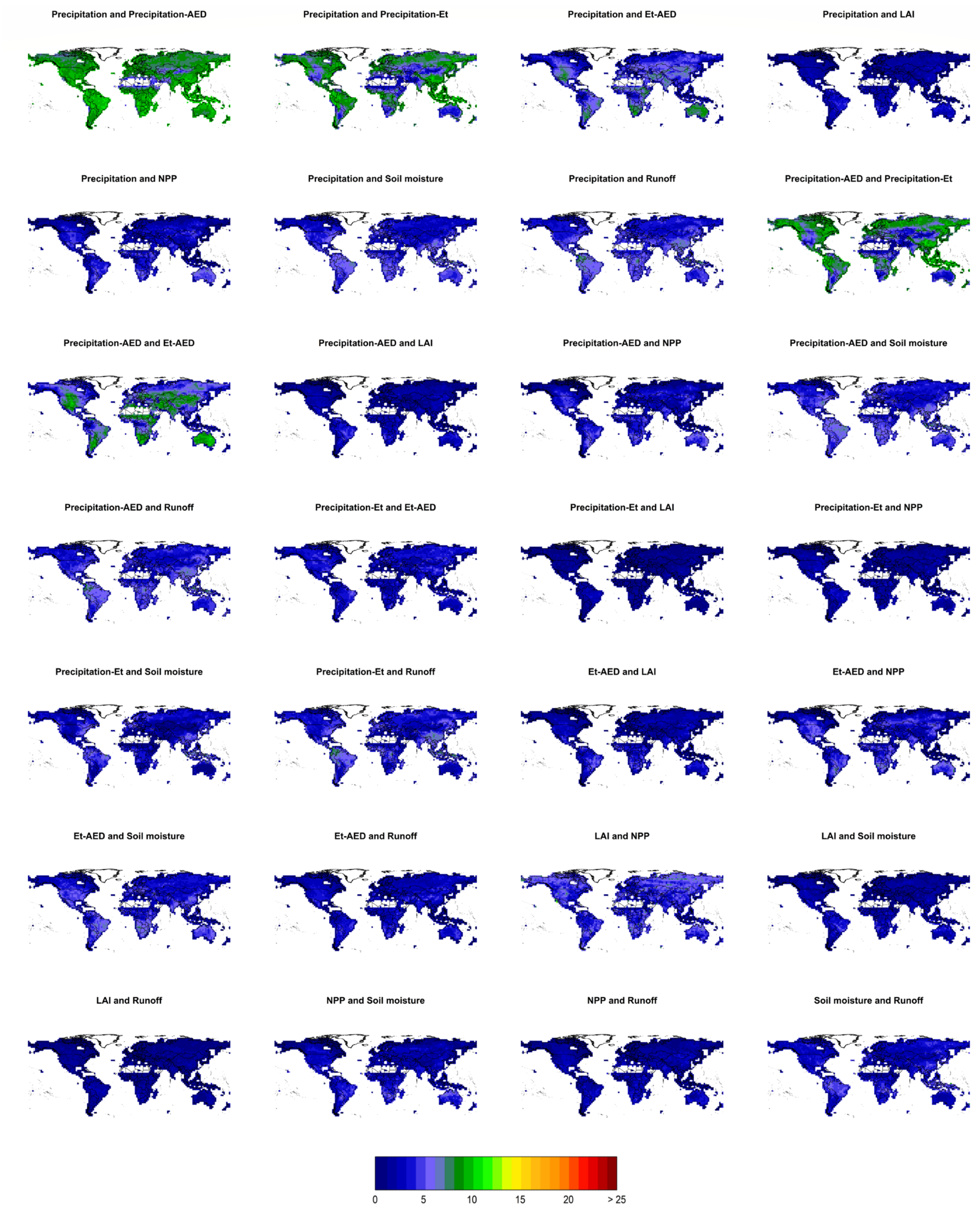

Figure S9. Average percentage of temporal agreement among the various metrics in the historical period (1850-2014) for the different models

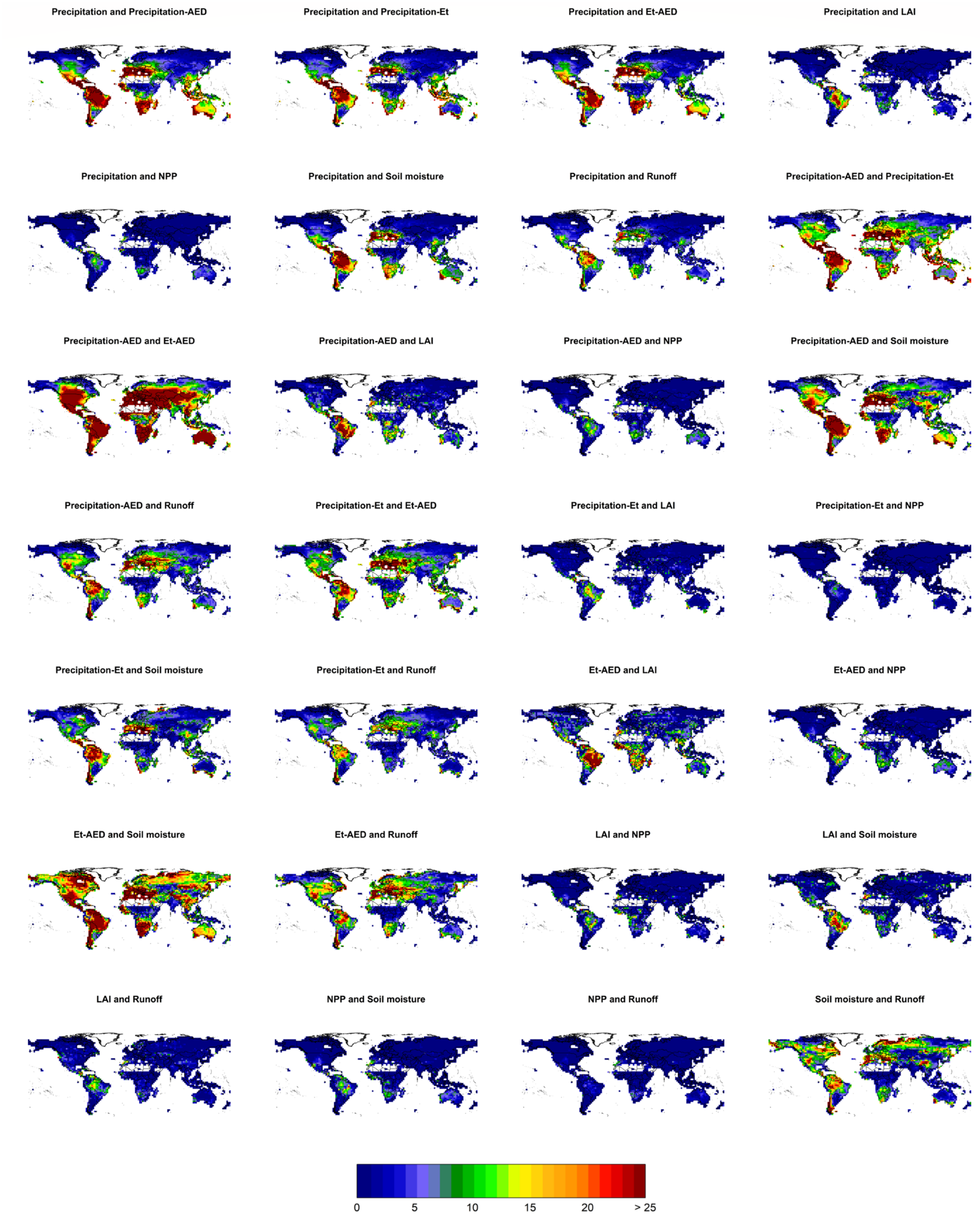

Figure S10. Average percentage of temporal agreement among the various metrics in the projected period (2015-2100) for the different models

MODEL NAME	INSTITUTION	NATIVE SPATIAL RESOLUTION (lon x lat)
ACCESS-CM2	CSIRO-ARCCSS	1.875° x 1.25°
ACCESS-ESM1-5	CSIRO	1.875° x 1.25°
CanESM5-CanOE	CCCma	2.8125° x 2.767272°
CanESM5	CCCma	2.8125° x 2.767272°
CMCC-ESM2	CMCC	1.25° x 0.9424084°
CNRM-CM6-1-HR	CNRM-CERFACS	0.5° x 0.49512°
CNRM-CM6-1	CNRM-CERFACS	1.40625° x 1.38903°
CNRM-ESM2-1	CNRM-CERFACS	1.40625° x 1.38903°
FIO-ESM-2-0	FIO-QLNM	1.25° x 0.9424084°
GFDL-ESM4	NOAA-GFDL	1.25° x 1°
GISS-E2-1-G	NASA-GISS	2.5° x 2°
HadGEM3-GC31-LL	MOHC	1.875° x 1.25°
HadGEM3-GC31-MM	MOHC	0.8333333° x 0.5555556°
INM-CM4-8	INM	2° x 1.5°
IPSL-CM6A-LR	IPSL	2.5° x 1.267606°
MIROC-ES2L	MIROC	2.8125° x 2.767272°
MIROC6	MIROC	1.40625° x 1.38903°
MRI-ESM2-0	MRI	1.125° x 1.11209°

Table S1. CMIP6 models used in this study

Bibliography

Akaike, H. (1974). A new look at the statistical model identification. *IEEE Transactions on Automatic Control*, 19(6), 716-723. https://doi.org/10.1109/TAC.1974.1100705

Algarra, I., Eiras-Barca, J., Nieto, R., & Gimeno, L. (2019). Global climatology of nocturnal low-level jets and associated moisture sources and sinks. *Atmospheric Research*, 229, 39-59. https://doi.org/10.1016/j.atmosres.2019.06.016

Algarra, I., Nieto, R., Ramos, A. M., Eiras-Barca, J., Trigo, R. M., & Gimeno, L. (2020). Significant increase of global anomalous moisture uptake feeding landfalling Atmospheric Rivers. *Nature Communications*, 11(1), 5082. https://doi.org/10.1038/s41467-020-18876-w

Allan, R. P. (2023). Amplified seasonal range in precipitation minus evaporation. *Environmental Research Letters*, 18(9), 094004. https://doi.org/10.1088/1748-9326/acea36

Allan, R. P., Barlow, M., Byrne, M. P., Cherchi, A., Douville, H., Fowler, H. J., ... & Zolina, O. (2020). Advances in understanding large-scale responses of the water cycle to climate change. *Annals of the New York Academy of Sciences*, 1472(1), 49-75. https://doi.org/10.1111/nyas.14337

Amador, J. A. (2008). The intra-Americas sea low-level jet: Overview and future research. *Annals of the New York Academy of Sciences*, 1146(1), 153-188. https://doi.org/10.1196/annals.1446.012

Batibeniz, F., Ashfaq, M., Önol, B., Turuncoglu, U. U., Mehmood, S., & Evans, K. J. (2020). Identification of major moisture sources across the Mediterranean Basin. *Climate Dynamics*, 54, 4109-4127. https://doi.org/10.1007/s00382-020-05224-3

Beck, H. E., Wood, E. F., Pan, M., Fisher, C. K., Miralles, D. G., Van Dijk, A. I., ... & Adler, R. F. (2019). MSWEP V2 global 3-hourly 0.1 precipitation: methodology and quantitative assessment. *Bulletin of the American Meteorological Society*, 100(3), 473-500. https://doi.org/10.1175/BAMS-D-17-0138.1

Beguería, S. (2005). Uncertainties in partial duration series modelling of extremes related to the choice of the threshold value. *Journal of Hydrology*, 303(1-4), 215-230. https://doi.org/10.1016/j.jhydrol.2004.07.015

Beguería, S., Angulo-Martínez, M., Vicente-Serrano, S.M., López-Moreno, J.I. and El-Kenawy, A. (2011). Assessing trends in extreme precipitation events intensity and magnitude using non-stationary peaks-over-threshold analysis: a case study in northeast Spain from 1930 to 2006. *International Journal of Climatology*, 31: 2102-2114. https://doi.org/10.1002/joc.2218

Beirlant, J., Goegebeur, Y., Segers, J., & Teugels, J. L. (2006). *Statistics of extremes: theory and applications*. John Wiley & Sons.

Bell, J. E., Brown, C. L., Conlon, K., Herring, S., Kunkel, K. E., Lawrimore, J., ... & Uejio, C. (2018). Changes in extreme events and the potential impacts on human health. *Journal of the Air & Waste Management Association*, 68(4), 265-287. https://doi.org/10.1080/10962247.2017.1401017

Bevacqua, E., De Michele, C., Manning, C., Couasnon, A., Ribeiro, A. F., Ramos, A. M., ... & Zscheischler, J. (2021). Guidelines for studying diverse types of compound weather and climate events. *Earth's Future*, 9(11), e2021EF002340. https://doi.org/10.1029/2021EF002340

Bevacqua, E., Suarez-Gutierrez, L., Jézéquel, A., Lehner, F., Vrac, M., Yiou, P., & Zscheischler, J. (2023). Advancing research on compound weather and climate events via large ensemble model simulations. *Nature Communications*, 14(1), 2145. https://doi.org/10.1038/s41467-023-37847-5

Brioude, J., Arnold, D., Stohl, A., Cassiani, M., Morton, D., Seibert, P., ... & Wotawa, G. (2013). The Lagrangian particle dispersion model FLEXPART-WRF version 3.1. *Geoscientific Model Development*, 6(6), 1889-1904. https://doi.org/10.5194/gmd-6-1889-2013

Byrne, M. P., & O'Gorman, P. A. (2018). Trends in continental temperature and humidity directly linked to ocean warming. *Proceedings of the National Academy of Sciences*, 115(19), 4863-4868. https://doi.org/10.1073/pnas.1722312115

Casella, G., & Berger, R. (2024). *Statistical inference*. CRC Press.

Cheng, T. F., & Lu, M. (2023). Global Lagrangian tracking of continental precipitation recycling, footprints, and cascades. *Journal of Climate*, 36(6), 1923-1941. https://doi.org/10.1175/JCLI-D-22-0185.1

Coles, S. (2001). *An introduction to statistical modeling of extreme values*. Springer, London.

Crausbay, S. D., Ramirez, A. R., Carter, S. L., Cross, M. S., Hall, K. R., Bathke, D. J., ... & Sanford, T. (2017). Defining ecological drought for the twenty-first century. *Bulletin of the American Meteorological Society*, 98(12), 2543-2550. https://doi.org/10.1175/BAMS-D-16-0292.1

Czado, C. (2019). *Analyzing dependent data with vine copulas*. Lecture Notes in Statistics, Springer, 222.

Danabasoglu, G., Lamarque, J. F., Bacmeister, J., Bailey, D. A., DuVivier, A. K., Edwards, J., ... & Strand, W. G. (2020). The community Earth system model version 2 (CESM2). *Journal of Advances in Modeling Earth Systems*, 12(2), e2019MS001916. https://doi.org/10.1029/2019MS001916

Dee, D. P., Uppala, S. M., Simmons, A. J., Berrisford, P., Poli, P., Kobayashi, S., ... & Vitart, F. (2011). The ERA-Interim reanalysis: Configuration and performance of the data assimilation system. *Quarterly Journal of the Royal Meteorological Society*, 137(656), 553-597. https://doi.org/10.1002/qj.828

Douville, H., Raghavan, K., Renwick, J., Allan, R. P., Arias, P. A., Barlow, M., Cerezo-Mota, R., Cherchi, A., Gan, T. Y., Gergis, J., Jiang, D., Khan, A., Pokam Mba, W., Rosenfeld, D., Tierney, J., & Zolina, O. (2021). Water Cycle Changes. In V. Masson-Delmotte, P. Zhai, A. Pirani, S. L. Connors, C. Péan, S. Berger, N. Caud, Y. Chen, L. Goldfarb, M. I. Gomis, M. Huang, K. Leitzell, E. Lonnoy, J. B. R. Matthews, T. K. Maycock, T. Waterfield, O. Yelekçi, R. Yu, & B. Zhou (Eds.), *Climate Change 2021: The Physical Science Basis. Contribution of Working Group I to the Sixth Assessment Report of the Intergovernmental Panel on Climate Change* (pp. 1055–1210). Cambridge University Press. https://doi.org/10.1017/9781009157896.010

Drumond, A., Stojanovic, M., Nieto, R., Vicente-Serrano, S. M., & Gimeno, L. (2019). Linking anomalous moisture transport and drought episodes in the IPCC reference regions. *Bulletin of the American Meteorological Society*, 100(8), 1481-1498. https://doi.org/10.1175/BAMS-D-18-0111.1

Durán-Quesada, A. M., Reboita, M., & Gimeno, L. (2012). Precipitation in tropical America and the associated sources of moisture: a short review. *Hydrological Sciences Journal*, 57(4), 612-624. https://doi.org/10.1080/02626667.2012.673723

Eiras-Barca, J., Algarra, I., Nieto, R., Schröder, M., Hegglin, M. I., & Gimeno, L. (2022). Analysis of the main source regions of moisture transport events with the new ESA

CCI/CM-SAF total column water vapour climate data record (v2). *Quarterly Journal of the Royal Meteorological Society*, 148(748), 3272-3286. https://doi.org/10.1002/qj.4358

Emori, S., & Brown, S. J. (2005). Dynamic and thermodynamic changes in mean and extreme precipitation under changed climate. *Geophysical Research Letters*, 32(17). https://doi.org/10.1029/2005GL023272

Eyring, V., Bony, S., Meehl, G. A., Senior, C. A., Stevens, B., Stouffer, R. J., & Taylor, K. E. (2016). Overview of the Coupled Model Intercomparison Project Phase 6 (CMIP6) experimental design and organization. *Geoscientific Model Development*, 9(5), 1937-1958. https://doi.org/10.5194/gmd-9-1937-2016

Fernández-Alvarez, J. C., Pérez-Alarcón, A., Eiras-Barca, J., Rahimi, S., Nieto, R., & Gimeno, L. (2023a). Projected changes in atmospheric moisture transport contributions associated with climate warming in the North Atlantic. *Nature Communications*, 14(1), 6476. https://doi.org/10.1038/s41467-023-41915-1

Fernández-Alvarez, J. C., Pérez-Alarcón, A., Eiras-Barca, J., Ramos, A. M., Rahimi-Esfarjani, S., Nieto, R., & Gimeno, L. (2023b). Changes in Moisture Sources of Atmospheric Rivers Landfalling the Iberian Peninsula With WRF-FLEXPART. *Journal of Geophysical Research: Atmospheres*, 128(8), e2022JD037612. https://doi.org/10.1029/2022JD037612

Fernández-Alvarez, J. C., Vázquez, M., Pérez-Alarcón, A., Nieto, R., & Gimeno, L. (2023c). Comparison of moisture sources and sinks estimated with different versions of

FLEXPART and FLEXPART-WRF models forced with ECMWF reanalysis data. *Journal of Hydrometeorology*, 24(2), 221-239. https://doi.org/10.1175/JHM-D-22-0018.1

Fleig, A. K., Tallaksen, L. M., Hisdal, H., & Demuth, S. (2006). A global evaluation of streamflow drought characteristics. *Hydrology and Earth System Sciences*, 10(4), 535-552. https://doi.org/10.5194/hess-10-535-2006

Gao, S., Liu, P., & Lall, U. (2021). Seasonal precipitation predictability for the Northern Hemisphere using concurrent and preseason atmospheric water vapor transport and sea surface temperature. *Journal of Hydrometeorology*, 22(1), 183-199. https://doi.org/10.1175/JHM-D-20-0107.1

Genest, C., Rémillard, B., & Beaudoin, D. (2009). Goodness-of-fit tests for copulas: A review and a power study. *Insurance: Mathematics and economics*, 44(2), 199-213. https://doi.org/10.1016/j.insmatheco.2007.10.005

Gimeno, L., Algarra, I., Eiras-Barca, J., Ramos, A. M., & Nieto, R. (2021a). Atmospheric river, a term encompassing different meteorological patterns. *WIREs Water*, 8(6), e1558. https://doi.org/10.1002/wat2.1558

Gimeno, L., Dominguez, F., Nieto, R., Trigo, R., Drumond, A., Reason, C. J., ... & Marengo, J. (2016). Major mechanisms of atmospheric moisture transport and their role in extreme precipitation events. *Annual Review of Environment and Resources*, 41, 117-141. https://doi.org/10.1146/annurev-environ-110615-085558

Gimeno, L., Drumond, A., Nieto, R., Trigo, R. M., & Stohl, A. (2010a). On the origin of continental precipitation. *Geophysical Research Letters*, 37, L13804. https://doi.org/10.1029/2010GL043712

Gimeno, L., Eiras-Barca, J., Durán-Quesada, A. M., Dominguez, F., van der Ent, R., Sodemann, H., ... & Kirchner, J. W. (2021b). The residence time of water vapour in the atmosphere. *Nature Reviews Earth & Environment*, 2(8), 558-569. https://doi.org/10.1038/s43017-021-00181-9

Gimeno, L., Nieto, R., & Sorí, R. (2020a). The growing importance of oceanic moisture sources for continental precipitation. *Npj Climate and Atmospheric Science*, 3(1), 27. https://doi.org/10.1038/s41612-020-00133-y

Gimeno, L., Nieto, R., Trigo, R. M., Vicente-Serrano, S. M., & López-Moreno, J. I. (2010b). Where does the Iberian Peninsula moisture come from? An answer based on a Lagrangian approach. *Journal of Hydrometeorology*, 11(2), 421-436. https://doi.org/10.1175/2009JHM1182.1

Gimeno, L., Nieto, R., Vázquez, M., & Lavers, D. A. (2014). Atmospheric rivers: A mini-review. *Frontiers in Earth Science*, 2, 2. https://doi.org/10.3389/feart.2014.00002

Gimeno, L., Sorí, R., Vázquez, M., Stojanovic, M., Algarra, I., Eiras-Barca, J., Gimeno-Sotelo, L., & Nieto, R. (2022). Extreme precipitation events. *WIREs Water*, 9(6), e1611. https://doi.org/10.1002/wat2.1611

Gimeno, L., Stohl, A., Trigo, R. M., Dominguez, F., Yoshimura, K., Yu, L., ... & Nieto, R. (2012). Oceanic and terrestrial sources of continental precipitation. *Reviews of Geophysics*, 50(4). https://doi.org/10.1029/2012RG000389

Gimeno, L., Vázquez, M., Eiras-Barca, J., Sorí, R., Stojanovic, M., Algarra, I., ... & Dominguez, F. (2020b). Recent progress on the sources of continental precipitation as revealed by moisture transport analysis. *Earth-Science Reviews*, 201, 103070. https://doi.org/10.1016/j.earscirev.2019.103070

Gimeno-Sotelo, L., Bevacqua, E., Fernández-Alvarez, J. C., Barriopedro, D., Zscheischler, J., & Gimeno, L. (2024a). Projected changes in extreme daily precipitation linked to changes in precipitable water and vertical velocity in CMIP6 models. *Atmospheric Research*, 304. https://doi.org/10.1016/j.atmosres.2024.107413

Gimeno-Sotelo, L., Bevacqua, E., & Gimeno, L. (2023). Combinations of drivers that most favor the occurrence of daily precipitation extremes. *Atmospheric Research*, 294, 106959. https://doi.org/10.1016/j.atmosres.2023.106959

Gimeno-Sotelo, L., & Gimeno, L. (2022). Concurrent extreme events of atmospheric moisture transport and continental precipitation: The role of landfalling atmospheric rivers. *Atmospheric Research*, 278, 106356. https://doi.org/10.1016/j.atmosres.2022.106356

Gimeno-Sotelo, L., & Gimeno, L. (2023). Where does the link between atmospheric moisture transport and extreme precipitation matter?. *Weather and Climate Extremes*, 39, 100536. https://doi.org/10.1016/j.wace.2022.100536

Gimeno-Sotelo, L., El Kenawy, A., Franquesa, M., Noguera, I., Fernández-Duque, B., Domínguez-Castro, F., Peña-Angulo, D., Reig, F., Sorí, R., Gimeno, L., Nieto, R. & Vicente-Serrano, S. M. (2024b). Assessment of the global relationship of different types of droughts in model simulations under high anthropogenic emissions. *Earth's Future*, 12, e2023EF003629. https://doi.org/10.1029/2023EF003629

Gimeno-Sotelo, L., Fernández-Alvarez, J. C., Nieto, R., Vicente-Serrano, S. M., & Gimeno, L. (2024c). The increasing influence of atmospheric moisture transport on hydrometeorological extremes in the Euromediterranean region with global warming. Submitted.

Gimeno-Sotelo, L., Sorí, R., Nieto, R., Vicente-Serrano, S. M., & Gimeno, L. (2024d). Unravelling the origin of the atmospheric moisture deficit that leads to droughts. *Nature Water*, 2, 242-253. https://doi.org/10.1038/s44221-023-00192-4

Gimeno-Sotelo, L., Stojanovic, M., Sorí, R., Nieto, R., Vicente-Serrano, S. M., & Gimeno, L. (2024e). Nexus between the deficit in moisture transport and drought occurrence in regions with projected drought trends. *Environmental Research Letters*, 19, 074035. https://doi.org/10.1088/1748-9326/ad560b

Guan, B., & Waliser, D. E. (2015). Detection of atmospheric rivers: Evaluation and application of an algorithm for global studies. *Journal of Geophysical Research: Atmospheres*, 120(24), 12514-12535. https://doi.org/10.1002/2015JD024257

Gvoždíková, B., & Müller, M. (2021). Predictability of moisture flux anomalies indicating central European extreme precipitation events. *Quarterly Journal of the Royal Meteorological Society*, 147(739), 3335-3348. https://doi.org/10.1002/qj.4131

Hausfather, Z., & Peters, G. P. (2020). Emissions – the 'business as usual' story is misleading. *Nature*, 577, 618–620. https://doi.org/10.1038/d41586-020-00177-3

Held, I. M., & Soden, B. J. (2006). Robust responses of the hydrological cycle to global warming. *Journal of Climate*, 19(21), 5686-5699. https://doi.org/10.1175/JCLI3990.1

Helfand, H. M., & Schubert, S. D. (1995). Climatology of the simulated Great Plains low-level jet and its contribution to the continental moisture budget of the United States. *Journal of Climate*, 8(4), 784-806. https://doi.org/10.1175/1520-0442(1995)008<0784:COTSGP>2.0.CO;2

Hersbach, H., Bell, B., Berrisford, P., Hirahara, S., Horányi, A., Muñoz-Sabater, J., ... & Thépaut, J. N. (2020). The ERA5 global reanalysis. *Quarterly Journal of the Royal Meteorological Society*, 146(730), 1999-2049. https://doi.org/10.1002/qj.3803

Huang, W., & Prokhorov, A. (2014). A goodness-of-fit test for copulas. *Econometric Reviews*, 33(7), 751-771. https://doi.org/10.1080/07474938.2012.690692

Hurrell, J. W. (1995). Decadal trends in the North Atlantic Oscillation: Regional temperatures and precipitation. *Science*, 269(5224), 676-679. https://doi.org/10.1126/science.269.5224.676

IPCC (2021). *Climate Change 2021: The Physical Science Basis. Contribution of Working Group I to the Sixth Assessment Report of the Intergovernmental Panel on Climate Change*[Masson-Delmotte, V., Zhai, P., Pirani, A., Connors, S.L., Péan, C., Berger, S., Caud, N., Chen, Y., Goldfarb, L., Gomis, M.I., Huang, M., Leitzell, K., Lonnoy, E., Matthews, J.B.R., Maycock, T.K., Waterfield, T., Yelekçi, O., Yu, R., and Zhou, B. (eds.)]. Cambridge University Press, Cambridge, United Kingdom and New York, NY, USA.

Jahn, M. (2015). Economics of extreme weather events: Terminology and regional impact models. *Weather and Climate Extremes*, 10, 29-39. https://doi.org/10.1016/j.wace.2015.08.005

Joe, H. (2014). *Dependence modeling with copulas*. CRC press.

John, A., Douville, H., Ribes, A., & Yiou, P. (2022). Quantifying CMIP6 model uncertainties in extreme precipitation projections. *Weather and Climate Extremes*, 36, 100435. https://doi.org/10.1016/j.wace.2022.100435

Jones, C. (2019). Recent changes in the South America low-level jet. *Npj Climate and Atmospheric Science*, 2(1), 20. https://doi.org/10.1038/s41612-019-0077-5

Khouakhi, A., Villarini, G., & Vecchi, G. A. (2017). Contribution of tropical cyclones to rainfall at the global scale. *Journal of Climate*, 30(1), 359-372. https://doi.org/10.1175/JCLI-D-16-0298.1

Kim, S., Sharma, A., Wasko, C., & Nathan, R. (2022). Linking total precipitable water to precipitation extremes globally. *Earth's Future*, 10(2), e2021EF002473. https://doi.org/10.1029/2021EF002473

Kunkel, K. E., Stevens, S. E., Stevens, L. E., & Karl, T. R. (2020). Observed climatological relationships of extreme daily precipitation events with precipitable water and vertical velocity in the contiguous United States. *Geophysical Research Letters*, 47(12), e2019GL086721. https://doi.org/10.1029/2019GL086721

Lavers, D. A., Pappenberger, F., & Zsoter, E. (2014). Extending medium-range predictability of extreme hydrological events in Europe. *Nature Communications*, 5(1), 5382. https://doi.org/10.1038/ncomms6382

Lavers, D. A., Simmons, A., Vamborg, F., & Rodwell, M. J. (2022). An evaluation of ERA5 precipitation for climate monitoring. *Quarterly Journal of the Royal Meteorological Society*, 148(748), 3152-3165. https://doi.org/10.1002/qj.4351

Lavers, D. A., & Villarini, G. (2013). The nexus between atmospheric rivers and extreme precipitation across Europe. *Geophysical Research Letters*, 40(12), 3259-3264. https://doi.org/10.1002/grl.50636

Lavers, D. A., & Villarini, G. (2015). The contribution of atmospheric rivers to precipitation in Europe and the United States. *Journal of Hydrology*, 522, 382-390. https://doi.org/10.1016/j.jhydrol.2014.12.010

Lavers, D. A., Waliser, D. E., Ralph, F. M., & Dettinger, M. D. (2016). Predictability of horizontal water vapor transport relative to precipitation: Enhancing situational awareness for forecasting western US extreme precipitation and flooding. *Geophysical Research Letters*, 43(5), 2275-2282. https://doi.org/10.1002/2016GL067765

Li, C., Zwiers, F., Zhang, X., & Li, G. (2019). How much information is required to well constrain local estimates of future precipitation extremes?. *Earth's Future*, 7(1), 11-24. https://doi.org/10.1029/2018EF001001

Lloyd-Hughes, B. (2014). The impracticality of a universal drought definition. *Theoretical and Applied Climatology*, 117, 607-611. https://doi.org/10.1007/s00704-013-1025-7

Lorente-Plazas, R., Montavez, J. P., Ramos, A. M., Jerez, S., Trigo, R. M., & Jimenez-Guerrero, P. (2020). Unusual atmospheric-river-like structures coming from Africa induce extreme precipitation over the western Mediterranean Sea. *Journal of Geophysical*

Research: Atmospheres, 125(2), e2019JD031280. https://doi.org/10.1029/2019JD031280

Marengo, J. A., Soares, W. R., Saulo, C., & Nicolini, M. (2004). Climatology of the low-level jet east of the Andes as derived from the NCEP–NCAR reanalyses: Characteristics and temporal variability. *Journal of Climate*, 17(12), 2261-2280. https://doi.org/10.1175/1520-0442(2004)017<2261:COTLJE>2.0.CO;2

McClenny, E. E., Ullrich, P. A., & Grotjahn, R. (2020). Sensitivity of atmospheric river vapor transport and precipitation to uniform sea surface temperature increases. *Journal of Geophysical Research: Atmospheres*, 125(21), e2020JD033421. https://doi.org/10.1029/2020JD033421

McKee, T. B., Doesken, N. J., & Kleist, J. (1993, January). The relationship of drought frequency and duration to time scales. In *Proceedings of the 8th Conference on Applied Climatology* (Vol. 17, No. 22, pp. 179-183).

Miralles, D. G., Nieto, R., McDowell, N. G., Dorigo, W. A., Verhoest, N. E., Liu, Y. Y., ... & Gimeno, L. (2016). Contribution of water-limited ecoregions to their own supply of rainfall. *Environmental Research Letters*, 11(12), 124007. https://doi.org/10.1088/1748-9326/11/12/124007

Naveau, P., Huser, R., Ribereau, P., & Hannart, A. (2016). Modeling jointly low, moderate, and heavy rainfall intensities without a threshold selection. *Water Resources Research*, 52(4), 2753-2769. https://doi.org/10.1002/2015WR018552

Nelsen, R. B. (2006). *An introduction to copulas*. Springer.

Nieto, R., Gallego, D., Trigo, R., Ribera, P., & Gimeno, L. (2008). Dynamic identification of moisture sources in the Orinoco basin in equatorial South America. *Hydrological Sciences Journal*, 53(3), 602-617. https://doi.org/10.1623/hysj.53.3.602

Nieto, R., & Gimeno, L. (2021). Addendum: A database of optimal integration times for Lagrangian studies of atmospheric moisture sources and sinks. *Scientific Data*, 8(1), 130. https://doi.org/10.1038/s41597-021-00902-1

Nogueira, M. (2020). Inter-comparison of ERA-5, ERA-interim and GPCP rainfall over the last 40 years: Process-based analysis of systematic and random differences. *Journal of Hydrology*, 583, 124632. https://doi.org/10.1016/j.jhydrol.2020.124632

O'Brien, T. A., Wehner, M. F., Payne, A. E., Shields, C. A., Rutz, J. J., Leung, L. R., ... & Zhou, Y. (2022). Increases in future AR count and size: Overview of the ARTMIP Tier 2 CMIP5/6 experiment. *Journal of Geophysical Research: Atmospheres*, 127(6), e2021JD036013. https://doi.org/10.1029/2021JD036013

O'Gorman, P. A., & Schneider, T. (2009). The physical basis for increases in precipitation extremes in simulations of 21st-century climate change. *Proceedings of the National Academy of Sciences*, 106(35), 14773-14777. https://doi.org/10.1073/pnas.0907610106

O'Neill, B. C., Tebaldi, C., Van Vuuren, D. P., Eyring, V., Friedlingstein, P., Hurtt, G., ... & Sanderson, B. M. (2016). The scenario model intercomparison project (ScenarioMIP) for CMIP6. *Geoscientific Model Development*, 9(9), 3461-3482. https://doi.org/10.5194/gmd-9-3461-2016

Payne, A. E., Demory, M. E., Leung, L. R., Ramos, A. M., Shields, C. A., Rutz, J. J., ... & Ralph, F. M. (2020). Responses and impacts of atmospheric rivers to climate change. *Nature Reviews Earth & Environment*, 1(3), 143-157. https://doi.org/10.1038/s43017-020-0030-5

Pendergrass, A. G., Meehl, G. A., Pulwarty, R., Hobbins, M., Hoell, A., AghaKouchak, A., ... & Woodhouse, C. A. (2020). Flash droughts present a new challenge for subseasonal-to-seasonal prediction. *Nature Climate Change*, 10(3), 191-199. https://doi.org/10.1038/s41558-020-0709-0

Pfahl, S., O'Gorman, P. A., & Fischer, E. M. (2017). Understanding the regional pattern of projected future changes in extreme precipitation. *Nature Climate Change*, 7(6), 423-427. https://doi.org/10.1038/nclimate3287

Pisso, I., Sollum, E., Grythe, H., Kristiansen, N. I., Cassiani, M., Eckhardt, S., ... & Stohl, A. (2019). The Lagrangian particle dispersion model FLEXPART version 10.4. *Geoscientific Model Development*, 12(12), 4955-4997. https://doi.org/10.5194/gmd-12-4955-2019

Pokhrel, Y., Felfelani, F., Satoh, Y., Boulange, J., Burek, P., Gädeke, A., ... & Wada, Y. (2021). Global terrestrial water storage and drought severity under climate change. *Nature Climate Change*, 11(3), 226-233. https://doi.org/10.1038/s41558-020-00972-w

Quante, M., & Matthias, V. (2006, December). Water in the Earth's atmosphere. In *Journal de Physique IV (Proceedings)* (Vol. 139, pp. 37-61). EDP sciences.

Ratna, S. B., Cherchi, A., Joseph, P. V., Behera, S. K., Abish, B., & Masina, S. (2016). Moisture variability over the Indo-Pacific region and its influence on the Indian summer monsoon rainfall. *Climate Dynamics*, 46, 949-965. https://doi.org/10.1007/s00382-015-2624-z

Rivoire, P., Martius, O., & Naveau, P. (2021). A comparison of moderate and extreme ERA-5 daily precipitation with two observational data sets. *Earth and Space Science*, 8(4), e2020EA001633. https://doi.org/10.1029/2020EA001633

Ropelewski, C. F., & Halpert, M. S. (1987). Global and regional scale precipitation patterns associated with the El Niño/Southern Oscillation. *Monthly Weather Review*, 115(8), 1606-1626. https://doi.org/10.1175/1520-0493(1987)115<1606:GARSPP>2.0.CO;2

Schumacher, D. L., Keune, J., Dirmeyer, P., & Miralles, D. G. (2022). Drought self-propagation in drylands due to land–atmosphere feedbacks. *Nature Geoscience*, 15(4), 262-268. https://doi.org/10.1038/s41561-022-00912-7

Seneviratne, S. I., Zhang, X., Adnan, M., Badi, W., Dereczynski, C., Di Luca, A., Ghosh, S., Iskandar, I., Kossin, J., Lewis, S., Otto, F., Pinto, I., Satoh, M., Vicente-Serrano, S. M., Wehner, M., & Zhou, B. (2021). Weather and Climate Extreme Events in a Changing Climate. In V. Masson-Delmotte, P. Zhai, A. Pirani, S. L. Connors, C. Péan, S. Berger, N. Caud, Y. Chen, L. Goldfarb, M. I. Gomis, M. Huang, K. Leitzell, E. Lonnoy, J. B. R. Matthews, T. K. Maycock, T. Waterfield, O. Yelekçi, R. Yu, & B. Zhou (Eds.), *Climate Change 2021: The Physical Science Basis. Contribution of Working Group I to the Sixth Assessment Report of the Intergovernmental Panel on Climate Change* (pp. 1513–1766). Cambridge University Press. https://doi.org/10.1017/9781009157896.013

Shemyakin, A., & Kniazev, A. (2017). *Introduction to Bayesian estimation and copula models of dependence*. John Wiley & Sons.

Sierra, J. P., Arias, P. A., Durán-Quesada, A. M., Tapias, K. A., Vieira, S. C., & Martínez, J. A. (2021). The Choco low-level jet: past, present and future. *Climate Dynamics*, 56, 2667-2692. https://doi.org/10.1007/s00382-020-05611-w

Skamarock, W. C., Klemp, J. B., Dudhia, J., Gill, D. O., Barker, D., Duda, M. G., … Powers, J. G. (2008). *A Description of the Advanced Research WRF Version 3* (No. NCAR/TN-475+STR). University Corporation for Atmospheric Research. https://doi.org/10.5065/D68S4MVH

Sklar, M. (1959). Fonctions de répartition à n dimensions et leurs marges. In *Annales de l'ISUP* (Vol. 8, No. 3, pp. 229-231).

Slette, I. J., Smith, M. D., Knapp, A. K., Vicente-Serrano, S. M., Camarero, J. J., & Begueria, S. (2020). Standardized metrics are key for assessing drought severity. *Global Change Biology*, 26(2). https://doi.org/10.1111/gcb.14899

Stohl, A., Forster, C., Frank, A., Seibert, P., & Wotawa, G. (2005). The Lagrangian particle dispersion model FLEXPART version 6.2. *Atmospheric Chemistry and Physics*, 5(9), 2461-2474. https://doi.org/10.5194/acp-5-2461-2005

Stohl, A., & James, P. (2004). A Lagrangian analysis of the atmospheric branch of the global water cycle. Part I: Method description, validation, and demonstration for the August 2002 flooding in central Europe. *Journal of Hydrometeorology*, 5(4), 656-678. https://doi.org/10.1175/1525-7541(2004)005<0656:ALAOTA>2.0.CO;2

Stohl, A., & James, P. (2005). A Lagrangian analysis of the atmospheric branch of the global water cycle. Part II: Moisture transports between Earth's ocean basins and river catchments. *Journal of Hydrometeorology*, 6(6), 961-984. https://doi.org/10.1175/JHM470.1

Sun, Q., Miao, C., Duan, Q., Ashouri, H., Sorooshian, S., & Hsu, K.-L. (2018). A review of global precipitation data sets: Data sources, estimation, and intercomparisons. *Reviews of Geophysics*, 56, 79–107. https://doi.org/10.1002/2017RG000574

Sun, Q., Zhang, X., Zwiers, F., Westra, S., & Alexander, L. V. (2021). A global, continental, and regional analysis of changes in extreme precipitation. *Journal of Climate*, 34(1), 243-258. https://doi.org/10.1175/JCLI-D-19-0892.1

Tallaksen, L. M., Madsen, H., & Clausen, B. (1997). On the definition and modelling of streamflow drought duration and deficit volume. *Hydrological Sciences Journal*, 42(1), 15-33. https://doi.org/10.1080/02626669709492003

Tan, X., Wu, X., Huang, Z., Fu, J., Tan, X., Deng, S., ... & Liu, B. (2023). Increasing global precipitation whiplash due to anthropogenic greenhouse gas emissions. *Nature Communications*, 14(1), 2796. https://doi.org/10.1038/s41467-023-38510-9

Tootoonchi, F., Sadegh, M., Haerter, J. O., Räty, O., Grabs, T., & Teutschbein, C. (2022). Copulas for hydroclimatic analysis: A practice-oriented overview. *WIREs Water*, 9(2), e1579. https://doi.org/10.1002/wat2.1579

Torres-Alavez, J. A., Das, S., Corrales-Suastegui, A., Coppola, E., Giorgi, F., Raffaele, F., ... & Sines, T. (2021). Future projections in the climatology of global low-level jets from CORDEX-CORE simulations. *Climate Dynamics*, 1-19. https://doi.org/10.1007/s00382-021-05671-6

Trenberth, K. E., Branstator, G. W., & Arkin, P. A. (1988). Origins of the 1988 North American drought. *Science*, 242(4886), 1640-1645. https://doi.org/10.1126/science.242.4886.1640

Trenberth, K. E., Dai, A., Rasmussen, R. M., & Parsons, D. B. (2003). The changing character of precipitation. *Bulletin of the American Meteorological Society*, 84(9), 1205-1218. https://doi.org/10.1175/BAMS-84-9-1205

Trenberth, K. E., Smith, L., Qian, T., Dai, A., & Fasullo, J. (2007). Estimates of the global water budget and its annual cycle using observational and model data. *Journal of Hydrometeorology*, 8(4), 758-769. https://doi.org/10.1175/JHM600.1

Ukkola, A. M., De Kauwe, M. G., Roderick, M. L., Abramowitz, G., & Pitman, A. J. (2020). Robust future changes in meteorological drought in CMIP6 projections despite uncertainty in precipitation. *Geophysical Research Letters*, 47(11), e2020GL087820. https://doi.org/10.1029/2020GL087820

Valenzuela, R. A., & Garreaud, R. D. (2019). Extreme daily rainfall in central-southern Chile and its relationship with low-level horizontal water vapor fluxes. *Journal of Hydrometeorology*, 20(9), 1829-1850. https://doi.org/10.1175/JHM-D-19-0036.1

Van de Pol, M., Jenouvrier, S., Cornelissen, J. H., & Visser, M. E. (2017). Behavioural, ecological and evolutionary responses to extreme climatic events: challenges and directions. *Philosophical Transactions of the Royal Society B: Biological Sciences*, 372(1723), 20160134. https://doi.org/10.1098/rstb.2016.0134

Van der Ent, R. J., Savenije, H. H., Schaefli, B., & Steele-Dunne, S. C. (2010). Origin and fate of atmospheric moisture over continents. *Water Resources Research*, 46(9). https://doi.org/10.1029/2010WR009127

Vázquez, M., Nieto, R., Liberato, M. L., & Gimeno, L. (2020). Atmospheric moisture sources associated with extreme precipitation during the peak precipitation month. *Weather and Climate Extremes*, 30, 100289. https://doi.org/10.1016/j.wace.2020.100289

Vicente-Serrano, S. M. (2016). Foreword: Drought complexity and assessment under climate change conditions. *Cuadernos de Investigación Geográfica*, 42(1), 7-11. https://doi.org/10.18172/cig.2961

Vicente-Serrano, S. M., Beguería, S., & López-Moreno, J. I. (2010). A multiscalar drought index sensitive to global warming: the standardized precipitation evapotranspiration index. *Journal of Climate*, 23(7), 1696-1718. https://doi.org/10.1175/2009JCLI2909.1

Vicente-Serrano, S. M., McVicar, T. R., Miralles, D. G., Yang, Y., & Tomas-Burguera, M. (2020). Unraveling the influence of atmospheric evaporative demand on drought and its response to climate change. *WIREs Climate Change*, 11(2), e632. https://doi.org/10.1002/wcc.632

Vicente-Serrano, S. M., Peña-Angulo, D., Beguería, S., Domínguez-Castro, F., Tomás-Burguera, M., Noguera, I., ... & El Kenawy, A. (2022). Global drought trends and future projections. *Philosophical Transactions of the Royal Society A*, 380(2238), 20210285. https://doi.org/10.1098/rsta.2021.0285

Vicente-Serrano, S. M., Peña-Angulo, D., Murphy, C., López-Moreno, J. I., Tomas-Burguera, M., Dominguez-Castro, F., ... & El Kenawy, A. (2021). The complex multisectoral impacts of drought: Evidence from a mountainous basin in the Central Spanish Pyrenees. *Science of the Total Environment*, 769, 144702. https://doi.org/10.1016/j.scitotenv.2020.144702

Wainwright, C. M., Allan, R. P., & Black, E. (2022). Consistent trends in dry spell length in recent observations and future projections. *Geophysical Research Letters*, 49(12), e2021GL097231. https://doi.org/10.1029/2021GL097231

Wang, K., & Dickinson, R. E. (2012). A review of global terrestrial evapotranspiration: Observation, modeling, climatology, and climatic variability. *Reviews of Geophysics*, 50(2). https://doi.org/10.1029/2011RG000373

Wang, S., Ma, X., Zhou, S., Wu, L., Wang, H., Tang, Z., ... & Gan, B. (2023). Extreme atmospheric rivers in a warming climate. *Nature Communications*, 14(1), 3219. https://doi.org/10.1038/s41467-023-38980-x

Wang, S., & Yuan, X. (2018). Extending seasonal predictability of Yangtze River summer floods. *Hydrology and Earth System Sciences*, 22(8), 4201-4211. https://doi.org/10.5194/hess-22-4201-2018

Westra, S., Alexander, L. V., & Zwiers, F. W. (2013). Global increasing trends in annual maximum daily precipitation. *Journal of Climate*, 26(11), 3904-3918. https://doi.org/10.1175/JCLI-D-12-00502.1

White, H. (1982). Maximum Likelihood Estimation of Misspecified Models. *Econometrica*, 50(1), 1–25. https://doi.org/10.2307/1912526

Wilhite, D. A., & Glantz, M. H. (1985). Understanding: the drought phenomenon: the role of definitions. *Water International*, *10*(3), 111-120. https://doi.org/10.1080/02508068508686328

WMO Atlas of Mortality and Economic Losses from Weather, Climate and Water Extremes (1970–2019) (World Meteorological Organization, 2021).

Xie, P., Chen, M., Yang, S., Yatagai, A., Hayasaka, T., Fukushima, Y., & Liu, C. (2007). A gauge-based analysis of daily precipitation over East Asia. *Journal of Hydrometeorology*, 8(3), 607-626. https://doi.org/10.1175/JHM583.1

Xu, G., Ma, X., Chang, P., & Wang, L. (2020). Image-processing-based atmospheric river tracking method version 1 (ipart-1) [software]. *Geoscientific Model Development*, 13(10), 4639–4662. https://doi.org/10.5194/GMD-13-4639-2020

Zhang, X., Alexander, L., Hegerl, G. C., Jones, P., Tank, A. K., Peterson, T. C., ... & Zwiers, F. W. (2011). Indices for monitoring changes in extremes based on daily temperature and precipitation data. *WIREs Climate Change*, 2(6), 851-870. https://doi.org/10.1002/wcc.147

Zhang, X., Hao, Z., Singh, V. P., Zhang, Y., Feng, S., Xu, Y., & Hao, F. (2022). Drought propagation under global warming: Characteristics, approaches, processes, and controlling factors. *Science of the Total Environment*, 838, 156021. https://doi.org/10.1016/j.scitotenv.2022.156021

Zhang, L., Zhao, Y., Cheng, T. F., & Lu, M. (2024). Future changes in global atmospheric rivers projected by CMIP6 models. *Journal of Geophysical Research: Atmospheres*, 129(3), e2023JD039359. https://doi.org/10.1029/2023JD039359

Zhou, S., Williams, A. P., Lintner, B. R., Berg, A. M., Zhang, Y., Keenan, T. F., ... & Gentine, P. (2021). Soil moisture–atmosphere feedbacks mitigate declining water availability in drylands. *Nature Climate Change*, 11(1), 38-44. https://doi.org/10.1038/s41558-020-00945-z

Zhu, Y., & Newell, R. E. (1998). A proposed algorithm for moisture fluxes from atmospheric rivers. *Monthly Weather Review*, 126(3), 725-735. https://doi.org/10.1175/1520-0493(1998)126<0725:APAFMF>2.0.CO;2

Zscheischler, J., Naveau, P., Martius, O., Engelke, S., & Raible, C. C. (2021). Evaluating the dependence structure of compound precipitation and wind speed extremes. *Earth System Dynamics*, 12(1), 1-16. https://doi.org/10.5194/esd-12-1-2021

Zscheischler, J., Westra, S., Van Den Hurk, B. J., Seneviratne, S. I., Ward, P. J., Pitman, A., ... & Zhang, X. (2018). Future climate risk from compound events. *Nature Climate Change*, 8(6), 469-477. https://doi.org/10.1038/s41558-018-0156-3

Universidade Vigo